QUANTIFYING UNCERTAINTIES IN LUNG DOSIMETRY WITH APPLICATION TO PLUTONIUM OXIDE AEROSOLS

By

THOMAS EDWARD HUSTON

A DISSERTATION PRESENTED TO THE GRADUATE SCHOOL
OF THE UNIVERSITY OF FLORIDA IN PARTIAL FULFILLMENT
OF THE REQUIREMENTS FOR THE DEGREE OF
DOCTOR OF PHILOSOPHY

UNIVERSITY OF FLORIDA

1995

Dedicated to Rhonda, my wife and friend--

without her encouragement this work would have been impossible.

ACKNOWLEDGMENTS

This work has been supported in part by Grant Number R23/CCR409769-01 from the Centers for Disease Control and Prevention (CDC); however, its contents are solely the responsibility of the author and do not necessarily represent the official view of CDC. Preliminary portions of the research were performed under appointment to the Environmental Restoration and Waste Management Fellowship Program administered by Oak Ridge Institute for Science and Engineering for the United States Department of Energy. I am especially grateful to these agencies for providing the financial assistance necessary to complete this work.

I wish to thank my supervisory committee members--Drs. William G. Vernetson (chair), W. Emmett Bolch (cochair), Marc Jaeger, David E. Hintenlang, William S. Properzio, and Wesley E. Bolch--for serving on the committee and for their guidance during the course of this study. I am especially thankful to Drs. William Vernetson, Emmett Bolch, and Marc Jaeger for their useful suggestions to improve content in early draft versions of the manuscript. I offer a special note of thanks to Dr. Emmett Bolch, who during the past two years provided me (through the resources of the CDC grant) with the financial backing to complete this research; his care for students is indeed a credit to his profession.

I am thankful to several others with whom I have had the privilege of associating throughout various stages of this work. These persons include, among many others, Drs. Gen Roessler, John Till, Helen Grogan, Tony James, and Alan Birchall. Dr. Gen Roessler served as a point of contact for me during the early stages of this work. She introduced me to Dr. Till, who (along with colleagues from Radiological Assessments Corporation) expressed a need for quantitative information regarding uncertainties in lung dose predictions for plutonium. Dr. Till assisted during the early stages of this work by helping me obtain draft reports from the National Council on Radiation Protection and Measurements (NCRP) and the International Commission on Radiological Protection (ICRP). At that time, both agencies were in the process of releasing independent models for respiratory tract dosimetry. I appreciate the willingness of the ICRP and NCRP to release these draft reports to me before publication. Drs. Tony James and Alan Birchall provided me with many useful materials and encouragement. Dr. Helen Grogan provided several helpful comments throughout the work.

I would like to thank my wife, Rhonda, for her constant encouragement throughout my "tenure" at the university. She kept me focused on my work, never complaining about the long hours I kept. She also helped organize the reference section of the manuscript. I have been truly blessed with a wonderful, caring wife and a best friend. I certainly look forward to spending the rest of my life (yes, I do plan to get one after graduation) with her. I want to thank our new son, Hayden Edward Huston (born

only days ago on July 24, 1995), for bringing me happiness and wonder while I have prepared this manuscript.

I would like to thank some (past and present) fellow students, Kaiss Al-Ahmady, Brian Birky, Thabet Tolaymat, George Harder, Louis Iselin, Susan Stanford, and Missy Jones, among others, for their friendship and stimulating discussions regarding the radiation sciences. I also appreciate the departmental staff in the Nuclear Engineering Sciences office (Barbara, Joan, Beth, Cess, and Donna) and the Environmental Engineering Sciences office (Sandy, Berdenia, and Shirley). Thanks also to Chuck, Al, Gene, and Gary for providing me with an outlet to this insanity by way of the Tuesday night trombone jazz sessions.

Finally, but certainly not least, I am very thankful to all of my family and friends back home in Arkansas for giving me hope and encouragement throughout the many, many years of my education. I miss them all greatly.

TABLE OF CONTENTS

page

ACKNOWLEDGMENTS iii

LIST OF TABLES x

LIST OF FIGURES xiv

ABSTRACT xviii

CHAPTERS

1 INTRODUCTION 1

1.1 Purpose of Study 3
1.2. Background Information 4
1.2.1. Radiation Exposure Pathways 4
1.2.2. Internal Radiation Dosimetry, Reference Man, and Risk 9
1.2.3. Advantages and Disadvantages of the Reference Man Approach 14
1.3. Previous Work 16
1.4. Description of Present Study 20
1.4.1. Assessment Problem Addressed 20
1.4.2. Units of Exposure 22
1.4.3. Summary of the Research Approach 24

2 METHODS FOR RESPIRATORY TRACT MODELING 27

2.1. Introduction 27
2.2. Development of Respiratory Tract Dose Models 31
2.3. Respiratory Tract Morphological Model 33
2.4. Respiratory Tract Deposition Model 35
2.5. Particle Size and Diffusion Characteristics 48
2.6. Respiratory Tract Clearance Model 51
2.7. Respiratory Tract Dose Model 63
2.8. Summary 70

page

3 METHODS FOR CONDUCTING PARAMETER UNCERTAINTY ANALYSES 72

3.1. Introduction 72
3.2. Quantifying Parameter Correlations and Uncertainties 75
3.2.1. Parameter Correlations 75
3.2.2. Parameter Uncertainties 78
3.2.3. Testing the Fit of an Assigned Distribution 84
3.2.4. Subjective Probability Judgements and Expert Opinion 86
3.3. Propagation of Parameter Uncertainty 88
3.3.1. Simple Random Sampling 89
3.3.2. Latin Hypercube Sampling 91
3.4. Presentation of Uncertainties in Model Predictions 96
3.5. Parameter Sensitivity Techniques 97
3.6. Description of the Lung Dose Uncertainty Code (LUDUC) 102
3.7. Summary 109

4 UNCERTAINTIES IN RESPIRATORY TRACT MODEL PARAMETERS 110

4.1 Deposition Model Parameters 112
4.1.1. Body Height 112
4.1.2. Body Mass Index 116
4.1.3. Airway Diameters and Lengths 123
4.1.4. Anatomical Dead Space 131
4.1.5. Regional Volumes of the Respiratory Tract 135
4.1.6. Functional Residual Capacity 137
4.1.7. Vital Capacity 139
4.1.8. Ventilation Rate and Volumetric Flow Rate 141
4.1.9. Tidal Volume 160
4.1.10. Fraction of Air Breathed Through the Nose 169
4.1.11. Uncertainty in Particle Inhalability 174
4.1.12. Regional Deposition Efficiency Uncertainty 176
4.2. Clearance Model Parameters 179
4.2.1. Introduction 179
4.2.2. Partition of Deposition in Clearance Model Compartments 180
4.2.3. Fractional Clearance Rate Constants 188
4.2.4. Absorption Rate Constants 190
4.3. Dose Model Parameters 200
4.3.1. Introduction 200
4.3.2. Measurements of the Bronchial Epithelium and Critical Cell Layers 201

page

4.3.3. Extrathoracic Regions 207
4.3.4. Bronchial Region 207
4.3.5. Bronchiolar Region 214
4.3.6. Surface Area of Bronchial and Bronchiolar Regions 219
4.3.7. Alveolar-Interstitial Region 222
4.3.8. Total Lung Mass 223
4.3.9. Mass of Lymph Nodes 225
4.3.10. Regional Risk-Apportionment Factors 226
4.3.11. Summary of Methods for Dose Model Parameters 228

5 APPLICATION OF LUDUC TO INHALED PLUTONIUM OXIDE AEROSOLS: RESULTS AND DISCUSSION 231

5.1. Introduction 231
5.2. Characteristics of $^{239}PuO_2$ Aerosols 233
5.3. Dose Uncertainty Results for Inhaled $^{239}PuO_2$ Aerosols 237
5.3.1. Exposure Scenario and Notational Conventions 237
5.3.2. Adult Males Exposed to $^{239}PuO_2$ Aerosols 239
5.3.3. Influence of Dose Integration Time 249
5.3.4. Influences of Age and Gender 252
5.3.5. Influences of Particle Size Dispersion 256
5.4. Dose Sensitivity Results for Inhaled $^{239}PuO_2$ 264
5.4.1. Combined Lung Dose 266
5.4.2. Regional Tissue Doses 270
5.5. Deposition Sensitivity Results 279
5.5.1. Bronchial Region 283
5.5.2. Bronchiolar Region 283
5.5.3. Alveolar-Interstital Region 284
5.6. Implications of Dose Results and Comparison to Reference Man Dose . 285
5.7. Summary of Results 292

6 CONCLUSIONS AND RECOMMENDATIONS 296

6.1. Summary of Research 296
6.2. Conclusions Based on Results for Plutonium Oxides 300
6.3. Recommendations for Future Research 305

page

APPENDICES

A COMPARISON OF ICRP AND NCRP MODELS 311

B THE CLEARANCE MODEL: SYSTEM OF DIFFERENTIAL EQUATIONS 323

C DOSE CALCULATIONS IN TRACHEOBRONCHIAL AIRWAYS 330

D TIDAL VOLUMES FOR CHILDREN 355

E DOSE DATA FOR INHALATION OF PLUTONIUM OXIDE 364

REFERENCES 410

BIOGRAPHICAL SKETCH 429

LIST OF TABLES

Table		page
1-1.	Selected intake-to-dose conversion factors for inhalation of some plutonium isotopes and other transuranics	11
1-2.	Organ and total risk per inhalation intake of plutonium compounds	12
1-3.	Specific information related to the assessment question and scenarios considered in this study.	21
2-1.	Recommended parameters for use in model of regional deposition for the fraction of intake inhaled and exhaled through the nose for any subject as functions of respiratory variables and anatomical size.	42
2-2.	Recommended parameters for use in model of regional deposition for the fraction of intake inhaled and exhaled through the mouth for any subject, as functions of respiratory variables and anatomical size.	43
2-3.	Description of input parameters required by the revised ICRP deposition model.	44
2-4.	Other parameters of use in modeling particle deposition in the respiratory tract.	46
2-5.	Reference values for mechanical clearance rates in the particle transport aspect of the ICRP human respiratory tract model.	56
2-6.	Reference values for partition of deposit among compartments in region.	56
2-7.	Assignment of compartments to source regions for short-range radiations in the revised ICRP respiratory tract model.	66
2-8.	Risk-apportionment factors recommended by the ICRP for weighting the dose to various respiratory tract target tissues	69
3-1.	Main steps involved in conducting a parameter uncertainty analysis.	74

Table		page
3-2.	Intervals paired for the Latin hypercube sample shown in Figure 3-6.	95
3-3.	Example of a hypothetical data set and its rank-transformed data set.	101
4-1.	Selected height data from the Second National Health and Nutrition Examination Study (NHANES II)	113
4-2.	Body mass index data from NHANES II	119
4-3.	Correlations between height and BMI.	119
4-4.	Dimensional model of the tracheobronchial tree in adult male	126
4-5.	Expressions relating airway lengths and diameters to body height	127
4-6.	Regression equations and related information for functional residual capacity.	138
4-7.	Regression equations and related information for vital capacity.	140
4-8.	Regression equations and related data characterizing basal metabolic rates for given age and gender classes	152
4-9.	Typical basal multiplier values for different activities	155
4-10.	Distributions assigned to basal multiplier for four physical exertion levels.	155
4-11.	Summary of distributions and methods used to predict variabilities in V_E.	157
4-12.	Fraction of ventilatory airflow passing through the nose in normal augmenters and in mouth breathers.	172
4-13.	Scaling constants used to account for uncertainties in regional deposition equations.	178
4-14.	Distributions and relationships describing partition of deposited material into compartments.	182
4-15.	Distributions adopted to describe uncertainties in fractional clearance rate constants used in mechanical clearance aspect.	189

Table page

4-16. Results of studies that examined long-term clearance of inhaled PuO_2 aerosols from the lungs. 191

4-17. Distributions and relationships adopted to describe the absorption clearance aspect for plutonium oxides. 199

4-18. Range of alpha particles in water for given energies. 201

4-19. Summary data for bronchial epithelium based on study by Gastineau et al. . . 204

4-20. Summary data for bronchial epithelium measurements based on study by Baldwin et al. 205

4-21. Summary data for bronchial epithelium measurements based on study by Mercer et al. 206

4-22. Summary of distributions used to model uncertainty in source and target tissue dimensions in the BB and bb regions. 229

4-23. Summary of methods to model uncertainties in source and target tissue volumes and masses. 230

4-24. Summary of distributions and relationships used to model uncertainties in risk apportionment factors. 230

5-1A. Combined equivalent dose to the lungs, H_{TH}/A_E: Ranking of selected variables 268

5-1B. Combined equivalent dose to the lungs, H_{TH}/A_E: Results of step-wise rank regression analysis 268

5-2A. Equivalent dose to BB secretory cell layer, $H(BB_{sec})/A_E$: Ranking of variables 271

5-2B. Equivalent dose to BB secretory cell layer, $H(BB_{sec})/A_E$: Results of step-wise rank-regression analysis 271

5-3A. Equivalent dose to BB basal cell layer, $H(BB_{bas})/A_E$: Ranking of variables . . 272

5-3B. Equivalent dose to BB basal cell layer, $H(BB_{bas})/A_E$: Results of step-wise rank-regression analysis 272

Table page

5-4A. Equivalent dose to bb secretory cell nuclei layer, $H(bb_{sec})/A_E$: Ranking of variables 273

5-4B. Equivalent dose to bb secretory cell nuclei layer, $H(bb_{sec})/A_E$: Results of step-wise rank-regression analysis 273

5-5A. Equivalent dose to AI tissue, $H(AI)/A_E$: Ranking of variables 274

5-5B. Equivalent dose to AI tissue, $H(AI)/A_E$: Results of step-wise rank-regression analysis 274

5-6A. Equivalent dose to thoracic lymph nodes (LNth), $H(LNth)/A_E$: Ranking of input variables 275

5-6B. Equivalent dose to LNth tissue, $H(LNth)/A_E$: Results of step-wise rank-regression analysis 275

5-7. Ranking of the top ten input variables as determined by standardized rank-regression coefficients for deposition fractions in respiratory tract regions 280

5-8A. Deposition fraction for BB region, DF_{BB}: Results of step-wise rank-regression analysis for the four top-ranked model parameters 281

5-8B. Deposition fraction for bb region, DF_{bb}: Results of step-wise rank-regression analysis for the four top-ranked model parameters 281

5-8C. Deposition fraction for AI region, DF_{AI}: Results of step-wise rank-regression analysis for the four top-ranked model parameters 281

5-9. Summary comparison of typical dose predictions for exposure of various population groups 293

5-10. Summary list of the variables contributing the most to uncertainties in equivalent doses to thoracic target tissues. 295

5-11. Summary list of variables contributing the most to uncertainties in deposition fractions to thoracic regions. 295

LIST OF FIGURES

Figure		page
1-1.	Factors to consider in radiological risk assessment	6
1-2.	Ratio of upper to lower 95% confidence bounds for committed effective dose equivalent per inhalation intake for adult male workers	18
2-1.	Components of a respiratory tract dosimetry model	28
2-2.	Anatomical representation of revised ICRP respiratory tract model	34
2-3.	Model of airway wall in the bronchial (BB) region	36
2-4.	Deposition model for the revised ICRP respiratory tract model	37
2-5.	Inhalability of particles as a function of the aerodynamic diameter for wind speeds of U = 1, 5, and 10 m/s.	39
2-6.	Particle transport model adopted by the ICRP to represent mucociliary and macrophage transport mechanisms to the gastrointestinal tract and lymph nodes.	52
2-7.	Compartment model recommended by ICRP to represent dissolution and absorption to blood and lung tissues for materials deposited in the respiratory tract.	57
2-8.	Alternate form for the dissolution/absorption model	59
2-9.	Schematic of the overall compartment model to represent clearance of material from the respiratory tract by mechanical and absorptive processes.	61
3.1.	Example of a uniform probability density function.	80
3.2.	Examples of triangular probability density functions	81
3-3.	Examples of two typical normal probability density functions.	82

Figure page

3-4. Examples of lognormal probability density functions. 83

3-5. Algorithm to generate a random number, ξ, on the interval (0,1). 90

3-6. Example of a Latin hypercube sample. 94

3-7. Schematic diagram showing the flow of computations in the Lung Dose Uncertainty Code (LUDUC). 103

4-1. Average body height as a function of age for males and females 115

4-2. Ratio of predicted to observed fractiles in body height for males 117

4-3. Average body mass index as a function of age for males and females 118

4-4. Ratio of predicted to observed fractiles in BMI for males 122

4-5. Average airway length versus airway generation at three body heights and residual standard errors of the linear regression equations used to predict lengths 128

4-6. Average airway diameter versus airway generation at three body heights and residual standard errors (RSE) of the linear regression equations used to predict diameters 128

4-7. Comparison of the cumulative probability for the observed residuals of $\ln(V_d)$ and the cumulative probability for E_{vd} 133

4-8. Anatomical dead space as a function of body height 134

4-9. Relationship between volumes at ambient temperature and pressure to volumes reported at body temperature and pressure 143

4-10. Predicted average values for V_E as a function of age for males and females . . 158

4-11. Comparison of ventilation rates at rest for males and females 160

4-12. Tidal volume at various physical exertion levels for males and females 167

4-13. Comparison of average resting tidal volumes in present study with other references 169

Figure page

4-14. Slow-clearing fraction of material deposited in the tracheobronchial region as a function of the volume-equivalent particle diameter. 185

4-15. Normal probability plot of the residuals for the slow-clearing thoracic deposit 186

4-16. Total ^{239}Pu disintegrations in the lung as a function of time for three values of s_s for the scenario specified 197

4-17. Surface area of the bronchial region as a function of height 221

4-18. Surface area of the bronchiolar region as a function of height 221

4-19. Total (blood-filled) lung mass as a function of age for males and females . . . 224

5-1. Fractiles predicted for the committed (50 year) equivalent dose per unit activity exposure to the lungs for a population group of 25-34 year-old males at light exertion 240

5-2. Dose quantities versus particle diameter in all thoracic target tissues for adult males exposed at light exertion 242

5-3. Equivalent dose to the lungs for adult males at four exertion levels: resting, sitting, light, and heavy exertion 245

5-4. Estimated values of median dose to all thoracic targets for adult males at four exertion levels: resting, sitting, light, and heavy exertion 247

5-5. Estimated values of the ratio of 95% to 5% dose fractiles for all thoracic targets for adult males at four exertion levels: resting, sitting, light, and heavy exertion 248

5-6. Influence of integration time on dose uncertainties 250

5-7. Influences of age and gender on dose uncertainties 255

5-8. Estimated values of median dose to all thoracic targets for nine different age/gender groups at light exertion 257

5-9. Estimated values of the ratio of 95% to 5% dose fractiles for all thoracic targets for nine different age/gender groups at light exertion 258

Figure page

5-10. Influence of activity-size dispersion on lung dose uncertainties 260

5-11. Estimated values of median dose versus activity median diameter for thoracic tissues in adult males at four activity-size dispersion values. 262

5-12. Estimated values of the ratio of 95% to 5% dose fractiles versus activity median diameter for thoracic tissues in adult males at four activity-size dispersion values 263

5-13. Lognormal probability plots for various equivalent doses in the respiratory tract 286

5-14. Estimated values of the geometric standard deviation, GSD, of equivalent dose per activity exposure in various target tissues for males at four broad exertion levels 288

5-15. Comparison of median dose values computed in this study to reference man dose values as predicted by LUDEP 290

Abstract of Dissertation Presented to the Graduate School of the University of Florida in Partial Fulfillment of the Requirements for the Degree of Doctor of Philosophy

QUANTIFYING UNCERTAINTIES IN LUNG DOSIMETRY WITH APPLICATION TO PLUTONIUM OXIDE AEROSOLS

By

Thomas Edward Huston

August 1995

Chairperson: William G. Vernetson
Cochair: W. Emmett Bolch
Major Department: Nuclear Engineering Sciences

A complete respiratory tract model for predicting lung dosimetry of inhaled radioactive aerosols involves several component models, including models for particle deposition in airways, biokinetic clearance and radiological decay of deposited materials, and radiological dose to critical target tissues. Each component depends on several parameters which can vary among members of a population group. The traditional approach has been to use reference values for parameters and to generate a single, deterministic reference dose. Based on conducting parameter uncertainty analyses, a methodology was developed in this study to incorporate parameter uncertainties into the respiratory tract modeling process. The methodology allows lung dose predictions to be determined as probability distributions, which better reflect the potential spread in doses for members of population groups than a single reference dose. The study involved

compilation and critical evaluation of previous studies to recommend defensible distributions representative of parameter uncertainties. Relationships were also identified to account for correlations between many model parameters. An interactive computer program, LUDUC (for LUng Dose Uncertainty Code), was developed to implement the methodology. Doses resulting from inhalation of plutonium oxide aerosols (aerodynamic diameters ranging from 0.1 to 50 microns) were investigated with LUDUC to demonstrate the methodology. This specific application of the methodology developed dose data which support an ongoing dose reconstruction study of plutonium released by the Rocky Flats Plant in Colorado. Resulting dose distributions followed a lognormal distribution shape for all scenarios examined. For many scenarios, the uncertainties in lung dose predictions were substantial--with geometric standard deviations approaching values of five. Uncertainties in doses increased by about a factor of ten from the smallest to the largest particle sizes. Differences in predicted dose distributions were small when comparing different age and gender groups from 2 to 35 years of age. Median doses for plutonium oxide generally agreed with reference dose values, providing some level of confidence in the reference-man approach. Parameter sensitivity analyses were conducted for inhaled plutonium oxides and revealed that dose uncertainties are generally attributable to only a few of the model parameters; parameter sensitivity depended on the inhaled particle diameter.

CHAPTER 1
INTRODUCTION

As knowledge of particle deposition, clearance, and radiation dosimetry in the human respiratory tract has increased, so have the sophistication and complexity of the conceptual and computational models used to describe these processes [e.g., International Commission on Radiological Protection (ICRP), 1960; Task Group on Lung Dynamics (TGLD), 1966; ICRP, 1979 and 1994]. In spite of recent advances in respiratory tract modeling, the reliability of model predictions should be addressed. A number of publications have focused on the techniques of model reliability assessment [e.g., Morgan and Henrion, 1990; International Atomic Energy Agency (IAEA), 1989; Organization for Economic Cooperation and Development (OECD), 1987; Hoffman and Gardner, 1983]. Although the general techniques of model reliability assessment can be applied to any mathematical model, past applications in the radiological dose assessment area (e.g., OECD, 1987; Desmet, 1988; Garten, 1980; Hoffman and Baes, 1979; Little and Miller, 1979) have primarily involved environmental transfer models (e.g., atmospheric, surface-water, groundwater, and terrestrial/aquatic food-chain transport models). Similar techniques have also been applied to light-water nuclear reactors to examine probabilities associated with accident scenarios (Rasmussen, 1975; Lewis, 1978). The current study

extends the application of reliability assessment techniques to include anatomical and physiological models adopted to simulate the human respiratory tract.

Several factors must be considered in a study of model reliability. According to a report by the International Atomic Energy Agency, model reliability is affected by:

> (1) uncertainty due to improper definition and conceptualization of the assessment problem or scenario,
> (2) uncertainty due to improper formulation of the conceptual model,
> (3) uncertainty involved in the formulation of the computational model,
> (4) uncertainty inherent within estimation of model parameter values, and
> (5) calculational and documentation errors in the production of results.
> (IAEA, 1989, p. 16)

The assessment problem and scope of this study, item (1), are discussed in detail in a following section. Uncertainties in the formulation of the conceptual and computational (or mathematical) models, items (2) and (3), were not examined here. In regard to items (2) and (3), an underlying assumption in this research has been that the conceptual and computational models adopted for this study appropriately represent the anatomy and physiology of the human respiratory tract. This study has used the revised respiratory tract model recently issued (ICRP, 1994) by the International Commission on Radiological Protection (ICRP). The model is based on recommendations by an ICRP task group composed of experts in the field of respiratory tract dosimetry. The effect of uncertainties in respiratory tract model parameters on model predictions, item (4), has been the primary focus of this research. These uncertainties were examined in detail by implementing parameter uncertainty and parameter sensitivity analyses of the revised ICRP respiratory tract model. Calculational errors, item (5), were examined to some level, since the probabilistic computer code developed to implement parameter uncertainty analyses of the

model was verified by comparison to a simpler, deterministic code, LUDEP, developed independently by the National Radiological Protection Board (Jarvis et al., 1993).

1.1 Purpose of Study

The primary purpose of this study was to develop a computational methodology for quantifying uncertainties (including stochastic variabilities) in respiratory tract model dose predictions for exposure of population groups to radioactive aerosols. The study is based on parameter uncertainty analyses of recommended biological models describing the fate of inhaled, radioactive aerosols in the human respiratory tract. A probabilistic computer code, LUDUC (Lung Dose Uncertainty Code), was developed in this study to perform these analyses. A secondary purpose of this study was to demonstrate this computational methodology by application to various inhalation exposure scenarios for plutonium oxide aerosols (while also providing guidance for application to other radionuclides and chemical forms). An objective of this study was not to develop a new respiratory tract model or to validate existing models, but rather to use a model currently recommended by national and/or international scientific advisory bodies (NCRP, 1993; ICRP, 1994) as the basis for conducting parameter uncertainty analyses. In addition, parameter sensitivity analyses also were performed in the study to identify the parameters that most influence model predictions.

The study was undertaken in an effort to improve current internal dose assessment methods by including parameter uncertainties in the dose modeling process. The methodology developed allows inhalation exposure-to-dose conversion factors (EDCFs),

among other assessment quantities, to be derived as probability distributions rather than as single, deterministic values--which are based solely on a reference human and do not account for parameter uncertainties arising from biological variability and lack of knowledge. Probabilistic characterization of respiratory tract model predictions is important for a many reasons.

First, probabilistic characterization helps to demonstrate the reliability of models adopted to represent the anatomical and physiological characteristics of the human respiratory tract. Second, it helps to improve the credibility of dose assessment calculations by estimating the potential distribution or range of values (including descriptive statistics such as medians, fractiles, means, and standard deviations) for quantities of interest. Finally, probabilistic characterization, when performed in conjunction with sensitivity analyses, helps to distinguish the more influential model parameters (with respect to model predictions) from the less influential ones. This latter sensitivity information can help guide future research efforts in respiratory tract modeling.

1.2. Background Information

1.2.1. Radiation Exposure Pathways

In scientific endeavors to quantify and predict human health risks from exposure to ionizing radiations, mathematical models are both appropriate and necessary. Numerous models exist for describing the release, environmental transport, food-chain propagation, human intake/usage, internal and external dosimetry, and subsequent health risks of radioactive materials (e.g., see Till and Meyer, 1983 and NCRP, 1984 for summary). An

illustration of the major factors considered in radiological risk assessment is shown in Figure 1-1. The upper aspect of this figure (boxes 1-5) involves release conditions and environmental transport factors, while the lower aspect (boxes 6-8) involves human lifestyle and biological factors. As indicated by bold print in Figure 1-1, this study focuses on components in the risk assessment chain that are associated with *usage rates* and *dose factors* (boxes 6 and 7) for inhalation of radioactive aerosols.

Within the context of inhalation of radioactivity, *usage rates* refer to the amounts of air and subsequently radioactivity inhaled per unit time by an individual. The amount of radioactivity inhaled per unit time is termed the *inhalation intake rate*. The time integral of the inhalation intake rate over the *exposure duration* is termed the *inhalation intake* (i.e., the total activity inhaled during the exposure period). Using the International System of units (SI), the inhalation intake is expressed in units of becquerels (Bq), where the becquerel is the special SI unit for radioactivity; one becquerel is equal to one radioactive disintegration (or transformation) per second.

A quantity of interest in this study, related to *usage rates*, is the *activity exposure*. In this study *activity exposure*, denoted by A_E and with units of Bq-hr/m^3, is defined as the time integral of the ambient *activity concentration*, $C_a(t)$ in Bq per m^3, over the *exposure duration*, D, in hours. Thus,

$$A_E = \int_0^D C_a(t)\,dt = D * \bar{C}_a \qquad (1\text{-}1)$$

where $\bar{C}_a$ represents the time-averaged ambient activity concentration over the exposure duration, D. The *activity concentration* represents the radioactivity per unit volume

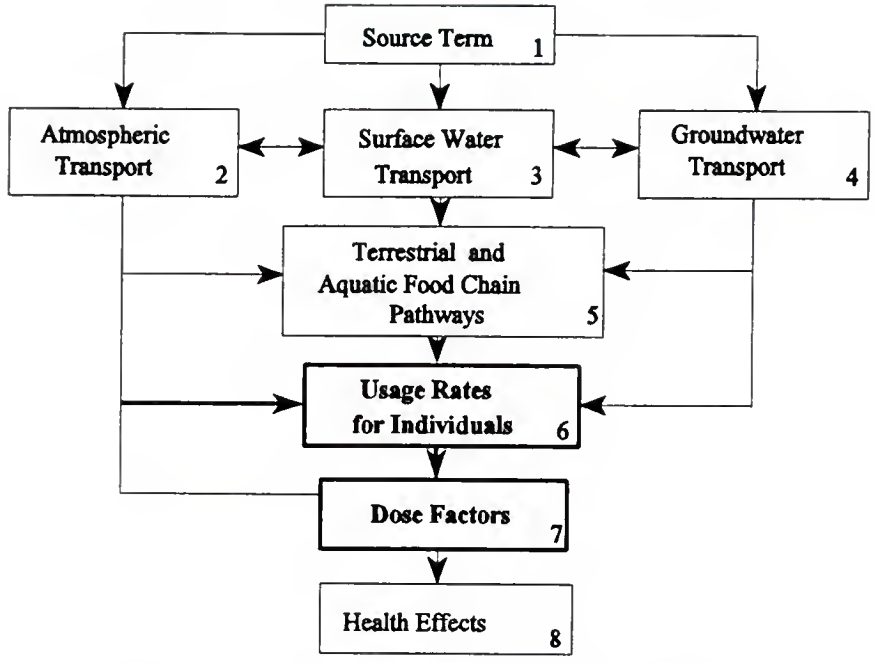

Figure 1-1. Factors to consider in radiological risk assessment. This study focuses on components represented by boxes 6 and 7 for inhalation. After NCRP 1984, Figure 1.

(ambient air) as a function of time for a specified radionuclide and a specified particle activity-size distribution. The *exposure duration*, D, represents the time a group of subjects is exposed to the specified activity concentration (i.e., the time over which the inhalation intake occurs). The activity-size distribution characterizes the fraction of the airborne activity associated with aerosol particles in various size ranges. Particle size characteristics and activity-size distributions are discussed in section 2.6.

As defined above, A_E is useful when the activity-size distribution and the physical exertion level of the population group do not change significantly over the exposure duration for the specified radionuclide. These conditions have been assumed in conducting the present study. Throughout this study a simplifying assumption was to

model the deposition of inhaled material as an acute event. This assumption is justified when the intake occurs over a relatively short exposure duration (during which ventilation rates remain relatively constant for individuals within the population group). For a long exposure duration (where ventilation and intake rates change), the mathematical model for biokinetic clearance requires mathematical expressions for the intake rates for individuals. Therefore, the methodology and results described herein are based on an acute activity deposition in the lungs.

Dose factors for inhalation refer to the radiation dose delivered over a specified time period to a tissue, organ, or the whole body per unit of inhaled activity. Dose quantities of interest for an *inhalation intake* include the *equivalent dose* to various body organs (including, but not limited to, the lungs) and the *effective dose* to the whole body. These dose quantities are described in later sections of this dissertation. Generally, these dose quantities represent the amount of radiation energy absorbed per unit mass (of the target tissue) and include various weighting factors to account for the biological effectiveness of different radiation types and for the differential radiation sensitivities of organs in the body. The special SI unit for *equivalent dose* and *effective dose* is the sievert, abbreviated Sv. The sievert has more fundamental units of joules per kilogram.

To compute radiation dose, the *dose integration time* must be specified. This integration time refers to the period, following the intake, over which the radiation dose is delivered. For radiation protection purposes, the ICRP (1991a) has recommended a dose integration time of 50 years for adults (18 years or older) and 70 years for children when

deriving equivalent and effective doses. However, for epidemiological studies or radiation litigation cases, other dose integration times might be desired.

It is important to distinguish clearly the *exposure duration*, D, from the *dose integration time*. As described above, the *exposure duration* refers to the time over which the intake occurs. The *dose integration time* refers to the time over which the dose rate is integrated to compute radiation doses to various body tissues and organs. For radionuclides that deposit in the body, dose continues to be delivered (in some cases over many years) after the intake has occurred since material is retained by various tissues.

Of the possible pathways for intake of a radionuclide into the body (i.e., inhalation, ingestion, absorption, and injection), inhalation is generally the most complex. Particles that deposit in the respiratory tract can undergo a number of processes including: (1) transport by mucociliary clearance to the gastro-intestinal (GI) tract, (2) phagocytosis by alveolar macrophages accompanied by possible transport to the lung-associated lymph nodes (where particles can be retained throughout the remainder of a person's life) or the GI tract via the mucociliary escalator, and (3) dissolution accompanied by absorption from lung tissues to the blood circulatory system. Therefore, in addition to being a region of concern with respect to radiation-induced risk, the respiratory tract is also a portal for inhaled radionuclides to other body tissues and organ systems. For example, animal studies involving inhalation of a number of transuranic compounds have demonstrated increased incidences of fatal cancer to the bones, liver, and kidneys, as well as the lungs (ICRP 1980).

1.2.2. Internal Radiation Dosimetry, Reference Man, and Risk

Radiation dose calculations for a given inhalation intake have traditionally involved deterministic techniques. In such techniques biological variabilities and uncertainties are ignored in the dose prediction yielding a single quantitative result. The traditional approach has been to define and apply anatomical and physiological models under the auspices of a *reference* or *standard man*, where reference man represents an individual comprising *typical* anatomical and physiological characteristics (e.g., ICRP, 1975, 1979). Such characteristics have been chosen by scientific consensus in order to provide a common (simplified and routine) basis for performing internal dose calculations. Acknowledging differences attributable to age and gender, the reference-man approach currently distinguishes between adult man, adult woman, and children of various ages (ICRP, 1989). Although a useful concept for simplifying computational effort, relatively few, if any, individuals in a given population group will match their reference man counterpart identically.

Using the reference-man approach, tables of intake-to-dose conversion factors (or DCFs) have been compiled for a number of specific intake conditions (e.g., Eckerman et al., 1988; ICRP, 1979; ICRP, 1989; USNRC, 1992). Such tables are used extensively in the nuclear industry and affect many decisions regarding past and future exposures of both workers and the general public to potential internal radiation sources.

Generally for internal dosimetry, the DCF represents either the radiation *equivalent dose* (to a tissue/organ) or the *effective dose* (to the whole body) per unit intake of radioactivity and has units of sieverts per becquerel (Sv/Bq). These quantities are defined

in ICRP *Publication 60* (1991a). These dose quantities include a *radiation weighting factor*, w_R, to account for the different biological effectiveness of various radiation types (e.g., photons, electrons, alpha particles, neutrons) per *absorbed dose*. When reflecting the effective dose, the DCF also incorporates tissue weighting factors, w_T, which account for the different radiation sensitivities of organs/tissues to induction of detrimental diseases.

Table 1-1 lists inhalation DCFs for some selected plutonium isotopes and transuranics. Except for Pu-241, the dose from these radionuclides is due primarily to energy deposited by alpha particles. Values in all but the last column are from Eckerman et al. (1988) and are for a working, reference adult male. These values are based on the dose methodology described in ICRP *Publication 30* and *Supplements* (ICRP, 1979). An aerosol with a 1 μm activity median aerodynamic diameter (AMAD, i.e., the diameter for which half of the activity is associated with particles of smaller aerodynamic diameter) with typical dispersion in size (i.e., geometric standard deviation or GSD < 3.5) has been used in deriving these values. The last column, labeled *effective dose* (denoted H_{eff}), was derived using the organ equivalent doses from Eckerman et al. (1988) and the tissue weighting factors adopted in ICRP *Publication* 60 (ICRP, 1991a). The clearance class refers to the residence time of various chemical forms of the radionuclide in the lungs. Clearance classes D, W, and Y (defined in ICRP, 1979) refer to materials having residence times that are on the order of days, weeks, and years in the lungs, respectively. Generally, plutonium oxides, which are of interest in this study, are assigned to class Y, while other chemical forms of plutonium are assigned to class W. The term denoted f_1 corresponds to

the fraction of the activity in the small intestine that is absorbed to the blood. An important point to note is that these tabulated DCFs have been listed without their associated uncertainties; the reason is that uncertainties in these DCFs have not been previously quantified.

Table 1-1. Selected intake-to-dose conversion factors (in Sv/Bq) for inhalation of some plutonium isotopes and other transuranics based on an activity median aerodynamic diameter, AMAD, of 1 μm.

Inhaled Nuclide	Class[a]; f_1[b]	Gonads[c]	Lungs[c]	Red Bone Marrow[c]	Bone Surfaces[c]	Liver[c]	H_{eff}[d]
Pu-238	W;1.0E-3	2.80E-05	1.84E-05	1.52E-04	1.90E-03	3.51E-04	6.26E-05
	Y;1.0E-5	1.04E-05	3.20E-04	5.80E-05	7.25E-04	1.37E-04	6.15E-05
Pu-239	W;1.0E-3	3.18E-05	1.73E-05	1.69E-04	2.11E-03	3.78E-04	6.87E-05
	Y;1.0E-5	1.20E-05	3.23E-04	6.57E-05	8.21E-04	1.51E-04	6.48E-05
Pu-240	W;1.0E-3	3.18E-05	1.73E-05	1.69E-04	2.11E-03	3.78E-04	6.87E-05
	Y;1.0E-5	1.20E-05	3.23E-04	6.57E-05	8.21E-04	1.51E-04	6.48E-05
Pu-241	W;1.0E-3	6.82E-07	7.42E-09	3.36E-06	4.20E-05	6.57E-06	1.29E-06
	Y;1.0E-5	2.76E-07	3.18E-06	1.43E-06	1.78E-05	3.01E-06	9.37E-07
Am-241	W;1.0E-3	3.25E-05	1.84E-05	1.74E-04	2.17E-03	3.91E-04	7.08E-05
Cm-244	W;1.0E-3	1.59E-05	1.93E-05	9.38E-05	1.17E-03	2.39E-04	4.04E-05

Source: All columns except last are from Eckerman et al. (1988). Last column is based on a weighted sum of organ/tissue doses with tissue weighting factors from ICRP (1991a).

[a] "Class" refers to clearance class (D,W, or Y) as defined in ICRP *Pub. 30* (ICRP 1979).

[b] The term f_1 represents the fraction of activity absorbed from the small intestines to the blood.

[c] Organ/tissue equivalent dose in sieverts per becquerel (Sv/Bq).

[d] Effective dose, H_{eff}: sum of organ/tissue equivalent doses weighted by tissue weighting factors as described by ICRP (1991a).

For all of the transuranics listed in Table 1-1, the bone surfaces (endosteal tissues) are predicted to receive the greatest equivalent dose (per inhalation intake). For class W forms, the liver is predicted to receive the second highest equivalent dose followed by the red bone marrow. For class Y forms, the lungs are predicted to receive the second highest

dose followed by the liver. In comparing organ DCFs, one should be aware that while DCFs indicate the typical equivalent doses to organs (of reference man), they do not necessarily reflect the radiation-induced health risks to these organs.

As a means to compare organs on a risk basis, the ICRP (1991a, Table B-20) has recommended organ/tissue risk factors. These risk factors quantify the additional probability (i.e., above the background or baseline probability) per organ equivalent dose that a person will experience a fatal cancer or contribute a severe genetic effect to offspring. The organ DCFs listed in Table 1-1 have been multiplied by respective organ risk factors (from Table B-20 of ICRP, 1991a) to determine organ risks per intake. Table 1-2 lists results of these computations for some of the radionuclides in Table 1-1.

For all radionuclides listed in Table 1-1 with clearance class W, the three organs having the greatest risk per unit intake (from highest to lowest risk) are: bone surfaces, red marrow, and liver; the lungs rank fifth and account for only about 5% of the total risk (based on data presented in Table 1-2). For clearance class Y, the order is lungs, bone surfaces, and red marrow; and the risk to the lungs contributes over 70% to the total risk from the intake. For both clearance classes, the order of organs as ranked by equivalent dose does not match the order as ranked by organ risk. The discrepancy is due to the fact that some organs are more sensitive to radiation than others.

As a practical example of what the numbers in Table 1-2 reflect, consider the total risk per intake for class Y Pu-239; the value is 3.84×10^{-6} per Bq. The annual limit on intake (ALI) for class Y Pu-239 is about 300 Bq (ICRP, 1991b). If one million (10^6) people experienced a 300 Bq intake, then about 1000 out of the 10^6 people

[i.e., (300 Bq)*(3.84x10^{-6} Bq^{-1})*(10^{6})] are predicted to develop a fatal cancer or pass on a severe genetic effect to offspring. It is predicted that 70% of those people, based on Table 1-2, would develop fatal lung cancers. A number of assumptions are implied in this methodology. The most important (and controversial) is that these risk factors, which are based on exposures of persons at high dose/high dose rate, are appropriate for the low dose/low dose rate exposures generally of interest in environmental exposure scenarios.

Table 1-2. Organ and total risk (of fatal cancer or severe genetic disorder) per inhalation intake of plutonium compounds for working adult male.

	Risk per Inhalation Intake (x 10^{-6} Bq^{-1})			
	Pu-238 [a]		Pu-239 [b]	
Organ	Class W	Class Y	Class W	Class Y
Lungs	0.156 (5.8%)	2.72 (73.7%)	0.147 (5.0%)	2.74 (71.4%)
Bone Surfaces	0.950 (35.2%)	0.290 (7.9%)	1.05 (35.5%)	0.410 (10.7%)
Red Marrow	0.760 (28.1%)	0.362 (9.8%)	0.845 (28.5%)	0.328 (8.5%)
Liver	0.526 (19.5%)	0.205 (5.6%)	0.567 (19.2%)	0.226 (5.9%)
Gonads[c]	0.280 (10.4%)	0.104 (2.8%)	0.318 (10.7%)	0.120 (3.1%)
Total Risk[d]	2.70 (99.0%)	3.69 (99.8%)	2.96 (98.9%)	3.84 (99.6%)

Notes: Values are based on product of dose factors from Eckerman et al. (1988) for working adult male (presented in Table 1-1) and organ risk factors from ICRP *Pub. 60* (1991a, Table B.20). Values in parentheses represent percent contribution of respective organs to the total risk.

[a] Values for Am-241 compounds are approximately equal to values for class W Pu-238.

[b] Values for Pu-240 are equal to values for Pu-239 (for respective classes).

[c] Risk of severe genetic effects for gonads. Risk of fatal cancer for other organs.

[d] Total risk includes contributions from other organs (e.g., stomach, bladder, breast, etc.) not listed in the table. Parenthetical values represent the percent contribution from organs listed in the table.

In summary, the above discussion indicates that inhalation of radioactive aerosols introduces risks to the lungs as well as to other body organs. Traditional methods provide

only point, deterministic predictions of organ dose/risk, not information on the uncertainty in these quantities. Regardless of which organs acquire higher risks after an inhalation intake, uncertainties in respiratory tract models are important and affect dose and dose-based risk predictions. For certain inhaled radionuclides which pose the greatest risk to lung tissues (e.g., the class Y transuranics listed in Table 1-1), uncertainties in all aspects (i.e., deposition, clearance, and dosimetry) of the respiratory tract model are potentially important. For inhaled radionuclides that pose greater risks to tissues other than the lungs (e.g., class W transuranics listed in Table 1-1), uncertainties in the deposition and clearance aspects of the respiratory tract model are nonetheless important because they influence the amounts of radioactivity that reach these tissues. In the present study, the focus is only on uncertainty in radiation dose to the lungs. However, the methodology developed can also be useful for quantifying uncertainties in other organ doses (inasmuch as they are influenced by the lung model).

1.2.3. Advantages and Disadvantages of the Reference-Man Approach

As discussed, the reference-man approach for dose assessment results in single, quantitative (deterministic) dose estimates for a given intake scenario. In many circumstances such an approach is adequate and useful. For example, the following situations are well served by this approach: (1) if the purpose of the dose assessment were simply to demonstrate compliance with radiation protection standards and regulatory limits or, (2) if the purpose of the assessment were to perform screening calculations in order to identify doses (and dose pathways) which might result in serious health effects.

However, if the dose assessment study were being performed to assess actual radiological health risks either to an exposed individual or to an exposed population group (e.g., as in radiation litigation cases or epidemiological studies), it is difficult to justify the reference-man approach (depending on the magnitude of the predicted risks). Individual and population-wide tissue doses might differ significantly from *typical* doses based on the reference-man methodology. In the former case, an exposed individual would likely differ from reference man with respect to anatomical and physiological characteristics. In the latter case, the problem is that the reference-man approach does not address the biological variabilities among individuals in a population group. Additionally, the reference-man approach does not include uncertainties due to lack of knowledge regarding model parameters.

A number of major studies are underway in the United States whose tasks are to assess radiation doses and risks to population groups exposed to past releases of radioactive and hazardous materials from nuclear weapons-related production and testing sites. Facilities under study include the U.S. Department of Energy Hanford Site in Washington, Rocky Flats Plant in Colorado, Savannah River Site in South Carolina, and Oak Ridge National Laboratory in Tennessee, among others. A difficult issue that all of these studies face is one of incorporating uncertainties in dose and risk estimates. Some of these studies have attempted to include uncertainties in environmental transfer models (e.g., PNL, 1991a, 1991b; 1991c); however, none have conducted a detailed examination of the uncertainties in human biological models (describing the fate of the radionuclide after it enters the body). It would be beneficial to know whether variabilities in predicted

dose attributable to uncertainties in the human biological models are negligible compared to variabilities in dose attributable to uncertainties in environmental transfer models (i.e., uncertainties in source-term, atmospheric/hydrogeologic dispersion, and terrestrial/aquatic food-chain models).

1.3. Previous Work

Upon conducting a literature search for previous work, three studies were found which dealt with uncertainties in inhalation radiation doses attributable to human respiratory tract models and associated parameters. Uncertainties have been examined for: (1) the effective dose (to whole body) due to inhaled U-238, Th-230, Ra-226, and Pb-210 (Wise, 1985), (2) dose to basal cells of the bronchial epithelium due to inhalation of radon decay products (Hofmann and Daschil, 1986), and (3) dose to the lungs due to inhalation of radon decay products based on the revised ICRP lung model (Birchall and James, 1994).

Based on measured deposition data from human experiments by Chan and Lippman (1980) and Yu et al. (1981), Wise (1985) examined uncertainties in the fitting parameters of empirical equations used to predict particle deposition in the respiratory tract. These uncertainties were propagated through the dose methodology recommended in ICRP *Publication* 30 (1979) to obtain uncertainty bounds for committed-effective-dose equivalents (i.e., dose integrated over 50 years post intake) for a number of selected inhalation scenarios. Uncertainties in organ committed dose to the lung were not presented; only the committed effective dose to the whole body. Selected statistics and

uncertainty limits were tabulated for a number of particle aerodynamic diameters, radionuclides, and solubility classes. Wise did not directly account for stochastic variabilities in the input parameters of the lung deposition model such as airway dimensions, tidal volumes, ventilation rates, etc. Wise's study also neglected uncertainties in the clearance aspect of the lung dose model. Furthermore, variability in parameters involved in systemic and excretion models for anatomical and physiological systems beyond the respiratory tract were not included. Thus, the extent of the uncertainty in effective dose was under-estimated.

With the above limitations, Wise found that uncertainties in deposition model predictions lead to committed effective dose equivalents whose lower and upper 95% confidence limits differed by less than a factor of about 10. If a log-normal distribution is assumed for dose predictions, this factor corresponds to a geometric standard deviation, GSD, of about 1.8 (i.e., $10^{1/4}$). Ratios of the upper 95% confidence bound to the lower 95% bound have been determined from results tabulated by Wise and are plotted in Figure 1-2. This plot represents a working adult male breathing (20 L/min) entirely through the nose. The ratio for the two largest particle sizes (5 and 6 μm) are not shown for U-238 since the lower 95% confidence limits were zero for these conditions. Wise also reported data for mouth breathers; the ratios obtained were slightly less than for nose breathers. While these results were important as a first attempt to quantify uncertainties in inhalation dose coefficients, they are incomplete.

Hofmann and Daschil (1986) performed a parameter uncertainty analysis on the respiratory tract models for radon progeny (Hofmann, 1982a, 1982b) in order to derive

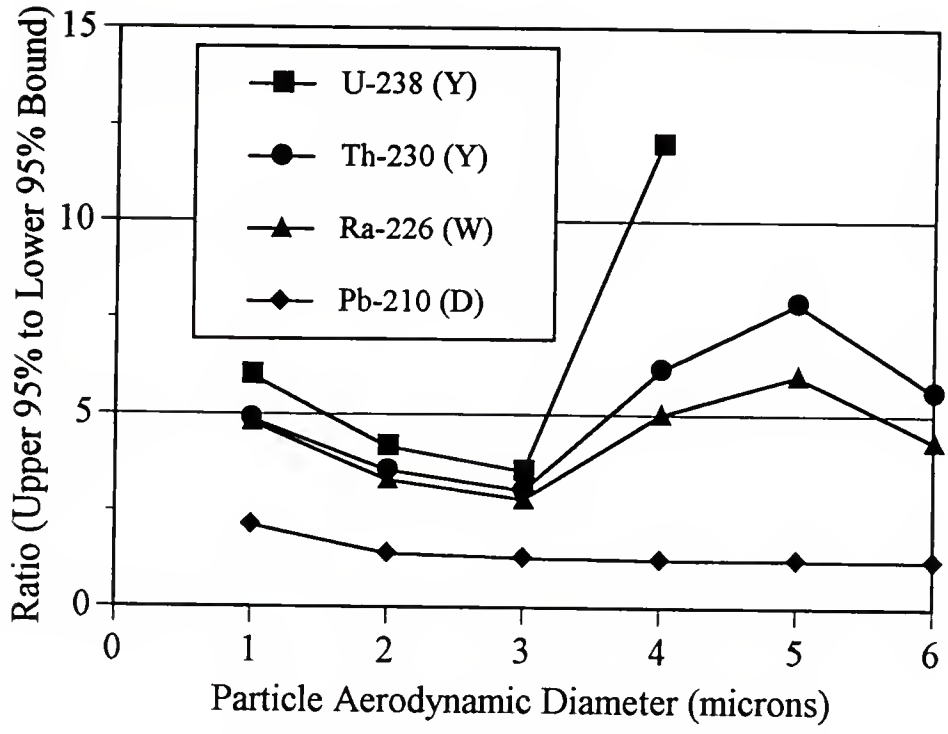

Figure 1-2. Ratio of upper to lower 95% confidence bounds for committed effective dose equivalent per intake for adult male workers. Based on results from Wise (1985). The ratio is undefined for the largest two diameters (5 and 6 μm) of U-238 because the lower bound was reported as zero.

distributions in radiation dose to the basal cells of various airway generations of the bronchial epithelium. For the target cells considered (basal cells), Hofmann and Daschil examined uncertainty in more detail than Wise (1985) by accounting for variabilities in a number of model input parameters (including deposition fractions, total surface area of bronchial generations, amount of inhaled activity, mucociliary clearance rates, translocation rates to blood, and basal cell depths).

However, the authors did not examine uncertainties in radiation doses arising in the pulmonary region of the lungs. Furthermore, doses were only examined for individual

basal cells as the targets. While dose at the cellular level is of interest, the approach adopted in the revised ICRP lung model (ICRP, 1994) is to compute average doses for critical tissues (composed of many critical cells). The authors found that doses to basal cells of the bronchial epithelium under specified conditions were approximately lognormally distributed and that the 50% and 99% fractiles differed by about a factor of five depending on the tracheobronchial generation. This value corresponds to a GSD of about two. This dispersion is similar to that which can be deduced from results of the study by Wise (1985).

Birchall and James (1994) recently performed an uncertainty analysis of the effective dose per unit exposure from radon progeny using the revised ICRP lung model (ICRP, 1994). This model is also used to conduct the present study. The primary purpose of their study was to reconcile dose factors derived from the revised lung model with those derived from epidemiological estimates. The study was performed for a working male with median ventilation rate of 20 L/min. Uncertainties were included for aerosol size characteristics, ventilation rate, deposition and clearance factors, source and target layer dimensions, and regional risk-apportionment factors (discussed later in Chapter 2), among other variables. Here Birchall and James found that model predictions were influenced largely by the choice of values for the regional risk-apportionment factors. Results indicated that effective dose per unit radon progeny exposure varied over about one order of magnitude based on parameter distributions selected.

While the study by Wise (1985) did produce results of a useful form for whole-body dose assessment activities, the results are incomplete since uncertainties only

pertained to the lung deposition portion of the dose model. Hofmann and Daschil (1986) produced results which accounted for more detail in the uncertainty and variability of lung model parameters but did not examine uncertainties in doses to the pulmonary region of the lungs. Consequently, it is difficult to apply results of that study to class Y materials such as plutonium oxides where a relatively large dose is expected to be delivered to the pulmonary region of the lungs. The study by Birchall and James (1994) included parameter uncertainties in the revised ICRP lung model but focused strictly on radon progeny. Furthermore, all of the above studies were performed for working reference man--not for other variants of the population (i.e., other age and gender groups).

1.4. Description of Present Study

1.4.1. Assessment Problem Addressed

According to the IAEA (1989), the reliability of model predictions can only be properly examined within the context of a well-defined assessment problem. The assessment problem of interest throughout this study was the following:

> Determine the *assessed quantity* (per unit activity exposure, i.e., per Bq-hr/m^3) to an *unspecified* individual in a population group exposed under the following scenario:
> (a) specified age/gender of the population group,
> (b) specified exertion level (resting, sitting, light exertion, or heavy exertion) of the population group,
> (c) specified radionuclide/chemical form,
> (d) specified aerosol activity-size distribution (including related parameters such as particle mass density and particle shape factor, defined in section 2.5),
> (e) specified dose integration time,
> (f) specified ambient temperature and barometric pressure over exposure duration.

The term *assessed quantity* in the above assessment problem serves simply as a placeholder for text describing specific quantities of interest in this study. Table 1-3 lists the *assessed quantities* and scenario information which were investigated in the present research. Quantities of interest included (1) the fraction of inhaled radioactivity that deposits in various respiratory tract (RT) regions, (2) the total number of radionuclide transformations that occur in various RT source components as functions of time, and (3) the radiation dose delivered to various RT target tissues for a specified dose integration time. For item (3), the *assessed quantity* corresponds to a dose conversion factor, expressed per unit activity exposure (i.e., an exposure-to-dose conversion factor, or EDCF). These assessed quantities are discussed in more detail in Chapter 2.

Table 1-3. Specific information related to the assessment question and scenarios considered in this study.

Radionuclide/ Chemical Form	Exertion Level	Population Age (years)[a]	Assessed Quantity[b]
$^{239+240}PuO_2$	Resting (Sleeping)	2	Deposition Fraction
	Sitting (Awake)	5	(activity deposited in RT
	Light Exertion	10	regions)
	Heavy Exertion	15	
		18-24	Number of Transformations
		25-34	(in RT source components)
		35-44	
		45-54	Equivalent Dose
		55-64	(to RT target regions)
			Equivalent Dose
			(to lung: weighted sum)

[a] Both males and females have been considered at these ages.

[b] Quantities assessed in this study pertain to respiratory tract regions or to combinations of regions; other organs/tissues are not examined. Assessed quantities and respiratory tract regions are discussed in detail in Chapter 2.

Since this assessment problem addresses *unspecified* individuals within a population group, it possesses a probabilistic rather than deterministic answer. In other words, stochastic variability exists in the *assessed quantity* among unspecified individuals in the population group. Therefore, the answer to the assessment question should be represented by a probability density function (distribution) rather than a single number.

In performing demonstration calculations in this study, the scope of the assessment problem has been narrowed to include only inhaled PuO_2-laden aerosols with radionuclides Pu-239 and Pu-240. These particular radionuclides/chemical form was selected to support a dose reconstruction study underway by the Colorado Department of Public and Environmental Health. One purpose of that study is to predict population risks arising from historical releases of plutonium from the Rocky Flats Plant (a facility that produces and stores nuclear weapons components and is located about 20 from downtown Denver, Colorado). $^{239+240}PuO_2$ emits primarily alpha particles and is relatively insoluble in lung fluids; also as shown by predictions in Table 1-2, this material (depending on the magnitude of the intake) can result in potentially large risks to the lungs. As further limitation on the work, aerosol particles were assumed to be non-hygroscopic (i.e., particles do not increase in size upon entering saturated conditions of the respiratory tract)

1.4.2. Units of Exposure

Traditional methods have predicted inhalation dose conversion factors per unit *intake*, where the *intake* represents the amount of radioactivity inhaled. However, in the assessment question defined above, the *intake* possesses stochastic variability among

individuals of the exposed population. In order to account for these variabilities, an improved reference unit for dose predictions is the *activity exposure*, A_E, defined earlier.

At least three reasons exist for expressing dose factors per unit activity exposure rather than per unit activity intake. First, in assessing doses to humans from inspirable radionuclides released to the environment, atmospheric dispersion models are usually implemented to estimate airborne activity concentration, i.e., $C_a(t)$ in Bq m^{-3} at specific locations. By expressing dose factors in terms of activity exposure rather than intake, a more efficient coupling of the results of dispersion models and inhalation dose factors can be achieved. If dose factors were per unit intake, one would still need to determine the inhalation intake in order to use the dose factor.

Second, intake depends on the human ventilation rate which is influenced by biological variability and lifestyle habits among members of a population. It is desirable in this study to account for variability in ventilation (and subsequently the intake) as a contributor to uncertainties in dose factors. The activity exposure, A_E, is not influenced by the ventilation rate.

Third, the ventilation rate is a parameter in the deposition component of the lung dose model (it is proportional to the average inspiratory flow rate); so the dose coefficient (expressed per unit intake) is correlated with the intake since both are mutually dependent on ventilation rate. Therefore, in this study inhalation dose coefficients were derived per unit activity exposure and have units of Sv per Bq·hr·m^{-3}.

1.4.3. Summary of the Research Approach

As discussed in the opening section of this chapter, the reliability of model predictions is affected by several uncertainties introduced through the modeling process. This study examined the uncertainty in model predictions attributable to parameter uncertainties. The respiratory tract model issued recently by the ICRP (1994) was selected to perform this study. The study was divided into three phases: I, II, and III.

Phase I involved development of a computer program to implement the adopted respiratory tract model and to couple the model with existing numerical random sampling programs. The program developed in this work accounts for all aspects of the RT model, including particle deposition, clearance, and radiation dosimetry. An existing program that performs Latin hypercube sampling (Iman and Shortencarier, 1984)--which is a form of random number sampling used to select values for the model parameters from their respective, assigned, probability distributions--was coupled with the program for solving the respiratory tract model. Sampled model parameter values are combined to form input vectors (or realizations) which are propagated through the model to produce numerical distributions in model predictions. An overview of the RT model, and the techniques implemented to solve it, are provided in Chapter 2 and related appendices. Techniques employed in this study for generating random samples of the joint probability density function for the combined ranges of all parameters for propagating parameter uncertainties through the model structure are discussed in Chapter 3. That chapter also presents techniques used to examine parameter sensitivities in the model predictions.

Phase II of the study involved quantifying uncertainties and variabilities in respiratory tract model parameters. Some of the general concepts involved in this phase of the study are discussed in Chapter 3. Based on an extensive literature review, Chapter 4 presents the specific parameter distributions adopted to perform uncertainty analyses in this study. This phase of the work was necessarily tedious since approximately seventy input parameters were assigned distributions in the RT model. Although many of these parameters were not primary input parameters, they were needed in order to account for correlations between and restrictions on the primary model parameters. Most of the parameter distributions presented in Chapter 4 are independent of radionuclide and chemical form; so techniques developed in this study could be applied with minimal effort to other radionuclides/forms. For example, except for hygroscopic materials, all parameters related to the deposition component of the model are generally independent of radionuclide and physico-chemical form. For the clearance model, only the parameters related to dissolution and absorption clearance processes and the radioactive decay constant depend on the radionuclide/form. For the dose model, all source and target geometrical dimensions are independent of nuclide/form; however, energy deposition computations do depend on the radionuclide decay scheme (radiation types, frequencies, and energies).

Phase III of the study involved application of the computational methodology (developed in Phase I) and recommended parameter distributions (developed in Phase II) to various assessment scenarios (i.e., substitution of entries in Table 1-3 into the assessment problem model). These scenarios involved inhalation exposures to plutonium

oxide aerosols by various population groups specified by age and gender. Equivalent doses to lung tissues and an overall, combined lung dose were examined for various particle sizes. This final phase also included sensitivity analyses with the primary model parameters to determine which parameters contributed most to the uncertainty in equivalent dose predictions for the lungs. The results of these activities are presented in Chapter 5. Chapter 6 presents a summary of the work, important conclusions and recommendations, and suggests future research to expand the methodology and the body of knowledge concerning uncertainties in human biological-radiological dosimetry models.

CHAPTER 2
METHODS FOR RESPIRATORY TRACT MODELING

2.1. Introduction

In this study, parameter uncertainty analyses have been conducted with the new respiratory tract model recommended by the International Commission on Radiological Protection (ICRP, 1994). The National Council on Radiation Protection and Measurements (NCRP, 1993) has also been working to issue guidance on respiratory tract modeling (independently of the ICRP). However, a comparison of the two models (see Appendix A) revealed difficulties in implementing the NCRP model in the numerical strategy employed by this study--which required solving the model repetitively and efficiently. In this study, Monte Carlo techniques have been employed to treat model parameters as random variables within the computational model recommended by the ICRP (these techniques are discussed in Chapter 3). The purpose of the current chapter is to provide an overview of the components of the new ICRP respiratory tract model and to outline the computational techniques for solving these components. A complete description of the model can be found in ICRP Publication 66 (ICRP, 1994).

Although generally cited as a single entity, a respiratory tract model for dose assessment involves a number of component models arising from many specialized areas of study. As illustrated in Figure 2-1, the overall model can be divided into three primary

components--deposition, clearance, and dosimetry models. Each component involves a number of input parameters which can depend on the exposure scenario. Topics which must be considered in developing the conceptual and computational models for the respiratory tract and in quantifying associated input parameters include respiratory tract morphology, radiation biology, and respiratory physiology. In this context, morphology refers to the anatomy and structure of the airways and associated tissues; radiation biology involves identification and sensitivities of various critical (target) cells in the respiratory tract; and respiratory physiology involves the functions and dynamics of the airways and associated tissues. Aerosol particle size characteristics must also be considered since they affect deposition mechanisms.

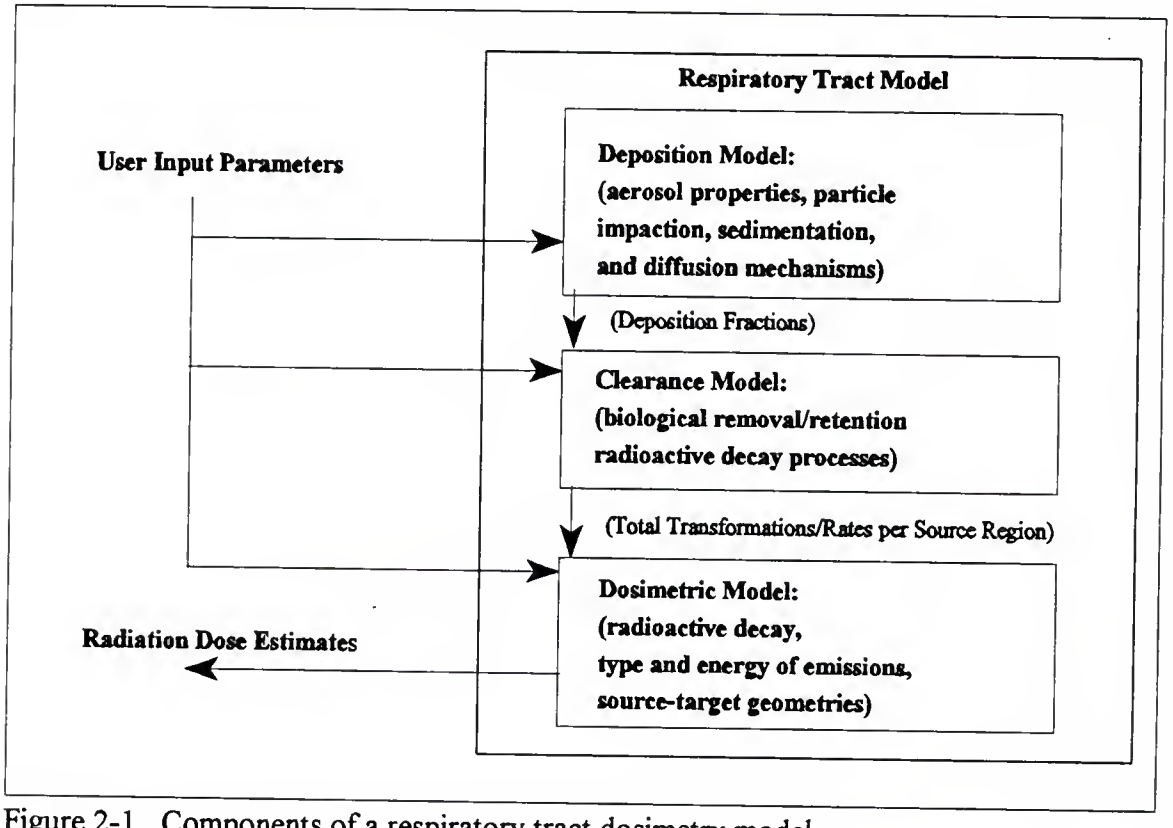

Figure 2-1. Components of a respiratory tract dosimetry model.

Particles deposit on airway walls by several interacting mechanisms including inertial impaction, gravitational sedimentation, Brownian diffusion, interception, and electrostatic attraction. The efficiencies of these deposition processes depend on a number of parameters including: particle physical characteristics (e.g., aerodynamic diameter, mass density, shape factor, and diffusion coefficient), airway diameters and lengths, airway branching and gravitational angles, tidal volume, functional residual capacity, and ventilation rate. Due to particle physical characteristics and air flow patterns in the lung, one or more of the above deposition mechanisms can dominate in various regions of the respiratory tract. Deposition generally does not depend on the radionuclide or its chemical form (except for hygroscopic materials). Predictions of the deposition component of the respiratory tract model include the fractions of inhaled activity which deposit in various respiratory tract regions. These deposition fractions are subsequently inputs to the clearance model.

Clearance of deposited materials refers to their biological and radiological removal from the respiratory tract. Three primary mechanisms exist for biological clearance in the respiratory tract: (1) mucociliary clearance of material to the gastrointestinal tract, (2) phagocytosis by alveolar macrophages followed by subsequent translocation to lymph nodes or to the mucociliary escalator, and (3) dissolution of material accompanied by absorption to airway tissues and/or to the blood circulatory system. When the material is radioactive a fourth removal mechanism exists--radioactive decay. Depending on the region of deposition and the physico-chemical form of the deposited material, various clearance mechanisms/patterns can occur. To model clearance, the respiratory tract is

compartmentalized and is traditionally described by a system of first-order, linear differential equations with respect to time. Except in very unique circumstances, deposition and clearance models are not intended solely for radioactive materials. From both a biological and mathematical perspective, the only difference between a radioactive and non-radioactive material with respect to deposition and clearance is the accommodation of radioactive decay as one removal mechanism. Two predictions are generally of interest for the clearance model as applied to inhaled radionuclides. One is the total number of radioactive transformations (or disintegrations) that occur in individual model compartments over a specified integration time; the other is the transformation rate (or activity) of the radionuclide in individual model compartments at a specified time. The latter model prediction is related to the radiation dose rate while the former is related to the radiation dose (i.e., the time-integrated dose rate).

The dosimetry component of a respiratory tract model is unique to radioactive materials. The radiation dose rate attributable to short-range radiation types (e.g., alpha particles, beta particles, and electrons) is directly related to the amount of radioactivity present in lungs; this activity is determined by solving the clearance model for the intake scenario of concern. For gamma rays and other penetrating radiation types, activity in other body organs can also contribute to the lung dose. The radiation dose is the integral of the dose rate over time and is related to the total number of radioactive transformations that occur in organs in the specified time interval. The dosimetry aspect depends on the radionuclide since different decay schemes (radiation types, frequencies, and energies) are characteristic of different radionuclides. Furthermore, for short-range radiations, the dose

to critical lung tissues is very sensitive to the source-target geometry. This geometry refers to the spatial relationship between tissues that contain the radioactive material (source regions) and tissues that contain the critical cells (target regions).

2.2. Development of Respiratory Tract Dose Models

A brief summary of the evolution of the model used in this study has been given by the ICRP (1994). The first coherent model integrating respiratory tract deposition, clearance, and dosimetry was issued in ICRP *Publication 2* (ICRP, 1960). Prior to that publication, discussions and recommendations concerning respiratory tract dosimetry were made at various conferences, such as the Tripartite Conferences on Radiation Protection held from 1949-1953 (Taylor, 1983). The model reported in ICRP *Publication 2* assumed that, lacking specific data, 75% of inhaled aerosol particles would deposit in the respiratory tract (50% deposited in upper airways; 25% deposited in the lungs; and 25% was exhaled). Concerning clearance, the model classified materials as either soluble or insoluble. Soluble materials that deposited in the lungs were assumed to be absorbed completely (by the blood) and translocated to other body tissues. For insoluble materials that deposited in the lungs, half of the material was assumed to clear (to the GI tract) with a biological half time of 24 hours (presumably to the GI tract); the other half was assumed to clear with a biological half time of 120 days (radiological decay would affect the overall clearance time).

In 1966, a revised lung model was published (TGLD, 1966) by the ICRP Task Group on Lung Dynamics. A slightly modified version of this model was ultimately

published by the ICRP in *Publication 30* (ICRP, 1979). Most of the current annual intake limits of radionuclides for workers (e.g., USNRC, 1992) are based upon the *Publication 30* model, which is a considerable improvement over the *Publication 2* model. The ICRP *Publication 30* model divides the thoracic region of the lungs into two regions (tracheobronchial and pulmonary) and includes a deposition model that accounts for particle size influences. The *Publication 30* model incorporates an improved clearance model which provides guidance for classifying materials into three (compared to only two in the former model) clearance classes. Clearance to lymph nodes, blood, and the gastrointestinal tract are all included in the model. The model is based on an adult lung morphology for deposition and on both human and animal data for clearance of materials. Dosimetry calculations are based on averaging energy deposition over the total lung mass.

In December of 1994, the ICRP issued a new respiratory tract model as ICRP *Publication 66* (ICRP, 1994). Among the reasons for revising the model were: (1) to provide a means for calculating doses to the nasal and oral passages; (2) to compute more biologically significant doses to critical target regions rather than simply averaging dose over the total lung mass; (3) to provide more flexibility for selecting various clearance rates so that predicted clearance patterns better match observed patterns; (4) to incorporate new data on particle deposition below 0.1 μm particle diameter; (5) to incorporate new knowledge and data on particle retention and clearance in various regions of the respiratory tract; and (6) to construct a model that applies to all members of the world's population consistent with age, gender, and race. A principal feature of the

revised lung model is that the relative radio-sensitivities of various respiratory tract tissues are taken into account when combining regional doses to obtain an overall lung dose.

As discussed in the opening paragraph, the NCRP (1993) has also been working, independently of the ICRP, to issue new guidance on respiratory tract modeling. Many of the items listed above for the ICRP *Publication 66* model are also addressed in the model adopted in principle, but not yet published, by the NCRP. The conceptual and computational models recommended by the NCRP and the ICRP (1994) differ in several ways. Differences exist in the deposition model resolution, specification of fractional clearance rates, and specification of target regions in the dosimetry model. Some of these differences between the models are discussed in more detail in Appendix A.

2.3. Respiratory Tract Morphological Model

The anatomical representation of the revised ICRP (1994) respiratory tract model is shown schematically in Figure 2-2. Based on structure and function, the model divides the respiratory tract into the following five primary regions:

(1) the extrathoracic region comprising the anterior nasal passages, ET_1,

(2) the extrathoracic region comprising the posterior nasal passages, larynx, pharynx, and mouth, ET_2,

(3) the bronchial region, BB, comprising airway generations 0 through 8 (trachea through the bronchi),

(4) the bronchiolar region, bb, comprising airway generations 9 through 15, and

(5) the alveolar-interstitial region, AI, comprising the first respiratory bronchioles through the alveolar sacs and including interstitial connective tissues.

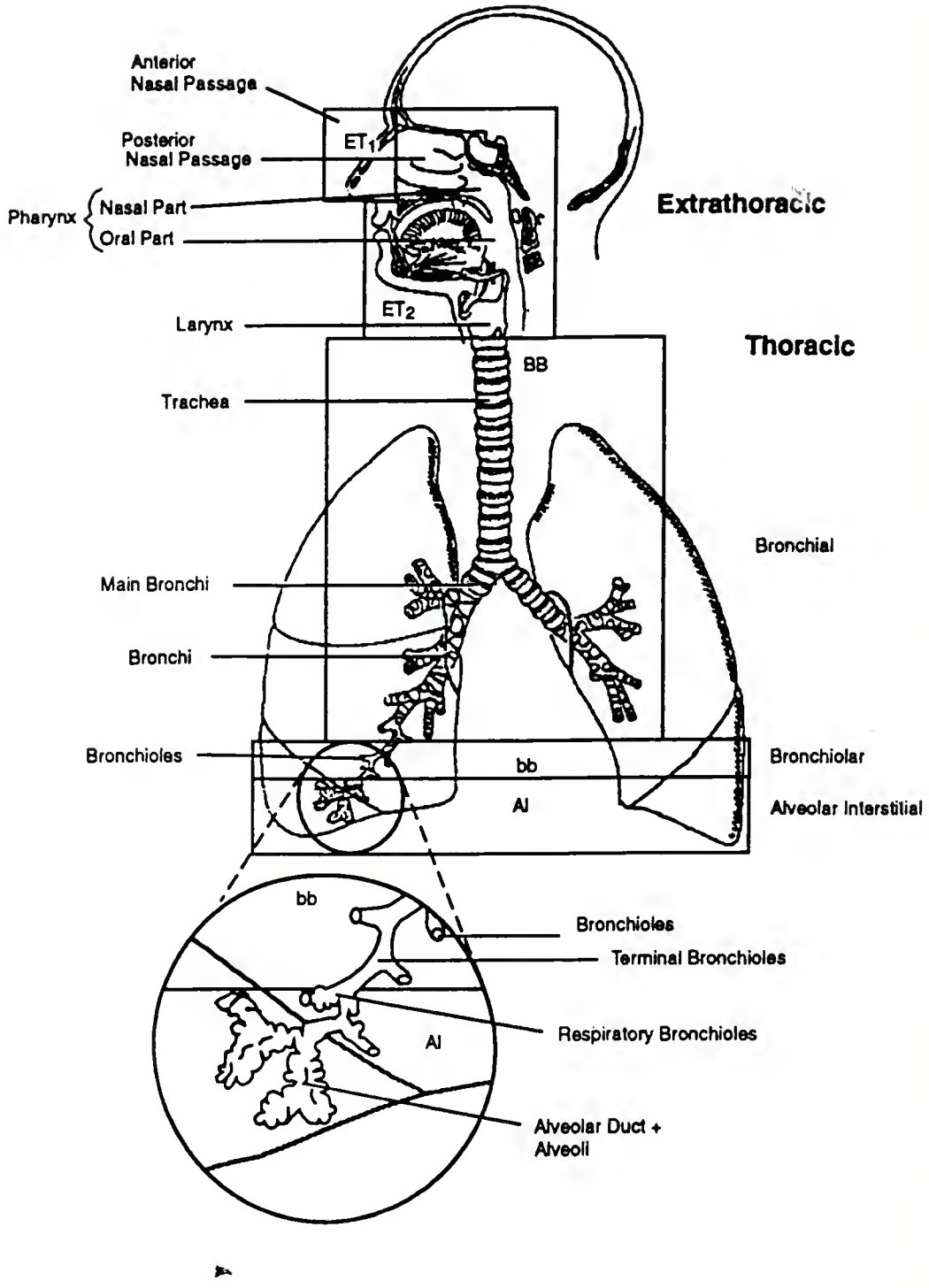

Figure 2-2. Anatomical representation of the revised ICRP respiratory tract model. The respiratory tract is divided into five primary regions (ET_1, ET_2, BB, bb, and AI) and two lymph node regions (not shown). Reproduced by permission from ICRP *Publication 66* (ICRP, 1994, p. 9).

In addition two lymph node regions are identified to represent the lymph nodes (LN_{ET}) which drain the extrathoracic regions (ET_1 and ET_2) and the lymph nodes (LN_{TH}) which drain the thoracic regions (i.e., BB, bb, AI).

To account for the morphological variation of the respiratory tract with respect to age, gender, and race, scaling factors are used in the deposition model. These factors allow regional deposition to be computed for any subject by scaling certain aspects of the model based on the ratio of subject airway dimensions to those of reference man. Scaling factors are based on the diameters of the trachea and airway generations 8 and 15. The thickness and cellular structure of surface and epithelial tissues in ET, BB, bb, AI regions are taken to be invariant with age, gender, and body size; however the surface area of the various airway regions does depend on body size and is accommodated in this study.

For ET, BB, and bb regions, the airways are modeled as cylinders. Source and target tissues residing within the airway wall are considered to be cylindrical shells. Figure 2-3 is a schematic of the cross sectional view of a typical airway wall for the bronchial region. Although there are some differences in thicknesses and tissue layer structure, similar geometries are used in the model to represent bb and ET airway wall tissues.

2.4. Respiratory Tract Deposition Model

The clearance pattern and regional doses are influenced by the amounts of radioactive material which deposit in the various respiratory tract regions. To compute the fraction of inhaled radioactivity which deposits in the five broad respiratory tract regions, the basic approach of the ICRP (1994) is to model the respiratory tract as a series

of filters, as illustrated in Figure 2-4. The first filter in the figure represents the inhalability of the aerosol--discussed below. The other filters represent the respiratory tract regions described above. Because deposition occurs during both inhalation and exhalation, some respiratory regions appear more than once in the filter chain.

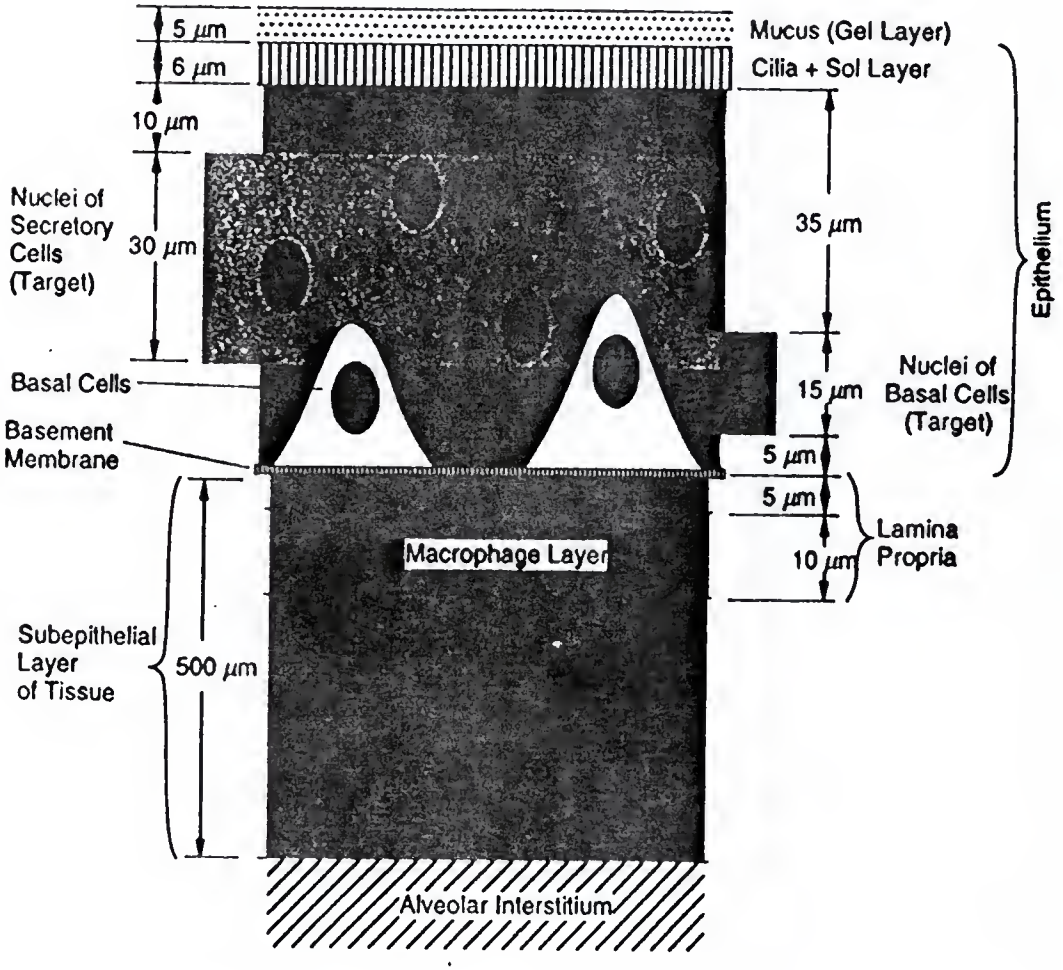

Figure 2-3. Model of airway wall in the bronchial (BB) region. Targets in this region include secretory cell nuclei and basal cell nuclei. The region is separated from the alveolar interstitium by a layer of subepithelial connective tissue. Reproduced with permission from ICRP *Publication 66* (ICRP, 1994, p. 15).

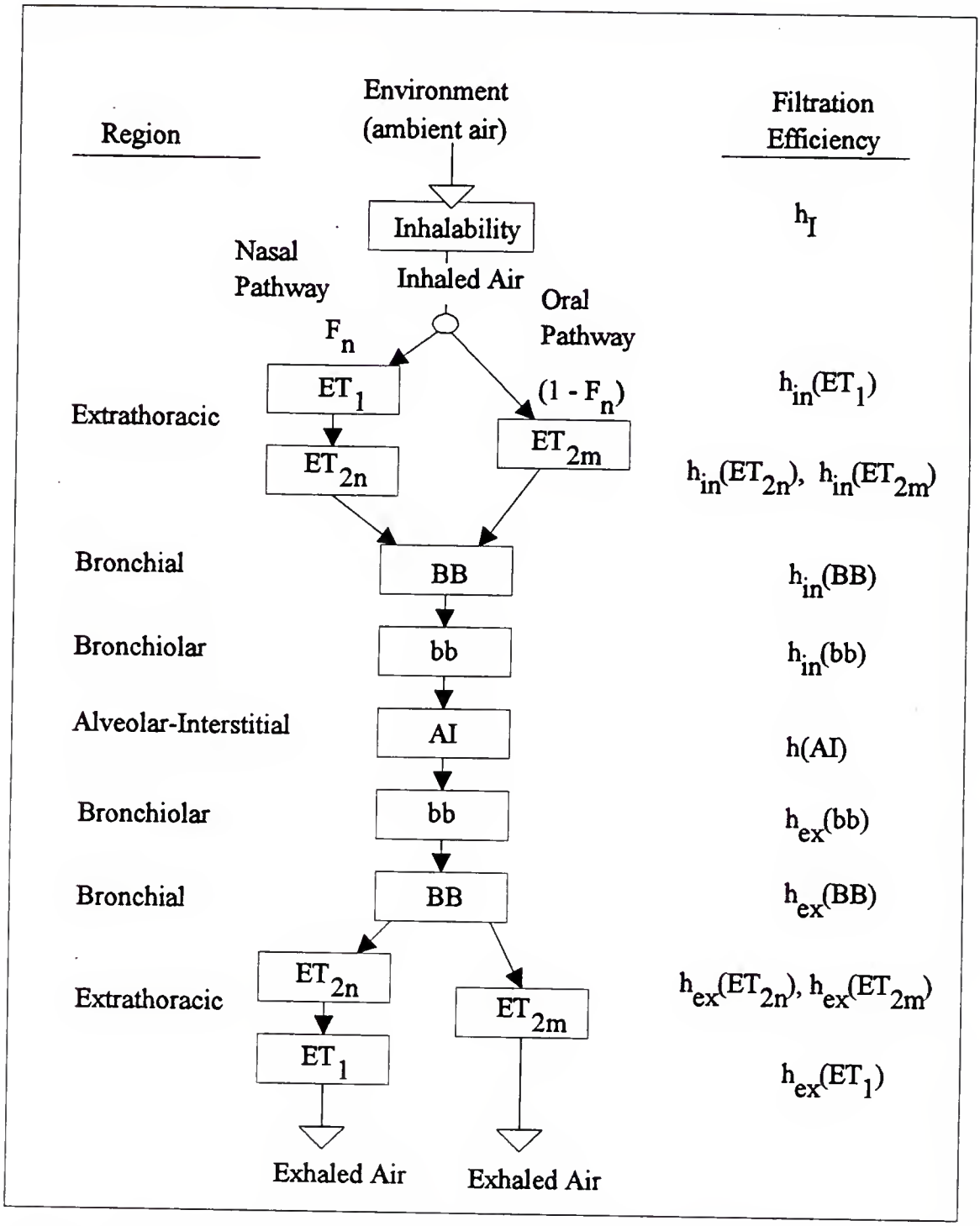

Figure 2-4. Representation of the deposition component of the revised ICRP respiratory tract model. The respiratory tract is modeled as a series of filters with characteristic volumes and deposition efficiencies. After Figure 8 in ICRP(1994).

Two pathways are considered for air flow in and out of the thoracic region--the nasal pathway (i.e., air inhaled via the nose) and the oral pathway (i.e., air inhaled via the mouth). Both pathways can coexist during breathing. The fraction of air inhaled which passes through the nose is denoted by F_n. These pathways are distinguished because the nasal pathway generally results in more filtration of particles than the oral.

Each deposition region (or filter) possesses two characteristic parameters--its volume, V, and its deposition (or filtration) efficiency, h. The deposition efficiency represents the overall efficiency of the region for removing aerosol particles (h = 1 - output/input particles). Denoting the tidal volume of the flow by V_T and the (dead space) volume of the *j*th filter by V_j, the volumetric fraction of the tidal air which reaches filter *j* is given by:

$$\phi_j = \begin{cases} 1 & \text{for } j = 0 \\ 1 - \dfrac{1}{V_T} \displaystyle\sum_{i=0}^{j-1} V_i & \text{for } 1 \le j \le (N+1)/2 \\ \phi_{N-j+1} & \text{for } (N+3)/2 \le j \le N \end{cases} \qquad (2\text{-}1)$$

where a value of zero for *j* denotes the inhalability (a virtual filter with $V_0 = 0$; discussed in following paragraph); N is the total number of filters (not counting inhalability) considered for the complete breathing cycle (inhalation and exhalation). Note that N = 9 for nose breathing, and N = 7 for mouth breathing. The middle component of Eq. 2-1 represents the fraction of air reaching filter *j* during inhalation. The bottom component represents the fraction of air reaching filter *j* during exhalation and assumes that the volume of air traversing a filter during inhalation equals the volume during exhalation.

Inhalability (the first "filter" in the chain) refers to the efficiency with which particles of a given diameter are able to be inspired by the nose and mouth. Inhalability effects arise due to the complex flow of particles around the human head and torso and is important only for particles with aerodynamic diameters larger than about 0.5 μm. For increased wind speeds and larger particles, the inhalability can be greater than one; this effect is attributable to non-isokinetic sampling conditions of the human head. Based on the model recommended by the ICRP (1994), the inhalability is plotted in Figure 2-5 as a function of the particle aerodynamic diameter. In the deposition model, inhalability can be regarded as a virtual filter which acts to remove particles from the air before they actually enter the airways.

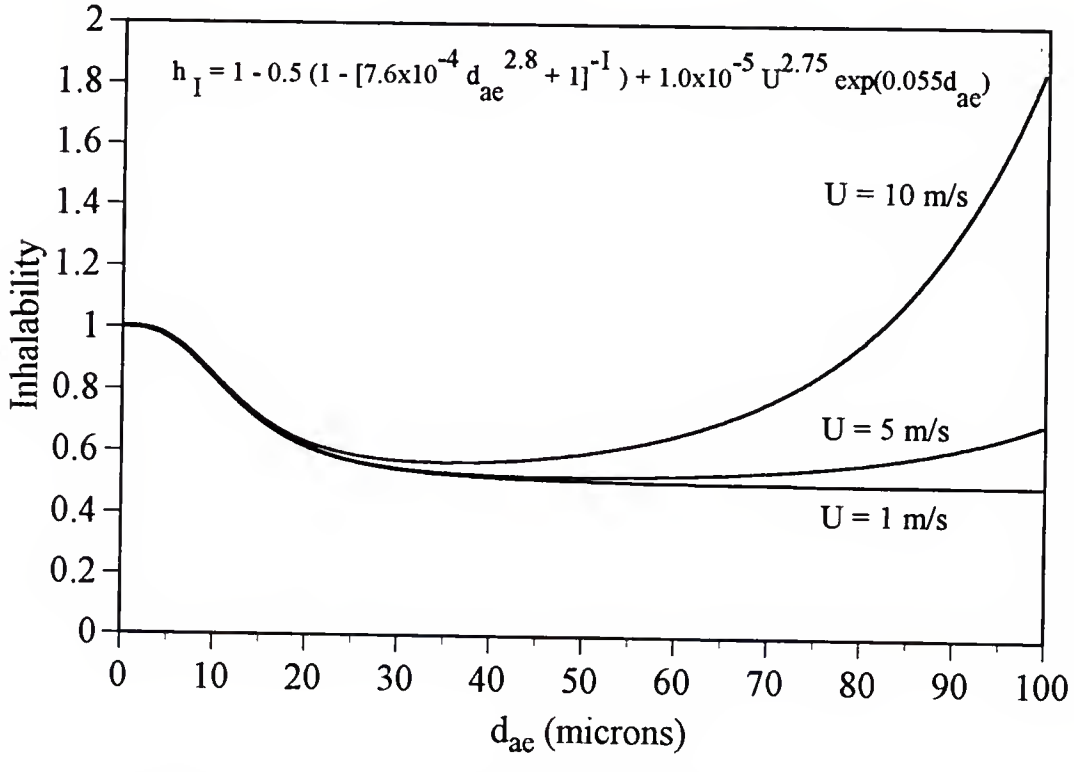

Figure 2-5. Inhalability of particles as a function of the aerodynamic diameter for various wind speeds of U = 1, 5, and 10 m/s.

In this sequential filtration system, the index *j* corresponds to a respiratory tract region as it is encountered by air during the respiratory cycle (both inspiration and expiration). The fraction of material inhaled which deposits in filter *j*, DE_j, is given by an expression involving the filtration efficiencies, h_i, of the preceding filters and the volumetric correction factor, ϕ_j such that:

$$DE_j = h_j \phi_j \prod_{i=0}^{j-1} (1 - h_i) \quad . \tag{2-2}$$

Deposition in each respiratory region results from both aerodynamic and thermodynamic processes. Aerodynamic processes include inertial impaction and gravitational settling; thermodynamic processes include particle diffusion and Brownian motion. Aerodynamic deposition mechanisms generally dominate for particles with aerodynamic diameter larger than about 0.2 μm while thermodynamic mechanisms dominate for particles less than this size. The model assumes that particles in the aerosol carry no net charge--i.e., electrostatic deposition mechanisms are not accommodated. Denoting h_{ae} as the aerodynamic deposition efficiency and h_{th} as the thermodynamic deposition efficiency, James et al. (1994b) have represented the combined deposition efficiency of region j by the quadratic expression:

$$h_j = (h_{ae,j}^2 + h_{th,j}^2)^{1/2} \quad . \tag{2-3}$$

James et al. (1994b) provide a detailed discussion of the mathematical expressions used to estimate h_{ae} and h_{th} for the various respiratory tract regions/filters. The expressions for extrathoracic regions are based upon regression analyses of experimental data involving both persons (e.g., Stahlhofen et al., 1989; Rudolf et al., 1986) and hollow

casts (e.g., Swift et al., 1992). Expressions for thoracic regions are based upon regression analyses of deposition data predicted by an underlying, more sophisticated, theoretical model developed by Egan and Nixon (1985), Nixon and Egan, 1987, and Egan et al. (1989). The equations adopted by the ICRP (1994) for regional deposition efficiencies are listed in Tables 2-1 and 2-2. Expressions presented in Table 2-1 are for air inhaled and exhaled through the nose; those in Table 2-2 are for air inhaled and exhaled through the mouth.

The primary difference between nose and mouth breathing is that the anterior nasal passages (region ET_1) are not part of the flow pathway for mouth breathing. The equations apply over a wide particle size range--from a 0.001 μm thermodynamic particle diameter to a 100 μm aerodynamic particle diameter.

As shown in Tables 2-1 and 2-2, the deposition model depends on a number of parameters. Parameters required as direct input to the deposition model are listed along with brief descriptions in Table 2-3. Reference values for parameters have been presented in ICRP *Publication 66* (ICRP, 1994) and are specified for various age and gender groups. Many of the parameters described in Table 2-3 depend on other, more fundamental, parameters such as body height, weight, and age. Other parameters, investigated during the course of this work to account for correlations between the direct input parameters, are listed in Table 2-4. Uncertainties and variabilities in these parameters are examined in detail in Chapter 4.

The outputs of the deposition model are the fractions of activity that deposit in the various respiratory tract regions--ET_1, ET_2, BB, bb, and AI. The deposition model does

Table 2-1. Expressions recommended by the ICRP to predict regional deposition for the fraction of intake inhaled and exhaled through the *nose* as functions of respiratory variables and anatomical size.

			Regional Deposition Efficiency, h_R						
	Filter j	Region	Aerodynamic $h_{ae} = 1 - \exp(-aR^P)$			Thermodynamic $h_{th} = 1 - \exp(-aR^P)$			Volumetric Fraction, ϕ_j [c]
			a	R	P	a	R	P	
Inhale	1	ET_1 [a]	3.0E-4	$d_{ae}^2 V_{Fn} SF_t^3$	1	18	$D(V_{Fn}SF_t)^{-1/4}$	1/2	1
	2	$ET_{2,n}$ [b]	5.5E-5	$d_{ae}^2 V_{Fn} SF_t^3$	1.17	15.1	$D(V_{Fn}SF_t)^{-1/4}$	0.538	1
	3	BB	4.08E-6	$d_{ae}^2 V_F SF_t^{2.3}$	1.152	$22.02\, SF_t^{1.24}\Psi_{th}$ [d]	Dt_B	0.6391	$1-V_D(ET)/V_T$
	4	bb	0.1147	$(0.056+t_b^{1.5}) \times d_{ae}\wedge(t_b^{-0.25})$	1.173	$-76.8+167\, SF_b^{0.65}$	Dt_b	0.5676	$1-[V_D(ET)+V_D'(BB)]/V_T$
	5	Al	$0.146\, SF_A^{0.98}$	$d_{ae}^2 t_A$	0.6495	$170+103\, SF_A^{2.13}$	Dt_A	0.6101	$1-\frac{[V_d(ET)+V_d'(BB)+V_d'(bb)]}{V_T}$
Exhale	6	bb	0.1147	$(0.056+t_b^{1.5}) \times d_{ae}\wedge(t_b^{-0.25})$	1.173	$-76.8+167\, SF_b^{0.65}$	Dt_b	0.5676	$1-[V_D(ET)+V_D'(BB)]/V_T$
	7	BB	2.04E-6	$d_{ae}^2 V_F SF_t^{2.3}$	1.152	$22.02\, SF_t^{1.24}\Psi_{th}$	Dt_B	0.6391	$1-V_D(ET) / V_T$
	8	$ET_{2,n}$ [b]	5.5E-5	$d_{ae}^2 V_{Fn} SF_t^3$	1.17	15.1	$D(V_{Fn}SF_t)^{-1/4}$	0.538	1
	9	ET_1 [a]	3.0E-4	$d_{ae}^2 V_{Fn} SF_t^3$	1	18	$D(V_{Fn}SF_t)^{-1/4}$	1/2	1

Source: ICRP (1994, Table 12)

(a) $h_{ae} = 0.5[1 - 1/(aR^p + 1)]$; $h_{th} = 0.5[1-\exp(-aR^p)]$

(b) $h_{ae} = 1-1/(aR^p+1)$; $h_{th} = 1-\exp(-aR^p)$

(c) $V_D'(BB) = V_D(BB)(1 + V_T/FRC)$; $V_D'(bb) = V_D(bb)(1 + V_T/FRC)$

(d) Ψ_{th} is an empirical correction factor accounting for nonlaminar bronchial airflow and is given by $\Psi_{th} = 1 + 80\exp\{-[\log_{10}(80+10/(d_{th}^{0.6}))]^2\}$.

Table 2-2. Expressions recommended by the ICRP to predict regional deposition for the fraction of intake inhaled and exhaled through the *mouth* as functions of respiratory variables and anatomical size.

			Regional Deposition Efficiency, h_R						
	Filter j	Region	Aerodynamic $h_{ae} = 1 - \exp(-aR^P)$			Thermodynamic $h_{th} = 1 - \exp(-aR^P)$			Volumetric Fraction, ϕ_j [(b)]
			a	R	P	a	R	P	
Inhale	1	$ET_{2,m}$ [(a)]	1.1E-4	$d_{ae}^2 (V_F SF_t^3)^{0.6} x (V_T SF_t^2)^{-0.2}$	1.4	9	$D(V_{Fm} SF_t)^{-1/4}$	1/2	1
	2	BB	4.08E-6	$d_{ae}^2 V_F SF_t^{2.3}$	1.152	$22.02\ SF_t^{1.24} \Psi_{th}$ [(c)]	Dt_B	0.6391	$1-V_D(ET) / V_T$
	3	bb	0.1147	$(0.056+t_b^{1.5}) x\ d_{ae}\hat{}(t_b^{-0.25})$	1.173	$-76.8+167\ SF_b^{0.65}$	Dt_b	0.5676	$1-[V_D(ET)+V_D'(BB)]/V_T$
	4	AI	$0.146 SF_A^{0.98}$	$d_{ae}^2 t_A$	0.6495	$170+103\ SF_A^{2.13}$	Dt_A	0.6101	$1-\frac{[V_d(ET)+V_d'(BB)+V_d'(bb)]}{V_T}$
Exhale	5	bb	0.1147	$(0.056+t_b^{1.5}) x\ d_{ae}\hat{}(t_b^{-0.25})$	1.173	$-76.8+167\ SF_b^{0.65}$	Dt_b	0.5676	$1-[V_D(ET)+V_D'(BB)]/V_T$
	6	BB	2.04E-6	$d_{ae}^2 V_F SF_t^{2.3}$	1.152	$22.02\ SF_t^{1.24} \Psi_{th}$	Dt_B	0.6391	$1-V_D(ET) / V_T$
	7	$ET_{2,m}$ [(a)]	1.1E-4	$d_{ae}^2 (V_F SF_t^3)^{0.6} x (V_T SF_t^2)^{-0.2}$	1.4	9	$D(V_{Fm} SF_t)^{-1/4}$	1/2	1

Source: ICRP (1994, Table 13).

(a) $h_{ae} = 1-1/(aR^P+1)$; $h_{th} = 1-\exp(-aR^P)$

(b) $V_D'(BB) = V_D(BB)(1 + V_T/FRC)$; $V_D'(bb) = V_D(bb)(1 + V_T/FRC)$

(c) Ψ_{th} is an empirical correction factor accounting for nonlaminar bronchial airflow and is given by $\Psi_{th} = 1 + 80\exp\{-[\log_{10}(80+10/d_{th}^{0.6})]^2\}$.

Table 2-3. Description of input parameters required by the revised ICRP deposition model.

Quantity (units)	Symbol	Description/Comments
Aerodynamic Diameter (μm)	d_{ae}	Diameter of a unit density sphere with same settling velocity as the particle of interest. Used to quantify aerodynamic deposition mechanisms (important for particles larger than about 0.2 μm).
Thermodynamic Diameter (μm)	d_{th}	Diameter of spherical particle with same diffusion coefficient as the particle of interest.
Diffusion coefficient (cm^2/s)	D	Physical constant for particle characterizing its diffusivity in specified medium (air in this case); depends on particle size, air temperature, and pressure, among other quantities. Used to quantify thermodynamic deposition mechanisms (important for particles smaller than about 0.2 μm).
Volumetric Flow Rate (mL/s)	V_F	Total flow rate of air entering the respiratory tract (nasal + oral pathways).
Nasal Volumetric Flow Rate (mL/s)	V_{Fn}	Flow rate for air entering by nose; $V_{Fn}=V_F F_n$; F_n= fraction of air inhaled by nasal pathway.
Oral Volumetric Flow Rate (mL/s)	V_{Fm}	Flow rate for air entering by mouth; $V_{Fm}=V_F(1-F_n)$
Tracheal Scaling Factor	SF_t	Scaling factor to relate regional deposition efficiencies in ET and BB regions of subject of interest to reference man. $SF_t = 1.65/d_0$ (d_0 = diameter of trachea in subject, cm).
Bronchiolar Scaling Factor	SF_b	Scaling factor to relate regional deposition efficiencies in bb region of subject of interest to reference man. $SF_b = 0.165/d_8$ (d_8 = diameter of airway generation 8 in subject, cm).
Alveolar Scaling Factor	SF_A	Scaling factor to relate regional deposition efficiencies in AI region of subject of interest to reference man. $SF_A = 0.051/d_{16}$ (d_{16} = diameter of generation 16 in subject, cm).
Residence time in BB Region (sec)	t_B	Time constant for conduction of air through BB region. The ICRP has recommended the following expression to compute t_B from other quantities: $t_B = V_D(BB)(1 + 0.5\ V_T/FRC)/V_F$

Table 2-3 --continued.

Quantity	Symbol	Description/Comments
Residence time in bb Region (sec)	t_b	Time constant for conduction of air through bb region. ICRP has recommended the following expression to compute t_b from other quantities: $t_b = V_D(bb)\ (1 + 0.5\ V_T/FRC)/V_F$.
Residence time in AI region (sec)	t_A	Time constant for residence of air in the alveolar region. ICRP has recommended the following expression to compute t_A from other quantities: $t_A = [V_T - V_D]\cdot[1 + 0.5\ V_T/FRC]/V_F$ where $V_D = V_D(ET) + V_D(BB) + V_D(bb)$.
Tidal Volume (mL)	V_T	Volume of air inhaled or exhaled per breath; depends on temperature and saturation conditions. Tidal volume is specified at body temperature, ambient pressure, and saturated with water vapor.
Volume of ET Region (mL)	$V_D(ET)$	The (dead space) volume of the ET region airways (anterior nose + oro/nasopharynx+larynx).
Volume of BB Region (mL)	$V_D(BB)$	The (dead space) volume of the BB region airways (trachea + airway generations 1-8).
Volume of bb Region (mL)	$V_D(bb)$	The (dead space) volume of the bb region airways (generations 9 to 15).
Functional Residual Capacity (mL)	FRC	Volume of air remaining in the lungs at the end of a normal exhalation.

Table 2-4. Other parameters of use in modeling particle deposition in the respiratory tract.

Quantity	Symbol	Description/Comments
Age (y)	A	Age of subject of interest in years.
Body Height (cm)	Ht	Height of subject of interest.
Body Mass (kg)	Wt	Body mass (or weight) of subject of interest.
Body Mass Index (kg/m^2)	BMI	$BMI = (Wt)/(Ht^2)$
Anatomical Dead Space (mL)	V_D	Total volume of the conducting airways including extrathoracic region: $V_D = V_D(ET) + V_D(BB) + V_D(bb)$
Ventilation Rate (L/min)	V_E	Amount of air inhaled or exhaled per unit time.
Oxygen Consumption Rate (mL/min)	V_{O2}	The amount of oxygen consumed by the body per unit time.
Ventilatory Equivalent Ratio	VQ	Ratio of the ventilation rate to the oxygen consumption rate, $VQ = V_E/V_{O2}$.
Basal Metabolic Rate (MJ/day)	BMR	Energy consumption rate needed to sustain basic life activities.
Basal Multiplier	B_{mult}	Multiplication factor to relate the metabolic rate at a specified exertion level to the basal metabolic rate.
Oxygen Consumption Factor (L/kJ)	H_{oxy}	Amount of oxygen needed to produce 1 kJ of energy.
Vital Capacity (mL)	VC	The amount of air present in lungs at maximal inhalation.

not depend on the total activity inhaled, only on the fraction of the total activity that is associated with a given particle size. The fraction of activity associated with given particle sizes are quantified by the activity-size distribution, where *size* in this case refers to either the aerodynamic diameter or the thermodynamic particle diameter. These distributions are probability density functions which express the fraction of activity associated with particles in an incremental size range. Generally, measurements have shown that particles are log-normally distributed with respect to size. Therefore, the size distributions are usually characterized by a geometric mean aerodynamic (or thermodynamic) diameter and a geometric standard deviation (GSD). The activity median aerodynamic (or thermodynamic) diameter, denoted by AMAD (or AMTD) is the diameter of the particle for which half of the activity is associated with particles less than that diameter.

The ICRP (1994) has suggested four physical exertion levels be used to classify the physical activities of persons. The levels are: resting (or sleeping), sitting awake, light exertion, and heavy exertion. Based on these four exertion levels, the ICRP has recommended age and gender-specific reference values characterizing the ventilation rate, tidal volume, respiratory frequency, and fraction of time spent in these levels. The present study considers all of these parameters except the fraction of time spent in various levels; subsequently, computations developed in this work assume a subjects are exposed while at only one of these four levels over the duration of the exposure. More details concerning the types of activities assigned to exertion levels in this study are given in Chapter 4.

2.5. Particle Size and Diffusion Characteristics

This section presents some of the relationships needed to compute parameters in the deposition model which are related to particle size. Most of these relationships have been discussed in more detail in Hinds (1982). The two parameters required by the model that depend on particle size (and air temperature and pressure) are the aerodynamic diameter, d_{ae}, and the particle diffusion coefficient, D. Other quantities that are used to relate these two parameters are the equivalent volume diameter, d_e, and the thermodynamic diameter, d_{th}, which are discussed below. For a dispersion-type aerosol (e.g., windborne surface soil), the aerodynamic diameter (or more generally the distribution of aerodynamic diameters) would likely be determined from measurements, for example, employing cascade impactors. For an aerosol produced by a chemical reaction (e.g., oxidation processes), the thermodynamic diameter (or more generally the distribution of thermodynamic diameters) would likely be determined from measurements, for example, employing graded screen arrays or diffusion batteries.

The aerodynamic diameter, d_{ae}, of a particle (defined as the diameter of a unit density sphere with the same settling velocity as the particle) is related to the equivalent volume diameter, d_e (defined as the diameter of a sphere with the same volume as the particle), by the following expression:

$$d_{ae} = d_e \left[\frac{\rho C(d_e)}{\chi \rho_o C(d_{ae})} \right]^{1/2} \qquad (2\text{-}4)$$

where χ is the particle (dynamic) shape factor; ρ is the mass density of the particle; ρ_o is unit density (1 g/cm^3); $C(d_e)$ and $C(d_{ae})$ are particle slip correction factors (Hinds, 1982). If d_{ae} is given, d_e can be computed from Equation 2-4.

The particle mass density is difficult to measure, especially for aggregates (clusters of particles attached as a result of thermal coagulation). Generally, if the source of the aerosol particles is known, the mass density of the particulates is assumed equal to the mass density of the bulk material. James et al. (1994b) have suggested a reference value of 3 g cm^{-3} for environmental aerosols because it is typical of many natural materials.

The slip correction factor generally depends on air temperature and pressure. For particles in the respiratory tract (saturated air at 37°C) at atmospheric pressure P (cm Hg), the slip factor has been reported by James et al. (1994b) as:

$$C(d_e, P) = 1 + [13.57 + 4.31 \exp(-0.102\ Pd_e)]/[Pd_e] \quad . \qquad (2\text{-}5)$$

The slip factor for d_{ae}, $C(d_{ae})$, is also computed with Equation 2-5 by replacing d_e with d_{ae}.

The particle (dynamic) shape factor, χ, is the ratio of the actual drag force on an irregular particle, F_D, to the drag force predicted by Stoke's law, F_S, using the particle's equivalent volume diameter, d_e;

$$\chi = \frac{F_D}{F_S} = \frac{F_D}{3\pi\eta u d_e} \qquad (2\text{-}6)$$

where η is the viscosity of air in the respiratory tract and u is the particle velocity. For a spherical particle $\chi = 1$; typical values of χ range from 1 to 2 (Hinds, 1982). Shape factors must generally be determined experimentally.

The diffusion coefficient, D (cm^2/s), for a particle is estimated by the following expression (Hinds, 1982):

$$D = \frac{C(d_{th})kT}{3\pi\eta d_{th}} \tag{2-7}$$

where k is Boltzmann's constant, T is the absolute temperature (K), and d_{th} is the thermodynamic diameter (diameter of sphere with same thermal diffusivity as particle of interest). Consistent units must be used for quantities in Equation. 2-7. Based on the discussion in James et al. (1994b), the following expression determines the value of the thermodynamic diameter to be used in Equation 2-7 (d_{th} and d_e in μm):

$$d_{th} = \begin{cases} d_e & \text{for } d_e > 0.005\ \mu m \\ d_e[1 + 3\exp(-2.20 \times 10^3 d_e)] & \text{for } d_e \le 0.005\ \mu m \end{cases} \tag{2-8}$$

The lower portion of Equation (2-8) is based on recommendations, by Ramamurthi and Hopke (1989), that a correction be made to Eq. 2-7 for particles less than about 2 nm. A value of 5 nm was chosen as the application point for their results in this study, since it can be shown that the error in assuming d_{th} equals d_e is less than 0.01% for $d_e > 5$ nm.

Solving Eqs. 2-4 and 2-5 for d_e involves an iterative approach since the solution cannot be obtained analytically. James et al. (1994b) have recommended an approximate, initial solution by setting $d_e = d_{ae}(\chi/\rho)^{1/2}$; convergence to the correct value by iteration is reportedly rapid (usually requiring less than 10 iterations).

2.6. Respiratory Tract Clearance Model

The clearance model adopted by the ICRP (1994) is based on an approach introduced by Cuddihy and colleagues (Cuddihy, 1976, 1984; Cuddihy et al., 1979; Cuddihy and Yeh, 1988). In this approach clearance from various regions is based on competitive clearance processes. In all regions but the anterior nasal passages, ET_1, clearance is achieved (1) by mechanical translocation processes (such as macrophage uptake and transport in fluids over surfaces by mucociliary action to the gastrointestinal tract), (2) by transport to lymph nodes, and (3) by dissolution and absorption to lung tissues and/or to blood. Radioactive decay can also be considered a form of removal. These processes compete to remove material from various regions. In the anterior extrathoracic region (ET_1) material is removed by external pathways (such as nose blowing, sneezing, or coughing) and by radioactive decay.

Three major working assumptions have been made in the clearance model (discussed by Bailey and Roy, 1994). These assumptions are as follows:

(1) clearance rates due to mechanical transport processes (mucociliary and macrophage transport) and dissolution/absorption processes (to blood) are independent; therefore, the overall fractional clearance rate from a model compartment is represented by the sum of the rates due to individual processes;

(2) mechanical transport rates are the same for all materials; i.e., the chemical form of the material does not influence the fractional clearance rate due to particle transport processes; and

(3) the dissolution/absorption rate of a material to blood is the same for all regions of the respiratory tract except the anterior nasal passages ET_1, where no absorption is assumed to occur.

The compartment model which has been adopted by the ICRP (1994) to represent mechanical clearance processes (including particle transport by the mucociliary mechanism and by alveolar macrophages) to the gastrointestinal tract and lymph nodes is shown in Figure 2-6. This figure does not include absorption pathways. Arrows represent routes (and directions) for particle transport in the clearance model. According to the second assumption above, these routes and their associated fractional clearance rates are generally independent of the chemical form of the material.

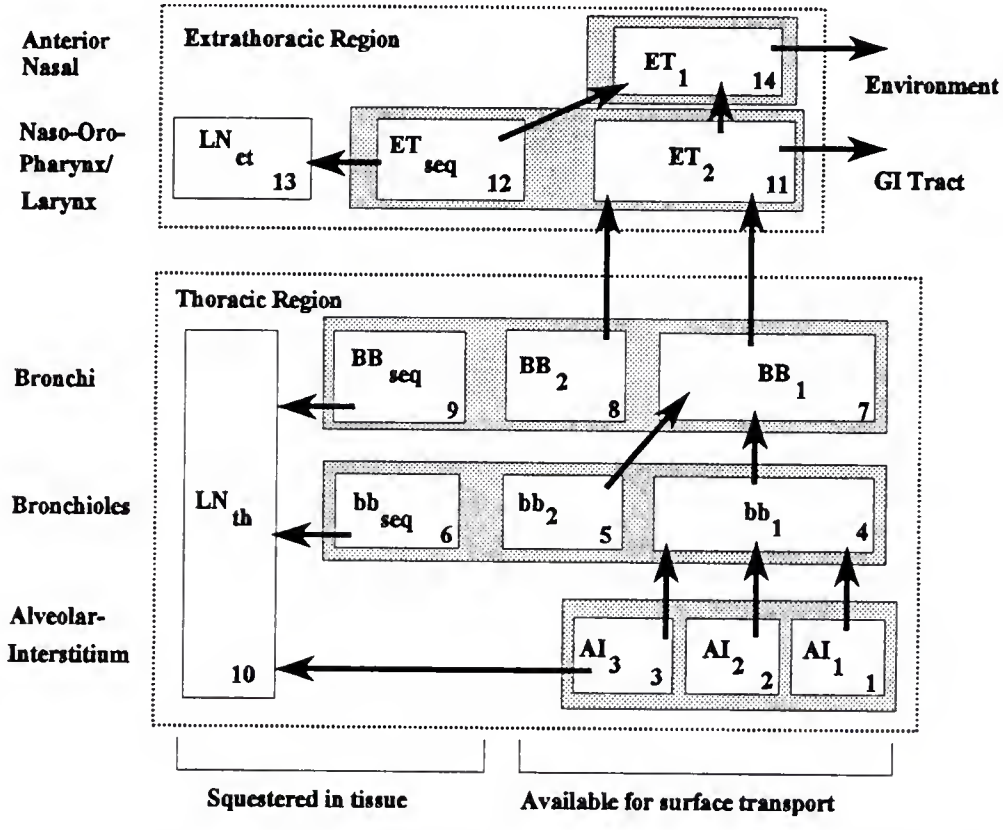

Figure 2-6. Representation of particle transport model recommended by the ICRP (1994) for mucociliary and macrophage transport mechanisms to the gastrointestinal tract and lymph nodes (no absorption pathways shown).

Material that deposits in the respiratory tract is assigned to those compartments which that are shaded in Figure 2-6. The deposition model predicts the overall amount of material that deposits in a given broad region (i.e., ET_1, ET_2, BB, bb, and AI; represented by the grouped boxes in Fig. 2-6). This regional deposition is then partitioned among the shaded compartments within the region to account for observed clearance patterns. An exception to the second assumption exists for the BB and bb regions. For these regions the partition of the deposition to regional compartments is based on particle size. This aspect of the model is discussed in more detail in Chapter 4.

Clearance of materials from respiratory tract regions does not always occur at a constant rate with respect to time. To accommodate time-varying clearance rates in a practical manner, the model designers have represented the broad respiratory regions (ET, BB, bb, and AI) by a number of compartments (representing materials in different clearance states) clearing at different rates. Uncertainties in the fraction of the initial deposition assigned to these states (or compartments) and in clearance rates for these compartments are discussed in section 4.2 and are included in parameter uncertainty analyses. These compartments are discussed below.

The ET_1 region is modeled by a single compartment in which all material is deposited and cleared at a constant rate. The ET_2 region is modeled by two compartments, ET_2 and ET_{seq}. Based on animal data, the ICRP (1994) has suggested that ~0.05% of the regional deposition be associated with ET_{seq} and the rest (99.95%) with the ET_2 compartment. The ET_{seq} compartment represents material that is

sequestered by the airway walls in the ET_2 region and can only be cleared to lymph nodes or to blood (as do all following compartments subscripted by *seq*).

Mechanical clearance from the BB region is represented by three compartments, BB_1, BB_2, and BB_{seq}. Based on animal data, the ICRP (1994) recommends that ~0.7% of the material deposited in BB be assigned to the BB_{seq} compartment. The rest is partitioned between BB_1 (a fast-clearing compartment) and BB_2 (a slow-clearing compartment) based on particle size. The bb region is represented in an analogous manner by compartments labeled bb_1, bb_2, bb_{seq}. These bb compartments are assumed to receive the same partition of deposition as their BB region counterparts.

Mechanical clearance from the AI region is modeled by three compartments, AI_1, AI_2, and AI_3, representing compartments that clear fast, slow, and very slow, respectively. The ICRP (1994) recommends partitioning the overall deposition in AI by fractions of 0.3, 0.6, and 0.1 for compartments AI_1, AI_2, and AI_3, respectively. These values, along with reference values for all other compartments, are subject to uncertainties and variabilities which are addressed in Chapter 4.

In the conceptual model structure, the mechanical clearance rates for compartments in Figure 2-6 are taken to be independent of particle size and physico-chemical form of the deposited material. For reference, the compartments in Fig. 2-6 have been numbered. Denoting the mechanical clearance rate from compartment *i* to compartment *j* in Fig. 2-6 as $m_{i,j}$, the ICRP (1994) reference values for mechanical

clearance rates are listed in Table 2-5. One interpretation of these rates is that they represent the fraction of material in compartment *i* that passes from compartment *i* to *j* per unit time by the specified pathway. Denoting the fraction of the regional deposition assigned to a compartment as f_d, Table 2-6 lists reference values for the partition of deposition among compartments.

Unlike particle transport mechanisms represented by the compartment scheme in Fig. 2-6, absorptive processes do depend on the physico-chemical properties of the radionuclide. Such properties include solubility of material within, and transportability through, lung tissues. The model adopted by the task group to describe these processes is shown in Figure 2-7. According to the third assumption listed in the beginning of this section, absorption rates are taken to be the same from all regions (except ET_1 where no absorption is assumed) and depend on the chemical form of the radionuclide. Similar to the processes represented in Figure 2-6, experimental evidence suggests that for some materials the fractional absorption rate of materials to blood is time-varying. Rather than using time-varying clearance rates (which would lead to a system of differential equations with time-varying coefficients), the ICRP (1994) has modeled absorption to blood by multiple compartments with constant fractional absorption rates.

In the model, particles are deposited into "initial state" compartments. These initial-state compartments correspond to the shaded compartments in Fig. 2-6. After deposition, competing mechanisms act either to remove material from a location or to change the state of the material. Material deposited in the initial state can be

Table 2-5. Reference values for (fractional) mechanical clearance rates in the particle transport aspect of the ICRP human respiratory tract model.

Pathway	From	To	Rate (d^{-1})	Half Time[a]
$m_{1,4}$	AI_1	bb_1	0.02	35 d
$m_{2,4}$	AI_2	bb_1	0.001	700 d
$m_{3,4}$	AI_3	bb_1	0.0001	7000 d
$m_{3,10}$	AI_3	LN_{th}	0.00002	
$m_{4,7}$	bb_1	BB1	2	8 h
$m_{5,7}$	bb_2	BB1	0.03	23 d
$m_{6,10}$	bb_{seq}	LN_{th}	0.01	70 d
$m_{7,11}$	BB_1	ET_2	10	100 min
$m_{8,11}$	BB_2	ET_2	0.03	23 d
$m_{9,10}$	BB_{seq}	LN_{th}	0.01	70 d
$m_{11,15}$	ET_2	GI tract	100	10 min
$m_{12,13}$	ET_{seq}	LN_{et}	0.001	700 d
$m_{14,16}$	ET_1	Environment	1	17 h

Source: ICRP (1994, Table 17A).

[a] Half times are approximate since they are based on rounded values for the rates (half-time = ln(2)/rate). No half-time is reported for $m_{3,10}$; the rate for this route was chosen simply to direct the desired amount of material to the lymph nodes. Units: d = day; h = hour; min = minutes.

Table 2-6. Reference values for partition of deposition among compartments in region.

Respiratory Tract Region	Clearance Compartment	Fraction, f_d, of Regional Deposition Assigned to Compartment[a]	
ET_2	ET_2	$f_d(ET_2)$	= 0.9995
	ET_{seq}	$f_d(ET_{seq})$	= 0.0005
BB	BB_1	$f_d(BB_1)$	= 0.993 - f_s
	BB_2	$f_d(BB_2)$	= f_s
	BB_{seq}	$f_d(BB_{seq})$	= 0.007
bb	bb_1	$f_d(bb_1)$	= 0.993 - f_s
	bb_2	$f_d(bb_2)$	= f_s
	bb_{seq}	$f_d(bb_{seq})$	= 0.007
AI	AI_1	$f_d(AI_1)$	= 0.3
	AI_2	$f_d(AI_2)$	= 0.6
	AI_3	$f_d(AI_3)$	= 0.1

Source: ICRP (1994, Table 17B).

[a] The term f_s represents the slow-clearing fraction of particles deposited in the tracheobronchial airways; it depends on particle size (discussed in section 4.2.2.1).

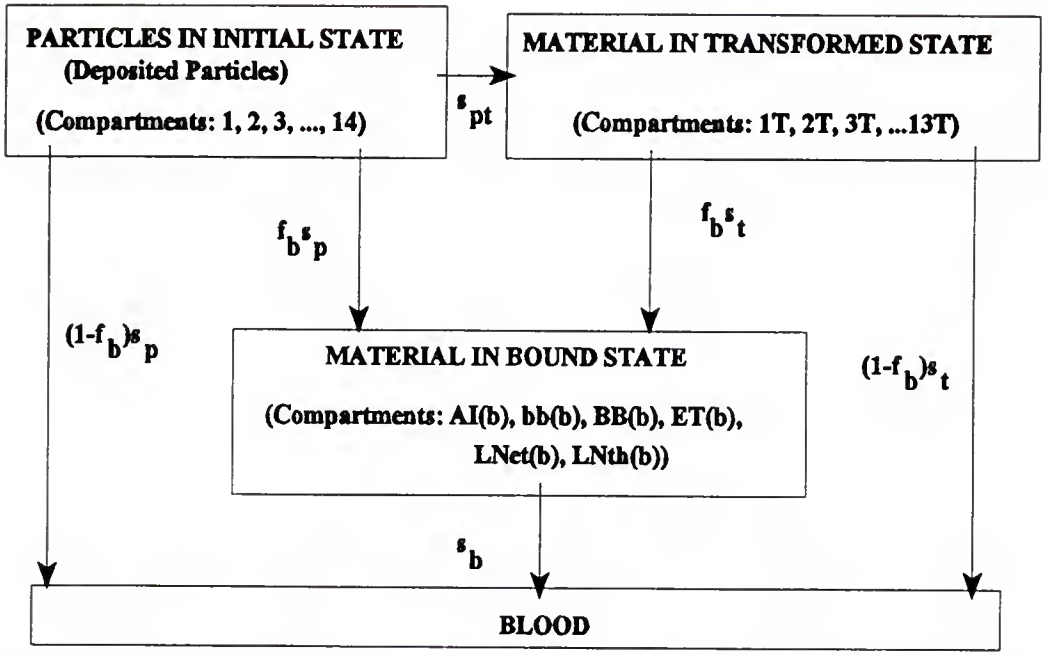

Figure 2-7. Compartment model recommended by ICRP (1994) to represent dissolution and absorption to blood and lung tissues for materials deposited in the respiratory tract.

(1) transported mechanically between initial state compartments by the pathways indicated in Figure 2-6, (2) transformed to a different clearance state (i.e., "transformed state") represented by a different compartment although in the same spatial location, or (3) absorbed from the initial state to either a "bound state" or to the blood. The bound state represents material that chemically binds to the tissues in the airway wall after dissolving in lung fluids. The total fractional clearance rate for materials from initial state compartments to the blood and to the bound state is denoted by s_p. The fraction of material that clears from the initial state to the bound state is given by f_b so that the net fractional clearance rates to the bound state and the blood are $f_b s_p$ and $(1-f_b)s_p$, respectively.

The transformed state represents material that is absorbed to the blood and bound state at a different rate, s_t, than initial state material. The fractional clearance rate from initial state to transformed state is represented by s_{pt}. According to the clearance model adopted by the ICRP (1994), material in the transformed state can either be (1) transported mechanically among transformed state compartments by assuming the same pathways apply as in Figure 2-6 or (2) absorbed to the blood and bound state. The total fractional clearance rate for materials from the transformed state to the blood and the bound state is denoted by s_t. The fraction of material that clears from the transformed state to the bound state is given by f_b (assumed to equal the fraction to bound state from initial state) so that the net fractional clearance rates to the bound state and the blood are $f_b s_t$ and $(1-f_b)s_t$, respectively.

The ICRP (1994) has also examined an alternate form for the absorption model which has parameters that are generally easier to determine from experimental data than the model shown in Figure 2-7. This alternate model is depicted in Figure 2-8. In this alternate form, material is assumed to be deposited in either a rapid dissolution state (or rapid absorption phase) or a slow dissolution state (or slow absorption phase). The fraction of material in the rapid phase is denoted by f_r (so that the fraction in the slow phase is $1-f_r$). Fractional clearance rates from the rapid and slow states to the blood and bound states are given by s_r and s_s, respectively. As before, f_b represents the fraction of cleared material that goes to the bound state. Concerning the amount of material that is absorbed to blood over a specified time period, this alternate form provides the same

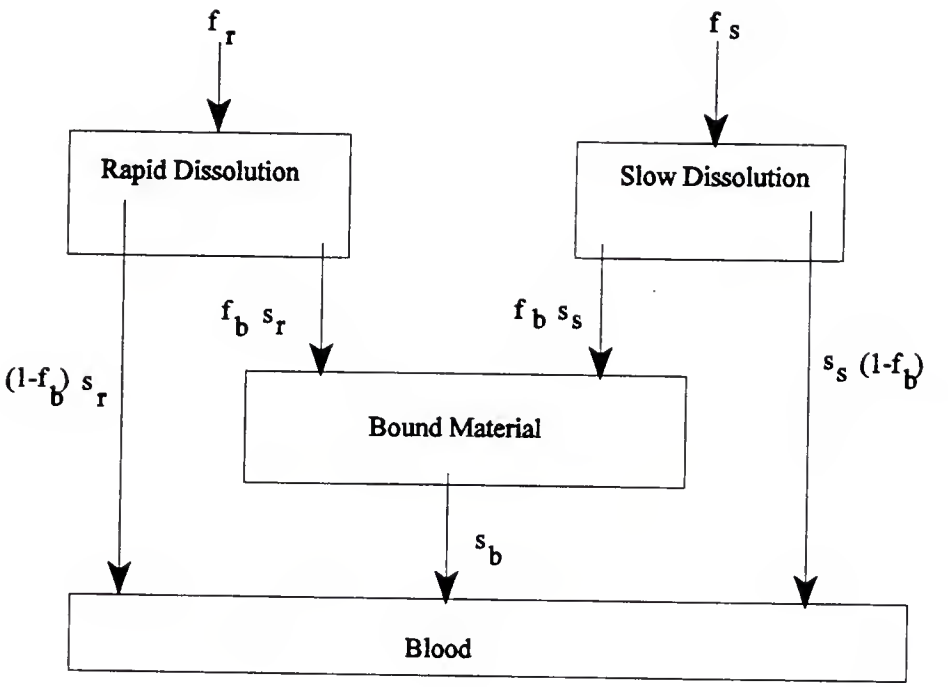

Figure 2-8. Alternate form for the dissolution/absorption model. This model form is related to the form in Figure 2-7 through Equation 2-9.

numerical results as the form in Figure 2-7. The following expressions can be derived which relate the two models:

$$\begin{aligned} s_p &= s_s + f_r(s_r - s_s) \\ s_{pt} &= (1 - f_r)(s_r - s_s) \\ s_t &= s_s \end{aligned} \quad . \qquad (2\text{-}9)$$

When reliable human data exist, the absorption aspect of the model can use observed rates of absorption to blood; when data is not available, the absorption rate is classified as *slow*, *moderate* and *fast* (denoted S, M, and F) and is based on reference values recommended by the ICRP. In the present study, literature related to absorption

of plutonium oxides was investigated (section 4.2.4) to develop distributions for the absorption rate constants for that specific material.

Upon coupling the absorption model of Figure 2-7 with the particle transport model of Figure 2-6, the overall compartmental clearance model is obtained; it is represented schematically in Figure 2-9. The overall clearance model is presented in its complete mathematical form (i.e., as a system of first-order differential equations) in Appendix B, where the mathematical form of the older ICRP *Publication* 30 lung model (ICRP, 1979) is also presented for comparison. The revised lung model possesses 33 compartments compared to only 10 for the older model.

Since the mathematical form of the clearance model involves linear, first-order differential equations with constant coefficients, the model can be solved analytically for simple exposures of interest. Due to mathematical complexity in accounting for changes in activity intake rates over time (e.g., due to changes in ventilation rate with level of physical exertion), this study has focused on an acute intake scenario. For an acute activity intake, material is deposited instantaneously at time t_o in the respective initial state compartments (shaded regions in Fig. 2-6). This assumption simplifies the solution to the differential equations presented in Appendix B for the clearance model. This simplifying assumption is appropriate when ventilation rates remain relatively constant over the *exposure duration* (which is less at most a few hours) and when the exposure duration is much less than the *dose integration time*. A relatively simple solution to the differential equations also exists for relatively constant, non-acute intakes however, such scenarios are reserved for future study.

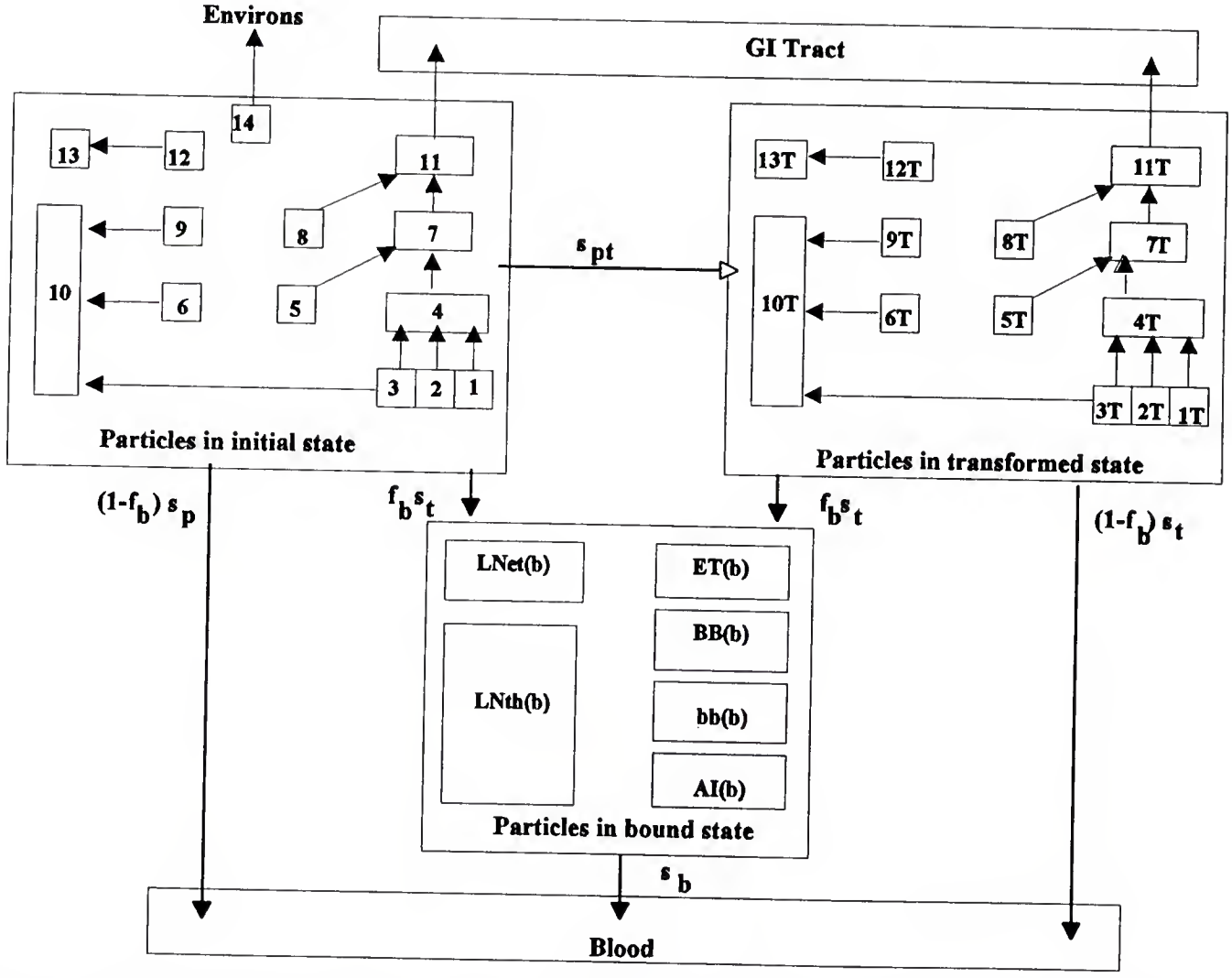

Figure 2-9. Schematic of the overall compartment model to represent clearance of material from the respiratory tract by mechanical and absorptive processes.

Several methods are available for solving clearance models represented by systems of linear first-order differential equations in this exposure situation. In this study, a computational algorithm described by Birchall (1986) has been employed. This algorithm is based on analytical equations (so-called Bateman equations) presented by Skrable et al. (1974), which originate from equations first suggested by Bateman (1910). The algorithm is restricted to first-order, non-recycling compartment models, such as the clearance model described here. Non-recycling models are those which do not allow material to re-enter clearance compartments (i.e., routes do not allow material to return to previous compartments of residence). The algorithm can solve the clearance model for both acute and constant, chronic activity intake scenarios. Given the initial number of atoms deposited into initial state compartments, the algorithm can solve the clearance model for two quantities: (1) the number of atoms remaining in compartments at time t, and (2) the total number of radioactive transformations occurring in compartments over an integration time τ. For a compartment of interest, the algorithm operates by first finding all pathways that lead to that compartment. For each pathway leading to the compartment the algorithm uses the Bateman equations to compute the contribution made to (1) the activity in compartment at time, t and (2) to the total transformations in compartment over time τ. Contributions from all pathways are then summed. Provisions are included to avoid duplicating contributions from overlapping pathways. A complete description of the algorithm and a listing of the source code for computer implementation can be found in the original paper by Birchall (1986).

2.7. Respiratory Tract Dose Model

Dose calculations in the revised ICRP respiratory tract model are based on the methodology presented in ICRP *Publication 30* (ICRP, 1979) for radiation workers and later expanded for exposures to the general population in ICRP *Publication 56* (ICRP, 1989). In that methodology, the committed equivalent dose to a tissue T, denoted $H_T(\tau)$ with special SI unit of Sv, is the time-integrated equivalent dose rate for that tissue, where τ is the integration time. For radiation protection purposes the ICRP (1989 and 1991a) has recommended an integration time of $\tau = 50$ years for adults and $\tau = 70$ years for children. However, other integration times can be specified if desired. The equivalent dose rate at time t for target tissue T is given by:

$$\dot{H}_T(t) = c \sum_s \sum_j q_{s,j}(t)\, SEE\,(T \leftarrow S;t)_j \qquad (2\text{-}10)$$

where c is a constant accounting for conversion of units, $q_{s,j}(t)$ is the activity of radionuclide j in source region S for a subject at time t; SEE(T← S; t) represents the specific effective energy for tissue T irradiated by radionuclide j in source S and is defined below. Due to source-target geometry effects, the SEE generally depends on the age of the subject at time t. The summation over s is over all source regions, S, that irradiate the target. The summation over j is over all radionuclides in source region S. The double summation over s and j then accounts for all radionuclides in all source regions that affect the target tissue.

The specific effective energy, $SEE(T \leftarrow S)_j$ for radionuclide j is expressed by:

$$SEE\ (T \leftarrow S;t) = \sum_{R} \frac{w_R E_R Y_R AF(T \leftarrow S;t)_R}{M_T(t)} \qquad (2\text{-}11)$$

where w_R is the radiation weighting factor for radiation type R emitted from radionuclide j; E_R is the energy of radiation R; Y_R is the yield of radiation type R per transformation of radionuclide j; $AF(T \leftarrow S; t)_R$ is the fraction of energy of radiation R emitted by source S that is absorbed in target T and depends, among other things, on the age of subject at time t; and $M_T(t)$ is the mass of target tissue T for the subject at time t.

Assuming an acute intake at time t_o, the committed equivalent dose at time t due to the intake is computed as:

$$H_T(t) = \int_{t_o}^{t} \dot{H}_T(t')\,dt' = c \sum_{s} \sum_{j} \left[\int_{t_o}^{t} q_{s,j}(t')\ SEE\ (T \leftarrow S;t')_j\,dt' \right]. \qquad (2\text{-}12)$$

If the SEE is assumed to be independent of time t (e.g., for adults where growth is negligible), the term enclosed in brackets becomes:

$$\left[\int_{t_o}^{t} q_{s,j}(t')\ SEE\ (T \leftarrow S;t')_j\,dt' \right] = U_{s,j}(\tau)\ SEE\ (T \leftarrow S)_j\ , \qquad (2\text{-}13)$$

where

$$U_{s,j}(\tau) = \int_{t_o}^{t} q_{s,j}(t')\,dt' \qquad (2\text{-}14)$$

and where $U_{s,j}(\tau)$ equals the total number of transformations of radionuclide j that occur in source region S over an integration time of $\tau = t - t_o$. When a respiratory tract region is the source, $U_{s,j}(\tau)$ depends on both the deposition and clearance models described

above and is determined by integrating, with respect to time, the solutions to the differential equations that are presented in Appendix B.

The present study focuses on doses to various lung tissues as the targets. The scope of the present study has been limited to include only source regions within the respiratory tract. The scope is further limited to include only those doses which are contributed by alpha particles. For an inhalation of primarily alpha-emitting radionuclides with negligible photon, electron, and beta emissions--such as Pu-238, Pu-239, Pu-240--the dose to lung tissues is due almost exclusively to alpha particles which originate within the lung tissues. To justify this statement, the computer program LUDEP (Jarvis et al., 1993) has been run for a class S (insoluble) ^{239}Pu-laden aerosol having an AMAD of 5 μm and a GSD of 2.5; the scenario involved a reference adult male at light exertion. The lung model described here and the ICRP (1979) metabolic models for other organ systems were used with reference values for all parameters. Results indicated negligible contributions to the *lung* dose from source organs other than the lungs (<<0.1%) and from radiations other than alpha particles that originated within the lungs (<<0.1%). Methods developed in this study are applied to Pu-239 and Pu-240 oxides in Chapter Five; for these radionuclides doses contributed by radiations other than alpha particles are negligible.

For short-range alpha, beta, and electron emitters, source regions in the lungs are identified in Table 2-7. In total the ICRP (1994) has identified 17 source components to be considered for short-range radiation emitters. These regions have been modeled to correspond with anatomical regions in the airway wall as shown earlier in Fig. 2-3. The

thicknesses and depths of various source and target layers are important determinants of the fraction of energy that can reach the target layers. These dimensions are examined in more detail in Chapter 4.

Table 2-7. Assignment of compartments to source regions for short-range radiations in the revised ICRP respiratory tract model.

Target[a]	Source Region	Clearance Compartments Comprising Sources in the Respiratory Tract[b]
ET_1	Surface deposit	14
ET_2	Surface fluid	11 + 11T
	Particles sequestered in airway wall	12 + 12T
	Bound material	ET(b)
LN_{et}	All transformations in LN_{et}	13 +13T + LN_{et}(bnd)
BB	Mucous gel layer	7 + 7T
	Mucous sol layer	8 + 8T
	Particles sequestered in airway wall	9 + 9T
	Bound material	BB(b)
	Alveolar-interstitium	1 + 2 + 3 + 1T + 2T + 3T + AI(bnd)
bb	Mucous gel	4 + 4T
	Mucous sol	5 + 5T
	Particles sequestered in airway wall	6 + 6T
	Bound material	bb(bnd)
	Alveolar-interstitium	1 + 2 + 3 + 1T + 2T + 3T + AI(bnd)
AI	All transformations in AI and LNth	1 + 2 + 3 + 1T + 2T + 3T + AI(bnd) + 10 + 10T + LN_{th}(bnd)
LNth	All transformations in LNth	10 + 10T + LN_{th}(bnd)

Source: ICRP (1994)

[a] Target cell nuclei layers in respective respiratory tract regions are discussed in text.

[b] See Figs. 2-6 and 2-7 and Appendix B for additional clarification of model compartments.

Target tissues in the revised model include the following tissue and cell layers. For the extrathoracic tissues the target regions are: (1) the basal cell nuclei layer in the epithelium of region ET_1; (2) the basal cell nuclei layers in the epithelium of the naso-

oropharynx and larynx in region ET_2; and (3) the total mass of the extrathoracic lymph nodes, LN_{ET}. For the thoracic tissues (or lungs) the target tissues are: (1) the secretory cell nuclei layer in the epithelium of the BB region; (2) the basal cell nuclei layer in the epithelium of the BB region; (3) the secretory cell nuclei layer in the epithelium of the bb region; (4) the total mass of the alveolar-interstitial tissues, AI; and (5) the total mass of the thoracic lymph nodes, LN_{TH}. This aspect of the revised model (computing doses to target regions within the lungs) differs from the ICRP *Publication 30* model (ICRP, 1979) in which a single dose was computed to the lung by averaging over the total lung mass.

Based on a review of human epidemiological studies, Masse and Cross (1989) have suggested that target tissues in the respiratory tract be assigned varying degrees of radiation sensitivity in the new model. To account for varying sensitivities, the revised respiratory tract model (ICRP, 1994) has incorporated regional weighting factors to partition the risk from irradiation of lung tissues. The approach adopted in the model specifies that combined equivalent doses to extrathoracic and thoracic (lung) tissues be computed by the following expressions:

$$H_T(ET) = H_{T,ET(1)}\, A_{ET(1)} + H_{T,ET(2)}\, A_{ET(2)} + H_{T,LN(ET)}\, A_{LN(ET)} \qquad (2\text{-}15)$$

$$H_T(TH) = H_{T,BB}\, A_{BB} + H_{T,bb}\, A_{bb} + H_{T,AI}\, A_{AI} + H_{T,LN(TH)}\, A_{LN(TH)}\,, \qquad (2\text{-}16)$$

where $H_T(ET)$ and $H_T(TH)$ are the detriment-adjusted equivalent doses to the extrathoracic and thoracic (lung) tissues, respectively; $H_{T,ET(1)},\ldots$, etc., are the equivalent doses to targets in the extrathoracic regions; $H_{T,BB},\ldots$, etc., are equivalent doses to targets in the thoracic regions; $A_{ET(1)},\ldots$, etc., are *detriment apportionment factors* for

the partition of risk in ET tissues; and A_{BB},..., etc., are detriment apportionment factors for the partition of risk in the thoracic (lung) tissues.

The detriment apportionment factors are used to weight the doses to the individual regions and reflect the relative sensitivity of the target regions to radiation-induced effects. The values recommended by the ICRP in Publication 66 are listed below in Table 2-8; it is important to note that these values are quite uncertain. Concerning the values reported in the table, the following statement was made:

> It was concluded that there was no basis for deriving factors to represent regional differences in radiation sensitivity with any acceptable degree of confidence. Therefore, the weighting factors given in Table 31 [Table 2-8] are recommended. These factors may be revised by the Commissions as better information becomes available. Revisions can be made without changing the respiratory tract dosimetry model itself. (ICRP, 1994, p. 114)

Based on this statement, the focus of this study has been more toward regional doses than an overall, combined lung dose. Uncertainties in the apportionment factors do not influence regional doses (only their interpretation on a radiological risk basis). Nonetheless, the methodology developed in this study (1) predicts uncertainties in the combined lung dose and (2) provides a means to change the detriment-apportionment (actually their assigned uncertainties) for the thoracic region with little effort. It is noted that although methods are provided for predicting doses to the extrathoracic tissues, these tissues are not included in the list of organs that receive tissue weighting factors in the ICRP (1991a) system of radiological protection. Consequently, these tissues do not receive as much emphasis in this study.

Table 2-8. Risk-apportionment factors recommended by the ICRP for weighting the dose to various respiratory tract target tissues.

Extrathoracic Regions	Detriment Apportionment Factors (A)[a]	Thoracic Regions	Detriment Apportionment Factors (A)
ET_1	0.001	BB	0.333
ET_2	1	bb	0.333
LN_{ET}	0.001	AI	0.333
		LN_{TH}	0.001
Total =	1.002	Total =	1.000

Source: ICRP (1994).

[a] Values are as listed in the reference; do not sum to one.

Masses for target layers associated with ET, BB, and bb regions can be estimated from the products of the regional surface area and the target layer thickness. The regional surface areas are both age- and sex-dependent and must generally be estimated from airway dimensions, which depend on body size. Absorbed fractions for short-range radiations in ET, BB, and bb tissues depend primarily on the source and target layer thicknesses and depths. Measurements (e.g., Gehr, 1987) suggest that dimensions for source and target layers in the airways are independent of age or body size. Furthermore, computations have shown that the airway diameter is of secondary importance to absorbed fractions. Based on these findings, the ICRP (1994) has suggested that absorbed fractions for short-range radiations in the lung are independent of age.

The computational methods used to compute energy absorption in BB and bb target tissues in this study are discussed in detail in Appendix C. The approach for ET regions has been to use the simplified expressions for the absorbed fractions, AF, as

presented by James et al. (1994a). For ET regions, the uncertainties in source and target dimensions are not included in the present study since these regions are relatively resistant to radiation effects and for reasons discussed above. For AI and lymph node tissues, the absorbed fractions suggested by the ICRP(1994) for short-range radiations are used to compute doses. These absorbed fractions (AF) in these regions for alpha particles may be summarized as:

$$AF(AI \leftarrow BB) = AF(AI \leftarrow bb) = AF(AI \leftarrow ET) = 0 \qquad (2\text{-}17)$$

$$AF(AI \leftarrow AI) = AF(LN_{TH} \leftarrow LN_{TH}) = AF(LN_{ET} \leftarrow LN_{ET}) = 1. \qquad (2\text{-}18)$$

Equation 2-17 simply states that alpha particles emitted from sources in the BB, bb, or ET regions deposit a negligible amount of energy in the AI region. Equation 2-17 has been suggested by the ICRP since the additional energy deposited in the AI region from sources in other respiratory tract regions is negligible compared to the energy deposited in the AI region due to sources in the AI region (due primarily to the thickness of tissues separating these regions and to large surface area and mass of the AI region). Equation 2-18 states that alpha particles emitted by the AI and lymph node tissues (as source regions) are completely absorbed by the those regions (as target tissues).

2.8. Summary

The purpose of this chapter has been to provide an overview of the new ICRP respiratory tract model (ICRP, 1994). In this chapter, the deposition, clearance, and dosimetry components of the respiratory tract model have been presented, and model parameters have been introduced. The following chapter presents the methods

employed to treat model parameters and associated quantities as random variables within the (computational) model framework. Chapter 4 examines the respiratory tract model parameters in greater detail by providing results of a formidable literature review--undertaken to assign probability distributions to parameters and to account for relationships (or correlations) among parameters.

CHAPTER 3
METHODS FOR CONDUCTING PARAMETER UNCERTAINTY ANALYSES

3.1. Introduction

A computational methodology has been developed to quantify uncertainties in lung dose quantities for population groups exposed to radioactive aerosols. This methodology is based on conducting parameter uncertainty analyses using the revised ICRP respiratory tract model described in Chapter 2 within the scope of the assessment problem defined in Chapter 1. The purpose of a parameter uncertainty analysis is to quantify variabilities in model predictions attributable to uncertainties (including stochastic variability and lack of knowledge) in model parameters. Additionally, parameter sensitivity analyses of the model are desired in order to determine the relative importance of parameters in affecting model predictions (i.e., which parameters contribute most to variability of the predictions). Specific methods involved in performing such analyses for complex mathematical models have been the subject of many studies and reports (IAEA, 1989; Morgan and Henrion, 1990; OECD, 1987; Hoffman and Gardner, 1983; Iman and Helton, 1985; Iman and Conover, 1982; Hamby, 1995; Iman and Helton, 1988; Nowak and Hofer, 1987; Paschoa and Wrenn, 1987). The purpose of this chapter is to provide a description of methods used in the current study to perform such analyses with the selected respiratory tract model.

The International Atomic Energy Agency (IAEA, 1989) has listed the main steps involved in conducting a parameter uncertainty/sensitivity analysis. These steps are repeated in Table 3-1 and have been followed in the current study. To examine the concepts and techniques associated with these steps, this chapter is divided into five additional sections. In section 3.2 parameter uncertainties and correlations are addressed. Section 3.3 involves a discussion of the numerical methods used to sample the joint probability density function (i.e., the probability density for combined parameter values) and to propagate this joint density function through the model. In section 3.4, some measures of model prediction uncertainty and formats for presenting results are discussed. Section 3.5 provides a discussion of techniques employed to determine parameter sensitivities in the model (i.e., methods to determine dominant parameters and their contributions to model prediction uncertainty). Section 3.6 provides a description of the computer code developed to implement the respiratory tract model and to integrate it with the methods described in this chapter.

Due to the mathematical nature of the respiratory tract model and the large number of model parameters involved, a numerical approach has been adopted for propagating parameter uncertainties through the model. A Latin hypercube sampling technique (McKay et al., 1979; described in section 3.3) has been used in this study to generate a numerical representation of the joint probability density function for the combined range of parameter values. This technique involves numerical generation of n values from each of the m hypothesized parameter distributions. A special pairing process is then implemented to combine values randomly for the m model parameters into n input vectors which can be

used to solve the model for *n* output values for each desired model prediction. Various aspects of the technique are discussed in more detail in the following sections of this chapter.

Table 3-1. Main steps involved in conducting a parameter uncertainty analysis.

(1) List all of the parameters that are potentially important contributors to uncertainty in the final model prediction.
(2) For each parameter listed, specify the maximum reasonable range of applicable alternative values.
(3) Specify the degree of belief (in percentage) that the appropriate parameter value is not larger than specific values selected from the range established in Step 2 above and select a probability distribution that best fits the quoted degrees of belief.
(4) Account for dependencies among model parameters by introducing suitable restrictions, by incorporating appropriate conditional degrees of belief, or by specifying suitable measures of degree of association.
(5) Set up a subjective probability density function (*pdf*) for the combined range of parameter values. This will subsequently be referred to as a joint *pdf*. Propagate this joint *pdf* through the model to generate a subjective probability distribution of predicted values.
(6) Derive quantitative statements about the effects of parameter uncertainties on the model prediction.
(7) Rank the parameters with respect to their contribution to the uncertainty in the model prediction [sensitivity of parameters].
(8) Present and interpret the results of the analysis.

Source: IAEA (1989, pp. 31-32) with minor alterations.

3.2. Quantifying Parameter Correlations and Uncertainties

The first four steps listed in Table 3-1 involve identifying model input parameters and quantifying their correlations and uncertainties. Primary input parameters for the respiratory tract model have been identified in Chapter 2. In this section, the techniques used to account for parameter correlations and uncertainties are discussed. Chapter 4 contains a detailed discussion of individual respiratory tract model parameters, focusing on the distributions and relationships adopted in this study to accommodate parameter uncertainties and correlations.

3.2.1. Parameter Correlations

Two approaches for accommodating parameter correlations/dependencies have been considered. One approach involves specifying and using a rank correlation matrix and is implemented during the pairing process for the m parameter values. The other approach involves using regression equations along with random error terms. The latter approach generally accounts for correlations directly by incorporating detailed relationships between parameters into the uncertainty analysis; consequently, this approach is used here and is more heavily weighted in the following discussion. However, the methodology accommodates the rank correlation matrix approach (as discussed below and in section 3.6).

The correlation matrix approach uses a restricted pairing technique (Iman and Conover, 1982) to induce correlation between the ranks of two numerically sampled input variables. Iman and Shortencarier (1984) have developed a computer code which

implements this approach within the Latin hypercube sampling scheme (discussed in section 3.3). Use of the code requires the user to specify rank correlation coefficients for pairs of parameters. If an appropriately sampled data set exists for two parameters, for example parameters X and Y, then the rank correlation coefficient (also known as Spearman's correlation coefficient) can be estimated by the sample correlation coefficient of the rank-transformed data. The rank correlation coefficient expresses the degree of *linear* relationship between the ranks of X and Y (i.e., it is a measure of the monotonic relationship between parameters). For example, if an increase in X always results in an increase in Y, the rank correlation coefficient would be (positive) one. If an increase in X always resulted in a decrease in Y, the rank correlation coefficient would be negative one. This approach is discussed in more detail by Iman and Conover (1982) and by Liebetrau and Doctor (1987).

A second approach for accommodating relationships between parameters (and the one used in this study) is to use reported regression equations which predict the value of one variable (or input parameter) as a function of another variable (or input parameter). Consider a hypothetical example involving two variables, X and Y. Assume a literature survey has revealed that Y can be predicted (to some degree) by a regression equation relating Y to X; for example, $Y = aX^b$ (i.e., a power function with fitting parameters *a* and *b* determined, for example, by the least squares method). This expression is equivalent to $\ln Y = \ln(a) + b*\ln(X)$, and the associated coefficient of determination, R^2, provides a measure of the variance in Y that is unexplained by the variance in X. For example, a value of $R^2 = 0.90$ means that 90% of the variance in Y is explained by the regression. A

residual, or random, error term can be introduced to explain the remaining uncertainty in Y. For this example, the expression above could be multiplied by an error term, $E_{Y,X}$, so that $Y = (aX^b)*E_{Y,X}$; equivalently, $\ln Y = \ln(a) + b*\ln(X) + \ln(E_{Y,X})$. A distribution for Y, that accounts for its correlation with X, is then obtained by sampling values from a distribution for X and from a distribution for $E_{Y,X}$. The parameter Y does not, in this case, need to be assigned a distribution of its own since it is determined by sampled values for X and $E_{Y,X}$.

The choice of the distribution shape for the residual error term depends on the type of regression equation used. For linear, quadratic, and higher-order polynomial regression models the error term is customarily *added* to the regression expression and assigned a normal distribution with mean value of zero and standard deviation estimated by the standard deviation of the residual errors. The residual errors are given by the differences between the observed values of Y and the values predicted by the regression equation without the random error term. For exponential and power-function regression models, the error term is customarily *multiplied* into the regression expression and assigned a lognormal distribution with geometric mean of one and geometric standard deviation estimated by the sample standard deviation of the *log residuals*, where *log residuals* refer to the differences between *ln*(observed Y) and *ln*(predicted Y). The term *ln* refers to the natural logarithm. Given the data set for the residuals or log residuals, the assigned distribution for the residuals can be subjected to various statistical tests (section 3.2.3) to determine whether the assigned (or hypothesized) distribution is accepted or rejected based on the data.

Throughout this study, parameter correlations have been handled directly (when possible) by using reported regression equations and accompanying residual error terms. This approach allows all random variables to be sampled independently in the Latin hypercube sampling scheme, improving computational efficiency. More details are given for specific model parameters in Chapter 4, where literature is reviewed, parameter uncertainties and regression relationships are discussed, and distributions are assigned. Although a mechanism exists in the methodology for its inclusion (see section 3.6), the rank correlation pairing approach for inducing parameter correlations has not been employed in this study.

3.2.2. Parameter Uncertainties

Uncertainties in respiratory tract model parameters are accommodated by introducing continuous *random variables*. Such variables can attain any real value within their allowed range. Associated with each random variable is a probability density function, or *pdf*. The *pdf* characterizes uncertainties (and variabilities) of the random variable by describing the probability associated with a specified range of values for the random variable. For a continuous random variable, a continuous probability density function is used. All of the parameters investigated in this study possess uncertainties due both to lack of knowledge and to stochastic variability. Since lack of knowledge exists, the *pdf*s generally incorporate some subjective information. One interpretation of the distributions assigned in Chapter 4 is that all represent subjective prior distributions in which distribution parameters (e.g., mean and standard deviation) are Bayesian estimators

(Morgan and Henrion, 1990, p. 83). Future information and data for model parameters can be used to update these prior distributions by employing Bayesian statistics (DeGroot, 1970) to compute the posterior distributions. Notwithstanding these issues, one must work in the present with limited data sets and attempt to assign, on a case by case basis, distributions to model parameters that realistically reflect the current state of knowledge (as perceived by the assessor). If measured data exist for model parameters, graphical and statistical tests can be used to determine whether to reject an assigned (hypothesized) *pdf*; however, no tests exist which can unequivocally prove that an assigned distribution is the correct one.

Many distribution shapes can be used to represent parameter uncertainties. Among the *pdf*s considered in this study are the uniform (or rectangular), triangular, normal, and lognormal probability density functions. The choice of distribution depends on the information available for the specific parameter being considered. A description of each of these distribution shapes follows.

The uniform *pdf* represents the simplest distribution shape for continuous random variables. For this *pdf* the random variable has an equal probability of assuming any value between a specified minimum and maximum value. If the minimum value is represented by *a* and the maximum by *b*, the *pdf* for the uniform distribution is given as:

$$f(x) = \frac{1}{(b-a)}, \qquad a \le x \le b \tag{3-1}$$

where x refers to a specific value of the random variable, denoted as X. The integral of the *pdf* over a specified range of values Δx is the probability of X taking on a value in that

range. A typical uniform distribution is shown in Figure 3-1. This distribution shape is useful when the only information known about the parameter is the *range* of possible values and when no other sufficiently detailed information exists to justify one of the other *á priori pdfs*.

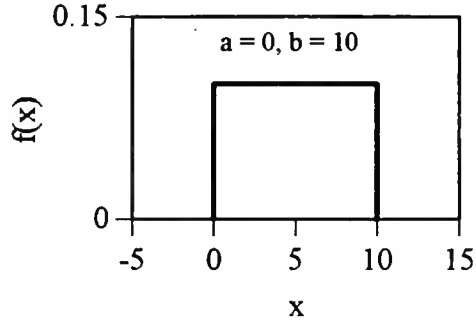

Figure 3-1. Example of a uniform probability density function with a = 0 and b = 10.

The triangular probability density function has three parameters, the minimum value *a*, the mode (or most probable value) *b*, and the maximum value *c*. Three cases can be identified for triangular distributions. For case one, $a < b < c$; for case two, $a = b < c$; and for case three, $a < b = c$. Typical distribution shapes associated with these cases are shown in Figure 3-2. Functions representing the *pdf* are given by the following equations for these three cases:

Case one (a < b < c):

$$f(x) = \begin{cases} \dfrac{2(x-a)}{(c-a)(b-a)} & a \le x \le b \\ \dfrac{2(c-x)}{(c-a)(c-b)} & b \le x \le c \end{cases}; \qquad (3\text{-}2)$$

Case two (a = b < c): $$f(x) = \frac{2(c-x)}{(c-a)^2} \quad a \le x \le c \ ; \tag{3-3}$$

Case three (a < b = c): $$f(x) = \frac{2(x-a)}{(c-a)^2} \quad a \le x \le c \ . \tag{3-4}$$

This distribution shape is useful for model parameters with values that tend toward a single most likely value (i.e., stochastic variability is not expected to be large), but the paucity of data precludes that value from being specified exactly.

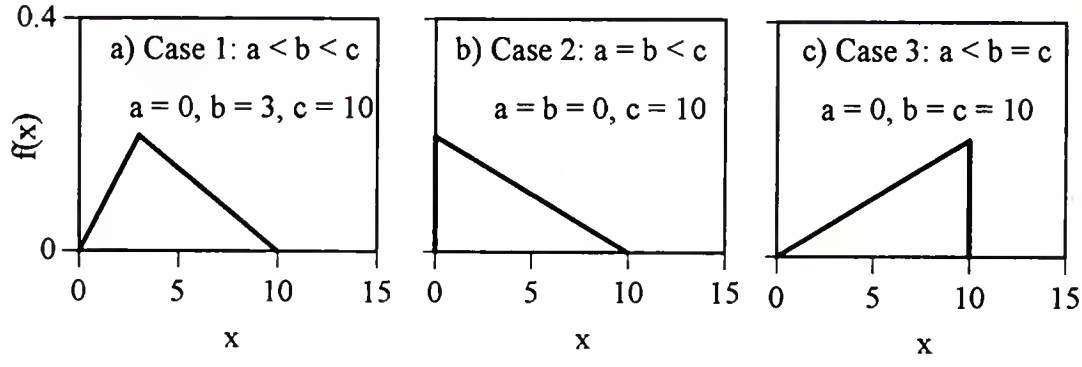

Figure 3-2. Examples of triangular probability densities for the three possible cases discussed in text: (a) Case one: *a*<*b*<*c*, (b) Case two: *a*=*b*<*c*, and (c) Case three: *a*<*b*=*c*.

The normal (or Gaussian) probability density function is specified by two parameters, μ and σ, where μ represents the mean value and σ represents the standard deviation. The *pdf* for the normal distribution is:

$$f(x) = \frac{1}{\sqrt{(2\pi)}\,\sigma} \exp\left(-\frac{(x-\mu)^2}{2\sigma^2}\right) \quad -\infty \le x \le \infty \ . \tag{3-5}$$

Two examples of this distribution are represented in Figure 3-3. In the figure, the distributions are truncated at 2.5σ; however, mathematically the tails go to infinity. This distribution is useful for representing random data that generally follow a bell-shaped distribution. Many biological parameters have been found to be well represented by a normal distribution (e.g., body height). This distribution is also useful for accommodating random error or uncertainty in mean values according to the central limit theorem.

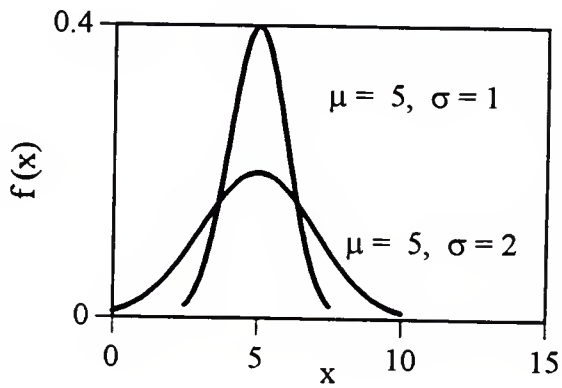

Figure 3-3. Examples of two typical normal probability density functions.

The (two-parameter) lognormal density function is related to the normal distribution by a simple transformation of the random variable, X. If X is lognormally distributed, then ln(X) follows a normal distribution. Specification of the lognormal distribution requires two parameters, γ and ϕ, where γ is the mean value of ln X and ϕ is the standard deviation of ln X. The *pdf* for the lognormal distribution is given by:

$$f(x) = \frac{1}{\sqrt{(2\pi)}\,\phi\,x} \exp\left(-\frac{(\ln x - \gamma)^2}{2\phi^2}\right) \qquad 0 \le x \le \infty \ . \tag{3-6}$$

Two quantities related to the parameters of the lognormal distribution are the geometric mean, μ_{geo} and the geometric standard deviation, σ_{geo} (also denoted by GSD throughout this document). These quantities are given by the following expressions:

$$\mu_{geo} = \exp(\gamma) \; ; \qquad \sigma_{geo} = \exp(\phi) \; . \tag{3-7}$$

Two examples of lognormal distributions are plotted in Figure 3-4 for two values of σ_{geo}. As σ_{geo} (or ϕ) increases, so does the dispersion of the random variable. A value of σ_{geo} equal to one represents no dispersion (i.e., variable has only one possible value).

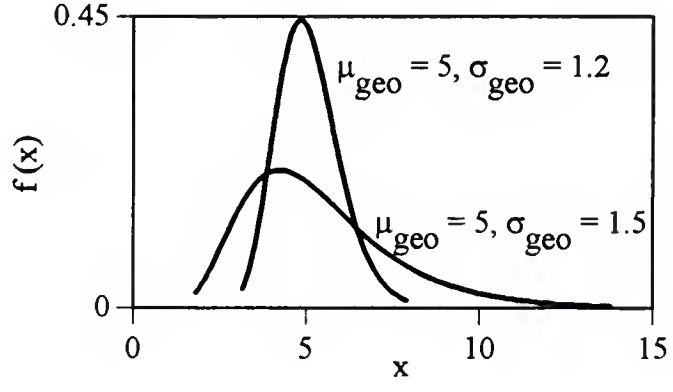

Figure 3-4. Examples of lognormal probability density functions.

The lognormal distribution often provides a good representation for quantities constrained to be non-negative and positively skewed. Many biological quantities are represented well by lognormal distributions. For quantities possessing a lognormal distribution, the following expressions relating the (arithmetic) mean and standard deviation (μ and σ) to the geometric mean and GSD (μ_{geo} and σ_{geo}) are useful:

$$\mu_{geo} = \frac{\mu}{\sqrt{\sigma^2/\mu^2 + 1}}; \qquad \sigma_{geo} = \exp\sqrt{\ln(\sigma^2/\mu^2 + 1)} \; . \tag{3-8}$$

Expressions in Eq. (3-8) have been derived from equations presented in Table 5.2 of Morgan and Henrion (1990).

3.2.3. Testing the Fit of an Assigned Distribution

If sampled data exist for a model parameter, then techniques exist for evaluating the fit of an assigned (hypothesized) *pdf* with respect to the data set. Distributions based purely on subjective judgement or expert opinion (i.e., no adequate data set exists), however, cannot be tested by any statistical means. Furthermore, as a result of the scientific method, a hypothesized *pdf* cannot be proved, only rejected based on the data set. Tests of distribution fit considered in this study can be categorized as either graphical or statistical; both involve an analytical component.

Graphical tests involve plotting distributions and comparing shapes. One commonly used graphical test involves the probability plot (Hahn and Shapiro, 1967; King, 1971; Filliben, 1975; Vogel, 1986). Such a plot possesses a cumulative probability axis and a value axis for the random variable. The scale of the probability axis is designed so that the cumulative probability of the specified distribution shape (i.e., the distribution shape which is being tested, e.g., a normal distribution) plots as a straight line versus the random variable. An observed data set can be tested to determine if it is consistent with the specified distribution shape by plotting the cumulative probability of the data set versus the data values. If the graphed data can be approximated well by a straight line, then the

data set is at least consistent with the specified distribution. Normal and lognormal probability distributions are examples of distribution shapes which have been used to create probability plots. These plots are also useful in selecting mean values and standard deviations for the variable being investigated. Other graphical techniques simply involve comparing various predicted fractiles (based on an assigned distribution) to the measured, or observed, fractiles.

Statistical tests involve computing various *test statistics* and comparing them to tabulated values to determine whether a sampled data set is consistent with the hypothesized distribution. Such statistical *goodness-of-fit* tests are numerous. The more popular tests are: (1) the chi-squared test; (2) the non-parametric Kolmogorov-Smirnov test (e.g., see Sachs, 1984, pp. 320-332; Conover, 1980); (3) Lilliefors' test (Lilliefors, 1967, 1969); (4) the W test developed by Shapiro and Wilk (1965); and (5) D'Agostino's test (D'Agostino, 1971). The chi-squared test is technically suitable only for discrete random variables; however, it can be applied to continuous variables with some effort and caution in interpreting results. The Kolmogorov-Smirnov goodness-of-fit test is useful for evaluating the fit of any continuous hypothesized distribution; however, it may not be valid if parameters of the hypothesized distribution are estimated from the data set. Lilliefors' test allows the parameters of the hypothesized distribution to be estimated from the data set but only applies to tests involving a hypothesized normal or lognormal distribution. The W test is also limited to an hypothesized normal or lognormal distribution. As published by Shapiro and Wilk (1965), the W test could be performed for samples with

$n \leq 50$. D'Agostino's test extended the W test to n between 50 and 1000. Royston (1982, cited in Gilbert, 1987) developed a procedure allowing the W test for n up to 2000. The W test has been discussed and applied by Gilbert (1987), who described it as one of the most powerful tests available for detecting departures from a hypothesized normal or lognormal density function.

3.2.4. Subjective Probability Judgements and Expert Opinion

Many of the parameters examined in this study are not associated with direct data sets. The problem is that many quantities of interest in respiratory tract modeling cannot be reliably measured nor have they been the subject of direct investigation. For such parameters, this study has relied on a subjective approach in assigning distributions. Even with measured data sets, some level of subjectiveness remains in the assignment process since a variety of distribution shapes are generally acceptable by available statistical tests.

In some cases (e.g., regarding the particle transport aspect of the clearance model), parameter uncertainties have been discussed by individuals who can be considered "experts" with respect to the parameter of interest. In such cases, the distributions recommended by these individuals have been adopted to represent parameter uncertainties. In cases where no expert opinion exists, this study has attempted to collect as much information as possible in order to make a defensible recommendation for the distribution shape. In the case where conflicting expert opinion exists, one approach may be an attempt to combine the opinions, for example, by sampling parameter values from two (or more) weighted distributions. Ultimately, the effort directed toward quantifying

uncertainties in a particular parameter should be kept in perspective concerning the relative contribution that parameter makes to uncertainty in model predictions (i.e., the parameter might not influence results significantly compared to other variables in the model; or disagreement among experts is insignificant with respect to model output).

An interesting discussion of subjective probability and various techniques for eliciting probability judgements from experts and others can be found in Chapters 6 and 7 of Morgan and Henrion (1990). In their discussion of elicitation techniques, Morgan and Henrion note that "a strong and consistent tendency to overconfidence" generally exists among assessors. Overconfidence, as discussed by those authors, refers to the tendency of an assessor to assign more events to the tails of a distribution than actually exist. In other words, assessors tend to broaden the distribution somewhat, increasing the probability associated with unlikely (or rare) events. As an example of overconfidence, the authors show a plot of the estimated deaths per year (by a group of 40 well-educated people, but not necessarily experienced actuarians) versus the actual deaths per year from a variety of causes. Actual deaths per year caused by tornadoes are about 80; the group of people estimated that about 800 deaths per year were caused by tornados. It is obvious that for some types of rare events (e.g., *death* due to a tornado), emotions play a key role in influencing judgement and opinion. The authors also discuss situations in which "experts" might under-estimate or over-estimate the probabilities associated with unlikely events in efforts to influence decisions made as a result of an uncertainty analysis (e.g., the decision to fund research and development in which the assessor is involved).

3.3. Propagation of Parameter Uncertainty

Once distributions have been assigned to parameters and correlations defined, both analytical and numerical techniques exist for propagating parameter uncertainties through mathematical models (e.g., for an overview see IAEA, 1989; Morgan and Henrion, 1990). The most common analytical methods are variance propagation and moment matching. Both of these methods require an algebraic representation for the model. In the present study such a formulation is not practical since numerical algorithms must be employed to solve certain aspects of the model (e.g., energy deposition in target regions). Therefore, numerical techniques for uncertainty propagation have been used in this study.

For sake of discussion, it is convenient to consider the respiratory tract model as a function, g, of the m model parameters (input variables X_1, X_2, X_3, ..., X_m in following discussions), which are characterized by assigned probability distributions. If Y is taken as a model prediction, then $Y = g(X_1, X_2, X_3, ..., X_m)$. A single set of sampled values $\{x_1, x_2, x_3, ..., x_m\}$ required to solve the model for a single trial is defined as an *input vector*. In a numerical propagation of parameter uncertainties, n input vectors (comprised of n sampled values for each of m variables) are determined by either *simple random sampling* or *Latin hypercube sampling* techniques. These n input vectors are then used in the model to produce n *realizations* of Y. Numerical techniques employed to sample values from parameter distributions, for purposes of propagating uncertainties through the model structure, are discussed in following sections.

3.3.1. Simple Random Sampling

In simple random sampling *n* values are randomly selected for each parameter (or input variable) using a straightforward Monte Carlo technique. The technique involves two components, a random number generator and a numerical representation for the inverse cumulative distribution function for the input variable. The approach is as follows: (1) a value, ξ, is selected at random between 0 and 1 based on a uniform distribution; (2) the inverse cumulative distribution function for input variable X, denoted as $F^{-1}[F(x)]$, is then evaluated at $F(x) = \xi$ to determine a sampled value, $x = F^{-1}(\xi)$, for input variable X.

In practice ξ is actually a *pseudo*-random number since it is determined by a numerical algorithm. Many pseudo-random number generators are available for sampling values for ξ. This study has used an algorithm suggested by Park and Miller (1988). The algorithm is efficient and works on any computer system for which the maximum value of an integer variable is $(2^{31} - 1)$ or larger. For most computer systems, this value corresponds to an integer which is allocated at least four bytes (32 bits) of memory. The algorithm is shown in Figure 3-5.

Specification of the inverse cumulative distribution function is the more difficult component of the Monte Carlo technique. The cumulative distribution function, F(x), represents the probability that a parameter X is less than or equal to some value x and is related to the probability density function, f(x), by the following expression:

$$F(x) = \int_{x_{min}}^{x} f(x`)dx` \quad . \tag{3-9}$$

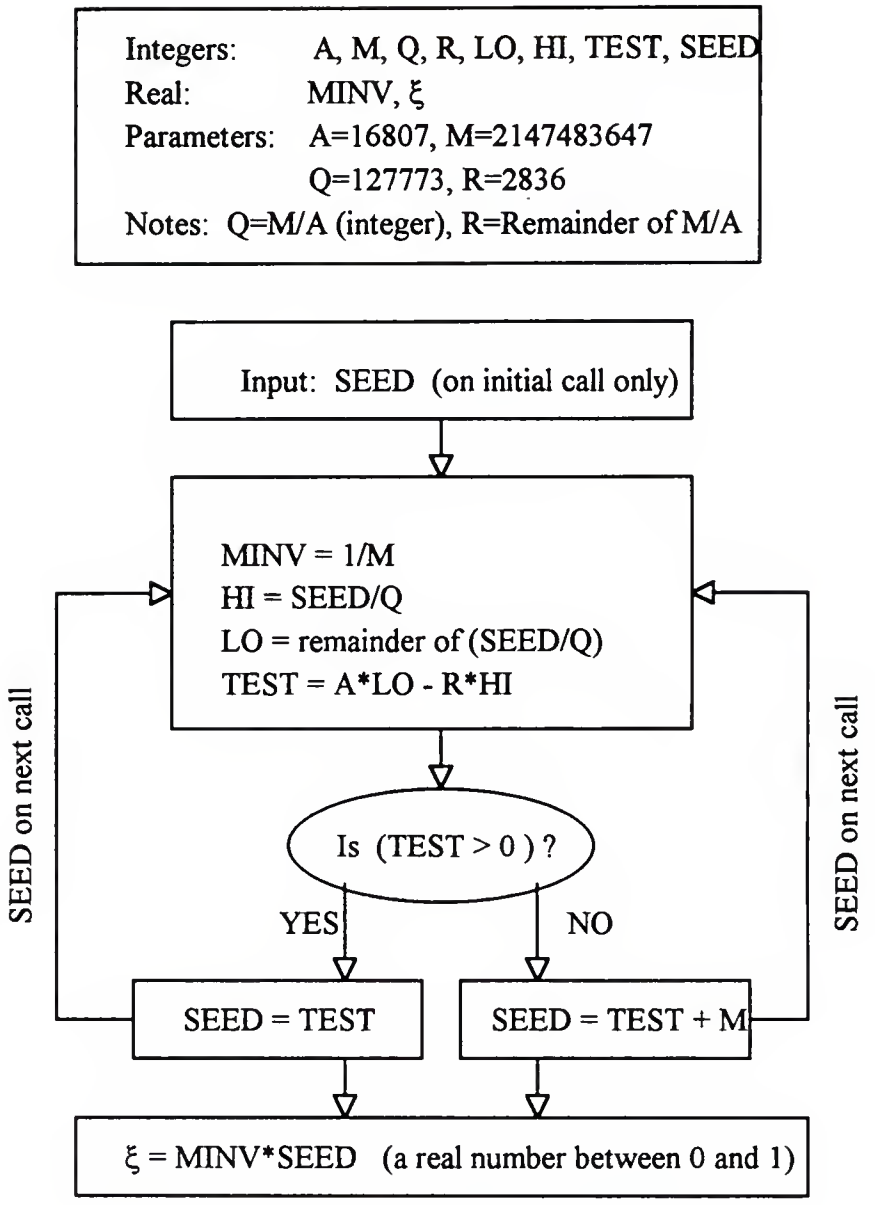
Integers: A, M, Q, R, LO, HI, TEST, SEED
Real: MINV, ξ
Parameters: A=16807, M=2147483647
Q=127773, R=2836
Notes: Q=M/A (integer), R=Remainder of M/A
Input: SEED (on initial call only)
MINV = 1/M
HI = SEED/Q
LO = remainder of (SEED/Q)
TEST = A*LO - R*HI
Is (TEST > 0) ?
YES
NO
SEED = TEST
SEED = TEST + M
SEED on next call
SEED on next call
ξ = MINV*SEED (a real number between 0 and 1)

Figure 3-5. Algorithm to generate a random number, ξ, on the interval (0,1).

Solving Equation 3-9 for x as a function of F(x) yields the inverse cumulative function, $F^{-1}[F(x)]$. For some simple distributions, an analytical expression can be obtained for $F^{-1}[F(x)]$. For example, for an input parameter uniformly distributed between *a* and *b*, $F(x) = (x-a)/(b-a)$, so that $x = F^{-1}[F(x)] = a + F(x)*(b-a)$. However, for a normal (or lognormal) distribution, an explicit, analytical form for the inverse cumulative distribution does not exist. In these circumstances numerical approximations must be used.

For example, the *Box-Muller* method (e.g., Press et. al., 1986) is a technique that uses two randomly sampled values of ξ (i.e., ξ_i and ξ_{i+1}) to generate pairs of values sampled from an approximate normal distribution. Other numerical approximations have also been suggested for evaluating the inverse cumulative function of normal and other distributions (Abramowitz and Stegun, 1964; Hastings, 1955; Press et al., 1986). For more details on the Monte Carlo method and its applications the reader is referred to discussions by Cashwell and Everett (1959), Carter and Cashwell (1975), Rubinstein (1981), and Bouleau (1994).

3.3.2. Latin Hypercube Sampling

Latin hypercube sampling (abbreviated LHS; developed by McKay et al., 1979) involves a constrained Monte Carlo sampling scheme. In LHS the cumulative probability distribution, F(x), is partitioned into *n* non-overlapping intervals of equal probability, and simple random sampling is used within each interval to generate *n* sampled values for parameter X. The feature of LHS is that it results in a smoother sample from the assigned parameter distribution with fewer trials (smaller *n*) than would be required by simple

random sampling. The effect of this smoother sample for parameters is a potentially smoother output distribution for the model predictions (with fewer trials). The Latin hypercube sampling method derives its name from fractional factorial sampling schemes such as Latin squares (Liebetrau and Doctor, 1987).

A Latin hypercube sample of size *n* is generated as follows (Iman and Shortencarier, 1984). The range for each of the *m* variables (i.e., X_1, X_2, X_3, ..., X_m) is divided into *n* non-overlapping intervals (numbered from 1 to *n* from smallest to largest values) having equal probability (i.e., each interval is associated with a probability of $1/n$). One value is randomly selected from each of the *n* intervals with respect to the probability density function using the Monte Carlo techniques outlined above. This selection process results in *n* values for the *m* variables. The *n* values obtained for X_1 are paired in a random manner with the *n* values of X_2. These *n* pairs $\{X_{1i}, X_{2i}\}_{i=1,n}$ are then combined in a random manner with the *n* values of X_3 to form *n* triplets $\{X_{1i}, X_{2i}, X_{3i}\}_{i=1,n}$, and so on, until finally *n m*-tuples are formed. These *n m*-tuples comprise a numerical sample of the joint subjective *pdf* for the combined range of parameter values. The model is solved for each of the *n m*-tuples to yield *n* predicted values. These *n* predicted values form a numerical sample of the subjective *pdf* for the prediction.

If desired, special techniques can be used in the pairing process to induce correlations between sampled variables. A technique for inducing correlations in Latin hypercube samples has been suggested by Iman and Conover (1982). In the present study correlations have been handled more directly by using reported regression equations and associated residual error terms. Subsequently, in this study, the LHS samples are assumed

to be composed of independent random variables (i.e., random pairing techniques have been used without inducing correlations). However, the computational code used in this study to generate the n m-tuples is capable of implementing the restrictive pairing technique, if desired in future work.

To illustrate the LHS method, Figure 3-6 shows a typical LHS sample of size $n = 5$ for $m = 2$ input variables, X_1 and X_2. Uncertainty in X_1 is characterized by a lognormal distribution; uncertainty in X_2 is represented by a triangular distribution. The distributions are first divided into $n = 5$ intervals each having a probability of $1/n = 0.2$. One value is then randomly selected with respect to the probability distribution from each of the five intervals for each variable. The values are then paired by associating random permutations of the integer set $\{1, 2, 3,..., n\}$ with the intervals sampled for each input variable. The permutation is selected at random from the $n!$ possibilities. For the example shown in Figure 3-6, the random permutation for variable X_1 is $\{2, 5, 3, 4, 1\}$; for variable X_2 the random permutation is $\{5, 2, 1, 4, 3\}$. These permutations correspond to the intervals that are paired to form each of the $n = 5$ trials and are indicated by O's in the figure. Table 3-2 shows the intervals paired for each indicated trial.

Principal features of the LHS method (Andres, 1987) are: (1) LHS produces unbiased estimators for the population mean and cumulative density function of any output variable Y (as determined by the specified parameter distributions and mathematical model), and (2) LHS potentially provides a more efficient means for estimating various quantities for the model prediction (e.g., mean, variance, fractiles) than simple random sampling since estimates (from LHS) are expected to exhibit less variation from sample to

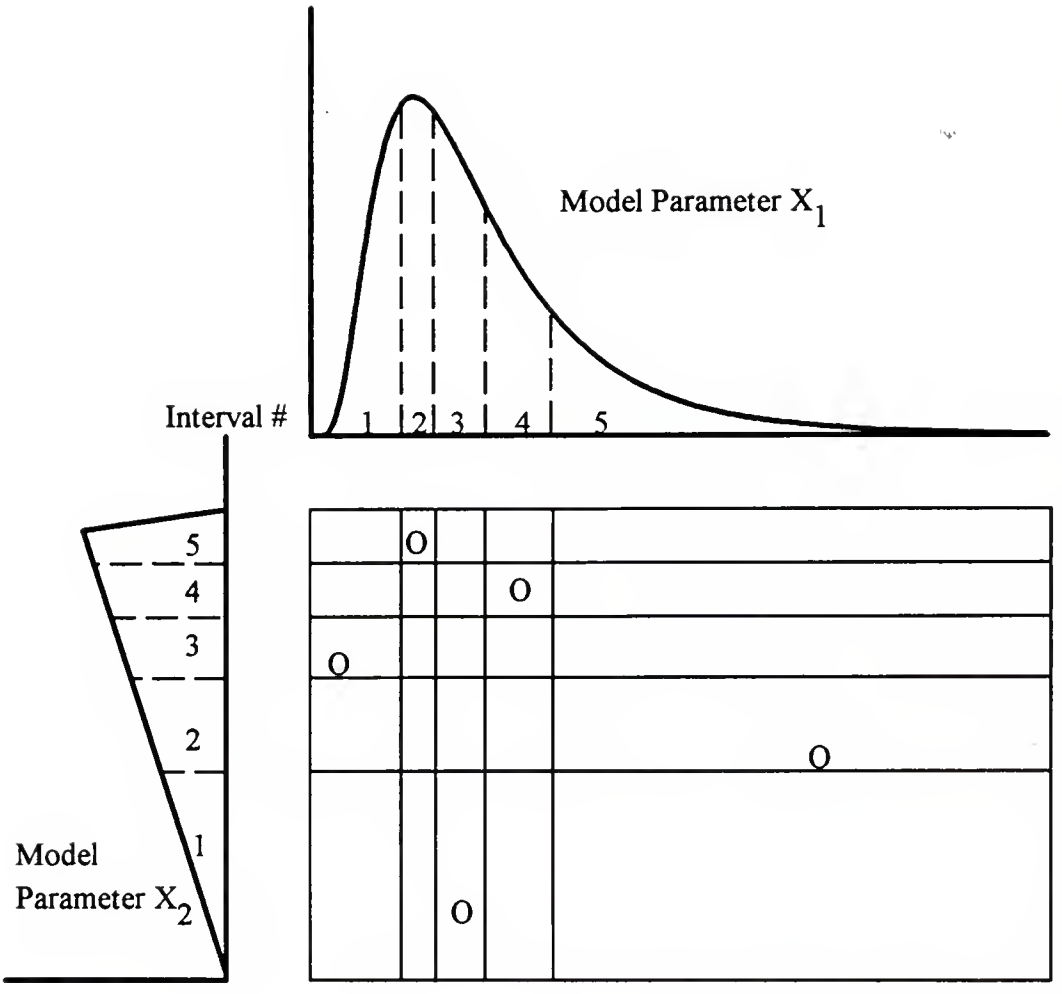

Figure 3-6. Example of a Latin hypercube sample of size $n = 5$ drawn for two input variables, X_1 and X_2.

Table 3-2. Intervals paired for the Latin hypercube sample shown in Figure 3-6.

Trial	Interval for X_1	Interval for X_2
1	2	5
2	5	2
3	3	1
4	4	4
5	1	3

sample (for the same sample size, *n*). Disadvantages of LHS include: (1) Potentially large memory storage requirements since a the sample be produced in its entirety before solving the model (simple random sampling does not have this restriction). This limitation has not been a problem in the current study because memory requirements did not exceed capacities. An estimate of the LHS memory requirement for 32-bit variables (on most systems) is given by the product (4 bytes per variable)*(*m* variables)*(*n* trials). For example in this study, n=1000 was used with about 70 variables; so roughly 280 kilobytes were needed for the LHS data (not including additional memory to store executable program and output data). (2) No simple methods exist for obtaining confidence limits for estimators (e.g., estimated fractiles) derived by LHS techniques. The only solution is to draw a second independent sample of size *n*, compute a new estimate of the fractile, and compare it to the first to get an idea of the sampling error. Simple random sampling does not have this limitation. (3) LHS can be influenced by the degree of monotonic relationship between the model predictions versus input variables. If the model is not a monotonic function of each input variable then, according to Andres (1987), the LHS technique may be no better than simple random sampling.

3.4. Presentation of Uncertainties in Model Predictions

Many useful quantities exist for summarizing the results of an uncertainty analysis. Among the quantities considered in this study are various distribution-free fractile estimates, means (arithmetic and geometric), and standard deviations (arithmetic and geometric). Cumulative probability plots of the n predicted values for various assessed quantities also provide a useful format for presentation. While these plots allow various fractiles to be ascertained graphically, they also permit a graphical test to determine whether the distribution of values is consistent with a particular distribution shape (e.g., lognormal). Normalized frequency histograms are also useful for comparing distribution shapes among different assessed quantities.

Upon generating the n values for the predicted quantity as described above, the *distribution-free* (sample) fractiles can be obtained in the following manner. First the predicted values are arranged in increasing order. Then an empirical cumulative probability of $1/n$ is assigned to the smallest value, $2/n$ is assigned to the next value, and so on. This process results in an empirical cumulative distribution function. This function can be used to estimate various fractiles (or percentiles) of the numerical sample. For example the k-th ordered prediction value provides an estimate of the $(k/n)*100\%$ sample fractile. These estimates are *distribution-free* since they do not depend on any assumed distribution shape for predicted values. Fractiles of general interest include the 2.5%, 5%, 25%, 50%, 75%, 95%, and 97.5%. The 50% fractile corresponds to the median of the distribution and is a measure of the central tendency of the distribution. The 95% fractile

is of interest in many regulatory standards. The 2.5% and 97.5% fractiles are of interest since they represent the lower and upper bounds, respectively, of the 95% confidence interval for the prediction. The 95% confidence interval provides an indication of the spread in predicted values.

3.5. Parameter Sensitivity Techniques

Several techniques exist for performing both local and global parameter sensitivity analyses (e.g., see Hamby, 1995; IAEA, 1989; Iman and Helton, 1988; Crick et al., 1987; Iman and Conover, 1982). Local sensitivity analyses involve variations in a single model parameter with all other parameters set to a nominal scenario (e.g., reference or default values). Local analyses are generally easy to implement (the model can be solved without using random sampling techniques); however, their results cannot be easily extrapolated to other scenarios, and interactions among parameters cannot be easily incorporated. Global sensitivity analyses involve a multivariate approach where all parameters are allowed to vary over their range simultaneously. The global approach accounts for the joint probability density function for the combined range of all parameters (i.e., parameter interactions and probabilities are included). For the model examined in this study, the desire is to examine sensitivities from a global perspective. Due to the mathematical complexity of the model, a numerical approach, consistent with the random sampling techniques discussed in previous sections, has been adopted to examine parameter sensitivities in the respiratory tract model.

Previous sections have addressed techniques for representing parameter uncertainties and correlations and for generating appropriate numerical samples of the joint probability density function for the combined range of parameter values. Once the *n* *m*-tuples $\{X_{1i}, X_{2i}, X_{3i}, ..., X_{mi}\}_{i=1,n}$ have been generated and the respiratory tract model has been solved for *n* values of the assessed quantity $\{Y_i\}_{i=1,n}$, parameter sensitivities can be estimated from the resulting data set $\{X_{1i}, X_{2i}, X_{3i}, ..., X_{mi}, Y_i\}_{i=1,n}$ by use of regression methods. For models which are not linear with respect to input variables (such as the respiratory tract model), the IAEA (1989) has suggested computing and using various correlation and regression coefficients of the data set as measures of parameter sensitivity.

Regression coefficients are determined by fitting a multivariate regression model to the rank-transformed data set associated with *n* trials. Using the set of the *n* multivariate observations, $\{X_{1i}, X_{2i}, X_{3i}, ..., X_{mi}, Y_i\}_{i=1,n}$, the following multiple linear regression model can be fit to the data by the least squares method:

$$\hat{Y} = b_o + \sum_{j=1}^{m} b_j X_j \qquad (3\text{-}10)$$

where $\hat{Y}$ represents the regression prediction; b_0 is a constant and b_j is the regression coefficient for parameter X_j. The regression coefficient represents the partial derivative of the regression model with respect the associated input variable. Thus, the regression coefficient provide a measure of the change in the model prediction per unit change in the input parameter. One measure for the degree of fit of the regression model is provided by its R^2 value (or coefficient of determination) which is computed as:

$$R_y^2 = \frac{\sum_i^n (\hat{Y}_i - \bar{Y})^2}{\sum_i^n (Y_i - \bar{Y})^2} \quad (3\text{-}11)$$

The value of R_y^2 is equal to the fraction of the variance in the assessed quantity, Y, that is explained by the regression on the X's. For simple linear regression involving one independent variable X, R_y^2 corresponds to the correlation coefficient squared for X and Y. For multiple linear regression, involving more than one independent variable, R_y^2 corresponds to the multiple correlation coefficient squared (as defined, for example, in Conover, 1980). Assuming that (multiple) linear regression is an appropriate approximation of the actual model, step-wise regression can be performed in which input parameters are added to the regression one-at-a-time; the increase in R^2 provides a measure of the variance in the assessed quantity that is explained by the added parameter.

The regression coefficient b_j in Eq. 3-10 provides a measure of the sensitivity of the output variable, Y, with respect to changes in the associated input variable X_j. However, the set of regression coefficients cannot generally be compared since they are influenced by the units used to express the input variables (e.g., grams, kilograms, liters/minute,..., etc.). To remove the influence of parameter units on the regression coefficients, Iman et al. (1985) have suggested that the data be "standardized" and the regression coefficients be determined from the standardized data set. The data are standardized by the following transformation: $X_j^* = (X_j - \bar{X}_j)/s_{xj}$ where $\bar{X}_j$ is the sample

mean and s_{xj} is the sample standard deviation for variable X_j. Using the standardized data set $\{X^*_{1i}, X^*_{2i}, X^*_{3i}, \ldots, X^*_{mi}, Y^*_i\}_{i=1,n}$, the regression model can be rewritten as:

$$\hat{Y}^* = \sum_{j=1}^{m} b^*_j X^*_j \qquad (3\text{-}12)$$

where b_j^* is the standardized regression coefficient (SRC) for parameter X_j. The standardized regression coefficient of a parameter (or input variable, X) "indicates by how many standard deviations s_Y the approximate model prediction changes if this parameter is changed by one standard deviation s_X, all other parameters remaining constant. (IAEA, 1989, p. 55)" The values of b_j^* can be compared directly since the influence of units has been removed. The larger the magnitude of b_j^*, the more sensitive the model predictions are to changes in X_j^*. A negative value indicates that an increase in X_j^* results in a decrease in Y^*. By ranking the standardized regression coefficients based on their magnitudes, the most important model parameters can be determined.

A major assumption in this treatment is that the regression model provides an adequate representation of the more complex computational model. The R^2 value for the regression provides a measure of the adequacy of the regression. For mathematical models that are not linearly related to all input parameters (e.g., the model examined in this study), the linear regression models discussed above are expected to be inadequate. In such cases, the IAEA (1989) has suggested that the regression model be based on the rank-transformed data set.

The rank-transformed data set is obtained by ranking the *n* sampled (and predicted) values in the data set for each variable while retaining the association of values

for the *i*-th trial. As an example, Table 3-3 lists a hypothetical data set with $n = 5$ trials, $m = 3$ input parameters, and one prediction. The rank-transformed data set is shown in the right portion of the table.

Table 3-3. Example of a hypothetical data set and its rank-transformed data set.

Original Data Set (n = 5, m = 3)					Rank-Transformed Data Set				
Trial	X_1	X_2	X_3	Y	Trial	RankX_1	RankX_2	RankX_3	RankY
1	2.4	1.2	4.2	29.0	1	2	2.5[a]	3	4
2	2.2	1.3	4.1	31.1	2	1	4	2	5
3	3.1	1.1	4.3	22.3	3	5	1	4	1
4	2.7	1.4	4.4	24.2	4	3	5	5	2
5	3.0	1.2	3.9	27.6	5	4	2.5[a]	1	3

[a] For ties, an average rank is assigned.

The coefficients of the multiple linear regression equation based on the rank-transformed data are known as standardized rank regression coefficients (SRRC). Whether the sampled data or the standardized data are used is not important since the ranks will be the same. Basing the regression on the rank-transformed data increases explanatory power of the regression model (by reducing effects of model nonlinearity on the regression analysis results). For a given model parameter, the standardized rank regression coefficient provides a measure of the degree of monotonic relationship between that parameter and the model prediction. A negative value corresponds to a negative monotonic relationship. The magnitude of the SRRC has been used to rank parameters in this study. The associated R^2 value for the regression on ranked data reflects the adequacy of the regression in explaining the variance in the rank transformed data. To

perform the necessary manipulations and computations required to estimate SRRCs and R^2 values a computer program developed by Iman et al. (1985) has been employed.

3.6. Description of the Lung Dose Uncertainty Code (LUDUC)

As discussed in Chapter 1, the first phase of this work has involved developing a computational code to solve the revised ICRP (1994) respiratory tract model for given values of parameters and to couple that model with an existing code (Iman and Shortencarier, 1984) for generating simple random samples and Latin hypercube samples of the input parameters. The overall code package has subsequently been named LUDUC (for Lung Dose Uncertainty Code). The computer code consists of the following program modules (all but the second were developed in the current study): (1) scenario specification and input module, (2) LHS module (developed by Iman and Shortencarier, 1984), (3) respiratory tract particle deposition module, (4) respiratory tract clearance module, (5) short-range radiation dose matrix module, (6) respiratory tract dosimetry module, and (7) data presentation/ output module. A schematic diagram of these modules indicating the flow of computations is shown in Figure 3-7.

The module listed as item (1) in Fig. 3-7 was written in the Visual Basic™,[1] programming language and runs in the Microsoft©,[2] Windows™,[3] environment. This programming language makes full use of the graphical user interface and multi-tasking

---

[1]Visual Basic™ is a trademark of the Microsoft Corporation.

[2] Microsoft Corporation, One Microsoft Way, Redmond, WA 98052-6399.

[3]Windows™ is trademark of the Microsoft Corporation.

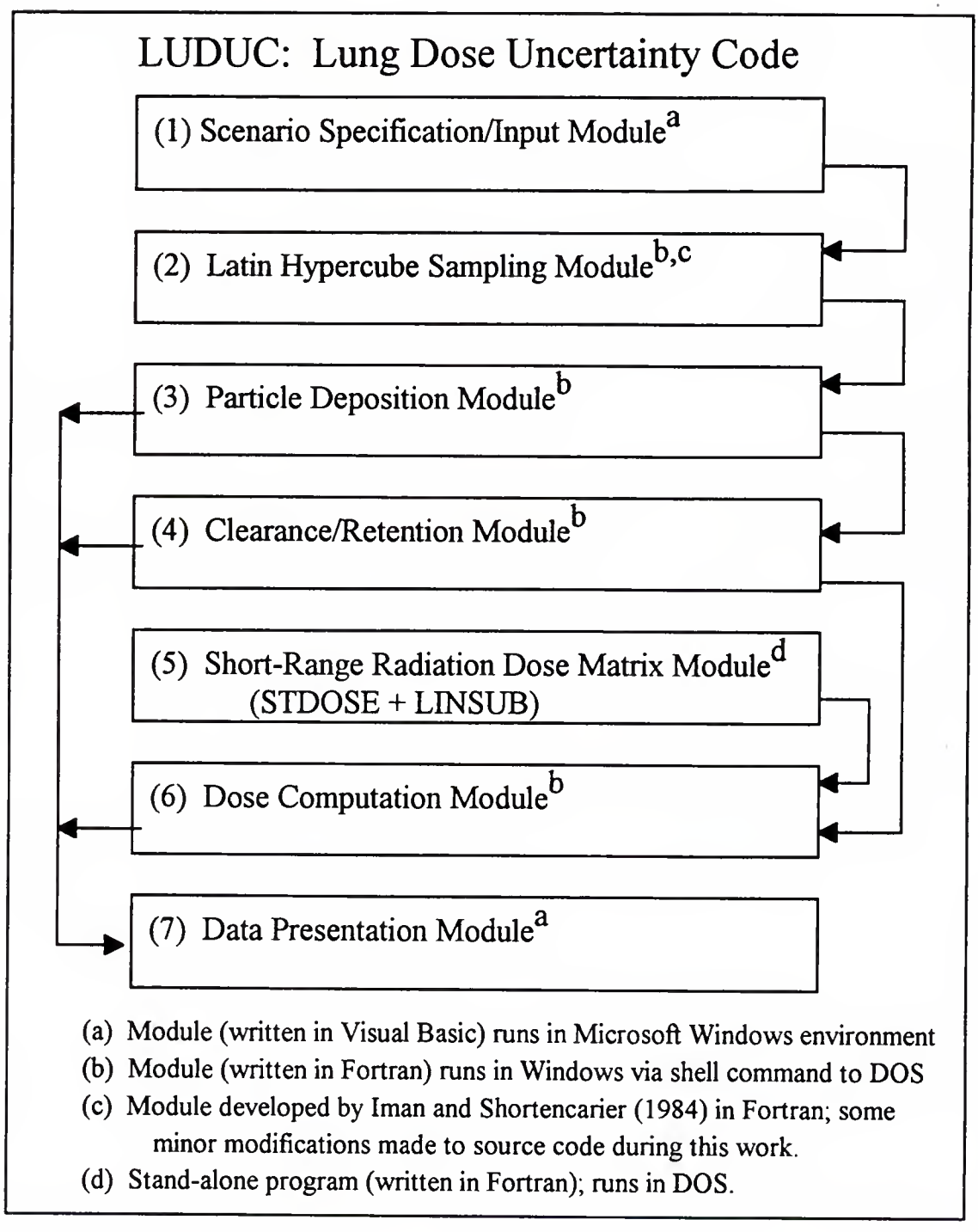
LUDUC: Lung Dose Uncertainty Code
(1) Scenario Specification/Input Module[a]
(2) Latin Hypercube Sampling Module[b,c]
(3) Particle Deposition Module[b]
(4) Clearance/Retention Module[b]
(5) Short-Range Radiation Dose Matrix Module[d] (STDOSE + LINSUB)
(6) Dose Computation Module[b]
(7) Data Presentation Module[a]
(a) Module (written in Visual Basic) runs in Microsoft Windows environment
(b) Module (written in Fortran) runs in Windows via shell command to DOS
(c) Module developed by Iman and Shortencarier (1984) in Fortran; some minor modifications made to source code during this work.
(d) Stand-alone program (written in Fortran); runs in DOS.

Figure 3-7. Schematic diagram showing the flow of computations in the Lung Dose Uncertainty Code (LUDUC).

capabilities offered by the Microsoft© Windows™ environment. This module allows the user of LUDUC to specify the exposure scenario and other input information. As discussed in Chapter 1, an uncertainty analysis is conducted within the context and scope of an assessment problem. As posed, the assessment problem requires the exposure scenario to be defined by specifying: (1) the age and gender of the exposed population group, (2) the physical exertion level of the group during the exposure (assumed to be acute for computational purposes), (3) the activity-particle size distribution (in terms of the aerodynamic diameter), the particle shape factor, and the particle density, and (4) the ambient temperature and pressure. If desired, the user can also specify an ambient activity concentration level, and an exposure duration (otherwise quantities are assessed per unit exposure). The code allows either monodisperse particles, a lognormal particle size distribution, uniform size distribution, or a user-supplied histogram (normalized) to be specified for the activity-size distribution. This module also allows the user to specify control variables that store the number of trials to perform, the integer seed for the random number generator, and the truncation level desired for normal and lognormal distributions (e.g., sample from distributions truncated at two standard deviations). This module also allows the input distributions (discussed and assigned in Chapter 4) to be modified to some degree by giving the user an opportunity to change distribution shape and parameters. The primary function of the module is to set up the input files which are required by subsequent modules, including the Latin hypercube sampling code developed by Iman and Shortencarier (1984).

The second module listed above was developed by Iman and Shortencarier (1984) at Sandia National Laboratories. The module is available from those authors as a FORTRAN source code. Three modifications have been made to the source code during the current study: (1) Beta distribution capabilities were disabled since these distribution types were not used in the current study. (2) A feature was added to the program that allows the user to specify truncation levels (in the input file read by the program) for samples drawn from normal and lognormal distributions. The truncation level corresponds to the confidence interval from which values are sampled from these distribution types. A truncation level of 95% was used for all normal and lognormal distributions in applying methods to plutonium oxides (Chapter 5). Truncation is needed since theoretical extreme values of these distributions go to infinity. A truncation level of 95% is consistent with standards recommended for medicine (Bo, 1969). (3) The random number generator shown in Figure 3-5 is incorporated into the code. As LUDUC runs, the LHS module reads an input file created by the first module (input/scenario module) and creates a large computer file, *lhs.raw*, to store the n m-tuples generated by the LHS process. This module runs in the MS-DOS®,[4] environment by a shell command. Although not utilized in this research, this program accommodates a user-supplied rank correlation matrix to induce correlations between various input parameter pairs.

The third module solves the deposition component of the ICRP respiratory tract model discussed in Chapter 2. This module reads both *lhs.raw* and the input file storing the scenario data and solves the deposition model n times to generate n predictions for the

[4]MS-DOS is a registered trademark of the Microsoft Corporation.

desired output quantities (deposition fractions). The code employs numerical techniques to integrate over polydisperse particle size distributions by breaking the distribution into discrete size ranges and weighting the deposition fraction for that size range by its probability. The source code for this module is written as a FORTRAN subroutine and is portable to other computer systems supporting FORTRAN. The executable module also runs in the MS-DOS® environment and has been compiled/linked using Lahey[5] FORTRAN (Version 5.20).

The fourth module solves the clearance component of the respiratory tract model. This module implements the algorithm described by Birchall (1986) to solve the system of differential equations listed in Appendix B. The module reads from an output file created by the deposition module to determine the initial activity deposited in model compartments. This module also reads both *lhs.raw* and the input file storing the scenario data. The purpose of the module is to solve the clearance model n times to generate n predictions for the desired output quantities. Depending on specifications in the input/scenario module, the clearance module computes either the number of nuclear transformations or the transformation rate in source components (see Table 2-7 for components) after a specified time. These computations are stored in an output file which is subsequently read by the dose computation module (sixth module). The source code for this module is written as a FORTRAN subroutine. The executable module runs in the MS-DOS® environment and has been compiled/linked using Lahey FORTRAN.

---

[5]Lahey FORTRAN is a product of Lahey Computer Systems, Inc., P.O. Box 6091, Incline Village, NV 89450.

The fifth module is a stand-alone program that computes a dose matrix used as input to the dose computation module. This program, named STDOSE, computes the equivalent dose to targets at various depths in tissues due to sources comprising 0.5 μm thick cylindrical shells (geometrical model for BB and bb the airways). In Appendix C, mathematical techniques employed by the code are described, and the program is listed. The source-target geometry in the BB and bb regions is complex and generally requires evaluation of a complex volume integral in cylindrical coordinates. The dose matrix created by STDOSE stores results from these integrations thereby allowing the dose computation module (sixth module) to execute much faster. For a given radionuclide two dose matrices are needed--one for the BB region and one for the bb region. Use of the dose matrix generated by STDOSE greatly improves the speed of dose computations in the bronchial and bronchiolar target layers of the respiratory tract model and essentially makes this study feasible. Without this component, computational runs took roughly 300 times as long to complete (e.g., ~30 versus 0.1 hours for n=1000 trials) for a specified scenario on a (486DX) 66MHz personal computer. The source code for this module is written as a FORTRAN subroutine. The executable module runs in the MS-DOS® environment and has been compiled/linked using Lahey FORTRAN.

The sixth module has been developed to compute equivalent doses in target regions of the respiratory tract. The model also computes the combined lung dose (i.e., weighted sum of the regional doses). This module couples results from clearance model computations with target and source geometries. Using data generated by the LHS module for target and source dimensions, masses,..., etc. (based on assigned input

distributions), this module solves the dose model (n times) for n values for dose quantities. Dose matrices generated by STDOSE are used to compute doses to BB and bb regions. Doses to the AI region and to the lymph node regions are predicted as described in ICRP *Pub. 66* (ICRP, 1994). The executable module runs in the MS-DOS® environment and has been compiled/linked using Lahey FORTRAN.

The final module (seventh module) presents the numerical results from the deposition, clearance, and dose modules as histograms. In addition to histograms the module presents minimum, maximum, median, mean, standard deviation, geometric mean, geometric standard deviation, and various fractile values for predicted quantities. Predicted quantities include the following: (1) deposition fractions in ET_1, ET_2, BB, bb, AI, total thoracic, and total respiratory tract; (2) total radionuclide transformations (or transformation rates) at time t since exposure for all source components in the respiratory tract; (3) equivalent doses to ET_1 (basal cell layer), ET_2 (basal cell layer), LNet (total mass), BB (basal cell layer), BB (secretory cell layer), bb (secretory cell layer), AI (total mass), LNth (total mass), and the combined thoracic region dose (weighted sum of regional doses). This module was written in Visual Basic™ and runs in the Microsoft© Windows™ environment.

Modules (1), (2), (3), (4), (6), and (7) can all be run from a single computational platform in Microsoft© Windows™. Modules (2), (3), (4), and (6) are run by a shelling command which temporarily transfers control from the Windows™ environment to the MS-DOS® environment. For sample size of $n = 1000$, this platform runs in less than five minutes on a 66 MHz personal computer system. Module (5) must be run in the DOS

environment and reads from input files storing appropriate stopping power, range, and energy data.

Modules (3), (4), (6), and (7) have been verified by direct comparison with results from a program developed, independently, by the National Radiological Protection Board (Jarvis et al., 1993). That program is called LUDEP (for Lung Dose Evaluation Program). The program LUDEP solves the ICRP lung model for a deterministic scenario (i.e., all input parameters set to single values). Using the same input parameter values, lung deposition and clearance model predictions (modules [3] and [4]) for the two programs agreed well (relative differences were less than 0.1%). Differences between dose model predictions (module [6]) for plutonium were generally less than 5%.

3.7. Summary

This chapter has presented discussions of the techniques adopted for this work to perform parameter uncertainty analyses of the respiratory tract model discussed in Chapter 2. The approach has been to use numerical techniques to propagate parameter uncertainties through the model. A computer program, LUDUC, has been developed to perform analyses. Details for various model parameters are presented in Chapter 4. Chapter 5 gives results for a specific application of LUDUC to inhaled $^{239}PuO_2$ aerosols.

CHAPTER 4
UNCERTAINTIES IN RESPIRATORY TRACT MODEL PARAMETERS

Previous chapters present the respiratory tract model selected for this work and the techniques involved in performing a parameter uncertainty analysis of the model. The purpose of this chapter is to present results from Phase II of this study. In this phase literature on model parameters (i.e., both direct and indirect input parameters) was compiled and examined, and probability density functions and restrictive relationships were assigned to parameters. Assignment of appropriate distributions and relationships to parameters was necessarily tedious due to the large number of parameters required by the model. As discussed in Chapter 3, many of these distributions are subjective since direct measurements have not been made for all parameters. The discussion focuses primarily on model *input* parameters; however, uncertainties in some *embedded* model parameters are also addressed. In total sixty-nine model parameters (including direct and indirect input parameters and embedded parameters) were assigned distributions. Recommendations were based on a direct review of over one hundred references. Many of these references are compilation studies which are, in turn, based on numerous other references.

Information was not generally adequate to quantify directly the correlations between all parameters. However, many correlations were accommodated by an indirect approach. For example, many of the deposition model input parameters are correlated

with body height and/or mass. By accounting for the mutual correlation of these parameters with height and/or mass, correlations between many of the deposition parameters are implicitly addressed.

This chapter is divided into three primary sections. Section 4.1 presents methods used in this study to model uncertainties and correlations in deposition model parameters; section 4.2 examines uncertainties in parameters involved in the clearance/retention component of the model; and section 4.3 examines the dosimetry (energy absorption and geometry) parameters of the model. The section on deposition parameters is quite detailed compared to other sections; one reason is that several age- and gender-related differences in lung dosimetry exist in this component of the model. Also many of the quantities required to model particle deposition have been studied in more detail than those required by other model components. Consequently, correlations are better quantified for the deposition aspect; whereas for the other components (clearance and dose models), parameters are generally assumed to be statistically independent--lacking more definitive information.

The relationships and distributions presented in this chapter are based, whenever possible, on studies performed with healthy persons. The approach was to use body height (per gender and age population subgroups) for the United States population at large as the starting point for the study. The possibility exists that these and other data (and relationships) discussed in this chapter might not be representative of populations residing at specific geographic locations. Consequently, use of the methods discussed in this chapter could introduce a bias for site-specific estimates. Nevertheless, the

"population-at-large" distributions in height and mass (and associated quantities) were a practical point of departure in the investigation of uncertainties and variability in lung dose coefficients. One advantage of using "at-large" population data is that the results of this work are more broadly applicable. In the computer program developed to implement the methodology, LUDUC, the user is able to modify all suggested parameter distributions--should better information become available.

4.1 Deposition Model Parameters

The primary input parameters for the particle deposition model have been listed previously in Table 2-3. Other quantities, which are important in order to derive these parameters and to account for correlations between them, have been listed in Table 2-4. The purpose of this section is to present available information on deposition model parameters and to suggest distributions for them. Correlations between parameters are addressed when sufficient information exists.

4.1.1. Body Height

Body height, Ht, is a variable that correlates well with a number of the deposition parameters listed in Table 2-3. Age- and gender-specific distributions in body height have been inferred from studies conducted by the National Center for Health Statistics (NCHS, a branch of the U.S. Department of Health and Human Services). The most recent study is the second National Health and Nutrition Examination Study (NHANES II) conducted from 1976 to 1980. Body height, body mass, and body mass index data collected during this study for the United States population were recently analyzed by Najjar and Rowland

(1987). Results from that study include descriptive statistics per yearly age increment for ages 2-19 years and per ten year age groupings (e.g., 25-34 years) for adults. Selected estimates of the arithmetic means and standard deviations in height are listed in Table 4-1.

Table 4-1. Selected Height Data from the Second National Health and Nutrition Examination Study (NHANES II) Conducted from 1976-1980.

Age (years)	Gender[a]	Arithmetic Mean (cm)	Standard Deviation (cm, % of mean)	Number Examined
2	M	91.2	4.3, 4.7%	375
	F	89.7	4.2, 4.7%	336
5	M	112.6	5.4, 4.8%	397
	F	111.6	5.3, 4.8%	364
10	M	141.6	7.3, 5.2%	157
	F	141.9	6.5, 4.6%	136
15	M	170.8	6.7, 3.9%	184
	F	177.0	7.1, 4.0%	145
18-24	M	177.0	7.1, 4.0%	988
	F	163.4	6.6, 4.0%	1066
25-34	M	176.7	6.7, 3.8%	1067
	F	163.1	6.3, 3.9%	1170
35-44	M	176.3	7.3, 4.1%	745
	F	162.8	6.3, 3.9%	844
45-54	M	175.2	6.6, 3.8%	690
	F	161.3	6.4, 4.0%	763
55-64	M	173.7	6.9, 4.0%	1227
	F	160.1	6.4, 4.0%	1329
65-74	M	171.3	7.1, 4.1%	1199
	F	158.1	6.2, 3.9%	1416

Source: From Najjar and Rowland, 1987.

[a] M = males; F = females.

Expressed as a percent of the mean, the standard deviations indicate that the variability in body height is relatively constant over all ages. For children, the standard deviation is roughly 5% of the mean. For ages greater than or equal to about 15 years the standard deviation is roughly 4% of the mean and changes little with increasing age. Figure 4-1 plots the relationship between body height and age for males and females; the data points are based on results from NHANES II and earlier studies conducted by the NCHS (namely, Cycles I, II, and III of the Health Examination Survey, HES and the first National Health and Nutrition Survey, NHANES I). A small increase in the average height of the adult population can be discerned when comparing recent to earlier studies over two decades.

The data presented in Table 4-1 and Figure 4-1 are for the U.S. population as a whole and include all races examined in the NHANES II survey. No information was given in that study comparing regional population groups to the at-large population data. The NHANES II study did compare blacks and whites for all adult age brackets; generally, negligible differences existed between estimated mean values and only minor differences between estimated standard deviations.

In the present study, body height (for a given age/gender group) was assigned a normal distribution with mean and standard deviation estimated from values in Table 4-1. To help justify this approach, observed (distribution-free) fractiles in height from Najjar and Rowland (1987) were compared to ones predicted by the assigned normal distribution in height for a given population class. The predicted fractiles in height were estimated from an approximate inverse function (Abramowitz and Stegun, 1964) for the normal

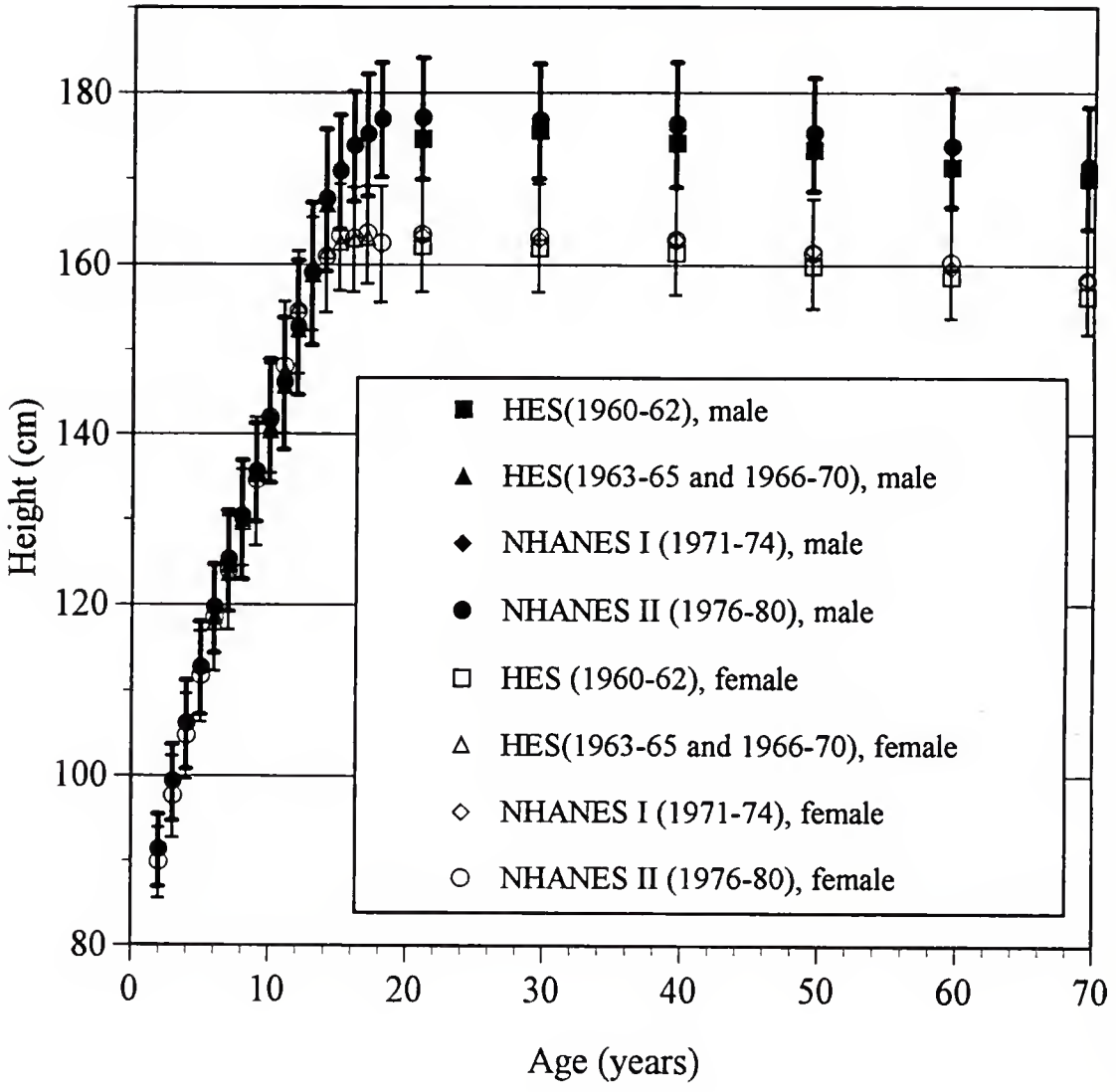

Figure 4-1. Average body height as a function of age for males and females. Error bars indicate one standard deviation from the mean value. Heavier bars are for males.

cumulative distribution. For example, the observed 0.25 fractile (i.e., 25th percentile) in height for 10 year old males is 137.0 cm (Najjar and Rowland, 1987). Assuming a normal distribution with mean of 141.6 cm and standard deviation of 7.3 cm (as listed in Table 4-1), the predicted 0.25 fractile is 136.7 cm. Therefore, the ratio of the predicted-to-observed 0.25 fractile is (136.7)/(137.0) = 0.998. Ratios of predicted to observed fractiles for selected population classes are plotted in Figure 4-2. The fact that all ratios are close to unity supports the inference that height is normally distributed. The plot shows that there is less than a one-percent difference between observed fractiles and those predicted with a normal distribution. In addition to computing the ratios described, Kolmogorov-Smirnov goodness-of-fit tests (e.g., see Sachs, 1984, pp. 330-332) were performed using predicted and observed fractiles. Normal distributions in height were not rejected by these tests for the population groups listed in Table 4-1 at a high level of significance ($\alpha = 0.1$).

4.1.2. Body Mass Index

While a number of the quantities listed in Table 2-3 correlate well with body height, others are found to correlate better with body mass (or weight). Therefore, distributions in body mass were also needed for each population class. However, body mass is known to be correlated with body height. For example, Smalley et al. (1990) recently examined height and mass in 363 adult subjects and reported a correlation coefficient of 0.46. In using Monte Carlo sampling techniques, the desire is to work with statistically independent variables whenever possible. To account for correlations between height and mass, the body mass index (BMI) was utilized in the present study.

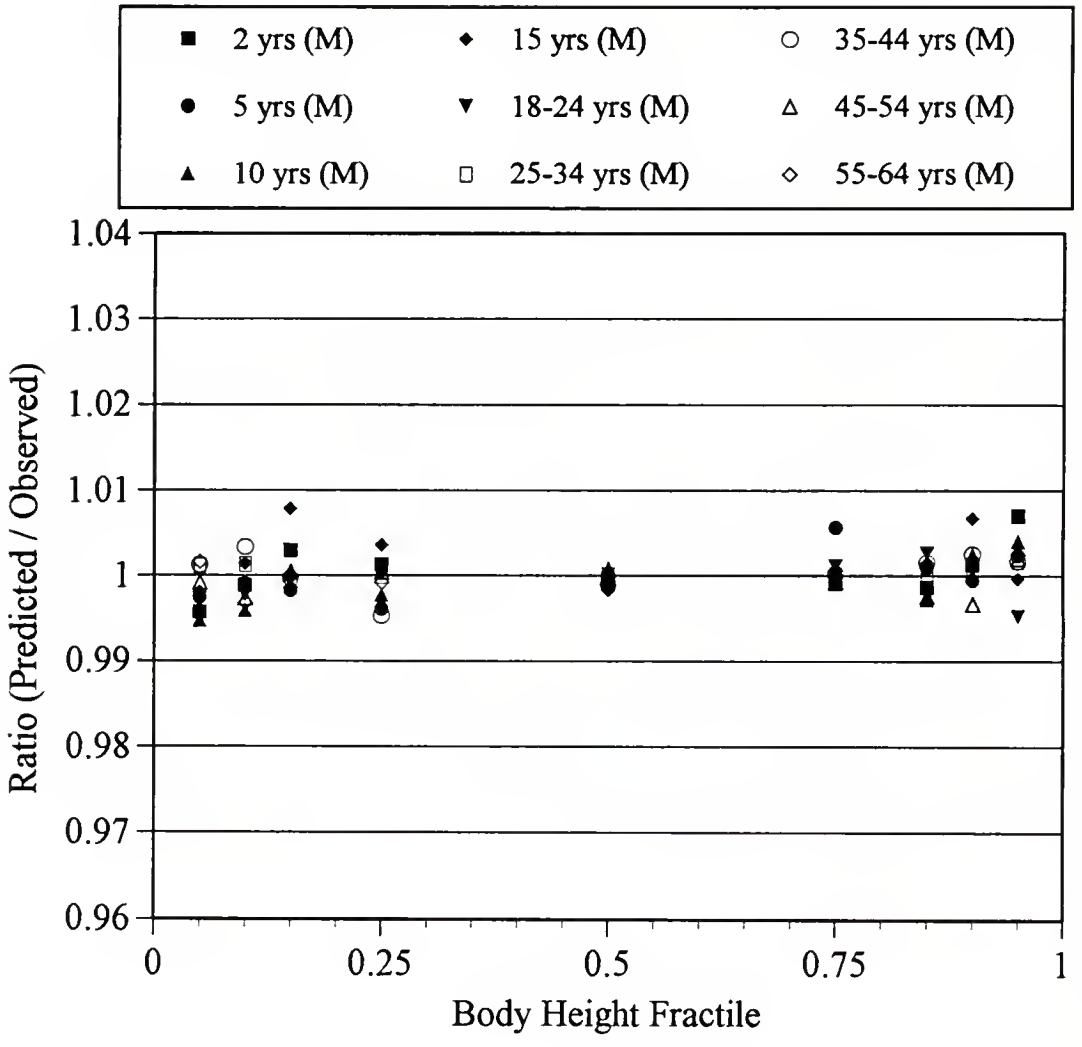

Figure 4-2. Ratio of predicted (assuming normal distribution) to observed fractiles in body height for males (M) at selected age groups. Although not shown, females showed similar values and trends.

The BMI is defined as the quotient of body mass and height squared (i.e., units: kg/m^2). For a given height and BMI, the body mass, denoted by Wt, is then estimated as the product of BMI and height squared;

$$Wt = BMI * Ht^2. \quad (4\text{-}1)$$

Arithmetic averages and standard deviations for BMI, as determined by Najjar and Rowland (1987) from NHANES II, are listed in Table 4-2 for selected age and gender classes. The geometric means and standard deviations were derived from their arithmetic counterparts (using Equation 3-8). Figure 4-3 shows the relationship between the average BMI and age for males and females. Error bars indicate one (arithmetic) standard deviation. Generally, the variability in BMI for females is greater than for males.

Height and BMI were assumed to be statistically independent within a given population class. Over broad age ranges in which growth is occurring at a fast rate, this assumption does not hold since both BMI and height increase with age--compare Figures 4-1 and 4-3. However, within small age intervals (i.e., yearly increments up to 18 years age; and intervals as delineated in Table 4-2 for ages greater than 18 years), limited information exists which supports independence. A necessary (albeit insufficient) condition for two quantities to be statistically independent is that their correlation coefficient equal zero. Two studies were located which examined correlations between BMI and height. Smalley et al. (1990) computed a correlation coefficient of 0.02 for BMI and height based on data from 363 adult males and females. Based on data from the first National Health and Nutrition Examination Survey (NHANES I), Garn et al. (1986)

computed sample correlation coefficients for a number of gender-specific age groups; these are listed in Table 4-3.

Table 4-2. Body mass index data from NHANES II (1976-1980).

Age (years)	Gender	Arithmetic Mean, kg/m^2 (Std. Deviation, kg/m^2)	Geometric Mean, kg/m^2 (Geometric Std. Dev.)[a]	Number Examined
2	M	16.3 (1.3)	16.3 (1.08)	375
	F	16.1 (1.3)	16.1 (1.08)	336
5	M	15.6 (1.5)	15.5 (1.09)	397
	F	15.6 (1.8)	15.5 (1.12)	364
10	M	18.0 (2.9)	17.8 (1.17)	157
	F	17.8 (3.2)	17.5 (1.20)	136
15	M	20.8 (3.1)	20.6 (1.16)	184
	F	20.6 (3.0)	20.4 (1.16)	145
18-24	M	23.5 (3.6)	23.2 (1.17)	988
	F	22.6 (4.2)	22.2 (1.20)	1066
25-34	M	25.2 (4.0)	24.9 (1.17)	1067
	F	24.1 (5.5)	23.5 (1.25)	1170
35-44	M	26.0 (3.9)	25.7 (1.16)	745
	F	25.3 (5.8)	24.7 (1.25)	844
45-54	M	26.3 (4.1)	26.0 (1.17)	690
	F	26.1 (5.8)	25.5 (1.25)	763
55-64	M	26.1 (3.8)	25.8 (1.16)	1227
	F	26.5 (5.6)	25.9 (1.23)	1329
65-74	M	25.5 (3.9)	25.2 (1.16)	1199
	F	26.7 (5.4)	26.2 (1.22)	1416

Source: All data except those in fourth column are from Najjar and Rowland (1987). Geometric data in column four were derived here based on an assumed lognormal distribution for BMI using Eq. 3-8 with reported sample means and standard deviations.

Table 4-3. Correlations Between Height and BMI.

Age Group (years)	Males[a]		Females	
	n	R	n	R
5-10	1112	0.32	1165	0.27
11-15	897	0.24	895	0.17
16-19	596	0.04	614	-0.08
20-35	1706	-0.02	3766	-0.08
36-50	1485	-0.05	2513	-0.08

Source: Garn et al. (1986).

[a] R = sample correlation coefficient; n = number of subjects.

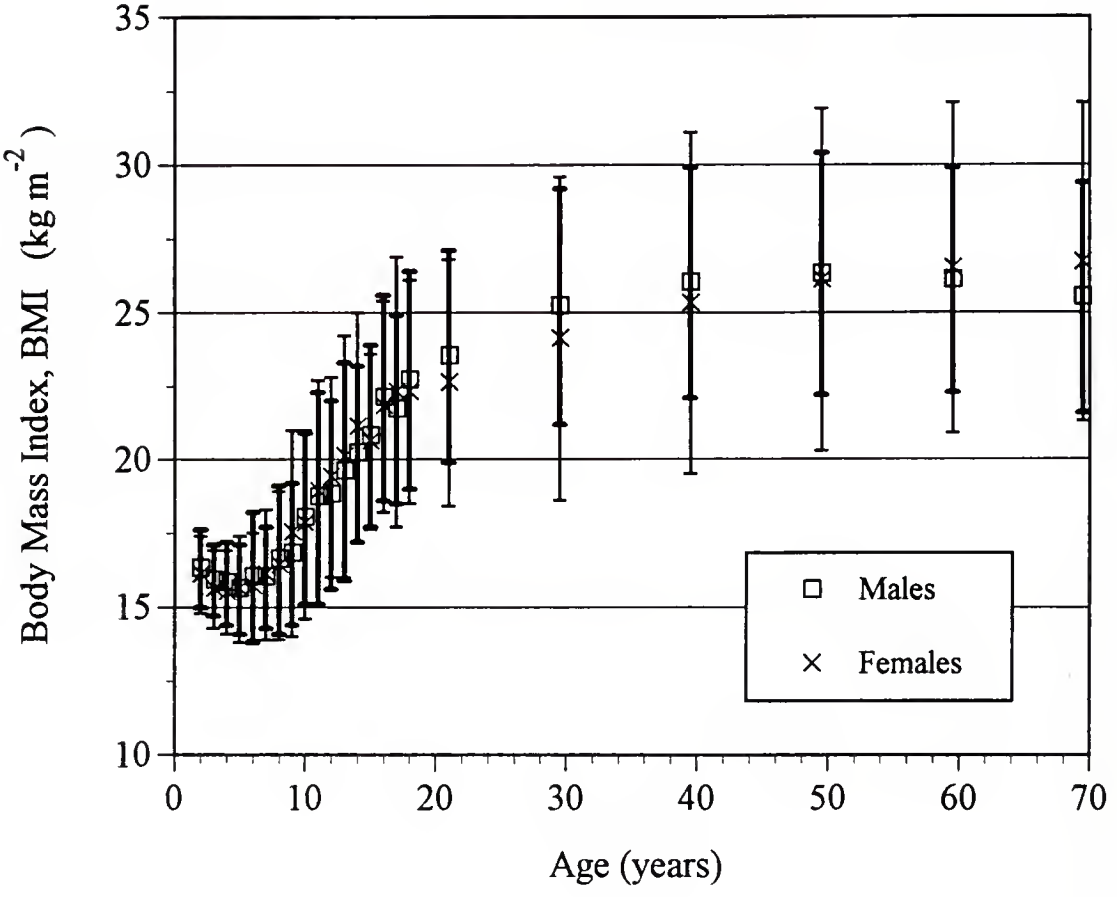

Figure 4-3. Average body mass index as a function of age for males and females. Error bars indicate one standard deviation from the mean value. Heavier bars are for males.

Correlation coefficients in Table 4-3 for age groups older than 16 years are approximately zero supporting (although not proving) statistical independence of BMI and Ht for older population groups. However, for the younger age groups the correlation is relatively high. This result is likely attributable to the broad age groupings (~ 5 year intervals) used in computing correlation coefficients for children--growth occurs at a high rate within these groupings. Although speculative, an assumption in this study was that correlations (between BMI and height) for yearly age intervals for children less than 16 years old are negligible. This assumption allows independent selection of BMI and height from their respective distributions while setting up the input vectors for trials.

Two distribution shapes, normal and lognormal, were investigated for describing variabilities in BMI. A better fit was found with a lognormal distribution shape; so in the present study the assumption was that body mass index, BMI, (for a given age/gender group) is lognormally distributed with geometric averages and standard deviations as listed in Table 4-2. To help justify this assumption, Figure 4-4 plots the ratio of the predicted to observed fractiles for BMI. Observed (distribution-free) fractiles are from the study by Najjar and Rowland (1987). The predicted fractiles for BMI were estimated from an approximate inverse function (Abramowitz and Stegun, 1964) for the lognormal cumulative distribution. As indicated in Figure 4-4, the predicted fractiles are slightly less than the observed fractiles below the 50% fractile and generally higher than observed fractiles above the 50% fractile. This result indicates that, for all groups examined, a lognormal distribution tends to over-estimate slightly the variability in BMI; however since the predicted fractiles are generally within 2-5% of the observed values, this discrepancy is

not expected to be significant. In fact, this figure indicates that a lognormal distribution provides a slightly conservative model of the variability. In addition to this graphical test for distribution fit, quantitative Kolmogorov-Smirnov goodness-of-fit tests were performed using the observed fractiles for these population classes. The result was that lognormal distributions in BMI with parameters from Table 4-2 were not rejected at high levels of significance ($\alpha = 0.1$).

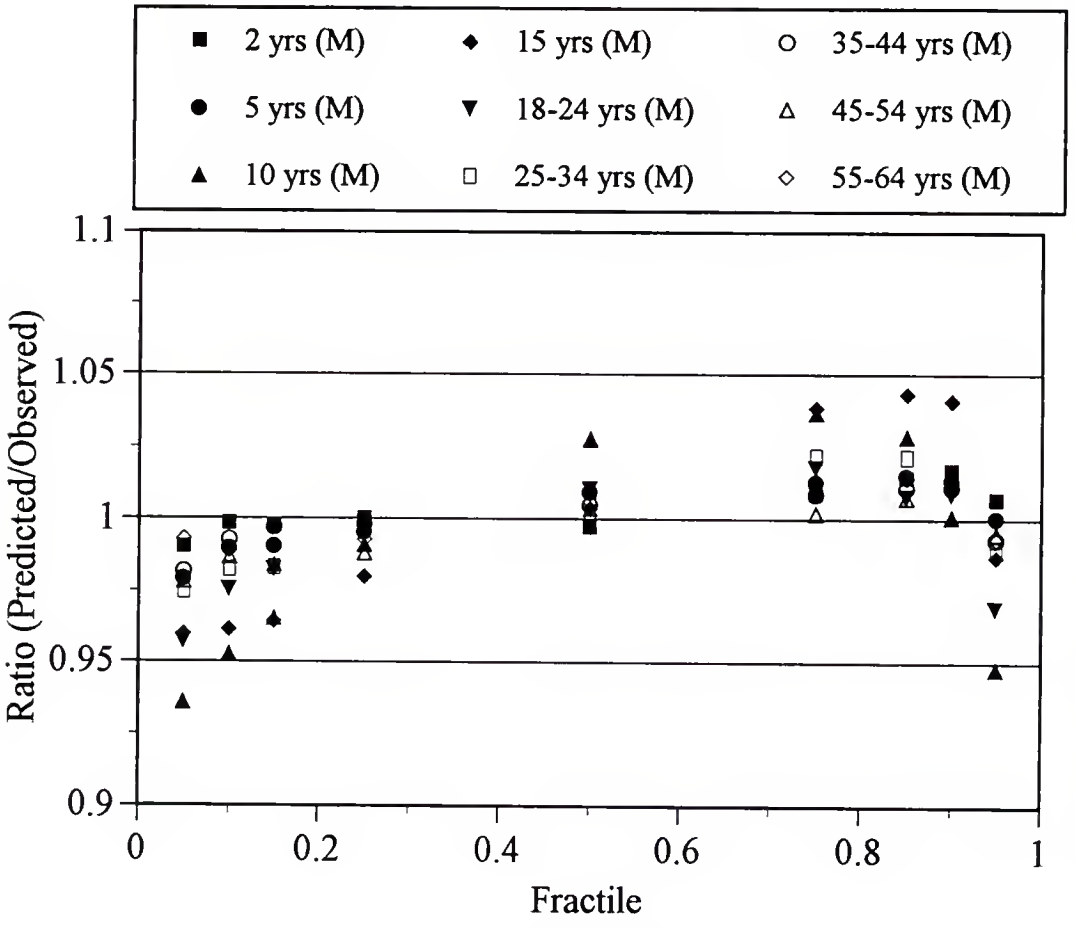

Figure 4-4. Ratio of predicted (assuming lognormal distribution) to observed fractiles in BMI for males (M) in selected age groups. Although not shown, values for females demonstrated a similar trend.

4.1.3. Airway Diameters and Lengths

Airway diameters are used to compute scaling factors in the ICRP respiratory tract deposition model. Three scaling factors are needed to adjust regional deposition efficiencies, which are based on reference-man airway dimensions, to the dimensions of sampled individuals from the population group of interest. The scaling factors, denoted by SF_t (for ET_1, ET_2, and BB regions), SF_b (for the bb region), and SF_A (for the AI region), are defined as the ratios of the appropriate airway diameters in reference man to diameters in the sampled individual. The diameters of airway generations 0, 9, and 16 are recommended by the ICRP (1994) for computing SF_t, SF_b, and SF_A, respectively. For the ICRP reference adult male, the following values have been recommended (ICRP 1994): $d_{0,ref} = 1.65$ cm, $d_{9,ref} = 0.165$ cm, and $d_{16,ref} = 0.051$ cm, where $d_{i,ref}$ denotes the diameter of the airway generation *i* in reference man and the trachea is generation zero. Therefore, with consistent units for diameters (cm):

$$SF_t = \frac{1.65}{d_0};\ SF_b = \frac{0.165}{d_9};\ SF_A = \frac{0.051}{d_{16}} \quad . \tag{4-2}$$

where d_i is the average diameter for airway generation *i* in the sampled individual (or trial).

Airway diameters and lengths are also needed to estimate the surface area and volume of the various deposition regions. The airway surface area is an important quantity for the dosimetry component of the model. The volumes of the deposition regions, $V_D(ET)$, $V_D(BB)$, and $V_D(bb)$, are needed to estimate volumetric correction terms, ϕ_i, in the deposition model (e.g., see Tables 2-1 and 2-2).

A number of studies involved determination of airway lengths and diameters in humans (e.g., Engel, 1913; Rohrer, 1925; Weibel, 1963; Horsfield and Cumming, 1968; Horsfield et al., 1971; Yeh and Schum, 1980; and Phalen et al., 1985). All of these studies involved measurements on the lungs of deceased subjects; and most of the studies only examined lungs from one or two subjects. However, the study by Phalen et al. (1985) included a larger number of subjects (n = 20) and provided analyses which can indirectly accommodate correlations between airway dimensions (length and diameter) and other respiratory parameters (e.g., anatomical dead space, tidal volume, functional residual capacity, etc.).

Measurements of airway diameters and lengths were made by Phalen et al. (1985) for the trachea, the first eight generations of the bronchial tree, and the terminal bronchioles. The measurements were made on silicon replicas of the lungs of twenty deceased subjects (males and females) aged 11 days to 21 years at time of death. The average diameters and lengths for generations 0-8 in subjects were found to correlate well with body height. Linear regression equations for diameters and lengths as functions of height were presented in that study, and residual standard errors (of the regression fit) were reported for these airway generations. Similar expressions for the diameters and lengths of generations 9-15 were derived by Phalen et al. (1985) based on interpolations of a more limited data set for generations 9, 10 and 15.

Modified versions of the equations derived by Phalen et al. (1985) were used in the current study to estimate airway dimensions as a function of body height. The ICRP (1994) adopted airway dimensions reported by James (1988) for the reference adult male

lungs. These dimensions are repeated in Table 4-4 and are averages of the values reported for the adult male by three of the studies cited above (Weibel 1963; Yeh and Schum 1980; and Phalen et al. 1985). The expressions developed by Phalen et al. (1985) were modified to be consistent with the airway dimensions recommended by the ICRP (1994, listed in Table 4-4) for reference man (Ht = 176 cm). The modified expressions are based on simple multiplication factors, equal to the ratio of the diameter (or length) for reference man (Table 4-4) to the estimate given for the diameter (or length) by the original expression evaluated at Ht = 176 cm. These factors were multiplied into the original expressions--changing the slope and intercept values. The modified expressions used in the current study to predict average airway dimensions as functions of height, are shown in Table 4-5.

The expressions for airway length and diameter in Table 4-5 are plotted in Figures 4-5 and 4-6, respectively, for body heights of 100, 150, and 200 cm. Comparison of these dimensions to Table 4-1 shows that these heights cover ages greater than about 2 years. As discussed by Phalen et al. (1985), the expressions in Table 4-5 imply that growth becomes less influential on diameters and lengths for deeper-lying airway generations.

An expression for generation 16 (i.e., first respiratory bronchiole) was not given; so data for generation 15 (the terminal bronchioles) are used to compute SF_A (where d_{15} = 0.053 cm for reference adult male). Since SF_A is a ratio (reference man: subject), the value predicted using generation 15 is not expected to differ significantly from the value predicted by generation 16.

Table 4-4. Dimensional model of the tracheobronchial tree in reference adult male as recommended in ICRP *Publication 66* (based on reference body height of 176 cm).

Airway Generation	Number	Diam.[a] (cm)	Length (cm)	SA[b] (cm^2)	Σ SA[c] (cm^2)	Vol[d] (cm^3)	Σ Vol[e] (cm^3)
0 Trachea	1	1.65	9.10	47.2	47.2	19.5	19.5
1 Main Bronchi	2	1.20	3.80	28.7	75.9	8.6	28.1
2	4	0.86	1.50	16.2	92.1	3.5	31.5
3	8	0.61	0.83	12.7	104.8	1.9	33.5
4	16	0.44	0.90	19.9	124.7	2.2	35.7
5	32	0.36	0.81	29.3	154.0	2.6	38.3
6	64	0.29	0.66	38.5	192.5	2.8	41.1
7	128	0.24	0.60	57.9	250.4	3.5	44.6
8	256	0.20	0.53	85.3	335.6	4.3	48.8
9	512	0.165	0.437	116.0	451.6	4.8	53.6
10	1024	0.135	0.362	157.0	608.6	5.3	58.9
11	2048	0.109	0.301	211.4	820.0	5.8	64.7
12	4096	0.088	0.250	283.7	1104	6.3	70.9
13	8192	0.072	0.207	383.4	1487	6.9	77.8
14	16384	0.060	0.170	527.6	2014	8.0	85.8
15 Terminal Bronchioles	32768	0.053	0.138	757.2	2772	10.1	95.9

Source: Data in columns 3 and 4 are from ICRP (1994); Data in column 2 based on dichotomously branching airways; Data in columns 4 to 7 are based on cylindrical airways.

[a] Airway diameter

[b] SA = surface area of airway generation;

[c] ΣSA = cumulative surface area for generations less than or equal to the one specified.

[d] V = volume of airway generation.

[e] ΣVol = cumulative volume of generations less than or equal to the one specified.

Table 4-5. Expressions relating airway lengths, l, and diameters, d, to body height, Ht for generations 0 - 15.

Gen.[a]	Length, l (mm)	R^2[b]	RSE[c]	Diameter, d (mm)	R^2	RSE
0[d]	l_0 =0.5084*Ht+1.5251[e]	0.9	----	d_0 =0.0902*Ht+0.6225	0.94	----
1	l_1 =0.1778*Ht+6.7070	0.90	3.0	d_1 =0.0635*Ht+0.8160	0.94	0.84
2	l_2 =0.0710*Ht+2.4966	0.77	1.7	d_2 =0.0431*Ht+0.9195	0.85	0.92
3	l_3 =0.0416*Ht+0.9739	0.86	1.0	d_3 =0.0298*Ht+0.8474	0.96	0.37
4	l_4 =0.0388*Ht+2.1724	0.56	1.6	d_4 =0.0187*Ht+1.1014	0.69	0.57
5	l_5 =0.0385*Ht+1.3193	0.77	0.91	d_5 =0.0159*Ht+0.8062	0.72	0.43
6	l_6 =0.0291*Ht+1.4808	0.50	1.1	d_6 =0.0131*Ht+0.5914	0.61	0.51
7	l_7 =0.0216*Ht+2.2056	0.44	0.74	d_7 =0.0097*Ht+0.6889	0.61	0.30
8	l_8 =0.0145*Ht+2.7514	0.18	0.86	d_8 =0.0067*Ht+0.8296	0.61	0.17
9	l_9 =0.0136*Ht+1.9685			d_9 =0.0049*Ht+0.7930		
10	l_{10} =0.0100*Ht+1.8516			d_{10} =0.0032*Ht+0.7770		
11	l_{11} =0.0078*Ht+1.6429			d_{11} =0.0017*Ht+0.7903		
12	l_{12} =0.0059*Ht+1.4671			d_{12} =0.0013*Ht+0.6531		
13	l_{13} =0.0043*Ht+1.3159			d_{13} =0.0008*Ht+0.5806		
14	l_{14} =0.0029*Ht+1.1835			d_{14} =0.0005*Ht+0.5180		
15[f]	l_{15} =0.0018*Ht+1.0670			d_{15} =0.0002*Ht+0.4917		

Source: Equations were modified from Phalen et al. (1985) to agree with ICRP dimensions given in Table 4-4. Values for R^2 and RSE are taken from Phalen et al. (not modified).

[a] Gen = airway generation.

[b] R^2 = correlation coefficient squared (coefficient of determination for regression).

[c] RSE = residual standard error (of regression equation) reported by Phalen et al. (1985).

[d] Trachea

[e] Ht (body height) is in units of centimeters for all equations.

[f] Terminal bronchioles

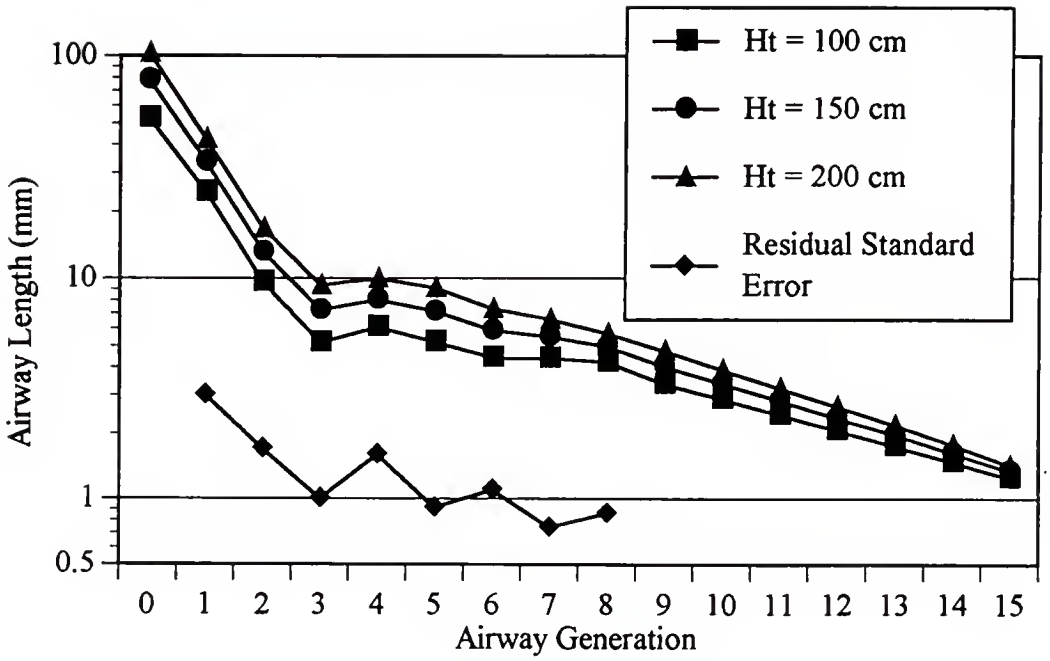

Figure 4-5. Average airway length versus airway generation at three body heights (top three curves) and residual standard errors (RSE) of the linear regression equations used to predict lengths (see Table 4-5). Lengths are correlated with body height (which depends on age and gender).

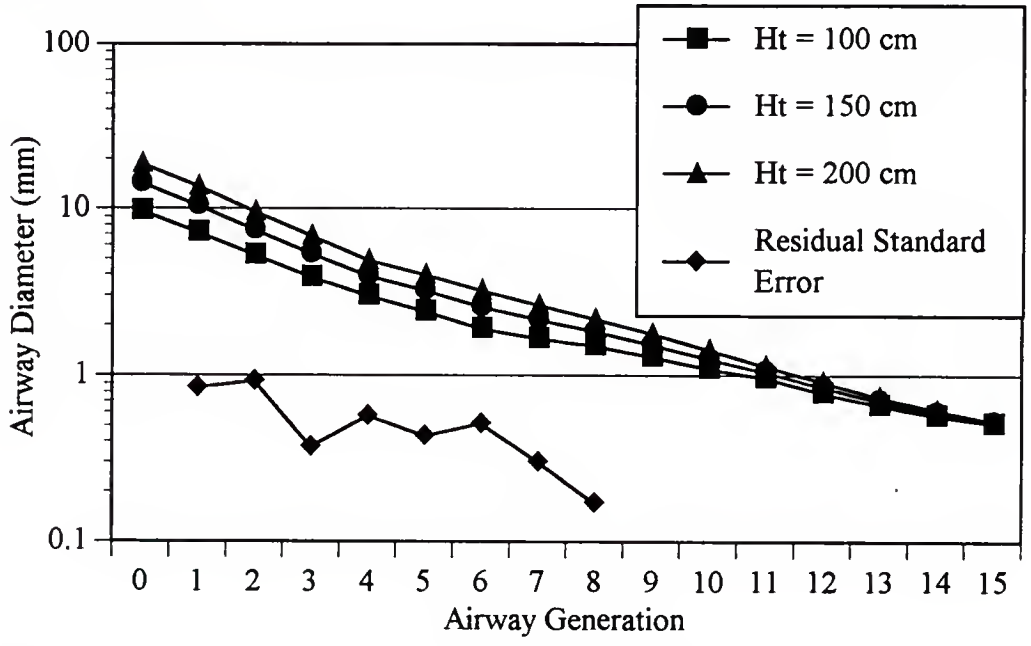

Figure 4-6. Average airway diameter versus airway generation at three body heights (top three curves) and residual standard errors (RSE) of the linear regression equations used to predict diameters (from Table 4-5). Diameters are correlated with body height (which depends on age and gender).

The residual standard errors (RSE) listed in Table 4-5 provide some information regarding the magnitude of uncertainty in the regression expressions (i.e., the variability unexplained by the correlation of airway dimensions with height). Unfortunately, the paper by Phalen et al. (1985) did not report the residual standard errors for equations describing generations 0 and 9-15. That no RSE value was given for trachea diameter is unclear since 18 tracheal measurements were made; however, the value of the coefficient of determination for the linear regression for tracheal diameter with height ($R^2 = 0.94$) implies that the RSE is likely to be small. Nevertheless, estimates of RSE values not determined were determined by extrapolation from values computed for generations 1-8. The bottom-most curves in Figures 4-5 and 4-6 are plots of the standard residual errors (RSE) vs. airway generations reported by Phalen et al. (1985).

Regression errors for diameters of generations 0, 9, and 15 were needed to quantify uncertainties in the scaling factors--SF_t, SF_b, SF_a. Based on the RSE values plotted in Figure 4-6, conservative estimates for the residual error terms appear to be 2 mm, 0.3 mm, and 0.1 mm for diameters of generations 0, 9, and 15, respectively. The value for generation 15 was determined by visually fitting an exponential curve (i.e., a straight line on a semi-log plot) through available RSE (vs. generation) data. Although inconclusive for airway generations for which the RSE is unavailable, a trend in the residual errors appears to exists. The residual standard errors appear to be roughly 10-20% of the predicted average airway diameters.

To predict airway diameters for generations 0, 9, and 15 (needed to compute the deposition scaling factors: SF_t, SF_b, SF_A) and to account for uncertainties/variabilities, the following expressions were employed in this study:

$$d_0 = (d_{0,reg,Ht})(1 + E_{d0});\ \ d_9 = (d_{9,reg,Ht})(1 + E_{d9});\ d_{15} = (d_{15,reg,Ht})(1 + E_{d15}). \qquad (4\text{-}3)$$

In this expression, $d_{i,reg,Ht}$ is the diameter predicted for generation *i* using the appropriate *regression* expression in Table 4-5 and depends on the sampled value for body height, *Ht*. The term E_{di} is a random error term used to introduce uncertainty into the regression prediction for generation *i*. Lacking more complete information, the random error terms were assumed to be normally distributed with mean values of zero and standard deviations given as 0.10, 0.10, and 0.20 for generations 0, 9, 15, respectively. These values of standard deviation introduce errors of 10%, 10%, and 20% to the regression model predictions for diameters of generations 0, 9, and 15, respectively. The error term is increased for generation 15 since it is based on extrapolation of the RSE data (e.g., plotted as lower curve in Figure 4-6) far from reported values.

As an example of how Equation 4-3 was used in the current study, assume that a Latin hypercube sample of size *n* is generated for all random variables in the model. For a single trial (i.e., input vector, or *m*-tuple), values are specified for body height, Ht, and for the random error terms E_{d0}, E_{d9}, and E_{d15}. For this trial, the sampled value of body height is used along with the sampled values of E_{di} to determine values of d_i. These diameters are then used to solve the model for that specific trial (and so forth with other trials). The standard deviations of the random error terms, E_{di}, can be updated should better information becomes available.

4.1.4. Anatomical Dead Space

The anatomical dead space, V_D, is the total internal volume of the conducting airways (i.e., the mouth, nasal vestibules and sinuses, pharynx, larynx, trachea, bronchi and non-respiratory bronchioles). This volume is termed *dead space* because air in it does not participate significantly in gas exchange processes with the blood. From the perspective of particle deposition, V_D is useful in estimating the fractional volume of inhaled aerosols which reach given lung regions (i.e., factors ϕ_j in Tables 2-2 and 2-3); therefore, the dead space influences how much material is deposited in various lung regions.

Anatomical dead space is a measurable quantity which a number of studies have investigated (e.g., see Altman and Dittmer, 1971, pp. 64-69, for a compilation). Two studies are especially useful for the present study due to the number of subjects and range of ages examined and to the regressions of dead space on height. Hart et al. (1963) measured dead space in 73 normal persons (42 males, 31 females) with ages ranging from 4 to 42 years. Wood et al. (1971) measured dead space in 46 healthy persons (19 adults, 27 children).

Unfortunately data from Hart et al. and Wood et al. were available only in a graphical format. Plots of the data were scanned into a computer and coordinates (Ht, V_D) were reconstructed with an appropriate computer software package. The reconstructed data from the two studies were combined and reanalyzed using an exponential regression model to predict the resting-level dead space as a function of body height. Based on the method of least squares the following expression was obtained:

$$V_D\,(\text{ml}) = 8.72 \cdot e^{(1.62 \times 10^{-2}\,\text{Ht})} \quad . \tag{4-4}$$

This expression has a coefficient of determination of $R^2 = 0.84$. In other words, about 84% of the variance in V_D is explained by the regression on body height.

The remaining variance in dead space (unexplained by Equation 4-4) can be accommodated by introducing a random error term, denoted here as E_{VD}, into the model as follows:

$$V_D = 8.72 \cdot e^{(1.62 \times 10^{-2}\,\text{Ht})} \cdot E_{VD} \tag{4-5}$$

The random error term accounts for statistical fluctuations due both to experimental uncertainties and to biological variability at a given height. In this study the random error term, E_{VD}, was assigned a lognormal distribution [i.e., $\ln(E_{VD})$ was assumed to be normally distributed] with a geometric mean value of one and geometric standard deviation (GSD) estimated as

$$\text{GSD}\,(E_{VD}) = \exp\left[\sqrt{\frac{1}{n}\sum_{i=1}^{n}\left[\ln(V_{D,\text{obs},i}) - \ln(V_{D,\text{pred},\text{Ht}_i})\right]^2}\right] = \exp(0.160) = 1.17 \tag{4-6}$$

where $V_{D,\text{obs},i}$ refers to the i^{th} observed value (from the combined data set) for dead space and $V_{D,\text{pred},\text{Ht}i}$ refers to the value of V_D predicted for observed height Ht_i using Eq. 4-4.

To provide some justification that E_{VD} follows a lognormal distribution, Figure 4-7 compares the cumulative distribution for the observed residual logarithms of dead space [i.e., $\ln(V_{D,\text{obs},i}) - \ln(V_{D,\text{pred},\text{Ht}i})$, based on observed values and predictions from Eq. 4-4] to the cumulative distribution predicted by assuming a normal distribution for $\ln(E_{VD})$ with

mean value zero and standard deviation equal to 0.16 [i.e. ln(GSD)]. The two curves generally agree, providing some degree of justification for assigning E_{VD} a lognormal distribution with parameters discussed above.

The data reconstructed from the two studies cited above are plotted along with Equation 4-4 in Figure 4-8. Dotted lines represent the 95% confidence bounds of the regression prediction, based on the assumed lognormal distribution for E_{VD}. All but about 5 (out of a total of 119, or ~4%) of the data points lie within the 95% confidence bounds; so the model is acceptable. In order to generate values of V_D for this study, Ht and E_{VD} must be sampled from their respective distributions and substituted into Equation 4-5.

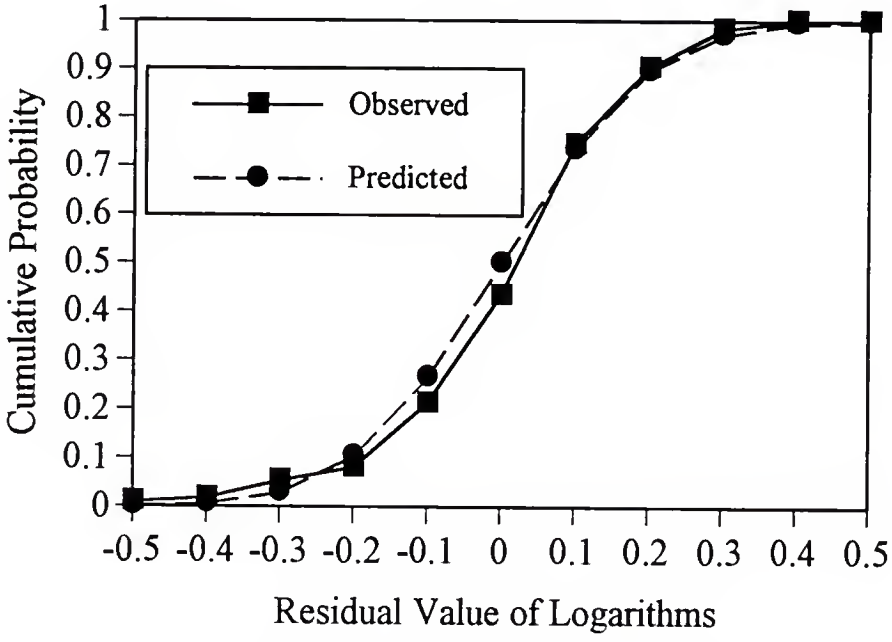

Figure 4-7. Comparison of the cumulative probability for the observed residuals of $\ln(V_D)$ and the cumulative probability for E_{VD} (assuming E_{VD} is lognormally distributed with geometric mean of 1.0 and GSD of 1.17).

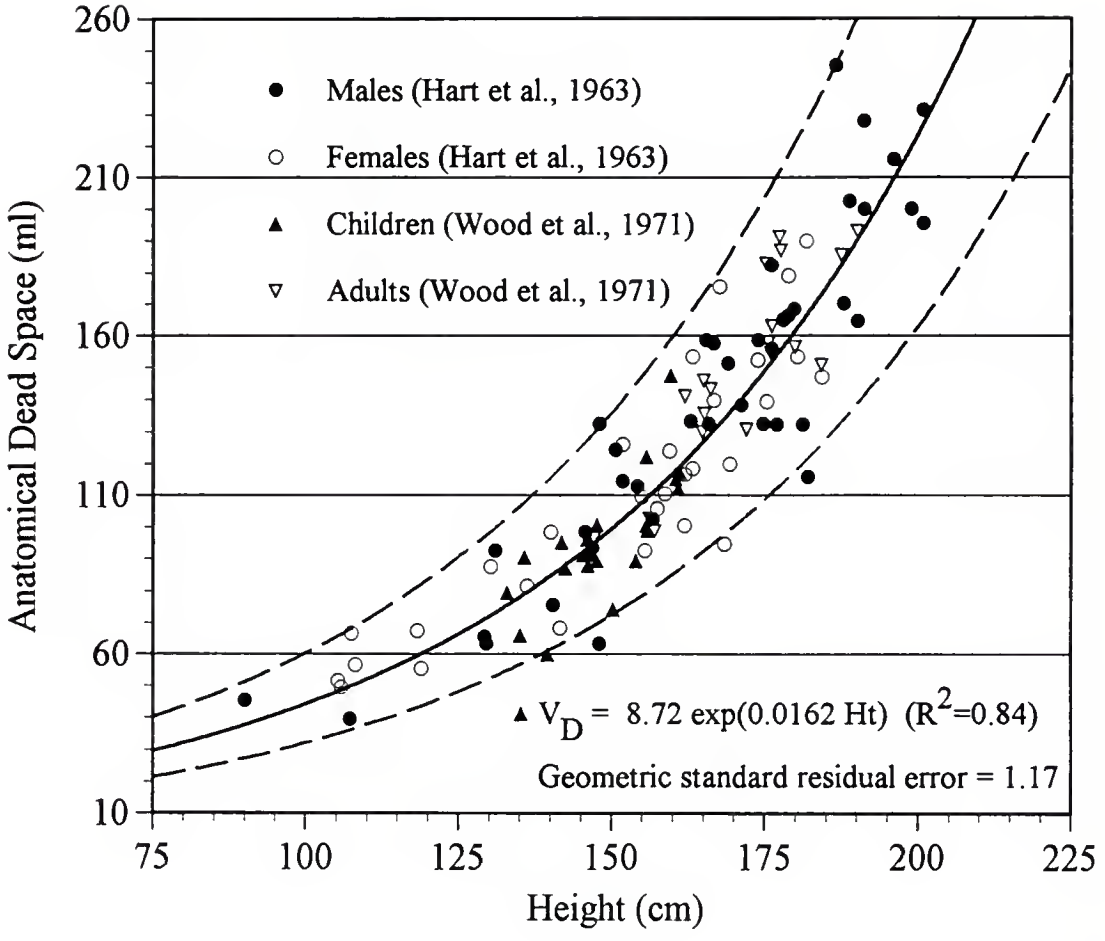

Figure 4-8. Anatomical dead space as a function of body height. Data are based on plots from Hart et al. (1963) and Wood et al. (1971). Exponential regression curve has been fit to data based on least squares method. Dotted lines represent 95% confidence bounds predicted by assuming the log residuals of V_d are normally distributed with mean of zero and standard deviation of 0.16 (discussed in text). All but about 5 of the data points fall within these bounds.

4.1.5. Regional Volumes of the Respiratory Tract

Little experimental information exists for dividing the total anatomical dead space into the regional volumes required by the deposition model (Tables 2-1 and 2-2), $V_D(ET)$, $V_D(BB)$, and $V_D(bb)$. All studies located relied on assumed values for the volume of extrathoracic airways, $V_D(ET)$. Landahl (1950) suggested a value of 40 ml for the volume of the mouth and pharynx for a reference adult; Yeh and Shum (1980) assumed a volume of 50 ml for the nasopharyngeal region; and Schum et al. (1991) assumed a cumulative volume of 50 ml for the adult mouth, oropharynx, and larynx. Only Schum et al. (1991) have addressed the volume of the extrathoracic airways with respect to ages below 18 years. In their work $V_D(ET)$ was assumed to scale in linear proportion to the ratio of the tracheal cross-sectional area. Lacking better information, this approach was adopted in the present work. Based on an adult reference value of $V_D(ET) = 50\ cm^3$ and reference tracheal diameter of $d_0 = 1.65$ cm (Table 4-4), the following expression results for estimating $V_D(ET)$ as a function of height:

$$V_D(ET) = \frac{50\ cm^3}{(1.65\ cm)^2} d_0^2 = 18.37\ d_0^2 \qquad (4\text{-}7)$$

where d_0 is in units of cm. Variability in $V_D(ET)$ is accommodated by uncertainties in d_0 as discussed above (i.e., see Eq. 4-3 and accompanying discussion).

The volumes of the bronchial (BB) and bronchiolar regions (bb) have not been measured directly. However, based on total dead space and airway diameter measurements, estimates can be made regarding the partition of the anatomical dead space

between these two regions and the ET region. In a study by Yu and Diu (1982), a number of lung models based on independent measurements of airway dimensions were compared. The models compared were from Weibel (1963), Olson et al. (1970), Hansen and Ampaya (1975), and Yeh and Schum (1980). Based on data reported in Yu and Diu (1982, Tables II, III, IV, and V), the ratio of the volume of the bb region (airway generations 9 to 15) to the volume of the BB region (airway generations 0 to 8), i.e., $V_D(bb):V_D(BB)$, equals 1.20 for the model of Weibel, 1.02 for the model of Olson et al., 1.02 for the model of Hansen and Ampaya), and 1.005 (model of Yeh and Schum). An additional value of 0.77 for the ratio is derived from the reference model described in Phalen et al. (1985). The average of these values is 1.003. In conclusion, these ratios help justify an assumption that the volume of the bronchial (BB) region is equal to the volume of the bronchiolar (bb) region. Therefore, since $V_D = V_D(ET) + V_D(BB) + V_D(bb)$, the following expression was adopted in the present study to predict $V_D(BB)$ and $V_D(bb)$:

$$V_D(BB) = V_D(bb) = 0.5 * [V_D - V_D(ET)]. \quad (4\text{-}8)$$

Variabilities in the regional volumes are accommodated through variabilities in V_D and $V_D(ET)$ as discussed above.

It is important to note the agreement between the regression expressions adopted above for airway dimensions (Table 4-5) and the one adopted for total anatomical dead space (Eq. 4-4). The studies cited above for airway dimensions are independent of the studies cited for total dead space. If the equations in Table 4-5 are used with this body height and airways are assumed to be right cylinders, the volume $V_D(BB)+V_D(bb)$ can be computed as the total cumulative volume of airway generations 0 to 15 and equals about

96 cm^3. If $V_D(ET)$ is equal to 50 cm^3 (as discussed above) then a total dead space of 96+50 = 146 cm^3 is derived for a reference (or typical) adult male. This value agrees well with the value of 150 cm^3 which can be computed for Ht = 176 cm with the empirical expression given in Eq. 4-4.

4.1.6. Functional Residual Capacity

The functional residual capacity, FRC, is the volume of gas in the respiratory tract at the end of a normal expiration. The FRC can be measured by gas dilution techniques (e.g., helium dilution) or by body plethysmography. In addition to age, gender, and body height, functional residual capacity has been found to vary slightly with exertion level, posture, and body fat content, e.g., see Altman and Dittmer (1971) for a compilation of references. The functional residual capacity is used in the deposition model (i.e., Tables 2-1 and 2-2) to correct for increases in the (resting-level) anatomical dead space, V_D, during increased tidal breathing. Data compiled by Altman and Dittmer (1971, p. 68) indicate an increase of about 30-50% in dead space for high- versus normal-level breathing.

Based on measured data, linear regression models have been proposed (Quanjer et al., 1983) to predict the mean FRC as functions of body height and age for adult men and women. For children, both linear and power function models have been proposed (e.g., Helleisen et al., 1958; Gaultier et al., 1979; Taussig et al., 1977; Zapletal et. al, 1987). The residual standard errors (RSE) of the regression models provide an estimate of the uncertainty and variability at a given height (and age) for a specified population class. The equations and error terms listed in Table 4-6 were adopted for use in the present study.

Similar equations with slightly different fitting parameters have been presented by Cotes (1979) and by Altman and Dittmer (1971). Results of these references generally agree with the expressions presented in Table 4-6.

Table 4-6. Regression equations and related information for functional residual capacity.

Population Class Age and Gender	Notes/comments	Regression Equation Mean FRC (ml)	R^2	RSE (ml)
Infants: 0-3 years[a] (36 boys, 34 girls)	French infants; $p < 0.001$; He dilution technique	FRC = 6.57*Ht - 246.9	0.81	27.8
Infants: 0-3 years[b] (19 boys, 15 girls)	U.S. infants; $p < 0.001$; He dilution technique	FRC = 7.740*Ht - 347.7	0.80	44.9
Children: 3-6 years[b] (51 boys, 36 girls)	U.S. children; He dilution technique	FRC = 12.76*Ht - 760.9	0.48	94.6
Children: 6-18 years[c] (70 boys, 74 girls)	He dilution technique.	$FRC = 1.29x10^{-3}*Ht^{2.82}$	0.81	1.14[e]
Adult Males[d]	Based on compilation of many studies representing many nationalities.	FRC=23.48*Ht + 9.0*A - 1093	0.26	600
Adult Females[d]	Same as "Adult Males."	FRC=22.45*Ht + 1.0*A - 1003	0.35	500

Sources: [a]Gaultier et al. (1979), [b]Taussig et al. (1977), [c]Zapletal et al. (1987), [d]Quanjer et al. (1983).
Notes: All volumes are at body temperature and saturated with water vapor, BTPS.
Ht = height (cm); A = age (years); RSE = residual standard error.
[e] This value corresponds to the geometric residual standard error (no units).

Given the information presented in Table 4-6, the following expressions were used as appropriate to sample values of FRC for the *n* trials:

$$FRC = FRC_{reg} + E_{FRC} \quad (4\text{-}9)$$

or

$$FRC = FRC_{reg} * E_{FRC} \quad (4\text{-}10)$$

where FRC_{reg} refers to the appropriate regression equation in Table 4-6 and is a function of height and possibly age; E_{FRC} is a residual error term added to or multiplied into the

regression expression to introduce variability and uncertainty not explained by the regression expression. Equation 4-10 was used when FRC_{reg} is described by a power function; otherwise Equation 4-9 was used. When Eq. 4-9 was used, the error term E_{FRC} was assumed to follow a normal distribution with mean of zero and standard deviation given by the appropriate RSE value in Table 4-6. When Eq. 4-10 was used, E_{FRC} was assumed to be lognormally distributed with geometric mean of one and geometric standard deviation given by the appropriate RSE value in Table 4-6.

For adults and 3 to 6 year-old children, the regression expressions presented in Table 4-6 account for little of the variability in FRC. For example, only 26% and 35% of the variance in FRC for adult males and females, respectively, are explained by the regression model in Table 4-6. This observation is in sharp contrast to equations for other age groups (0-3 years and 6-18 years), where the regression appears relatively successful in explaining much of the variance.

4.1.7. Vital Capacity

Vital capacity, VC, is the volume of air inhaled from a maximal expiratory level to a maximal inspiratory level (inspiratory VC) or the volume exhaled from maximal inspiratory level to maximal expiratory level (expiratory VC), depending on measurement techniques used. Vital capacity is generally measured with a spirometer. Although not a direct input parameter to the deposition model, the vital capacity (one half of VC) has been suggested (Hey et al., 1966; discussed in section 4.1.9) as an upper limit to the tidal volume at high breathing levels. Quanjer et al. (1983) compiled results of a number of

experimental studies of VC for adult males and females and--based on this compilation--recommended standard regression expressions for VC. Zapletal et al. (1987) measured VC in children and adolescents with ages ranging from 6 to 18 years. For 0 to 3 year-old children, the crying vital capacity (CVC) has been measured by Gaultier et al. (1979) using an adapted mouth piece connected to a spirograph. The crying vital capacity refers to the amount of air breathed in or out while an infant is crying. In all of the cited studies, data were summarized with regression equations giving VC as functions of height, Ht, and in some cases height and age. These equations, accompanied by their residual standard error (RSE) and R^2 values, are listed in Table 4-7. The R^2 values indicate that the regression equations explain the variability in VC reasonably well, accounting for over 80% of the variability in all cases.

Table 4-7. Regression Equations and Related Information for Vital Capacity.

Population Class	Notes/comments	Regression Equation, VC(ml)	R^2	RSE[d] (ml)
Infants: 0-3yrs[a] (45 subjects)	Crying vital capacity measured.	$CVC = 12.28*Ht - 539$	0.92	42.8
Children: 6-18 yrs[b] (86 boys, 87 girls)		$VC = 3.38x10^{-3}*Ht^{2.72}$	0.88	1.10[e]
Adult Males[c]	Average of many studies.	$VC = 61.0*Ht - 28.0*A - 4650$	0.88	560
Adult Females[c]	" "	$VC = 46.6*Ht - 24.0*A - 3280$	0.81	420

Sources: [a] Gaultier et al. (1979), [b]Zapletal et al. (1987), [c] Quanjer et al. (1983).
Notes: All volumes are at BTPS; Ht = height (cm); A = age (years).
[d] RSE = Standard error of the estimate (residual error of the regression).
[e] This value corresponds to the geometric residual standard deviation (no units).

Given the information presented in Table 4-7, the following expressions were used, as appropriate, to sample values of VC for the *n* trials:

$$VC = VC_{reg} + E_{VC} \tag{4-11}$$

or $VC = VC_{reg} * E_{VC}$ (4-12)

where VC_{reg} refers to the appropriate regression equation in Table 4-7 and is a function of height and possibly age; E_{VC} is a residual error term added to or multiplied into the regression expression to introduce variability and uncertainty not explained by the regression expression. Equation 4-12 was used when VC_{reg} is a power function; otherwise Equation 4-11 was used. For Eq. 4-11, the error term E_{VC} was assumed to follow a normal distribution with mean value of zero and standard deviation equal to the RSE reported in Table 4-7. For Eq. 4-12, E_{VC} was assumed to be lognormally distributed with geometric mean of one and geometric standard deviation estimated by the RSE value reported in Table 4-7. Furthermore, the results of Zapletal et al. (1987) were assumed to apply to 4- and 5-year olds since data are lacking for this age.

4.1.8. Ventilation Rates and Volumetric Flow Rate

The ventilation rate, V_E, is defined as the volume of air expired from the respiratory tract per minute (or minute ventilation). The ventilation rate is equal to the product of the tidal volume, V_T (volume of air expired during a breath), and the respiratory rate (number of breaths per minute). Coupled with the airborne concentration of a contaminant, the ventilation rate determines the potential intake of an inhaled substance. The ventilation rate is also used to estimate the average volumetric flow rate, V_F, of air through the airways during inhalation and exhalation. This flow rate is an important parameter in the deposition model and influences impaction efficiencies and

residence times of aerosol particles in various airway regions. The deposition model (see Tables 2-1 and 2-2) requires the average flow rates during inhalation and exhalation.

Although measured at ambient temperature and pressure (ATP), the ventilation rate is defined and reported at body temperature and pressure, saturated (BTPS) with water vapor. Volumes at BTPS must be corrected to ATP to determine the volume of ambient air *inhaled*. The volume of the inhaled, rather than exhaled, air is important to assess the activity intake. Based on the ideal gas law, volumes under these two conditions are linked by the following equation (Cotes, 1979):

$$\frac{V_{ATP}}{V_{BTPS}} = \left(\frac{P'_B - 47\,\text{mmHg}}{P_B - P_{H_2O}(t)} \right) * \left(\frac{273 + t}{273 + 37} \right) \qquad (4\text{-}13)$$

where V is the gas volume under conditions specified by the subscript; P_B denotes the barometric pressure at ATP (in mm Hg); P'_B denotes the barometric pressure for the volume expressed at BTPS; t denotes the ambient temperature in °C (body temperature is 37 °C); and $P_{H20}(t)$ is the water vapor pressure at temperature t (P_{H2O} = 47 mmHg at 37 °C). The vapor pressure for water (mmHg) can be estimated from the following empirical formula for temperatures between 0 and 60 °C (Hinds, 1982):

$$\log_{10} P_{H_2O}(t) = 8.11 - \frac{1750}{(t+235)} \; . \qquad (4\text{-}14)$$

Most of the studies examined in this research do not specify the barometric pressure at which ventilation data are reported; so the assumption is made that volumes are reported at standard pressure (i.e., P'_B = 760 mmHg is used in Eq. 4-13).

Using Eqs. (4-13) and (4-14), the ratio of inhaled volumes (ATP) to exhaled volumes (at BTPS) was computed as a function of (ambient) temperature and is plotted in Figure 4-9 for some ambient barometric pressures. A pressure of 0.8 atm (608 mmHg) corresponds to a standard elevation of about 2000 m (6560 ft) above sea level; a pressure of 0.9 atm (684 mmHg) corresponds to an elevation of about 1000 m (3280 ft). For an ambient temperature of 20 °C (68 °F) and pressure of 1 atm, Figure 4-9 shows that volumes at ATP are 10% less than volumes at BTPS. Thus, use of ventilation rates at BTPS without volume corrections would slightly over-predict the intake of an airborne substance by approximately 10% at these conditions. Eqs. (4-13) and (4-14) were used in this work to determine ventilation rate and radionuclide intake.

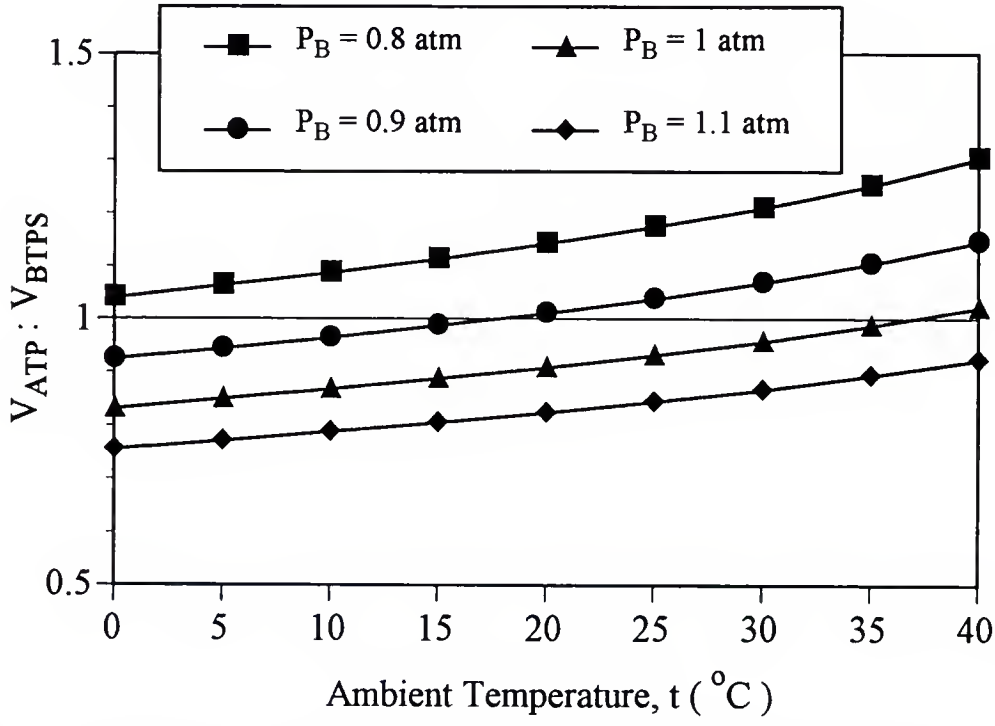

Figure 4-9. Relationship between volumes at ambient temperature and pressure to volumes reported at body temperature and pressure (BTPS). A collection pressure of 760 mmHg (1 atm) has been assumed.

As mentioned, the ventilation rate is used to approximate an average volumetric flow rate, V_F, of air moving into and out of the respiratory tract. This flow rate is needed to determine regional deposition fractions. Assuming that the instantaneous flow rate follows a sinusoidal pattern (e.g., as depicted by Cotes, 1979, p. 74), the root mean square flow rate, denoted $V_{F,rms}$, can be derived as:

$$V_{F,rms}(mL/s) = \left[\frac{1000\ mL \cdot min}{60\ L \cdot s}\right] * \pi \frac{V_E(L/min)}{\sqrt{2}} = \frac{1000}{60} * 2.22 * V_E \quad . \qquad (4\text{-}15)$$

where conditions of BTPS are retained to represent volumes associated with the flow rate.

An assumption made in deriving Equation 4-15 was that the inpsiratory time, T_I, is equal to the expiratory time, T_E; or T_I/T_{tot} equals 0.5, where $T_{tot} = T_I + T_E$. Several studies have examined breathing patterns regarding inspiratory, expiratory, and total breathing cycle times (Kay et al., 1975; Clark et al., 1983; Lind and Hesser, 1984; Poon, 1989; Younes, 1991; Caretti et al., 1992). Poon (1989) found values for T_I/T_{tot} ranging from 0.4 to 0.6; however, no trend could be discerned from the data plotted. Lind and Hesser (1984) reported average values of T_I/T_{tot} ranging from about 0.35 to 0.42 for eight male subjects at various exercise levels; as the exercise level increased from rest (0.38 average at rest), the average ratio decreased initially, reached a minimum (of 0.35), and then increased to 0.42. Caretti et al. (1992) examined 14 adult males during cycling and treadmill exercises and found the average value of T_I/T_{tot} to increase from approximately 0.40 to 0.53 in cycling and from about 0.38 to 0.53 during treadmill exercise as the ventilation rate increased. Younes (1991) listed typical values of T_I/T_{tot} during exercise that ranged from 0.42 (at power output of 50 Watts) to 0.49 (at 250 Watts). These

studies indicate that inspiration time is slightly shorter than expiration time at resting levels and that these times become approximately equal during increased exercise. This level of detail in the breathing pattern is acknowledged here but not incorporated into the present work. In preliminary investigations of the deposition model in this work, indications were that differences between inspiratory and expiratory times at the levels discussed above did not significantly affect deposition predictions.

For intake assessment activities V_E values for different ages and gender have traditionally been estimated as the product of the tidal volume and respiratory frequency (e.g., ICRP, 1975; Roy and Courtay, 1991), where these two factors are selected for broad physical exertion levels (such as resting, light exertion,..., etc.). While useful for estimating typical or reference ventilation rates, this approach leads to difficulties when trying to accommodate uncertainties and variabilities in ventilation rates. One problem is that tidal volume and respiratory frequency are not statistically independent. Furthermore, this traditional approach provides no simple means to account for correlations between ventilation rates and various lung volumes (including airway dimensions). A solution to this problem is possible if an approach based on energy expenditure and oxygen consumption is utilized to determine ventilation rates. Among other things, this approach accounts for variabilities in body weight, age, and exertion level. Furthermore, by using this approach, correlations between many deposition model parameters--such as airway diameters, dead space, functional residual capacity, and vital capacity--are indirectly accommodated since these parameters have also been related to body size, age, and gender. In this study ventilation rate is assumed to be linearly proportional to the oxygen

consumption rate; and the oxygen consumption rate is assumed to be linearly proportional to the metabolic rate. The following discussion provides some support for this assumption.

A fundamental equation, based on steady-state mass balance considerations, for relating the alveolar ventilation rate V_A (the amount of air expired from the alveolar region of the respiratory tract per minute at BTPS) to other ventilatory factors is the following:

$$V_A = f * (V_T - V_D) = \frac{V_{CO_2}}{P_{ACO_2}} * 863 \qquad (4\text{-}16)$$

where f is the respiratory frequency (breaths per minute); V_T is the tidal volume (expressed in liters at BTPS); V_D is the dead space (expressed in liters at BTPS); V_{CO2} is the CO_2 production rate (at standard temperature and pressure, dry air, or STPD); and P_{ACO2} is the partial pressure (mmHg) of CO_2 in the alveolar region of the lungs. The constant term, 863, accounts for the partial pressure of gases in the alveolar air (= 760 - 47 mmHg) and a conversion factor for volumes from STPD to BTPS conditions (= 1.21). The carbon dioxide production rate, V_{CO2}, is related to the oxygen consumption rate, V_{O2}, by the following ratio, defined as the respiratory exchange ratio: $R_e = V_{CO2}/V_{O2}$. The value of R_e is typically around 0.8 since less CO_2 is added than O_2 removed from alveolar air during gas exchange. Since $V_E = f * V_T$ and $R_e = V_{CO2}/V_{O2}$, the following expression can be derived from Equation 4-16 to relate V_E to the oxygen consumption rate (among other factors):

$$V_E = \left[\frac{863 * R_e}{P_{ACO_2}(1 - V_D/V_T)}\right] * V_{O2} \quad (4\text{-}17)$$

Based on mass balance considerations, this expression indicates that the ventilation rate is proportional to the oxygen consumption rate; however, since other ventilatory factors are present in the expression, a *linear* proportionality may not be strictly true. Values of R_e and P_{ACO2} are relatively constant and independent of age, gender, and exertion level (typical values are 0.8 and 40 mmHg, respectively). The ratio V_D/V_T is influenced by the exertion level according to data compiled by Altman and Dittmer (1971, p. 65). As the breathing level increases, V_D/V_T generally decreases; therefore, in theory, V_E and V_{O2} are not strictly linearly related.

However, empirical plots of V_E versus V_{O2} for adults show a linear relationship up to an oxygen uptake rate of about 2.5 l/min (e.g., Layton, 1993, Figure 2; Guyton, 1991, Figure 41-9; Powers and Howley, 1990, P. 231; Brooks and Fahey, 1984, p. 257; Grodins, 1950). At V_{O2} values higher than about 2.5 l/min (for adults), the slope of V_E versus V_{O2} increases slightly with increasing values of V_{O2}. Layton (1993) recently combined and reanalyzed data from several studies reporting V_E and V_{O2} and found that the following regression equation provided a good fit to data:

$$V_E = 27(V_{O2})^{0.99}, \quad (4\text{-}18)$$

with $R^2 = 0.96$ and V_{O2} ranging from about 0.25 to 6.0 L/min (STPD). The coefficient of determination (R^2) implies that 96% of the total variance in the measured ventilation values is explained by the above regression on V_{O2}. This empirical result supports an assumption that changes in V_E are linear with respect to changes in V_{O2} (at least up to a

level). An empirical quantity known as the ventilatory equivalent ratio, VQ, relates Equations 4-17 and 4-18. The ventilatory equivalent ratio, VQ, is defined as the ratio of V_E (in L-air/min at BTPS) to V_{O2} (in L-O_2/min at STPD). The ventilatory equivalent ratio has a typical value of 27 as indicated by Equation 4-18 and is relatively constant during exercise.

Based on discussions above and on suggestions by Layton (1993), the following model was adopted in this study to sample ventilation rates for members of population groups (in specified physical exertion levels):

$$V_E = VQ * V_{O2} \quad . \tag{4-19}$$

Variability in VQ is discussed in a following subsection. At least two approaches exist for estimating variabilities (and uncertainties) in oxygen consumption rates for population groups (e.g., 5 year-old males) exposed at a specified exertion level (e.g., resting). One approach is to estimate values of V_{O2} at different exertion levels based on a multiplier of the resting, or basal, V_{O2}; the other approach is to estimate values based on a multiplier of the maximal oxygen uptake rates, or V_{O2} max. In this study the former approach was adopted (as suggested by Layton, 1993), and the oxygen consumption rate was estimated from the following expression:

$$V_{O2} = (C * BMR * H_{oxy}) * B_{mult} \tag{4-20}$$

where the term in parentheses represents the basal oxygen consumption rate; C is a constant factor to account for conversion of units; BMR denotes the basal metabolic rate; and H_{oxy} is an oxygen consumption factor representing the amount of oxygen (liters)

required to produce 1 kJ of energy by metabolizing various energy sources (fats, proteins, and carbohydrates) in the body. The term B_{mult} is the basal multiplier which depends on the level of exertion. Units for these factors are as follows: BMR (MJ/day), H_{oxy} (liters O_2 per kJ); B_{mult} (no units). Based on these units, C is equal to 0.694 (kJ-day)/(MJ-min). The factors BMR, B_{mult}, H_{oxy} are discussed in more detail in the following subsections.

4.1.8.1. Ventilatory equivalent ratio, VQ

In an attempt to infer a distribution for VQ, Layton (1993) combined and reanalyzed data from a number of earlier studies. From 159 measurements in 75 subjects (most were males; many were athletes), he found that a lognormal distribution having a geometric mean of 27 and a geometric standard deviation (GSD) of 1.18 provided a good fit to the data. As an independent source of verification, Layton (1993) cited typical values of VQ determined by other authors; for example, Grodins (1950) in a summary of earlier work on ventilation and oxygen consumption examined the relationship between V_E and VO_2 (based on 611 respiratory measurements on 86 subjects). The slope of the linear portion of the curve corresponded to a typical value of VQ = 25. In a literature review conducted for the current study, two additional studies were found which examined VQ. Matheson and Gray (1950) examined 100 healthy, young male medical students on two different days. For the first day, a geometric mean and GSD of 27 and 1.17, respectively, can be estimated for VQ from the data presented. For the second day, these values were 25 and 1.13, respectively. Filley et al. (1954) examined 34 normal males (23 to 60 years of age) during moderately severe treadmill exercise; a geometric mean of 27 and GSD of

1.15 were deduced for VQ from the data presented. Averaging the results from Layton (1993), Matheson and Gray (1950), and Filley et al. (1954) yields an average geometric mean of 26.5 and GSD of 1.16. These parameters were adopted to model variabilities in VQ in the current study. With respect to variability, the upper and lower 95% confidence bounds of VQ can be estimated as 20 and 35, respectively (corresponding to a relative difference of about 75%).

Most of the above studies were based on adult males; however, values of VQ for other females and for children are not expected to differ greatly. As cited by Layton (1993), Stahlman and Meece (1957) studied 44 newborns and the resulting geometric mean value for VQ was 28.1 with a GSD of 1.3. Cook et al. (1955) studied 17 newborns and found a geometric mean of 24.6 with a GSD of 1.23. Lacking additional data, the lognormal distribution assigned above (geometric mean of 26.5 and GSD of 1.16) was used in this study for all population classes. Additional data are needed to characterize VQ for other ages.

4.1.8.2. Basal metabolic rate, BMR

The basal metabolic rate, BMR, is the rate at which energy must be consumed by the human body to sustain the most basic activities of life. Although not technically correct, the resting metabolic rate has been used to approximate the basal metabolic rate in many studies. Energy consumed in the basal state by the liver, brain, heart, and kidneys contribute 26.4%, 18.3%, 9.2%, and 7.2%, respectively to the BMR (Lentner, 1981). Skeletal muscle contributes another 25.6% for a total of 86.7%. The additional 13.3% of

energy consumption is associated with other organs. The basal metabolism is a function of a number of factors including gender, height, mass, body composition, age, and hormonal balance.

Standard values of BMR have been recommended per age and gender by a number of authors (e.g., DuBois, 1936; Fleisch, 1951; Altman and Dittmer, 1968, p. 345; and Schofield, 1985). Schofield (1985) reviewed past studies and provided improved estimates for the average BMR by developing linear regressions of BMR on body weight and age. The equations were derived by least squares regression using over 7000 data points classified by age and gender. These regression equations are listed in Table 4-8. The residual standard errors (RSE) reported in that table are measures of the uncertainty in BMR for given body weight, age and gender. Use of the linear regression model assumes that the residual errors are normally distributed about a mean of zero and standard deviation approximated by the RSE. Using histograms and probability plots, Schofield (1985) examined the residual errors for each age group; the results supported the assumption that the residuals were normally distributed. Values of R^2 shown in Table 4-8 indicate that between about 40% and 90% of the variance in BMR is explained by the regression on body weight for given age/gender groups.

For the present study, the BMR (for specified age and gender class) was sampled by means of the following expression:

$$BMR = BMR_{reg} + E_{BMR} \qquad (4\text{-}21)$$

where BMR_{reg} represents the appropriate regression equation from Table 4-8 and E_{BMR} is a residual error term introduced to accommodate variability in BMR not explained by the regression equation. The error term E_{BMR} was assigned a normal distribution with mean value of zero and standard deviation equal to the appropriate residual standard error (RSE) value given in Table 4-8. Body weight, needed for computation of BMR, was determined from sampled values for body height and the body mass index as outlined earlier in sections 4.1.1 and 4.1.2 in this chapter.

Table 4-8. Regression equations and related data characterizing basal metabolic rates for given age and gender classes.

Age	Gender	N[a]	Regression Equation BMR (MJ/24 hr)	R^2	RSE	Typical Value[b]
Under 3 years	Male	162	BMR = 0.249*Wt - 0.127	0.90	0.2925	1.51
	Female	137	BMR = 0.244*Wt - 0.130	0.92	0.2456	1.54
3 to 10 years	Male	338	BMR = 0.095*Wt + 2.110	0.69	0.2803	4.14
	Female	413	BMR = 0.085*Wt + 2.033	0.66	0.2924	3.85
10 to 18 years	Male	734	BMR = 0.074*Wt + 2.754	0.86	0.4404	5.86
	Female	575	BMR = 0.056*Wt + 2.898	0.64	0.4661	5.04
18 to 30 years	Male	2879	BMR = 0.063*Wt + 2.896	0.42	0.6407	6.87
	Female	829	BMR = 0.062*Wt + 2.036	0.53	0.4967	5.33
30 to 60 years	Male	646	BMR = 0.048*Wt + 3.653	0.36	0.6997	6.75
	Female	372	BMR = 0.034*Wt + 3.538	0.46	0.4653	5.62
Over 60 years	Male	50	BMR = 0.049*Wt + 2.459	0.51	0.6865	5.59
	Female	38	BMR = 0.038*Wt + 2.755	0.46	0.4511	4.85

Source: Schofield (1985, pp. 17-18).

[a] N = number of subjects in study

[b] Values of BMR (MJ/24 hr) reported in using typical weight and age for group.

As an example of the spread in BMR values, the 18 to 30 year old adult male population class is examined here. A typical BMR value of 6.87 MJ/day is reported for this class in the last column of Table 4-8. Estimates for the 95% confidence bounds of

BMR are approximated by the typical BMR value plus or minus twice the RSE. This computation leads to a relative difference of about 45% for the upper and lower 95% confidence bounds. Examinations of other population classes show similar spreads in the values of BMR.

4.1.8.3. Oxygen consumption factor, H_{oxy}

The oxygen consumption factor, H_{oxy}, is equal to the volume of oxygen (at conditions of standard temperature [273 K] and pressure [1 atm] for dry air, or STPD) consumed in the production of 1 kJ of energy. Thus, H_{oxy} has units of LkJ^{-1}. Energy (and CO_2 and H_20) is produced when the body catabolizes (oxidizes) fats, proteins, and carbohydrates. The amount of oxygen consumed in such processes depends on the energy source. Oxidation of one gram of fat, protein, or carbohydrate consumes 2.0 L, 0.97 L, or 0.83 L of O_2 and releases 39.4 kJ, 18.3 kJ, and 17.4 kJ of energy, respectively. Therefore, H_{oxy}(fat) = 0.0508; H_{oxy}(protein)= 0.0529; H_{oxy}(carbohydrate) = 0.0476. The normal diet includes a mixture of these three energy sources. Layton (1993) examined results from two major studies on food intake (USDA 1984 and U.S. DHHS 1983) and arrived at the same weighted-average value for H_{oxy} of about 0.05 L kJ^{-1}. This average is approximately equal to the unweighted average of H_{oxy}(fat), H_{oxy}(protein), and H_{oxy}(carbohydrate). In the present study, a uniform distribution with a minimum value of 0.0476 and maximum value of 0.0529 was used to model uncertainties in H_{oxy}. This distribution was further assumed to apply to all exertion levels and to all age/gender groups. There are limitations to this approach. For example, during exercise, especially heavy, short term exercise, it is known

that the body preferentially catabolizes carbohydrates (since less oxygen is needed to oxidize these sources). In the current methodology, such detail in metabolism, although acknowledged here, was not incorporated since a relative difference of only about 10% exists between minimum and maximum H_{oxy} values. This influence of this variability on ventilation rate is small compared to variabilities in VQ (~75%), BMR (~45%), and B_{mult} (discussed below).

4.1.8.4. Basal multiplication factor, B_{mult}

The basal multiplication factor, B_{mult}, represents the ratio of the energy expenditure rate to the basal metabolic rate (or supine resting metabolic rate as an approximation) and depends on the physical activity being performed. Layton (1993) listed some typical values for B_{mult} in some common physical activities; these values are repeated in Table 4-9. Values for B_{mult} can also be estimated from a biological handbook on metabolism compiled by Altman and Dittmer (1968, pp. 355-361). In the latter publication, over 300 different energy expenditure values (compiled from 49 references) for males and females were presented as percents over the supine level.

The ICRP (1994) has specified four broad exertion levels in an effort to group different activities--resting (sleeping), sitting (awake), light exertion, and heavy exertion. Based on the data in Table 4-9 and (more so) on the over 300 data points in Altman and Dittmer (1968), the distributions listed in Table 4-10 were assigned to B_{mult} per broad physical exertion level to model uncertainties and variabilities.

Table 4-9. Typical basal multiplier values, B_{mult}, for different activities.

Activity Level	Basal Multiplier	Activity Level	Basal Multiplier
Sedentary Activity	1.2	Moderate Activities (cont'd)	
Light Activities		Table tennis	3.0
Knitting/sewing	1.3	Light industry	3.1
Standing	1.5	Walking	3.5
Floor sweeping	1.8	Bed Making	3.8
Preparing vegetables	1.8	Vacuuming	3.8
Office work	1.8	Cycling	5.3
Moderate Activities		Swimming	5.3
Carpet sweeping	2.7	Dancing	5.3
Cooking	2.7	Heavy Activities	
Preparing a meal	2.7	Various sports events	10 to 22
Dish washing	2.7	Heavy industry work	10
Volleyball	3.0		

Source: Layton (1993, p. 28)

Table 4-10. Distributions assigned to B_{mult} in this study for four broad physical exertion levels.

Exertion Level	Distribution Shape	Minimum value	Maximum value
Resting	Uniform	1.0	1.1
Sitting	Uniform	1.2	1.7
Light Exertion	Uniform	2.0	5.0
Heavy Exertion	Uniform	5.0	10.0

Note: Minimum and maximum values based on values reported in Altman and Dittmer (1968) and, to a lesser degree, on Table 4-9.

The range chosen for each distribution depends on the activities that were assigned to each exertion level. The assignment process is a potential source of uncertainty in these distributions. For example, depending on the physical health of the subject, walking might qualify as a heavy exercise. The distributions in Table 4-10 are based on average or typical data for healthy persons. The value of B_{mult} varies not only with the type of activity being performed (as indicated by typical values in Table 4-9), but B_{mult} is expected to demonstrate high variability among individuals performing the same type of activity. Data

were not found which quantified this latter aspect of the variability (i.e., variability among individuals performing the same activity). Another potential source of error is that values for B_{mult} are presumably based on steady-state metabolic activity. Situations exist where persons exposed during a very short period might not reach a steady state level.

For the resting level, energy expenditure was taken to range from the basal metabolic level (B_{mult}=1) to 10% greater than the BMR (B_{mult} = 1.10). The upper value was chosen to account for increased metabolism (over basal) due to such processes as digestion and fluctuations in metabolism during sleep. For example, DuBois (1936) suggested a rise in metabolism of 5-10% for an average diet due to the specific action of food. The limits chosen for sitting are based primarily on data from Altman and Dittmer (1968) who presented energy expenditure for several sitting activities (e.g., calculating, writing, listening to radio, reading, eating, etc.). The values for light exertion are based on activities such as showering, dressing, driving a car, walking (< 4.0 mi/hr), cooking and cleaning. The values for heavy exertion are based on activities such as walking (> 4.0 mi/hr), bicycling, basketball, football, walking in snow, skiing, and heavy industrial work (e.g., mining). From data presented by Altman and Dittmer (1968), a value of B_{mult} = 21 was found for ladder climbing at a 90° angle, 12 m/min, with a 50-lb load. Other high values included walking up stairs (B_{mult}= 15.5), ski running (B_{mult} = 18.7) and rowing 30 strokes/min (B_{mult} = 16.2). These activities were not expected to be performed often by the majority of the population and were not used to set the upper limit on B_{mult}.

4.1.8.5. Summary of methods to model variabilities in ventilation rates

The methods adopted in this study to predict variabilities in ventilation rates are summarized in Table 4-11. To examine the predictability of the methodology, Latin hypercube sampling techniques (discussed in Chapter 3) were used to perform 1000 trials for each of the selected population groups. Average values of V_E computed from these trials are plotted in Fig. 4-10 for (a) males and (b) females. For population groups at rest, sitting, light exertion, and heavy exertion, the sample standard deviations (as percentages of the mean value) ranged from 15-20%, 18-22%, 29-32%, and 25-28%, respectively.

Table 4-11. Summary of distributions and methods used to predict variabilities in V_E.

Relationship/Distribution[a,b]	Units
$V_E = C*BMR*B_{mult}*H_{oxy}*VQ$, (Eqs. 4-19 and 4-20 combined)	l/min
C = (1000 kJ/MJ)/(1440 min/day) = 0.694	
$BMR = BMR_{reg}(Wt) + E_{BMR}$; $BMR_{reg}(W)$ is regression expression in Table 4-8; $Wt = Ht^2*BMI$; $Ht \sim N(\mu,\sigma)$--μ,σ from Table 4-1. $BMI \sim LN(\mu_{geo}, \sigma_{geo})$--$\mu_{geo},\sigma_{geo}$ from Table 4-2. $E_{BMR} \sim N(0, \sigma)$--$\sigma$ = RSE, from Table 4-8; linear regression random error term.	MJ/day
B_{mult} see Table 4-10 for distribution (depends on exertion level).	none
$H_{oxy} \sim U(0.0476, 0.0529)$	l O_2/kJ
$VQ \sim LN(\mu_{geo} = 26.5; GSD = 1.16)$	l air/min (BTPS) per l O_2/min (STPD)

[a] "Reg" denotes that the value depends on a regression function.
[b] The letter *N* denotes a normal distribution; *LN* denotes a lognormal distribution; *U* denotes a uniform distribution. Values in parentheses indicate distribution parameters: N(mean, standard deviation), U (minimum, maximum), LN (geometric mean, GSD).

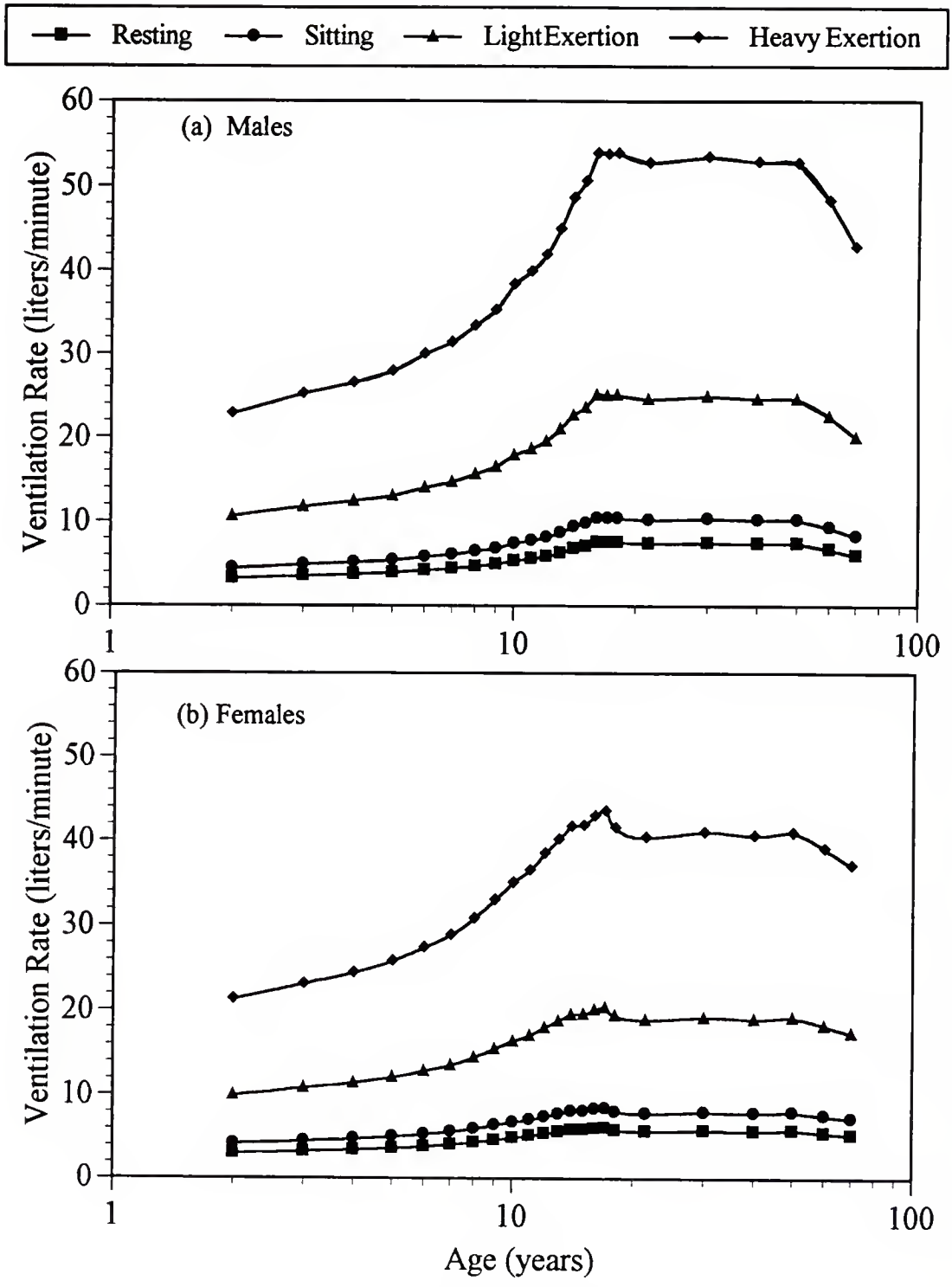

Figure 4-10. Predicted average values for V_E as a function of age. (a) For males. (b) For females. Each data point is based on 1000 trials using Latin hypercube sampling techniques. Standard deviations are discussed in text.

Figure 4-10 indicates an increase in ventilation rate with age up to about 18 years of age. The ventilation rate is roughly constant from an age of about 18 to 55 years; and it decreases slightly with age for older population groups. Based on measurements, several studies have reported the influence of age on V_{O2} max in children and adults (Mercier, 1991; Cooper and Weiler-Ravell, 1984; Bruce, 1984; Flandrois et al., 1982). The trends demonstrated in Figure 4-10 for average V_E in various exertion levels are consistent with those demonstrated by measured values of V_{O2} max.

In the current methodology, changes in the *average* V_E versus age are explained by changes in the *average* basal metabolic rate, which increases up to about 18 years of age and decreases for older persons. The abrupt change in average V_E for females between 15 and 18 years of age at heavy exertion is believed to be an artifact of the methodology--arising from the regression expressions used to predict BMR (in Table 4-8). These regression equations were based on discrete age intervals; discontinuities exist at the ages of 3, 10, 18, 30, and 60 years, where expressions change. Efforts were implemented to smooth effects of discontinuities at these ages by taking the average of the BMR predicted by the two relevant regression equations. The smoothing efforts were successful for all age transitions except 18 year old females.

Figure 4-11 compares the predicted average V_E values to standard values suggested by Roy and Courtay (1991) for subjects resting and sitting. The values generally agree; this agreement helps justify the approach adopted in the present work. Roy and Courtay (1991) derived values from a number of sources (including ICRP, 1975; Cotes, 1979; Gaultier, 1978; Gaultier et al., 1981; Godfrey et al., 1971; Godfrey, 1973;

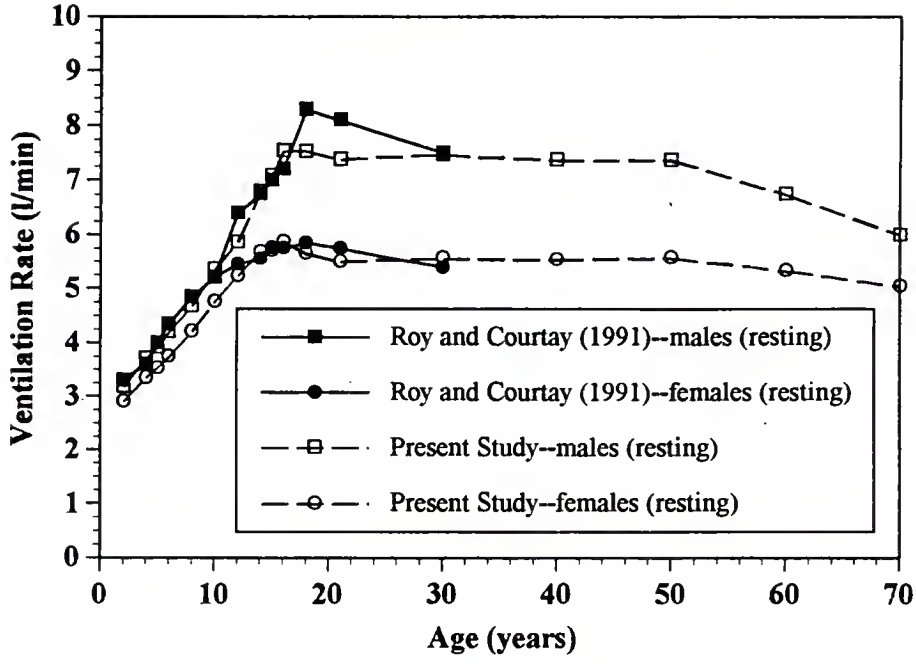

Figure 4-11. Comparison of ventilation rates at rest for males and females. The plot shows good agreement among data predicted by two independent methods.

Cooper and Weiler-Ravell, 1984; Flandrois et al., 1982; and Zapletal et al., 1987). Subsequently, the ICRP (1994) has adopted the ventilation values suggested by Roy and Courtay as the recommended reference values in their new lung model. The values determined in the present study are independent of those references cited in the study by Roy and Courtay.

4.1.9. Tidal Volume

The method described above for computing ventilation rates based on oxygen and energy consumption requirements does not include the tidal volume. (Traditionally the ventilation rate has been estimated as the product of the tidal volume and the respiratory

frequency). However, the tidal volume is still required by the particle deposition model. The tidal volume, V_T, is defined as the volume of air inhaled (or exhaled) during a breath, and it depends on the physical exertion level of the subject. Tidal volume is influenced to some degree by the anatomical dead space; the tidal volume must be larger than the dead space for inhaled air to reach the gas exchange region of the lungs. In the deposition model, tidal volume along with regional dead space volumes are needed to determine the fractions of inhaled and exhaled air that reach given respiratory regions. These volumetric fractions multiply into the regional deposition efficiencies in order to predict total regional deposition fractions.

At rest the tidal volume normalized per unit body weight is relatively constant throughout the human population and is on the order of about 10 ml/kg (+/- 2) for ages 4-30 years (Gaultier et al., 1981). As ventilation increases from the resting state, tidal volume increases. Generally, the increase in tidal volume is approximately linear with respect to the increase in ventilation rate (Hey et al., 1966). However, at very high ventilation rates, the tidal volume eventually reaches a plateau; and further increases in ventilation are effected by increases in respiratory frequency.

A number of studies have examined the relationship between tidal volume and ventilation rate in individuals (Hey et al., 1966; Gilbert et al., 1971; Patrick and Howard, 1972; Paek and McCool, 1992). Hey et al. (1966) examined 62 adult subjects and found that the relationship between tidal volume and ventilation rate could be expressed well by a linear model of the form:

$$V_E = M * (V_T - K) \quad , \tag{4-22}$$

where M and K are fitting parameters. The slope, M (min^{-1}), was found by Hey et al. to exhibit inter-subject variability but was relatively constant from day to day for an individual. The constant K (liters) was found to differ little between subjects and was suspected to be related to anatomical dead space or other physical body dimensions. Other studies, cited below, have confirmed this model. The study by Hey et al. also found that the relationship between V_E and V_T was essentially unaltered by moderate muscular exercise, posture, metabolic acidosis, and wide variations in alveolar gas pressures (oxygen and carbon dioxide partial pressures); however, the relationship was affected by changes in body temperature.

Hey et al. presented experimentally derived values for M and K for 26 adult subjects (23 men, 3 women); analysis of these data resulted in average values of M = 28.4 ± 5.7 min^{-1} (mean ± standard deviation) and K = 0.32 ± 0.13 liters. Gilbert et al. (1971) examined the breathing pattern in 10 adults and found a similar relationship between tidal volume and ventilation rate with average values of M = 23.4 ± 7.8 and K = 0.16 ± 0.24, respectively. Patrick and Howard (1972) examined the influences of age, gender, and body size on breathing patterns in 63 subjects (28 young men, 26 young women, and 9 older men). They obtained the average values of M = 24.9 ± 9.5 and K = 0.37 ± 0.41 for young adult males, M = 26.1 ± 13.2 and K=0.25 ± 0.26 for young adult females, and M = 17.1 ± 0.48 and K = 0.48 ± 0.53 for older adults. Average values for M and K for adults

from all references cited above are comparable for all but the older adult class reported by Patrick and Howard (1972).

Patrick and Howard (1972) concluded that the relationship between V_E and V_T was not influenced significantly by gender differences; however, they did find that age had a significant effect on the value of M. Within an age range of 19 to 51 years they found a significant negative correlation between M and age ($p < 0.05$). Assuming a linear decline, the following (regression) expression was presented for the average value of M versus age:

$$M\,(\text{min}^{-1}) = 31.8 - 0.33 * \text{Age}\,(\text{years}) \quad . \tag{4-23}$$

No residual standard error (RSE) of fit or R^2 value was reported. The authors also found that body size had some influence on the relationship of V_E and V_T. The parameter K was found to be correlated with height and was described by:

$$K\,(\text{liters}) = 0.0114 * \text{Ht}\,(\text{cm}) - 1.65 \tag{4-24}$$

where Ht is the body height; again no RSE and R^2 values were given.

The studies discussed above were for adult subjects. No similar studies were found relating tidal volume and ventilation rate for children. However, data collected in a study by Godfrey et al. (1971) provided a basis for evaluating M and K for children. Godfrey et al. examined 119 children ages 6-15 years at rest and at two steady-state exercise levels in an investigation of the breathing patterns of children. The data were analyzed by those authors in a number of ways; however, simple attempts to relate ventilation rate and tidal volume were not successful. The data collected for that study

were obtained from the Librarian of the Royal Society of Medicine (London, England) and reanalyzed in the present study; the data and results are presented in Appendix D. The analyses show that for single individuals the relationship between tidal volume and ventilation rate is represented well by the model given in Eq. (4-22). Additionally, values for M and K were found to be correlated with age. The resulting expressions for M and K as functions of age are (based on n=71 subjects):

$$M\ (\text{min}^{-1}) = 1.48 \times 10^{2} * \exp(-7.32 \times 10^{-2} * \text{Age}),\ R^2 = 0.35 \qquad (4\text{-}25)$$

and

$$K\ (\text{liters}) = 8.75 \times 10^{-2} * \text{Age}^{0.487},\ R^2 = 0.10 \qquad (4\text{-}26)$$

where *Age* is in years. A number of other regressions were investigated for both M and K (linear, power, and exponential models on both age and height); however, the above best fitting models were adopted for the present work.

The results presented above for adults and children provide a basis for predicting an average tidal volume given the age, height, and ventilation rate. However, the variability in tidal volume must also be quantified. Based on data presented in Appendix D, an examination of the tidal volumes at various exertion levels for children grouped in yearly age intervals yielded an average geometric standard deviation (GSD) of about 1.27. Similar values were found by Zapletal et al. (1987), who examined 173 healthy children (age 6-18 years) at rest and presented a power function relationship between: (1) the resting tidal volume and height ($R^2 = 0.42$) and (2) the resting tidal volume and age ($R^2 = 0.32$). For the regression on height, the GSD of the residuals was 1.23; for the regression

on age, it was 1.25. Both of these values obtained for the GSD by Zapletal et al. generally agree with the value of 1.27 derived in Appendix D. These GSD values provide a measure of the residual variability in the tidal volume after variabilities attributable to height and/or age are removed.

For adults, Matheson and Gray (1950) reported coefficient of variations (standard deviation divided by the mean) of 28.5% and 25.9% in tidal volume for 100 young adult males for data collected on two consecutive days. A number of references investigating tidal volume have been compiled by Altman and Dittmer (1971, e.g., pp. 54-60); based on data presented for adults in that reference, coefficients of variation ranged from 14% to 28% for tidal volume.

Based on discussions above for children and adults, the tidal volume (including variabilities and uncertainties) was sampled for trials in this study by the following model:

$$V_T = \left(\frac{V_E}{M_{(Age)}} + K_{(Ht,Age)} \right) * E_{VT} \qquad (4\text{-}27)$$

where the term in brackets represents the average tidal volume (a function of the ventilation rate, age, and height) and is based on Eqs. 4-22 through 4-26). For adults (Age ≥ 18 years), Equations 4-23 and 4-24 are used for M and K, respectively. For children, Equations 4-25 and 4-26 are used for M and K, respectively. The subscripts on M and K serve as reminders that these parameters are correlated with age and possibly height. The last factor, E_{VT}, is a random error term which introduces uncertainty into tidal volume predictions and was assigned a lognormal distribution with geometric mean of 1.0 and GSD = 1.25 (based on the discussion in the preceding two paragraphs). The random

error term was sampled by LHS techniques in order to generate variability in the tidal volume. Equation 4-27 accommodates both variability and correlations of tidal volume with ventilation rate, age, and height.

As discussed, the tidal volume reaches a plateau value at high ventilation rates (e.g., heavy exertion). Based on recommendations of Hey et al. (1966), the tidal volume in this work was confined to a maximum value given by one-half of the vital capacity, VC.

$$V_T \leq \frac{1}{2} * VC \tag{4-28}$$

This upper value is generally reached only at the heavy exertion level. As a lower limit, the tidal volume was further confined to a minimum value of 40% of the anatomical dead space, V_D; so the following constraint is applied in sampling tidal volumes in this study:

$$\frac{V_T}{V_D} > 0.4 \tag{4-29}$$

This lower limit is primarily a concern only at the resting (sleeping) activity level and is based on data reported by Altman and Dittmer (1971, pp. 65-66).

Using the methods described above, average tidal volumes were computed at the four broad exertion levels for various population classes. Figure 4-12 is a plot of the average tidal volume as a function of age and is based on a (Latin hypercube) sample size of 1000. The standard deviations (as percentages of mean) ranged from 15-19%, 18-22%, 29-32%, and 25-28% for population classes at rest, sitting, at light exertion, and at heavy exertion, respectively. These ranges of standard deviations for subjects resting and sitting

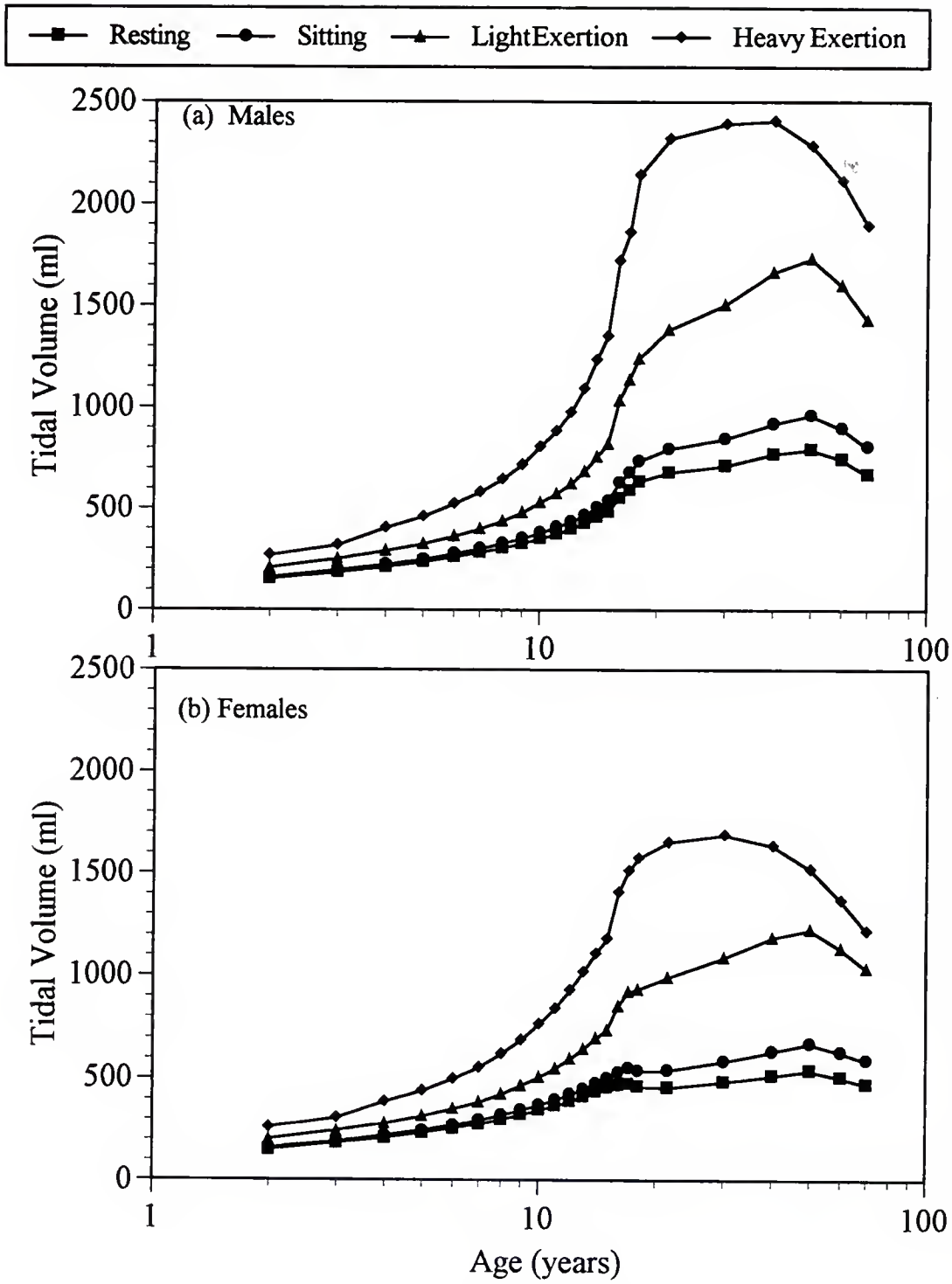

Figure 4-12. Tidal volume at various physical exertion levels for (a) males and (b) females at different ages. Based on 1000 realizations using a Latin hypercube sampling techniques.

agree with values reported by authors above (e.g., Matheson and Gray, 1950; Altman and Dittmer, 1971). The decrease in tidal volume seen in Fig. 4-12 for ages greater than about 30-50 years is due in part to the decrease in ventilation rate (ages greater than about 50 years) and in part to the decrease in vital capacity (which poses a limit on tidal volume during the heavy exertion).

As some verification of the methodology, the average tidal volumes plotted in Figure 4-12 for heavy exertion are less than (average) values reported for maximal tidal volume, V_{Tmax}, by Altman and Dittmer (1971, pp. 82-83) for males and females. For example, the average V_{Tmax} for 20-25 year-old females is around 2100 ml; for 20-33 year-old males the average V_{Tmax} is around 3000 ml. For heavy exertion, Figure 4-12 indicates average tidal volumes of about 1700 ml for females and 2400 ml for males. These values are about 80% of the maximal values reported by Altman and Dittmer.

As additional verification of the methodology, Figure 4-13 shows a comparison of the average resting values predicted by methods in this study and those estimated by others. The values reported by Roy and Courtay (1991) are based on compilations from many references. The values associated with Zapletal et al. (1987) and Taussig et al. (1977) are based on regression equations derived from measured values of tidal volume at rest. Subsequently, the ICRP (1994) has adopted the values recommended by Roy and Courtay as reference values for use in its lung dosimetry model. The data presented in Figure 4-13 provide support for the methods adopted to model V_T in the present study.

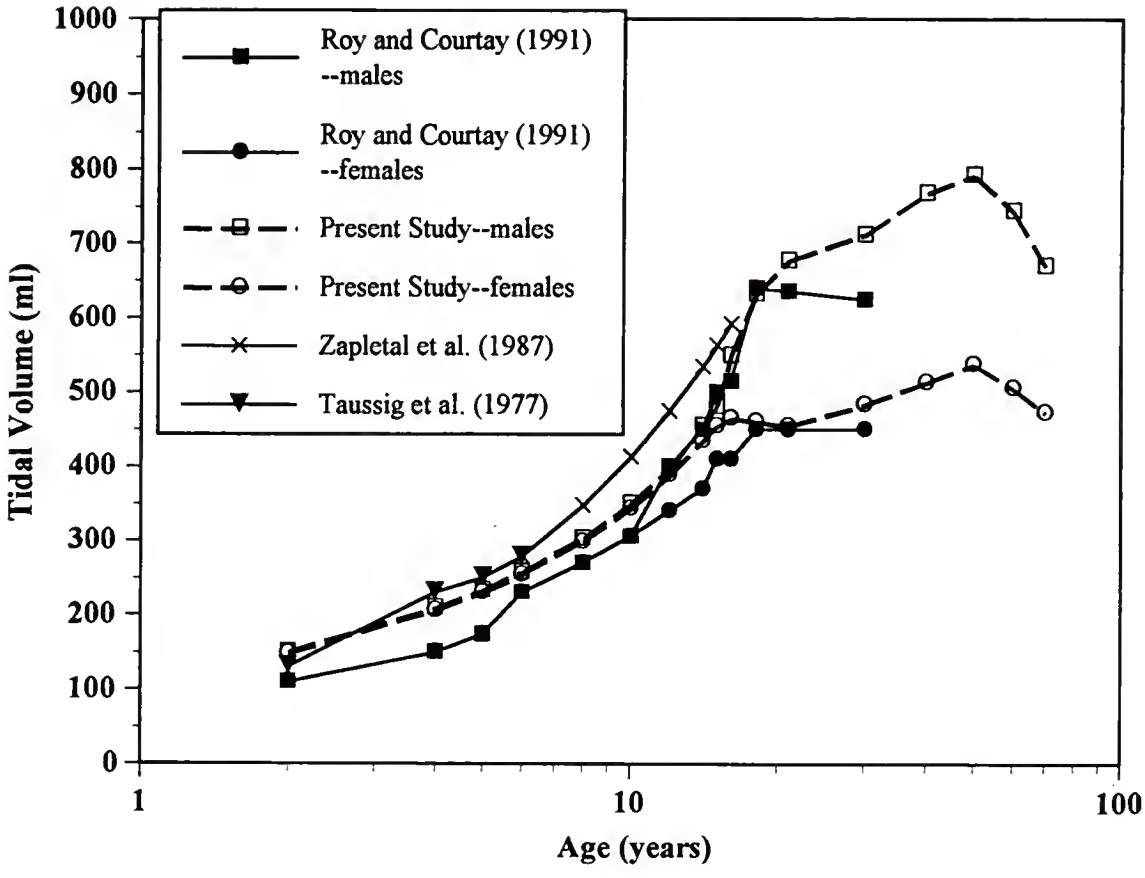

Figure 4-13. Comparison of average resting tidal volumes in present study with other references including Roy and Courtay (1991) which is the basis for ICRP reference values (ICRP 1994).

4.1.10. Fraction of Air Breathed Through the Nose

Air is inhaled through the nose, the mouth, or a combination of the two. Characterization of the breathing mode is an important aspect of particle deposition modeling. For example, Miller et al. (1988) showed that the thoracic deposition fraction was potentially larger for habitual mouth breathers compared to those breathing primarily through the nose. In the deposition aspect of the ICRP respiratory tract model (ICRP

1994), the fraction of air inhaled via the nose, F_n, is needed to account for different filtration efficiencies of mouth versus nose breathing. According to the ICRP deposition model, nose breathing involves a series of nine filtration regions while mouth breathing only involves seven (i.e., region ET_1, the anterior nasal region is not present during mouth breathing).

Past studies indicate that more than 80% of normal adult subjects breathe exclusively through the nose while at rest (Uddstromer 1940; Camner and Bakke 1980; Niinimaa et al. 1981; Rodenstein and Stanescu 1984). This pattern of breathing generally persists until moderate to heavy exertion levels are reached; at these levels nasal breathing becomes augmented by mouth breathing (Niinimaa et al. 1981; Chadha et al. 1987). Persons following this breathing mode are classified as normal augmenters. Other persons are classified as mouth breathers and represent those persons who habitually augment nasal breathing with oral breathing at all levels of physical exertion, including rest. It is important to note that these classifications represent healthy persons. Various respiratory problems can cause a normal augmenter to become a mouth breather (temporarily or chronically). The switching point from nasal to oronasal breathing in normal augmenters has been shown to occur at a total ventilation of about 35-40 l/min in adult subjects (Chadha et al., 1987; Niinimaa et al., 1981; Saibene et al., 1978).

Several investigations have resulted in useful information regarding breathing mode in adults; however, few studies exist for children. Warren et al. (1990) examined 120 normal children (6 to 15 years of age) at rest. The authors found that the mean

percentage of nasal breathing by age increased approximately linearly from about 50% at 6 years of age to about 90% at 14 years.

For five adult subjects, Wheatley et al. (1991) showed the nasal flow fraction did not change significantly from inspiration to exhalation within individuals. The authors also demonstrated that intrasubject variability in the nasal fraction was very small compared to intersubject variability. Niinimaa et al. (1981) studied the breathing mode in 30 adults at rest and at exercise. For normal augmenters, Niinimaa et al. found that all subjects breathed through the nose exclusively up to a switching point of 35 ± 10.8 l/min. After the switching point, the subjects breathed about 60% of the air nasally. At the highest ventilation rates achieved (~90 l/min) subjects breathed about 40% nasally. Mouth breathers consistently breathed less air nasally as the exertion level (and total ventilation rate) increased. Niinimaa et al. summarized the results of their work by the following equations for normal augmenters (NA) and mouth breathers (MB):

$$V_{En}(NA) = \begin{cases} V_E & (V_E < V_{switch}) \\ 0.29\,V_E + 9.9 & (V_E \geq V_{switch})\ (RSE = 6.31) \end{cases} \tag{4-30}$$

$$V_{En}(MB) = 0.26\,V_E + 4.6 \qquad (RSE = 5.79) \tag{4-31}$$

where V_{En} represents the nasal component of the ventilation rate (l/min); V_{switch} is the switching point ventilation at which normal augmenters change from total nasal to oronasal breathing; and RSE (l/min) denotes the residual standard error (of the estimate) for the regression equation.

The ICRP (1994) has suggested reference values for F_n at various exertion levels based on a paper by Miller et al. (1988), who subsequently derived values from Niinimaa et al. (1981). These data are repeated in Table 4-12. The ICRP approach requires that nasal augmenters and mouth breathers be treated separately. However, in the present study the desire is to predict results for whole population classes--accounting for both breathing modes in the output dose distribution.

Table 4-12. Fraction of ventilatory airflow passing through the nose in normal augmenters and in mouth breathers.

	F_n	
Level of Exertion	Normal Augmenters	Mouth Breathers
Sleep	1.0	0.7
Sitting (awake)	1.0	0.7
Light exercise	1.0	0.4
Heavy exercise	0.5	0.3

Source: ICRP Publication 66 (ICRP 1994)--based on Miller et al. (1988).

The desire in the present study was to account for the variabilities and uncertainties in model parameters for all ages. Based on the information presented above, the following approach was adopted. First, the fraction of the population that can be classified as normal augmenters (NA) versus mouth breathers (MB) was estimated. For adults, the assumption (based on measurements by Uddstromer 1940; Camner and Bakke 1980; Niinimaa et al. 1981; Rodenstein and Stanescu 1984) was that 90% of the population comprises NA, and 10% comprises MB. For children, a simple straight line fit (graphically) through Fig. 6 of Warren et al. (1990) predicts the fraction of NA by age. Based on that figure, about 50% of the six-year-old population and 90% of the fourteen-year-old population are NA. Using this information, the following expression was derived

to predict the fraction of the population at a given age (in years) that can be classified as normal augmenters, NA:

$$NA(\%) = \begin{cases} 5 * Age + 20\% & (Age < 14 years) \\ 90\% & (Age \geq 14 years) \end{cases} \quad (4\text{-}32)$$

so that MB(%) = 1 - NA(%).

Given that a subject is either a normal augmenter or a mouth breather, F_n can be predicted by dividing Eqs. 4-30 and 4-31 by the total ventilation rate, V_E, to yield:

$$F_n(NA) = \begin{cases} 1.0 & (V_{Ea} < V_{switch}) \\ 0.29 + (9.9 + E_{NVn})/V_{Ea} & (V_{Ea} \geq V_{switch}) \end{cases} \quad (4\text{-}33)$$

$$F_n(MB) = 0.26 + (4.6 + E_{MVn})/V_{Ea} \quad (4\text{-}34)$$

where E_{NVn} and E_{MVn} represent random error terms introduced into the expressions to account for uncertainties and variabilities in F_n; and V_{Ea} is used as the ventilation rate to stress the fact that these expressions are based on ventilation data from adult subjects. The random error terms were assigned the following distributions based on the RSE values reported in Eqs. 4-30 and 4-31: E_{NVn} ~N(0, 6.3) and E_{MVn} ~ N(0, 5.8) where N denotes a normal distribution with specified mean and standard deviation, respectively, in parentheses. The value for V_{switch} was taken to be 35 l/min (average value reported by Niinimaa et al., 1981). An adult-equivalent ventilation rate, V_{Ea}, must be determined to use the above expressions for children. To determine an adult equivalent ventilation, ventilation rates were scaled based on the basal metabolic rate of a reference adult to that sampled for the trial in question. Using the expression in Table 4-8 for a 25 year old male,

the standard basal metabolic rate for an adult is estimated as 7.3 MJ/day. Therefore, V_{Ea} is given by:

$$V_{Ea} = V_E(\text{sampled}) * \frac{\text{BMR (adult)}}{\text{BMR (sampled)}} = V_E(\text{sampled}) * \frac{7.3\ \text{MJ/day}}{\text{BMR (sampled)}} \quad (4\text{-}35)$$

Implementation of this approach involves: (1) determining whether the subject sampled in the trial is a nose breather or a mouth breather based on a binomial distribution (with probability of being a nose breather predicted by equation Eq. 4-32), (2) computing the BMR and V_E for the trial based on techniques presented in previous sections, (3) computing V_{Ea} for the trial from Eq. 4-35, and finally (4) computing F_n from either Equation 4-33 or 4-34. A number of assumptions are implicit in this approach. The population of persons older than 14 years is assumed to be composed of 90% nose breathers. The trend estimated by Niinimaa et al. (1981) for adults is assumed to apply to children (all ages) by simple adjustment of the ventilation rates to an adult equivalent. And although no data were found for ages less than 6 years, extrapolation of available data to the lower age limit of this study, i.e., 2 years, is assumed appropriate.

4.1.11. Uncertainty in Particle Inhalability

Inhalability of aerosol particles is defined as the efficiency with which particles enter the human nasal or oral airways. The inhalability determines the fraction of particles of a given size which enter the airways and therefore influences deposition of particles in airways. Previous experiments using mannequins have showed that inhalability depends on particle size, wind speed, ventilation rate, and head orientation with respect to wind

direction (Ogden and Birkett 1977; Armbruster and Breuer 1982; Vincent and Mark 1982; and Vincent et al., 1990). These experiments were performed using adult dimensions. A recent paper by Chung et al. (1993) presented results of a numerical model predicting inhalability in children and adults. The results, although limited, showed that children inhale larger fractions of particles of a given aerodynamic diameter than adults. No reasons were given for the increase. The scope of that latter study was very limited (e.g., the torso was not included in the model) and only a couple of scenarios were examined.

By averaging results from the first three studies cited above over all orientations and wind speeds, the American Conference of Governmental Industrial Hygienists (ACGIH, 1985) recommended the following empirical expression as a standard for instruments designed to sample the inhalable fraction, I, of airborne particulates:

$$I = 0.5 * [1 + \exp(-0.06 * d_{ae})] \qquad (4\text{-}36)$$

where d_{ae} represents the particle aerodynamic diameter (discussed in section 2.5) and the expression covers diameters less than or equal to 100 microns. Vincent et al. (1990) recently collected additional data characterizing the effects of wind speed on inhalability for speeds up to 9 m/s. A correction to the ACGIH expression was proposed for wind speeds, U, greater than 4 m/s but less than 10 m/s (i.e., ~9 to 22 miles/hr) resulting in

$$I = 0.5 * [1 + \exp(-0.06 * d_{ae})] + 10^{-5} * U^{2.75} * \exp(0.055 * d_{ae}) \; . \qquad (4\text{-}37)$$

This equation accounts for about 60% of the variance in the observed values of inhalability. For wind speeds less than 4 m/s, Vincent et al. stated that the ACGIH expression is adequate. James et al. (1994b) further refined the expression to increase the

accuracy (with respect to the experimental data) for d_{ae} less than 10 μm. The resulting expression, which was adopted by the ICRP (1994), is:

$$I = 1 - 0.5 * \{1 - [7.6 \times 10^{-4} d_{ae}^{2.8} + 1]^{-1}\} + 10^{-5} * U^{2.75} * \exp(0.055\ d_{ae}) \quad . \qquad (4\text{-}38)$$

This equation is plotted in Figure 2-5 of Chapter 2 for some wind speeds.

Regarding the uncertainty in inhalability, Vincent et al. (1990) suggested that "inhalability may vary from this curve by up to ± 0.1 for each value of d_{ae}." Examination of data plotted in Figure 5 of Vincent et al. (1990) supports this statement. Therefore, to account for uncertainty in the inhalability, a random error term, E_{Inh}, was added to Equation 4-38 and was assumed to follow a normal distribution with a mean value of zero and a standard deviation of 0.10. No studies were located which measured inhalability for particles with d_{ae} less than about 5 μm. Presumably as the aerodynamic diameter decreases below about 1 μm, the inhalability increases to unity and the uncertainty decreases to zero (i.e., all particles are able to follow the flow lines since the inertial mechanisms, primarily responsible for variations in inhalability, become negligible). In this study, for particles with $d_{ae} < 0.5$ μm the inhalability was assumed to be unity with no error term. Because experimental data are lacking for children, the approach described in this section was applied to all ages.

4.1.12. Regional Deposition Efficiency Uncertainty

As discussed in Chapter 2, the particle deposition aspect of the ICRP respiratory tract dosimetry model uses simplified mathematical expressions to predict both aerodynamic and thermodynamic deposition efficiencies for the five broad deposition

regions of the respiratory tract. For extrathoracic regions these mathematical expressions are based on regression analyses of experimental data. For thoracic regions the expressions are based on nonlinear curve fitting of primarily theoretical data predicted by an underlying, more sophisticated model. The ICRP (1994) has provided guidance to account for variabilities in deposition efficiencies that are not explained by the regression equations. In other words, the ICRP has recommended methods to account for uncertainty in the mathematical structure of the deposition model. These methods are incorporated in the current study as explained in following paragraphs.

Based on experimental data from large groups of subjects [primarily studies by Lippmann (1977) and Chan and Lippmann (1980)], Rudolf et al. (1994) estimated the upper and lower 95% confidence bounds for equations very similar to those presented in Tables 2-1 and 2-2 to predict aerodynamic deposition efficiencies in single subjects. Because experimental data on deposition are scarce for submicron-sized particles, the ICRP (1994) proposed comparable values to obtain the 95% confidence bounds for thermodynamic deposition efficiencies. The confidence bounds are determined through the use of dimensionless scaling constants, c_i (for region i), that act on parameters a_i in deposition model equations (i.e., Tables 2-1 and 2-2). The lower and upper 95% bounds for deposition efficiencies are estimated as $a_i \div c_i^2$ and $a_i * c_i^2$. The ICRP has recommended (ICRP 1994, pp. 48-49) the values in Table 4-13 for use as the scaling constants, c_i. In regard to using these scaling constants to account for model uncertainties, James et al. (1994b) state the following:

> To estimate the overall probability distribution of regional lung (and extrathoracic) deposition, it would be reasonable to assume that the deposition efficiencies in each region are not correlated, and that these are sampled at random from...distributions centered on the predictions of the recommended algebraic model. (James et al., 1994b, p. 281)

Based on this statement, uncertainties in aerodynamic and thermodynamic regional deposition efficiencies were accounted for by multiplying a_i (in Tables 2-1 and 2-2) by random variables $C_{ae}(i)$ and $C_{th}(i)$ which were all assigned lognormal distributions with geometric means of one and geometric standard deviations (GSD) given by $(c_i)^{1/2}$. Values for c_i (i.e., GSD^2) are listed in Table 4-13 for aerodynamic and thermodynamic efficiencies. In this approach, the error term, sampled for a specific trial and for a specific deposition region, was assumed to be appropriate for both inhalation and exhalation deposition efficiencies in that region. As stated above by James et al., all random variables were assumed to be statistically independent and were sampled independently from their respective probability distributions.

Table 4-13. Dimensionless scaling constants used to account for uncertainties in aerodynamic and thermodynamic deposition efficiencies.

	Aerodynamic Efficiency[a]		Thermodynamic Efficiency[b]	
Region	Random Variable	Scaling Constant, c_i (GSD^2)	Random Variable	Scaling Constant, c_i (GSD^2)
ET_1[c]	$C_{ae}(ET_1)$	3.3	$C_{th}(ET_1)$	1.4
ET_2	$C_{ae}(ET_2)$	3.3	$C_{th}(ET_2)$	1.4
BB	$C_{ae}(BB)$	2.5	$C_{th}(BB)$	1.5
bb	$C_{ae}(bb)$	2.5	$C_{th}(bb)$	1.5
AI	$C_{ae}(AI)$	1.7	$C_{th}(AI)$	1.5

Source: Adapted from Table 14 in ICRP Publication 66 (ICRP 1994, p. 49).
Notes: See Tables 2-1 and 2-2 for model equations; GSD = geometric standard deviation.
[a] Aerodynamic scaling constants are based on a study by Rudolf et al. (1994).
[b] Thermodynamic scaling constants are based on (ICRP 1994).
[c] Region ET_1 is for nasal pathway only.

4.2. Clearance Model Parameters

4.2.1. Introduction

Uncertainties in parameters required for modeling the clearance of materials deposited in the respiratory tract are examined in this section. The clearance model has been discussed in Chapter 2. More than twenty input parameters are required by the clearance model; however, depending on the physico-chemical properties of the deposited material and the elapsed time since deposition, some parameters are more important than others.

Bailey and Roy (1994) recently reviewed past studies and available information on the mechanical aspects of particle clearance in the respiratory tract. The purpose of their work was to recommend (best estimate) reference values for parameters used in the revised ICRP (1994) clearance model. In making recommendations, Bailey and Roy provided details on the uncertainties for many of the parameters. Consequently, their work is the basis for much of the information presented in this section. The approach was to adopt the parameter uncertainties suggested by Bailey and Roy (1994) as a form of expert opinion. With regard to the suggested uncertainties in clearance model parameters, Bailey and Roy made the following statement:

> In general, reference values are based on indirect information and therefore involve a considerable element of judgement. Some rates are based entirely on data from animal studies, and extrapolating results to humans involves a possible systematic error which could be large...Thus the combination of a high degree of intersubject variation and possible systematic errors means that uncertainties in reference values are large and difficult to quantify. It is therefore assumed that the uncertainty in the reference value is log-normally distributed, and thus that there is

a 95% probability that the true mean value lies within a factor of Φ_u of the chosen reference value (Bailey and Roy, 1994, p. 306).

As discussed in Chapter 1, one purpose of this study was to examine uncertainties in respiratory tract doses from inhaled plutonium oxides. Many of the clearance model parameters depend on the physico-chemical form of the material; therefore, some of the parameter distributions presented in this section are based on clearance of plutonium oxides only. These distributions must be revised for other materials. The affected parameters are only those four associated with the absorption component of the model (discussed in section 4.2.4).

For all materials, mechanical clearance (to gastrointestinal tract and lymph nodes) and absorption (to blood and to bound state compartments within lung tissues) compete to remove material from the respiratory tract. For radioactive material, decay must also be considered as a removal mechanism; however, for some long-lived radionuclides, removal by decay is negligible (such is the case for Pu-239). Depending on the nature of the material, a single mechanism might dominate; however, generally all mechanisms must be considered.

4.2.2. Partition of Deposition in Clearance Model Compartments

The deposition model predicts the amount of material (or activity) that deposits in the broad respiratory tract regions: ET_1, ET_2, BB, bb, and AI. Material deposited in a specific region is then divided among the appropriate initial-state clearance compartments within that region. The fraction of the regional deposition that is assigned to compartment

i is denoted here by $f_d(i)$. For example, the fraction of the deposit that is assigned to compartment BB_1 is $f_d(BB_1)$ and represents the ratio of material deposited in compartment BB_1 to the total deposition in the BB region. Distributions and relationships adopted to quantify uncertainties in $f_d(i)$ for relevant compartments are listed in Table 4-14. Unless additional details are given below, these distributions are based directly on recommendations of Bailey and Roy (1994). Compartments not listed in the table receive no initial deposition in the model. Since these quantities represent fractions of deposited material, sampled values cannot be greater than one or less than zero. Furthermore, the deposition fractions within a region (e.g., BB) must sum to unity. Methods were implemented in sampling algorithms to truncate distributions so that values are within the allowable range. For example, valid values of $f_d(AI_1)$ must be between 0 and 1; and $f_d(AI_1)+f_d(AI_2)+f_d(AI_3) = 1$. Some of the values of f_d are based primarily on animal data; for these values, Bailey and Roy (1994) suggested an uncertainty factor of $\Phi_u = 3$. This factor corresponds to the number by which the reference value must be multiplied (or divided) to obtain upper (or lower) 95% confidence limits (for the true mean value) assuming a lognormal distribution (i.e., $\Phi_u \approx GSD^2$).

4.2.2.1. The slow-clearing thoracic deposition fraction

The term f_s in Table 4-14 represents the slow-clearing fraction of material from the tracheobronchial region (regions BB + bb). A slow-clearing thoracic component was introduced into the ICRP 66 clearance model (ICRP 1994) by designers as a result of

Table 4-14. Distributions and relationships describing partition of deposited material into compartments of the ICRP clearance model.

Parameter	Clearance Compartment	Reference Values	Distribution or Relationship Adopted in this Study
$f_d(ET_2)$	ET_2	0.9995	$f_d(ET_2) = 1 - f_d(ET_{scq})$
$f_d(ET_{scq})$	ET_{scq}	0.0005[a]	$f_d(ET_{scq}) \sim LN(0.0005, 1.73)$[c]
$f_d(BB_1)$	BB_1	0.993-f_s	$f_d(BB_1) = 1 - f_s - f_d(BB_{scq})$
$f_d(BB_2)$	BB_2	f_s	$f_d(BB_2) = f_s$
$f_d(BB_{scq})$	BB_{scq}	0.007[a]	$f_d(BB_{scq}) \sim LN(0.007, 1.73)$[c]
$f_d(bb_1)$	bb_1	0.993-f_s	$f_d(bb_1) = 1 - f_s - f_d(bb_{scq})$
$f_d(bb_2)$	bb_2	f_s	$f_d(bb_2) = f_s$
$f_d(bb_{scq})$	bb_{scq}	0.007[a]	$f_d(bb_{scq}) \sim LN(0.007, 1.73)$[c]
f_s	(slow-clearing TB fraction)	See Eq. 4-39 and discussion in section 4.2.2.1.	$f_s = f_{s,average} + E(f_s)$[b] $f_{s,average}$ given by Eq. 4-41 in text. $E(f_s) \sim N(0, 0.1)$
$f_d(AI_1)$	AI_1	0.3	$f_d(AI_1) \sim LN(0.3, 1.10)$[d]
$f_d(AI_2)$	AI_2	0.6	$f_d(AI_2) = 1 - f_d(AI_1) - f_d(AI_3)$
$f_d(AI_3)$	AI_3	0.1	0.1 (discussed, section 4.2.2.2)

Source: Reference values, distributions, and relationships are based on Bailey and Roy (1994) unless otherwise indicated by note (b).

Notes:

~N(x,y) signifies that quantity is assigned a normal distribution with mean value of x and standard deviation of y.

~LN(w,z) signifies that quantity is assigned a lognormal distribution with geometric mean of w and geometric standard deviation of z. The 95% confidence interval for a lognormal distribution is approximately ($w \div z^2$, $w * z^2$).

[a]Indicates that reference value is based only on animal data.

[b]Signifies that modifications were made with respect to original recommendations of Bailey and Roy (1994). Modifications are discussed in text.

[c]Based on a proposed uncertainty factor of $z^2 = 3$ for the 95% confidence interval.

[d]Based on a proposed uncertainty factor of $z^2 = 2$ for the 95% confidence interval.

inhalation experiments by Stahlhofen (1989, 1991), Stahlhofen et al. (1986a, 1986b, 1987a, 1987b, 1990, 1994), Scheuch (1991), and Scheuch et al. (1993). Based on data presented in Table E.11 of Bailey and Roy (1994), the following relationship was suggested by those authors for f_s as a function of the particle equivalent-volume diameter, d_e (i.e., the diameter of a sphere with the same volume as the particle):

$$f_s = \begin{cases} 0.5 & (d_e \leq 2.5\ \mu m) \\ 0.5e^{-0.63(d_e - 2.5)} & (d_e > 2.5 \mu m) \end{cases} \quad (4\text{-}39)$$

where the d_e is related to d_{ae} (defined in section 2.5) by

$$d_e = d_{ae}\sqrt{\frac{\chi}{\rho}} \quad (4\text{-}40)$$

and χ is the particle dynamic shape factor (Hinds, 1982) and ρ is the mass density of the particle (g/cm^3). This expression was subsequently adopted by the ICRP (1994) for use in the revised lung model.

Bailey and Roy (1994) provided no suggestions to accommodate uncertainties in Equation 4-39. Furthermore, it is not clear from their text which data (in Table E-11 of Bailey and Roy, 1994) were used to obtain Equation 4-39. An independent analysis of the data (listed in Table E-11 of Bailey and Roy) was conducted in the present study using a similar model form. To minimize complications in interpreting data, only data associated with a bolus front depth of $V_{BF} < 80$ ml were used. The bolus front depth, V_{BF}, corresponds to the volume of air that passes the larynx from the time the leading edge passes it to the end of inspiration. As discussed previously, the anatomical dead space in

adults is about 150 ml. Assuming a value of about 50 ml for the extrathoracic airways during mouth breathing (mouth, oropharynx, and larynx), the tracheobronchial airways represent about 100 ml of this volume. By selecting only data with $V_{BF} < 80$ ml, the bolus material is expected to deposit primarily in the tracheobronchial airways (BB + bb). This cutoff point is in accordance with Scheuch and Stahlhofen (1988), who found that for a bolus with $V_{BF} < 80$ ml, most of the material deposited in airways with effective diameters greater than 2 mm (i.e., little reached the alveolar region--where effective diameters are generally less than 1 mm). Data meeting this condition (n = 41) are plotted in Figure 4-14. Using the same model form as Bailey and Roy with these data, the following expression was obtained in the present study:

$$f_s = \begin{cases} 0.58 & (d_e \leq 2.5\ \mu m) \\ 0.58\, e^{-0.76(d_e - 2.5)} & (d_e > 2.5 \mu m) \end{cases} \qquad (4\text{-}41)$$

where f_s is set equal to the average value of the data in Figure 4-14 associated with $d_e <$ 2.5 μm. For data associated with $d_e > 2.5$ μm, the factor -0.76 in the expression was obtained by forcing $f_s = 0.25$ at $d_e = 3.6$ μm (similar to approach used by Bailey and Roy). Figure 4-14 also plots Equations 4-39 and 4-41. As demonstrated in Fig. 4-14, the modified model predicts the (sample) average values of f_s slightly better for particles with $d_e < 2.5$ μm; however, uncertainties in f_s are still quite large.

To examine uncertainties in Eq. 4-41, the residuals (i.e., difference of measured and predicted values for f_s) were examined. The normal probability plot of the residuals is shown in Figure 4-15. Since the plotted data are approximated well by a straight line,

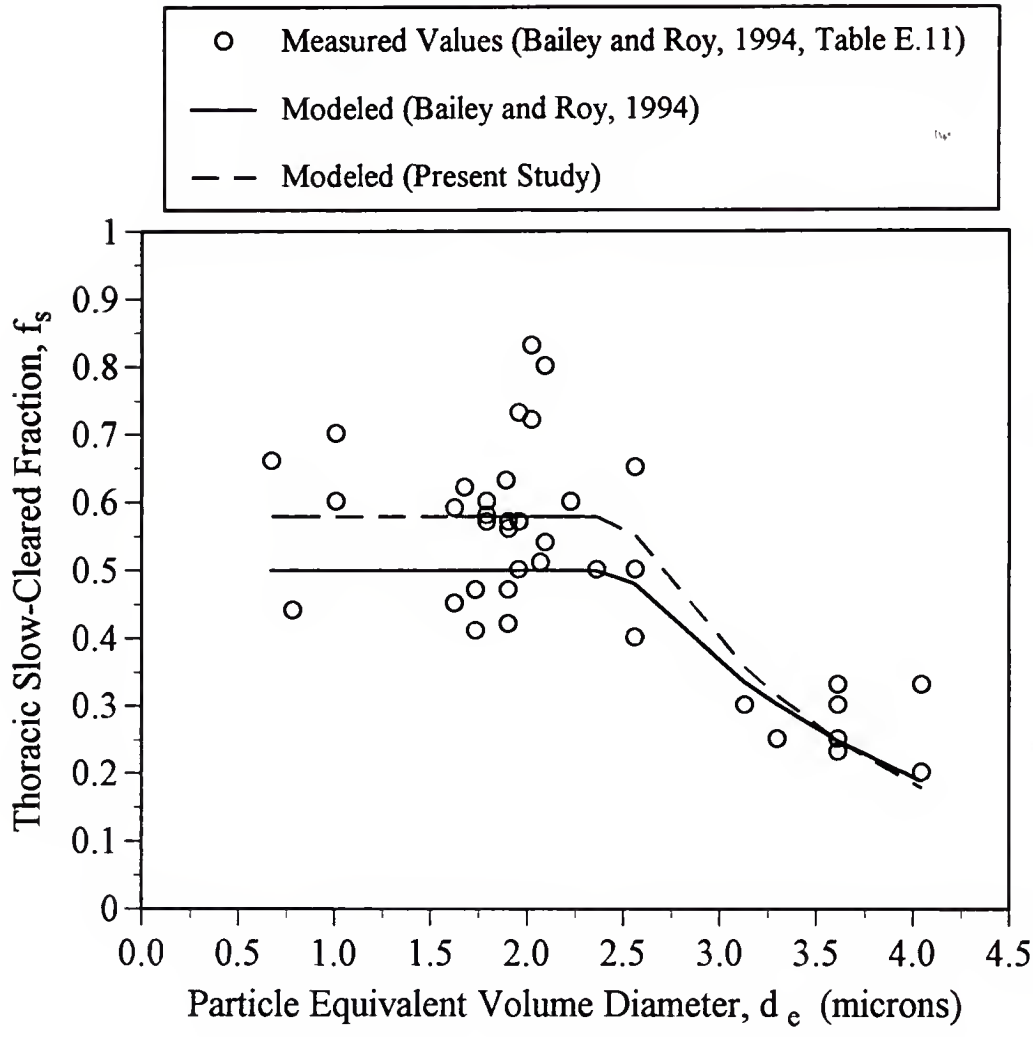

Figure 4-14. Plot of the slow-clearing fraction of material deposited in the tracheobronchial region (BB + bb) as a function of the volume-equivalent particle diameter. Based on data (with $V_{BF} < 80$ ml) compiled in Table E-11 of Bailey and Roy (1994). The solid line represents the model suggested by Bailey and Roy (Eq. 4-39); the dashed line represents the model derived (from these data) in the present study (Eq. 4-41).

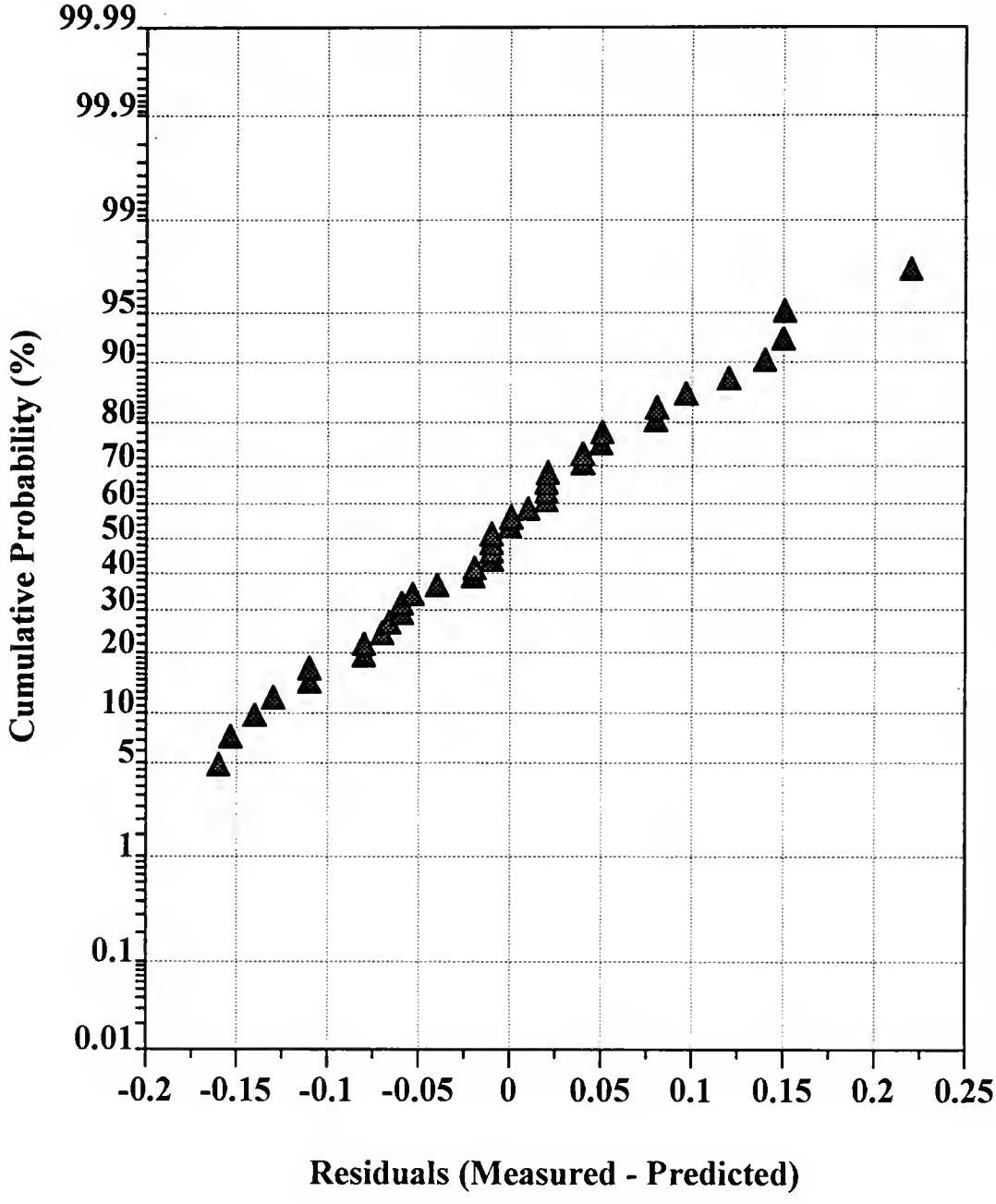

Figure 4-15. Normal probability plot of the residual errors for the slow-clearing tracheobronchial deposition fraction determined from data in Fig. 4-14 (measured values) and predictions of Eq. 4-41. The plot indicates that residuals are approximated by a normal distribution with mean of zero (50th percentile) and standard deviation of 0.1 (difference between 84th and 50th percentile).

the residuals follow (approximately) a normal distribution with a mean value of zero (i.e., the 50% fractile) and a standard deviation of about 0.1 (i.e., difference between the 84% and 50% fractiles). Therefore, for purposes of modeling uncertainties in f_s, the approach in this study was to compute an average value for f_s from Eq. 4-41 and to add a random error term, $E(f_s)$, to this value to introduce uncertainty, where $E(f_s)$ was assigned a normal distribution with mean value of zero and standard deviation of 0.1.

4.2.2.2. Clearance parameters associated with AI compartments

Three compartments are included in the clearance model to represent mechanical clearance of initial-state material from the AI (or pulmonary) region of the lungs--AI_1, AI_2, and AI_3. These compartments differ from those used in other regions (e.g., BB and bb) in that they correspond to different phases of clearance within the *same* spatial location. Compartments in other lung regions correspond both to different phases and to different spatial locations (or source regions) in the lungs when dosimetry computations are performed. In discussing uncertainty in reference values for mechanical clearance from these AI compartments, Bailey and Roy (1994) suggest that variability for all of the associated parameters not be considered. Rather, they suggest that either the fraction of material assigned to a compartment, f_d, or the fractional rate constant for clearance from that compartment, m, be considered variable--not both. This suggestion was due partly to lack of knowledge and partly to the fact that "considerable variation in the retention pattern can be achieved by altering either the amount in each compartment [i.e., value for f_d] or the clearance rates [i.e., values for m]." In order to achieve a desired level of

variability in the retention pattern (consistent with observed values for retention and clearance rates), the distributions listed in Tables 4-14 and 4-15 were recommended by those authors for $f_d(AI_1)$, $m_{2,4}$ (i.e., fractional clearance rate from compartment AI_2 to BB_1), and $m_{3,4}$ (i.e., fractional clearance rate from AI_3 to BB_1). Other relevant parameters [viz., $f_d(AI_2)$, $f_d(AI_3)$, and $m_{1,4}$] were assigned reference values. [Note that $f_d(AI_2) = 1 - f_d(AI_1)-f_d(AI_3)$ and is not an independent parameter since it depends on other partition fractions]. These recommendations were followed in the present work. However, in the computer program developed to implement methods in the current work, LUDUC, provisions are included which allow future users to specify distributions for all parameters associated with these compartments (should better information become available).

4.2.3. Fractional Clearance Rate Constants

Fractional clearance rate constants reflect the rates at which a unit of material (or activity) in a given compartment leaves that compartment by specified pathways (in this case mechanical clearance pathways, the absorption pathways, or radioactive decay). For mechanical clearance pathways, others have examined clearance rates by inhalation experiments involving both humans and animals with insoluble (radiolabelled) photon-producing materials such as ^{99m}Tc-, ^{51}Cr-, ^{59}Fe-, ^{57}Co-, or ^{85}Sr-labeled particulates composed of various iron oxides, fused aluminosilicate, teflon, polystyrene, and albumin. For absorption pathways, rates have been determined through mass balance studies using both humans and animals and results depend on the particular physico-chemical form of

Table 4-15. Distributions to describe uncertainties in fractional clearance rate constants used in mechanical clearance aspect of the ICRP *Publication 66* lung model.

Clearance Parameter	From	To	Reference Value, d^{-1}	(Half time)	Distribution (Adopted in this Study)
$m_{1,4}$	AI_1	bb_1	0.02	(≈35 d)	See note (b)
$m_{2,4}$	AI_2	bb_1	0.001	(≈700 d)	~LN(0.001, 1.41)[c]
$m_{3,4}$	AI_3	bb_1	0.0001	(≈7000 d)	~LN(0.0001, 1.73)[d]
$m_{3,10}$	AI_3	LN_{th}	0.00002		~LN(0.00002, 1.41)[c]
$m_{4,7}$	bb_1	BB_1	2	(≈8 h)	~LN(2, 1.41)[c]
$m_{5,7}$	bb_2	BB_1	0.03	(≈23 d)	~LN(0.03, 1.73)[d]
$m_{6,10}$	bb_{seq}	LN_{th}	0.01[a]	(≈70 d)	~LN(0.01, 1.73)[d]
$m_{7,11}$	BB_1	ET_2	10	(≈100 min)	~LN(10, 1.22)[c]
$m_{8,11}$	BB_2	ET_2	0.03	(≈23 d)	~LN(0.03, 1.73)[d]
$m_{9,10}$	BB_{seq}	LN_{th}	0.01[a]	(≈70d)	~LN(0.01, 1.73)[d]
$m_{11,15}$	ET_2	GI_{tract}	100	(≈10 min)	~LN(100, 1.73)[d]
$m_{12,13}$	ET_{seq}	LN_{et}	0.001[a]	(≈700 d)	~LN(0.001, 1.73)[d]
$m_{14,16}$	ET_1	Environs	1	(≈17 h)	~LN(1, 1.73)[d]

Source: Reference values and distributions are based on values proposed by Bailey and Roy (1994).

Note: ~LN(w, z) signifies that quantity is assigned a lognormal distribution with geometric mean of w and geometric standard deviation of z.

[a] Indicates that reference value is based only on animal data.

[b] As discussed by Bailey and Roy (1994), variabilities in this quantity are not specified; uncertainties in the clearance from AI_1 (the fastest-clearing AI compartment) are accommodated by uncertainties in $f_d(AI_1)$.

[c] Based on a proposed uncertainty factor ($\Phi_u \approx z^2$) of 3 for the 95% confidence interval. The 95% confidence interval for a lognormal distribution is approximately ($w \div z^2$, $w * z^2$).

[d] Based on a proposed uncertainty factor ($\Phi_u \approx z^2$) of 2 for the 95% confidence interval.

[e] Based on a proposed uncertainty factor ($\Phi_u \approx z^2$) of 1.5 for the 95% confidence interval.

the material used. Uncertainties in the mechanical clearance rate constants were extracted from discussions in the report by Bailey and Roy (1994) and are listed in Table 4-15. As with some f_d reference values, some rate constants are based on animal data; for these constants, the authors again suggested an uncertainty factor of Φ_u=3.

4.2.4. Absorption Rate Constants

The model parameters presented in Tables 4-14 and 4-15 are assumed by the ICRP *Publication 66* lung model to be independent of the radionuclide or its physico-chemical form (except for particle size characteristics). The parameters which are dependent on the radionuclide chemical form are now discussed. The discussion focuses on plutonium dioxide, $^{239}PuO_2$; consequently, the distributions for these parameters must be revised before applying methods in this study to other radionuclides/forms. Two important summaries of primarily *in vivo* studies with plutonium and other actinides were published by the ICRP (1972, 1986). The purpose of these studies was to examine the metabolism of compounds of these radionuclides arising from all routes of exposure (inhalation, ingestion, and injection/absorption). To demonstrate variability in the long-term clearance of $^{239}PuO_2$ from the lungs, information extracted from these publications is shown in Table 4-16. This information reflects long-term clearance attributable to all pathways--including mechanical and absorptive processes--from the respiratory tract. Neglecting species and other differences, long-term (fractional) clearance rates reported in the table for $^{239}PuO_2$ vary over about a factor of 10 (highest to lowest values)--from about 0.0004 to 0.004 d^{-1}. And within a given species, clearance of PuO_2 is affected by the temperature at which the

oxide was formed and by the activity median aerodynamic diameter (AMAD) of the inhaled particles. Also, the matrix or mixture of materials in which the PuO_2 exists (e.g., mixed oxides of Pu and U) has been found to influence clearance rates (ICRP 1972).

Table 4-16. Results of studies that examined long-term biological clearance of inhaled PuO_2 aerosols from the lungs.

PuO_2 Formation Temp (C)	Origin	Species	Particle Size	Long-Term Retention Halftime (days)	Long-Term Clearance Rate[c] ($days^{-1}$)	Reference
750	Oxalate	Beagle	AMD=2.3, GSD=1.9	1100	6.30E-04	Par85[a]
1000	Peroxide	Baboon	CMD=0.6, GSD=1.3	500-1300	1.39E-03 to 5.33E-04	Bair80[a]
350	Oxalate	Beagle	MMD=4.3	370	1.87E-03	Bair68[a]
450	Oxalate	Beagle	MMD=4.8	840	8.25E-04	Bair68[a]
1000	Oxalate	Beagle	MMD=2.8	780	8.89E-04	Bair68[a]
325	Chloride	Beagle	AMD=1.9, GSD=1.2	180	3.85E-03	Mew76[a]
600	Chloride	Beagle	AMD=1.9, GSD=1.2	340	2.04E-03	Mew76[a]
900	Chloride	Beagle	AMD=1.9, GSD=1.2	>500	<1.39E-03	Mew76[a]
1150	Chloride	Beagle	AMD=1.9, GSD=1.2	>500	<1.39E-03	Mew76[a]
1150	Chloride	Beagle	AMD=0.7	760	9.12E-04	Gu80a[a]
1150	Chloride	Beagle	AMD=1.4	1450	4.78E-04	Gu80a[a]
1150	Chloride	Beagle	AMD=2.8	1600	4.33E-04	Gu80a[a]
		Man		500	1.39E-03	Wa75[a] Ra70,78[a]
		Mouse	CMD=0.2	490	1.41E-03	Bair61a[b]
		Dog	MMD=4.3	1600	4.33E-04	Bair61b[b]
123	Metal	Dog	MMD=1.3	690	1.00E-03	Bair68[b]

Notes: AMD = Activity Median Aerodynamic Diameter; CMD = Count Median Diameter; MMD = Mass Median Diameter; GSD = Geometric Standard Deviation.
Data for "Man" were not from controlled experiments, but rather involved accidental inhalation scenarios.

[a] Reference cited in ICRP *Publication 48* (ICRP 1986).

[b] Reference cited in ICRP *Publication 19* (ICRP 1972).

[c] Rate derived from long-term retention half time; rate = ln(2)/halftime.

Note that Table 4-16 pertains to overall clearance from the lungs and includes both mechanical and absorption processes. It is important to consider what portion of the overall clearance is attributable to absorption to blood. The most reliable data come from mass balance studies with beagles and baboons. For a polydisperse aerosol of $^{239}PuO_2$ (prepared by calcining plutonium peroxide at 1000 °C), Bair et al. (1980, cited in ICRP 1986) reported translocation rates (to blood) of ~0.0001 d^{-1} at one thousand days after exposure for both beagles and baboons. For rats exposed to aerosols of $^{239}PuO_2$ prepared at 1200 °C, the absorption rate was almost an order of magnitude less ~0.000025 d^{-1} (cited in ICRP 1986). For hamsters exposed to mixed oxides of $^{239}PuO_2$:UO_2, the Pu was translocated to blood at even slower rates of ~0.000012 d^{-1} (cited in ICRP 1986). These values indicate that about 1-10% of the overall long-term clearance may be attributed to the absorption pathway to blood.

In addition to *in vivo* studies, a number of *in vitro* studies examining dissolution of plutonium-laden soils and aerosols in simulated lung serums have been published (e.g., Lee et al., 1982; Vashi et al., 1980; Eidson and Mewhinney, 1983; and Voillequé et al., 1987). While these studies are not generally able to provide definitive information regarding absorption rates, they can be useful for determining the fraction of the material which is rapidly solubilized in lung fluids and potentially (rapidly) absorbed to the blood. Some results of these studies are discussed below.

Lee et al. (1982) examined Pu-contaminated soils and sediments from four DOE sites--the Nevada Test Site (NTS, soil samples) , Rocky Flats (RF, soil samples), Oak Ridge National Laboratory (ORNL, pond sediment samples), and Mound Laboratory

(ML, canal sediment samples). The form of Pu was expected to be primarily PuO_2 for samples from these sites. The authors found that 0.02% (NTS and ORNL samples), 0.43% (ML sample), and 0.70% (RF sample) of the plutonium dissolved in the serum simulant after 1 day of equilibration. It is not clear whether these dissolved fractions represent PuO_2 that dissolved or other more-soluble trace forms of plutonium (e.g., $PuCl_4$) which might have been present in the samples.

Vashi et al. (1980) examined dissolution characteristics of aerosol samples of Pu collected on glass-fiber filter paper in a nuclear reprocessing plant. Two types of samples were collected. One type was "oxide aerosol samples from glove boxes." The other type was "field aerosol samples from the working environment." No other information on the samples was provided. For plutonium oxide particles in plain lung serum simulant, about 0.12% (0.0012) of the Pu dissolved within about 10 days (less than 0.2% had dissolved after 90 days); for the field Pu aerosol sample in the serum, about 4% of the Pu dissolved in 10 days (less than 7% had dissolved after 70 days). The values for the "oxide samples" are comparable to the values reported by Lee et al. (1982) for Pu-contaminated soil samples (above). From the facility sampled, mixed oxides of Pu and U might have been present in the "field samples."

Eidson and Mewhinney (1983) examined in vitro dissolution of aerosols from industrial uranium and plutonium mixed oxide fuels. Of interest here are results from the dissolution studies with aerosols generated with PuO_2 powder (calcined at 850 °C) alone (not mixed with UO_2). Results with aerosols of the PuO_2 powder indicated that less than about 0.4% of the Pu dissolved after 100 days (less than about 0.04% after 10 days) in the

serum simulant. However, for Pu in aerosols of the mixed oxide powders, anywhere from 0.4 - 4.6% of the Pu was dissolved within a couple of days.

Voilleque et al. (1987) used dissolution studies to estimate dissolution rate constants for transuranic radionuclides in a steam-generator work environment at a nuclear power plant. Dissolution rates, averaged over 21 days, for various plutonium compounds were all <0.0003 d^{-1}; in other words < 0.6% (i.e., 0.0003 d^{-1} x 21 d) of the Pu dissolved into the serum simulant in 21 days. No information was provided regarding the chemical form of the Pu (e.g., oxides, chlorides, etc.); however, it is expected that Pu was primarily in the oxide form (most likely a result of neutron absorption by ^{238}U nuclei in uranium oxide reactor fuel).

4.2.4.1. Uncertainty in the rapidly absorbed component

The ICRP (1994) suggests that a small fraction, $f_r = 0.001$ (or 0.1%), of Class S (formerly Class Y) material deposited in the lungs is rapidly absorbed to the blood with a fractional absorption rate of $s_r = 100\ d^{-1}$. This rate was chosen to make the absorption of this small fraction virtually immediate and corresponds to a half time of about ten minutes. The other 99.9% of the material is assumed to be absorbed to blood at a very slow fractional rate of about 0.0001 d^{-1} (corresponding half time ~ 7000 days). Since the fraction that clears rapidly is very small (i.e., ~0.1% of the activity), uncertainties in this quantity are not expected to be important to the overall variability in *lung* doses. However, if one were concerned with systemic organ doses from Pu (e.g., dose to

endosteal surfaces, bone marrow, liver, or gonads), uncertainties in f_r could be very important. The present study was concerned with uncertainties in lung dose only.

Based on information from the *in vitro* studies above, f_r (for PuO_2) was assigned a uniform distribution from 0.0005 to 0.005 (or 0.05 - 0.5%). This distribution covers the range of most of the results reported above and provides a median value equal to the ICRP reference value for class S materials. If site-specific solubility information were available, this distribution could (and should) be adjusted to match the rapidly dissolved fraction of Pu for aerosols from that site. The absorption rate constant, s_r, for the rapidly absorbed fraction was assigned a lognormal distribution with geometric mean equal to the ICRP (1994) recommended value of 100 d^{-1} and a GSD of 3.2. This GSD value was chosen to introduce an uncertainty factor of about $\Phi_u = 10$ for this parameter. This parameter is not expected to be important for plutonium oxides since it corresponds to such a short clearance half time (~minutes).

4.2.4.2. Uncertainty in the slowly absorbed component

The ICRP recommends a fractional rate constant of $s_s = 0.0001$ d^{-1} for absorption of the slow-clearing component of Class S (formerly Class Y) materials to the blood. This value agrees with beagle and baboon experiments by Bair et al. (1980). To accommodate uncertainties in the fractional clearance rate of the slowly absorbed component of plutonium oxides, s_s was assigned a lognormal distribution with a median value of 0.0001 d-1 (ICRP reference value) and a GSD of 3.2. This GSD corresponds to an uncertainty factor of about 10 (i.e., $GSD^2 \sim 10$ and the lower and upper 95% confidence bounds are

~0.00001 and ~0.001, respectively). The lower bound agrees with the very slow absorption rates presented for rats exposed to mixed U:Pu oxides; the upper bound agrees with the data presented in Table 4-16 for overall clearance of plutonium oxide from the lungs. Figure 4-16 shows the relative impact of uncertainties in parameter s_s (= s_l) on the total number of ^{239}Pu disintegrations that occur in the lungs as a function of the integration time. Data in this figure were derived by solving the deposition and clearance models; reference values were used for all parameters but s_s. Values used for s_s are indicated in the figure and correspond to the lower 95% confidence limit (or 2.5 percentile--0.00001d^{-1}), the median (50 percentile--0.0001 d^{-1}), and the upper 95% confidence limit (97.5 percentile--0.001 d^{-1}) of the distribution suggested above. Generally, for an acute activity intake, a variability of s_s over the range of 0.00001 to 0.001 d^{-1} (i.e., two orders of magnitude) results in a variability of about a factor of four (upper to lower 95% bounds) for the total disintegrations. The same computations were performed for other particle aerodynamic diameters ranging from 0.1 to 10 μm; and although not shown, the results were similar. Dose is generally proportional to the total disintegrations; these results show that, within the range of values examined, the model is not too sensitive to changes in s_s which possesses a large degree of uncertainty.

The absorption model accommodates mechanisms which can bind dissolved material to the tissues in the lungs. The ICRP (1994, p. 74) stated that "the need to use the bound state will mainly arise for materials that are soluble in water but bind to tissues." The model parameters necessary to quantify this bound state are denoted as f_b and s_b. The parameter f_b represents the fraction of the deposited material that transfers to the bound

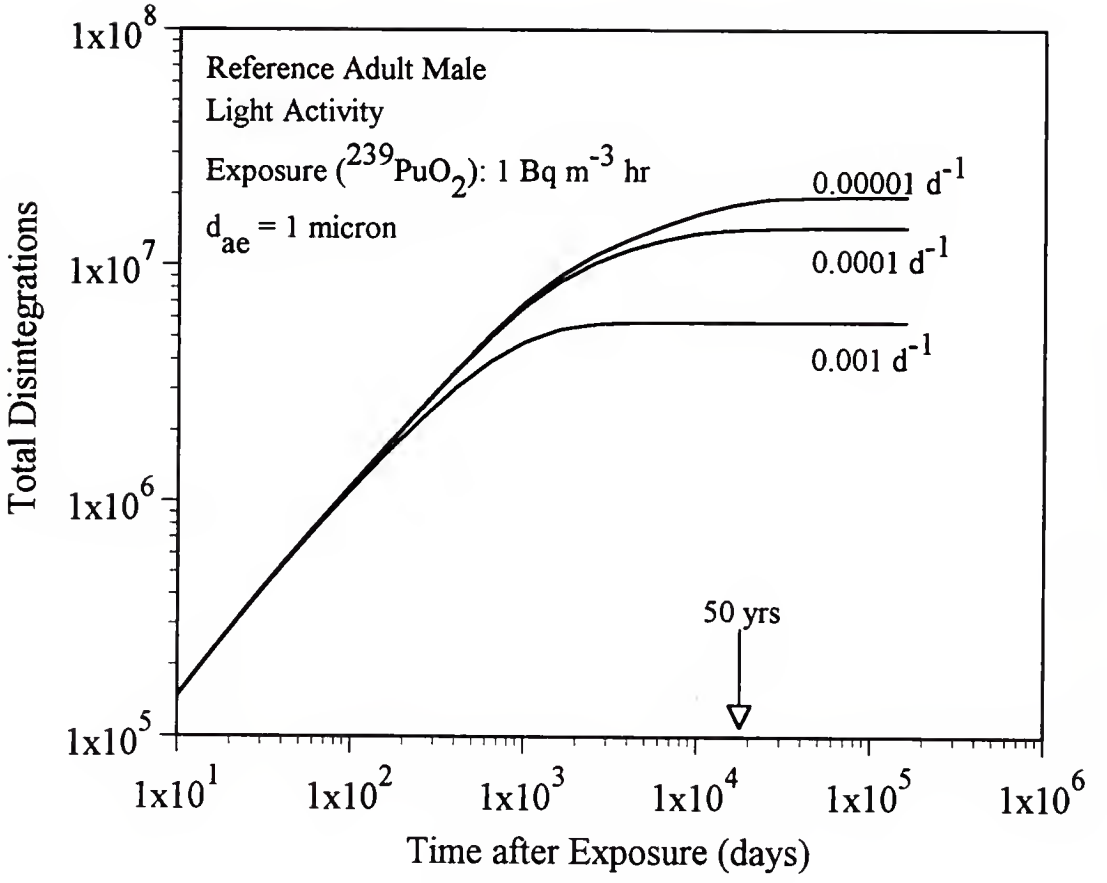

Figure 4-16. Total ^{239}Pu disintegrations in the lung as a function of time for three values of s_s (the fractional absorption rate for the slow-clearing component) representing minimum, median, and maximum values adopted in this study. An acute exposure scenario has been assumed (A_E = 1 Bq-hr/m^3 of $^{239}PuO_2$; d_{ae} = 1 μm, monodisperse, unit density sphere) for reference adult man at light activity (i.e., V_E = 1.5 m^3/hr).

state and s_b represents the fractional clearance rate for materials from the bound state to blood. In the case of plutonium oxides (relatively insoluble in water), the bound state compartments (e.g., see equations for ET_{bnd}, BB_{bnd}, bb_{bnd}, AI_{bnd} in Appendix B) are not needed. The ICRP (1994) recommends that f_b be set equal to zero for class S materials that are insoluble in water. This approach was adopted in this research ($f_b = 0$) ; and no uncertainties were considered in f_b. Since f_b equals zero, there was no need to quantify s_b. However, provisions were included in the computational code developed to implement this research (i.e., LUDUC; discussed in section 3.6) which allow future users to specify distributions (uniform, triangular, normal, or lognormal) for both f_b and s_b.

4.2.4.3. Summary of distributions for absorption aspect

Table 4-17 summarizes distributions selected for parameters related to the absorption aspect of the clearance model. The upper panel lists parameters required by an alternative but equivalent form of the absorption model. The lower panel lists the parameters directly required by the mathematical model and their relationships to the alternative (upper panel) model parameters (e.g., see Appendix B for mathematical model). Parameters in the upper panel are generally more easily determined from experimental results than parameters in the lower panel.

Table 4-17 Distributions and relationships adopted to describe the absorption aspect of clearance in the ICRP *Publication 66* lung model based on $^{239}PuO_2$ aerosols.

Parameter	Description (f.c. = fractional clearance)	Reference Value[a]	Distribution[b,c] or Relationship
f_r	fraction of material rapidly dissolved	0.001	~LN(0.001, 3.2)
s_r	fractional absorption/dissolution rate for fast phase	100 d^{-1}	~LN(100, 3.2)
s_s	fractional absorption/dissolution rate for slow phase	0.0001 d^{-1}	~LN(0.0001, 3.2)
s_p	f.c. rate from initial state to blood compartments	0.1 d^{-1}	$s_p = s_s + f_r (s_r - s_s)$
s_{pt}	f.c. rate from initial state to transformed state compartments	100 d^{-1}	$s_{pt} = (1 - f_r)(s_r - s_s)$
s_t	f.c. rate from transformed state to blood compartments	0.0001 d^{-1}	$s_t = s_s$
f_b	fraction of material reaching bound state compartment	0	0 (see note d)
s_b	f.c. rate from bound state to blood compartments	---	see note d

[a] Reference values are based on ICRP *Publication 66* (ICRP 1994, p. 76) for Type *S* materials (relatively insoluble in the respiratory tract; or slow solubilization).

[b] ~LN(w, z) signifies that quantity is assigned a lognormal distribution with geometric mean of w and geometric standard deviation of z. The geometric standard deviation for distributions in the table (z = 3.2) corresponds to an assumed 95% confidence interval given by a factor of 10 (w÷10, w·10).

[c] The dividing line in the table separates two alternate models for absorption. The models are related by the equations in the last column of the table.

[d] The bound state compartment, although defined in the model, has not been assigned reference values for Type S materials since the fraction of material translocated to the bound state is taken to be zero.

4.3. Dose Model Parameters

4.3.1. Introduction

Dose model parameters consist primarily of quantities which characterize source and target tissue geometries for the various respiratory tract regions. Of interest are variabilities in source and target tissue depths and thicknesses. These dimensions are important for short range radiations such as low energy beta and alpha particles. Source and target regions defined for the ICRP *Publication 66* respiratory tract model have been described in Chapter 3. The target regions of interest include the basal cell nuclei layer in the ET regions, basal and secretory cell nuclei layers in the BB region, the secretory (Clara) cell nuclei layer in the bb region, and the total tissue mass of the AI region. In addition to depths and thicknesses, variabilities in the surface area of ET, BB, and bb airway regions are needed in order to estimate uncertainties in the source region volumes and target region masses. The volume of a given source/target region is approximated by the product of the surface area of the region and the thickness of the source/target region. Finally, variabilities in certain target tissue masses (e.g., AI and lymph node masses) must also be determined.

Dimensions of the bronchial epithelium and of the target cell layers contained within it are important for short range radiations such as alpha and beta particles. The ranges of alpha particles at some selected energies are shown in Table 4-18 for unit density water. For comparison, average alpha-particle energies for Pu-239 and Am-241 are 5.1 and 5.5 MeV, respectively, corresponding to tissue ranges of about 40-45 μm.

Alpha particles emitted by Po-214 (an important radon daughter) have energies of 7.7 MeV, corresponding to tissue depths greater than about 70 μm. Water at unit density is a close approximation to soft tissues with respect to energy absorption from alpha particles. Alpha particles in the 4-7 MeV range penetrate to distances on the order of the thickness of the epithelium in the bronchial (BB) region; therefore, dimensions of the bronchial epithelium and layers of target cells are expected to be sensitive factors in lung dosimetry.

Table 4-18. Range of alpha particles in water for given energies.

Energy (MeV)	Range (μm)	Energy (MeV)	Range (μm)
4.0	27	6.0	50
4.5	32	6.5	56
5.0	38	7.0	63
5.5	43	7.5	71

Source: Based on density range values reported in ICRU Report 49 (ICRU 1993). Assumes unit density water.

4.3.2. Measurements of the Bronchial Epithelium and Critical Cell Layers

A literature search for published work on lung tissue dimensions identified the following useful studies--Gehr (1994), Trevisani et al. (1992), Baldwin et al. (1991), Mercer et al. (1991), Bowden and Baldwin (1989), Gies et al. (1987), and Gastineau et al. (1972). The study by Bowden and Baldwin (1989) apparently involved the same data and results as Baldwin et al. (1991). One difficulty in estimating tissue thicknesses in the lung epithelium is that tissue specimens generally come from surgical procedures to remove diseased tissue from subjects; the possibility for bias then exists in many of the results reviewed here.

Gehr (1994, Tables A.2, A.3, and A.4) reported estimates of various dimensions of the trachea, bronchus, and bronchioles. These were "unpublished, preliminary data, based on a few randomly selected samples only" and covered ages from 26 days to 39 years. Data reported for children of ages 5 yrs down to 26 days indicate that cilia length, epithelium thickness, and airway wall thickness in both bronchi and bronchioles are not different from those found in adults. In the bronchial region, cilia length ranged from 5.3 - 8.0 μm; epithelium thickness ranged from 27 - 35 μm; wall thickness ranged from about 400-1300 μm; and connective tissue (musculature thickness) ranged from 250 - 1260 μm. In bronchioles, cilia ranged from 5-7 μm; epithelium height ranged from 11-21 μm; wall thickness ranged from 33-93 μm; and connective tissue (musculature thickness) ranged from 12-75 μm. For a bronchus (~generation 4), Gehr reported the thickness of the subepithelial layer at about 500 μm; for a bronchiole (~generation 15) this thickness was only about 20μm.

Trevisani et al. (1992) examined 70 biopsy specimens taken from the bronchial epithelium (main bronchus, generation 1) of 40 smokers (27 with chronic bronchitis and 13 asymptomatic). The authors found significant differences in the mean thickness of the bronchial epithelium ($p < 0.001$), the number of layers of basal cells ($p < 0.001$), and the thickness of the zone occupied by basal cells ($p < 0.01$), among other quantities, in chronic bronchitics compared to asymptomatic smokers. For asymptomatic smokers the epithelium thickness was 47.3 ± 2.0 μm (mean ± standard error of mean, n=13); the number of basal cell layers was 2.55 ± 0.26 (n=13); and the thickness of the zone occupied by basal cells was 19.95 ± 1.41 μm. For chronic bronchitics all of these values

were significantly larger. Gies et al. (1987) examined effects of cigarette smoking in dogs and found no differences in the thickness of the epithelium for smoking compared to non-smoking group of dogs. Baldwin et al. (1991, discussed below) also found no significant differences between epithelium height in human smokers versus non-smokers. As a general conclusion, dimensions of the epithelium for smokers do not seem to differ from nonsmokers, unless symptoms of respiratory disease (e.g., bronchitis) exist. A major limitation of this study is that it was based on measurements from only the main bronchi (generation 1); no comparisons (smokers versus nonsmokers) were found for smaller airways (bronchioles).

Based on 116 measurements of human tissue specimens (from an unknown number of persons), Gastineau et al. (1972) published summary data characterizing a number of dimensions in the bronchial epithelium. Quantities measured were thickness of epithelium, length of cilia, and basal cell layer thickness for main-stem, lobar, segmental, and subsegmental, and transitional bronchi, and bronchioles. Summary data are repeated in Table 4-19, where approximate airway generation numbers have been added to clarify the relationship with the respiratory tract regions defined for modeling purposes. The distance from the epithelial surface to basal cell layer is approximately the difference between the epithelial thickness and the basal cell layer thickness. The authors suggested a mucus layer thickness of 7 μm, although this quantity was not measured. With regard to uncertainty and variability, Gastineau et al. presented histograms (Fig. 1 in that paper) for the relative number of measurements of epithelial thickness that fell within 10 μm intervals. The

histogram curves for lobar/segmental bronchi and bronchioles gave an indication of a bell shaped curve for the distribution in epithelium thickness among subjects.

Table 4-19. Summary data for bronchial epithelium based on study by Gastineau et al. (1972).

Bronchus Region (airway generation)	Epithelium Thickness (μm)	Cilia Length (μm)	Basal Cell Layer Thickness (μm)	Number Measured
Main-stem (1)	80 (70-85)[a]	7.5 (7.5-10)	10 (7.5-10)	6
Lobar (2)	50 (25-70)	7.5 (5-12.5)	7.5 (5-10)	20
Segmental (3)	50 (15-100)	7.5 (2.5-10)	7.5 (5-10)	63
Subsegmental (4)	50 (50-70)	8.5 (7.5-10)	7.5 (7.5-15)	3
Transitional (~ 8-9)	20 (12.5-30)	7.5 (5-7.5)	7.5 (5-7.5)	12
Bronchioles (~ 9-15)	15 (5-30)	5 (2.5-7.5)	Not present	12[b]

Source: Gastineau et al. (1972)
[a] Format for all table entries is median value (observed range in parentheses).
[b] Only n = 6 measurements for basal cell layer thickness column (n = 12 for others).

Baldwin et al. (1991) recently reported results of measurements of epithelium surface-to-nuclear distances in the human bronchial epithelium. The authors examined 29 surgically removed tissue specimens from patients undergoing lobectomy or pneumonectomy for various conditions (26 of the samples were from smokers). Measurements were made for airway generations 1-16. The authors found no significant difference in epithelial thickness between smokers and nonsmokers. The composite data (smokers and non-smokers) are listed in Table 4-20. The authors recommended a value of 5 μm for the mucus layer thickness, although this quantity was not measured. A few dust-laden macrophages were also identified in the tissue region beyond the basement

membrane (in generations 4-16); the authors found distances from these macrophages to range from 4.11-9.03 μm for typical basal cell nuclei and for 3.4-4.0 μm for "atypical" basal cells.

Table 4-20. Summary data for bronchial epithelium measurements based on study by Baldwin et al. (1991).

Airway Generation	Ciliary Height (μm)	Surface to Basement Membrane Distance[b] (μm)		Surface to Cell Nuclei Distance[c] (μm)		
		Ciliated[d]	Non-ciliated	Non-Ciliated	Basal (typical)	Basal (atypical)
1	6.52[a]	31.17	29.57	10.08	26.65	23.34
	(0.21)	(2.23)	(4.77)	(2.49)	(2.36)	(2.40)
2	6.40	31.98	32.91	13.05	25.83	21.33
	(0.41)	(4.87)	(2.90)	(1.67)	(3.96)	(5.07)
3	6.29	29.02	23.65	9.10	24.08	17.19
	(0.21)	(3.03)	(3.07)	(1.59)	(2.22)	(1.36)
4	6.02	25.32	24.99	9.10	22.02	20.11
	(0.18)	(2.13)	(1.24)	(1.09)	(1.29)	(1.84)
5-7	5.84	27.35	21.51	7.32	24.59	18.15
	(0.13)	(1.63)	(1.67)	(0.53)	(1.76)	(1.08)
7-16	5.58	20.94	17.76	6.41	17.46	15.98
	(0.12)	(1.37)	(1.19)	(0.59)	(0.93)	(1.19)

Source: Baldwin et al. (1991).
[a] Format for all table entries is mean value (standard error of mean--below mean).
[b] Distance from epithelial surface to basement membrane for indicated cell type.
[c] Distance from epithelial surface to nuclei of indicated cell type.
[d] Cilia height subtracted from value.

Mercer et al. (1991) examined the depth distribution of nuclei in human and rat lungs. The human lobar tissue samples were obtained from surgical resections of three nonsmokers who had normal pulmonary function tests and normal chest radiographs, except for small lesions. Epithelial thicknesses determined in that study are shown in Table 4-21. The authors commented on the procedures used in the work, implying that

Table 4-21. Summary data for bronchial epithelium measurements based on study by Mercer et al. (1991).

Airway Diameter (mm) (approx. generation)	Epithelial Thickness[a] (μm)	Basal Cell Nuclei Depth Range[c] (μm)	Secretory/Clara Cell Nuclei Depth Range[c] (μm)
5 - 3 mm (4 - 6)	57.8 (~2.9)[b]	20 - 52	10 - 50
3 - 1 mm (6 - 11)	50.0 (~2.1)	20 - 50	20 - 48
< 1 mm (11 - 15)	~16 (~1.4)	not reported	not reported
Terminial bronch. (15-16)	9.8 (~1.4)	basal cells not present	2 - 8

Source: Mercer et al. (1991).
[a] Format for entries in column is mean and (standard error of mean in parentheses, N = 3).
[b] Values preceded by "~" were estimated graphically (from Fig.4 of Mercer et al., 1991).
[c] Values in these columns were estimated from Tables 1, 2, and 3 in Mercer et al. (1991).

their methods resulted in improved measurements compared to those of Gastineau et al. (1972). The thickness of the interstitial space between the bronchiolar airway epithelium and the adjacent alveoli was 11.2 ± 4 μm (mean ± SE, N=3). For bronchi the interstitial space varied from 169 μm (d=1-2 mm) to 516 μm (d=3-5 mm). This range of distances for the bronchi is well outside of the range (in tissue) of alpha particles emitted by radionuclides. The authors reported that the epithelial thickness in different bronchial rings varied by as much as 35% from the mean. Another finding was that only minor differences existed between distributions of nuclei in large and small bronchi (5-3 mm versus 3-1 mm). The authors reported mucus thickness measurements of about 15 μm. The authors also reported the distribution of various cell types (including ciliated, preciliated, basal, goblet, Clara and other secretory cells) per distance into the epithelium. From data reported, secretory cells appeared to be uniformly distributed over the range of

the epithelium; basal cells appeared at a depth of about 30% of epithelium thickness with increasing occurrence as the basement membrane was approached.

4.3.3. Extrathoracic Region

The extrathoracic region (comprising compartments ET_1, ET_2, ET_{seq}, and ET_{bnd}) is relatively resistant with respect to biological effects of radiation. In fact, critical cell layers in ET regions are not included as target tissues in the ICRP (1991a) system of radiation protection (i.e., ET tissues receive no effective-dose tissue weighting factors). For this reason the default tissue parameters recommended by the ICRP (1994) were used in the present work to model dose in these regions without accounting for variability in tissue parameters. However, parameter variabilities in the deposition and clearance components for the ET regions (discussed in previous sections) were included in analyses.

4.3.4. Bronchial Region

Source components in the bronchial (BB) region (airway generations 0 to 8) include radionuclides: (1) located in the mucus/gel layer (represented by compartments: $BB_1 + BB_{1T}$), (2) located in the sol/cilia layer ($BB_2 + BB_{2T}$), (3) sequestered by macrophages, etc., in the airway wall ($BB_{seq} + BB_{seq,T}$), (4) bound chemically in the airway wall (BB_{bnd}), and (5) located in the AI region with sufficient energy to irradiate targets in the BB region ($AI_1 + AI_2 + AI_3 + AI_{1T} + AI_{2T} + AI_{3T} + AI_{bnd}$). The ICRP lung model assumes that radioactive material present in these source regions is uniformly dispersed throughout the volume of the region.

Radiation dosimetry in the BB region is computed for two target tissues, (1) the secretory cell (nuclei) layer, BB_{sec}, and (2) the basal cell (nuclei) layer, BB_{bas}. These cell types are believed to be susceptible to radiation effects since both are capable of division and are suspected to be progenitors of other bronchial cells (e.g., Keenan et al. 1982a, 1982b; McDowell et al. 1984, 1985, Evans et al. 1986, Ayers and Jeffery 1988). The geometry of these tissue layers (depths and thicknesses of layers in the epithelium) must be specified for dosimetry computations to be performed.

This research focused on alpha particle radiation types only. For such radiations the source component (5) does not contribute to the dose in the BB region. The thickness of interstitial tissues between AI region and BB epithelium is greater than the range of alpha particles (Table 4-18); e.g., Mercer et al. (1991) reported interstitial tissue thicknesses greater than 100 μm.

4.3.4.1. Mucus/gel layer (BB_1+BB_{1T})

The mucus (or gel) layer thickness for bronchial airways was reported by the references above as 5 μm (Baldwin et al., 1991), 7 μm (Gastineau et al., 1972), and 15 μm (Mercer et al. 1991). Harley and Pasternack (1972) also suggested a value of 15 μm for the mucus layer. From the context, the values reported by Mercer et al. and Harley and Pasternack included the thickness of the ciliary layer; so these values should be decreased by about a factor of two. In addition Gehr (1994) reported a mucus layer thickness of 5 μm for a bronchus (approximately generation 4). Based on these limited data, the thickness of the mucus layer (BB region) was modeled in this study by a triangular

distribution with minimum, mode, and maximum values equal to 4, 6, and 8 μm, respectively.

4.3.4.2. Cilia/sol layer (BB_2+BB_{2T})

The cilia (or sol) layer is between the mucus (gel) layer and the epithelium surface; the cilia move the mucus layer toward the pharynx. Gastineau et al. (1972) reported values for cilia length in generations 1-7 ranging from 2.5 - 12.5 μm (all generations), with a median value of about 7.5 μm. This range is based on the extreme values for all generations (see Table 4-19). Baldwin et al. (1991) reported values in bronchi ranging from about 5.7 - 6.7 μm (based on means and standard errors, Table 4-20). Gehr (1994, Table A.3) reported values from about 5 - 8 μm. Based on this limited information, the cilia layer thickness (BB region) was modeled in this study by a triangular distribution with minimum, mode, and maximum values equal to 4, 7, and 10 μm, respectively.

4.3.4.3. Sequestered material (BB_{seq}+$BB_{seq,T}$)

Sequestered material in the airway wall of the BB region is assumed by designers of the ICRP respiratory tract model (ICRP 1994) to reside in a macrophage layer in the lamina propria (at a default depth of 5 μm beyond the basement membrane). The only values located which helped to quantify the depth and thickness of this layer were reported by Baldwin et al. (1991). They identified dust-laden macrophages, albeit a limited number, in airway generations 4 - 16 and found distances from these macrophages to typical basal cell nuclei to range from about 4 - 9 μm. Using the difference in these reported ranges, a thickness of about 5 μm can be inferred for the macrophage layer. This

thickness is on the order of the diameter of the macrophage (~10 μm). A reference thickness of 10 μm is adopted by the ICRP (1994). Lacking better data, and noting the ICRP recommendation, the uncertainty in the thickness of this source region was modeled by a uniform distribution with minimum and maximum values of 5 and 15 μm. Based on the ranges cited above, the depth of this layer with respect to basal cells is about 5 to 10 μm. The ICRP recommends a reference value of 5 μm for the depth with respect to the basement membrane of the epithelium; this value is reasonable if basal cells are located approximately 5 μm from the basement membrane. The depth of the (sequestered material) macrophage layer (with respect to basement membrane) was taken to be uniformly distributed from 0 to 10 μm with a mean of 5 μm.

4.3.4.4. Thickness of BB epithelium

To compute the depth of the sequestered material as well as the range of possible depths for basal and secretory cells, the thickness of the BB epithelium is needed. The ICRP (1994) recommends a default value of 55 μm for the thickness. However, from the data presented in previous tables, a large discrepancy is seen in epithelial thicknesses for airways in the BB region.

The dose model assumes that source material is uniformly distributed with respect to surface area of the airways in the region. Based on the ICRP reference man morphological model listed in Table 4-6, generation 6 represents the median generation with respect to surface area in the BB region (i.e., half of the surface area is associated

with generations 0 to 6 while half is associated with generations 6 to 8). Therefore, the thickness of the epithelium in generation 6 is most representative for the BB region.

For generation 6, Mercer et al. reported thicknesses between about 50 and 58 μm; Baldwin et al. reported a thickness of about 27 μm (based on ciliated cells); Gehr (1994, Table A.3) reported preliminary values from 27 to 35 μm for bronchial airways (no generations specified); and a value between about 20 and 50 μm was deduced from results of Gastineau et al. Based on these values, the thickness of epithelium in the BB region was modeled by a uniform distribution with a minimum value of 25 μm and a maximum value of 60 μm. This distribution results in a median value of 42.5 μm which is much less than the default value of 55 μm, chosen by the ICRP.

The consistently lower values of epithelial thickness provided by Baldwin et al. (1991) lead one to question whether shrinkage or expansion of samples was a factor in the experimental protocol. The authors did perform tests to determine the influence of shrinkage and found that samples shrunk by about 4%; however, this effect was compensated by expansion (~3%) in another aspect of the sample preparation. No information was provided regarding shrinkage or expansion corrections for results of Mercer et al. (1991). Gastineau et al. (1972) addressed shrinkage by calibration procedures.

4.3.4.5. Bound material (BB_{bnd})

For materials which become chemically bound in the airway wall, the radionuclide concentration is assumed (ICRP 1994, p. 86) to be uniform throughout the epithelium and

to a depth of 5 μm beyond the epithelium. Therefore, the thickness of this region is equal to the thickness of the epithelium plus an additional 5 μm. Although this bound compartment is included in the clearance and dosimetry models, it only becomes important when the bound material fraction f_b is greater than zero. As discussed in section 4.2.4, for plutonium oxides, $f_b = 0$; so this source region accumulates no radioactive material and its thickness is irrelevant. For future use with other materials, however, the thickness of this region was assumed to equal the thickness of the epithelium plus 5 μm (as described by the ICRP 1994). Uncertainties in thickness are then accommodated by uncertainties in the epithelium thickness discussed above.

4.3.4.6. Secretory cell layer (BB_{scc})

Depths and thicknesses of secretory cells in the bronchial epithelium of the BB region have been measured by Baldwin et al. (1991) and by Mercer et al. (1991). These dimensions were summarized in Tables 4-20 and 4-21 above. Baldwin et al. (1991) reported that the distances between the epithelial surface and nuclei of these cells "do not vary significantly throughout the bronchial tree [generations 0 to 16]." Measurements by Mercer et al. (1991) indicate that secretory cell nuclei are located throughout the bronchial epithelium--except that these nuclei were not generally seen within a few microns of either the epithelial surface or the basement membrane. Baldwin et al. (1991) reported values of about 10 to 7 μm (generations 1 to 7) for the average depth (to surface) of nonciliated cell nuclei in the epithelium. However, Mercer et al. (1991) reported a minimum depth of nuclei of about 10 μm in generations 3 to 6 (5 to 3 mm diameter) and a depth of about 20

μm in generations 6 to 11 (3 to 1 mm diameter). Based on these measurements, the depth of secretory cell nuclei layer is modeled by a uniform distribution spanning 5 to 15 μm (median value of 10 μm). The thickness of this target layer is determined from the following expression:

(thickness of BB_{scc}) = (BB epithelium thickness) - (depth of BB_{scc}) - (5 μm) (4-42)

where 5 μm is subtracted to agree with results that secretory nuclei were not seen within a few microns of the basement membrane. A further constraint on the thickness is that it be at least 5 μm (roughly the diameter of the cell nucleus). The ICRP (1994) suggests reference values of 10 μm for the depth and 30 μm for the thickness of this target tissue. Using the distribution above results in a median thickness of about 30 μm and a median depth of 10 μm; both agree with ICRP recommendations.

4.3.4.7. Basal cell layer (BB_{bas})

According to measurements by Gastineau et al. (1972) the basal layer thickness ranged from 5 to 15 μm, and the thickness of the layer did not change significantly throughout the bronchial region (generations 1 to 8). Mercer et al. (1991) indicated the thickness of the basal cell layer (nuclei) to be about 15 μm for generations 4 to 11 (airway diameters 5 to 1 mm); their results, although numerically different from Gastineau et al., also indicate that the thickness is relatively constant throughout the bronchial region. Similar to secretory cell nuclei, no basal cell nuclei were reported within a few microns of the basement membrane by Mercer et al. Baldwin et al. (1991) reported a relatively constant average depth of basal cell nuclei to about 25 μm for generations 1to 7. Based

on these limited data, the thickness of the basal cell nuclei layer is modeled by a uniform distribution between 10 and 20 microns. The depth of the basal layer with respect to the epithelium surface is assumed to be given by:

(depth of BB_{bas}) = (BB epithelium thickness) - (BB_{bas} thickness) - 5 μm (4-43)

where the 5 μm term is included to account for the fact that nuclei were not observed within a small distance of the basement membrane (Mercer et al. 1991). A constraint included in the methodology is that the depth be at least 5 μm into the epithelium. The ICRP (1994) has suggested a depth of 35 μm and a thickness of 15 μm for the basal cell nuclei layer. A median epithelium thickness of 45 μm (above) and median basal cell (nuclei) layer thickness of 15 μm results in a median basal nuclei depth of about 25 μm using Eq. 4-43. This value agrees with the results of Baldwin et al. (1991)--average basal cell nucleus depth of about 25 μm.

4.3.5. Bronchiolar Region

Source components in the bronchiolar (bb) region (airway generations 9 to 15) include radionuclides: (1) located in the surface mucus/gel layer (model compartments: bb_1 + bb_{1T}), (2) located in the cilia/sol layer (bb_2 + bb_{2T}), (3) sequestered (e.g., by macrophages) in the airway wall (bb_{seq} + $bb_{seq,T}$), (4) bound chemically in the airway wall (bb_{bnd}), and (5) located in the AI region that can irradiate targets in the bb region (AI_1 + AI_2 + AI_3 + AI_{1T} + AI_{2T} + AI_{3T} + AI_{bnd}). The ICRP model assumes that radioactive material present in these source regions is uniform throughout the volume of the regions.

Radiation dosimetry in the bb region is computed for one target tissue, the secretory, or Clara, cell (nuclei) layer. Basal cells are rarely found in the bronchioles (Bartels, 1983; Mercer et al., 1991) and are not included as targets in the bb region. The geometry of the secretory cell (nuclei) layer (depths and thickness of layer in the epithelium) must be specified for dosimetry computations to be performed.

4.3.5.1. Mucus/gel layer ($bb_1 + bb_{1T}$)

Gehr (1994) reported a mucus layer thickness of 2 μm for a bronchiole (approximately generation 15); no other values were found. This value has been adopted by the ICRP (1994). As an upper limit, the minimum value for the mucus layer in the BB region was about 4 μm. Uncertainty in the mucus layer thickness is accommodated by a uniform distribution from 1 to 3 μm. The measured value of 2 μm then represents the median value. The uncertainty in this thickness is not expected to influence dose calculations significantly since the thickness is only about 5% of the range of most alpha particles (based on a 5 MeV particle in soft tissue).

4.3.5.2. Cilia/sol layer ($bb_2 + bb_{2T}$)

The thickness of the cilia (or sol) layer in the bb region is smaller than the thickness for larger airways. Baldwin et al. (1991) reported an average value of 5.6 μm for the cilia height in generations 7 to 16. Gehr (1994, Table A.2) recently reported values of 4 to 5 μm in generation 15 bronchioles. Based on this limited information, the cilia layer thickness (BB region) is modeled by a uniform distribution with minimum and maximum

values equal to 3 and 6 μm, respectively. The ICRP has adopted a value of 4 μm for the thickness of the cilia region.

4.3.5.3. Sequestered material ($bb_{seq} + bb_{seq,T}$)

Sequestered material in the airway wall of the bb region is assumed by designers of the ICRP respiratory tract model to reside in a (5 μm thick) macrophage layer in the lamina propria (at a depth of 5 μm beyond the basement membrane). As reported above, Baldwin et al. (1991) identified a limited number of dust-laden macrophages in airway generations 4 to 16 and found distances from these macrophages to basal cell nuclei to range from 4 to 9 μm (typical basal cells). Using the difference in these reported ranges, a thickness of about 5 μm can be inferred for the macrophage layer and a distance from basal cells is about 4 to 10 μm. Lacking additional data, the uncertainty in the thickness of this source region is modeled by a uniform distribution with minimum and maximum values of 4 and 10 μm, respectively. The depth of the (sequestered material) macrophage layer with respect to the basement membrane is represented by a uniform distribution with minimum and maximum of 0 and 10 μm, respectively.

4.3.5.4. Thickness of epithelium in bb region

To compute the depth of the sequestered material as well as the range of possible depths for secretory cell nuclei (target layer), the epithelium thickness in the bb region is needed. The ICRP (1994) has recommended a default value of 15 μm for the thickness. Gastineau et al. (1972) observed a range of 5 to 30 μm (15 μm median) for the thickness of the epithelium in bronchioles; Baldwin et al. (1991) reported an average value of about

20 μm for generations 7 to 16; Mercer et al. (1991) reported a thickness of ~10 μm for terminal bronchioles; and Gehr (1994, Table A.2) reported a value of 16 μm for generation 15 (approximately terminal bronchioles). Based on these values, the thickness of epithelium in the bb region is modeled by a uniform distribution with a minimum value of 10 μm and maximum value of 20 μm. This distribution results in a median value of 15 μm which agrees with the default value chosen by the ICRP (1994).

4.3.5.5. Bound material (BB_{bnd})

For radioactive material which becomes chemically bound in the airway wall, the concentration is assumed (ICRP 1994, p. 86) to be uniform throughout the epithelium and to a depth of 5 μm beyond the epithelium. Therefore, the thickness of this region is equal to the thickness of the epithelium and an additional 5 μm. Although this bound compartment is included in the clearance and dosimetry models, it only becomes important when the fraction f_b is not zero. In this research (applied to plutonium oxides), $f_b = 0$; and the bound region is neglected. However, for future work, the uncertainty in the dosimetry/geometry aspect of this source compartment is assumed to be accommodated by the uncertainty in the thickness of the epithelium.

4.3.5.6. AI (AI_1+AI_2+AI_3+AI_{1T}+AI_{2T}+AI_{3T}+AI_{bnd}) as a source for bb target layers

Tissues between alveoli and bronchioles are thin enough to allow some energy from alpha particles originating in the AI region to be absorbed in secretory/Clara cells in the bronchiolar region. The tissue separating the alveolar interstitium and the basement membrane of the bronchiolar epithelium is termed the subepithelial layer by the ICRP

(1994); this layer includes the lamina propria, connective and musculature tissues. Few measurements were found for the thickness of this layer. Mercer et al. (1991, p. 122) reported a value of 11.2 ± 4 μm (mean ± SE, N=3) for the "thickness of the interstitial space between the airway epithelium and the adjacent alveoli of human bronchioles." Based on preliminary values ranging from 12 to 75 μm, Gehr (1994) recommended a value of 20 μm for the subepithelial layer thickness. As a result of Gehr's work, the ICRP (1994) has recommended a thickness of 20 μm. This thickness represents a very important parameter for relatively insoluble radioactive material deposited in the AI region because biological clearance from this region is slow. For radiations that can penetrate the subepithelial layer, the AI region can add significantly to the dose in the bb region. Based on the very limited data, the thickness of the subepithelial layer is modeled by a uniform distribution with minimum and maximum values of 10 and 30 μm. The upper value of 30 μm was selected for this distribution for two reasons. First, this value results in an average value of 20 μm, which agrees with the ICRP recommendation. Second, the values above reported by Gehr (1994) were preliminary--choosing a smaller value is more conservative (with respect to dose) since more energy can reach the bb target tissues from the AI source components. No other guidance for selecting any other value was found.

4.3.5.7. Secretory/Clara cell layer (bb_{scc})

Depths and thicknesses of secretory cells in the bronchial epithelium of the bb region have been measured by Baldwin et al. (1991) and by Mercer et al. (1991). These measurements were summarized in Tables 4-20 and 4-21 above. Baldwin et al. (1991)

reported a value of about 6 to 7 μm (generations 7 to 16) for the average depth (to surface) of nonciliated cell nuclei in the epithelium. Mercer et al. (1991) reported a minimum depth of secretory cell nuclei of about of about 2 μm in terminal bronchioles (approximately generation 15). Based on these measurements, the depth of secretory cell nuclei layer is modeled by uniform distribution from 2 to 7 μm (median value of roughly 4 μm). The thickness of this target layer is assumed to be:

(thickness of bb_{scc}) = (bb epithelium thickness) - (depth of bb_{scc}) - (2 μm) (4-44)

where 2 μm is subtracted to agree with observations (Mercer et al. 1991) that secretory nuclei were not seen within a couple of microns of the basement membrane. Since the maximum thickness of the epithelium is taken to be 10 μm, the possibility exists for a value of zero to be sampled for the thickness of the secretory layer. A constraint implemented in the present study is that the thickness be at least 4 μm (roughly the diameter of the secretory cell nucleus). The ICRP (1994) suggested values of 4 μm for the depth, 8 μm for the thickness, and 3 μm for the distance from the basement membrane.

4.3.6. Surface Area of Bronchial and Bronchiolar Regions

Surface area of airways in the bronchial (BB) and bronchioar (bb) regions are needed to estimate the volumes of source regions. Volumes are estimated by the product of the source region thickness and the regional surface area. For example, the volume of the mucus/gel layer in the BB region is equal to the product of the mucus thickness in that region and the surface area of airways comprising generations 1to 8. The trachea (generation 0) is not included in the dose aspect of the model (per ICRP [1994]

recommendations) since it is relatively resistant to radiation damage. Typical values for the surface area of airways were given in Table 4-4 for reference adult male.

To account for age and gender effects, the equations previously listed in Table 4-5 for airway lengths and diameters have been used to compute surface area (assuming cylindrical geometry) with a range of values for height (75 to 200 cm). These equations represent average airway dimensions for a given body height. The resulting relationships between surface area and height are shown graphically in Figures 4-17 and 4-18 for the BB and bb regions, respectively. Using linear fitting (method of least squares), polynomial curves have been estimated for the data. The regression equations provide estimates forthe average surface area given the body height. To account for variability in the surface area in these regions which is not explained by the regression on height, a random error term, E(SA), has been included in the methodology. This error term is assumed to have a lognormal distribution with geometric mean of 1.0 and geometric standard deviation of 1.1. The product of the error term and the value predicted by the regression expression gives the value of the surface area for a specific realization. As an example, given a height of 175 cm (typical adult male), these methods yield a 95% confidence interval for surface area of the BB region of about 235 to 350 cm^2 ; for the bb region the interval is about 2000 to 2900 cm^2.

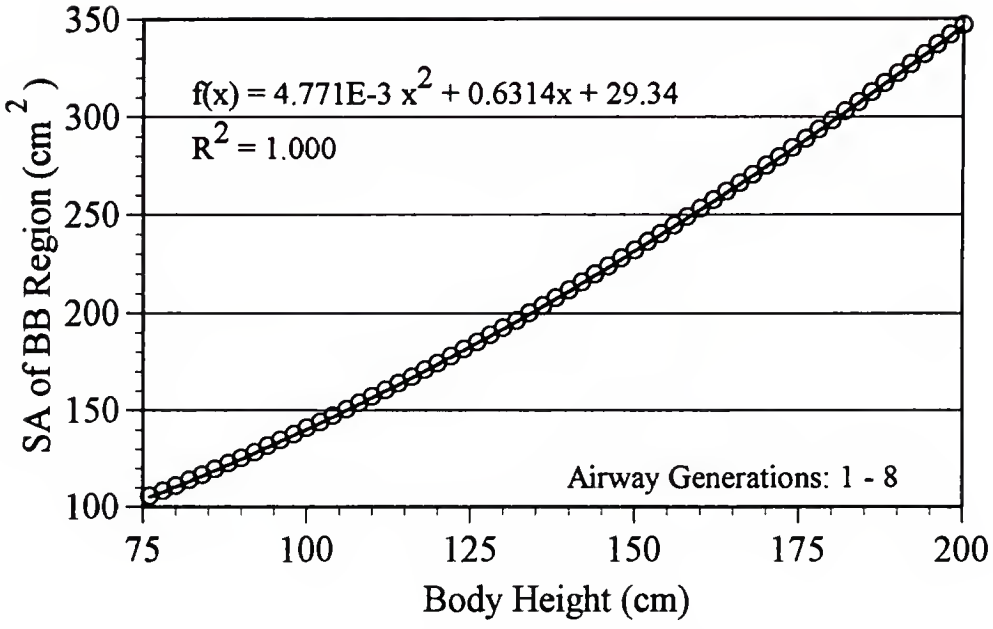

Figure 4-17. Surface area (SA) of the bronchial (BB) region (not including trachea) as a function of height. Based on symmetrical, dichotomously branching, cylindrical airways with dimensions estimated by equations in Table 4-5.

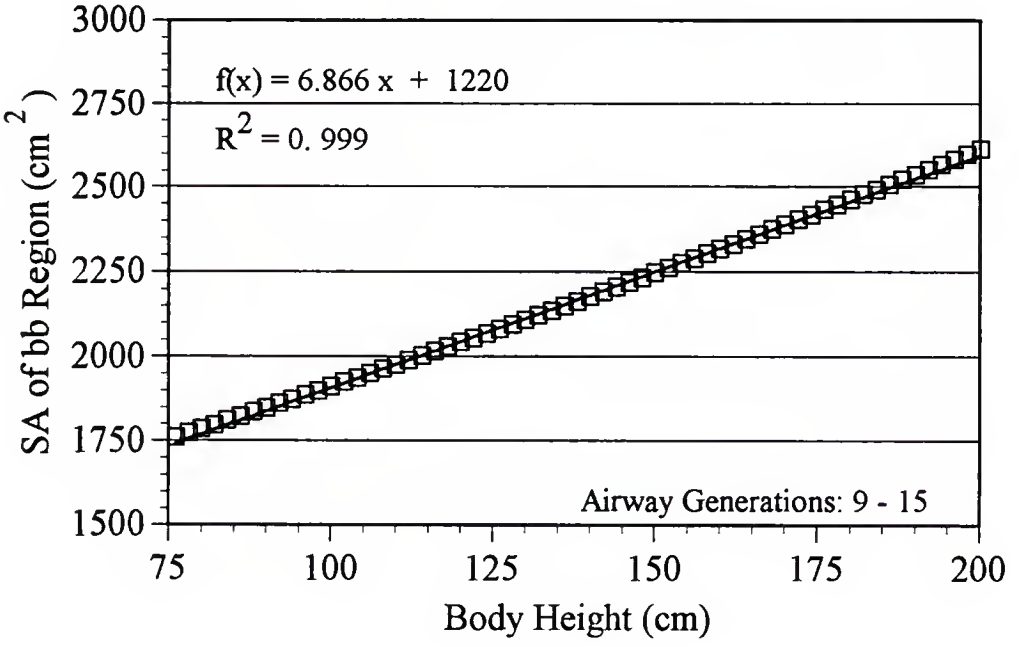

Figure 4-18. Surface area (SA) of the bronchiolar (bb) region as a function of height. Based on symmetrical, dichotomously branching, cylindrical airways with dimensions estimated by equations in Table 4-5.

4.3.7. Alveolar-Interstitial Region

The tissues in the alveolar-interstital (AI) region are very thin. For example, Gehr (1994) reported a mean value for the (alveolar) tissue barrier in the gas exchange region of the lung as 2.2 μm for humans (based on measurements from 8 individuals). Because tissues are thin compared to the range of alpha particles (on the order of 10's of microns in soft tissue), the energy absorbed by target tissues (Type II epithelial cells) in the AI region is assumed to be uniform throughout the region. Dose in the AI region is computed as the total energy deposited in the AI region divided by the mass of the AI region. Parameters describing tissue dimensions in this region are not needed. However, variabilities in the mass of the AI region are needed.

The mass of the AI region is needed to compute radiation doses in AI tissues. The mass of the AI region includes all alveolar-interstitial tissues and the blood. Associated lymph nodes are not included in the AI mass; lymph nodes are treated as separate targets in the dose model. On a mass basis the AI region is much larger than the BB and bb regions. The ICRP (1975, Table 69) estimated the total weight of the tracheo-bronchial structure of the airways (trachea to terminal bronchioles) to be about 40 g. Without the trachea the value was approximately 30 g. This weight is < 3% of the average total lung mass (i.e., 1100 g) reported for adult males (ICRP 1975, Table 65). Based on this information, the AI region mass, M_{AI}, is assumed to equal the total lung mass, M_{lung}.

4.3.8. Total Lung Mass

Using data reported in ICRP *Publication 23* (1975, Table 65), Walker (1991) recently suggested an empirical model describing postnatal growth of the lungs. The model provided a good fit to the ICRP data and is used to predict average lung mass as a function of age and is given for males as

$$M(X) = 0.050 + 0.297\,[1 - \exp(-0.033\,X)] + \frac{0.831}{[1 + \exp(-0.028\,(X - 198.200))]} \quad (4\text{-}45)$$

and for females as

$$M(X) = -0.035 + 0.185\,[1 - \exp(-0.051\,X)] + \frac{0.770}{[1 + \exp(-0.014\,(X - 144.900))]} \quad (4\text{-}46)$$

where $0 \le X \le X_{maturity}$ for both expressions; X is the age in months after birth; $X_{maturity}$ is the age when the lungs reach their mature size; and M is the average lung mass given in kg. The value for $X_{maturity}$ is taken to be 360 months since observed values of lung mass increase at least up to this age (age interval of 20-40 years showed an increase compared to 19-20 years). Equations 4-45 (males) and 4-46 (females) are plotted in Figure 4-19 along with data from ICRP *Pub. 23* (1975, Table 65). The data points represent average values at given ages. Walker (1991) examined residuals of the models for both sexes and found model errors to be about 10%. In discussing the model, the Walker stressed that the models are representative of reference individuals only and that using the model for

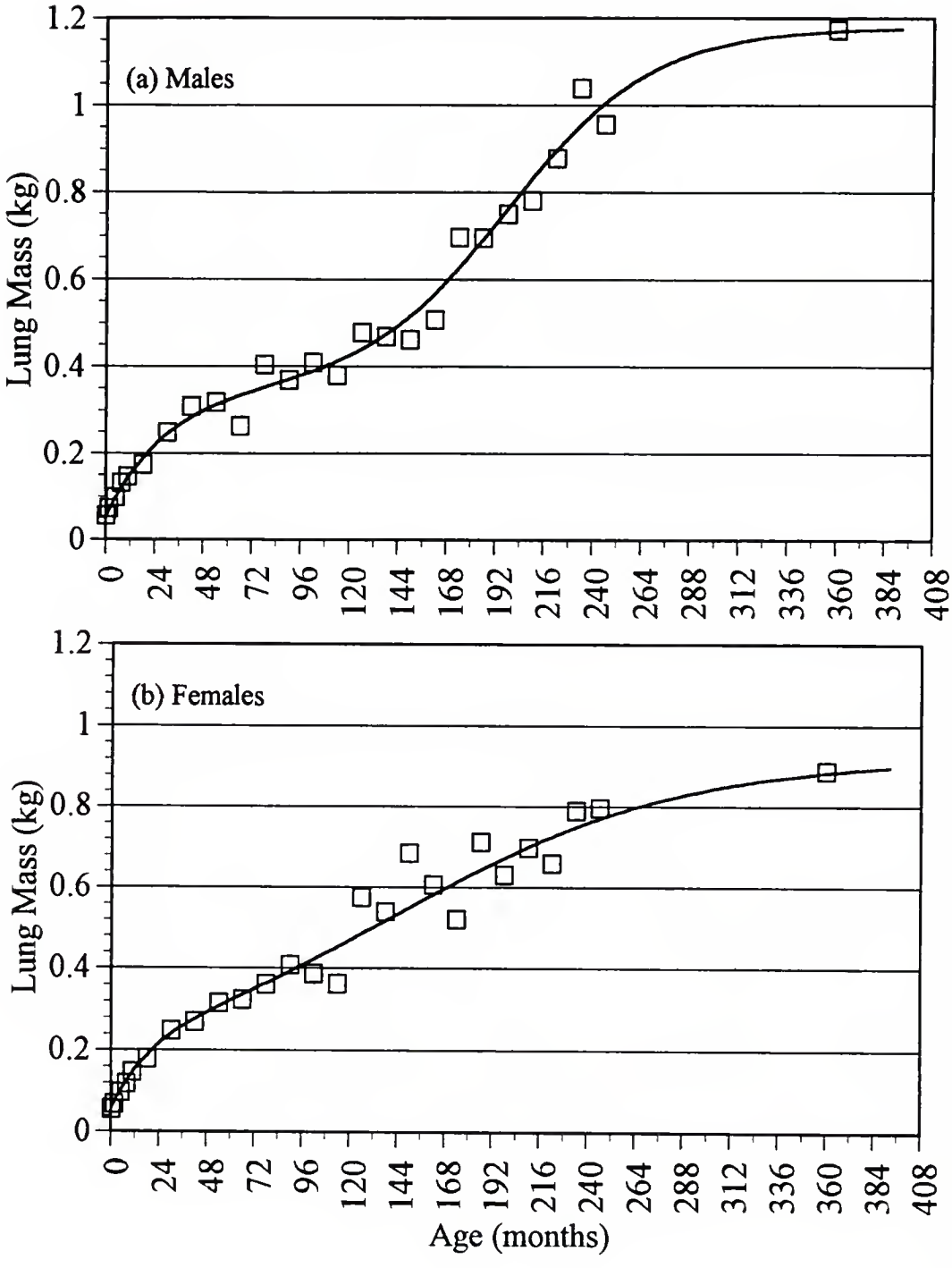

Figure 4-19. Total (blood-filled) lung mass as a function of age for (a) males and (b) females. Data are from ICRP (1975, Table 65). Curves represent empirical models by Walker (1991).

"estimating lung mass sizes of average individuals in today's population will introduce secular, genetic, and geographical biases." However, these are still the best models available for estimating lung mass to perform this study.

In the present study the empirical models above (Eqs. 4-31 and 4-32) are used to provide estimates for mean lung mass given the age and gender of a specified population class (e.g., 6 year old males). Latin hypercube sampling techniques are then used to select an error term, denoted by E_{lung}, which is used to produce variability about that mean value. The error term is assumed to be normally distributed with a mean value 0 and a standard deviation equal to 10% of the mean lung mass estimated from the expression. The model then adopted in this work for the total lung mass is:

$$M_{lung}(X) = M(X)*[1+E_{lung}] \qquad (4\text{-}47)$$

where M(X) is given by Eq. 4-45 or 4-46 as appropriate.

4.3.9. Mass of Lymph Nodes

Lymph nodes in general have been found to be relatively resistant to radiation-induced cancers (Masse and Cross, 1994). Consequently, the radiation doses delivered to lymph nodes associated with extrathoracic (ET) and thoracic (TH) regions have been assigned regional weighting factors of 0.001 by the ICRP (1994) for purposes of summing lung regions in order to estimate an overall lung dose. The masses of these tissues are derived for a subject by scaling the value reported for reference man in ICRP *Publication 23* (ICRP 1975) to the lung mass (1100 g for reference man). In that publication a value of 15 g was assumed for lymph nodes associated with ET and thoracic (TH) regions.

Both ET and TH lymph node masses, denoted here as M_{LN} since they are assumed equal, are estimated in this methodology as:

$$M_{LN} = (0.015/1.1)*M_{lung} \quad (4\text{-}48)$$

where M_{lung} (in kg) is determined from Eq. 4-47. Besides incorporating the variability in the lung mass for a given age/gender group, no additional steps are taken to model variability in lymph node masses since they are relatively radio-resistant.

4.3.10. Regional Risk-Apportionment Factors

Regional risk apportionment factors are required to compute overall, combined organ equivalent doses for the extrathoracic and thoracic (lung) regions. These doses, along with the associated apportionment factors, were defined in Chapter 2 (i.e., section 2.7, Eqs. 2-15 and 2-16). The overall, combined (effective) lung dose is needed to compute the committed effective dose equivalent, CEDE, (USNRC, 1992) and the effective (whole body) dose equivalent, H_E (ICRP, 1991).

In this study, the default values reported in ICRP *Publication 66* (ICRP, 1994) have been adopted for ET regions since these regions are generally insensitive to radiation damage. For the thoracic regions the approach suggested by Birchall and James (1994) has been used to accommodate uncertainties in the regional risk apportionment factors. Let W_{BB} represent relative sensitivity of the BB region to the total tracheobronchial region (BB+bb) so that

$$W_{BB} = \frac{A_{BB}}{(A_{BB} + A_{bb})} \quad . \quad (4\text{-}49)$$

Further, note that the BB region possesses two target regions, the basal cell nuclei and the secretory cell nuclei layer. Therefore, the apportionment factor for the BB region, denoted A_{BB}, is actually the sum of two apportionment factors for these two targets. Denoting the apportionment factor for the BB basal cell layer as $A_{BB(basal)}$ and for the BB secretory cell layer as $A_{BB(secretory)}$, the following relationship must then hold:

$$A_{BB} = A_{BB(basal)} + A_{BB(secretory)} \quad (4\text{-}50)$$

Let W_{basal} represent the fraction A_{BB} that is assigned to the BB basal cell nuclei layer.

$$W_{basal} = \frac{A_{BB(basal)}}{A_{BB}} \quad (4\text{-}51)$$

Therefore, if values are specified for A_{AI} (AI region apportionment factor), W_{BB}, and W_{basal}, the remaining apportionment factors can be computed as follows:

$$A_{BB} = W_{BB}*(1 - A_{AI}) \quad (4\text{-}52)$$

$$A_{BB(basal)} = W_{basal}*A_{BB} = W_{basal}*W_{BB}*(1 - A_{AI}) \quad (4\text{-}53)$$

$$A_{BB(secretory)} = (1 - W_{basal})*A_{BB} = (1 - W_{basal})*W_{BB}*(1 - A_{AI}) \quad (4\text{-}54)$$

$$A_{bb} = (1 - W_{BB})*(1 - A_{AI}) \quad (4\text{-}55)$$

This approach for estimating apportionment factors accounts for correlations between factors and also satisfies the constraint that the sum of A_{BB}, A_{bb}, and A_{AI} be unity.

For the AI apportionment factor, A_{AI}, Birchall and James (1994) suggested a uniform distribution with minimum and maximum equal to 0 and 0.666 (this distribution results in a mean value of 0.333 for A_{AI}--the reference value). For factor W_{BB} a uniform

distribution from 0 to 1 was suggested. This distribution reflects total lack of knowledge as to which region, BB or bb, is more sensitive to radiation damage. For W_{basal} a uniform distribution from 0 to 1 was suggested. This distribution similarly reflects a total lack of knowledge regarding which cells, basal or secretory, are most sensitive in the bronchial epithelium. Use of these distributions results in mean values that are consistent with the ICRP reference values for the apportionment factors (e.g., see Table 2-8).

4.3.11. Summary of Methods for Dose Model Parameters

Summaries of the methods used to estimate uncertainties in dose model parameters are presented in Tables 4-22 and 4-23. Table 4-22 focuses on source and target tissue dimensions--depths and thickness of the regions. Table 4-23 focuses on regional surface areas, volumes, and masses of various source and target regions. Table 4-24 presents distributions for apportionment factors and related parameters defined to accommodate correlations.

Table 4-22. Summary of distributions used to model uncertainty in source and target tissues dimensions in the BB and bb regions.

Region/Source/Target	Equivalent Compartment	Dimension	Distribution (parameters)[a]	ICRP Default[a,b]
BB Region:				
Mucus/Gel Layer	$BB_1 + BB_{1T}$	Thickness	Triangular (4, 6, 8)	5
Cilia/Sol Layer	$BB_2 + BB_{2T}$	Thickness	Triangular (4,7.5,10)	6
Sequestered Material	$BB_{seq} + BB_{seq,T}$	Thickness Depth[c]	Uniform (5, 15) Uniform (0,10)	10 5
BB Epithelium, BB_{epithk}		Thickness	Uniform (25, 60)	55
Bound Material Layer	BB_{bnd}	Thickness	(BB_{epithk} + 5 μm)	60
Basal Cell Nuclei Layer	(Target tissue)	Thickness Depth[d]	Uniform (10, 20) see note (e)	15 35
Secretory Cell Nuclei Layer	(Target tissue)	Depth[d] Thickness	Uniform (5, 15) see note (f)	10 30
bb Region:				
Mucus/Gel Layer	$bb_1 + bb_{1T}$	Thickness	Uniform (1, 3)	2
Cilia/Sol Layer	$bb_2 + bb_{2T}$	Thickness	Uniform (3, 6)	4
Sequestered Material	$bb_{seq} + bb_{seq,T}$	Thickness Depth[c]	Uniform (4, 10) Uniform (0, 10)	5 5
bb Epithelium, bb_{epithk}		Thickness	Uniform (10, 20)	15
Bound Material Layer	bb_{bnd}	Thickness	bb_{epithk} + 5 μm	20
Subepithelial Layer		Thickness	Uniform (10, 40)	20
Secretory (or Clara) Cell Nuclei Layer	(Target tissue)	Depth[d] Thickness	Uniform (2, 8) see note (f)	4 8

[a] All parameters have units of microns. For uniform distributions parameters represent minimum and maximum values; for triangular distributions parameters represent minimum, mode, and maximum values, respectively.

[b] Values suggested in ICRP *Publication 66* (ICRP 1994); for comparison.

[c] Depth with respect to basement membrane of epithelium.

[d] Depth with respect to epithelium surface (lumen surface, excluding mucus and cilia).

[e] Depth = (Epithelium Thickness) - (Basal Nuclei Layer Thickness) - 5 μm.

[f] Thickness = (Epithelium Thickness) - (Secretory Nuclei Layer Depth) - X, where X = 5 μm for BB region and X = 2 μm for bb region; minimum thickness of 5 μm.

Table 4-23. Summary of methods to model uncertainties in source and target tissue volumes and masses.

Quantity	Relationship	Distribution/Comments
SA for BB Region (Units: cm^2, Ht in cm)	$SA(BB) = SA_{mean}(BB)*SA_{error,BB}$	$SA_{mean}(BB) = 4.771x10^{-3}\ Ht^2 + 6.314x10^{-1}\ Ht + 2.934x10^{1}$ $SA_{error,BB}$ ~Lognormal (1, 1.1)
SA for bb Region (Units: cm^2, Ht in cm)	$SA(bb) = SA_{mean}(bb)*SA_{error,bb}$	$SA_{mean}(bb) = 6.866*Ht + 1220$ $SA_{error,bb}$ ~Lognormal (1, 1.1)
Volume of source tissues in BB and bb regions (Units: cm^3)	V = SA(BB or bb)*Sthk Sthk (cm) = thickness of source layer	Variability accomodated by uncertainties in SA and Sthk. See Table 4-22 for Sthk.
Mass of target tissues in BB and bb regions (Units: kg)	$M_{BB,bb} = SA(BB\ or\ bb)*Tthk*\rho_{tissue}$ Tthk (cm) = thickness of target layer ρ_{tissue} = tissue density (kg/cm^3)	Variability accommodated by uncertainties in SA and Tthk. See Table 4-22 for Tthk
Mass of AI region (Units: kg)	$M_{AI}=M_{lung} = M(X)*(1+E_{lung})$	M(X) given by Eqns. 4-45 and 4-46 in text. E_{lung} ~Normal (0, 0.1)
Mass of Lymph Nodes (Units: kg)	$M_{LN} = (0.015/1.1)*M_{lung}$ X = age (months)	

Notes: Ht = body height (cm); SA = surface area (cm^2); Distribution parameters indicate (mean, standard deviation) for normal and (geometric mean, geometric standard deviation) for lognormal distributions.

Table 4-24. Summary of distributions and relationships used to model uncertainties in risk apportionment factors.

Quantity	Symbol	Distribution or Relationship
Sensitivity ratio of BB:(BB+bb)	W_{BB}	W_{BB} ~Uniform (0, 1)
Sensitivity ratio of BB_{basal}:BB	W_{basal}	W_{basal} ~Uniform (0, 1)
AI Apportionment	A_{AI}	A_{AI} ~Uniform (0, 0.666)
BB(basal) Apportionment	$A_{BB(basal)}$	$A_{BB(basal)} = W_{basal}*W_{BB}*(1-A_{AI})$
BB(secretory) Apportionment	$A_{BB(secretory)}$	$A_{BB(secretory)} = (1-W_{basal})*W_{BB}*(1-A_{AI})$
bb Apportionment	A_{bb}	$A_{bb} = (1-W_{BB})*(1-A_{AI})$

Note: Distribution parameters indicate (minimum, maximum) for uniform distributions.

UNIVERSITY OF FLORIDA
3 1262 05482 0013

CHAPTER 5
APPLICATION OF LUDUC TO INHALED PLUTONIUM OXIDE AEROSOLS: RESULTS AND DISCUSSION

5.1. Introduction

A methodology for quantifying uncertainties in radiation doses to the respiratory tract has been discussed in previous chapters. The methodology is based on conducting parameter uncertainty analyses using the revised ICRP respiratory tract model (ICRP, 1994) within the scope of specified exposure scenarios. Exposure scenarios of interest were presented in Chapter 1. All of the methods presented in previous chapters have been implemented in a probabilistic computer code, LUDUC (for LUng Dose Uncertainty Code; discussed in section 3.6), which has been developed during the course of this study. The program LUDUC uses random sampling techniques along with parameter distributions and relationships discussed in Chapter 4 to solve the respiratory tract model a specified number of times (trials). The purpose of this chapter is to demonstrate LUDUC by application to exposure scenarios involving inhalation of plutonium oxide aerosols. Plutonium oxide was selected since results for population dose uncertainty can benefit an ongoing dose reconstruction study of releases from the Rocky Flats nuclear weapons facility in Colorado.

In this chapter equivalent dose uncertainties are examined for the five target regions of the lungs (described in Chapter 2) and for the combined, or total, lung

(weighted sum of the target regions; see Eq. 2-16). The five target regions include: (1) the secretory cell nuclei layer in the bronchial epithelium, denoted as BB_{sec}; (2) the basal cell nuclei layer in the bronchial epithelium, denoted BB_{bas}; (3) the secretory cell nuclei layer of the bronchiolar epithelium, denoted as bb_{sec}; (4) the total mass of the alveolar-interstitial region, AI; and (5) the total mass of the thoracic lymph node region, LNth. The following nine age/gender population groups were included in the investigation of plutonium oxide: 2-year olds, 5-year olds, 10-year olds ,15 year-old females, 15 year-old males, 18-24 year-old females, 18-24 year-old males, 25-34 year-old females, and 25-34 year-old males. The 2-, 5-, and 10-year old groups were based on males, although gender has very little influence on model parameters at these ages. For each age/gender group, equivalent doses have been computed at the four broad physical exertion levels discussed in previous chapters (e.g., section 4.1.8.2). These levels were defined as resting (sleeping), sitting (awake), light exertion, and heavy exertion. Doses were examined for a range of aerosol particle diameters from 0.1 to 50 μm. Unless otherwise stated, all doses were integrated over 50 years post intake for adults (age ≥ 18 years old) or 70 years for children (< 18 years), where an acute intake was assumed to simplify solution to differential equations (listed in Appendix B).

Methods employed to model deposition of aerosol particles in the respiratory tract assumed electrostatically neutral, nonhygroscopic, and nonfibrous aerosol particles. Hygroscopicity refers to the tendency of particles to increase in size upon entering the human respiratory tract due to the absorption of water molecules from the saturated air. Generally, if the particle material is soluble in water, it is hygroscopic. Although

techniques are suggested elsewhere (e.g., James et al., 1994b, pp. 283-291) to deal with hygroscopic aerosols, they were not implemented in this work. Aerosol particles composed solely of PuO_2 meet the condition of nonhygroscopicity. Most host particles (e.g., dust particles) to which PuO_2 might attach in the outdoor environment are likely to be non-hygroscopic as well, since hygroscopic materials are generally removed from topsoil by percolation of rain water.

5.2. Characteristics of $^{239}PuO_2$ Aerosols

Plutonium oxide, $^{239}PuO_2$, was selected to demonstrate the methodology developed in this study for two reasons. First, $^{239}PuO_2$ possesses a combination of nuclear and chemical characteristics that makes it a radiological hazard to the lungs if inhaled in sufficient quantities. Second, historical exposures to $^{239}PuO_2$ -laden aerosols are currently under investigation for residents living near the Rocky Flats Plant (a U.S. nuclear weapons complex located near Denver, Colorado). Methods are needed to account for uncertainties in radiation doses to the lungs of members of population groups which have inhaled $^{239}PuO_2$-laden aerosol particles. Based on a parameter uncertainty analysis of the revised ICRP lung model (ICRP, 1994), LUDUC has been used to estimate numerical probability distributions in lung dose (per activity exposure) for population groups.

The radionuclide ^{239}Pu decays primarily by alpha emission over 99% of the time; it has a half life of approximately 24,400 years and an average alpha particle energy of 5.15 MeV. Alpha particles are roughly twenty times more effective than gamma rays or beta particles in producing biological effects in living cells (ICRP, 1991a). Concerning

chemical characteristics, the oxide form of ^{239}Pu is relatively insoluble in lung tissues. If deposited in the pulmonary region of the lungs, plutonium oxides clear very slowly (with biological half-lives of years), primarily by macrophage transport to lung-associated lymph nodes and to the gastrointestinal tract via the mucociliary escalator in the tracheobronchial region, with little absorption to blood (ICRP, 1986). Slow clearance from the pulmonary region coupled with the increased biological effectiveness of alpha particles (compared to other radiation types) leads to a high risk to the lungs per unit inhalation intake of $^{239}PuO_2$ (as demonstrated earlier in Table 1-2)--such a scenario is generally true for inhalation of all alpha-emitting radionuclides that are in a relatively insoluble chemical form.

Plutonium possesses many isotopes (mass numbers from 232 to 246); the radionuclides that generally receive the most attention are ^{238}Pu, ^{239}Pu, ^{240}Pu, ^{241}Pu, and ^{242}Pu. The first of these, ^{238}Pu, is formed by neutron capture by ^{235}U (following some intermediate transmutations) or directly by an (n, 2n) reaction with ^{239}Pu. ^{239}Pu, ^{240}Pu, and ^{241}Pu are formed as a result of neutron irradiation of ^{238}U. Both ^{235}U and ^{238}U are present in the fuel of light water nuclear reactors. All of these isotopes of Pu, except ^{241}Pu, decay primarily by alpha particle emission. ^{241}Pu decays (100%) by beta emission (14 y half-life), transmuting to ^{241}Am (which is primarily an alpha emitter). A mixture of these isotopes usually exists in plutonium metal. Sutherland (1983) reported the percent radioactivity in Rocky Flats weapons grade plutonium to be 0.34% ^{238}Pu, 11.29% ^{239}Pu, 2.58% ^{240}Pu, 83.22% ^{241}Pu, and <0.001% ^{242}Pu. (Am-241 made up an additional 2.58%). For an inhalation intake, the primary contribution to the equivalent dose in critical lung tissues is from the alpha-particle emitters. Although ^{241}Pu is present in large quantities, it is a beta

emitter with an average energy of about 5 keV (compared to the ~5 MeV alpha particles from other nuclides); furthermore, energy deposited in human biological tissues by alpha particles receives a radiation weighting factor of $w_R = 20$ compared to $w_R = 1$ for beta particles. Consequently, for targets in range of both radiation types, ^{241}Pu (in the mixture cited above) would contribute a negligible amount to the dose in lung tissues. Subsequently, for this particular mixture (Rocky Flats weapons grade plutonium), ^{239}Pu and ^{240}Pu account for most of the dose due to plutonium.

A complicating factor in plutonium dosimetry is that the resolution of current alpha spectrometry systems does not allow distinction between ^{239}Pu and ^{240}Pu. Consequently, the total activity of $^{239+240}Pu$ is often reported in measurement results. Computations with LUDUC (confirmed by predictions with LUDEP for the reference man case) have revealed that per activity exposure ^{239}Pu and ^{240}Pu result in the same numerical distributions for equivalent doses to all target tissues. Therefore, in all of the text that follows, $^{239}PuO_2$ can be replaced with $^{239+240}PuO_2$ with negligible error (i.e., an activity exposure to ^{239}Pu is mathematically equivalent to the same activity exposure to $^{239+240}Pu$).

The formation of plutonium aerosols as well as several measurements regarding activity-size distributions have been discussed by Chamberlain (1991). Chamberlain listed four modes of plutonium aerosol formation including: (1) oxidation or volatilization of Pu metal, (2) oxidation or volatilization of irradiated U or UO_2, (3) dispersion of droplets from aqueous solutions or suspensions of Pu, and (4) resuspension of soil or dust which is contaminated with Pu. The activity size-distribution for $^{239}PuO_2$ aerosols depends on the mode of formation. The plutonium aerosols produced during activities at Rocky Flats

(ChemRisk, 1994) primarily involved modes (1), (3), and (4). Two major fires (in 1957 and 1969) have occurred at the Rocky Flats Plant, both resulting in the release of plutonium oxide particles to the air (by mode 1). Releases also occurred from the late 1950s and throughout the 1960s as a result of leaking waste oil drums (at the site of the 903 pad at the Rocky Flats plant). The waste oil contaminated soil with plutonium which was subsequently dispersed by wind to off-site receptors (by mode 4). During routine operations, evaporation of Pu-laden solvents occurred in working areas (by mode 3); these were ultimately released via the ventilation exhaust. The aerosol activity-size distributions produced by these varied modes can differ, as discussed below.

Chamberlain (1991) has summarized several measured activity-size distributions for plutonium aerosols. For oxidation processes, the temperature of the atmosphere in which oxidation occurs is important. Higher oxidation temperatures usually lead to larger particle sizes. When controlled oxidation was conducted at 20 °C, an activity median aerodynamic diameter, or AMAD, of about 3 μm and a geometric standard deviation, or GSD, of about 3 were measured; at 450 °C, an AMAD larger than 50 μm and GSD of still about 3 were found (Carter and Stewart, 1971). For plutonium fumes from a fire, Mann and Kirchner (1967) reported an AMAD of about 0.3 μm and GSD of about 2. For a spill, Moss et al. (1961) reported that Pu was associated with inert dust particles having a mass median diameter of about 7 μm. Elder et al. (1974) examined plutonium-laden aerosol particles with a multi-stage cascade impactor in ventilation ducts at three plutonium processing plants. Depending on the type of activity being performed (research and development, fabrication, or recovery), AMADs were reported from 0.1 to 4 μm and

GSDs were reported from 1.5 to 4. In applying LUDUC to Pu-laden aerosols, a range of (carrier) particle aerodynamic diameters between 0.1 and 50 μm were examined; this range covers the particle sizes reported above.

5.3. Dose Uncertainty Results for Inhaled $^{239}PuO_2$ Aerosols

5.3.1. Exposure Scenario and Notational Conventions

The probabilistic computer code LUDUC, developed in this study to implement the methodology discussed in previous chapters, was applied to inhaled $^{239}PuO_2$ aerosols. Several model predictions have been produced to characterize the uncertainty in doses. These include various estimated fractiles, ratios of fractiles, geometric means, and geometric standard deviations for the six equivalent dose quantities described above (section 5.1). The output data for these dose quantities for some selected age groups, exertion levels, and particle sizes are listed in Appendix E; only a subset of that data is presented in following sections. Sensitivity analyses of dose predictions with respect to model parameters have also been performed. Results of these analyses are presented in this chapter.

In most of the computations for this work, a monodisperse aerosol (i.e., single-sized particles) was assumed. $^{239}PuO_2$-laden aerosol particles were further assumed to consist of unit density spheres (i.e., having shape factor of $\chi = 1.0$ and mass density of $\rho = 1.0$ g/cm^3). Therefore, by definition (see section 2.5), the physical particle diameter corresponds to the aerodynamic diameter.

Equivalent dose, H, was predicted per unit *activity exposure*, A_E (defined in Chapter 1). Therefore, the symbol H/A_E (units: Sv per Bq-hr/m^3) is used to present dose predictions. These doses then correspond to activity exposure-to-dose-conversion factors, EDCFs. If A_E is other than 1 Bq-hr/m^3, the linear nature of the model allows one to simply multiply H/A_E values (presented in this section and in Appendix E) by the actual activity exposure to predict the equivalent dose. However, it is again noted that the respiratory tract model was solved under the assumption that activity was deposited instantaneously (acute deposition at time zero) in the appropriate initial state compartments. This assumption is justified if the ventilation rate is relatively constant over the exposure duration.

Another notational convention used in this section has been to denote dose fractiles by $(H/A_E)_F$ where F represents the percent fractile. For example the 50% fractile is denoted as $(H/A_E)_{50\%}$. This represents the value of H/A_E at which half (50%) of the trials resulted in doses less than this value and is a measure of the central tendency of the distribution in H/A_E. The ratio of the 95% fractile to the 5% fractile has been used as a distribution-free (i.e., independent of any underlying distribution for H/A_E) measure of the dispersion, or uncertainty, in H/A_E. This ratio is denoted by $(H/A_E)_{95\%:5\%}$ and is dimensionless. For example, a value of 100 for this ratio means that the 95% fractiles are 100 times higher than the 5% fractiles; therefore some quantitative measure of "uncertainty" is provided. Since 90% of the dose values lie between the 5% and 95% dose fractiles, this ratio also represents the ratio of the upper to lower 90% confidence bounds. If the distribution shape for the dose data could be well approximated by a

lognormal distribution, this ratio (of the 90% to 5% dose fractiles) can be related to a geometric standard deviation for the dose, GSD, by the following expression:

$$\text{ratio (95\%:5\% fractile)} \approx [GSD^{1.64}]^2 = GSD^{3.28}. \quad (5\text{-}1)$$

As discussed, the equivalent dose to the *lungs* (or thoracic region of the respiratory tract) is actually a weighted sum of the equivalent doses to the five target tissues of the thoracic region (discussed in Chapter 2). Consistent with notation in Equation 2-50, the equivalent dose to the *lungs* is denoted in this chapter by H_{TH}. The equivalent doses to the five thoracic region target tissues are denoted as $H(BB_{bas})$, $H(BB_{scc})$, $H(bb_{scc})$, H(AI), and H(LNth) (see discussion in section 5.1 on target regions).

5.3.2. Adult Males Exposed to $^{239}PuO_2$ Aerosols (Monodisperse)

Using LUDUC, distribution-free fractiles have been estimated for H_{TH}/A_E (in Sv per Bq-hr/m^3), for a population group comprising 25-34 year old adult males at light physical exertion. These dose fractiles are shown as a function of particle diameter in Figure 5-1 and include the 5%, 10%, 25%, 50%, 75%, 90%, and 95% fractiles. As shown in Figure 5-1, H_{TH}/A_E is sensitive to particle size for diameters larger than about 2 μm. Additionally, the spread (or uncertainty) in H_{TH}/A_E, as indicated by the relative difference between the 5% and 95% fractiles, tends to become larger as particle diameter increases. For particle diameters between about 0.1 and 2 μm, the dose distribution is relatively constant with H_{TH}/A_E being distributed over about an order of magnitude (from the 5% to 95% fractile). As particle diameter increases above 2 μm the dose distribution shifts toward lower dose values, accompanied by an increase in the dose uncertainty. For

particle diameters larger than about 5 μm, H_{TH}/A_E is distributed over about two orders of magnitude. For a population group of 25-34 year old males, a wide spread in H_{TH}/A_E can exist--depending on particle size--among members of the group.

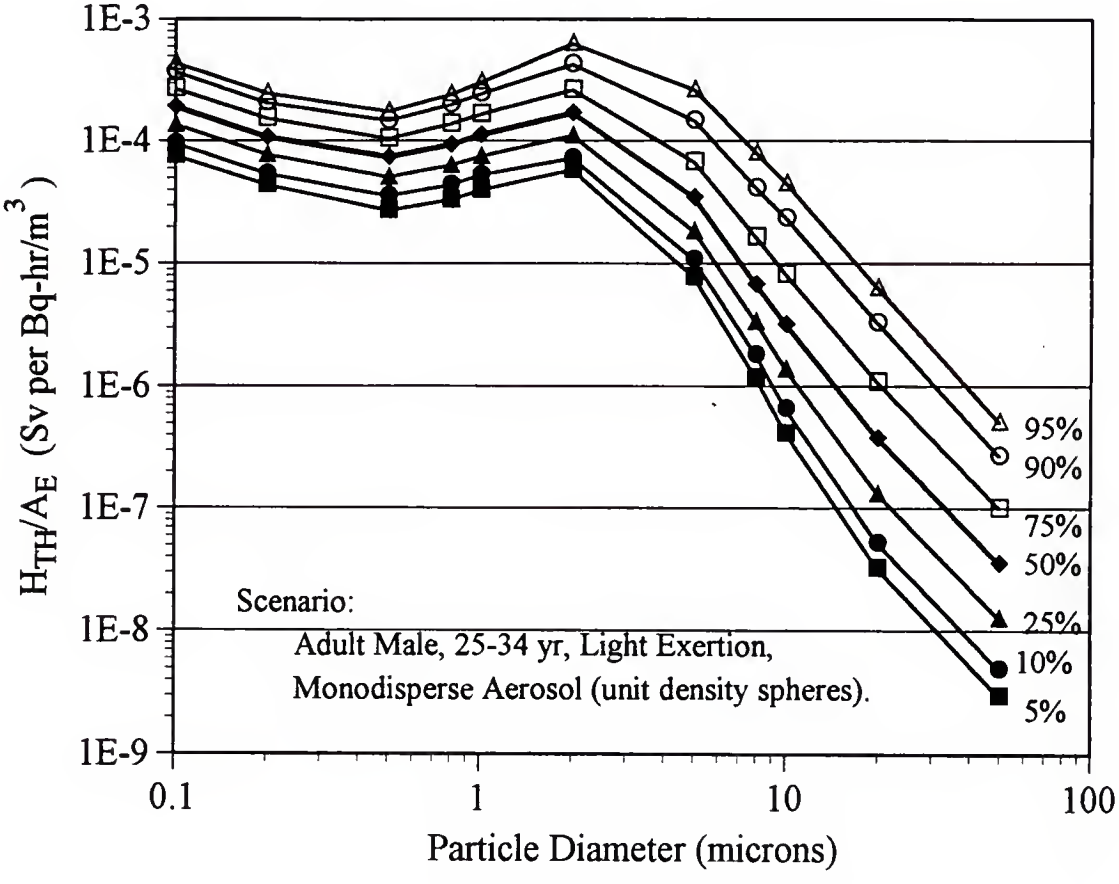

Figure 5-1. Fractiles predicted for the committed (50 year) equivalent dose per unit activity exposure, H_{TH}/A_E (Sv per Bq-hr/m^3), to the lungs (weighted sum of tissue doses) for a population group of 25-34 year-old males at light exertion. Based on exposure to monodisperse $^{239}PuO_2$ -laden aerosol particles comprising unit density spheres.

The change seen for the median dose as a function of particle size is due primarily to the sensitivity of the deposition model to particle size. For particle diameters larger than about 1 μm, less particles reach the lung since the filtration efficiencies of ET regions increase with particle size. The increase in the spread of dose values (i.e., increase in dose uncertainty) with particle size above 1 μm is attributed to an increase in the sensitivity of the deposition model with respect to the particle size; for larger particles, regional deposition efficiencies are sensitive to the diameter. This sensitivity is clearly demonstrated by the slope of the curve plotting the median dose versus diameter in Figure 5-1. Model sensitivity is examined in sections 5.4 and 5.5 of this chapter.

The values in Figure 5-1 are based on a weighted sum of doses to the five target tissues of the thoracic region. For the same scenario, Figure 5-2 presents information on equivalent dose to these five individual target regions. Panel (a) shows a plot of the median dose per exposure to the various target regions and includes the weighted sum for the lungs. Panel (b) shows the ratio of the 95% to 5% dose fractiles for each region and for the lung. The median doses to target tissues, in panel (a), all follow similar trends with respect to particle size. However, for given particle sizes, median doses differ by about a factor of 100 (more for larger particles). For smaller particles (d_p < 5 microns), panel (b) indicates that although uncertainties can be quite high for doses to BB_{bas} and LNth, uncertainties in H_{TH} are relatively small--the ratio of the 95% to 5% dose fractile is only about 5. This ratio increases by over an order of magnitude as larger particle sizes are approached. Note again that these results are based on monodisperse particles.

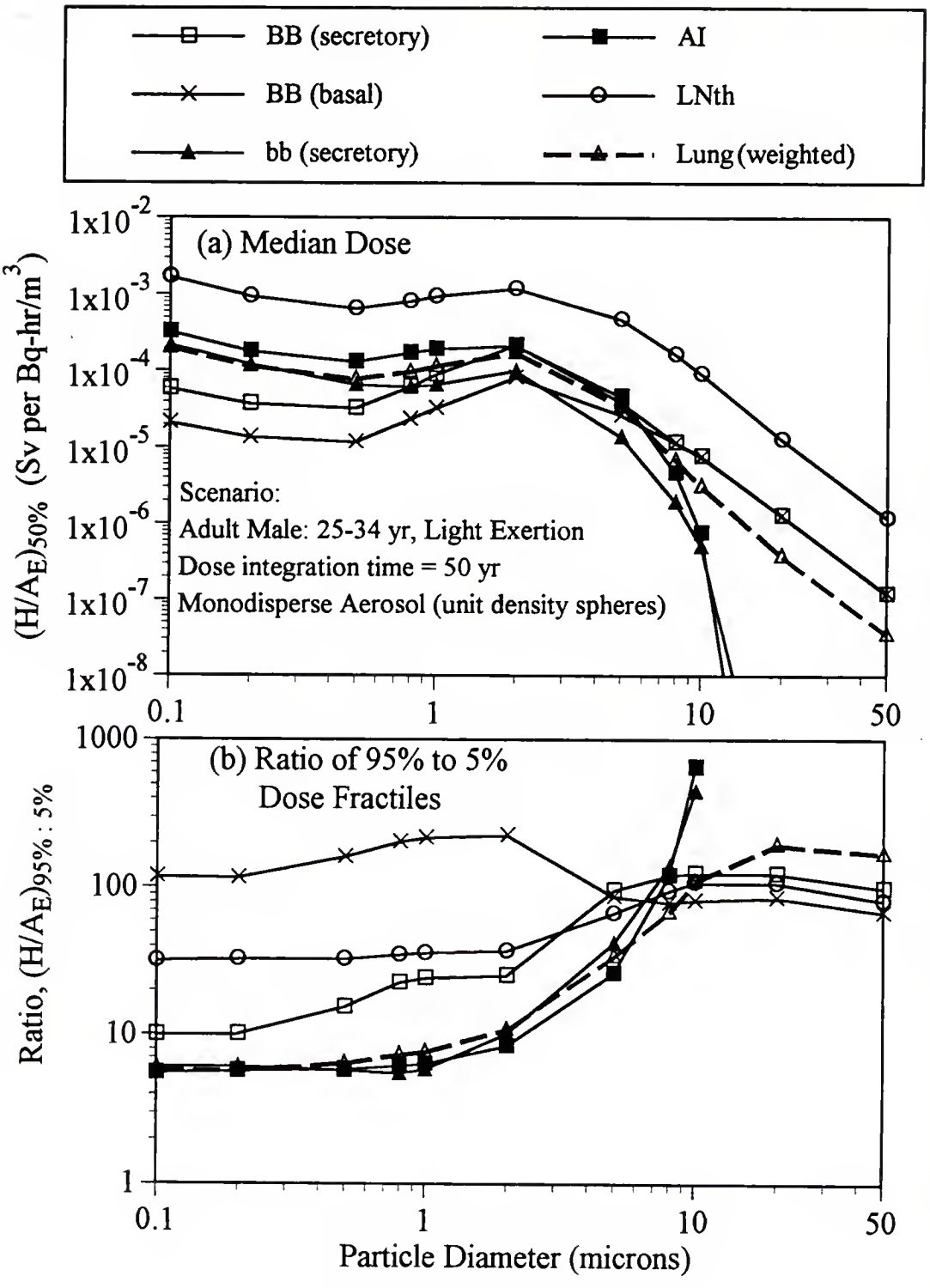

Figure 5-2. Dose quantities versus particle diameter in all thoracic target tissues for adult males (25-34 years old) exposed at light exertion. (a) Estimated median for H/A_E (Sv per Bq-hr/m^3). (b) Estimated ratios of 95% to 5% dose fractiles, $(H/A_E)_{95\%:5\%}$. Based on exposure to $^{239}PuO_2$ -laden aerosol particles (monodisperse, unit density spheres).

For the BB basal cell layer, BB_{bas}, the uncertainty in dose (as indicated by the ratio in panel [b]) is predicted to be much greater than for other regions for $d_p < 5$ μm. This result is due primarily to the uncertainty in the thickness of the bronchial epithelium (discussed in a later section). The uncertainty decreases slightly for BB_{bas} at larger particle sizes. This effect is thought to arise from a shift in the dose contributed to BB_{bas} from various source components. Dose is contributed to BB_{bas} by three source components: (1) transformations in the BB mucus/gel layer (fast mechanical transport phase), (2) transformations in the BB cilia/sol layer (slow mechanical transport phase); and (3) transformations in the BB sequestered layer (or macrophage layer). For smaller particles, component (2) contributes the most of the dose (see Fig. 4-14). For larger particles component (2) becomes less important as component (3) becomes more important. Doses from the sequestered layer are influenced less by the thickness of the bronchial epithelium.

Even though the same three source components described above for BB_{bas} exist for the BB secretory cell layer, BB_{sec}, the dose uncertainty for this target does not follow the same trend. This target tissue comprises almost the entire thickness of the BB epithelium. Consequently, doses to BB_{sec} are not as sensitive as BB_{bas} to the shifts in source components.

For the bb secretory cell layer (bb_{sec}) and AI tissues, the uncertainty increases (over about two orders of magnitude as indicated by the fractile ratio) for particle diameters approaching and surpassing 10 μm; however, median doses to these regions decrease sharply with particle diameter since few or no particles are predicted to deposit in the bb and AI regions for $d_p > 10$ microns. Consequently, for larger particles the ratio of dose

fractiles has little meaning for bb and AI. In fact, when $d_p > 10$ microns, the 5% dose fractile is zero, and the ratio is undefined in these targets (and subsequently is not plotted in Fig. 5-2[b]). As doses become small in these targets, the relative importance of these regions diminishes such that uncertainty in these doses are not important with respect to the total lung dose (weighted sum of regions). Furthermore, the doses to AI and bb tissues at these larger particle sizes would likely be of little consequence for polydisperse particle-size distributions since smaller particles would likely dominate the dose.

Median doses to thoracic lymph nodes, LNth, are an order of magnitude or more higher than doses to other tissues (per particle diameter). This result simply reflects the facts that (1) materials cleared from the lungs to the lymph nodes remain there virtually indefinitely and (2) the small mass of the lymph nodes results in a higher dose (i.e., energy absorbed per unit target mass). However, because the lymph nodes are relatively insensitive to radiation damage (as reflected by the low risk-apportionment weighting factor assigned to this region; $A_{LNth} = 0.001$ in Table 2-8), doses in LNth are not usually of much interest relative to other target regions. The contribution of H(LNth) to the weighted lung dose is negligible for the scenarios examined.

Values in Figure 5-1 and 5-2 were based on a population group involved in light physical exertion. The influence of exertion level on the dose values and their uncertainties is also of interest. Panel (a) of Figure 5-3 is a plot of the 50% fractiles (medians) for equivalent dose to the lungs (weighted sum of regional doses) at all four exertion levels (resting, sitting, light and heavy exertion). Panel (b) is a plot comparing the ratio of the 95% to 5% dose fractiles.

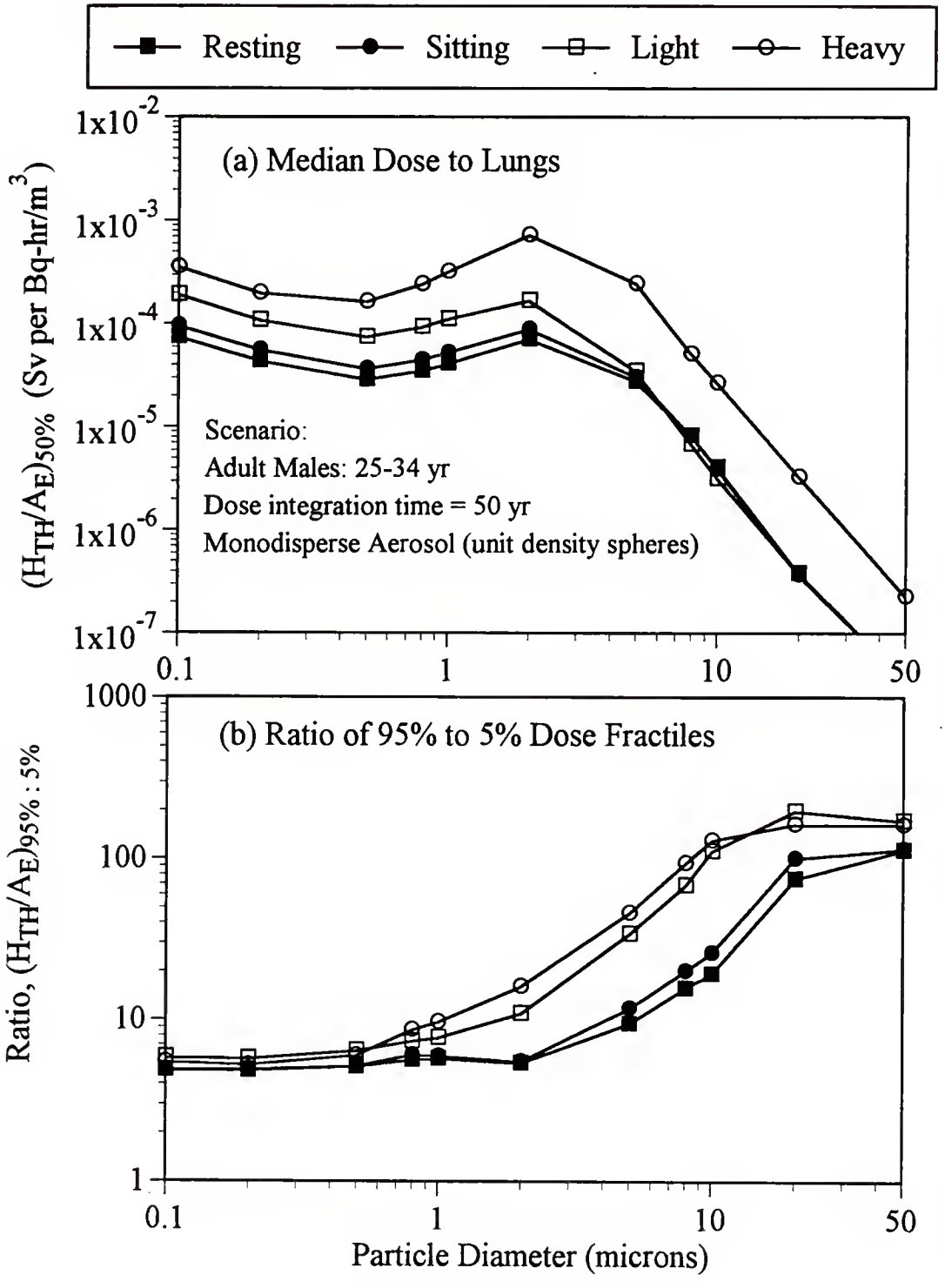

Figure 5-3. Equivalent dose to lungs for adult males at four exertion levels: resting, sitting, light and heavy exertion. (a) Estimated values for median dose, $(H_{TH}/A_E)_{50\%}$. (b) Estimated values of the ratio of dose fractiles, $(H_{TH}/A_E)_{95\%:5\%}$. Based on exposure to $^{239}PuO_2$ -laden aerosol particles (monodisperse, unit density spheres).

About an order of magnitude difference exists between median lung doses for exposure at heavy exertion compared to resting (and sitting). This effect is attributed to differences in the central tendency of the ventilation rate (and hence intake rate) since it increases by about a factor of ten from rest to heavy exertion (see Figure 4-10). Another feature of the plot in panel (a) is that, for particles larger than about 5 μm, $(H_{TH}/A_E)_{50\%}$ is roughly equal for resting, sitting, and light exertion; but it is almost an order of magnitude higher (than those levels) for heavy exertion. This result is due primarily to the deposition pattern at these size ranges and to an abrupt change in the oronasal breathing pattern (i.e., tendency to breathe more through mouth than nose; see section 4.1.10) in most persons in going from light to heavy exertion activities.

As shown in panel (b) of Fig. 5-3, the uncertainty in dose values (as measured by the ratio of fractiles) is relatively small and insensitive to change in the exertion level (i.e., ratio ~ 5) for particle diameters less than about 1 μm. However, for larger particles an increase in the uncertainty generally occurs. As particle diameter increases from 1 to 20 μm (2-20 μm for resting and sitting), the value of $(H_{TH}/A_E)_{95\%:5\%}$ for light exertion increases by about a factor of 40. This increase in dose uncertainty is due primarily to sensitivities in the deposition model (discussed later in section 5.5).

Figure 5-4 shows values of $(H/A_E)_{50\%}$ (for the same exposure scenario as Figure 5-3) for the five individual target tissues of the thoracic region (in panels [a]-[e]) and for the lung (in panel [f]). The purpose of this figure is to compare median doses among the target tissues for different exertion levels. Generally, the trends at the regional scale are similar to those shown by and discussed for Fig. 5-3. Figure 5-5 shows values of the ratio

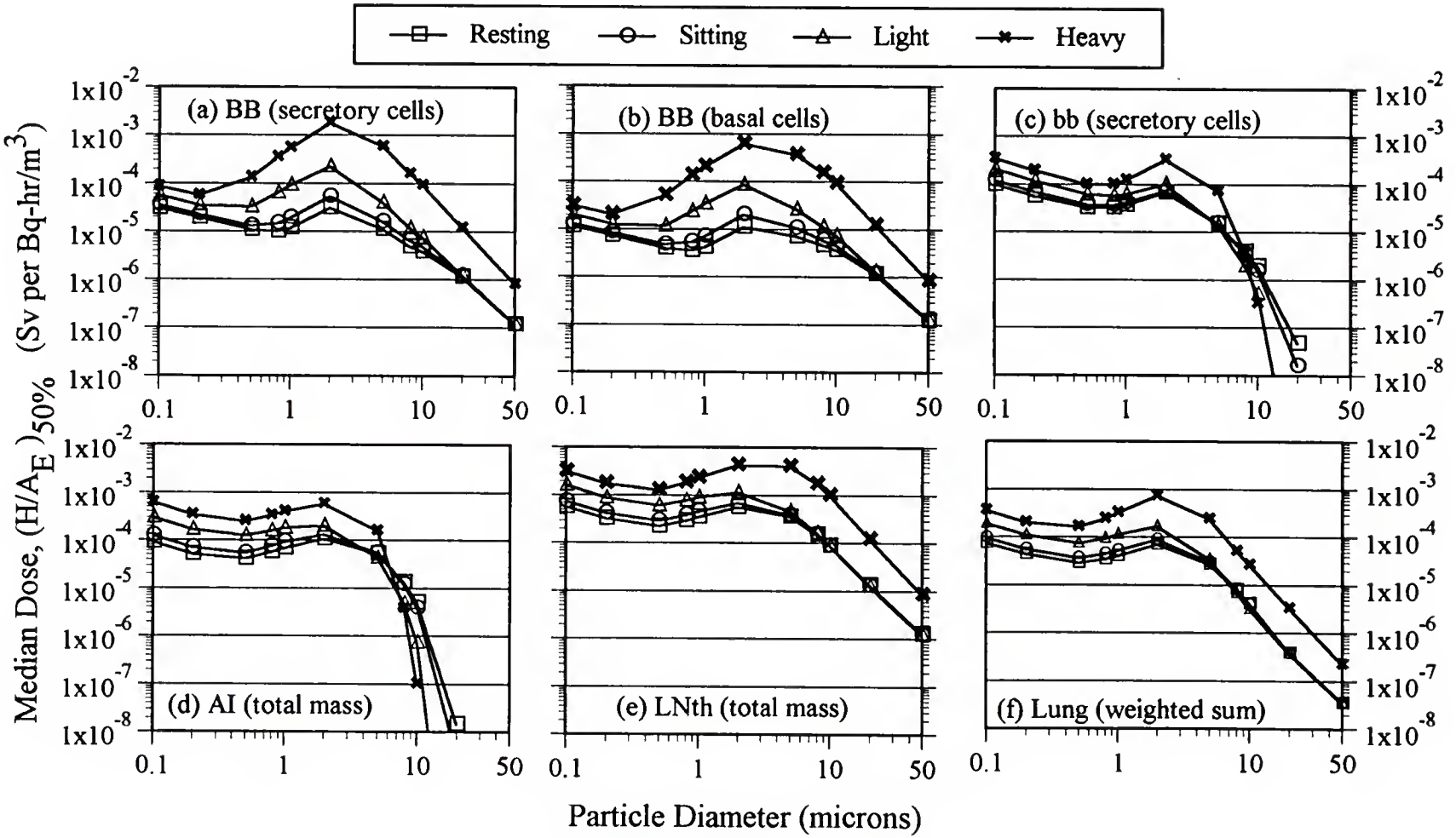

Figure 5-4. Estimated values of $(H/A_E)_{50\%}$ to all thoracic targets for adult males (25-34 years) at four exertion levels: resting, sitting, light, and heavy exertion. Based on exposure to $^{239}PuO_2$ -laden aerosol particles (monodisperse, unit density spheres).

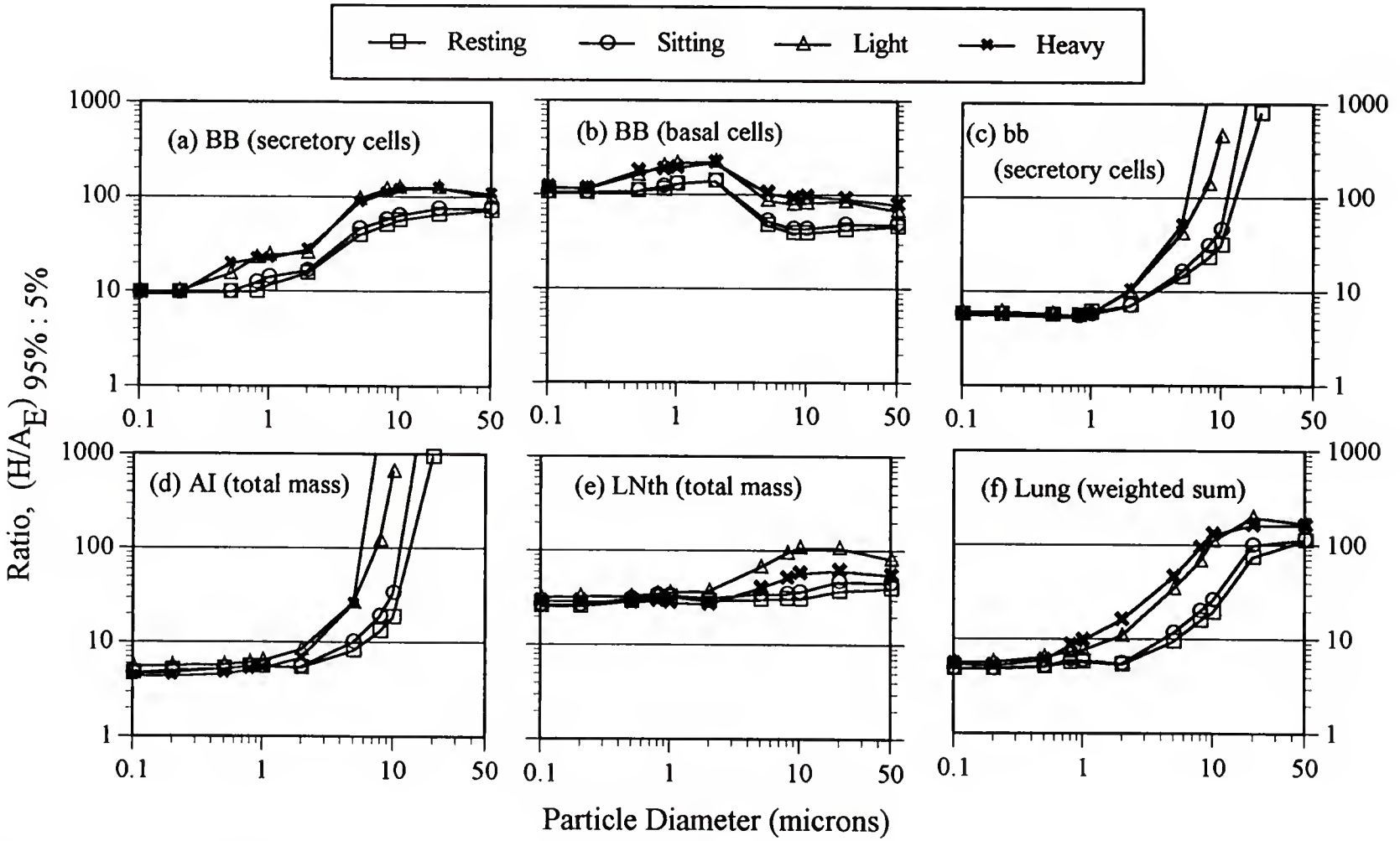

Figure 5-5. Estimated values of the ratio $(H/A_E)_{95\%:5\%}$ for all thoracic targets for adult males (25-34 years) at four exertion levels: resting, sitting, light, and heavy exertion. Based on exposure to $^{239}PuO_2$ -laden aerosol particles (monodisperse, unit density spheres).

$(H/A_E)_{95\%:5\%}$ for the five target tissues (panels [a]-[e]) and for the lungs (weighted sum of five targets, panel [f]). Although the uncertainty increases sharply with particle size for bb secretory cells and AI tissues, this increase is accompanied by a sharp decrease in equivalent dose values (Fig. 5-4) to these tissues. Thus, the contribution of doses in bb_{scc} and AI tissues to $(H_{TH}/A_E)_{50\%}$ and $(H_{TH}/A_E)_{95\%:5\%}$ is expected to be negligible (relative to other target tissues) for particle diameters larger than about 5 microns.

5.3.3. Influence of Dose Integration Time

The 25-34 year-old male population group was examined at light exertion (for an acute activity deposition) by employing several *dose integration times* (see section 1.2.1) to provide information on the influence of integration time on dose uncertainties for $^{239}PuO_2$ aerosols. The following integration times were selected: 10 days, 100 days, 365 days (1 year), 3650 days (10 years), 10950 days (30 years), 18250 days (50 years), and 25550 days (70 years). A (monodisperse) particle diameter of 1 μm was used to provide typical results (similar calculations at 5 μm revealed similar trends). Figure 5-6 summarizes these results. Panel (a) is a plot of the median dose values predicted. Panel (b) plots the percent contribution with respect to the 50-year median dose and was derived for targets by dividing median values in panel (a) by the respective median value (for the respective target tissue) at an integration time of 50 years. Panel (c) is a plot of the ratio of the 95% to 5% fractiles.

Results plotted in panel (b) show that virtually 100% of the 50-year dose in BB target tissues is delivered within the first year post intake. For bb secretory cells over 75%

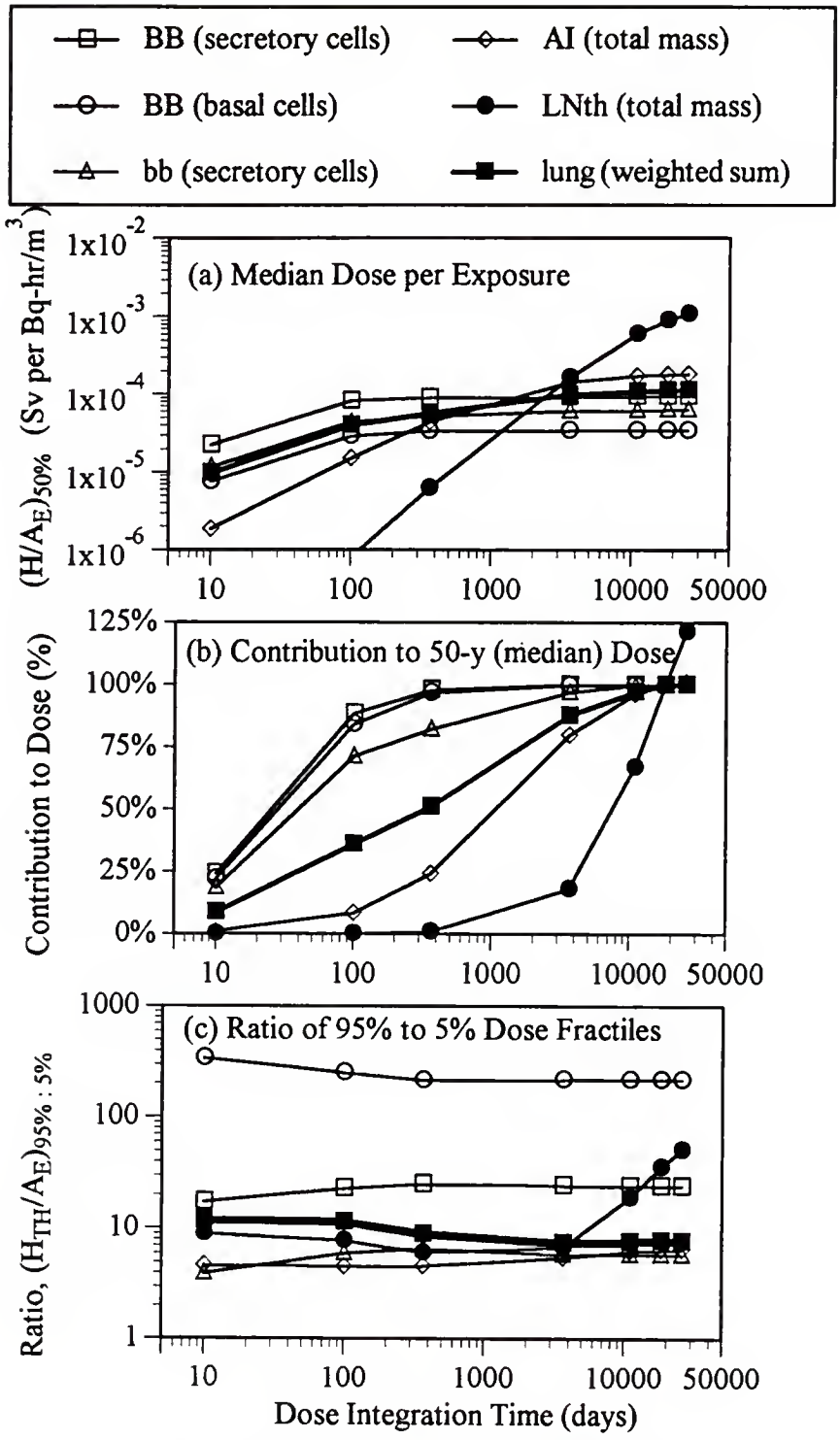

Figure 5-6. Influence of integration time on dose uncertainties. (a) Estimates of $(H/A_E)_{50\%}$ for various thoracic target tissues. (b) Percent of 50-year median dose contributed by stated integration times. (c) Ratio of 95% to 5% dose fractiles $(H_{TH}/A_E)_{95\%:5\%}$ versus integration time. Results based on 25-34 year-old males at light exertion inhaling a $^{239}PuO_2$-laden aerosol (monodisperse, unit density spheres with d_p = 1 μm).

of the 50-year dose is predicted to have been delivered within the first year post intake. The remaining 25% of the dose to bb_{scc} results primarily from the AI source component (i.e., alpha particles that cross the subepithelial layer between AI source and the bb_{scc} layer). For the AI tissues, about 25% of the (50-year) dose is delivered by the first year; about 50% is delivered in three years; 75% is delivered by 10 years; and virtually all of the 50-year dose is delivered by 30 years. For the thoracic lymph nodes (that receive a very low risk apportionment, or weighting, factor), model predictions indicate that only about 25% of the dose is delivered in the first ten years post intake; the rest is delivered over the next 40 years. Two reasons exist to explain the large difference in lymph node doses compared to other targets. First, no inhaled particles deposit in the lymph nodes; material is transported from other regions of the respiratory tract to lymph nodes (primarily by macrophages for insoluble materials). In contrast all other regions (BB, bb, and AI) receive an initial deposit of material and associated target layers (BB_{scc}, BB_{bas}, bb_{scc}, AI) are in immediate range of source emissions. Second, insoluble material cleared to lymph nodes can only be removed by absorption to blood (which is quite slow for relatively insoluble materials).

Although a complex pattern is seen for the median dose values in most targets with respect to integration time, panel (c) of Figure 5-6 indicates that the uncertainty in dose values (as quantified by the ratio of 95% to 5% dose fractiles) is relatively constant for most targets. Only the LNth tissues demonstrate a sharp increase in uncertainty with integration time (for times greater than 10 years). Sensitivity of doses to lymph nodes are

examined in section 5.4; indications are that most of the variability in dose is due to variabilities in the clearance rate constant for slow-phase absorption to blood, s_s.

Practical implications of results in Figure 5-6 are that dose uncertainties in most of the target tissues (including the weighted lung) can be characterized at a 50 year integration time (e.g., by the ratio in panel [c] or by a geometric standard deviation which could be derived from the ratio) and applied at other times without much error (in all except lymph nodes). Only the median values (central tendency of the dose distribution, panel [a]) change significantly with the dose integration time.

5.3.4. Influences of Age and Gender

The influences of the age and gender on dose uncertainties for various target regions are also of interest. To compare doses for various age/gender groups, a dose integration time of 70 years was used for ages less than 18 years; an integration time of 50 years was used for adults. These integration times are based on recommendations of the ICRP (1991a) and are meant to provide conservative dose predictions for radiation protection purposes. For example, if an adult is exposed at age 40, a 50-year integration implies that the person lives to an age of 90 years. Similarly for 15 year old, a 70-year integration time implies that the person lives to an age of 85 years. However, as indicated previously in Fig. 5-6, the addition of 20 years to the dose integration time has a negligible effect on doses to all tissues examined here but the thoracic lymph nodes.

Before presenting results, some limitations must be acknowledged. While integrating over time, it was assumed that the source-target geometry (e.g., including mass

of target tissues and surface areas of airway regions) remained fixed over the dose integration time (i.e., dimensions were assigned based on age at intake and growth was ignored). This assumption allowed simplification of the mathematical complexity involved in computing doses (i.e., time dependency of many factors were removed and Equation 2-13 could be used). Although not a problem for adults, this limitation leads to potentially conservative dose estimates for children in this work.

Consider first doses to BB and bb target tissue layers. Results shown previously in Figure 5-6 indicate that most of the doses to BB and bb tissues (due $^{239}PuO_2$ inhalation) are contributed by the first year so that the error introduced by assuming negligible growth is not a problem in these tissues. Consider next doses to AI tissues. Figure 5-6 indicates that dose to this region is delivered over a longer time (over ~30 years post intake). The mass of the AI region (approximately equal to the total lung mass; see Figure 4-19) increases by about a factor of five from 2 years of age to maturity. For children, a considerable portion of the total dose to the AI region (from an acute intake) can be delivered during growing years. The AI mass would then be under-estimated during all but the first year after the intake; and consequently, the AI dose would be over-estimated (since dose is inversely proportional to the target mass). Generally, the over-estimation would be less than a factor of five. A similar conservative effect is expected for LNth tissues, since the mass is modelled as proportional to the total lung mass (Eq. 4-48). Since the dose to the lungs (weighted sum) includes all targets, the conservative effect would be less (than that seen in AI and LNth) for the weighted lung dose.

Based on these conditions, Figure 5-7 shows values for (a) the median lung dose, $(H_{TH}/A_E)_{50\%}$, and (2) the ratio of 95% to 5% dose fractiles, $(H_{TH}/A_E)_{95\%:5\%}$, versus particle diameters for several age-gender groups at the light exertion level. Data in panel (a) indicate that age and gender of the exposed population group has only minor effects on the median dose to the lungs (weighted sum) per particle diameter. Ages groups are generally indistinguishable (with respect to median dose) for particle diameters less than about 2 μm. For diameters greater than about 2 μm, median doses for 2- and 5-year olds are predicted to be close to a factor of 2 greater than other age groups. The spread in doses as indicated by the ratio $(H_{TH}/A_E)_{95\%:5\%}$ in panel (b) follows a similar trend for all ages--increasing by about a factor of 10 with increasing particle diameter (from 1 to 20 μm). Except for ages of 2, 5, and 10 years (at $d_p > 1$ μm), all population groups are indistinguishable with respect to the ratio of fractiles (i.e., uncertainties in lung dose are relatively the same). The larger relative spread in doses for 2, 5, and 10 year olds is likely due to uncertainties in the breathing mode. For children, the methodology developed for this study results in a large fraction of children being classified as mouth breathers (see Eq. 4-32) compared to adults. Sensitivity studies of the deposition model (discussed in section 5.5) indicate that the fraction of air breathed by the nose, F_n, is an important parameter in the deposition model. Although sensitivity studies have not been performed for younger age groups, it is suspected that uncertainties in this parameter are responsible for the increased relative uncertainty demonstrated in Figure 5-7(b). This model parameter likely explains the increased median doses seen for 2 and 5 year olds as well (in Figure 5-7[a]).

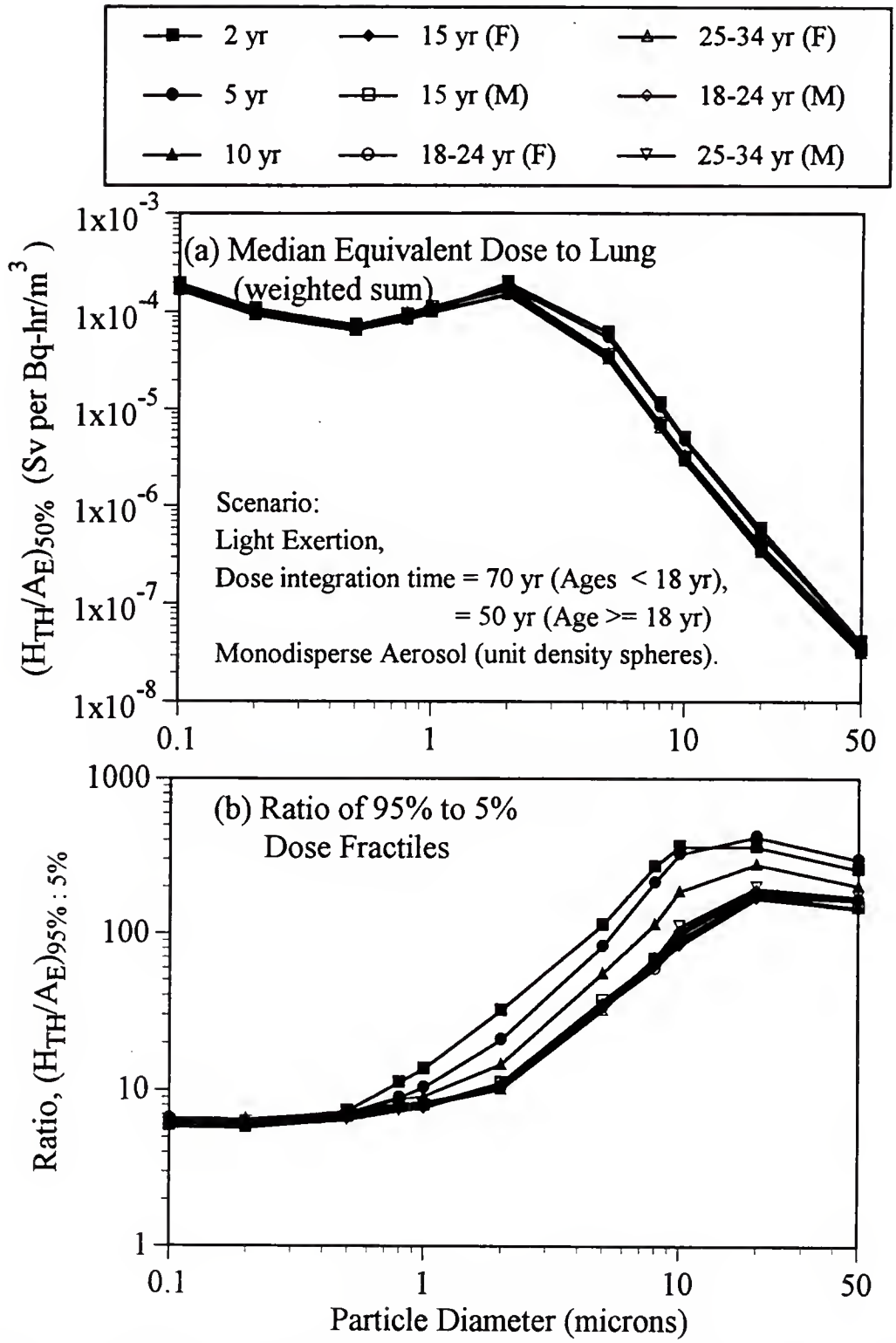

Figure 5-7. Influences of age and gender on dose uncertainties (versus particle diameter). (a) Estimates of $(H_{TH}/A_E)_{50\%}$. (b) Ratio of 95% to 5% dose fractiles $(H_{TH}/A_E)_{95\%:5\%}$. Based on inhalation of $^{239}PuO_2$-laden aerosol (monodisperse, unit density spheres) at light exertion.

Figure 5-8 shows increased resolution in lung dose by plotting median doses to each of the five target tissues (versus particle diameter) for these age groups. Panels (a-e) are for the regional targets and panel (f) is for the lungs (weighted sum of targets; the same as Figure 5-7[a]). This figure indicates more differences on a regional scale than are seen for the combined lung dose; however, differences are still quite small. The differences are generally much less than those indicated in Figure 5-4, which compared median doses for a single age group at different exertion levels.

As an indication of the uncertainty, Figure 5-9 accompanies Figure 5-8 and shows plots of the ratio of the 95% to 5% dose fractiles (versus particle diameter) for the nine age groups examined. The panels in Figure 5-9 indicate that for particles larger than 1 μm the 2, 5, and 10 year age groups generally have higher relative spreads in dose values compared to other groups. Again this difference is likely attributable to an increased sensitivity of the deposition model with respect to F_n at these younger ages.

5.3.5. Influences of Particle Size Dispersion

Dose predictions presented up to this point were based on monodisperse activity-size distributions. In other words, for a specified exposure scenario all radioactivity was assumed to be associated with a single particle diameter. Generally, except under controlled conditions, activity is associated with a distribution of particle sizes. Most often this activity-size distribution is unimodal and approximated by a lognormal probability distribution. An activity median (aerodynamic or thermodynamic) diameter and a geometric standard deviation, denoted here as $GSD(d_p)$, are used to characterize the

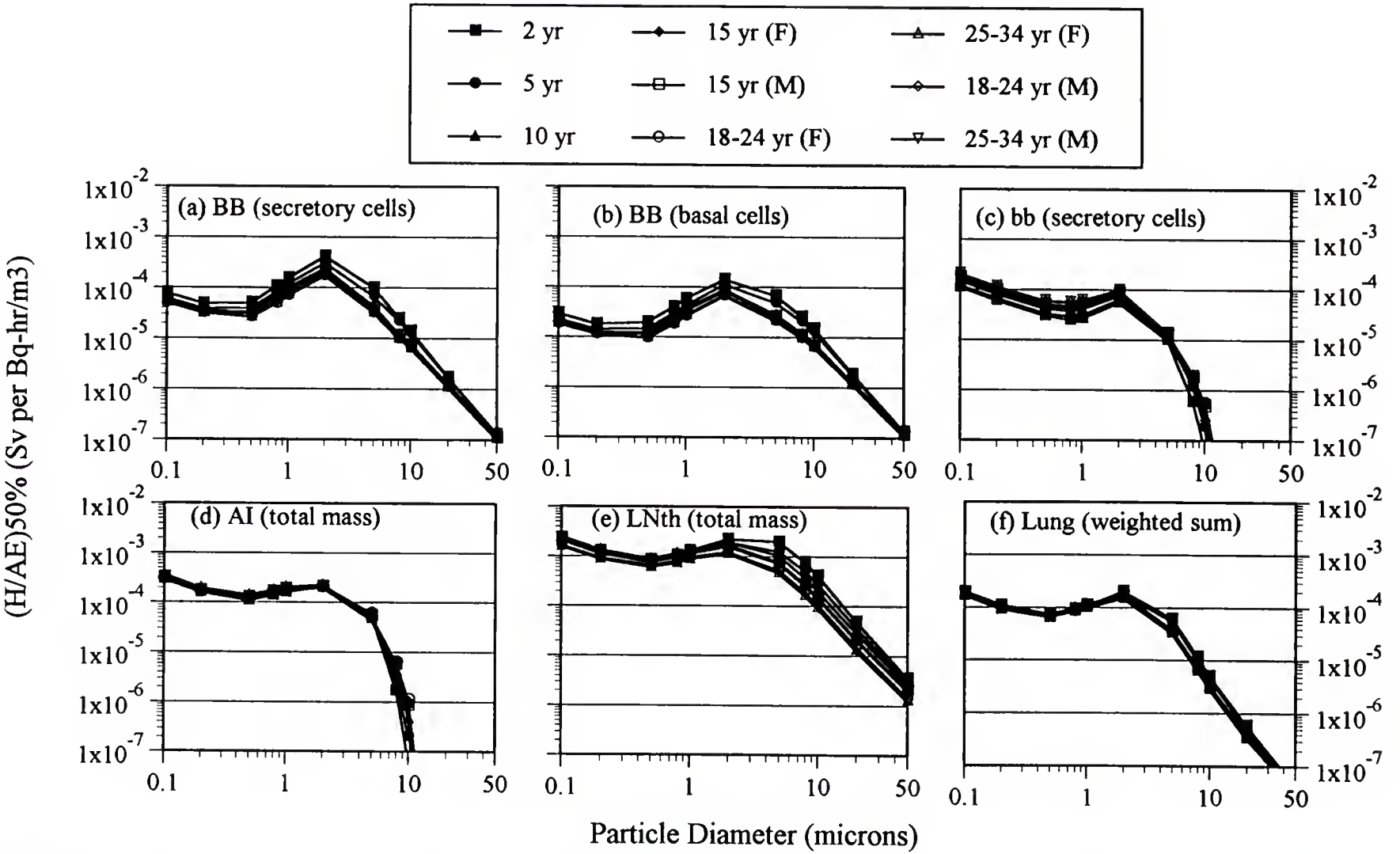

Figure 5-8. Estimated values of $(H/A_E)_{50\%}$ versus particle diameter to all thoracic targets (versus particle diameter) for nine different age groups, all at light exertion. Based on exposure to $^{239}PuO_2$ -laden aerosol particles (monodisperse, unit density spheres).

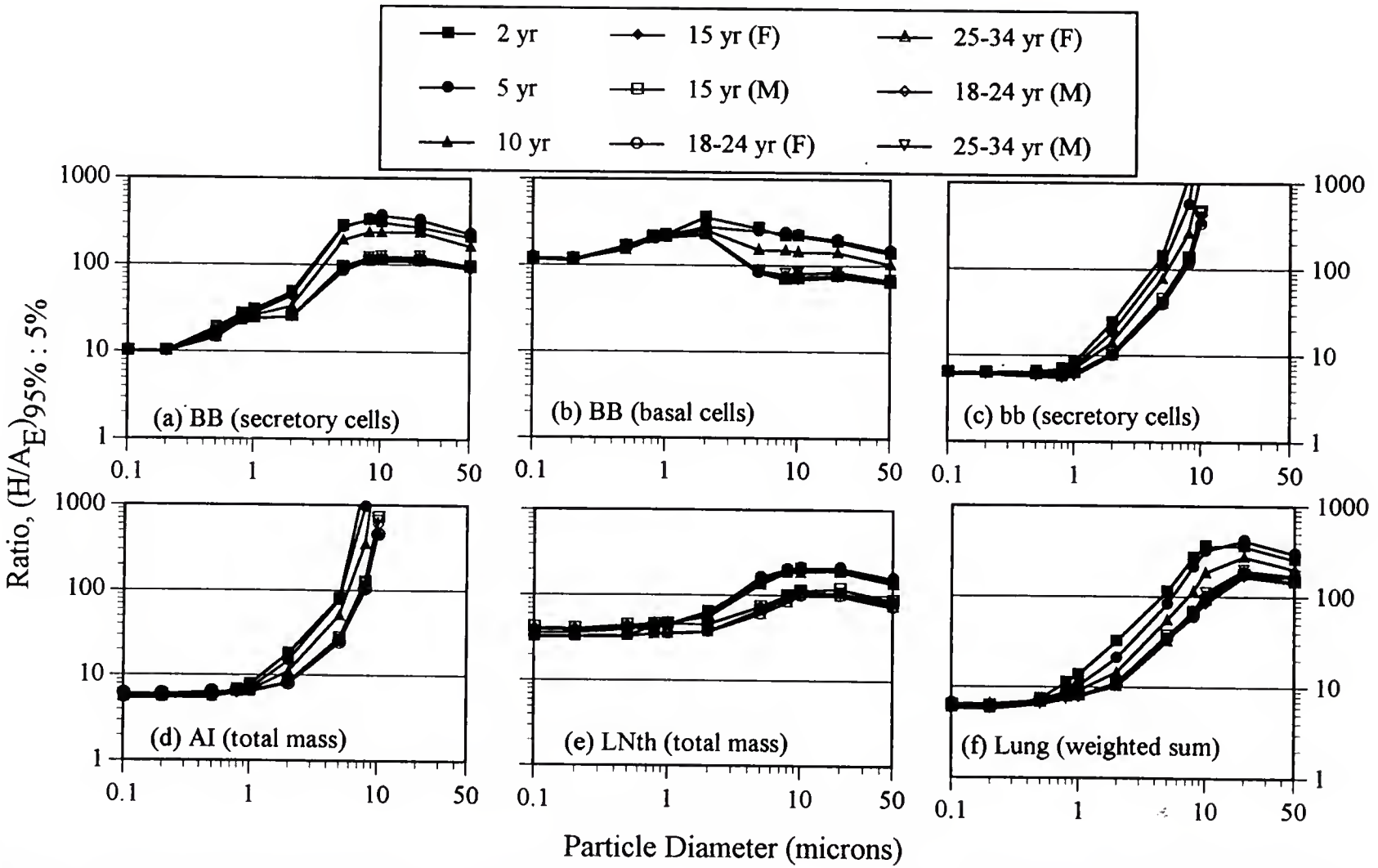

Figure 5-9. Estimated values of the ratio $(H/A_E)_{95\%:5\%}$ for all thoracic targets (versus particle diameter) for nine age groups at light exertion. Based on exposure to $^{239}PuO_2$ -laden aerosol particles (monodisperse, unit density spheres).

distribution. To examine the influence of the activity-size distribution on predicted dose distributions, LUDUC was run for various activity median diameter (AMD) and GSD(d_p) values for the 25-34 year-old male population group (at light exertion). In computations particles were assumed to comprise unit density spheres (so that the physical diameter, aerodynamic diameter, and thermodynamic diameters are all equal). Values of one, two, three, and four were selected for the GSD(d_p). A GSD(d_p) value of one corresponds to monodisperse (or single-sized) aerosol particles. As the GSD(d_p) increases, the activity-size distribution widens, with respect to particle size, and the airborne activity concentration is associated with a larger range of particle diameters.

Figure 5-10 plots results for the dose to the lungs, H_{TH}/A_E (weighted sum of target tissues), for various GSD(d_p) and activity median diameters, or AMDs. Panel (a) shows the median dose; panel (b) shows the ratio of the 95% to 5% dose fractiles. Results in panel (a) indicate that an increase in GSD(d_p) generally leads to an increase in $(H_{TH}/A_E)_{50\%}$ for a specific AMD. These effects are due to particle deposition mechanisms--particles with diameters less than ~2 μm generally have a greater probability of depositing in the lungs (versus extrathoracic airways) than larger particles (in the size range examined). Results in panel (b) of Fig. 5-10 indicate that size dispersion has a negligible effect on dose uncertainty (i.e., spread in dose values) for size distributions with AMD < ~1 μm. But for larger AMDs, an increase in the size dispersion, or value of GSD(d_p), leads to a decrease

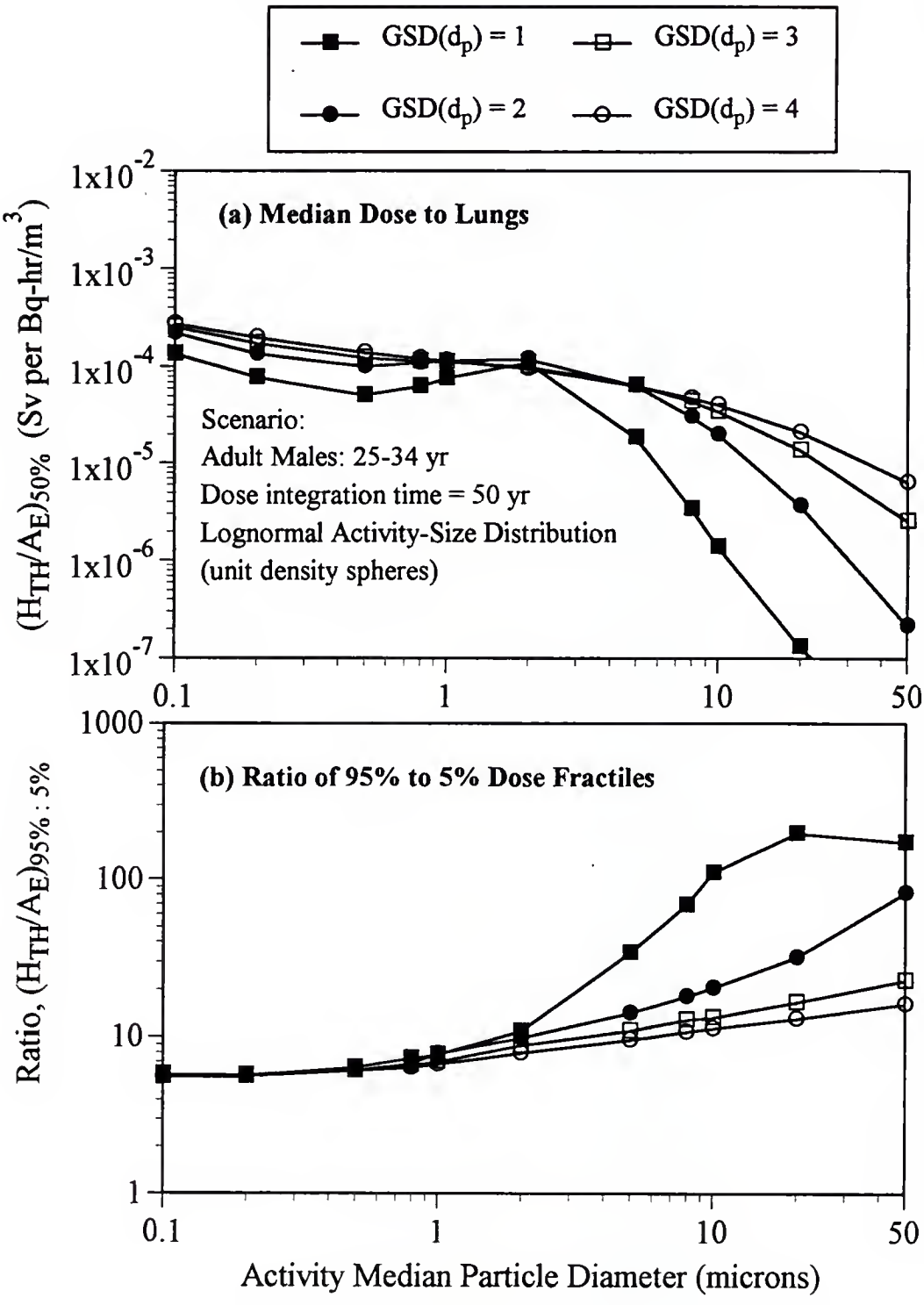

Figure 5-10. Influence of activity-size dispersion on lung dose uncertainties; shown for various activity median diameters (assumes unit density spheres). (a) Estimated median values for H_{TH}/A_E (Sv-hr/m^3). (b) Ratios of 95% to 5% dose fractiles, $(H_{TH}/A_E)_{95\%:5\%}$ for lungs. Based on exposure to $^{239}PuO_2$-laden aerosol particles.

in the dose uncertainty (indicated by a decrease in the ratio of the 95% to 5% dose fractiles). The dose uncertainty for a monodisperse aerosol decreases slightly at the largest size shown.

To better understand the trends shown for the weighted dose to the lungs, doses to the five thoracic target tissues are examined. Figure 5-11 shows median doses to the five target tissues (panels [a]-[e]) and for the lungs (a weighted sum of the targets, panel [f]). A similar trend in the median dose is seen for all target tissues. A more disperse activity-size distribution generally lessens the sensitivity of the median dose with respect to changes in the activity median particle diameter. Also for a given AMD, the median dose increases with increasing GSD(d_p). This increase is quite large for AMD > ~2 μm. Figure 5-12 shows the ratio of the 95% to 5% dose fractiles for the five target tissues (panels [a]-[e]) and the lungs (weighted sum; panel [f]). The ratio is undefined for particles larger than 10 microns in bb and AI tissues because the 5% dose fractile is zero. Except for the BB basal cells, there is generally an increase in the dose uncertainty with AMD for all scenarios and all regions; for AMD > ~2 μm, a steeper increase in relative dose uncertainty occurs for monodisperse particles (GSD[dp] = 1) compared to polydisperse aerosols.

For a polydisperse aerosol, half of the activity is associated with particles having d_p<AMD. This half of the activity contributes more to the dose than the other half associated with larger particles. Since uncertainties are generally less for the smaller particle sizes (which contribute more to the dose), the overall effect is a narrower

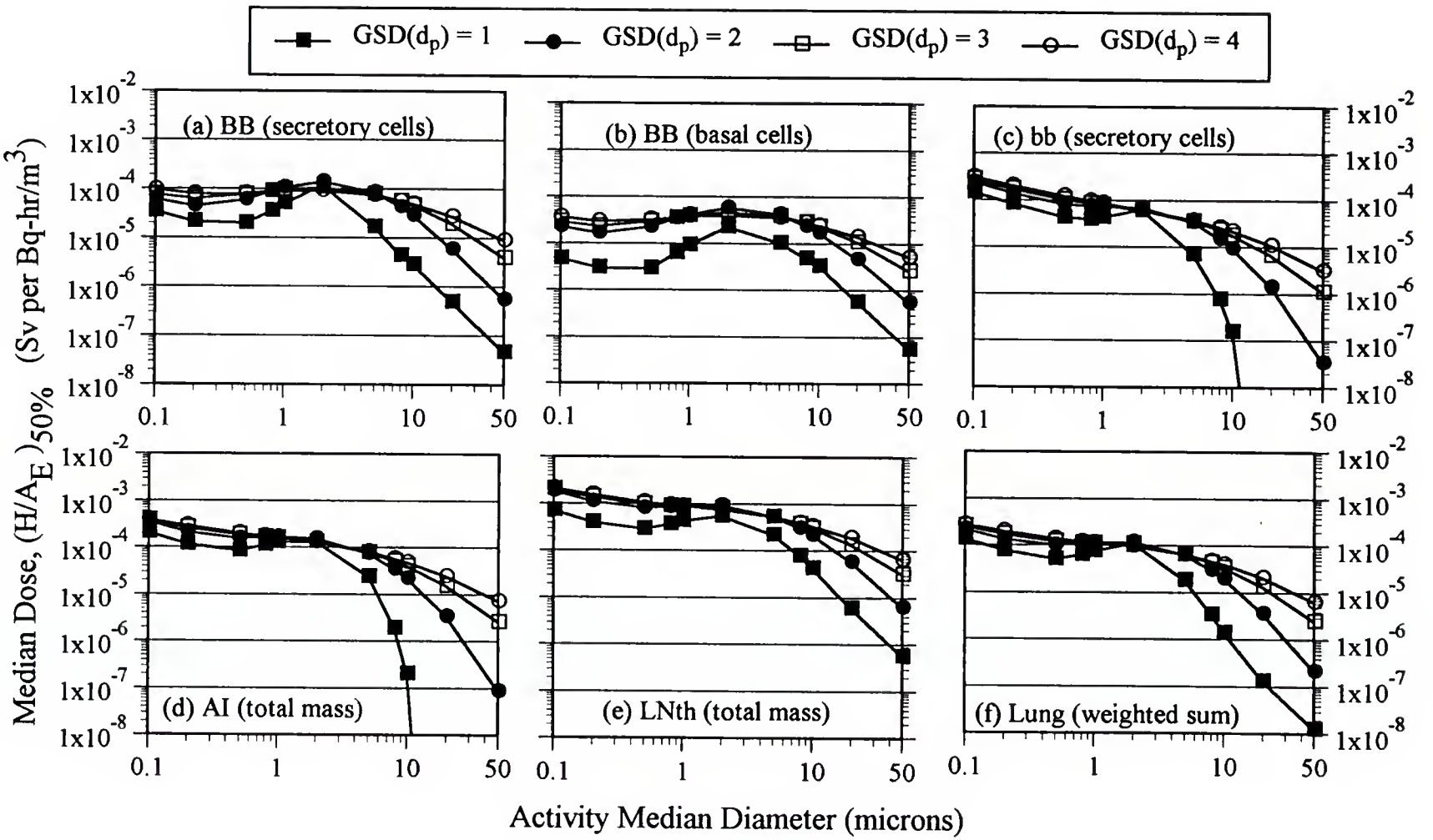

Figure 5-11. Estimated values of $(H/A_E)_{50\%}$ versus activity median diameter for thoracic tissues in adult males (25-34 years, light exertion) at four GSD(d_p) values. Based on exposure to $^{239}PuO_2$-laden aerosol particles (unit density spheres).

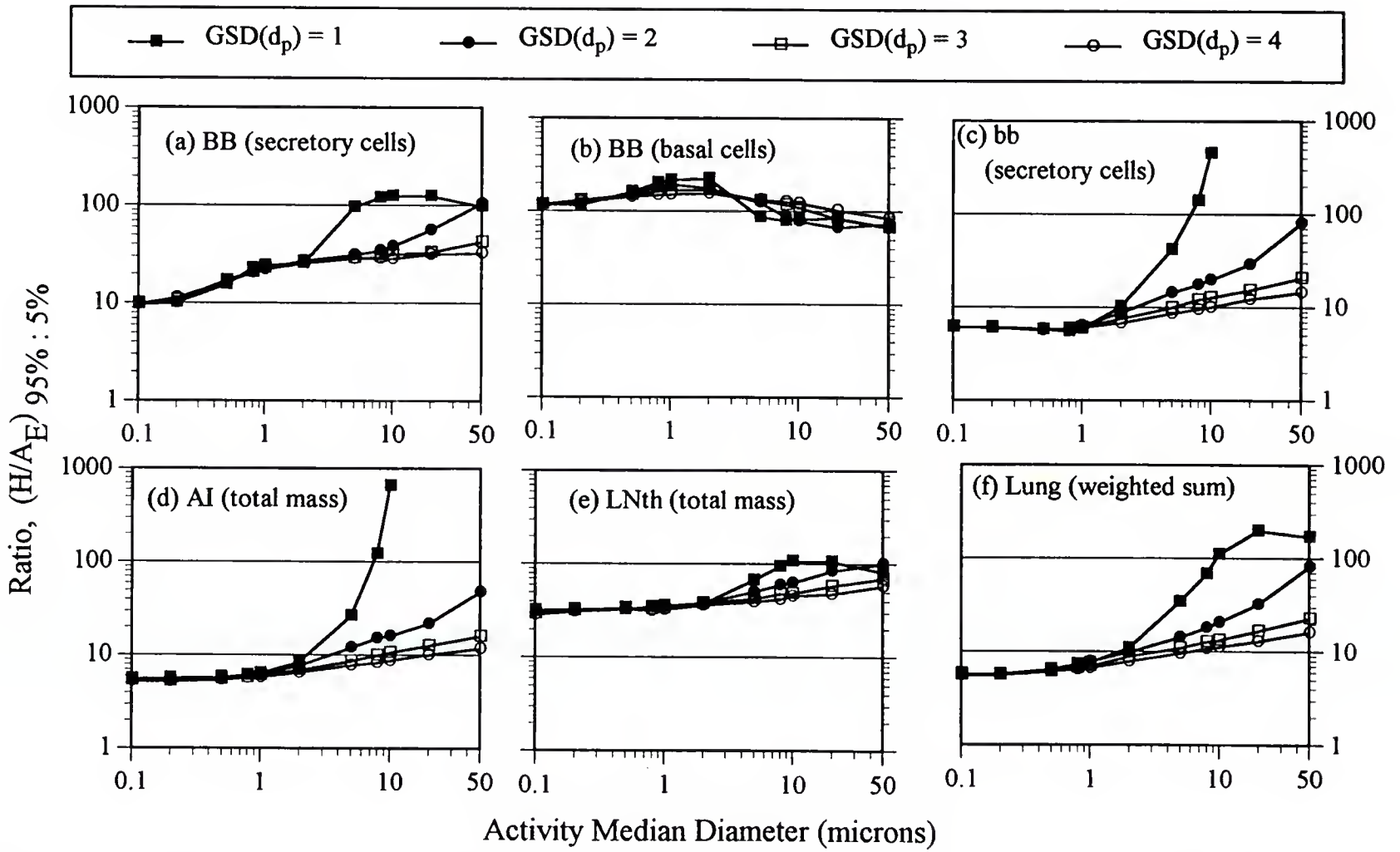

Figure 5-12. Estimated values of the ratio $(H/A_E)_{95\%:5\%}$ versus activity median diameter for thoracic tissues in adult males (25-34 years, light exertion) at four GSD(d_p) values. Based on exposure to $^{239}PuO_2$-laden aerosol particles (unit density spheres).

distribution in dose (less uncertainty) than is seen for a monodisperse aerosol with particle diameter equal to the AMD.

As an overall conclusion, Figures 5-10, 5-11, and 5-12 indicate that the value of $GSD(d_p)$ can have a significant influence on the distribution in dose values, depending on the value of the AMD. Assuming the AMD remains fixed, an increase in the $GSD(d_p)$ generally results in the following: (1) an increase in the median dose to a specific region (shown in Figures 5-10[a] and 5-11[all panels]) and (2) a decrease in the relative uncertainty for the dose (as indicated by a decrease in the ratio of the 95% to 5% dose fractiles in Figures 5-10[b], 5-12[a, c, d, e, f]). However, such generalization does not appear to hold for very large particles (e.g., Figure 5-12[e]) and for doses to the BB basal cell layer (Figure 5-12[b]).

5.4. Dose Sensitivity Results for Inhaled $^{239}PuO_2$

Sensitivity analyses were conducted for adult males (25-34 years old) exposed to $^{239}PuO_2$ aerosols at the light exertion level (acute deposition assumed). As discussed in Chapter 3, the objectives of a sensitivity analysis are to identify which model parameters most influence model predictions (i.e., rank input parameters with respect to their sensitivity) and to determine the contribution made by parameter variabilities to variabilities (or uncertainties) in model predictions. Sensitivity has been examined in this study by means of regression analyses (also discussed in Chapter 3) using the rank-transformed dose and deposition data generated by LUDUC. The data were generated by performing $n = 1000$ trials using Latin hypercube sampling techniques.

The sensitivities of model predictions on input variables have been investigated by determining the standardized rank regression coefficients (SRRCs) of selected input variables. The SRRC was discussed in Chapter 3. Based on *absolute* values of their associated SRRC's, input variables were ranked from one on up, where the most important variable (i.e., most sensitive) is assigned a rank of *one*. Concerning sensitivity, the sign of the SRRC (i.e., negative versus positive value) is not important; the magnitude is. A large, negative SRRC still indicates a strong monotonic association between output and input variables. A negative SRRC simply indicates that the output value decreases as the input value increases (or vice versa). In the results that follow input variables with negative SRRC values are enclosed in parentheses. This demarcation is to aid in interpreting results (i.e., to help in understanding the association between a specific input variable and the predicted quantity).

The SRRC only provides a measure by which to rank parameters based on their ability to affect model predictions; it is a normalized measure of the change in the model prediction per change in parameter value (or slope). To determine what fraction of the variability in the model prediction (e.g., equivalent dose to a specified target tissue) is attributable to variabilities in selected input quantities, step-wise rank-regression analyses are then performed. As discussed in Chapter 3, step-wise rank regression involves adding input variables to the regression model one at a time (generally starting with the most sensitive variable) and computing an R^2 value (i.e., coefficient of determination) for the regression. The R^2 value represents the fraction of the variance in the output variable (i.e., model prediction) that is explained by the input variable(s) included in the regression. As

a new variable is added to the regression model, the R^2 value increases. The value of this increase is a measure of the uncertainty contributed to the output variable by the added input variable. The present approach actually involves the rank-transformed data so that ultimately the R^2 values are a reflection of the variance in the ranks of the data. The data are rank-transformed in an effort to remove non-linear effects of the underlying model. The result of using rank-transformed data is that non-linear, monotonic relationships (with respect to input variables) are transformed into linear relationships. Hence, a larger fraction of the variance in the predictions of a non-linear, monotonic model can be explained by simple multiple-linear regression analysis.

5.4.1. Combined Lung Dose

To examine parameter sensitivities for H_{TH}/A_E, the approach was first to examine the sensitivity with respect to the equivalent doses in the five thoracic target tissues and with respect to parameters related to the risk-apportionment factors for those tissues. Following this step, a more detailed analysis was performed for the dose predictions in each of the five thoracic target tissues, namely, (1) the BB secretory cell layer, BB_{sec}, (2) the BB basal cell layer, BB_{bas}, (3) the bb secretory cell layer, bb_{sec}, (4) the AI tissues, and (5) the LNth tissues.

For H_{TH}/A_E, Table 5-1A shows the ranking of the selected input variables (based on the SRRC's). Generally, the sensitivity depends on the size of particles being inhaled. For $d_p \leq 5$ μm, results indicate that the equivalent dose to the AI region, $H(AI)/A_E$, (along with its associated risk-apportionment factor, A_{AI}) has the greatest influence on H_{TH}/A_E.

For $d_p > 5$ μm, the results indicate a shift in the most sensitive quantity to $H(BB_{scc})/A_E$ (along with parameters associated with its risk-apportionment, or weighting, factor). This shift occurs primarily since fewer particles deposit in the AI and bb regions at these larger sizes, while a relatively larger fraction of the activity deposits in the upper airways (BB region).

In efforts to determine how much of the variability in H_{TH}/A_E is explained by variabilities in regional doses and associated weighting factors, step-wise rank regression analyses have been performed for the four particles diameters referenced in Table 5-1A. The results of these step-wise regressions for H_{TH}/A_E are shown in Table 5-1B. The first row of entries (i.e., below column headings) corresponds to regression analyses (of rank-transformed data) performed with only the top ranked variable (i.e., rank = 1 in Table 5-1A, and variable as indicated in row for specific particle diameters). The second row of entries corresponds to the regression that results by adding the variable ranked second (in Table 5-1A) to the regression model; at this point only two "input" variables are included in the regression model. These steps continue until the all of the top four variables have been included (corresponding to the fourth data row of the table). As required, the value of R^2 increases as more variables are included in the regression model. Expressed as a percentage, the absolute increase in R^2, in going from one row down to the next, is a measure of the contribution the added variable makes to the variance in H_{TH}/A_E.

As an example of the information provided by results of these analyses consider particles with a diameter of $d_p = 5$ μm. Based on SRRC values, results in Table 5-1A

Table 5-1A. Combined equivalent dose to the lungs, H_{TH}/A_E: Ranking of selected variables based on standardized rank regression coefficients (SRRC) for inhalation of $^{239}PuO_2$-laden aerosols.

		Particle Diameter (μm)			
Description of Variable	Symbol	0.1	1	5	10
Equivalent Dose to BB (secretory cell nuclei)	$H(BB_{sec})$	5	3	2	1
Equivalent Dose to BB (basal cell nuclei)	$H(BB_{bas})$	6	4	3	3
Equivalent Dose to bb (secretory cell nuclei)	$H(bb_{sec})$	2	5	4	4
Equivalent Dose to AI tissues	H(AI)	1	1	1	5
Equivalent Dose to LNth tissues	H(LNth)	8	8	8	6
AI risk apportionment factor	A_{AI}	3	2	5	(7)
BB: (BB+bb) Relative Risk Factor	W_{BB}	(4)	7	6	2
BB_{bas}: (BB_{bas} +BB_{sec}) Relative Risk Factor	W_{basal}	(7)	(6)	(7)	8
Coefficient of Determination	R^2	0.82	0.82	0.88	0.89

Notes: Most sensitive parameter is assigned a rank of one. Values enclosed in parentheses denote a negative rank regression coefficient. Only top ten parameters are shown in listings. Exposure scenario: Adult Males, 25-34 yrs, light exertion, 50 yr dose integration time, monodisperse aerosol particles comprising unit density spheres.

Table 5-1B. Combined equivalent dose to the lungs, H_{TH}/A_E: Results of step-wise rank regression analysis for the four top-ranked respiratory tract model parameters. Based on inhalation of $^{239}PuO_2$-laden aerosols at specified particle diameters, d_p.

	$d_p = 0.1$		$d_p = 1$		$d_p = 5$		$d_p = 10$	
Ranks Included	Variable Added	R^2	Variable Added	R^2	Variable Added	R^2	Variable Added	R^2
1	H(AI)	0.39	H(AI)	0.45	H(AI)	0.55	$H(BB_{sec})$	0.67
1,2	$H(bb_{sec})$	0.56	A_{AI}	0.58	$H(BB_{sec})$	0.81	W_{BB}	0.79
1,2,3	A_{AI}	0.68	$H(BB_{sec})$	0.77	$H(BB_{bas})$	0.82	$H(BB_{bas})$	0.81
1,2,3,4	W_{BB}	0.79	$H(BB_{bas})$	0.78	$H(bb_{sec})$	0.83	$H(bb_{sec})$	0.87

Notes: First column lists the variables (by rank) included in regression analysis steps. Columns labeled "Variable Added" identify the variable added to the regression model at each step (these are described in the previous table). Columns labeled "R^2" report the coefficient of determination, R^2, for the (multiple) linear regression model (based on rank-transformed data) constructed with the variables indicated in the first column (by rank).

show that the dose to the lungs (H_{TH}; weighted sum of targets) is most sensitive to the following top-ranked variables: H(AI), $H(BB_{sec})$, $H(BB_{bas})$, and $H(bb_{sec})$. Based on step-wise rank regression with these four top-ranked variables, results in Table 5-1B (d_p = 5μm) indicate that variabilities in H(AI) accounts for 55% of the variance in H_{TH}; $H(BB_{sec})$ accounts for an additional 26% (i.e., 0.81 minus 0.55) of the variance; and $H(BB_{bas})$ and $H(bb_{sec})$ only account for an additional 2% of the variance. Therefore, these four variables together account for 83% of the variance in H_{TH}/A_E. To understand uncertainties in H_{TH}/A_E better, the focus of analyses then shifts (for d_p = 5 μm) to sensitivities related to H(AI) and $H(BB_{sec})$, since these two variables contribute 81% of the variance in H_{TH}/A_E.

Note that correlations may exist between some input variables in the regression model. If a variable is ranked high and is highly correlated with another variable, the SRRC ranking method could result in both variables receiving a high rank. However, if two variables are highly correlated and the second variable is added during step-wise regression, little or no increase in the R^2 value is expected to occur, providing a signal that a strong correlation exists. If only a mild correlation exists, then addition of the second variable can still result in an increased R^2 value--meaning that the second variable did in fact offer some additional explanatory power to the overall variance in the predicted quantity. Therefore, depending on the specific variables, a high rank as predicted by the SRRC value can, in the case of strong correlations, result in a minor contribution to the explanatory power of the step-wise regression model.

Results in Tables 5-1A and 5-1B indicate that the dose to the AI tissues, as a single variable, contributes the most to the variance in H_{TH}/A_E for $d_p < \sim 10$ μm. As d_p

approaches 10 μm, the dose to the BB secretory cell layer along with parameters associated with its apportionment factors, namely W_{BB}, become the larger contributors to uncertainties in H_{TH}/A_E. For a polydisperse aerosol with an activity median diameter within the range of sizes examined here and a GSD(d_p) of about 3, it is expected that the dose to the AI region would generally dominate as the most sensitive contributor to variabilities in the lung dose. This dominance is expected because activity associated with smaller particle sizes (where dose to the AI dominates the uncertainty) generally contributes more to the lung dose than activity associated with larger particles. This concept was illustrated in section 5.3.5.

5.4.2. Regional Tissue Doses

Investigations of parameter sensitivities for equivalent dose (per activity exposure) were conducted for all five thoracic target tissues. Results are shown in Tables 5-2A and 5-2B for $H(BB_{scc})/A_E$; in Tables 5-3A and 5-3B for $H(BB_{bas})/A_E$; in Tables 5-4A and 5-4B for $H(bb_{scc})/A_E$; in Tables 5-5A and 5-5B for $H(AI)/A_E$; and in Tables 5-6A and 5-6B for $H(LNth)/A_E$. The R^2 values that appear in Tables 5-2A, 5-3A, 5-4A, 5-5A, and 5-6A provide measures of the validity of the rank-regression approach for explaining model sensitivity. Generally, for all target tissues and all particle sizes examined, the rank-regression approach was able to explain over 90% of the variability in dose quantities. Although the results in these tables provide support for a very detailed discussion (for exposure to given particle sizes), the discussion in following paragraphs is limited to more general findings. It is stressed that these results apply to inhaled $^{239}PuO_2$; however, for

Table 5-2A. Equivalent dose to BB secretory cell layer, $H(BB_{scc})/A_E$: Ranking of variables based on standardized rank regression coefficients (SRRC) for inhalation of $^{239}PuO_2$-laden aerosols.

		Particle Diameter (μm)			
Description of Variable	Symbol	0.1	1	5	10
Particle clearance rate constant: BB_1 to ET_2	$m_{7,11}$	(10)			
Particle clearance rate constant: BB_2 to ET_2	$m_{8,11}$	(1)	(2)	(5)	(8)
Particle clearance rate constant: BB_2 to LNth	$m_{9,10}$			(7)	(6)
Fraction of BB deposit assigned to BB_{seq}	$f_d(BB_{seq})$	9	9	6	5
BB cilia/sol layer thickness	BB_{cilthk}	(8)	(8)		
BB epithelium thickness	BB_{epithk}	(2)	(3)	(4)	(4)
BB macrophage layer thickness	BB_{seqthk}				(10)
BB macrophage layer depth	BB_{seqdep}			(10)	(7)
BB secretory cell nuclei layer depth	BB_{secdep}	(5)	(5)	(9)	
BB surface area	SA(BB)	(7)	(7)		(9)
BB deposition fraction	DF_{BB}	4	1	2	1
AI deposition fraction	DF_{AI}		10	8	
Slow-cleared fraction of BB deposit (to BB_2)	f_s	6	6	1	2
Ventilation rate	V_E	3	4	3	3
Coefficient of Determination	R^2	0.94	0.93	0.94	0.89

Notes: See notes for Table 5-1A.

Table 5-2B. Equivalent dose to BB secretory cell layer, $H(BB_{scc})/A_E$: Results of step-wise rank-regression analysis for the four top-ranked model parameters. Based on inhalation of $^{239}PuO_2$-laden aerosols at specified particle diameters, d_p.

	d_p = 0.1 μm		d_p = 1 μm		d_p = 5 μm		d_p = 10 μm	
Ranks Included	Variable Added	R^2	Variable Added	R^2	Variable Added	R^2	Variable Added	R^2
1	$m_{8,11}$	0.34	DF_{BB}	0.49	f_s	0.34	DF_{BB}	0.33
1,2	BB_{epithk}	0.61	$m_{8,11}$	0.69	DF_{BB}	0.69	f_s	0.67
1,2,3	V_E	0.67	BB_{epithk}	0.81	V_E	0.74	V_E	0.72
1,2,3,4	DF_{BB}	0.80	V_E	0.88	BB_{epithk}	0.81	BB_{epithk}	0.78

Notes: See notes for Table 5-1B.

Table 5-3A. Equivalent dose to BB basal cell layer, $H(BB_{bas})/A_E$: Ranking of variables based on standardized rank regression coefficients (SRRC) for inhalation of $^{239}PuO_2$-laden aerosols.

		Particle Diameter (μm)			
Description of Variable	Symbol	0.1	1	5	10
Particle clearance rate constant: BB_2 to ET_2	$m_{8,11}$	(2)	(3)	(8)	(8)
Particle clearance rate constant: BB_2 to LNth	$m_{9,10}$	(7)	(7)	(6)	(5)
Fraction of BB deposit assigned to BB_{seq}	$f_d(BB_{seq})$	6	6	5	3
BB cilia/sol layer thickness	BB_{cilthk}	(10)	(9)		
BB epithelium thickness	BB_{epithk}	(1)	(1)	(2)	(6)
BB macrophage layer depth	BB_{seqdep}			(7)	(7)
BB basal cell nuclei layer thickness	BB_{basthk}	5	5		
BB surface area	SA(BB)	(9)	(10)	(10)	(9)
BB deposition fraction	DF_{BB}	4	2	1	1
AI deposition fraction	DF_{AI}			9	10
Slow-cleared fraction of BB deposit (to BB_2)	f_s	8	8	3	2
Ventilation rate	V_E	3	4	4	4
Coefficient of Determination	R^2	0.94	0.94	0.93	0.84

Notes: See notes for Table 5-1A.

Table 5-3B. Equivalent dose to BB basal cell layer, $H(BB_{bas})/A_E$: Results of step-wise rank-regression analysis for the four top-ranked model parameters. Based on inhalation of $^{239}PuO_2$-laden aerosols at specified particle diameters, d_p.

	d_p = 0.1 μm		d_p = 1 μm		d_p = 5 μm		d_p = 10 μm	
Ranks Included	Variable Added	R^2	Variable Added	R^2	Variable Added	R^2	Variable Added	R^2
1	BB_{epithk}	0.82	BB_{epithk}	0.68	DF_{BB}	0.32	DF_{BB}	0.39
1,2	$m_{8,11}$	0.85	DF_{BB}	0.84	BB_{epithk}	0.54	f_s	0.51
1,2,3	V_E	0.86	$m_{8,11}$	0.87	f_s	0.65	$f_d(BB_{seq})$	0.60
1,2,3,4	DF_{BB}	0.89	V_E	0.89	V_E	0.71	V_E	0.66

Notes: See notes for Table 5-1B.

Table 5-4A. Equivalent dose to bb secretory cell nuclei layer, $H(bb_{scc})/A_E$: Ranking of variables based on standardized rank regression coefficients (SRRC) for inhalation of $^{239}PuO_2$-laden aerosols.

		Particle Diameter (μm)			
Description of Variable	Symbol	0.1	1	5	10
Particle clearance rate constant: bb_1 to BB_1	$m_{4,7}$		(9)	(7)	(6)
Particle clearance rate constant: bb_2 to BB_1	$m_{5,7}$	(1)	(1)	(5)	(5)
Particle clearance rate constant: bb_2 to LNth	$m_{6,10}$				(9)
Fraction of bb deposit assigned to bb_{seq}	$f_d(bb_{seq})$				7
bb cilia layer thickness	bb_{cilthk}	(9)			
bb epithelium thickness	bb_{epithk}	(5)	(7)	(8)	(8)
bb subepithelial layer depth	bb_{subthk}	(7)	(4)	(6)	(10)
bb secretory cell nuclei layer depth	bb_{secdep}	(8)	(10)	(10)	
bb surface area	SA(bb)	(6)	(8)	(9)	
bb deposition fraction	DF_{bb}	3	3	1	1
AI deposition fraction	DF_{AI}	10	5	4	4
Slow-cleared fraction of bb deposit (to bb_2)	f_s	4	6	2	2
Ventilation rate	V_E	2	2	3	3
Coefficient of Determination	R^2	0.93	0.89	0.92	0.95

Notes: See notes for Table 5-1A.

Table 5-4B. Equivalent dose to bb secretory cell nuclei layer, $H(bb_{scc})/A_E$: Results of step-wise rank-regression analysis for the four top-ranked model parameters. Based on inhalation of $^{239}PuO_2$-laden aerosols at specified particle diameters, d_p.

	d_p = 0.1 μm		d_p = 1 μm		d_p = 5 μm		d_p = 10 μm	
Ranks Included	Variable Added	R^2	Variable Added	R^2	Variable Added	R^2	Variable Added	R^2
1	$m_{5,7}$	0.52	$m_{5,7}$	0.37	DF_{bb}	0.55	DF_{bb}	0.78
1,2	V_E	0.65	V_E	0.47	f_s	0.76	f_s	0.90
1,2,3	DF_{bb}	0.78	DF_{bb}	0.68	V_E	0.81	V_E	0.91
1,2,3,4	f_s	0.83	bb_{subthk}	0.74	DF_{AI}	0.83	DF_{AI}	0.92

Notes: See notes for Table 5-1B.

Table 5-5A. Equivalent dose to AI tissue, $H(AI)/A_E$: Ranking of variables based on standardized rank regression coefficients (SRRC) for inhalation of $^{239}PuO_2$-laden aerosols.

		Particle Diameter (μm)			
Description of Variable	Symbol	0.1	1	5	10
Particle clearance rate constant: AI_2 to bb_1	$m_{2,4}$	(4)	(4)	(4)	(4)
Particle clearance rate constant: AI_3 to bb_1	$m_{3,4}$	(6)	(5)	(6)	(6)
Particle clearance rate constant: AI_3 to LNth	$m_{3,10}$	(8)	(9)	(9)	(8)
Fraction of deposit absorbed rapidly (blood)	f_r	(9)	(8)	(8)	9
Blood absorption rate constant (rapid phase)	s_r	10	10	(10)	10
Blood absorption rate constant (slow phase)	s_s	(3)	(3)	(3)	(3)
Fraction of AI deposit assigned to AI_1	$f_d(AI_1)$	(7)	(7)	(7)	(7)
Lung mass	M(lung)	(5)	(6)	(5)	(5)
AI deposition fraction	DF_{AI}	2	1	1	1
Ventilation rate	V_E	1	2	2	2
Coefficient of Determination	R^2	0.93	0.92	0.95	0.99

Notes: See notes for Table 5-1A.

Table 5-5B. Equivalent dose to AI tissue, $H(AI)/A_E$: Results of step-wise rank-regression analysis for the four top-ranked model parameters. Based on inhalation of $^{239}PuO_2$-laden aerosols at specified particle diameters, d_p.

	d_p = 0.1 μm		d_p = 1 μm		d_p = 5 μm		d_p = 10 μm	
Ranks Included	Variable Added	R^2	Variable Added	R^2	Variable Added	R^2	Variable Added	R^2
1	V_E	0.36	DF_{AI}	0.33	DF_{AI}	0.78	DF_{AI}	0.94
1,2	DF_{AI}	0.60	V_E	0.61	V_E	0.86	V_E	0.96
1,2,3	s_s	0.81	s_s	0.80	s_s	0.92	s_s	0.98
1,2,3,4	$m_{2,4}$	0.88	$m_{2,4}$	0.88	$m_{2,4}$	0.93	$m_{2,4}$	0.98

Notes: See notes for Table 5-1B.

Table 5-6A. Equivalent Dose to thoracic lymph nodes (LNth), $H(LNth)/A_E$: Ranking of input variables based on standardized rank regression coefficients (SRRC) for inhalation of $^{239}PuO_2$-laden aerosols.

		Particle Diameter (μm)			
Description of Variable	Symbol	0.1	1	5	10
Particle clearance rate constant: AI_3 to bb_1	$m_{3,4}$	(5)	(5)	(10)	
Particle clearance rate const.: AI_3 to LNth	$m_{3,10}$	3	4	7	9
Particle clearance rate const.: bb_{seq} toLNth	$m_{6,10}$				10
Particle clearance rate const.: BB_{seq} to LNth	$m_{9,10}$				
Fraction of deposit absorbed rapidly (blood)	f_r	(9)			
Blood absorption rate constant: rapid phase	s_r	(10)			
Blood absorption rate constant: slow phase	s_s	(1)	(1)	(1)	(2)
Fraction of BB deposit assigned to BB_{seq}	$f_d(BB_{seq})$		8	5	3
Fraction of bb deposit assigned to bb_{seq}	$f_d(bb_{seq})$	7	9	8	8
Lymph node mass (LNth)	M(LNth)	(6)	(6)	(9)	(7)
BB deposition fraction	DF_{BB}		7	3	1
bb deposition fraction	DF_{bb}	8	10	6	5
AI deposition fraction	DF_{AI}	4	3	2	6
Ventilation rate	V_E	2	2	4	4
Coefficient of Determination	R^2	0.94	0.93	0.92	0.91

Notes: See notes for Table 5-1A.

Table 5-6B. Equivalent dose to LNth tissue, $H(LNth)/A_E$: Results of step-wise rank-regression analysis for the four top-ranked model parameters. Based on inhalation of $^{239}PuO_2$-laden aerosols at specified particle diameters, d_p.

	d_p = 0.1 μm		d_p = 1 μm		d_p = 5 μm		d_p = 10 μm	
Ranks Included	Variable Added	R^2	Variable Added	R^2	Variable Added	R^2	Variable Added	R^2
1	s_s	0.73	s_s	0.67	s_s	0.38	DF_{BB}	0.36
1,2	V_E	0.83	V_E	0.76	DF_{AI}	0.69	s_s	0.76
1,2,3	$m_{3,10}$	0.87	DF_{AI}	0.85	DF_{BB}	0.81	$f_d(BB_{seq})$	0.79
1,2,3,4	DF_{AI}	0.91	$m_{3,10}$	0.90	V_E	0.86	V_E	0.80

Notes: See notes for Table 5-1B.

similar materials (i.e., long-lived, relatively insoluble, primarily alpha-emitting materials), the results are expected to be very similar.

5.4.2.1. Bronchial region: secretory cell layer, BB_{scc}

Over the particle size range examined, various subsets of the five following input variables explain about 80% of the variability in $H(BB_{scc})/A_E$: (1) the fraction of activity deposited in the BB region, DF_{BB}, (2) the slow-clearing fraction of the tracheobronchial deposition, f_s, (3) the ventilation rate, V_E, (4) the thickness of the bronchial epithelium, BB_{epithk}, and (5) the clearance rate constant for particle transport from compartment BB_2 to ET_2 (see Figure. 2-6 and Table 2-5). As an example, Table 5-2B indicates that for particles with $d_p > \sim 5$ μm, roughly 70% of the variability in $H(BB_{scc})/A_E$ is explained by variabilities in only two parameters, DF_{BB} and f_s. For smaller particles ($d_p \sim 0.1$ μm), $m_{8,11}$ and BB_{epithk} together account for about 60% of the variability in $H(BB_{scc})/A_E$. The ventilation rate contributes about 5-8% to the variability in $H(BB_{scc})/A_E$ over the range of sizes examined.

5.4.2.2. Bronchial region: basal cell layer, BB_{bas}

Generally, the same variables are important for this target tissue as discussed above for BB_{scc}. As above, $H(BB_{bas})/A_E$ was found to be sensitive to DF_{BB}, f_s, BB_{epithk}, $m_{8,11}$, and V_E. For the largest particle size examined ($d_p = 10$ μm), the fraction of activity deposited in the BB region which is assigned to the sequestered compartment, $f_d(BB_{seq})$, was also among the four top-ranked variables. For smaller particles ($d_p \sim 0.1$ μm), the dose is very sensitive to thickness of the bronchial epithelium; roughly 80% of the

variability in dose is explained by variation in thickness, BB_{epithk}. As size increases, dose to the BB basal cell layer becomes increasingly more sensitive to changes in DF_{BB} and f_s; however, as indicated by the decreasing value of R^2 in the fourth row of Table 5-3B, the model is also sensitive to a larger number of variables (the top-four ranked variables only account for 66% of the variance at $d_p = 10$ μm).

5.4.2.3. Bronchiolar region: secretory cell layer, bb_{sec}

Tables 5-4A and 5-4B show results of sensitivity analyses for $H(bb_{sec})/A_E$. Six input variables described most of the variability in $H(bb_{sec})/A_E$. As listed in Table 5-4B these six variables include DF_{bb}, f_s, V_E, DF_{AI}, $m_{5,7}$ (clearance rate constant from compartment bb_2 to BB_1, e.g., see Fig. 2-6), and bb_{subthk} (the thickness between the AI region and the basement membrane of the bronchiolar epithelium). Results indicate that for smaller particle diameters, the dose is most sensitive to $m_{5,7}$--over 50% of the variability in dose is explained by this variable for $d_p = 0.1$ μm. For larger particles $H(bb_{sec})/A_E$ is most sensitive to the deposition fraction, DF_{bb}--over 50% of the variability in the dose is explained by this variable for $d_p \geq 5$ μm.

5.4.2.4. Alveolar-interstitial region: AI tissues

The variability in $H(AI)/A_E$, while influenced by particle diameter, depends primarily on four variables: DF_{AI}, V_E, s_s (the absorption rate constant for clearance of the slow-cleared phase of the deposited material to the blood), and $m_{2,4}$ (the clearance rate constant associated with particle transport from compartment AI_2 to bb_1). Generally, for smaller particles ($d_p < \sim 1$ μm), DF_{AI} and V_E contribute (approximately) equally to the

variability in $H(AI)/A_E$--accounting for about 60% of the variability together. The rate constant representing slow-phase absorption from the AI compartments to the blood, s_s, contributes an additional 20% to the uncertainty in $H(AI)/A_E$. For larger particles, the AI deposition fraction, DF_{AI}, dominates the dose variability--accounting for 78% of the variability at $d_p = 5$ μm and 94% of the variability at $d_p = 10$ μm.

5.4.2.5. Thoracic lymph node region: LNth tissues

Although the dose to the thoracic lymph nodes is generally not of much concern from a risk perspective, the variability in $H(LNth)/A_E$ is examined, for completeness, in Tables 5-6A and 5-6B. These tables indicate that $H(LNth)/A_E$ is sensitive primarily to s_s (which represents the rate constant for slow-phase absorption of material from all respiratory tract regions, except ET_1, to the blood) and to V_E, DF_{AI}, and DF_{BB}. A large sensitivity with respect to DF_{BB} occurs only for larger particle sizes ($d_p \sim 5$ μm and greater). For the particle diameters from about 0.1 to 1 μm, s_s appears to account for about 70% of the variance in $H(LNth)/A_E$. As d_p increases to larger sizes, the contribution made by s_s to the variability in $H(LNth)/A_E$ decreases to about 40%. The ventilation rate contributes about 10% to the variance at smaller sizes (~ 0.1 μm); however, this contribution decreases to ~1% at larger sizes (~10 μm). At larger sizes the deposition fraction in the BB region becomes important--accounting for ~35% of the variability in the dose at $d_p = 10$ μm.

5.5. Deposition Sensitivity Results

The results shown in the previous tables do not include detailed analyses with input variables of the deposition model; rather, these tables summarize results of analyses with deposition fractions as inputs to the clearance and dose models. Generally, the previous results indicate that uncertainty in deposition fractions are among the larger contributors to the uncertainty in the predicted equivalent doses to target tissues in the lungs. For example, Tables 5-5A and 5-5B indicate that a large amount (~24% to 94% depending on particle size) of the variability in $H(AI)/A_E$ is due to variability in the fraction of inhaled activity deposited in the AI region, denoted DF_{AI}. So the next logical step in examining model sensitivity was to perform sensitivity analyses on input variables for the deposition model. Sensitivity results for deposition model predictions (i.e., deposition fractions) are presented in Table 5-7 and in Tables 5-8A, 5-8B, and 5-8C for the BB, bb, and AI regions, respectively. Table 5-7 shows the ranks of various deposition model variables as predicted by SRRC analysis. Some measure of the validity of this approach is indicated by the R^2 values shown in Table 5-7; generally, again rank regression is able to account for over 90% of the variance in deposition fractions. Table 5-8 shows results of step-wise regression analyses (at four particle diameters) for the top four variables identified in Table 5-7. As in previous tables, these results are based on regression analyses with the rank-transformed (input and output) data for the adult male population group (25-34 years at light exertion).

Table 5-7. Ranking of the top ten input variables as determined by standardized rank-regression coefficients (SRRCs) for deposition fractions in respiratory tract regions. Based on unit density spheres (monodisperse) and a population group of 25-34 year old males at light exertion.

		Output: DF_{BB} d_p (μm)				Output: DF_{bb} d_p (μm)				Output: DF_{AI} d_p (μm)			
Description of Variable	Symbol	0.1	1	5	10	0.1	1	5	10	0.1	1	5	10
Anatomical dead space	V_D	4		(9)		3	3	(7)	(7)	(5)	(9)		7
Ventilation rate	V_E	(3)	2	(7)	(4)	(2)	(2)	(5)	(1)	(3)	(1)	(2)	(1)
Tidal volume	V_T	5			10	6		(9)	(9)	1	2	6	9
Functional residual capacity	FRC	(7)				(9)			10	6			
Vital capacity	VC												
Nasal flow fraction	F_n		(5)	(1)	(1)		(5)	(1)	(4)		(6)	(1)	(3)
Tracheal diameter	d_0	(1)	(3)	4	3	(5)		2	2	8	7	4	4
Generation 9 diameter	d_9	9				(4)	(9)			10			
Generation 15 diameter	d_{15}	6		10		8				(4)	(4)	(10)	(10)
Inhalability	I_o		4	5	6	10	4	8	8		5	8	8
Aero. uncertainty term for ET_1	$c_{ae}(ET_1)$		(7)	(6)	(8)		(8)	(10)			(10)		
Aero. uncertainty term for ET_2	$c_{ae}(ET_2)$		(6)	(2)	(2)		(6)	(3)	(5)	(9)	(8)	(3)	(6)
Aero. uncertainty term for BB	c_{ae}(BB)		1	3	5			(6)	(3)			(5)	(2)
Aero. uncertainty term for bb	c_{ae}(bb)						1	4	6			(9)	(5)
Aero. uncertainty term for AI	c_{ae}(AI)		(8)		9		(10)				3	7	
Thermo. uncertainty term, ET_1	$c_{th}(ET_1)$	(10)											
Thermo. uncertainty term, ET_2	$c_{th}(ET_2)$		10	8	7								
Thermo. uncertainty term for BB	c_{th}(BB)	2											
Thermo. uncertainty term for bb	c_{th}(bb)					1	7			(7)			
Thermo. uncertainty term for AI	c_{th}(AI)	(8)				(7)				2			
Coefficient of Determination	R^2	0.95	0.95	0.90	0.90	0.94	0.92	0.90	0.91	0.92	0.91	0.90	0.90

Notes: See notes for Table 5-1A. Methods have assumed non-hygroscopic aerosols. Parentheses indicate negative values for the SRCC.

Table 5-8A. Deposition fraction for BB region, DF_{BB}: Results of step-wise rank-regression analysis for the four top-ranked model parameters in Table 5-7. Based on inhalation of non-hygroscopic aerosols with specified particle diameters, d_p.

	d_p = 0.1 μm		d_p = 1 μm		d_p = 5 μm		d_p = 10 μm	
Ranks Included	Variable Added	R^2	Variable Added	R^2	Variable Added	R^2	Variable Added	R^2
1	d_0	0.23	c_{ae}(BB)	0.48	F_n	0.35	F_n	0.36
1,2	c_{th}(BB)	0.51	V_E	0.78	$c_{ae}(ET_2)$	0.69	$c_{ae}(ET_2)$	0.72
1,2,3	V_E	0.72	d_0	0.88	c_{ae}(BB)	0.86	d_0	0.80
1,2,3,4	V_D	0.94	l_o	0.90	d_0	0.87	V_E	0.86

Notes: See notes for Table 5-1B; exposure scenario and variables same as in Table 5-7.

Table 5-8B. Deposition fraction for bb region, DF_{bb}: Results of step-wise rank-regression analysis for the four top-ranked model parameters in Table 5-7. Based on inhalation of non-hygroscopic aerosols with specified particle diameters, d_p.

	d_p = 0.1 μm		d_p = 1 μm		d_p = 5 μm		d_p = 10 μm	
Ranks Included	Variable Added	R^2	Variable Added	R^2	Variable Added	R^2	Variable Added	R^2
1	c_{th}(bb)	0.43	c_{ae}(bb)	0.46	F_n	0.28	V_E	0.19
1,2	V_E	0.63	V_E	0.65	d_0	0.45	d_0	0.43
1,2,3	V_D	0.76	V_D	0.74	$c_{ae}(ET_2)$	0.62	c_{ae}(BB)	0.65
1,2,3,4	d_9	0.89	l_o	0.79	c_{ae}(bb)	0.74	F_n	0.82

Notes: See notes for Table 5-1B; exposure scenario and variables same as in Table 5-7.

Table 5-8C. Deposition fraction for AI region, DF_{AI}: Results of step-wise rank-regression analysis for the four top-ranked model parameters in Table 5-7. Based on inhalation of non-hygroscopic aerosols with specified particle diameters, d_p.

	d_p = 0.1 μm		d_p = 1 μm		d_p = 5 μm		d_p = 10 μm	
Ranks Included	Variable Added	R^2	Variable Added	R^2	Variable Added	R^2	Variable Added	R^2
1	V_T	0.15	V_E	0.33	F_n	0.26	V_E	0.34
1,2	c_{th}(AI)	0.49	V_T	0.61	V_E	0.47	c_{ae}(BB)	0.50
1,2,3	V_E	0.62	c_{ae}(AI)	0.80	$c_{ae}(ET_2)$	0.66	F_n	0.62
1,2,3,4	d_{15}	0.88	d_{15}	0.88	d_0	0.82	d_0	0.77

Notes: See notes for Table 5-1B; exposure scenario and variables same as in Table 5-7.

In contrast to sensitivity results for dose predictions, which were based on $^{239}PuO_2$, the sensitivity results for deposition predictions are generally applicable to many other exposure scenarios (involving different radionuclides and chemical forms). This assertion is supported because the deposition model is generally independent of the radionuclide and its chemical form. However, an exception exists for hygroscopic aerosols which tend to increase in size upon entering the saturated conditions of the respiratory tract. The results in Table 5-7 and 5-8 apply to nonhygroscopic (and non-fibrous) aerosols. In deriving these results conditions similar to those used in Tables 5-1 through 5-6 have been assumed. Namely, particles are assumed to be monodisperse (single size), unity density spheres (so that physical diameters equal aerodynamic diameters) and the population group was taken to be 25-34 year old males at light exertion.

Data in Tables 5-7 and 5-8 generally indicate a rather complex pattern of sensitivity for the deposition model that depends on particle size. This result is expected since primary deposition mechanisms change from thermodynamic (e.g., diffusion to airway walls) to aerodynamic (e.g., impaction with walls and gravitational settling) as particle size increases from 0.1 to 10 μm. Although a limited range of particles diameters has been examined in this study, the deposition model can be used for smaller particles (down to thermodynamic diameters of ~0.001 μm). The present application of the model is limited to sizes that are of more practical concern for plutonium oxide aerosols (discussed in section 5.2). More specific findings are discussed below.

5.5.1. Bronchial Region

As indicated in Table 5-7 and 5-8A, the sensitivity of DF_{BB} with respect to its input variables changes with particle diameter. For $d_p = 0.1$ μm, Table 5-8A indicates that d_0, $c_{th}(BB)$, V_E, and V_D each contribute over about 20% to the variability in DF_{BB}. The tracheal diameter, d_0, determines the BB deposition scaling factor, SF_t, used to adjust deposition efficiencies from reference man to agree with airway dimensions sampled during individual trials. The ventilation rate, V_E, is directly proportional to the volumetric flow rate and influences residence time of particles in various deposition regions (important for diffusion deposition mechanisms) and the velocity of particles in airway generations (important for aerodynamic deposition mechanisms). The volume of the BB region is related to the anatomical dead space, V_D. If V_D increases, the residence time of particles in the BB region increases--resulting in a larger thermodynamic deposition efficiency. For a given tidal volume, an increase in the volume of the BB region also results in less inhaled particles reaching other deposition regions. For larger particles the fraction of air breathed via the nasal pathway, F_n, becomes influential--contributing about 35% of the variability in DF_{BB}. The error term for the aerodynamic deposition efficiency of the ET_2 region, $c_{ae}(ET_2)$ (e.g., see section 4.1.12), also becomes important--accounting for an additional ~35% of the variability in the deposition fraction.

5.5.2. Bronchiolar Region

Sensitivity of the deposition model to input variables in the bb region shows a similar pattern as the BB region. For small particle diameters ($d_p = 0.1$ μm) sensitive

parameters include the error term to account for uncertainties in the deposition efficiency in the bb region, c_{th}(bb)--which accounts for over 40% of the variability in DF_{bb}. Other parameters of importance include the ventilation rate, the anatomical dead space, and the diameter of airway generation 9, d_9 (which is used to compute the deposition scaling factor, SF_b, for the bb region). As for the BB region, for larger particle diameters F_n becomes important--contributing 28% of the variability at d_p = 5 μm and about 17% at d_p = 10 μm. At these larger diameters, the tracheal diameter, d_0, is also found to be an influential parameter, accounting for some 20% of the variability in DF_{bb}. This finding is not obvious; however, an explanation is possible. As discussed, d_0 is used to compute SF_t, which is a factor in the mathematical expressions adopted to predict aerodynamic deposition efficiencies in the ET_2 and BB regions. As d_0 increases, SF_t ($SF_t = 1.65/d_0$) decreases; this decrease results in smaller aerodynamic deposition efficiencies in ET_2 and BB (i.e., see Table 2-1 and 2-2, noting footnotes)--so that more inhaled activity is available to deposit in bb. Therefore, d_0 is (positively) correlated with DF_{bb} for larger particles (where aerodynamic deposition mechanisms dominate).

5.5.3. Alveolar-Interstitial Region

Sensitivity results for DF_{AI} are shown in Table 5-8C. For the smallest particles examined (d_p = 0.1 μm), thermodynamic mechanisms continue to dominate (as for DF_{BB} and DF_{bb} at this particle size) as indicated by an added contribution to R^2 of about 35% by c_{th}(AI). Note also that for this particular size, the rank based on SRRC values resulted in V_T as the most sensitive parameter; however, step-wise regression analysis indicates that

c_{th}(AI) contributes more to the variability in DF_{AI}. This result is not contradictory since the most sensitive variable does not necessarily have to contribute the most to the uncertainty in the model output. For example, a sensitive variable that possesses negligible variability will generally not contribute much to the variability in the model prediction. For larger particle sizes ($d_p > 5$ μm), the sensitivity is almost the same as that seen for the bb region. The values of DF_{AI} and DF_{bb} are both sensitive to parameters affecting deposition in BB and ET_2 regions--since less deposition in these regions results in a potentially larger depositions in bb and AI.

5.6. Implications of Dose Results and Comparison to Reference Man Dose

As shown above, uncertainty and sensitivity analyses of complex models lead to a very large amount of numerical information. It is desirable to find a practical, yet defensible, manner to use the information produced by such analyses in dose assessment activities. Based on the distributions assigned to various model parameters and on the model structure, it has been observed that the resulting numerical distributions obtained for specific model predictions (e.g., DF_{BB}, $H(AI)/A_E$, H_{TH}/A_E, etc.) are generally represented well by lognormal distributions. To support this statement, Figure 5-13 shows a log-probability plot of various equivalent doses in the thoracic target tissues and the lungs (weighted sum). These data are based on an exposure to an assumed lognormal activity size distribution with an AMAD of 5 μm and a typical $GSD(d_p)$ of 2.5. A typical mass density of ρ=3 g/cm^3 and shape factor of χ = 1.5 were assumed for particles, and a population group of males aged 25-34 years was selected at the light exertion level.

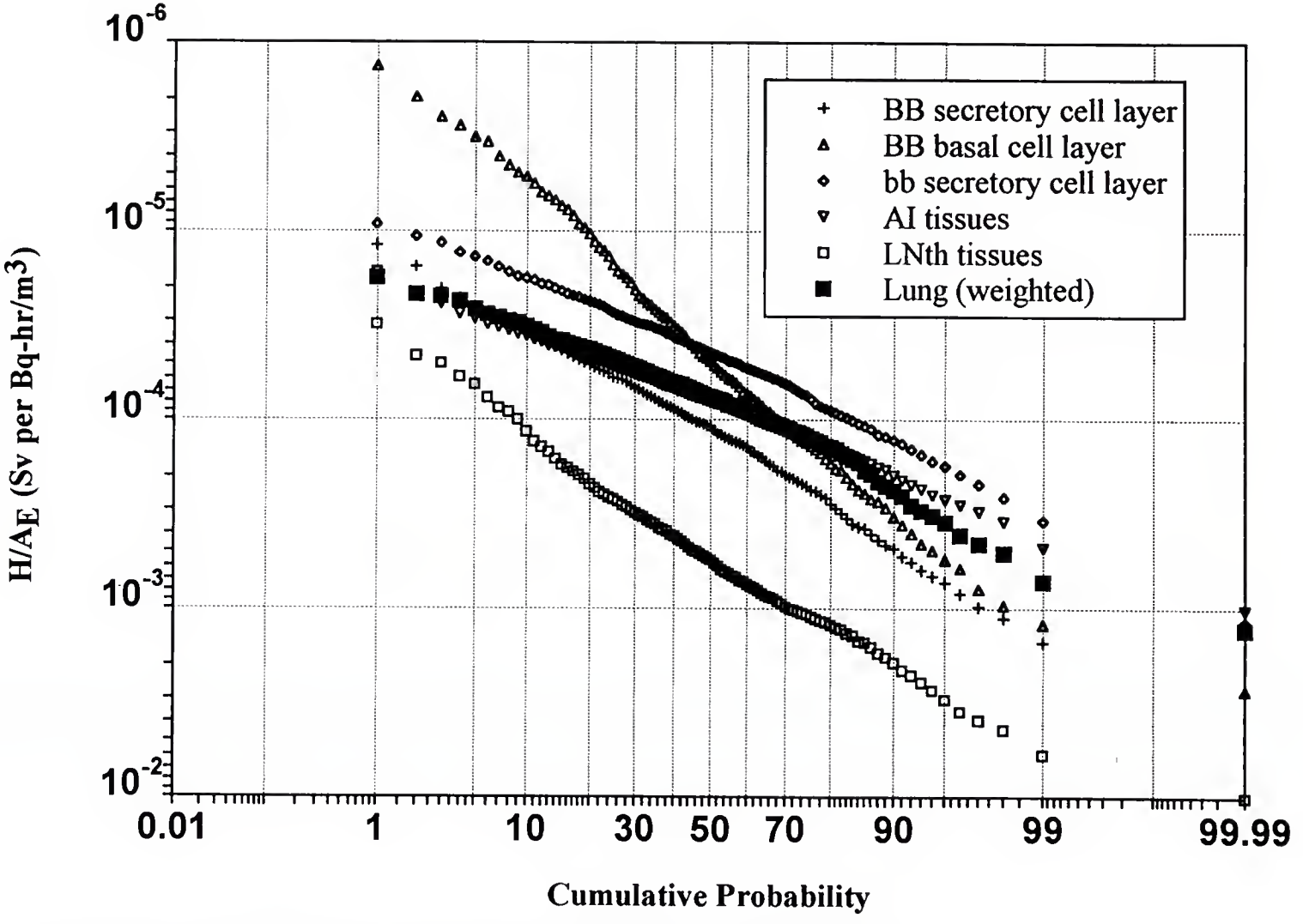

Figure 5-13. Lognormal probability plots for various equivalent doses in the respiratory tract. Computations based on inhalation of a polydisperse $^{239}PuO_2$ aerosol with 5 micron AMAD (activity median aerodynamic diameter) and GSD(d_p) = 2.5 and on a population group of 25-34 year old males at light exertion.

Generally, the distribution in predicted dose for each target tissue forms a straight line on the log-probability plot indicating that these dose distributions can be approximated by a lognormal probability density function. Although not shown, this same general result is also seen for deposition model predictions (i.e., regional deposition fractions) and for clearance model predictions (i.e., the total number of disintegrations occurring in source components). Therefore, as a practical result, results of uncertainty analyses presented in this chapter for $^{239}PuO_2$ can be approximated by two quantities: the geometric mean, GM, and the geometric standard deviation, GSD, of the predicted quantity.

Data for both geometric means and geometric standard deviations are listed in Table E-3 of Appendix E for most of the exposure scenarios discussed in this chapter. Values were computed for the GM and GSD for equivalent doses to thoracic target tissues and for the weighted dose to the lungs. As with fractiles, these estimates are basedon 1000 trials using LHS techniques. Figure 5-14 is a plot of the GSD in H/A_E for various target tissues of interest in this study. The values are based on the same population group (25-34 year-old males) and exposure scenario as that depicted previously in Figures 5-4 and 5-5. The GSD is not influenced greatly by exertion level at $d_p < \sim 1$ μm (the size range examined); however, for $d_p > \sim 1$ μm the GSD generally increases for all targets tissues but the BB basal cells (panel b of Fig. 5-14). As discussed previously, a shift in the dominant source component occurs for this tissue when the particle size increases due to the decrease in the slow-cleared tracheobronchial deposition fraction, f_s (discussed in section 4.2.2.1). For bb and AI tissues, GSD values increase

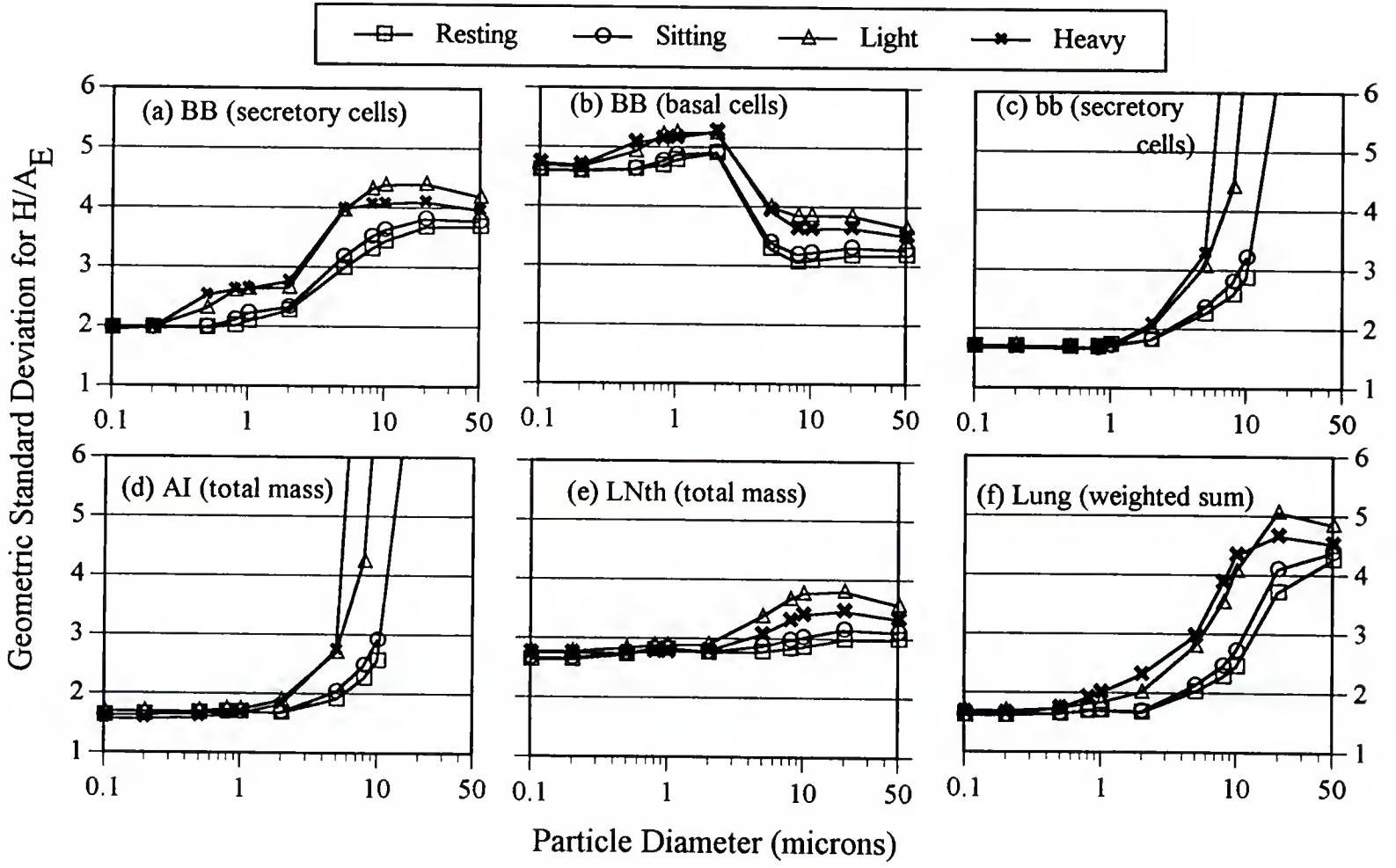

Figure 5-14. Estimated values of the geometric standard deviation, GSD, of H/A_E in various target tissues for males (25-34 years) at four broad exertion levels. Based on exposure to $^{239}PuO_2$-laden aerosol particles (monodisperse, unit density spheres).

sharply with particle diameter as less material deposits in these regions and as the dose goes to zero. In fact, inspection of Table E-3 in Appendix E shows that the GSD in dose is undefined for these tissues at larger particle diameters since zero dose values were predicted for some trials.

General conclusions are that (1) dose uncertainties in the lung can be modeled by lognormal distributions and that (2) GSD values for most tissues are less than about 5 for particle diameters examined in this demonstration of LUDUC. This result, for plutonium oxide, is expected to hold for polydisperse aerosols as well, since the dose uncertainty generally decreases with larger values of GSD(d_p) (shown in Figures 5-10 and 5-12). In other words, in the particle size range examined, the monodisperse scenario generally sets an upper limit on the GSD (in dose) values.5.7. Comparison with Reference Man Doses

A final issue of interest in this examination of dose uncertainties for plutonium oxide is how reference man-based dose values compare with computational results in this study. Workers at the National Radiological Protection Board have developed a code that implements the new ICRP respiratory tract model for reference man (Jarvis et al., 1993). This program is called LUDEP (LUng Dose Evaluation Program). LUDEP has been run in this study for the same exposure scenarios as above (monodisperse, unit density, $^{239}PuO_2$-laden particles), where input parameters for reference man and for a class S material (i.e., relatively insoluble material; see section 2.6) have been used. By means of a ratio, the results predicted by LUDEP are compared to the median values computed in this study (for the 25-34 year-old male population group). Figure 5-15 plots the ratio of $(H/A_E)_{50\%}$ to the reference man dose (as predicted by LUDEP). Generally, except for the

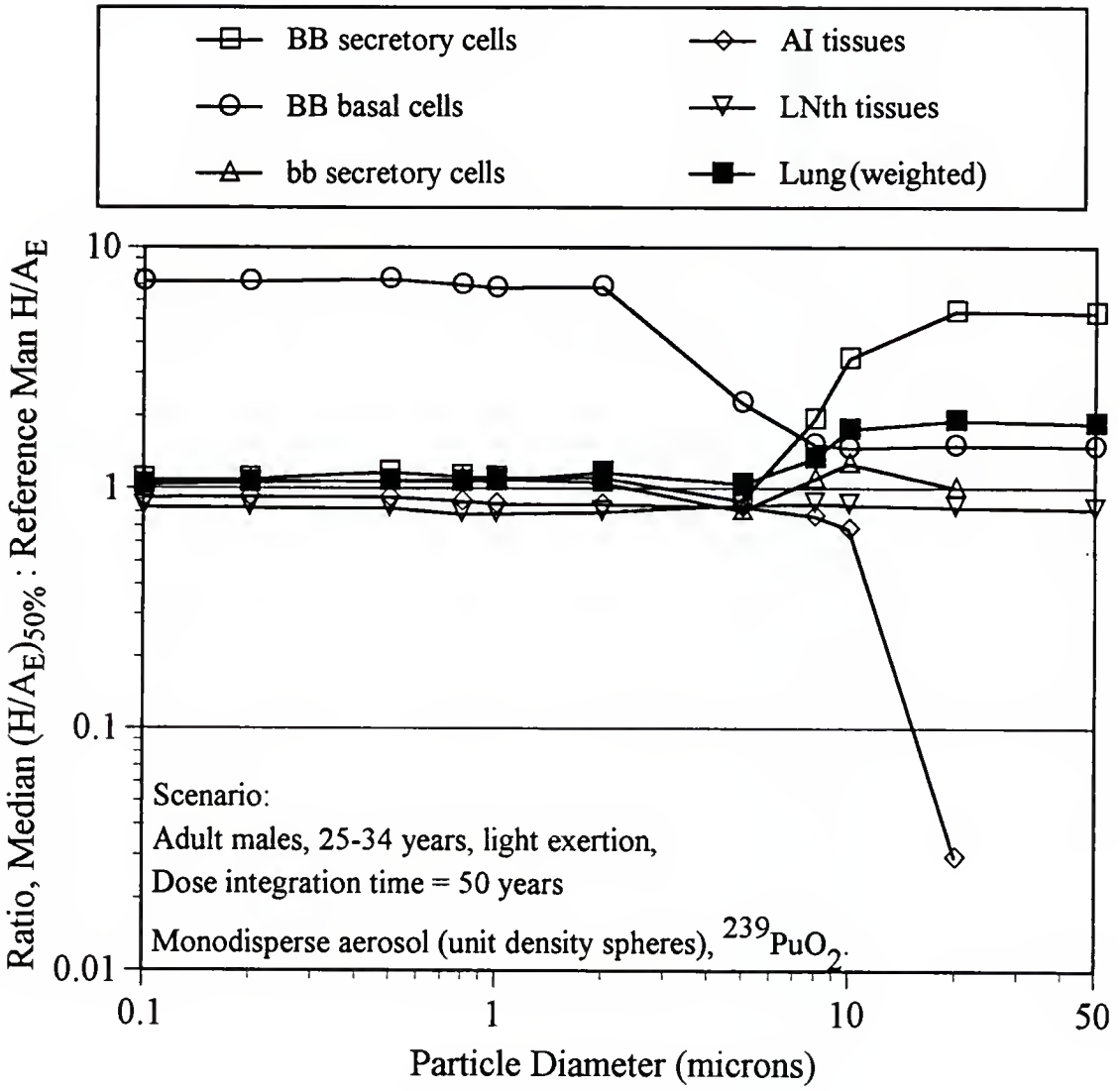

Figure 5-15. Comparison of median dose values computed in this study to reference man dose values as predicted by LUDEP. Median values are same as in Figure 5-2(a).

BB basal cell layer and for BB secretory cells in the larger particle size range, all median dose values agree well (within ~10 - 20%) with the reference man doses. (Note that this study predicts a median dose of zero for the bb and AI tissues at $d_p > 20$ μm [light exertion]; and dose to the AI region is negligible compared to other regions for $d_p > 10$ μm; e.g., see Figure 5-4).

The distribution in equivalent dose to the BB basal cell layer is shifted toward higher dose values in this study with respect to the reference man dose. This shift is due to the lower values used in this study for the median thickness of the bronchial epithelium compared to the reference value. The ICRP (1994) recommends a reference value of about 55 μm for the BB epithelium thickness. Based on literature examined in this study, the epithelium thickness (BB region) was assigned a uniform distribution with minimum value of 20 μm and maximum of 60 μm. Therefore, the median thickness is 40 μm (15 μm less than the ICRP reference value). Consequently, since the tissue barrier between the source region and the target region is less, a higher median dose is predicted in this study for the BB basal cell layer.

The increase in the ratio for BB secretory cells for $d_p > \sim 5$ μm is a result of the error term assigned to the slow-cleared deposition fraction, f_s, in the tracheobronchial airways (see section 4.2.2.1). Tables 5-2A and B indicate that f_s is among the most important parameters at these particles sizes. In the methodology developed in this study, a residual error term was added to Eq. 4-30 to model variability in the value of f_s. Based on experimental data, this error term was modeled as a normal distribution with mean of zero and standard deviation of 0.1. As the particle diameter increases, the value predicted

by Eq. 4-30 goes to zero. However, the value of f_s is restricted to be greater than or equal to zero. The result for large particles (d_p approaching 10 μm) is that the error term leads to an average value of f_s that is between 0 and 0.1. The reference value for f_s is predicted by Eq. 4-28 and is effectively zero for $d_p > \sim 8$ μm . The overall effect of this discrepancy in f_s (in this size range) is that the present study predicts slightly more material deposited in the slow-clearing compartments of the BB and bb regions, and the result is dose distributions that are shifted upward with respect to the reference man dose value in the BB secretory cell layer.

5.7. Summary of Results

In this chapter the probabilistic computer program, LUDUC (developed in this study to implement uncertainty and sensitivity analyses of the new ICRP respiratory tract model) has been demonstrated by application to inhaled $^{239}PuO_2$ particles. Results indicate that uncertainties in dose equivalents to target tissues of concern within the lungs can be substantial. Calculated uncertainties generally increase as the particle diameter increases from 0.1 to 50 μm; however, the calculated median dose decreases with increasing particle diameter over this same size range. Generally, uncertainties in lung and tissue equivalent doses can be modeled by lognormal distributions. As an upper limit a GSD of about 5 is predicted for larger particles. A GSD of about 2 can be estimated for smaller particles (at least down to the lower limit diameter considered in this application, 0.1 μm). To show and compare typical results from the various exposure scenarios investigated, Table 5-9 presents summary data for 1 μm diameter particles. The 95% confidence interval was

Table 5-9. Summary comparison of typical dose predictions for exposure of various population groups to $^{239}PuO_2$-laden aerosol particles (unit density spheres) with d_p = 1 μm. All values are reported in μSv per Bq-hr/m^3.

Population Group	Exertion Level	Dose Region	LUDEP	Median	95% Confidence Interval
2 year olds	light	lung	n.a.	108	23 - 518
5 year olds	light	lung	n.a.	106	26 - 437
10 year olds	light	lung	n.a.	114	30 - 438
15 year-old females	light	lung	n.a.	99	28 - 348
15 year-old males	light	lung	n.a.	110	31 - 393
18-24 year-old females	light	lung	n.a.	98	28 - 350
18-24 year-old males	light	lung	n.a.	113	33 - 387
25-34 year-old females	light	lung	n.a.	98	28 - 345
25-34 year-old males	light	lung	104	111	32 - 380
25-34 year old males	resting	lung	48	39	14 - 112
	sitting	lung	49	50	17 - 145
	light	lung	104	111	32 - 380
	heavy	lung	209	326	82 - 1300
25-34 year old males	light	BB_{bas}	5	30	1 - 821
	light	BB_{sec}	84	94	14 - 647
	light	bb_{sec}	58	62	21 - 180
	light	AI	207	177	59 - 536
	light	LNth	1140	774	93 - 6420
	light	lung	104	111	32 - 380

Notes: All values have units of μSv per Bq-hr/m^3 (equivalent dose per unit activity exposure). The dose region "lungs" corresponds to a weighted sum of the five primary target regions. Last two columns of table are based on results in Table E-3 (Appendix E), where a lognormal distribution is assumed. Data under column labelled "LUDEP" were computed with the code by Jarvis et al. (1993). Cells marked as "n.a." indicate that LUDEP was not applicable for the scenario.

based on an assumed lognormal distribution for dose values (as supported by Figure 5-13) and used GM and GSD values from Table E-3 in Appendix E. The lower and upper 95% confidence bounds are approximated by [GM÷GSD^2, GM*GSD^2].

Sensitivities in dose predictions differ between target tissues and are influenced by particle size, due primarily to dependencies in the deposition model. Table 5-10 provides a summary list of the most important variables influencing uncertainties in equivalent doses to target tissues in the lungs. This list is based on standardized rank-regression coefficients, which are determined by rank-regression analyses of model inputs versus outputs. This technique is generally able to explain over 90% of the variability in dose and deposition predictions. Table 5-11 gives a similar listing of important variables for the deposition component of the respiratory tract model. Indications are that a larger portion of the variability in deposition and dose model predictions are attributable to only a few model parameters. Future efforts should focus on improving the knowledge base for these parameters if uncertainties in the lung dose modeling process are to be minimized. This effort should proceed on two fronts. The first involves repeating the literature survey on a more intense level--seeking out additional information, including various esoteric reports that might have not been acquired during the initial literature review phase--to ensure that all available sources of information are used to assign probability density functions to sensitive model parameters. The second front involves performing experimental work to develop improved data sets for the most sensitive model parameters. Additional data can be used to update prior distributions (e.g., by using a Bayesian approach).

Table 5-10. Summary list of the variables contributing the most to uncertainties in equivalent doses (per activity exposure), H/A_E, to thoracic target tissues.

Target Tissue	Most Sensitive Variables
BB_{sec}	$m_{8,11}$, BB_{epithk}, V_E, DF_{BB}, f_s
BB_{bas}	$m_{8,11}$, BB_{epithk}, V_E, DF_{BB}, f_s, $f_d(BB_{scq})$
bb_{sec}	$m_{5,7}$, V_E, DF_{bb}, f_s, bb_{subthk}, DF_{AI}
AI	V_E, DF_{AI}, s_s, $m_{2,4}$
LNth	s_s, V_E, DF_{AI}, DF_{BB}, $f_d(BB_{scq})$, $m_{3,10}$

Notes: Variables are in no particular order. List based on top four ranked variables reported in Tables 5-2A, 5-3A, 5-4A, 5-5A, and 5-6A for exposure of 25-34 year-old males (at light exertion) to $^{239}PuO_2$ monodisperse aerosols (unit density spheres). Only particle diameters of 0.1, 1, 5, and 10 μm were examined.

Table 5-11. Summary list of variables contributing the most to uncertainties in deposition fractions to thoracic regions.

Deposition Region	Most Sensitive Variables
BB	$c_{th}(BB)$, $c_{ac}(BB)$, $c_{ac}(ET_2)$, d_0, V_E, V_D, F_n
bb	$c_{th}(bb)$, $c_{ac}(bb)$, $c_{ac}(BB)$, $c_{ac}(ET_2)$, d_0, d_9, V_E, V_D, F_n
AI	$c_{th}(AI)$, $c_{ac}(AI)$, $c_{ac}(BB)$, $c_{ac}(ET_2)$, d_0, d_{15}, V_T, V_E, F_n

Notes: Variables are in no particular order. List based on top four ranked variables reported in Tables 5-7 for exposure of 25-34 year-old males (at light exertion) to $^{239}PuO_2$ monodisperse aerosols (unit density spheres). Only particle diameters of 0.1, 1, 5, and 10 μm were examined in sensitivity analyses.

CHAPTER 6
CONCLUSIONS AND RECOMMENDATIONS

6.1. Summary of Research

The primary objective of this research was to develop a methodology for quantifying uncertainties in radiological dose (and related) predictions for respiratory tract tissues of population groups exposed to radioactive aerosols. A second objective of the research was to demonstrate the methodology by application to plutonium oxide aerosols. The methodology developed is a significant result of this study and involves conducting parameter uncertainty analyses using the respiratory tract model recently published by the ICRP (1994). A probabilistic computer program, LUDUC (for LUng Dose Uncertainty Code), was developed (as described in section 3.6) to carry out the methodology. The executable program and source code are available from the author.

The current study was based on the premise that a deterministic model can be used in a probabilistic format by treating input parameters as random variables within the model structure. By such treatment, predictions were generated as numerical probability distributions (and various estimated fractiles of these distributions) which contain information about uncertainties in model predictions. Quantitative information on these uncertainties provides insight into the reliability of the respiratory tract model. The ultimate assessment of model reliability would, of course, be to compare model

predictions with direct measurements. However, validation of lung dosimetry predictions by measurement is difficult, if not impossible, for most short-range radiations. For example, no direct *measurement* technique exists for radiological equivalent dose from alpha particles to tissues layers of the bronchial epithelium for a living person. So a practical alternative is to base uncertainty estimates on parameter uncertainty analyses.

The study involved three phases. In the first phase, the respiratory tract model was selected and potentially important parameters were identified. This phase involved translating conceptual and mathematical aspects of the model into a computer code so that it could be solved efficiently and accurately. This phase further involved coupling the program for solving the respiratory tract model with existing codes for generating random samples based on user-assigned input distributions (using Monte Carlo and Latin hypercube sampling techniques). The most difficult programming problem encountered in the work involved development of a technique to solve the source-target geometry component of the dose model efficiently and accurately for short-range radiations. Initially the feasibility of the work was hampered by numerical integrations required to compute equivalent dose in the tracheobronchial airways (where targets are modeled as embedded in a hollow cylindrical shell and irradiated by concentric source layers). To speed computational time, an algorithm and code were developed to solve this geometry by producing a dose-response matrix that stored results of the more complex integrations for later use. This code decreased computational time by a factor of 300 (from about 30 to 0.1 hours on a [486DX]66 MHz personal computer system)--making this work feasible. Mathematical details of this code are discussed in Appendix C.

In the second phase of the work, an extensive and critical literature review was conducted. These previous studies formed a basis for assigning distributions to the almost seventy random variables needed to conduct a detailed parameter uncertainty analysis of the respiratory tract model. This phase was tedious due to (1) the large volume of information available for some model parameters and (2) the lack of information available for many parameters. The review involved over one hundred publications (many of these were compilation studies and were, in turn, based on many additional references). The results of this review are presented in Chapter 4. Parameter distributions and accompanying relationships were based, whenever possible, on results published for normal, healthy persons, where persons in those studies were assumed to be representative samples of their associated age and gender groups. Often, uncertainties had to be pieced together from several studies and involved reanalyzing data collected by others. For example, data reanalysis was performed to find a relationship between tidal volume and ventilation rate for children (e.g., Appendix D). Although the results of this literature review were incorporated into the methodology, much freedom exists for parameter distributions and relationships to be updated interactively by users of LUDUC. In addition to parameter uncertainties, relationships were also identified and incorporated into the methodology to account for parameter correlations when possible.

In the third phase of the work, the parameter distributions and relationships (adopted in phase two) were used as inputs into the probabilistic code (developed in phase one) and uncertainties in lung doses from inhaled $^{239}PuO_2$ aerosols were examined. Dose values are reported per *activity exposure* (defined in section 1.2.1) and include

uncertainties in ventilation rates. These dose factors have units of Sv per Bq-hr/m^3 and allow a more efficient coupling of dose factors to results from atmospheric dispersion models (e.g., see section 1.4.2). Results for specific exposure scenarios involving $^{239}PuO_2$-laden aerosols are discussed in Chapter 5. These results involve both uncertainties in doses and sensitivities of various model parameters with respect to these doses. One important finding (Fig. 5-14) is that median values of dose distributions agree, in most cases, with dose values obtained using reference values for all model parameters. This finding provides support for the parameter values selected for the reference man case--which claims to represent a *typical* man. However, based on this general result, it can be argued that the reference-man approach (which is intended for radiation protection activities) is not *conservative* since it predicts only the median dose (i.e., 50% versus 95% dose fractile).

Three broad, but significant, summary results of this study are identified. First, the critical evaluation of previous studies (to recommend probability distributions and relationships for parameter uncertainties and correlations in the lung model) is a significant result of this study. It provides an evaluation of many quantities (e.g., body height, body weight, airway dimensions [diameters, lengths, surface areas, and volumes], ventilation rates, tidal volumes, tissue masses) important to inhalation hazard assessment and provides recommendations for handling uncertainties in these quantities. This evaluation also identified weaknesses in available data upon which parameter values are based. Second, the computational methodology developed (and the associated probabilistic computer code, LUDUC) is a significant result of the work. It provides a technique for generating

numerical probability distributions in model predictions (e.g., regional deposition fractions, total radioactive transformations in source regions, and radiation equivalent doses in target tissues). Finally, the application of the methodology to plutonium oxide aerosols is a significant result; data quantify uncertainties in equivalent dose to thoracic target tissues and to the lungs (as a weighted sum of the thoracic tissue doses). These data should be useful to an ongoing dose reconstruction study of plutonium releases from the Rocky Flats plant (near Denver, Colorado) and to plutonium processing and storage facilities around the world.

6.2. Conclusions Based on Results for Plutonium Oxides

Application of the probabilistic code developed in this work, LUDUC, to inhalation of plutonium oxides has lead to identification of several interesting trends which are believed to apply, in principle, to many other radioactive aerosols (especially relatively insoluble, alpha-emitting materials). However, note that actual dose values depend on the exact radionuclide and its chemical form. The more important trends are listed and discussed in the following paragraphs.

Numerical distributions predicted for equivalent doses were generally found to follow lognormal distribution shapes. Many results presented in this study involve distribution-free fractile estimates (e.g., 50% and 95% dose fractiles). These fractiles are used to present numerical results because they make no assumptions regarding distribution shape. However, indications (e.g., Fig. 5-13) are that lognormal distributions provide reasonable fits to all numerical distributions predicted for exposure to plutonium. Values

are listed in Appendix E for fractiles, geometric mean, and geometric standard deviation in dose for several $^{239}PuO_2$ exposure scenarios. The dose data produced in this work for $^{239}PuO_2$ are directly applicable to $^{240}PuO_2$ and to mixtures of $^{239+240}PuO_2$. The GSD values for other alpha-emitting radionuclides that are relatively insoluble in lung tissues are expected to be similar to those found in this work for plutonium. However, the geometric mean values (central tendencies of the dose distributions) will differ since alpha-particle energies and emission frequencies generally differ among radionuclides.

Dose uncertainty depends on the particle aerodynamic diameter. For plutonium oxides, this study shows that the spread in doses increases about tenfold for increasing particle diameters from 0.1 to 20 μm. For typical exposure scenarios, the 95% dose fractiles are about 10 times larger than the 5% fractiles (corresponding to a GSD of about 2) for particle diameters of about 0.1 to 5 μm; this difference increases to about a factor of 100 (corresponding to a GSD of about 5) as the particle diameter approaches 20 μm. However, doses become quite low at larger particle sizes since most of the deposition occurs in extrathoracic airways. The change in dose uncertainty with particle size is due primarily to changes in deposition model sensitivity.

For a constant activity median diameter, results show that dose uncertainties generally decrease for polydisperse compared to monodisperse aerosol particles (for a particle diameter range of 0.1 to 50 μm). Most of the computations performed in this work involved monodisperse (i.e., single-sized) particles. However, additional computations with polydisperse particles show that uncertainties generally decrease as doses are integrated over the particle activity-size spectrum. For larger particles, where

dose uncertainties are larger, a polydisperse aerosol with a GSD (in particle diameter) of 3 has an uncertainty (expressed here as the ratio of the 95% to 5% dose fractile) that is about 3 times less than a monodisperse aerosol. This effect is expected for other radionuclides and (nonhygroscopic) chemical forms as well since it is primarily an effect of the deposition model. Concerning the median dose value the converse is true--a polydisperse aerosol generally has a higher median dose than a monodisperse aerosol (assuming both aerosols have equal activity median diameters). As a useful summary result for $^{239}PuO_2$, the GSD values in equivalent dose to the lungs range from about 3 to about 5 for polydisperse aerosols in the 0.1 to 20 μm size range (i.e., activity median aerodynamic diameters).

The physical exertion level influences the dose uncertainty. For a given population group (i.e., specified age and gender), dose uncertainties are generally greatest when exposure is at light exertion. This finding is primarily a reflection of (1) uncertainties in ventilation rates at the light exertion level (due primarily to the basal multiplier, described in section 4.1.8) and (2) deposition model sensitivity to increases in the volumetric flow rate.

Investigation concerning the dose integration time (for an acute deposition of activity) showed that most of the committed equivalent dose from plutonium is delivered (1) by the first year post intake for targets in the tracheobronchial airways and (2) by about thirty years post intake for the AI region. Excluding the lymph nodes, the uncertainty in the dose (i.e., the spread in dose values) does not change significantly for any target tissue in the lungs after an integration time of about one hundred days.

Therefore, as a practical approach to accounting for uncertainty in dose with age after intake, the GSD value could be computed for doses at the conventional dose integration time of 50 years (using LUDUC) and used with typical median values (e.g., those from a reference man approach) to specify probability distributions (or derive confidence intervals) for dose.

The influences of age and gender of the population group on median dose predictions and dose uncertainties are generally negligible compared to influence of exertion level. For example, for a specified population group, median doses differ by about a factor of ten between resting and heavy exertion (due primarily to differences in the ventilation rates at rest and heavy exertion). However, for a specified exertion level (e.g., light exertion) median doses over all population groups differ by less than a factor of three. Age and gender can influence the pattern of dose on a regional scale (i.e., doses to the thoracic target tissues); however, these differences generally balance out for the weighted dose to the lungs.

Median dose values predicted by LUDUC for $^{239}PuO_2$ generally agree with the reference dose predictions for aerosol particle diameters ranging from 0.1 to 5 μm. Reference dose predictions are based on using the reference values for all model parameters as input to the independently developed computer code LUDEP. A major discrepancy is found, however, for doses to the basal cells of the bronchial epithelium. Calculated median doses in this region are about seven times higher than reference doses. This discrepancy is attributed to the selection of values for the thickness of the bronchial epithelium. Based on data reviewed in this study (section 4.3.4.4), the reference value

suggested by the ICRP (1994) for the epithelium thickness is believed to be too large--the result is less energy deposition in the basal cell layer for the reference scenario. For particle diameters larger than about 10 μm, the median dose values predicted for the secretory cell layer in the bronchial epithelium are about five times larger than the reference dose values. This discrepancy is due to uncertainties in the slow-clearing deposition fraction in the tracheobronchial airways (section 4.2.2.1).

Concerning parameter sensitivity, the results in this study suggest that most of the variability in the dose to a given target region is explained by only a few input variables. For example (for particle diameters between 0.1 and 5-10 μm), roughly 50% of the variability in the total lung dose (weighted sum of target tissues) for $^{239}PuO_2$ is due to variability in the dose to the alveolar-interstitial (AI) region. In turn, almost 90% of the variability in the dose to the AI region is attributable to uncertainties in only four variables in the model: the ventilation rate, the AI deposition fraction, the clearance rate constant for slow-phase absorption of deposited material to the blood, and the clearance rate constant for particle transport from the AI_2 to bb_1 compartment. A general conclusion is that many variables examined are unimportant regarding dose uncertainties. As a result, future research efforts can focus on improving distributions for those variables that contribute most to variability in dose values. If data can be collected for the most important variables, the distributions adopted in this study could serve as prior distributions in a Bayesian statistical approach to estimate posterior distributions.

6.3. Recommendations for Future Research

Nearly all radioactive materials, under conducive conditions, can form radioactive aerosols. The present study has addressed only some of the possible scenarios and has necessarily involved restrictions to limit the scope. Acknowledgment of the limitations of the methodology is important since they affect its applicability. Such acknowledgment also leads to recommendations for future development in the area of probabilistic dose assessment for inhaled radionuclides. The following paragraphs summarize the more important limitations while providing guidance for future development of the methodology. Final paragraphs deal with applicability of the methodology.

Uncertainties in environmental parameters (such as activity-size distribution of aerosol particles, particle mass density and dynamic shape factor, and ambient activity concentration) have not been included in the methodology. Such uncertainties are difficult to handle without focusing on actual site-specific aerosol conditions. The framework exists for generic inclusion of such uncertainties in the methodology (on a computational basis) with minimal effort. However, the actual distributions assigned to these parameters would require site-specific information.

Methods presently support only acute intakes at single exertion levels (resting, sitting, light, or heavy exertion). The simplifying assumption was that the ventilation rate did not change during the *exposure duration* (see section 1.2.1). A future extension of the methodology would be to allow intakes to occur over a mixture of exertion levels. Additional data are needed quantifying uncertainties in the fractions of times persons spend at different physical exertion levels (this information is possibly site-specific and

depends on the population group of interest). The source code must also be modified in LUDUC to include these uncertainties in computations. For chronic exposures (occurring over periods of years and decades), the methodology can be extended to provide for effects of growth (i.e., changes in airway dimensions, breathing rates, tissue masses, and other anatomical/physiological parameters--primarily an issue only for children).

The methodology presently accommodates only alpha particles. This limitation influences the dosimetry component of the methodology (deposition and clearance are independent of the radiation *type*). However, the methodology can be adapted for use with other short-range radiations (e.g., protons, electrons, beta particles) emitted by sources *in* the lungs with proper modifications to the dose-matrix module (i.e., computational module [5] in section 3.6; discussed in Appendix C). This module uses stopping-power, range, and energy data as inputs. These input data are currently based on alpha-particles; one needs only to supply the proper stopping-power, range, and energy data to this module to compute doses for other short-range radiations. Doses for gamma rays are based on a whole lung approach since gamma rays are more penetrating than radiations discussed above and since their energy is more uniformly deposited to total lung mass than is energy from short-range radiations. Specific absorbed fractions, SAFs, have been tabulated by others (ICRP, 1979) for various source-target organ pairs and could be incorporated into the methodology to allow gamma-ray dosimetry. Uncertainties in SAFs are not generally reported in the literature. So this approach would at least allow uncertainties in the total disintegrations (or cumulated activity) in source regions to be included in the gamma-ray dose predictions.

Although the computational methodology can accommodate materials of different solubilities (i.e., absorption types F, M, and S in the new ICRP [1994] lung model), parameter uncertainties have only been examined for plutonium oxides in this study. This restriction influences the absorption aspect of the clearance model and involves only five model parameters, f_r, s_r, s_s, f_b, and s_b (discussed in section 4.2.4). The parameters f_b and s_b are irrelevant for many materials, so that generally only the foremost three are required to solve the clearance model. To apply the present methodology to materials other than plutonium oxide (or similar type S materials), the absorption parameter distributions must be modified. Future research interests include compiling literature and collecting data to serve as bases for selecting absorption parameter distributions for other radioactive materials that pose inhalation-related risks. This work might best proceed on a site-specific level, since solubility of some materials depends on the process used to produce the material (ICRP, 1986).

The methodology presently accommodates only dose predictions for respiratory tract tissues. The purpose of this research was to quantify uncertainties in lung dosimetry only; however, many inhaled radionuclides are expected to pose a larger radiological risk to other body organs. By incorporating radiological/biological models for the gastrointestinal tract and the systemic organs into LUDUC, the methodology could be extended to predict uncertainties in the number of radioactive transformations in various other source regions of the body; and subsequently, uncertainties in dose due at least to uncertainties in the source transformations would be addressed.

The methodology accommodates only normal, healthy *population groups* (e.g., 18-24 year-old males) in the age range of 2 years up to 65 years. Uncertainty results produced by this methodology should not be interpreted within the context of a *specified individual* since parameter distributions are based on variabilities among unspecified individuals in population groups. To identify an individual and interpret results with respect to that individual would be misleading since a smaller uncertainty in the dose is expected for an individual. Furthermore, the health status of the lungs can influence virtually all of the parameters of the respiratory tract model. Age and gender influence several model parameters. This study has accounted for differences in many parameters due to age and gender; however, age and gender differences have not been included for clearance rate constants and deposition partition factors as discussed in section 4.2. All of these limitations can be addressed by modifying the parameter distributions to correspond to the desired group of persons (if relevant data are available). The methodology provides for changes in parameter distributions; however, additional research is needed to produce improved data sets from which to formulate parameter distributions.

Previous discussions in this section focus on extensions of the methodology and the associated computer program to allow uncertainties to be predicted for a wider range of potential inhalation exposure scenarios and target tissues other than lungs. But the methodology is sufficiently well developed to be applied directly to a number of lung dosimetry problems without major changes. For example, with only slight modification in the inputs to LUDUC (namely, distribution parameters for dissolution/absorption clearance rate constants, alpha-particle emission energies/frequencies, and radioactive half-

life), the methodology can be used to examine lung doses arising from acute inhalation of many alpha emitters, such as U-238, U-235, Pb-210, Th-230, Ra-226, and Am-241. Current limitations are that only doses from alpha emissions and parent radionuclides are accommodated. These limitations are important for short-lived radionuclides like Rn-222, since parent and progeny have relatively short half-lives (so the decay chain should be incorporated into the methodology). It is stressed that LUDUC does not presently predict dose for tissues beyond the respiratory tract. So for radionuclides/chemical forms that do not deliver a significant dose to the lungs (e.g., highly soluble chemical forms), LUDUC is not likely to be of great use without further development.

Since the deposition component of the respiratory tract model is independent of the nuclear stability (i.e., radioactive nature) and chemical form of the aerosol (except for hygroscopic materials--which are not presently accommodated by LUDUC), the methodology developed in this work can be readily applied to inhalation of (nonhygroscopic, nonfibrous) hazardous aerosols. The code LUDUC can accept a mass-size distribution (instead of activity-size distribution) for aerosol particles; in this case the code would predicts distributions for the fraction of inhaled mass that deposits in broad respiratory tract regions (including the thoracic region, extrathoracic region, and the total respiratory tract).

A future application of the methodology in occupational health physics could involve interpretation of bioassay measurements. Such measurements are usually required for persons who work with or near unsealed radioactive materials. Bioassay measurements involve *in vitro* analyses of blood, urine, and fecal samples and/or *in vivo*

counting of various body regions to determine the concentration and amounts of radioactive material in the body (and excretion rates from the body). From these measurements, it is possible (through use of appropriate biokinetic models) to work backwards to determine an activity intake (needed to predict internal doses). For inhalation, this back-calculation involves use of a respiratory tract model, such as the one implemented here. Depending on the magnitude of the intake, uncertainties in the model could be important. A future application of the methodology could focus on incorporating (respiratory tract model) parameter uncertainties into bioassay interpretation.

APPENDIX A
COMPARISON OF ICRP AND NCRP MODELS

Two respiratory tract models, developed independently by task groups of the International Commission on Radiological Protection (ICRP) and the National Council for Radiation Protection and Measurements (NCRP) have been considered in this study. Due to time constraints, only one model was selected. However, because the models possess many mutual input parameters, much information developed for the selected model should be useful in a similar investigation with the other model. Selection of the utilized model was based on information contained in published reports and on a recent draft report. The following section describes some of the key differences in the models and includes both scientific and practical considerations. The components compared include the morphological model, the deposition model, the clearance model, and the dose model. As discussed below, the conclusion was to use the ICRP model in the current investigation of respiratory tract dose uncertainties.

The ICRP (1994) recently issued its revised respiratory tract dosimetry model in December of 1994. The NCRP has also adopted, in principle, a new respiratory tract model for radiation protection; however, as of August 1995, the NCRP had not published a final report. A draft version of the report was obtained (in June 1993) from the NCRP scientific secretariat. The information reported in this appendix is based on that draft

report, since it was more recent than any other available publications. In addition to the draft report, details of the NCRP model were presented in the following sources: (1) proceedings of a workshop entitled *Respiratory Tract Dosimetry* were published by Radiation Protection Dosimetry (Vol. 38, Nos. 1-3, 1991) and (2) proceedings of the Twenty-Sixth Hanford Life Sciences Symposium (*Modeling for Scaling to Man: Biology, Dosimetry, and Response*) were published in the journal Health Physics (Vol. 57, Suppl. 1, 1989).

Comparison of Morphological Models

The morphological model represents the structure of the human respiratory tract. The respiratory tract can be divided into extrathoracic and thoracic regions. The extrathoracic region consists of the anterior and posterior nasal passages, the oral cavity, the naso- and oro-pharynx, and the larynx. The thoracic region comprises the tracheo-bronchial airways (including bronchi and bronchioles down to the terminal bronchioles) and the pulmonary region (including respiratory bronchioles, alveolar ducts and sacs, pulmonary capillaries, and interstitial tissues). An additional region identified by models is the lung-associated lymph nodes. Although lymph nodes are actually located within both thoracic and extrathoracic regions, they are distinguished from these regions due to their clearance characteristics and their relatively radio-resistant nature.

Only minor differences exist in ICRP and NCRP descriptions of the extra-thoracic region; consequently, these are not addressed here. Major differences are in the models' descriptions of the thoracic region. Both models consider the thoracic region to be

composed of a symmetrical, dichotomously branching, series of airways, or airway generations. Differences exist, however, in the grouping of these airway generations into deposition, clearance, and dose regions.

The ICRP model divides the conducting airways into two broad regions, the bronchial (BB) and bronchiolar (bb) regions; and the subsequent methodology predicts deposition and clearance in each broad region. The critical cell layers are believed to consist of both basal and secretory cells in the BB region and of only secretory (Clara) cells in the bb region. In order to obtain needed regional characteristics such as airway volumes and surface areas, the methodology incorporated airway dimensions averaged over a number of studies (James, 1988).

For the conducting airways, the NCRP models each airway generation separately for deposition and clearance and employs a typical path morphology for airways as recommended by Yeh and Schum (1980). The methodology is based on airway measurements made on a lung replica from a single 60 year old male cadaver. It was assumed by the authors that the measurement procedure revealed dimensions that corresponded to lungs inflated to total lung capacity (TLC). Airway dimensions for a desired lung volume are determined by scaling the dimensions at TLC using assumptions suggested by those authors. The NCRP model includes 25 airway generations. Generation 1 is the trachea; generations 2 - 16 are the remaining conducting airways; and generations 17 - 25 are the respiratory bronchioles, alveolar ducts, and alveoli. The NCRP model provides a general methodology for computing dose on a generation-by-generation basis for the first 16 generations; however, no specific recommendations were

made in the draft report with regard to target or source region dimensions. And indications are that measurements of the airway epithelium for each of these sixteen generations do not exist in enough detail to take advantage of this increased resolution in deposition (although information might be available in the future). The regional approach of the ICRP model for the tracheo-bronchial region, while having less resolution than the NCRP model, is easier to employ and subsequent accounting of doses is simpler. It is not clear whether the increased resolution of the NCRP model (deposition on a generation-by-generation basis) any better than the ICRP approach for developing an overall lung dose and risk as is desired for radiation protection activities.

Morphological models basically agree for the more distal airways and tissues (i.e., respiratory bronchioles; alveolar ducts and sacs) which are grouped into a single region for both models. The ICRP model calls this region the alveolar-interstitial region (AI); while the NCRP model retains the traditional term of pulmonary region (P). For both models the critical cells in this region are assumed to be the Type II epithelial cells. Because the tissues in this region are thin (a few microns thick) with respect particle penetration, the entire tissue of the AI or P region is included in the dose computation. This differs from the conducting airways where critical cells are taken to lie within certain depth intervals and doses are computed within these intervals only. This aspect of the revised models is in sharp contrast with the lung model described in ICRP Publication 30 (ICRP 1979). In that model equal weight was given to all lung tissues and dose was simply the energy deposited in the combined TB, P, and lymph node (L) regions divided by the total mass of these

regions. The revised respiratory tract models are considered more appropriate for risk assessment because only doses to critical tissues are included in computations.

The NCRP model includes a finer resolution of the respiratory-tract morphology than the ICRP model for the tracheo-bronchial airways. This resolution is interesting but may not be of much use in risk assessment. That more regions are included in the NCRP model implies that more mathematical manipulations are involved and that more data must be stored and passed along to solve the model. Such implications are important since the present research entails solving the model a large number of times using Monte Carlo techniques.

Comparison of Deposition Models

This section addresses some of the differences between the ICRP and NCRP deposition models. There are only minor differences in expressions used to model inhalability and deposition in extrathoracic regions; thus, these aspects are not considered in the following discussion. The major differences concern thoracic deposition and are outlined here.

In the NCRP model, deposition in thoracic airways (generations 0 to 25) is computed for each airway generation. Individual airways are modeled as cylinders, and semi-theoretical expressions for particle diffusion, impaction, and sedimentation are used to compute total deposition in each airway generation. Correction is made for the volume of tidal flow that reaches deeper-lying the airways. Each generation comprises a number of individual airways (e.g., assuming symmetrical branching, generation n has

approximately 2^n airways). In addition to physical characteristics of particles (e.g., mass density, shape factors, aerodynamic diameters, etc.), deposition probabilities depend on airway dimensions, branching angles, orientation angles with respect to the gravitational field, and flow velocities. The model considers deposition in all airway generations separately during inhalation and exhalation. Therefore, on the order of 150 calculations (i.e., 25 generations * 3 deposition mechanisms * 2 flow pathways--inhalation/exhalation) are necessary to compute deposition in the thoracic region for a single particle size, for a single subject. This number does not include supporting calculations needed to determine airway dimensions, flow velocities, diffusion coefficients, Reynolds' numbers, Stokes' numbers, volumetric corrections, etc. As will be discussed, the clearance model compartmentalizes the entire pulmonary region (generations 17-25) so that ultimately 17 deposition fractions need to be stored and passed as input to the clearance model for the thoracic region.

The ICRP deposition model uses a regional approach to predict thoracic deposition. There are three broad regions in which thoracic deposition is quantified. They are the bronchial (BB), bronchiolar (bb), and alveolar-interstitial (AI) regions. These regions are treated as a series of filters, each with a specified volume and deposition efficiency. The filter volume accounts for the inhaled air which does not reach subsequent filters. Two independent processes are considered in computing the deposition efficiency for a single filter (region); these are aerodynamic processes (which include impaction and settling) and thermodynamic processes (including deposition due to Brownian motion and diffusion). Equations giving deposition efficiencies for aerodynamic and thermodynamic

processes have been determined for each of the three thoracic regions by fitting regression equations to predictions of a theoretical model by Egan *et al.* (1989). Therefore, the use of a complex theoretical model is circumvented with simpler regression equations. From a computational standpoint, the ICRP model is much simpler than the NCRP in that there are fewer regions in which to compute deposition. Accounting for both inhalation and exhalation pathways, on the order of 12 calculations (3 regions * 2 deposition efficiencies/region * 2 pathways = 12) are necessary for the thoracic region for a single particle size in a single subject. As above, this computation neglects all supporting calculations of diffusion coefficients, volume correction factors, slip factors, etc. The ICRP model also accounts for the recent experiments of Stahlhofen and colleagues (Stahlhofen et al. 1986a, 1986b, 1987a, 1987b, 1990; Scheuch et al. 1993) by considering a slow-cleared fraction of the deposition in the conducting airway regions (BB and bb). This fraction is related to particle size and adds one more computation to the process. Ultimately only seven quantities need to be passed on to the clearance model.

With regard to scientific merit, both deposition models have their strengths and weaknesses. Model predictions of generational and regional deposition cannot be validated since adequate empirical data do not exist at this level. However, measurements of total thoracic deposition do exist, and predictions of total thoracic deposition by both models agree reasonably well with these measurements (despite computational differences). The NCRP deposition model is somewhat more flexible since it is based on a more direct model. Since the ICRP deposition model utilizes semi-empirical fits to an underlying theoretical model, it would be difficult to update the semi-empirical model if

significant changes were made to the underlying theoretical model structure. Two strengths of the ICRP model, from a practical standpoint, are that the model involves fewer calculations and fewer input quantities.

Finally, although a great amount of effort has been put into both models, the currently available documentation describing the ICRP deposition model has more mathematical detail than that describing the NCRP deposition model. The NCRP has not yet issued the final report of the respiratory tract model; drafts versions are available. To understand and use the NCRP deposition model, one must obtain, study, and understand the references cited in the task group's report. The ICRP (1994) has provided stand-alone documentation of the deposition model; subsequently, less effort was required to develop a computer code which successfully solved the ICRP deposition model. In conclusion, the ICRP deposition model appears more suitable for this study. It involves fewer calculations and requires that fewer quantities be stored for subsequent clearance calculations without compromising model validity. Also the model is published (versus draft form) and is easier to implement compared to the NCRP deposition model.

Comparison of Clearance Models

Both clearance models are based on compartment schemes and can be mathematically described by systems of linear, first-order differential equations in normal (canonical) form. The NCRP clearance model consists of 22 compartments comprising: 16 generations of conducting airways; the pulmonary region (a combination of generations 17-25 form this single compartment); 4 compartments comprising the naso-oro-

pharyngeal-laryngeal (NOPL) region; and the lung-associated lymph nodes (one compartment). The ICRP model is based on clearance of the broad respiratory regions described above; it has potentially 33 compartments with the following break down: extrathoracic regions (6 compartments), bronchial region (7 compartments), bronchiolar region (7 compartments), alveolar-interstitial region (7 compartments), thoracic lymph nodes (3 compartments), extrathoracic lymph nodes (3 compartments).

The primary difference in the models from a mathematical standpoint is that the NCRP clearance model employs fractional clearance rates that vary with time (i.e., some of the coefficients of the corresponding differential equations are functions of time), while the ICRP model has constant fractional clearance rates for all compartments. The ICRP model utilizes more compartments in order to avoid the difficulties involved with using time-varying coefficients. According to James et al. (1989, p. 273), "any model with monotonically changing clearance rates can be replaced by another, equivalent in complexity, that has constant rates." Consequently, the ICRP clearance model can be solved analytically for acute (and constant, chronic) intake scenarios. The NCRP model must generally be solved numerically over small, discrete time steps by a suitable numerical technique. Such techniques exist but generally require increased computational effort.

Recent experiments (e.g., Stahlhofen et al., 1990) using relatively insoluble materials have indicated that an appreciable fraction of material deposited in the tracheo-bronchial airways clears at a much slower rate than previously thought, the actual value depending on particle size. Previously, all slow-clearing components of the deposition

were assigned to the pulmonary region of the lungs. However, incorporation of the newer findings into the clearance model is important since the dose to the tracheo-bronchial region, which is believed to be the more radiosensitive region of the lung, is potentially increased. The ICRP model incorporates these findings; the NCRP model does not. The ICRP model accounts for the tracheobronchial slow-clearing component by providing three compartments for each region to describe mechanical clearance. For example, the bronchial region (denoted as BB and comprised of the trachea and the following eight airway generations) is subdivided into three compartments, BB_1, BB_2, and BB_{seq}; where BB_1 represents a fast clearing component of the deposition, BB_2 represents a slow clearing component, and BB_{seq} represents activity that is sequestered in airway walls (not available for mechanical clearance but can clear very slowly via lymphatics and absorption to blood).

Recommendation of one clearance model over the other is difficult without actually solving both under the circumstances of interest. However, the ICRP clearance model is believed to be more suitable for the present study simply because it can be solved with analytical expressions. Although it does involve roughly twice as many clearance compartments as the NCRP model, many of these only have a couple of pathways through which to clear and analytical techniques are likely to result in fewer overall computations. Also the ICRP model accounts for the recently-discovered slow-clearing fraction of the deposition, which potentially increases doses to the bronchial epithelium of the respiratory tract; the NCRP model does not account for this finding.

Comparison of Dosimetry Models

Although techniques used to model the transport of radiation from source to target regions are basically the same for both models, differences in the location of source regions lead to potentially different radiation doses to target tissues. Both the ICRP and the NCRP have considered similar critical cell layers as target regions. The primary difference is again related to the slow-clearing and sequestered tracheo-bronchial (TB) deposition fractions. The ICRP models the slow-clearing TB fraction as being associated with tissues in the sol/cilia layer of the bronchial epithelium. This places a portion of the activity closer to the layer of basal cells. The sequestered component is assumed to be associated with the a macrophage layer that accumulates in the interstitial tissues beyond the bronchial epithelium and the basement membrane; this location too is close to the basal cell layer. The result of both of these source components is that doses to the basal cells are potentially increased for short-range radiations compared to the doses derived by the NCRP model (in which material is assumed to clear over the mucociliary surface of the airways). Furthermore, the NCRP model assigns all of the slow-cleared and sequestered activity to the pulmonary region. So the dose to the pulmonary region would likely be larger for the NCRP model than for the ICRP model. Since more cancers have been observed in the tracheo-bronchial region than in the pulmonary region, it is possible that the NCRP model might not be as conservative with regard to overall risk compared to the ICRP model.

Furthermore, the NCRP has not provided any direction in the model which allows the various cell/tissue doses to be combined in order to yield an overall lung organ dose. The ICRP model has recommended regional risk-apportionment factors to arrive at an overall, combined lung dose. A single organ dose is needed to derive the effective dose (ICRP 1991a) and to compute potential organ risk/detriment.

Conclusion

As a result of the comparisons and discussions above, the ICRP respiratory tract model was selected for this research and served as the basis for deriving probabilistic inhalation dose coefficients for the lung. This study was not able to accommodate both models due to the amount of time and work involved in programming and solving the component models. However, many of the parameters investigated are similar for both ICRP and NCRP, and this study will nonetheless be useful to designers and users of both models.

APPENDIX B
THE CLEARANCE MODEL: SYSTEM OF DIFFERENTIAL EQUATIONS

The mathematical equations used to represent the clearance aspect of human respiratory tract dosimetry are presented in this appendix. Expressions are given for the compartmental model recently adopted by the International Commission on Radiological Protection (ICRP, 1994, *Publication 66*) and for the older lung model recommended in 1966 by the Task Group on Lung Dynamics (TGLD, 1966) and later adopted by the ICRP in *Publication 30* (ICRP, 1979). These models are both represented by first-order, linear, non-recycling differential equations.

ICRP Publication 66 Clearance Model

The ICRP recently adopted a clearance model that comprises a system of potentially 33 differential equations (ICRP, 1994). Abbreviations used to represent compartments are given in Table B-1 (these are discussed in more detail in Chapter 2). The amount of radioactivity in compartment *i* is denoted by q_i. The activity intake rate (Bq/sec) is denoted by *I* and is generally a function of time. The regional depositon fraction (i.e., fraction of inhaled activity that deposits in a given region) for the ET_1, ET_2, BB, bb, and AI regions are denoted as DE_{ET1}, DE_{ET2}, DE_{BB}, DE_{bb}, DE_{AI} , respectively (discussed in Chapter 2). The fraction of the regional deposit (e.g., DE_{BB}) that is assigned to compartment *i* is denoted by $f_d(i)$. For example, $f_d(BB_1)$ is the fraction of the activity

deposited in the BB region that is assigned to compartment BB_1 (see Table 2-6 in Chapter 2). Biological clearance rate constants from compartment *i* to *j* are denoted as $\lambda_{i,j}$. Radioactive decay constants for the radionuclide of interest is denoted as λ_r. The symbols s_p, s_{pt}, s_t, s_b represent rate constants describing particle dissolution and absorption processes.

Table B-1. Subscripts used in this appendix to describe the ICRP Publication 66 biokinetic clearance model.

Compartment	Subscript		
	Initial State	Transformed State	Bound State
AI_1	1	1T	AI(b)
AI_2	2	2T	
AI_3	3	3T	
bb_1	4	4T	bb(b)
bb_2	5	5T	
bb_{seq}	6	6T	
BB_1	7	7T	BB(b)
BB_2	8	8T	
BB_{seq}	9	9T	LN_{th}(b)
LN_{th}	10	10T	
ET_2	11	11T	ET(b)
ET_{seq}	12	12T	
LN_{et}	13	13T	LN_{et}(b)
ET_1	14		

Note: See Figure 2-9 for a diagram of the overall clearance model.

For a short-duration inhalation exposure in which the ventilation rate and ambient activity concentration in air remain relatively constant, an acute inhalation intake can be assumed and the system of differential equations shown below has an analytical solution (e.g., see Birchall, 1986). For an acute activity exposure of A_E (in Bq-hr/m^3, defined in Chapter 1) and ventilation rate V_E (in m^3/hr in this case), the intake rate *I* (in Bq/s) equals

$A_E * V_E * \delta(t-t_o)$, where $\delta(t-t_o)$ is a delta function with value of one at $t = t_0$ and zero for all other t. This intake scenario has been used in this study to solve the clearance component of the ICRP *Pub. 66* model; however, the equations listed below are represented in their general form in which *I* is any function of time. The following system of differential equations describe the ICRP *Publication 66* clearance model.

Initial State Compartments

$$\frac{dq_1}{dt} = DE(AI) \cdot f_d(AI_1) \cdot I - (m_{1,4} + \lambda_r + s_p + s_{pt})\, q_1 \tag{B-1}$$

$$\frac{dq_2}{dt} = DE(AI) \cdot f_d(AI_2) \cdot I - (m_{2,4} + \lambda_r + s_p + s_{pt})\, q_2 \tag{B-2}$$

$$\frac{dq_3}{dt} = DE(AI) \cdot f_d(AI_3) \cdot I - (m_{3,4} + m_{3,10} + \lambda_r + s_p + s_{pt})\, q_3 \tag{B-3}$$

$$\frac{dq_4}{dt} = DE(bb) \cdot f_d(bb_1) \cdot I + m_{1,4} q_1 + m_{2,4} q_2 + m_{3,4} q_3 - (m_{4,7} + \lambda_r + s_p + s_{pt})\, q_4 \tag{B-4}$$

$$\frac{dq_5}{dt} = DE(bb) \cdot f_d(bb_2) \cdot I - (m_{5,7} + \lambda_r + s_p + s_{pt})\, q_5 \tag{B-5}$$

$$\frac{dq_6}{dt} = DE(bb) \cdot f_d(bb_{seq}) \cdot I - (m_{6,10} + \lambda_r + s_p + s_{pt})\, q_6 \tag{B-6}$$

$$\frac{dq_7}{dt} = DE(BB) \cdot f_d(BB_1) \cdot I + m_{4,7} q_4 + m_{5,7} q_5 - (m_{7,11} + \lambda_r + s_p + s_{pt})\, q_7 \tag{B-7}$$

$$\frac{dq_8}{dt} = DE(BB) \cdot f_d(BB_2) \cdot I - (m_{8,11} + \lambda_r + s_p + s_{pt})\, q_8 \tag{B-8}$$

$$\frac{dq_9}{dt} = DE(BB) \cdot f_d(BB_{seq}) \cdot I - (m_{9,10} + \lambda_r + s_p + s_{pt})\, q_9 \tag{B-9}$$

$$\frac{dq_{10}}{dt} = m_{3,10}\, q_3 + m_{6,10}\, q_6 + m_{9,10}\, q_9 - (\lambda_r + s_p + s_{pt})\, q_{10} \tag{B-10}$$

$$\frac{dq_{11}}{dt} = DE(ET_2) \cdot f_d(ET_2) \cdot I + m_{7,11}\, q_7 + m_{8,11}\, q_8 - (m_{11,GI} + \lambda_r + s_p + s_{pt})\, q_{11} \tag{B-11}$$

$$\frac{dq_{12}}{dt} = DE(ET_2) \cdot f_d(ET_{seq}) \cdot I - (m_{12,13} + \lambda_r + s_p + s_{pt})\, q_{12} \tag{B-12}$$

$$\frac{dq_{13}}{dt} = m_{12,13}\, q_{12} - (\lambda_r + s_p + s_{pt})\, q_{13} \tag{B-13}$$

$$\frac{dq_{14}}{dt} = DE(ET_1) \cdot I - (m_{14,out} + \lambda_r)\, q_{14} \tag{B-14}$$

Transformed State Compartments

$$\frac{dq_{1T}}{dt} = s_{pt}\, q_1 - (m_{1,4} + \lambda_r + s_t)\, q_{1T} \tag{B-15}$$

$$\frac{dq_{2T}}{dt} = s_{pt}\, q_2 - (m_{2,4} + \lambda_r + s_t)\, q_{2T} \tag{B-16}$$

$$\frac{dq_{3T}}{dt} = s_{pt}\, q_3 - (m_{3,4} + m_{3,10} + \lambda_r + s_t)\, q_{3T} \tag{B-17}$$

$$\frac{dq_{4T}}{dt} = s_{pt}\, q_4 + m_{1,4}\, q_{1T} + m_{2,4}\, q_{2T} + m_{3,4}\, q_{3T} - (m_{4,7} + \lambda_r + s_t)\, q_{4T} \tag{B-18}$$

$$\frac{dq_{5T}}{dt} = s_{pt}\, q_5 - (m_{5,7} + \lambda_r + s_t)\, q_{5T} \tag{B-19}$$

$$\frac{dq_{6T}}{dt} = s_{pt} q_6 - (m_{6,10} + \lambda_r + s_t) q_{6T} \tag{B-20}$$

$$\frac{dq_{7T}}{dt} = s_{pt} q_7 + m_{4,7} q_{4T} + m_{5,7} q_{5T} - (m_{7,11} + \lambda_r + s_t) q_{7T} \tag{B-21}$$

$$\frac{dq_{8T}}{dt} = s_{pt} q_8 - (m_{8,11} + \lambda_r + s_t) q_{8T} \tag{B-22}$$

$$\frac{dq_{9T}}{dt} = s_{pt} q_9 - (m_{9,10} + \lambda_r + s_t) q_{9T} \tag{B-23}$$

$$\frac{dq_{10T}}{dt} = s_{pt} q_{10} + m_{3,10} q_{3T} + m_{6,10} q_{6T} + m_{9,10} q_{9T} - (\lambda_r + s_t) q_{10T} \tag{B-24}$$

$$\frac{dq_{11T}}{dt} = s_{pt} q_{11} + m_{7,11} q_{7T} + m_{8,11} q_{8T} - (m_{11,out} + \lambda_r + s_t) q_{11T} \tag{B-25}$$

$$\frac{dq_{12T}}{dt} = s_{pt} q_{12} - (m_{12,13} + \lambda_r + s_t) q_{12T} \tag{B-26}$$

$$\frac{dq_{13T}}{dt} = s_{pt} q_{13} - (\lambda_r + s_t) q_{13T} \tag{B-27}$$

Bound State Compartments

$$\frac{dq_{AI(b)}}{dt} = f_b s_p (q_1 + q_2 + q_3) + f_b s_t (q_{1T} + q_{2T} + q_{3T}) - (\lambda_r + s_b) q_{AI(b)} \tag{B-28}$$

$$\frac{dq_{bb(b)}}{dt} = f_b s_p (q_4 + q_5 + q_6) + f_b s_t (q_{4T} + q_{5T} + q_{6T}) - (\lambda_r + s_b) q_{bb(b)} \tag{B-29}$$

$$\frac{dq_{BB(b)}}{dt} = f_b s_p (q_7 + q_8 + q_9) + f_b s_t (q_{7T} + q_{8T} + q_{9T}) - (\lambda_r + s_b) q_{BB(b)} \tag{B-30}$$

$$\frac{dq_{LN_{th}(b)}}{dt} = f_b s_p q_{10} + f_b s_t q_{10T} - (\lambda_r + s_b) q_{LN_{th}(b)} \quad \text{(B-31)}$$

$$\frac{dq_{BT(b)}}{dt} = f_b s_p (q_{11} + q_{12}) + f_b s_t (q_{11T} + q_{12T}) - (\lambda_r + s_b) q_{BT(b)} \quad \text{(B-32)}$$

$$\frac{dq_{LN_{et}(b)}}{dt} = f_b s_p q_{13} + f_b s_t q_{13T} - (\lambda_r + s_b) q_{LN_{et}(b)} \quad \text{(B-33)}$$

ICRP Publication 30 Clearance Model

The lung model described in ICRP *Publication 30* (ICRP 1979) consists of a 10 compartment model (potentially) with compartments labeled from *a* to *j*. The fractions of intake which are deposited in the naso-pharyngeal, tracheobronchial, and pulmonary regions of the respiratroy tract are denoted as D_{NP}, D_{TB}, D_P, respectively. Fractional clearance rates out of compartments *a* through *j* are given by λ_a through λ_j, respectively; deposition partition fractions (i.e., fraction of material deposited in a specific deposition region, e.g., NP, TB, or P, that is assigned to a specified compartment within that region) are denoted by F_a to F_j. See ICRP *Publication 30* (ICRP 1979) for reference values of these parameters for various classes of materials. The first-order differential equations describing material clearance in that model are as follows:

$$\frac{dq_a}{dt} = I D_{NP} F_a - (\lambda_a + \lambda_r) q_a \quad \text{(B-34)}$$

$$\frac{dq_b}{dt} = I D_{NP} F_b - (\lambda_b + \lambda_r) q_b \quad \text{(B-35)}$$

$$\frac{dq_c}{dt} = I D_{TB} F_c - (\lambda_c + \lambda_r) q_c \tag{B-36}$$

$$\frac{dq_d}{dt} = I D_{TB} F_d + \lambda_f q_f + \lambda_g q_g - (\lambda_d + \lambda_r) q_d \tag{B-37}$$

$$\frac{dq_e}{dt} = I D_P F_e - (\lambda_e + \lambda_r) q_e \tag{B-38}$$

$$\frac{dq_f}{dt} = I D_P F_f - (\lambda_f + \lambda_r) q_f \tag{B-39}$$

$$\frac{dq_g}{dt} = I D_P F_g - (\lambda_g + \lambda_r) q_g \tag{B-40}$$

$$\frac{dq_h}{dt} = I D_P F_h - (\lambda_h + \lambda_r) q_h \tag{B-41}$$

$$\frac{dq_i}{dt} = F_i \lambda_h q_h - (\lambda_i + \lambda_r) q_i \tag{B-42}$$

$$\frac{dq_j}{dt} = F_j \lambda_h q_h - \lambda_r q_j \tag{B-43}$$

APPENDIX C
DOSE CALCULATIONS IN TRACHEOBRONCHIAL AIRWAYS

This appendix describes the methods used in this study to compute radiation equivalent doses in the bronchial (BB) and bronchiolar (bb) regions of the human respiratory tract. Dose computations are complex in these regions because source and target tissues are generally separated by intermediate layers with thicknesses approaching the range of alpha particles. Consequently, provisions are needed to account only for energy deposited by particles reaching BB and bb target tissue layers.

Although the general source-target geometries and resulting dose quantities in BB and bb regions are the same for this study compared to the ICRP (1994), the computational methods differ. A more rigorous approach was necessary in this work to include uncertainties in tissue dimensions (i.e., depth and thickness of source and target regions). As documented in ICRP Publication 66 (ICRP 1994, Annex H), only default absorbed fractions (based on reference tissue dimensions) are reported for short-range radiations (including alpha particles, electrons, beta particles, and positrons). Some algebraic expressions are also given by that reference to simplify computations. In performing parameter uncertainty analyses in this research, tissue parameters (thicknesses, depths, etc.) were sampled several times using Monte Carlo techniques; and the dose model was solved for each trial to generate a distribution of dose estimates for each target

region. Each trial required numerical integration to be performed for each source-target region pair. Methods were developed and are discussed in this appendix to solve the dose model efficiently and accurately for these trials. This aspect of the research has been limited to alpha-particle dosimetry; however, methods could be extended to other short-range radiations with appropriate stopping-power, range, and energy data.

Dose computations are performed for the target cell layers in respective regions based on an assigned airway diameter. Energy deposition in BB and bb regions was determined by modeling airways as hollow (air-filled) cylinders, as suggested by the ICRP (1994). Radiation source and target tissues were represented as concentric cylindrical shells within the airway walls. Figure C-1 shows a schematic of the geometry involved in BB and bb dosimetry. Source regions include the fast mucus/gel layer (BB_1+BB_{1T} or bb_1+bb_{1T}), the slower-moving cilia/sol layer (BB_2+BB_{2T} or bb_2+bb_{2T}), the sequestered material layer (BB_{seq} + BB_{seqT} or bb_{seq} + bb_{seqT}), and the bound material layers (BB_{bnd} or bb_{bnd}). For alpha particles, the AI region is also considered a source region since particles can cross the bb subepithelial layer to reach secretory cell nuclei. Target regions include the basal and secretory cell nuclei layers in the BB region (BB_{bas}, BB_{sec}) and the secretory (or Clara) cell nuclei layer in the bb region (bb_{sec}). Source and target layers can overlap (e.g., the bound material layer overlaps target cell layers in both BB and bb regions).

For BB and bb regions, representative airway diameters of 5 mm and 1 mm, respectively, were selected. These values were recommended by the ICRP (1994). Dose calculations were insensitive to changes (of roughly ± 50%) in these representative airway diameters; so these reference values were used throughout the work.

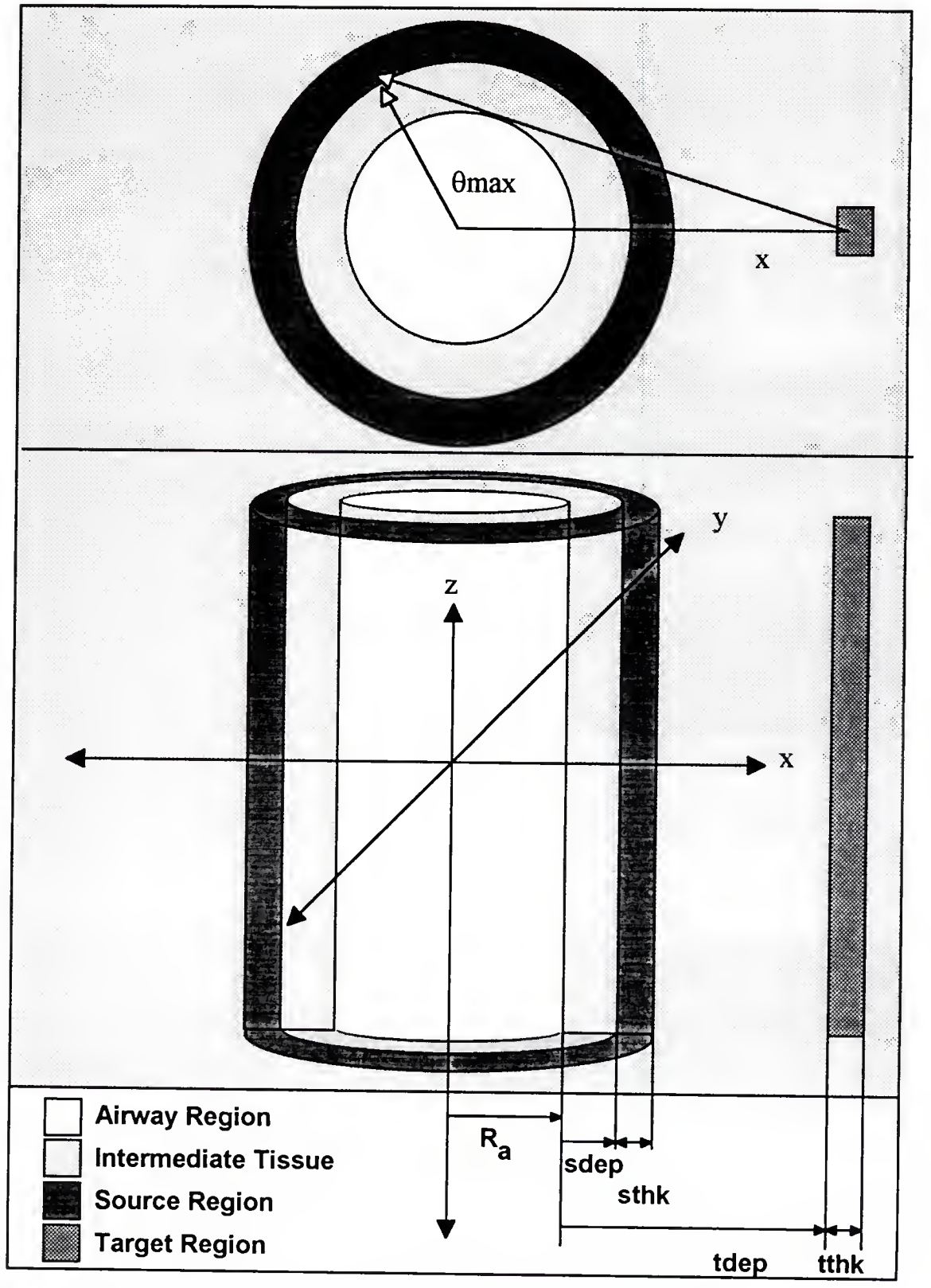

Figure C-1. Geometry used to compute radiation dose in the tracheobronchial airways.

To perform dose computations consider a cylindrical coordinate system (r, θ, z) with origin as depicted in Figure C-1 (on cylinder axis). For explanatory purposes, the cylindrical shell comprising the airway wall is considered infinite in length (z-dimension); however, alpha particle doses are only contributed by source points that are within a finite range of the target. This range depends on the initial energy of alpha particles emitted by the source. Let t_i denote the depth of a small target with respect to the airway surface. The average equivalent dose $H(t_i)$ in sieverts contributed by alpha particles from a source layer at a depth s_{dep} in the airway wall and having thickness s_{thk} is computed as

$$H_{tot}(t_i) = \sum_j H_j(t_i) \qquad \text{(C-1)}$$

where $H_j(t_i)$ is the equivalent dose contributed by the *j*th radionuclide and the summation is over all alpha-emitting radionuclides in the source region. The equivalent dose from the *j*th radionuclide is approximated by the following volume integral over the source region:

$$H_j(t_i) = C \cdot \sum_k \int_{s_1}^{s_2} \int_0^{2\pi} \int_{-z_{max,k}}^{z_{max,k}} \frac{f_{j,k} \cdot \tilde{A}_{v,j}}{4\pi d^2} \left(\frac{S}{\rho} \right)_{E_k(x)} Q(S_{E_k(x),\rho})\, dz\, r\, d\theta\, dr \qquad \text{(C-2)}$$

where summation is over all alpha particles (k) from the *j*th radionuclide and

C is a unit conversion factor and equals 1.602×10^{-10} J·g·MeV^{-1}·kg^{-1};

$f_{j,k}$ is the emission frequency for the *k*th alpha particle from the *j*th nuclide;

$\tilde{A}_{v,j}$ is total transformations (or disintegrations) of nuclide *j* per unit volume of the source region (trans/cm^3);

s_1 is the radial distance to the near boundary of the source region; $s_1 = R_a + s_{dep}$;

s_2 is the radial distance to the far boundary of the source region; $s_2 = R_a + s_{dep} + s_{thk}$;

R_a is a representative airway diameter for the BB (= 5 mm) or bb (= 1 mm) region;

d is the distance from source point at cylindrical coordinates (r, θ, z) to target at coordinates $(R_a + t_i, 0, 0)$; $d = [d_L^2 + z^2]^{1/2}$;

d_L is the projected distance in the plane $z = 0$ from the source point to the target at depth t_i; $d_L = [r^2 + (R_a + t_i)^2 - 2r(R_a + t_i)\cos\theta]^{1/2}$; this quantity equals the shortest distance between the target and a line of source points at constant r and θ;

$z_{max,k}$ is the maximum z value for a source point that is in range of the target and depends on the range, D_k, of the *k*th alpha particle in tissue; $z_{max,k} = [D_k^2 - d_L^2]^{0.5}$ for a homogenous intermediate tissue layer (between source and target).

x is the density thickness (i.e., density integrated over path length, g/cm^2) that an alpha particle travels between its emission point and the target; it depends on the source point location, (r, θ, z), and the target location--taken as $(R_a + t_i, 0, 0)$, and density of all intermediate matter (potentially tissue and air);

$(S/\rho)_{Ek(x)}$ is the mass stopping power ($MeVg/cm^2$) in the target tissue for the *k*th alpha and depends on the residual energy E_k of thethat has traveled a mass thickness of x;

$Q(S_{x,Ek,\rho})$ is the radiation quality factor, or radiation weighting factor, for alpha particles in tissue as a function of the stopping power (approximates the linear energy transfer, LET).

The radiation weighting factor, $Q(S_{x,Ek,\rho})$, is based on recommendations in ICRP Publication 60 (ICRP, 1991a). There the radiation weighting factor is given as a function of the unrestricted linear energy transfer, L (in keV μm^{-1}), where L represents the energy lost by a particle dE in traversing a distance dl. The unrestricted linear energy transfer is equal to the stopping power S in similar units, so that the following expressions (from ICRP, 1991a) relate the radiation weighting factor to the stopping power and are used in this study:

$$Q = \begin{cases} 1.0 & (S < 10) \\ 0.32\,S - 2.2 & (10 \le S \le 100) \\ 300/\sqrt{S} & (S > 100) \end{cases} . \qquad \text{(C-3)}$$

Equation (C-2) can be rewritten by factoring constant terms out of the integral, by utilizing the geometrical symmetry of a cylinder, and by bringing the summation over the k alpha emissions into the integral. Implementing these actions results in the following:

$$H_j(t_i) = C \cdot \frac{\tilde{A}_{vj}}{\pi} \int_{s_1}^{s_2} \int_{0}^{\pi} \left[\sum_k f_{j,k} \cdot \int_0^{z_{max,k}} \frac{1}{d^2} \left(\frac{S}{\rho} \right)_{E_k(x)} Q(S_{E_k(x),\rho})\, dz \right] r\, d\theta\, dr \quad . \quad \text{(C-4)}$$

Disregarding any conversion factors or constant terms at this point, the term enclosed in brackets in Equation (C-4) represents the average dose response at the target from an alpha-emitting line source (at specified values of r and θ) having one transformation per unit length. Using trigonometric substitution (i.e., $z = d_L \tan\phi$; so that $d^2 = d_L^2 \sec^2\phi$ and $dz = d_L \sec^2\phi\, d\phi$), the factor enclosed in brackets in Equation C-4 can be expressed as

$$\sum_k f_{j,k} \cdot \int_0^{z_{max,k}} \frac{1}{d^2} \left(\frac{S}{\rho} \right)_{E_k(x)} \cdot Q(S)\, dz = \frac{1}{d_L} \cdot \left[\sum_k f_{j,k} \int_0^{\phi_{max,k}} \left(\frac{S}{\rho} \right)_{E_k(x)} \cdot Q(S)\, d\phi \right] \qquad \text{(C-4)}$$

where ϕ represents the angle between the target-to-origin and target-to-source-point line segments. The maximum value of ϕ, ϕ_{max}, depends on the density ranges (or mass thickness, in g/cm^2) of the k^{th} radionuclide's alpha particles in tissue, $D_k \cdot \rho$ (g/cm^2) and on the density thickness of material between the target and the source line, x_L.

$$\phi_{max,k} = \arccos\left(\frac{x_L}{D_k \cdot \rho} \right) \qquad \text{(C-5)}$$

If x_L is greater than the range density for a given alpha particle *k'*, the target is out of range and no energy is deposited within the target by that particle (i.e., the integral for particle *k'* is zero and does not contribute to the summation).

The expression in brackets in Equation C-4 is denoted as $I_{L,j}$ and depends only on the radionuclide (indexed by *j*) and its alpha particle emission frequencies and energies (indexed by *k*) and on the density thickness of matter between the source line and the target, x_L. By incorporating Equation C-4 into Equation C-5, the following expression can be written as:

$$H_j(t_i) = \frac{C \cdot \tilde{A}_{vj}}{\pi} \int_{s_1}^{s_2} \int_{0}^{\pi} \left[\frac{I_{L,j}}{d_L} \right]_{r,\theta} r \, d\theta \, dr \quad . \tag{C-6}$$

A fortran computer code, LINSUB, was written to compute $I_{L,j}$ as a function of x_L (x_L is the mass density thickness between the target and a line comprised of source points at a given r and θ)using numerical integration techniques. The source code along with sample input files are listed at the end of the appendix in Tables C-1, C-2, and C-3A. The input files shown are for Pu-239. Values of $I_{L,j}$ versus x_L have been computed by LINSUB for four radionuclides: Pu-238, Pu-239, Pu-240, and Am-241. The results of these computations are shown in Figure C-2 for these radionuclides.

Based on Figure C-2, Pu-238 and Am-241 are seen to deliver the same dose to the target per disintegration in the source regions. Also Pu-239 and Pu-240 deliver approximately the same dose per disintegration in the source region. The reason is that

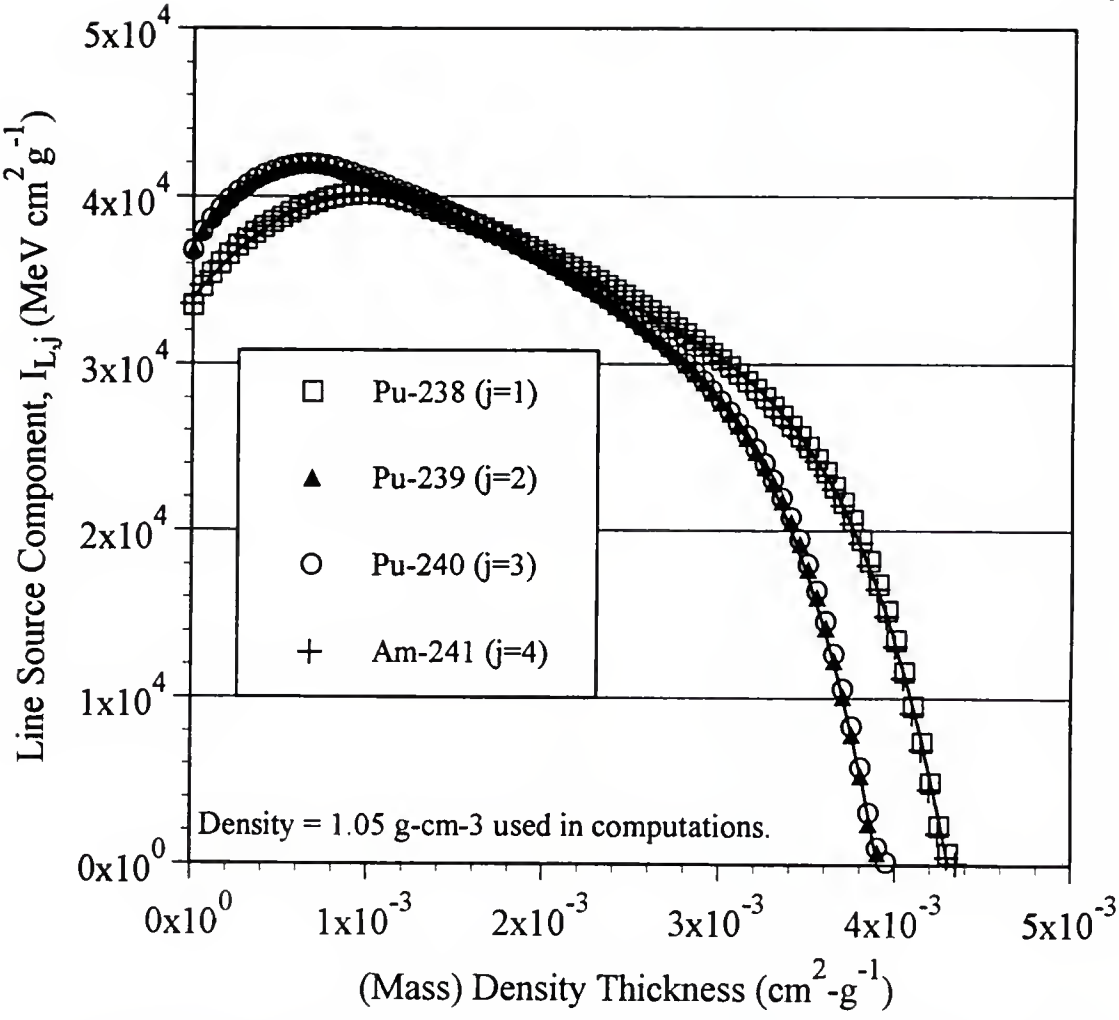

Results of Curve Fitting

Pu-238 and Am-241 (j=1,j=4):

$I_{L,j}(x_L)$ = -1.829E+17 x^5 + 1.145E+15 x^4 + -1.048E+12 x^3 + -7.019E+9 x^2 + 1.319E+7 x + 3.394E+4; R^2 = 0.9996

Pu-239 and Pu-240 (j=2, j=3):

$I_{L,j}(x_L)$ = -1.435E+17 x^5 + 2.094E+14 x^4 + 3.425E+12 x^3 + -1.421E+10 x^2 + 1.461E+7 x + 3.733E+4; R^2 = 0.9996

Figure C-2. Numerical results for the line source component ($I_{L,j}$) as a function of density thickness (x_L) for ^{238}Pu, ^{239}Pu, ^{240}Pu, and ^{241}Am radionuclides including polynomial curve fitting results.

Pu-238 and Am-241 emit alpha particles with approximately equal average energies per transformation; similarly Pu-239 and Pu-240 emit simlar average energies per transformation. As a practical result, total disintegrations for Pu-238 and Am-241 (and similarly for Pu-239 and Pu-240) can be added in source regions to simplify dose calculations when these mixtures of radionuclides are inhaled. It was found that polynomial regression equations could be fit to data points in Figure C-2 to further simplify dose computations for these radionuclides. These polynomials were used in a subsequent subroutine (ALINE) of the dose-matrix module STDOSE (discussed below) to further speed up the dose computation process.

Other alpha-emitting radionuclides nuclides can be investigated by modifying the input file to LINSUB shown in Table C-3A and the subroutie ALINE in STDOSE. Other short-range radiations that possess stopping-power- and range-energy data (as described below and shown in Table C-2) could also be used in this methodology to compute values for $I_{L,j}$. Similar polynomials could be fit for other radionuclides emitting short-range radiations with appropriate modifications to the input data to LINSUB.

Mass stopping power and range-energy data necessary to compute $I_{L,j}$ were obtained from Report 49 of the International Commission on Radiation Units and Measurements (ICRU, 1993). In selecting range and mass stopping power data, liquid water was chosen as the stopping medium. Soft tissues are very similar to liquid water with respect to alpha-particle mass stopping-power and mass density range. These data are listed in Table C-2; this is actually a listing of the file "table.dat" that is read by LINSUB. The range (i.e., density range in g/cm^2) is plotted as a function of alpha-particle

energy in Figure C-3. The mass stopping power versus the residual particle range is plotted in Figure C-4. This latter figure can be used to predict the mass stopping power of an alpha particle if the residual range of that particle in the stopping medium is known.

The density range ($D\rho$, g/cm^2) of an alpha particle is estimated by linear interpolation of the range-energy data in Table C-2 (or Fig. C-3). If x represents the mass (density) thickness between the source point and the target, the residual (density) range of the particle at the target can be estimated as [$D\rho$ - x]. This thickness corresponds to the (average) remaining distance, or the residual range, the particle can travel before stopping completely in the medium. Using linear interpolation a second time (with data plotted in Fig. C-3), the mass stopping power of the particle at the target can be estimated from this residual range. This technique is used in the present work to determine numerically the mass stopping powers needed to solve the numerical integration for $I_{L,j}$.

In computations, the airway wall was assumed to be homogeneous with a density of ρ_{tissue} = 1.05 g/cm^3. This density was recommended for the lung tissues by the ICRP (1975). Air in the (hollow) airway cavities was assumed to have a density of 1.15 g/l or 1.15×10^{-3} g/cm^3 (Weast, 1978, p. F-10; based on moist air at 760 torr and 35 °C).

With the polynomial fits to $I_{L,j}$ as a function of x_L, the next stage in the dose integration involves integration over θ and r. This integration is simplified by taking a small thickness of Δr = 0.5 microns (which is much less than the range of most alpha particles) and by assuming that the integrand in Equation 4-6 does not change significantly with r in this thickness. Integrations were performed for a large number of potential

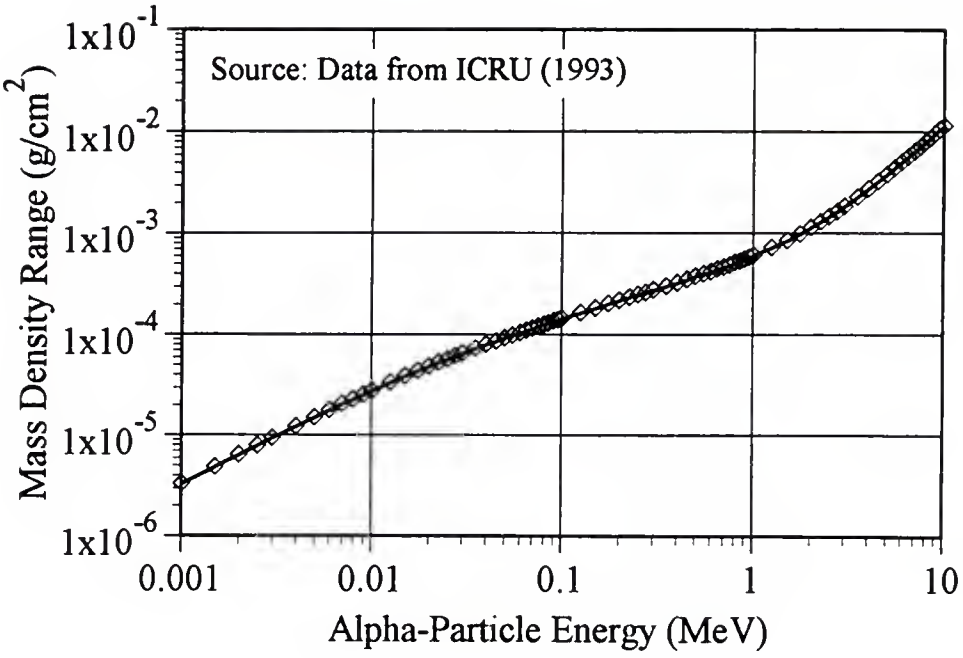

Figure C-3. Range versus alpha-particle energy based on liquid water.

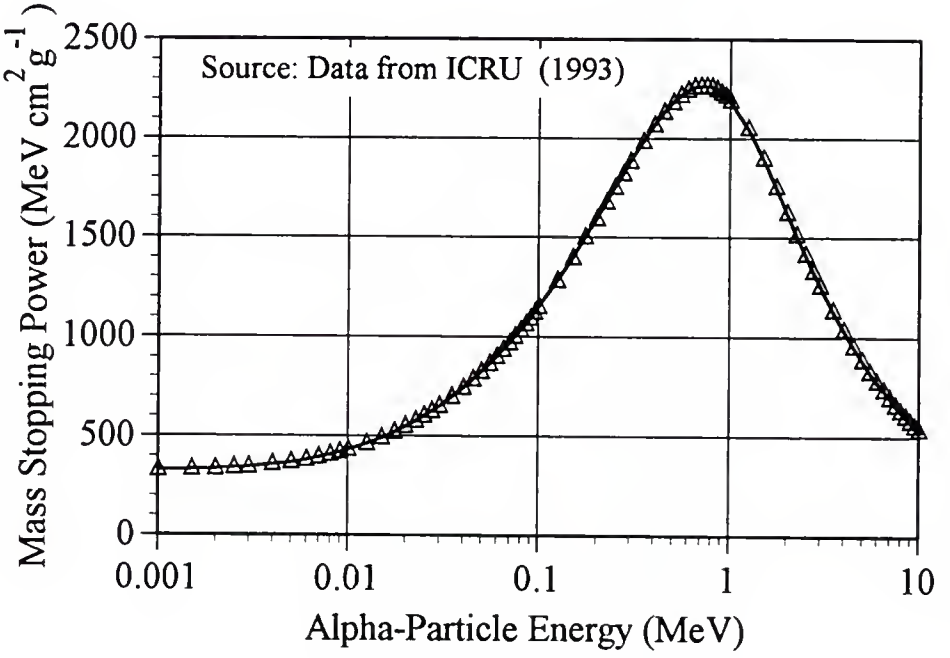

Figure C-4. Mass stopping power versus alpha-particle energy based on slowing down liquid water.

source and target depth pairs, (s_{dep}, t_{dep}) using another fortran code devloped in this work, STDOSE. This program is listed in Table C-4 at the end of the appendix. The function of STDOSE is to generate a dose-response matrix to store all possible source-target depth pairs for a particular radionuclide so that numerical integrations must only be performed one time for a target exposed to a source shell (of 0.5 micron thickness) at specified depths. The results of these computations are stored in a two-dimensional array $DOSE(s,t)_j$, where the first index, s, refers to a particular source depth (centered on a source shell thickness of 0.5 microns) and the second index refers to a specified target depth (t). The subscript *j* denotes that the dose-matrix of for a specific radionuclide. The dose module in LUDUC (Lung Dose Uncertainty Code) sums over these source shells very rapidly (by way of the dose-reponse matrix stored in the array DOSE) to generate the total target dose for a specified target depth. Use of this dose matrix allows doses for different values of source-layer depth and thickness and target depth and thickness to be computed quickly and accurately. Using this technique (versus the initial technique of solving the Equation C-2 anew with each trial), dose computation time was decreased by about a factor of 300 (from about 30 hours to 0.1 hours on a 66 MHz personal computer system)--making this study feasible.

Additional expressions were derived to perform the integration over θ and to account for "near wall" and "far wall" effects of the hollow cylinder. Some alpha particles are emitted from sources in the "far wall" of the airway and must traverse both tissue and air in route to the target. This fact complicates the integration over θ in Equation C-6. Expressions listed below were incorporated into STDOSE to handle particles that

originated from the "far wall." Additional notation introduced is described in the text following the expressions.

$$x_L = d_{L,air}\,\rho_{air} + d_{L,tissue}\,\rho_{tissue} \quad , \tag{C-7}$$

$$d_{L,air} = \begin{cases} 0 & (\theta < \theta_{max}) \\ 2\sqrt{(R_a^2 - h^2)} & (\theta \geq \theta_{max}) \end{cases} \quad , \tag{C-8}$$

$$h = (R_a + t_i)\, r \sin\theta / d_L \quad (\theta > \theta_{max}) \quad , \tag{C-9}$$

$$\theta_{max} = \arccos\left(\frac{R_a}{R_a + t_i}\right) + \arccos\left(\frac{R_a}{R_a + r}\right) \quad , \tag{C-10}$$

and $$d_{L,tissue} = d_L - d_{L,air} \quad . \tag{C-11}$$

Some notation was discussed above, directly following Equation C-2. The quantity $d_{L,air}$ is the thickness (cm) of air between the source line at (r, θ) and the target; $d_{L,tissue}$ is the thickness (cm) of tissue between the line and the target; d_L is the thickness (cm) between the line and the target (= $d_{L,air}$+ $d_{L,tissue}$). The condition to determine whether a particle must cross the hollow portion of the airway is to compare θ to θ_{max}, where θ_{max} denotes the angle at which $d_{L,air}$ becomes greater than zero. The term *h* is an intermediate term needed to determine $d_{L,air}$ when the particle orginates from the "far wall" (i.e., $\theta > \theta_{max}$).

Target and source tissues in extrathoracic (ET) regions are represented with geometries similar to BB and bb regions; however, because the ET regions are relatively insensitive to radiation-induced risk, uncertainties in source-target tissue dimensions (or more technically, absorbed fractions) are not examined in this research. In addition,

energy absorption in AI and lymph node tissues is assumed to be uniform and complete for alpha particles (i.e., alpha particles emitted by these tissues are absorbed locally, absorbed fractions of one); so dosimetry computations are simple for these regions once the mass and total number of transformations are known. However, variability still exists in doses to these regions due to uncertainties in the deposition and clearance aspects and due to uncertainties in regional tissue masses. The ICRP dose methodology is adopted for ET, AI, and LN regions. In that method, default absorbed fraction values (i.e., the fraction of energy emitted by source tissues absorbed in target tissues of the respective regions) are used to compute doses.

Table C-1. Listing of fortran source code for LINSUB

```
      PROGRAM LINSUB
C**** TO CALCULATE Equivalent Dose from an alpha-emitting line source.
C**** The code uses Simpson's Rule to integrate over geometry.
C**** Algorithms in subroutines QSIMP and TRAPZD came form
C****  the text Numerical Recipes (Press et al., 1986).
C**** Results of this code depend on the stopping medium and its density.
C**** Currently code reads stopping power and range data from TABLE.DAT
C****  which contains data for liquid water.  These data are from ICRU Report No. 49 (1993).
C
C****  AUTHOR:  T.E. HUSTON
C****  Last Revised: 10/19/94
C*************************************************************
C*************************************************************
      dimension tint(101),xl(101),ealf(10),rp(10),rmax(10),freq(10)
      common/dat1/ e(79),r(79),s(79),ni
      common/geom/ rpk,txl,dentrg

      OPEN(unit=5,file='linsub.dat',status='old')
      OPEN(unit=2,file='table.dat',status='old')
C** Table.DAT stores energy,range,and stopping power data from ICRU49 for water:
      READ(2,*) ni
      do i=1,ni
            read(2,*) e(i),r(i),s(i)
      enddo
C** dentrg=density of stopping medium (target,water) in g/cm^3.
c** ne=number of emissions (alphas) by source
c** ealf(i),freq(i) = energy and frequancy of alpha "i"
c** rp(i) is the mass range (g/cm^2) for alpha "i"  in water
c** rmax(i) (computed) is the range in microns for alpha "i" in water of density=dentrg
      READ(5,*) dentrg
      READ(5,*) ne
      do i=1,ne
            read(5,*) ealf(i),freq(i)
            rp(i)=range(ealf(i))
      enddo
c xlmin=minimum density thickness of interest (um), from target to line source.
c xlmax=maximum "
c nxl=number of steps in xl desired (sets thicknesses--step size--between calculations)
      READ(5,*) xlmin,xlmax,nxl
      READ(5,*) !skip next 4 lines in input file...these lines contain comments.
      READ(5,*)
      READ(5,*)
      READ(5,*)
      do i=1,ne
      WRITE(5,8005) ealf(i),rp(i)
      enddo
8005 FORMAT(/,5X,'MASS RANGE OF ',F8.4,
     1  ' MeV ALPHA PARTICLE IN WATER = ',F8.4,
     2  ' CM^2/G   Note: depends on density.')
```

Table C-1--cont'd.

```
      xlstp=(xlmax-xlmin)/real(nxl)
      do 10 i=1,nxl+1
            tint(i)=0.0
            xl(i)=xlmin+float(i-1)*xlstp   !total density thickness (targ to line) (g/cm^2)
            txl=xl(i)
            do 20 k=1,ne                   !sum over all emissions, weighted
              rpk=rp(k)
              if(txl.ge.rpk) go to 20      !compare density thickness to mass-density range
              a=0.                         !integrate from phi = a=0, phi is described in text.
              b=ACOS(dpt/rpk)              ! "        to phi = b
              tin=0.                       !initialize integral to 0.0
              call qsimp(a,b,tin)          !return tin (MeV/g per 1dis/um)
              tint(i)=tint(i)+tin*freq(k)  !weighted by frequency of emission and summed over "ith" alpha
   20   continue
   10 continue
C** to get to dose tint(i)=1./2/pi/(dt(i)+dv(j))*tint(i)*1.602E-10     !Dose (Sv per 1dis/um)
C** here the factors other than tint(i) are not included.
      print *,'Energies/frequencies:'
      print *, (ealf(i),i=1,ne)
      print *, (freq(i),i=1,ne)
      print *,'  xL      I(L,j)'
      do i=1,nxl+1
            print *,xl(i),tint(i)
            if(i.eq.18.or.i.eq.40) pause
            if(i.eq.18.or.i.eq.40) print *,'  xl        I(L,j)'
      enddo

      open(unit=3,file='linsub.out',status='unknown')
      write(3,900)
      write(3,*) (ealf(i),i=1,ne)
      write(3,*) (freq(i),i=1,ne)
      write(3,905) j
      do i=1,nxl+1
            write(3,*) xl(i),tint(i)
      enddo
  900 format('Energies/frequencies:')
  905 format('  xL      I(L,j) ')
      close(1)
      close(2)
      close(3)
      stop
      End
C
C*************************************************
      SUBROUTINE QSIMP(A,B,S)
      PARAMETER (EPS=1.E-4, JMAX=22)
c     jmax=10  !leads to nthet=512 for comparison to adose.for
c     EPS=1.e-4 means error is 0.0001 or 0.01%
      OST=-1.E30
      OS= -1.E30
```

Table C-1--cont'd.

```
      DO 11 J=1,JMAX
            CALL TRAPZD(A,B,ST,J)
            S=(4.*ST-OST)/3.
            IF (ABS(S-OS).LT.EPS*ABS(OS)) RETURN
            OS=S
            OST=ST
 11   CONTINUE
      PAUSE 'Too many steps.'
      END
c*********************************************
c*********************************************
      SUBROUTINE TRAPZD(A,B,S,N)
      IF (N.EQ.1) THEN
            S=0.5*(B-A)*(FUNC(A)+FUNC(B))
            IT=1
      ELSE
            TNM=IT
            DEL=(B-A)/TNM
            X=A+0.5*DEL
            SUM=0.
            DO 11 J=1,IT
             SUM=SUM+FUNC(X)
             X=X+DEL
 11    CONTINUE
            S=0.5*(S+(B-A)*SUM/TNM)
            IT=2*IT
      ENDIF
      RETURN
      END
C*****************************************
      real function func(z)
      common/geom/ rpk,txl,dentrg
      dpres=rpk-txl/cos(z)
      fz=0.
      if(dpres.gt.0.) then
            fz=stop(dpres)          !get mass stopping power.
            fz=fz*qfac(fz,dentrg)  !multiply by quality factor Q (depends on stopping power, fz*dentrg)
      endif
      func=fz
      return
      end
C*************************************************************
C**** SUBROUTINES, FUNCTIONS, ETC.**************************
C*************************************************************
      REAL FUNCTION RANGE(EX)
C-------------------------------------------------------
C**** PURPOSE: DETERMINES THE MASS RANGE (RX) OF ALPHA PARTICLE
C****       GIVEN ITS ENERGY (EX)
C****       REQUIRES PREVIOUSLY INPUT RANGE-ENERGY DATA
C****       E(I)=ENERGY VALUES, R(I)=RANGE VALUES,
```

Table C-1--cont'd.

```
C****       NI=# OF ENTREES IN RANGE-ENERGY TABLE.
C-------------------------------------------------------
      IMPLICIT REAL (A-H,O-Z)
      INTEGER NI
      Common/dat1/ e(79),r(79),s(79),ni
C**** FIND RANGE--USE INTERPOLATION BETWEEN TABLE VALUES
      DO 10 I=2,NI
      IF(EX-E(I).LE.0.) GO TO 50
   10 CONTINUE
   50 CONTINUE
      RANGE=R(I)-(E(I)-EX)*(R(I)-R(I-1))/(E(I)-E(I-1))
      RETURN
      END
C*********************************************************************
      REAL FUNCTION STOP(RXP)
C-------------------------------------------------------
C**** PURPOSE: DETERMINES Mass Stopping Power OF ALPHA PARTICLE
C****       GIVEN ITS Residual Mass Range (g/cm^2)
C****       REQUIRES PREVIOUSLY INPUT RANGE-ENERGY DATA
C****       E(I)=ENERGY VALUES, R(I)=RANGE VALUES,
C****       NI=# OF ENTREES IN RANGE-ENERGY TABLE.
C-------------------------------------------------------
      IMPLICIT REAL (A-H,O-Z)
      INTEGER NI
      common/dat1/ e(79),r(79),s(79),ni
C**** FIND SP--USE LINEAR INTERPOLATION BETWEEN TABLE VALUES-VALID
      DO 10 I=2,NI
      IF(RXP-R(I).LE.0.) GO TO 50
   10 CONTINUE
   50 CONTINUE
      STOP=S(I)-(R(I)-RXP)*(S(I)-S(I-1))/(R(I)-R(I-1))  !MeV cm^2/g
      RETURN
      END
C*************************************************************
C FUNCTION QFAC
C PURPOSE: DETERMINES RADIATION WEIGHTING FACTOR (QUALITY FACTOR) FOR
C       ALPHA PARTICLE GIVEN MASS STOPPING POWER AND MASS DENSITY.
C       ASSUMES MASS STOP POWER = LET OF PARTICLE IN MATERIAL.
C INPUTS:  SX  = MASS STOPPING POWER (MEV-UM^2/G)
C       dentrg = MASS DENSITY (G/CM^3)
C Based on ICRP Publication 60 (1991a); OR see page 101 in Rad Health Handbook(Ed. Shleien, 1992)
C*************************************************************
      REAL FUNCTION QFAC(SX,dentrg)
      REAL SX,dentrg,SXP
      SXP=SX*dentrg*0.1  !converts units: from Mev-cm^2/g to keV/um
      IF(SXP .LT. 10.) THEN
            QFAC=1.0
      ELSE IF (SXP .GT. 100.0) THEN
            QFAC=300.0/SQRT(SXP)
      ELSE
```

Table C-1--cont'd.

```
        QFAC=0.32*SXP-2.2
    ENDIF
    RETURN
    END
```

Table C-2. Listing of input file storing mass-stopping power and range data

Filename: table.dat

```
 79   !NI = # ENTRIES DOWN  Col 1: enrgy(MeV); Col 2: range(g/cm^2), Col 3: stopping power
(MeV-cm^2/g)
 0.000   0.000       0.000
 0.001   3.273E-06   3.271E+02
 0.0015  4.789E-06   3.305E+02
 0.002   6.294E-06   3.342E+02
 0.0025  7.781E-06   3.386E+02
 0.003   9.247E-06   3.435E+02
 0.004   1.211E-05   3.546E+02
 0.005   1.489E-05   3.667E+02
 0.006   1.757E-05   3.793E+02
 0.007   2.016E-05   3.921E+02
 0.008   2.267E-05   4.049E+02
 0.009   2.510E-05   4.177E+02
 0.01    2.746E-05   4.304E+02
 0.0125  3.307E-05   4.615E+02
 0.015   3.831E-05   4.916E+02
 0.0175  4.325E-05   5.205E+02
 0.02    4.793E-05   5.484E+02
 0.0225  5.238E-05   5.752E+02
 0.025   5.663E-05   6.012E+02
 0.0275  6.071E-05   6.253E+02
 0.03    6.462E-05   6.506E+02
 0.035   7.204E-05   6.971E+02
 0.04    7.900E-05   7.411E+02
 0.045   8.556E-05   7.830E+02
 0.05    9.179E-05   8.230E+02
 0.055   9.772E-05   8.612E+02
 0.06    1.034E-04   8.980E+02
 0.065   1.089E-04   9.333E+02
 0.07    1.141E-04   9.674E+02
 0.075   1.192E-04   1.000E+03
 0.08    1.241E-04   1.032E+03
 0.085   1.289E-04   1.063E+03
 0.09    1.335E-04   1.093E+03
 0.095   1.381E-04   1.122E+03
 0.1     1.425E-04   1.151E+03
 0.125   1.630E-04   1.281E+03
```

Table C-2--cont'd.

0.15	1.817E-04	1.397E+03
0.175	1.989E-04	1.500E+03
0.2	2.151E-04	1.593E+03
0.225	2.304E-04	1.677E+03
0.25	2.450E-04	1.753E+03
0.275	2.590E-04	1.820E+03
0.3	2.725E-04	1.881E+03
0.35	2.983E-04	1.985E+03
0.4	3.230E-04	2.069E+03
0.45	3.467E-04	2.134E+03
0.5	3.699E-04	2.184E+03
0.55	3.926E-04	2.220E+03
0.6	4.150E-04	2.245E+03
0.65	4.372E-04	2.260E+03
0.7	4.593E-04	2.266E+03
0.75	4.813E-04	2.266E+03
0.8	5.034E-04	2.260E+03
0.85	5.256E-04	2.248E+03
0.9	5.479E-04	2.233E+03
0.95	5.704E-04	2.215E+03
1.	5.931E-04	2.193E+03
1.25	7.107E-04	2.052E+03
1.5	8.374E-04	1.898E+03
1.75	9.744E-04	1.754E+03
2.	1.123E-03	1.625E+03
2.25	1.282E-03	1.512E+03
2.5	1.453E-03	1.415E+03
2.75	1.635E-03	1.330E+03
3.	1.829E-03	1.257E+03
3.5	2.249E-03	1.133E+03
4.	2.711E-03	1.035E+03
4.5	3.215E-03	9.535E+02
5.	3.759E-03	8.855E+02
5.5	4.344E-03	8.275E+02
6.	4.967E-03	7.777E+02
6.5	5.630E-03	7.340E+02
7.	6.330E-03	6.954E+02
7.5	7.067E-03	6.612E+02
8.	7.842E-03	6.306E+02
8.5	8.653E-03	6.030E+02
9.	9.500E-03	5.780E+02
9.5	1.038E-02	5.552E+02
10.	1.130E-02	5.344E+02

Source: Data are from ICRU (1993)

Table C-3. Listing of sample input files for (A) STDOSE and (B) LINSUB

(A) LINSUB.DAT--Input File for LINSUB (Based on Pu-239).

```
 1.05
 4
 5.1046  0.1150
 5.1429  0.1510
 5.1554  0.7330
 5.0075  0.001094
 0.0   0.0040   80
```

den = density (g/cm^3)
ne = # of alphas emitted by source (in spectrum)
ealf(ne), freq(ne) Note: ICRP23 (REF MAN) lists typical lung tissue
dtmin dtmax ndt (p163,bottom) density value of 1.05 (1.045-1.056) g/cm^3.

(B) STDOSE.DAT--Input File for STDOSE

```
2
5000.  0.0  110.0  10.0  75.0
1.1649E-3  1.05
'Pu9bbb.raw'
```

knuc (1=Pu238; 2=Pu239; 3=Pu240; 4=Am241)
calibre smin smax tmin tmax (assumes 0 is at mucus surface) all in microns
den1 den2 den1=airwaydensity; den2=tissue density
dfile=name of output file (created and written to).

Table C-4. Listing of Fortran Source Code for STDOSE

```
      PROGRAM STDOSE
C
C**** CALCULATES DOSE, DOSE EQUIVALENT PER BQ/CM^3 VOLUME ACTIVITY
C**** UNIFORMLY DISTRIBUTED IN A CYLINDRICAL SHELL CONCENTRIC ABOUT
C**** A COMMON AXIS AS THE TARGET SHELL.  AIRWAY MODEL: HOLLOW/AIR-FILLED
C**** CYLINDER, CONCENTRIC CYLINDERS OF SOURCE, INTERMEDIATE,AND TARGET
SHELLS.
C**** SOURCE IS AN ALPHA EMITTER.
C**** The code reads from stdose.dat and writes to stdose.raw; user must rename to pu9bbb.raw, etc.
C****      where "pu9" is radionuclide (Pu-239) and "bbb" denotes (BB region, "bb = bb Region).
C**** The output is the dose response matrix for a given alpha nuclide.
C**** The utility of the code is that it prevents another code from
C****   computing the same quantities over and over; saves CPUtime. Calculations
C****   are made once and can be used later.
C**** The code uses iterative version of Simpson'sRule to integrate over geometry.
C**** The algorithms for subroutines QSIMP and TRAPZD are from the text
C****  Numerical Recipes (Press et al., 1986).
C**** Use LINSUB to generate numerical data--> fit polynomial or some regression curve to data;
C**** Use the regression function in the subroutine ALINE to estimate the line source integral, I, for mass
C****  thickness x.
C****   AUTHOR:  T.E. HUSTON
C****   Last Revised: 10/9/94
C*************************************************************
      implicit REAL (a-h,o-z)
      real range(4),dose(150,250)  !(i,j)=(target,source)
      character*10 dfile
      data pi/3.14159/
      data range/0.0043431,0.0039408,0.0039559,0.0043992/
      data sthk/0.5/,tthk/0.5/
      common/geom/ rmax,radi,rs,rt,themax,den1,den2,knuc
      OPEN(unit=5,file='stdose.dat',status='old')
      READ(5,*) knuc
      READ(5,*) calib,smin,smax,tmin,tmax
      READ(5,*) den1,den2
      READ(5,*) dfile
      close(5)
C** knuc =1,2,3,4 for Pu-238,239,240,and Am-241 respectively
C** conc(knuc) = concentration of nuclide knuc in (dis/cm^2 for a surface source or dis/cm^3 for volume)
C** calib= airway calibre(i.e., diameter, um)
C** smin = minimum source depth (depth of source from airway surface, um)
C** smax = maximum source depth, um (if 0,source=surface)
C** tmin = minimum target depth from airway, um;
C** tmax=max target depth,um
C** den1=density of air in airway (at BTPS conditions)
C** den2  = density of airway wall, tissue (g/cm^3)
C** dfile = the name of the output file: e.g., pu9bbb.raw = Pu-239, BB region; this file is read by dose.exe.
C**  Get number of source depths and target depths to include in array dose(i,j)
C** 0.5 um thick source shells are assumed; 0.5 um steps in depths are taken for targets.
      ns=NINT((smax-smin)/sthk) !# of source shells considered(integrate over sthk)
      nt=NINT((tmax-tmin)/tthk)   !Note that 'tthk' micron thickness used.
```

Table C-4--cont'd.

```
      if(ns.eq.0) ns=1
      if(nt.eq.0) nt=1
      radi=calib/2.                    !airway radius in microns
      rmax=range(knuc)                 !rmax is mass range in g/cm^2
C Initialize array which will store elements in the alpha dose matrix.
      do i=1,nt
            do j=1,ns
              dose(i,j)=0.
            enddo
      enddo
C Begin loop over target points (shells) at depths td(i):
      do 110 i=1,nt
            td=tmin+FLOAT(i)*tthk-0.5*tthk
            rt=td+radi        !distance from center of airway to target shell.
C Begin loop over source shells at depth sd:
            do 100 j=1,ns
              sd=smin+FLOAT(j)*sthk-0.5*sthk
              if(sd.eq.td)sd=sd+0.025
              rs=sd+radi    !distance from center of airway to source shell.
              if(ABS(1.0e-4*den2*(rt-rs)) .ge. rmax) go to 90
              themax=ACOS(radi/rt)+ACOS(radi/rs)     !delineates near wall and far wall
C Common block "geom" passes other relevant info:
              CALL QSIMP(0.,PI,SS)   !integrate from 0 to pi, return SS (integral)
              ttl=SS/PI
              dose(i,j)=rs*sthk*ttl*1.602E-10*1.0E-8
C Note dose(i,j) = Dose response for target at td(i) and
C source shell at sd(j) units: Sv/(per dis/cm^3) per 0.5-um thick source shell.
 90     print *,td,sd,i,j,dose(i,j)
 100  CONTINUE
            print *, float(i)/float(nt)*100.0,'% complete'
 110  CONTINUE
C---------------------------WRITE RESULTS------------------C
C Note: this is strange, but I found that dimensions of dose(i,j) must remain
C the same as in this code for any code reading "dfile" (the binary file output file).
C I encountered problems otherwise!  Used Lahey FORTRAN compiler; other compilers
C might not have this problem.
C
      open(unit=2,file=dfile,access='sequential',
     *  form='unformatted')
      write(2) smin,smax,ns,sthk
      write(2) tmin,tmax,nt,tthk
      write(2) ((dose(i,j),j=1,ns),i=1,nt)
      close(2)
      STOP
      END
C*************************************************************
C  SUBROUTINES
C*************************************************************
C*******************************************
      SUBROUTINE QSIMP(A,B,S)
```

Table C-4--cont'd.

```
      PARAMETER (EPS=1.E-2, JMAX=21)
      REAL OS,OST,S,ST,A,B
      INTEGER J
C** jmax --->max # of iterations = 2^(jmax-1)
C** eps gives the relative difference between subsequent iterations before exiting
C** eps = the fractional difference from old and new interations when (new-old)/old < eps,
C**         code will assume convergence on integral value and return.
      OST=-1.E30
      OS= -1.E30
      DO 11 J=1,JMAX
            CALL TRAPZD(A,B,ST,J)
            S=(4.*ST-OST)/3.
            IF (ABS(S-OS).LE.EPS*ABS(OS)) RETURN
            if(j.eq.jmax) go to 11        !My line
            OS=S
            OST=ST
 11   CONTINUE
      Print 100, ABS(S-OS),EPS*ABS(OS)  !Added line to inform of convergence problem.
      PAUSE 'Too many steps.'                ! PAUSE execution
 100  FORMAT('ABS(NEW-OLD:',E12.4,' EPS*OLD:',E12.4)   !My Line
      END
C*************************************************
C*************************************************
      SUBROUTINE TRAPZD(A,B,S,N)
c Note subroutine stores IT and S between calls!
      IF (N.EQ.1) THEN
            S=0.5*(B-A)*(FUNC(A)+FUNC(B))
            IT=1
      ELSE
            TNM=IT          !REAL VALUE
            DEL=(B-A)/TNM
            X=A+0.5*DEL
            SUM=0.
            DO 11 J=1,IT
             SUM=SUM+FUNC(X)
             X=X+DEL
11      CONTINUE
            S=0.5*(S+(B-A)*SUM/TNM)
            IT=2*IT
      ENDIF
      RETURN
      END
C************************************************************
      REAL FUNCTION FUNC(Z)
      common/geom/ rmax,radi,rs,rt,themax,den1,den2,knuc
C LOCAL  VARIABLES:
C dtot=total line source to target distance
C dair=distance particle must travel in air (w.r.t line source)
C  dtis=mass distance particle must travel in tissue (wrt line source)
      dtot=SQRT(rs*rs+rt*rt-2.*rs*rt*COS(z))   !in um
```

Table C-4--cont'd.

```
      if(dtot.eq.0.) dtot=0.0001
      dair=0.     !dair=(line source) distance particle must travel in airway
      if(z.gt.themax) then
            ht=rt*rs*SIN(z)/dtot
            if(ht.lt.radi) dair=2.*SQRT(radi*radi-ht*ht)
      endif
C***** dtis=1.0E-4*den2*(dtot-dair)    !Mass tissue thickness(cm^2/g)
C***** dair=1.0E-4*den1*dair          !Mass airway distance
C***** dboth=dair+dtis
      dboth=1.0E-4*(den1*dair+den2*(dtot-dair)) !Mass distance total
      dtot=dtot*1.0E-4                  !convert from um to cm
      tint=0.
      if(dboth .lt. rmax) call aline(knuc,dtot,dboth,tint)
      func=tint
      return
      end
C*************************************************************
C*************************************************************
C***Uses line source response polynomial function generated as a result of LINSUB.
C*** Note that it is density specific (since quality factor depends on target density).
c*** den=1.05 g/cm^3 was used to genersate data for curves.
C**** k=1,2,3,4 = Pu-238,239,240,and Am-241, respectively.
C**** Based on polynomial fits to response obtained from data from lindose.sub
C****  being run with input values for X = x_L in text = density thickness from
C****  target to source line at rs, z = r,theta in text.
c****  LINSUB.FOR was written by T.E. Huston using algorithms similar to those in
C****  ALDOSE (ALDOSE is available from the Radiation Shielding and
C****  Information Center at Oak Ridge Nat. Lab., Oak Ridge, TN 37830).
      SUBROUTINE ALINE(K,D,X,TINT)
      dimension PC(2,6)
      data ( (PC(i,j), j=1,6), i=1,2)
     & /-1.829E+17,1.145E+15,-1.048E+12,-7.019E+9, 1.319E+7,3.394E+4,
     &  -1.435E+17,2.094E+14, 3.425E+12,-1.421E+10,1.461E+7,3.733E+4/
      kn=k
      if(k.eq.3) kn=2    !Response for PU-240 is approx = PU-239
      if(k.eq.4) kn=1    !Response for AM-214 is approx = PU=238
C Note: tint is in units of MeV-cm^2/g;
      tint = PC(kn,1)*X*X*X*X*X*X + PC(kn,2)*X*X*X*X*X + PC(kn,3)*X*X*X*X +
     &    PC(kn,4)*X*X + PC(kn,5)*X + PC(kn,6)
      if(tint.lt.0.) tint=0.
      tint = tint/D
C actual line dose is 2/4pi* tint; tint is in units of (MeV/g per 1dis/cm);
C constants (pi, etc.) are handled later.
      return
      end
```

APPENDIX D
TIDAL VOLUMES FOR CHILDREN

A study of the breathing pattern for children was performed by Godfrey et al. (1971). In that study, 117 boys and girls were examined at three steady-state exertion levels. The levels included rest, 1/3 and 2/3 of the maximum exercise energy-consumption level (denoted as W_{max}). The respiratory parameters measured included ventilation rate (V_E), tidal volume (V_T), oxygen consumption rate (V_{O2}), and respiratory frequency. A relationship between ventilation rate and tidal volume similar to that suggested by Hey et al. (1966) for adults is desired for children. Information on the variability in tidal volumes at specified ages is also desired. The data collected in the study by Godfrey et al. (1971) for subjects in steady-state exercise tests were obtained from the Librarian of the Royal Society of Medicine (see note below Table D-1). The data of use in the present study are listed in Table D-1. For those subjects having a complete set of data (consisting of values reported at all three exercise levels), the equation recommended by Hey et al. (1966) was fit to the ventilation rate and tidal volume data, $V_E = M(V_T - K)$. This equation denotes an assumed linear relationship between ventilation rate and tidal volume. The values of M (min^{-1}) and K (liters) along with the coefficient of determination (R^2) are listed for appropriate subjects in the last three columns of Table D-1. The coefficient of determination, or R^2, indicates the percentage of the variance described by the equation.

Both parameters M and K were found to be slightly correlated to the age of the subject. Values of M and K versus age are plotted in Figures D-1 and D-2. A best-fitting regression equation was determined for the relationship and is also plotted in these figures. For M the relationship with age is:

$$M\,(\text{min}^{-1}) = 1.48 \times 10^{2} \exp\,(-7.32 \times 10^{-2} * \text{Age}); \; R^{2} = 0.35; \; n = 71 \qquad \text{(A-1)}$$

For K the relationship with age is:

$$K\,(\text{liters}) = 8.75 \times 10^{-2} * \text{Age}^{\,4.87 \times 10^{-1}}; \quad R^{2} = 0.10, \quad n = 71 \qquad \text{(A-2)}$$

These expressions are used to estimate values for M and K as a function of the subject age. Given the ventilation rate for the subject, the average tidal volume is approximated by solving $V_T = V_E/M+K$.

To estimate the variability in the tidal volume, some measure of the spread of tidal volumes is needed. The data for tidal volumes in Table D-1 have been analyzed per single year age interval; the results are shown in Table D-2. The table gives the geometric means and geometric standard deviations for the three exertion levels. The geometric standard deviations (GSD) are similar for all ages/levels and range from 1.13 to 1.61. Averaging all GSD values in the table yields an average value of 1.27.

Table D-1. Ventilation data for 119 subjects 6-15 years of age including results from linear curve fitting of tidal volume and ventilation rate.

Subj.	Age (yrs)	Height (cm)	0 Wmax V_E (l/min)	0 Wmax V_T (ml)	0 Wmax VO_2 (l/min)	1/3 Wmax V_E (l/min)	1/3 Wmax V_T (ml)	1/3 Wmax VO_2 (l/min)	2/3 Wmax V_E (l/min)	2/3 Wmax V_T (ml)	2/3 Wmax VO_2 (l/min)	M (min^{-1})	K (l)	R^2
1	12.00	151.4	8.4	494	0.256	30.1	1070	1.100	40.9	1198	1.481	43.6	0.31	0.974
2	11.83	157.0	8.3	695	0.277	26.0	1304	1.100	47.7	1577	1.748	42.1	0.54	0.926
3	12.08	147.3	10.2	605	0.301	20.3	809	0.826	40.2	1044	1.296	68.8	0.48	0.979
4	14.67	170.7	10.0	721	0.342	27.8	1323	1.238	48.1	1769	2.101	36.0	0.48	0.985
5	12.50	146.9	16.1	860	0.360				33.9	764	1.168			
6[a]	13.58	156.2	10.9	786	0.361	23.4	979	0.360	50.9	990				
7[a]	12.58	137.7	8.0	477	0.226	22.2	914	0.915	46.1	919	1.264			
8[b]	12.58	152.1	18.4	955	0.310	25.6	819	1.252	49.2	1175	1.797			
9	11.83	137.9	6.8	633	0.249	17.8	713	0.690	30.9	883	1.054	93.4	0.54	0.976
10	11.75	146.5	7.7	408	0.259	19.4	586	0.723	30.9	676	0.968	83.6	0.33	0.967
11	11.75	136.7	10.4	545	0.242	21.7	805	0.838	38.9	887	1.254	73.7	0.42	0.841
12	11.67	147.4				23.6	534	0.786	34.1	717	1.059			
13	12.58	158.8	12.4	499	0.376	28.6	516	1.027	53.2	885	1.545	87.9	0.28	0.872
14	12.58	141.2	18.7	534	0.307	47.7	822	0.980						
15	11.75	144.5	8.6	365	0.238	21.0	649	0.800	34.7	673	1.074	67.5	0.24	0.785
16	11.75	152.5				24.4	855	0.877	44.3	1062	1.693			
17	11.33	151.9				31.8	751	0.900	52.2	907	1.520			
18	11.58	149.7	7.9	408	0.250	25.9	846	0.924	50.5	911	1.519	68.8	0.31	0.775
19	11.25	137.6	5.8	380	0.202	19.7	625	0.700	34.3	899	1.216	54.9	0.27	1.000
20	11.17	144.6	12.8	647	0.290	26.2	840	0.972	43.5	1116	1.380	65.3	0.45	0.999
21	10.42	150.3	6.7	400	0.184	18.3	605	0.600	37.6	825	1.089	72.9	0.32	0.985
22	10.75	144.4												
23	10.75	142.0	8.2	319	0.246	21.3	731	0.824	42.6	956	1.405	51.3	0.20	0.910
24	10.75	140.5	8.2	418	0.172	17.0	469	0.318						
25	10.17	143.9	9.3	745	0.240	18.2	877	0.782	33.5	960	1.110	108.4	0.67	0.922
26	10.33	142.3	8.0	523	0.265	23.6	652	0.728	35.0	742	1.042	123.1	0.46	1.000
27	10.42	135.6	6.4	311	0.202	18.7	622	0.683	28.1	749	0.916	47.7	0.19	0.974

Table D-1--cont'd.

Subj.	Age (yrs)	Height (cm)	0 Wmax V_E (l/min)	0 Wmax V_T (ml)	0 Wmax VO_2 (l/min)	1/3 Wmax V_E (l/min)	1/3 Wmax V_T (ml)	1/3 Wmax VO_2 (l/min)	2/3 Wmax V_E (l/min)	2/3 Wmax V_T (ml)	2/3 Wmax VO_2 (l/min)	M (min^{-1})	K (l)	R^2
28	10.25	126.5				20.1	496	0.619	33.9	598	0.924			
29	10.00	130.8	6.4	375	0.210	18.4	536	0.685	33.3	777	0.998	66.5	0.27	0.997
30	10.25	146.8	6.2	360	0.181	19.8	602	0.733	30.6	688	0.962	70.4	0.28	0.960
31	10.67	143.3	6.8	304	0.199	17.5	530	0.600	28.7	659	0.901	60.1	0.20	0.972
32	10.00	135.9	6.7	293	0.181	20.0	464	0.633	34.4	596	0.880	90.8	0.23	0.991
33	10.33	144.4	5.8	360	0.207	23.6	549	0.846	35.0	589	1.094	117.1	0.32	0.947
34	9.83	138.6	9.6	412	0.260	24.7	585	0.864	44.6	837	1.354	82.1	0.29	0.999
35	9.42	139.4	7.4	350	0.240	21.3	676	0.822	41.0	900	1.358	59.8	0.25	0.958
36[b]	9.50	137.8	7.4	685	0.230	21.7	509	0.692	36.6	713	1.020			
37	9.42	137.4				21.8	497	0.809	37.6	627	1.034			
38	9.33	136.7	9.5	313	0.261	25.0	503	0.725	42.1	700	1.107	84.3	0.20	1.000
39	9.42	132.3												
40	9.33	140.1												
41	10.08	133.7	5.2	311	0.170	17.5	468	0.675	32.5	645	0.950	81.9	0.25	0.999
42	10.08	132.3	6.8	326	0.164	23.8	567	0.821	36.9	851	1.095	57.0	0.19	0.985
43	9.42	140.1				20.8	441	0.731	30.8	422	0.860			
44	n.a	n.a.												
45	n.a.	n.a.												
46	8.91	131.8	5.9	335	0.193	17.7	577	0.648	32.0	672	0.970	71.8	0.27	0.912
47	9.17	126.6	4.6	314	0.148	15.7	479	0.518	28.9	548	0.787	97.2	0.28	0.922
48	8.50	131.6	5.8	306	0.190	20.4	554	0.514	20.6	549	0.561	59.9	0.21	0.999
49	8.75	135.5	7.6	337	0.176	15.4	515	0.500	30.0	663	0.880	67.9	0.24	0.950
50	8.25	129.0	5.7	296	0.163	17.3	439	0.536	32.7	604	0.921	87.1	0.24	0.998
51	8.25	124.4				14.7	355	0.448	22.6	505	0.633			
52	8.67	128.2	7.1	356	0.181	26.2	454	0.586	40.6	593	1.000	138.8	0.29	0.968
53	8.67	122.2	10.1	270	0.148	15.3	426	0.484	22.4	536	0.662	45.4	0.60	0.965
54	8.50	132.6	5.8	378	0.167	19.6	509	0.516						
55	8.50	133.1				23.1	657	0.782	37.4	702	1.020			

Table D-1--cont'd.

Subj.	Age (yrs)	Height (cm)	0 Wmax V_E (l/min)	0 Wmax V_T (ml)	0 Wmax VO_2 (l/min)	1/3 Wmax V_E (l/min)	1/3 Wmax V_T (ml)	1/3 Wmax VO_2 (l/min)	2/3 Wmax V_E (l/min)	2/3 Wmax V_T (ml)	2/3 Wmax VO_2 (l/min)	M (min^{-1})	K (l)	R^2
56[b]	8.50	144.1	8.9	514	0.187	17.5	494	0.565	33.1	737	1.019			
57[b]	7.83	132.8	6.5	549	0.224	17.7	520	0.638	30.6	694	0.987			
58	7.33	119.8	7.0	219	0.172	16.2	382	0.438	29.5	400	0.728	97.4	0.15	0.737
59	7.42	120.5	6.2	349	0.196	19.7	417	0.646	32.1	567	0.926	112.9	0.27	0.944
60	7.42	122.2				29.1	530	0.511	30.2	613	0.619			
61	8.75	134.1				30.9	529	0.753	41.1	728	1.036			
62	8.33	118.5	5.2	347	0.155	24.3	467	0.540						
63	12.58	146.4	8.0	482	0.237	21.3	884	0.833						
64	12.83	158.2	12.3	426	0.242	24.7	878	0.905	50.3	1383	1.468	39.9	0.17	0.973
65	12.67	148.1	9.7	261	0.191	21.6	701	0.793	38.2	1018	1.289	36.9	0.34	0.965
66	12.67	148.6	7.7	407	0.217	19.5	636	0.749	38.4	924	1.330	59.6	0.29	0.996
67	12.75	161.4				28.7	622	0.838	53.5	840	1.388			
68	7.42	120.8	8.7	338	0.191	12.6	407	0.434	19.0	443	0.634	92.6	0.25	0.902
69	7.25	124.6	5.6	258	0.181	20.0	534	0.615	33.4	594	0.892	73.3	0.19	0.892
70	7.25	119.3	4.9	332	0.176	23.2	650	0.705	31.4	646	0.873	70.6	0.26	0.902
71	7.85	131.0	6.9	291	0.168	20.1	583	0.600	36.8	666	0.978	70.7	0.21	0.863
72	7.42	124.0	5.3	290	0.128	18.5	587	0.659	26.4	685	0.886	51.3	0.19	0.981
73	13.83	161.5	10.3	362	0.289	23.2	907	0.907	41.6	1220	1.360	35.6	0.11	0.936
74	14.83	161.5	9.6	390	0.286	25.4	768	0.994	56.9	1282	1.635	53.5	0.24	0.990
75	14.83	152.8	12.4	593	0.277	26.4	919	0.835	41.2	1252	1.370	43.7	0.31	1.000
76	12.83	153.5	9.8	572	0.242	27.3	855	0.974	39.0	1127	1.208	52.7	0.37	0.990
77	14.83	167.9							53.2	1372	1.800			
78	13.83	164.6	7.9	544	0.234	28.7	1033	1.105	63.9	1198	1.689	75.8	0.48	0.829
79	13.83	157.4				27.2	730	0.836	52.3	1094	1.484			
80	13.75	158.7				24.2	1112	1.109	42.4	1289				
81	13.67	156.1				44.9	996	1.259						

Table D-1--cont'd.

Subj.	Age (yrs)	Height (cm)	0 Wmax V_E (l/min)	0 Wmax V_T (ml)	0 Wmax VO_2 (l/min)	1/3 Wmax V_E (l/min)	1/3 Wmax V_T (ml)	1/3 Wmax VO_2 (l/min)	2/3 Wmax V_E (l/min)	2/3 Wmax V_T (ml)	2/3 Wmax VO_2 (l/min)	M (min^{-1})	K (l)	R^2
82	13.91	160.1				22.5	833	0.879	57.0	955	1.612			
83	n.a.	n.a.												
86	7.17	127.1	5.7	250	0.142	16.8	337	0.447	24.4	498	0.697	71.9	0.14	0.925
87	n.a.	n.a.												
88	14.91	153.0				30.6	619	1.218	49.5	851	1.860			
89	14.42	166.6				29.3	988	1.251	61.0	1302	2.388			
90	13.33	148.1	11.5	328	0.253	18.9	606	0.689	32.3	760	1.033	45.6	0.11	0.896
91	13.91	170.6	9.2	366	0.197	22.6	717	0.813	53.6	1207	1.473	53.5	0.23	0.983
92	13.25	170.7	11.0	667	0.305	39.7	1002	1.348	67.3	1106	1.932	117.8	0.59	0.922
93	13.25	150.9	7.2	532	0.193	20.2	806	0.776	43.1	1364	1.323	42.8	0.35	0.999
94	13.42	156.5				26.5	681	0.831	51.2	897	1.270			
95	14.67	149.3	8.8	210	0.210	20.2	570	0.822	38.8	856	1.231	45.8	0.52	0.959
96	14.67	160.0	8.0	362	0.202	22.5	921	0.835	40.3	1164	1.200	37.8	0.19	0.922
97	14.83	160.0	10.7	476	0.323	25.5	837	0.916	47.6	1348	1.452	42.4	0.23	1.000
98	14.17	169.6	8.2	868	0.246	31.8	1069	1.184	63.5	1631	1.928	69.0	0.69	0.967
99	14.91	185.0				31.2	1371	1.108	60.7	2144	1.774			
100	15.25	181.0	10.4	752	0.258	30.5	1236	1.249	59.0	1758	2.423	48.4	0.56	0.995
101	15.67	172.0	13.3	566	0.298	32.8	1028	1.245	62.4	1657	2.026	45.1	0.28	0.999
102	15.67	182.1	11.9	563	0.311	32.6	1293	1.259	67.0	1943	2.294	39.7	0.33	0.969
103	15.17	170.0				27.6	1216	1.117	49.7	1328	1.904			
104	15.50	155.3	9.2	403	0.310	31.7	728	0.978	46.1	964	1.395	66.0	0.26	0.999
105	15.75	166.9	8.1	543	0.234	21.8	826	0.819	45.7	1365	1.539	45.6	0.36	1.000
106	15.33	167.1	10.6	381	0.302	16.7	888	0.732	40.9	1149	1.452	35.7	0.17	0.757
107	15.83	155.6	9.4	330	0.242	25.6	737	0.886	43.2	885	1.204	56.4	0.19	0.920
108	15.67	159.7	8.5	482	0.206	23.7	724	0.868	47.7	1022	1.369	72.9	0.38	0.995
109	15.75	163.9	10.5	376	0.263	28.5	923	0.972						

Table D-1--cont'd.

Subj.	Age (yrs)	Height (cm)	0 Wmax V_E (l/min)	0 Wmax V_T (ml)	0 Wmax VO_2 (l/min)	1/3 Wmax V_E (l/min)	1/3 Wmax V_T (ml)	1/3 Wmax VO_2 (l/min)	2/3 Wmax V_E (l/min)	2/3 Wmax V_T (ml)	2/3 Wmax VO_2 (l/min)	M (min^{-1})	K (l)	R^2
110	6.33	122.7	5.5	330	0.180	17.9	393	0.473	24.9	499	0.652	109.7	0.26	0.910
111	6.17	117.1	6.0	278	0.173	18.7	486	0.513	25.0	489	0.694	76.0	0.20	0.902
112[b]	6.75	114.8	4.6	244	0.132	15.1	503	0.438	27.0	478	0.673			
115	6.17	117.0	4.3	254	0.144	9.9	265	0.323						
116	6.08	112.8	4.3	251	0.124	14.6	294	0.500	21.4	378	0.618	127.3	0.20	0.912
117	6.33	118.9	5.6	466	0.152	14.6	400	0.457						
118	6.83	117.0	5.1	258	0.143	14.8	417	0.444						
119	6.08	114.8				13.7	357	0.419						

Notes: Data in first 12 columns are from Godfrey et al. (1971). Empty data blocks in these columns of the table are a result of the data set. The raw data were deposited by the authors with the Librarian of the Royal Society of Medicine, London, England as Clinical Science Table 40/2 and Clinical Science Table 40/3. The data in the last three columns were derived in the present study as described in the text.

[a] Tidal volume at level 2 was approximately equal to level 3; subject was not used.

[b] Tidal volumes did not increase with exertion level; subject was not used.

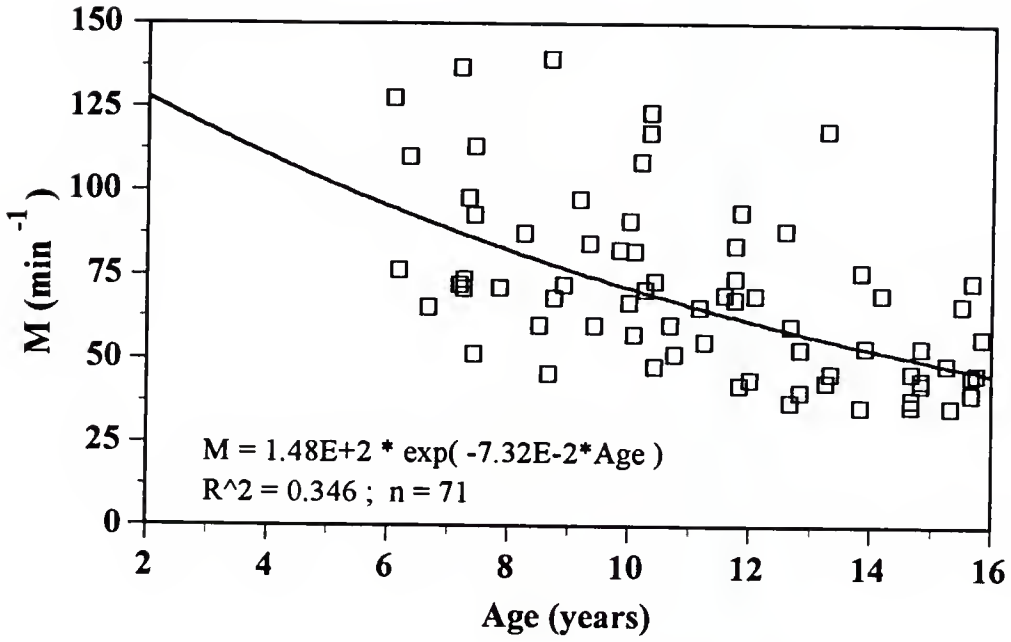

Figure D-1. Relationship between M and age for data listed in Table D-1.

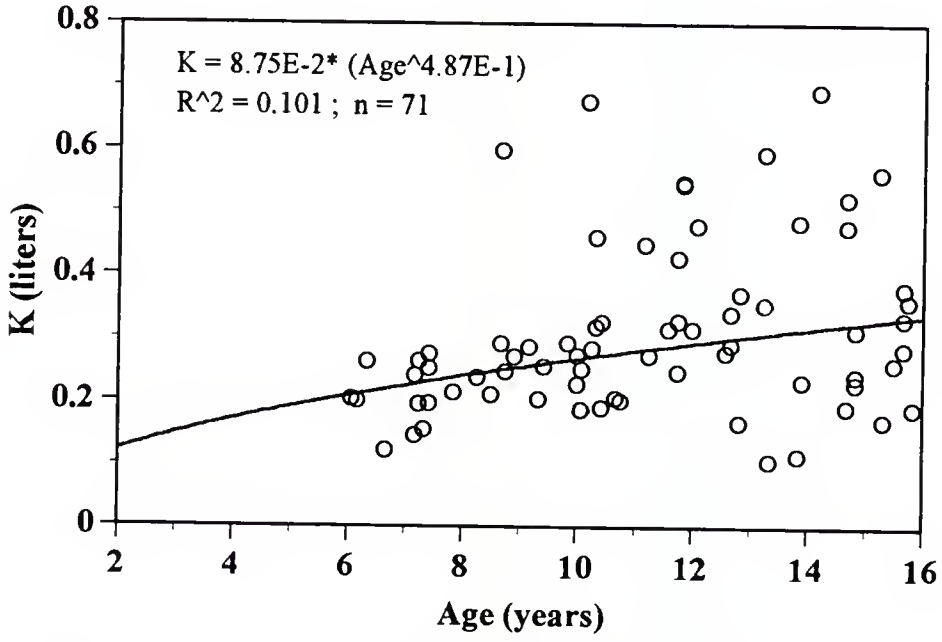

Figure D-2. Relationship between K and age for data listed in Table D-1.

Table D-2. Geometric mean tidal volumes and geometric standard deviations.

	0 Wmax		1/3 Wmax		2/3 Wmax	
Age (yrs)	V_T	GSD	V_T	GSD	V_T	GSD
6	281	1.26	389	1.24	446	1.13
7	306	1.29	489	1.29	557	1.22
8	343	1.20	492	1.17	624	1.14
9	396	1.39	522	1.15	660	1.29
10	374	1.30	574	1.20	731	1.19
11	495	1.30	752	1.27	910	1.28
12	520	1.40	780	1.22	1011	1.19
13	488	1.40	842	1.22	1074	1.20
14	472	1.61	940	1.35	1309	1.34
15	473	1.30	938	1.25	1296	1.32
Average GSD's:		1.34		1.24		1.23

Notes: Data derived from Table D-1.
All columns labeled V_T represent geometric means.
All columns labeled GSD repsresent geometric standard deviations.

APPENDIX E
DOSE DATA FOR INHALATION OF PLUTONIUM OXIDE

The probabilistic computer code LUDUC has been run for a number of exposure scenarios. Some of the dose data that resulted from these runs are listed in this appendix. These data represent the equivalent dose to the specified target tissue per activity exposure, denoted H/A_E (with units of Sv per Bq-hr/m^3). The radionuclide/chemical form was $^{239}PuO_2$ for all cases; however, for the same activity exposure (Bq-hr/m^3), the data are essentially the same for $^{240}PuO_2$ and for mixtures of $^{239+240}PuO_2$. The data include various fractiles (e.g., 5%, 50%, 95% fractiles), geometric means (GM), and geometric standard deviations (GSD). In all cases, aerosol particles were assumed to be comprised of monodisperse (single-sized aerosol particles), unit density spheres (i.e., mass density of 1 g/cm^3 and particle shape factor of 1). Dose calculations are based on an acute intake. Doses are integrated over 50 years post intake for adults (age $\geq$ 18 years) and 70 years post intak for children (age < 18 years). In all cases, each data point is based on a sample size of n = 1000 using Latin hypercube sampling techniques.

The five target tissues are (1) the secretory cells of the bronchial (BB) epithelium, (2) the basal cells of the bronchial epithelium, (3) the secretory cells of the bronchiolar (bb) epithelium, (4) the total mass of the alveolar-interstitium (AI), and (5) the total mass

of the lymph nodes associated with the thoracic region (LNth). The data presented for the "lung" represent a weighted sum of the equivalent doses to the five target tissues.

The first data set is listed in Table E-1 and is for exposure of adult males (25-34 years of age) at all exertion levels: resting, sitting, light exertion, and heavy exertion. Entries in the table represent various equivalent dose fractiles (in Sv per Bq-hr/m^3) obtained for exposure to several particle diameters (in microns). Particles were assumed to be unit density spheres so that diameters correspond to aerodynamic diameters.

The second data set is listed in Table E-2 and is for several age groups each at the light exertion level. The entries in this data set are similar to the those in Table E-1 and list various dose fractiles versus particle diameter (same units as Table E-1). The only difference is the age of the population group. For 2, 5, and 10 year-old groups the gender was taken to be males in the methodology; however, differences in fractiles between males and females were negligible.

The third data set is listed in Table E-3 and is for for all age groups and all exertion levels. This third set lists geometric means (GM) and geometric standard deviations (GSD) for the equivalent doses versus particle diameter (monodisperse, unit density spheres) for all target tissues. Geometric means have units of Sv per Bq-hr/m^3. Values listed as "-1" in the table correspond to cases in which the GM and GSD could not be computed due to zero dose values for some of the trials.

Table E-1. Various fractiles (versus particle diameter in μm) for equivalent dose per activity exposure, H/A_E (units: Sv per Bq-hr/m^3), for adult males (25-34 years) exposed to $^{239}PuO_2$ aerosols at four exertion levels (assumes monodisperse, unit density spheres).

BB Secretory Cells (Males, 25-34 years, Resting)

Diameter	5%	10%	25%	50%	75%	90%	95%
0.1	9.69E-06	1.27E-05	1.85E-05	2.99E-05	4.66E-05	6.86E-05	9.28E-05
0.2	6.17E-06	8.11E-06	1.19E-05	1.91E-05	3.01E-05	4.42E-05	5.94E-05
0.5	3.52E-06	4.56E-06	6.86E-06	1.07E-05	1.69E-05	2.52E-05	3.41E-05
0.8	3.33E-06	4.09E-06	6.36E-06	9.94E-06	1.59E-05	2.48E-05	3.28E-05
1	3.53E-06	4.57E-06	7.42E-06	1.16E-05	1.89E-05	2.97E-05	4.10E-05
2	7.97E-06	1.04E-05	1.83E-05	3.06E-05	5.12E-05	8.98E-05	1.22E-04
5	1.79E-06	2.57E-06	5.28E-06	1.11E-05	2.47E-05	4.59E-05	6.95E-05
8	7.71E-07	1.10E-06	2.19E-06	4.78E-06	1.12E-05	2.56E-05	3.85E-05
10	5.82E-07	8.07E-07	1.64E-06	3.77E-06	8.83E-06	2.13E-05	3.24E-05
20	1.62E-07	2.25E-07	4.74E-07	1.14E-06	2.82E-06	7.11E-06	1.04E-05
50	1.69E-08	2.43E-08	5.12E-08	1.19E-07	3.06E-07	7.62E-07	1.19E-06

BB Basal Cells (Males, 25-34 years, Resting)

Diameter	5%	10%	25%	50%	75%	90%	95%
0.1	7.93E-07	1.15E-06	2.56E-06	1.12E-05	3.14E-05	5.96E-05	8.27E-05
0.2	5.15E-07	7.39E-07	1.66E-06	7.13E-06	2.04E-05	3.81E-05	5.31E-05
0.5	2.74E-07	4.18E-07	9.38E-07	3.98E-06	1.16E-05	2.20E-05	2.95E-05
0.8	2.42E-07	3.69E-07	8.41E-07	3.54E-06	1.07E-05	2.07E-05	2.74E-05
1	2.67E-07	4.10E-07	9.71E-07	4.13E-06	1.25E-05	2.49E-05	3.44E-05
2	7.02E-07	1.05E-06	2.87E-06	1.11E-05	3.27E-05	6.85E-05	9.79E-05
5	1.12E-06	1.50E-06	3.12E-06	7.10E-06	1.51E-05	3.45E-05	5.28E-05
8	8.56E-07	1.18E-06	2.08E-06	4.56E-06	9.63E-06	2.18E-05	3.30E-05
10	7.06E-07	9.38E-07	1.73E-06	3.59E-06	8.04E-06	1.79E-05	2.75E-05
20	2.06E-07	2.94E-07	5.42E-07	1.14E-06	2.66E-06	6.12E-06	8.61E-06
50	2.06E-08	3.15E-08	5.73E-08	1.22E-07	2.82E-07	6.67E-07	9.39E-07

bb Secretory Cells (Males, 25-34 years, Resting)

Diameter	5%	10%	25%	50%	75%	90%	95%
0.1	4.14E-05	4.95E-05	6.73E-05	9.67E-05	1.38E-04	1.96E-04	2.33E-04
0.2	2.41E-05	2.86E-05	3.89E-05	5.60E-05	8.05E-05	1.14E-04	1.36E-04
0.5	1.33E-05	1.60E-05	2.15E-05	3.17E-05	4.46E-05	6.26E-05	7.41E-05
0.8	1.38E-05	1.60E-05	2.22E-05	3.22E-05	4.70E-05	6.37E-05	7.59E-05
1	1.52E-05	1.82E-05	2.53E-05	3.63E-05	5.50E-05	7.39E-05	9.20E-05
2	2.48E-05	3.12E-05	4.36E-05	6.66E-05	9.97E-05	1.43E-04	1.76E-04
5	3.90E-06	5.59E-06	8.61E-06	1.48E-05	2.64E-05	4.11E-05	5.54E-05
8	9.01E-07	1.33E-06	2.16E-06	3.92E-06	7.57E-06	1.42E-05	2.06E-05
10	3.77E-07	5.91E-07	1.01E-06	1.91E-06	3.81E-06	7.92E-06	1.17E-05
20	9.51E-10	2.96E-09	1.27E-08	4.62E-08	1.41E-07	3.75E-07	7.44E-07
50	0	0	0	0	2.05E-14	1.13E-12	8.33E-12

Table E-1--cont'd

AI Tissues (Males, 25-34 years, Resting)

Diameter	5%	10%	25%	50%	75%	90%	95%
0.1	4.01E-05	4.80E-05	6.46E-05	8.98E-05	1.25E-04	1.63E-04	1.87E-04
0.2	2.25E-05	2.73E-05	3.68E-05	5.11E-05	7.19E-05	9.55E-05	1.12E-04
0.5	1.70E-05	2.06E-05	2.81E-05	4.05E-05	5.63E-05	7.59E-05	8.86E-05
0.8	2.28E-05	2.82E-05	3.92E-05	5.60E-05	7.86E-05	1.05E-04	1.25E-04
1	2.75E-05	3.43E-05	4.81E-05	6.78E-05	9.51E-05	1.29E-04	1.51E-04
2	4.21E-05	5.39E-05	7.43E-05	1.05E-04	1.45E-04	1.92E-04	2.24E-04
5	1.70E-05	2.27E-05	3.37E-05	5.24E-05	7.63E-05	1.09E-04	1.38E-04
8	3.65E-06	4.90E-06	7.68E-06	1.32E-05	2.14E-05	3.43E-05	4.78E-05
10	1.14E-06	1.55E-06	2.56E-06	4.95E-06	8.61E-06	1.46E-05	2.08E-05
20	2.63E-10	6.43E-10	3.11E-09	1.45E-08	5.62E-08	1.40E-07	2.43E-07
50	0	0	0	0	0.00E+00	1.18E-16	1.46E-15

LNth Tissues (Males, 25-34 years, Resting)

Diameter	5%	10%	25%	50%	75%	90%	95%
0.1	7.06E-05	1.12E-04	2.58E-04	5.62E-04	9.61E-04	1.42E-03	1.80E-03
0.2	4.10E-05	6.51E-05	1.50E-04	3.24E-04	5.56E-04	8.28E-04	1.04E-03
0.5	2.65E-05	4.35E-05	1.07E-04	2.24E-04	3.91E-04	6.05E-04	7.55E-04
0.8	3.21E-05	5.44E-05	1.34E-04	2.90E-04	5.17E-04	8.03E-04	1.01E-03
1	3.79E-05	6.51E-05	1.63E-04	3.48E-04	6.17E-04	9.75E-04	1.21E-03
2	6.41E-05	1.04E-04	2.70E-04	5.61E-04	9.81E-04	1.58E-03	1.85E-03
5	4.42E-05	7.27E-05	1.68E-04	3.61E-04	6.75E-04	1.01E-03	1.33E-03
8	2.13E-05	3.50E-05	7.31E-05	1.50E-04	2.90E-04	4.62E-04	6.54E-04
10	1.35E-05	2.06E-05	4.40E-05	8.78E-05	1.74E-04	2.85E-04	4.12E-04
20	1.96E-06	3.28E-06	6.56E-06	1.33E-05	2.72E-05	4.60E-05	7.29E-05
50	1.82E-07	3.06E-07	6.20E-07	1.27E-06	2.61E-06	4.59E-06	7.15E-06

Lung, Combined (Males, 25-34 years, Resting)

Diameter	5%	10%	25%	50%	75%	90%	95%
0.1	3.27E-05	3.90E-05	5.47E-05	7.43E-05	1.00E-04	1.32E-04	1.58E-04
0.2	1.93E-05	2.29E-05	3.19E-05	4.33E-05	5.81E-05	7.75E-05	9.29E-05
0.5	1.17E-05	1.47E-05	2.03E-05	2.83E-05	3.87E-05	5.06E-05	5.92E-05
0.8	1.33E-05	1.63E-05	2.34E-05	3.43E-05	4.64E-05	6.17E-05	7.45E-05
1	1.57E-05	1.94E-05	2.79E-05	4.06E-05	5.58E-05	7.40E-05	8.95E-05
2	2.86E-05	3.59E-05	4.87E-05	7.04E-05	9.77E-05	1.28E-04	1.53E-04
5	8.18E-06	1.04E-05	1.69E-05	2.73E-05	4.33E-05	6.17E-05	7.66E-05
8	2.07E-06	2.97E-06	4.65E-06	8.14E-06	1.43E-05	2.30E-05	3.24E-05
10	9.98E-07	1.37E-06	2.33E-06	4.03E-06	7.27E-06	1.31E-05	1.91E-05
20	4.93E-08	7.81E-08	1.66E-07	3.79E-07	9.13E-07	2.22E-06	3.65E-06
50	3.20E-09	5.44E-09	1.30E-08	3.48E-08	8.84E-08	2.23E-07	3.59E-07

Table E-1--cont'd

BB Secretory Cells (Males, 25-34 years, Sitting)

Diameter	5%	10%	25%	50%	75%	90%	95%
0.1	1.15E-05	1.49E-05	2.17E-05	3.48E-05	5.51E-05	7.99E-05	1.09E-04
0.2	7.30E-06	9.45E-06	1.39E-05	2.23E-05	3.51E-05	5.09E-05	6.95E-05
0.5	4.28E-06	5.49E-06	8.35E-06	1.30E-05	2.09E-05	3.02E-05	4.18E-05
0.8	4.42E-06	5.81E-06	9.30E-06	1.47E-05	2.38E-05	3.93E-05	5.45E-05
1	5.42E-06	6.95E-06	1.18E-05	1.90E-05	3.16E-05	5.60E-05	7.60E-05
2	1.34E-05	1.85E-05	3.20E-05	5.33E-05	9.10E-05	1.65E-04	2.19E-04
5	2.37E-06	3.45E-06	7.33E-06	1.60E-05	3.65E-05	7.25E-05	1.07E-04
8	9.73E-07	1.31E-06	2.78E-06	6.33E-06	1.60E-05	3.71E-05	5.49E-05
10	6.94E-07	9.66E-07	1.99E-06	4.74E-06	1.19E-05	2.88E-05	4.34E-05
20	1.64E-07	2.38E-07	4.87E-07	1.19E-06	3.04E-06	7.97E-06	1.22E-05
50	1.63E-08	2.36E-08	5.01E-08	1.18E-07	3.09E-07	7.89E-07	1.23E-06

BB Basal Cells (Males, 25-34 years, Sitting)

Diameter	5%	10%	25%	50%	75%	90%	95%
0.1	9.25E-07	1.33E-06	3.03E-06	1.30E-05	3.75E-05	6.89E-05	9.73E-05
0.2	5.86E-07	8.46E-07	1.93E-06	8.33E-06	2.41E-05	4.39E-05	6.14E-05
0.5	3.27E-07	5.05E-07	1.15E-06	4.75E-06	1.39E-05	2.64E-05	3.54E-05
0.8	3.56E-07	5.26E-07	1.29E-06	5.35E-06	1.60E-05	3.26E-05	4.31E-05
1	4.56E-07	6.74E-07	1.73E-06	6.94E-06	2.05E-05	4.40E-05	5.95E-05
2	1.32E-06	1.88E-06	5.27E-06	2.01E-05	5.81E-05	1.23E-04	1.84E-04
5	1.56E-06	2.12E-06	4.53E-06	1.07E-05	2.33E-05	5.46E-05	8.24E-05
8	1.11E-06	1.50E-06	2.73E-06	5.84E-06	1.36E-05	3.15E-05	4.81E-05
10	8.68E-07	1.15E-06	2.13E-06	4.58E-06	1.06E-05	2.52E-05	3.73E-05
20	2.11E-07	3.00E-07	5.58E-07	1.20E-06	2.92E-06	7.22E-06	1.01E-05
50	2.01E-08	3.03E-08	5.57E-08	1.21E-07	2.99E-07	7.03E-07	9.81E-07

bb Secretory Cells (Males, 25-34 years, Sitting)

Diameter	5%	10%	25%	50%	75%	90%	95%
0.1	5.11E-05	6.10E-05	8.14E-05	1.18E-04	1.72E-04	2.41E-04	2.89E-04
0.2	2.94E-05	3.56E-05	4.66E-05	6.83E-05	9.89E-05	1.38E-04	1.66E-04
0.5	1.57E-05	1.93E-05	2.56E-05	3.73E-05	5.38E-05	7.39E-05	8.80E-05
0.8	1.56E-05	1.84E-05	2.51E-05	3.67E-05	5.15E-05	7.02E-05	8.32E-05
1	1.75E-05	2.09E-05	2.82E-05	4.11E-05	6.01E-05	8.06E-05	9.92E-05
2	2.74E-05	3.36E-05	4.74E-05	7.27E-05	1.09E-04	1.54E-04	1.92E-04
5	3.75E-06	5.16E-06	8.46E-06	1.51E-05	2.69E-05	4.56E-05	6.11E-05
8	7.15E-07	1.11E-06	1.84E-06	3.48E-06	6.85E-06	1.37E-05	2.17E-05
10	2.56E-07	4.26E-07	7.31E-07	1.56E-06	3.26E-06	7.28E-06	1.15E-05
20	6.27E-11	3.13E-10	2.69E-09	1.59E-08	6.16E-08	2.05E-07	3.74E-07
50	0	0	0	0	0	8.24E-15	1.41E-13

Table E-1--cont'd

AI Tissues (Males, 25-34 years, Sitting)

Diameter	5%	10%	25%	50%	75%	90%	95%
0.1	5.60E-05	6.47E-05	8.95E-05	1.22E-04	1.77E-04	2.27E-04	2.59E-04
0.2	3.16E-05	3.70E-05	5.04E-05	6.97E-05	9.98E-05	1.30E-04	1.50E-04
0.5	2.35E-05	2.77E-05	3.78E-05	5.35E-05	7.49E-05	1.00E-04	1.21E-04
0.8	3.08E-05	3.75E-05	5.16E-05	7.51E-05	1.04E-04	1.38E-04	1.68E-04
1	3.75E-05	4.50E-05	6.22E-05	8.91E-05	1.25E-04	1.68E-04	2.02E-04
2	5.16E-05	6.46E-05	9.07E-05	1.30E-04	1.80E-04	2.44E-04	2.80E-04
5	1.63E-05	2.17E-05	3.39E-05	5.42E-05	8.25E-05	1.24E-04	1.64E-04
8	2.82E-06	3.96E-06	6.50E-06	1.20E-05	2.07E-05	3.58E-05	5.29E-05
10	6.50E-07	1.06E-06	1.92E-06	3.86E-06	7.42E-06	1.40E-05	2.14E-05
20	8.62E-12	4.80E-11	4.10E-10	3.50E-09	2.01E-08	6.11E-08	1.13E-07
50	0	0	0	0	0	0	4.19E-19

LNth Tissues (Males, 25-34 years, Sitting)

Diameter	5%	10%	25%	50%	75%	90%	95%
0.1	9.28E-05	1.50E-04	3.39E-04	7.30E-04	1.28E-03	1.83E-03	2.44E-03
0.2	5.30E-05	8.57E-05	1.94E-04	4.16E-04	7.34E-04	1.07E-03	1.40E-03
0.5	3.31E-05	5.40E-05	1.37E-04	2.90E-04	5.07E-04	7.81E-04	1.02E-03
0.8	3.93E-05	6.74E-05	1.75E-04	3.73E-04	6.75E-04	1.02E-03	1.32E-03
1	4.72E-05	8.21E-05	2.11E-04	4.49E-04	8.02E-04	1.22E-03	1.58E-03
2	7.61E-05	1.29E-04	3.32E-04	6.97E-04	1.23E-03	1.89E-03	2.37E-03
5	4.78E-05	8.00E-05	1.82E-04	3.89E-04	7.50E-04	1.18E-03	1.64E-03
8	2.25E-05	3.50E-05	7.55E-05	1.54E-04	3.08E-04	5.58E-04	7.75E-04
10	1.36E-05	2.04E-05	4.39E-05	8.87E-05	1.78E-04	3.42E-04	4.91E-04
20	1.90E-06	3.09E-06	6.38E-06	1.31E-05	2.77E-05	5.38E-05	8.91E-05
50	1.72E-07	2.91E-07	6.07E-07	1.23E-06	2.62E-06	4.88E-06	7.74E-06

Lung, Combined (Males, 25-34 years, Sitting)

Diameter	5%	10%	25%	50%	75%	90%	95%
0.1	4.15E-05	4.93E-05	7.02E-05	9.56E-05	1.29E-04	1.71E-04	2.03E-04
0.2	2.42E-05	2.91E-05	4.05E-05	5.55E-05	7.51E-05	9.85E-05	1.18E-04
0.5	1.47E-05	1.85E-05	2.52E-05	3.62E-05	4.89E-05	6.48E-05	7.51E-05
0.8	1.65E-05	2.10E-05	3.01E-05	4.40E-05	5.99E-05	7.97E-05	9.92E-05
1	2.01E-05	2.48E-05	3.59E-05	5.17E-05	7.16E-05	9.63E-05	1.19E-04
2	3.56E-05	4.34E-05	6.16E-05	8.81E-05	1.23E-04	1.66E-04	1.95E-04
5	8.48E-06	1.14E-05	1.77E-05	3.02E-05	4.89E-05	7.53E-05	9.90E-05
8	1.93E-06	2.83E-06	4.55E-06	8.23E-06	1.46E-05	2.66E-05	3.85E-05
10	8.44E-07	1.23E-06	2.14E-06	3.88E-06	7.53E-06	1.47E-05	2.18E-05
20	4.09E-08	6.42E-08	1.51E-07	3.66E-07	9.73E-07	2.40E-06	4.05E-06
50	3.20E-09	5.36E-09	1.30E-08	3.48E-08	9.12E-08	2.34E-07	3.65E-07

Table E-1--cont'd

BB Secretory Cells (Males, 25-34 years, Light Exertion)

Diameter	5%	10%	25%	50%	75%	90%	95%
0.1	1.73E-05	2.33E-05	3.42E-05	5.49E-05	8.79E-05	1.27E-04	1.71E-04
0.2	1.08E-05	1.45E-05	2.14E-05	3.44E-05	5.52E-05	8.02E-05	1.08E-04
0.5	9.10E-06	1.17E-05	1.94E-05	3.19E-05	5.55E-05	1.03E-04	1.39E-04
0.8	1.48E-05	1.98E-05	3.45E-05	6.39E-05	1.17E-04	2.30E-04	3.33E-04
1	2.08E-05	2.84E-05	4.93E-05	9.21E-05	1.70E-04	3.41E-04	4.99E-04
2	4.84E-05	6.89E-05	1.17E-04	2.21E-04	4.30E-04	8.69E-04	1.22E-03
5	4.28E-06	6.60E-06	1.66E-05	3.95E-05	1.01E-04	2.45E-04	4.06E-04
8	1.47E-06	2.09E-06	4.39E-06	1.17E-05	3.53E-05	9.22E-05	1.76E-04
10	9.51E-07	1.38E-06	2.85E-06	7.47E-06	2.31E-05	6.01E-05	1.18E-04
20	1.54E-07	2.28E-07	4.88E-07	1.23E-06	3.81E-06	1.03E-05	1.90E-05
50	1.49E-08	2.18E-08	4.66E-08	1.17E-07	3.41E-07	9.42E-07	1.46E-06

BB Basal Cells (Males, 25-34 years, Light Exertion)

Diameter	5%	10%	25%	50%	75%	90%	95%
0.1	1.35E-06	2.04E-06	4.63E-06	1.99E-05	5.99E-05	1.07E-04	1.58E-04
0.2	8.65E-07	1.32E-06	2.96E-06	1.26E-05	3.72E-05	6.74E-05	9.91E-05
0.5	7.08E-07	1.09E-06	2.89E-06	1.16E-05	3.61E-05	7.68E-05	1.13E-04
0.8	1.32E-06	2.08E-06	6.22E-06	2.37E-05	6.62E-05	1.65E-04	2.66E-04
1	1.86E-06	3.06E-06	9.14E-06	3.43E-05	9.57E-05	2.44E-04	3.98E-04
2	4.43E-06	7.64E-06	2.26E-05	8.47E-05	2.39E-04	6.06E-04	9.92E-04
5	3.34E-06	5.01E-06	1.01E-05	2.64E-05	7.19E-05	1.76E-04	2.88E-04
8	1.81E-06	2.49E-06	4.67E-06	1.12E-05	3.07E-05	8.19E-05	1.42E-04
10	1.18E-06	1.64E-06	3.27E-06	7.42E-06	2.07E-05	5.42E-05	9.55E-05
20	1.88E-07	2.90E-07	5.58E-07	1.29E-06	3.47E-06	9.00E-06	1.59E-05
50	1.83E-08	2.82E-08	5.40E-08	1.24E-07	3.21E-07	8.17E-07	1.24E-06

bb Secretory Cells (Males, 25-34 years, Light Exertion)

Diameter	5%	10%	25%	50%	75%	90%	95%
0.1	8.49E-05	1.06E-04	1.44E-04	2.06E-04	3.01E-04	4.22E-04	5.15E-04
0.2	4.87E-05	5.99E-05	8.13E-05	1.16E-04	1.71E-04	2.41E-04	2.94E-04
0.5	2.58E-05	3.12E-05	4.26E-05	6.09E-05	8.84E-05	1.21E-04	1.47E-04
0.8	2.32E-05	2.88E-05	3.87E-05	5.68E-05	7.99E-05	1.07E-04	1.26E-04
1	2.48E-05	3.11E-05	4.22E-05	6.23E-05	8.89E-05	1.20E-04	1.43E-04
2	3.19E-05	4.03E-05	6.12E-05	9.88E-05	1.58E-04	2.46E-04	3.23E-04
5	2.63E-06	3.88E-06	6.90E-06	1.39E-05	2.95E-05	6.43E-05	1.09E-04
8	1.61E-07	3.49E-07	7.54E-07	1.96E-06	4.45E-06	1.21E-05	2.22E-05
10	1.62E-08	4.67E-08	1.54E-07	5.12E-07	1.42E-06	4.49E-06	7.24E-06
20	0	0	1.90E-13	3.52E-11	1.06E-09	1.06E-08	2.49E-08
50	0	0	0	0	0	0	0

Table E-1--cont'd

AI Tissues (Males, 25-34 years, Light Exertion)

Diameter	5%	10%	25%	50%	75%	90%	95%
0.1	1.21E-04	1.50E-04	2.03E-04	2.98E-04	4.35E-04	5.76E-04	6.61E-04
0.2	6.69E-05	8.17E-05	1.14E-04	1.66E-04	2.41E-04	3.24E-04	3.76E-04
0.5	4.80E-05	6.01E-05	8.26E-05	1.22E-04	1.71E-04	2.35E-04	2.78E-04
0.8	6.11E-05	7.77E-05	1.10E-04	1.57E-04	2.25E-04	3.11E-04	3.72E-04
1	6.82E-05	8.93E-05	1.26E-04	1.79E-04	2.57E-04	3.65E-04	4.30E-04
2	6.83E-05	8.68E-05	1.31E-04	1.98E-04	2.96E-04	4.29E-04	5.67E-04
5	9.61E-06	1.40E-05	2.37E-05	4.36E-05	8.32E-05	1.74E-04	2.51E-04
8	3.80E-07	7.34E-07	1.90E-06	4.79E-06	1.10E-05	2.68E-05	4.56E-05
10	1.78E-08	4.50E-08	2.01E-07	7.39E-07	2.27E-06	6.15E-06	1.15E-05
20	0	0	9.81E-17	3.64E-13	3.55E-11	7.39E-10	2.81E-09
50	0	0	0	0	0	0	0

LNth Tissues (Males, 25-34 years, Light Exertion)

Diameter	5%	10%	25%	50%	75%	90%	95%
0.1	1.78E-04	2.92E-04	7.06E-04	1.58E-03	2.80E-03	4.32E-03	5.60E-03
0.2	9.84E-05	1.63E-04	3.97E-04	8.82E-04	1.57E-03	2.44E-03	3.18E-03
0.5	6.94E-05	1.11E-04	2.87E-04	6.10E-04	1.10E-03	1.79E-03	2.25E-03
0.8	8.62E-05	1.37E-04	3.69E-04	7.56E-04	1.43E-03	2.22E-03	3.00E-03
1	9.99E-05	1.65E-04	4.30E-04	8.92E-04	1.69E-03	2.55E-03	3.54E-03
2	1.34E-04	2.26E-04	5.42E-04	1.15E-03	2.18E-03	3.50E-03	4.93E-03
5	6.18E-05	9.35E-05	2.17E-04	4.61E-04	9.60E-04	2.18E-03	4.11E-03
8	2.19E-05	3.54E-05	7.73E-05	1.63E-04	3.52E-04	9.81E-04	2.07E-03
10	1.21E-05	1.99E-05	4.23E-05	8.94E-05	2.00E-04	5.83E-04	1.30E-03
20	1.62E-06	2.76E-06	5.93E-06	1.27E-05	2.82E-05	8.67E-05	1.72E-04
50	1.58E-07	2.64E-07	5.72E-07	1.22E-06	2.65E-06	6.83E-06	1.28E-05

Lung, Combined (Males, 25-34 years, Light Exertion)

Diameter	5%	10%	25%	50%	75%	90%	95%
0.1	7.56E-05	9.55E-05	1.35E-04	1.90E-04	2.69E-04	3.66E-04	4.37E-04
0.2	4.34E-05	5.38E-05	7.70E-05	1.08E-04	1.52E-04	2.06E-04	2.46E-04
0.5	2.71E-05	3.53E-05	5.06E-05	7.38E-05	1.04E-04	1.45E-04	1.73E-04
0.8	3.30E-05	4.38E-05	6.28E-05	9.29E-05	1.37E-04	1.97E-04	2.41E-04
1	3.96E-05	5.22E-05	7.49E-05	1.11E-04	1.65E-04	2.42E-04	3.03E-04
2	5.78E-05	7.22E-05	1.10E-04	1.68E-04	2.62E-04	4.28E-04	6.25E-04
5	7.71E-06	1.08E-05	1.83E-05	3.44E-05	6.64E-05	1.45E-04	2.62E-04
8	1.17E-06	1.80E-06	3.35E-06	6.77E-06	1.64E-05	4.09E-05	7.96E-05
10	4.08E-07	6.48E-07	1.37E-06	3.16E-06	8.14E-06	2.33E-05	4.49E-05
20	3.21E-08	5.18E-08	1.31E-07	3.75E-07	1.08E-06	3.26E-06	6.26E-06
50	2.96E-09	4.85E-09	1.26E-08	3.53E-08	1.00E-07	2.69E-07	5.05E-07

Table E-1--cont'd

BB Secretory Cells (Males, 25-34 years, Heavy Exertion)

Diameter	5%	10%	25%	50%	75%	90%	95%
0.1	2.75E-05	3.62E-05	5.32E-05	8.35E-05	1.31E-04	1.92E-04	2.56E-04
0.2	1.87E-05	2.35E-05	3.54E-05	5.56E-05	9.06E-05	1.31E-04	1.75E-04
0.5	3.26E-05	4.23E-05	7.40E-05	1.33E-04	2.37E-04	4.63E-04	6.37E-04
0.8	7.84E-05	1.04E-04	1.86E-04	3.46E-04	6.28E-04	1.26E-03	1.71E-03
1	1.21E-04	1.59E-04	2.91E-04	5.43E-04	9.82E-04	1.96E-03	2.64E-03
2	3.18E-04	4.84E-04	9.05E-04	1.77E-03	3.23E-03	6.38E-03	8.67E-03
5	4.18E-05	7.68E-05	2.04E-04	5.75E-04	1.25E-03	2.40E-03	3.58E-03
8	1.13E-05	2.36E-05	6.19E-05	1.59E-04	3.85E-04	8.42E-04	1.23E-03
10	6.23E-06	1.39E-05	3.67E-05	9.01E-05	2.21E-04	4.92E-04	7.31E-04
20	8.37E-07	1.77E-06	4.64E-06	1.18E-05	2.90E-05	6.48E-05	1.02E-04
50	6.64E-08	1.23E-07	3.13E-07	8.15E-07	1.96E-06	4.46E-06	7.10E-06

BB Basal Cells (Males, 25-34 years, Heavy Exertion)

Diameter	5%	10%	25%	50%	75%	90%	95%
0.1	1.96E-06	3.00E-06	6.85E-06	3.03E-05	8.99E-05	1.66E-04	2.33E-04
0.2	1.34E-06	2.09E-06	4.72E-06	2.03E-05	6.12E-05	1.11E-04	1.53E-04
0.5	2.89E-06	4.53E-06	1.29E-05	5.02E-05	1.44E-04	3.46E-04	5.10E-04
0.8	7.43E-06	1.17E-05	3.37E-05	1.32E-04	3.74E-04	9.10E-04	1.37E-03
1	1.12E-05	1.84E-05	5.24E-05	2.02E-04	5.83E-04	1.40E-03	2.14E-03
2	3.33E-05	5.93E-05	1.73E-04	6.12E-04	1.89E-03	4.47E-03	7.22E-03
5	2.74E-05	6.17E-05	1.53E-04	3.65E-04	8.00E-04	1.91E-03	2.85E-03
8	1.12E-05	2.96E-05	6.92E-05	1.54E-04	3.34E-04	7.09E-04	1.02E-03
10	6.74E-06	1.84E-05	4.04E-05	9.30E-05	1.96E-04	4.15E-04	6.38E-04
20	9.47E-07	2.21E-06	5.33E-06	1.21E-05	2.63E-05	5.71E-05	8.57E-05
50	7.69E-08	1.52E-07	3.63E-07	8.36E-07	1.80E-06	3.92E-06	5.98E-06

bb Secretory Cells (Males, 25-34 years, Heavy Exertion)

Diameter	5%	10%	25%	50%	75%	90%	95%
0.1	1.47E-04	1.81E-04	2.42E-04	3.39E-04	4.87E-04	6.73E-04	8.12E-04
0.2	8.30E-05	1.00E-04	1.35E-04	1.89E-04	2.73E-04	3.76E-04	4.55E-04
0.5	4.42E-05	5.36E-05	7.13E-05	1.00E-04	1.45E-04	1.94E-04	2.34E-04
0.8	4.28E-05	5.20E-05	7.13E-05	1.00E-04	1.41E-04	1.88E-04	2.25E-04
1	5.00E-05	6.00E-05	8.35E-05	1.21E-04	1.72E-04	2.34E-04	2.85E-04
2	9.37E-05	1.28E-04	1.96E-04	3.26E-04	5.04E-04	7.66E-04	9.69E-04
5	7.36E-06	1.33E-05	3.23E-05	7.16E-05	1.38E-04	2.45E-04	3.75E-04
8	3.71E-08	1.57E-07	7.88E-07	3.66E-06	1.12E-05	2.63E-05	4.65E-05
10	1.45E-10	1.92E-09	3.06E-08	3.17E-07	1.56E-06	5.30E-06	9.73E-06
20	0	0	0	0	1.30E-13	3.32E-11	2.50E-10
50	0	0	0	0	0	0	0

Table E-1--cont'd

AI Tissues (Males, 25-34 years, Heavy Exertion)

Diameter	5%	10%	25%	50%	75%	90%	95%
0.1	2.82E-04	3.41E-04	4.43E-04	6.20E-04	8.25E-04	1.04E-03	1.21E-03
0.2	1.55E-04	1.86E-04	2.42E-04	3.38E-04	4.49E-04	5.74E-04	6.69E-04
0.5	1.09E-04	1.34E-04	1.79E-04	2.45E-04	3.31E-04	4.19E-04	4.92E-04
0.8	1.40E-04	1.71E-04	2.39E-04	3.28E-04	4.55E-04	5.84E-04	6.96E-04
1	1.59E-04	1.99E-04	2.84E-04	3.90E-04	5.46E-04	7.08E-04	8.37E-04
2	1.80E-04	2.54E-04	3.97E-04	5.67E-04	7.90E-04	1.06E-03	1.21E-03
5	1.85E-05	3.08E-05	7.73E-05	1.56E-04	2.66E-04	3.99E-04	4.74E-04
8	2.27E-08	1.10E-07	6.52E-07	3.77E-06	1.35E-05	2.98E-05	4.85E-05
10	1.42E-11	1.94E-10	4.87E-09	9.76E-08	7.59E-07	2.70E-06	5.44E-06
20	0	0	0	0	0	4.95E-15	1.67E-13
50	0	0	0	0	0	0	0

LNth Tissues (Males, 25-34 years, Heavy Exertion)

Diameter	5%	10%	25%	50%	75%	90%	95%
0.1	3.55E-04	5.68E-04	1.38E-03	3.09E-03	5.49E-03	7.80E-03	1.02E-02
0.2	1.97E-04	3.15E-04	7.60E-04	1.71E-03	3.07E-03	4.29E-03	5.64E-03
0.5	1.50E-04	2.48E-04	6.04E-04	1.27E-03	2.29E-03	3.36E-03	4.15E-03
0.8	2.18E-04	3.55E-04	8.49E-04	1.84E-03	3.32E-03	4.94E-03	6.30E-03
1	2.82E-04	4.48E-04	1.07E-03	2.31E-03	4.20E-03	6.23E-03	7.83E-03
2	5.52E-04	9.38E-04	2.03E-03	4.25E-03	8.03E-03	1.22E-02	1.46E-02
5	3.65E-04	7.45E-04	1.84E-03	4.05E-03	7.28E-03	1.18E-02	1.46E-02
8	1.40E-04	3.06E-04	7.98E-04	1.73E-03	3.31E-03	5.75E-03	7.06E-03
10	7.54E-05	1.65E-04	4.43E-04	1.00E-03	1.98E-03	3.44E-03	4.32E-03
20	1.00E-05	2.12E-05	5.30E-05	1.23E-04	2.58E-04	4.58E-04	6.12E-04
50	7.67E-07	1.48E-06	3.67E-06	8.42E-06	1.78E-05	3.13E-05	4.21E-05

Lung, Combined (Males, 25-34 years, Heavy Exertion)

Diameter	5%	10%	25%	50%	75%	90%	95%
0.1	1.38E-04	1.71E-04	2.50E-04	3.52E-04	4.82E-04	6.51E-04	7.49E-04
0.2	8.10E-05	9.95E-05	1.42E-04	1.98E-04	2.69E-04	3.64E-04	4.22E-04
0.5	6.40E-05	8.05E-05	1.13E-04	1.63E-04	2.24E-04	3.21E-04	3.81E-04
0.8	8.81E-05	1.08E-04	1.66E-04	2.41E-04	3.65E-04	5.58E-04	7.53E-04
1	1.13E-04	1.38E-04	2.13E-04	3.19E-04	4.94E-04	7.93E-04	1.09E-03
2	1.97E-04	2.88E-04	4.46E-04	7.22E-04	1.17E-03	2.24E-03	3.15E-03
5	2.88E-05	6.36E-05	1.30E-04	2.43E-04	4.33E-04	8.69E-04	1.32E-03
8	4.48E-06	7.86E-06	2.23E-05	5.05E-05	1.24E-04	2.72E-04	4.18E-04
10	1.85E-06	3.30E-06	1.05E-05	2.64E-05	6.81E-05	1.56E-04	2.37E-04
20	1.97E-07	3.73E-07	1.20E-06	3.27E-06	8.77E-06	2.01E-05	3.19E-05
50	1.35E-08	2.84E-08	8.30E-08	2.27E-07	5.90E-07	1.38E-06	2.18E-06

Table E-2. Various fractiles (versus particle diameter in μm) for the equivalent dose per activity exposure, H/A_E (units: Sv per Bq-hr/m^3), for several population groups (specified by age and gender) exposed to $^{239}PuO_2$-laden aerosols at the light exertion level only.

BB Secretory Cells (2 years, Light Exertion)

Diameter	5%	10%	25%	50%	75%	90%	95%
0.1	2.47E-05	3.18E-05	4.78E-05	7.75E-05	1.24E-04	1.87E-04	2.47E-04
0.2	1.52E-05	1.96E-05	2.98E-05	4.78E-05	7.75E-05	1.16E-04	1.54E-04
0.5	1.33E-05	1.74E-05	2.97E-05	5.02E-05	9.03E-05	1.73E-04	2.52E-04
0.8	2.32E-05	3.18E-05	5.53E-05	1.07E-04	2.07E-04	4.22E-04	6.31E-04
1	3.16E-05	4.46E-05	7.86E-05	1.56E-04	3.10E-04	6.37E-04	9.56E-04
2	6.11E-05	9.49E-05	1.79E-04	4.11E-04	9.28E-04	1.97E-03	2.95E-03
5	3.97E-06	8.55E-06	2.45E-05	9.92E-05	2.87E-04	6.49E-04	1.11E-03
8	9.36E-07	1.86E-06	6.24E-06	2.48E-05	8.21E-05	1.90E-04	3.07E-04
10	5.87E-07	1.05E-06	3.63E-06	1.39E-05	4.52E-05	1.16E-04	1.80E-04
20	8.53E-08	1.46E-07	5.08E-07	1.74E-06	5.51E-06	1.52E-05	2.33E-05
50	7.59E-09	1.34E-08	3.92E-08	1.27E-07	3.87E-07	1.03E-06	1.59E-06

BB Basal Cells (2 years, Light Exertion)

Diameter	5%	10%	25%	50%	75%	90%	95%
0.1	1.97E-06	3.00E-06	6.86E-06	2.89E-05	8.26E-05	1.54E-04	2.29E-04
0.2	1.25E-06	1.89E-06	4.35E-06	1.78E-05	5.10E-05	9.60E-05	1.38E-04
0.5	1.16E-06	1.75E-06	4.97E-06	1.94E-05	5.87E-05	1.29E-04	1.91E-04
0.8	2.12E-06	3.51E-06	1.07E-05	4.01E-05	1.20E-04	3.04E-04	4.52E-04
1	3.11E-06	5.18E-06	1.55E-05	5.75E-05	1.80E-04	4.53E-04	6.95E-04
2	6.32E-06	1.17E-05	3.90E-05	1.39E-04	4.77E-04	1.35E-03	2.28E-03
5	2.89E-06	4.78E-06	1.69E-05	6.75E-05	1.88E-04	4.43E-04	7.77E-04
8	1.20E-06	1.94E-06	7.00E-06	2.56E-05	7.16E-05	1.68E-04	2.61E-04
10	7.19E-07	1.16E-06	4.12E-06	1.49E-05	4.20E-05	9.53E-05	1.56E-04
20	1.04E-07	1.68E-07	5.37E-07	1.87E-06	5.20E-06	1.23E-05	1.95E-05
50	9.71E-09	1.62E-08	4.54E-08	1.34E-07	3.65E-07	8.41E-07	1.33E-06

bb Secretory Cells (2 years, Light Exertion)

Diameter	5%	10%	25%	50%	75%	90%	95%
0.1	4.38E-05	5.52E-05	7.75E-05	1.12E-04	1.66E-04	2.31E-04	2.78E-04
0.2	2.39E-05	3.06E-05	4.20E-05	6.09E-05	9.03E-05	1.26E-04	1.52E-04
0.5	1.16E-05	1.46E-05	2.02E-05	2.98E-05	4.51E-05	6.15E-05	7.53E-05
0.8	9.42E-06	1.12E-05	1.64E-05	2.53E-05	3.77E-05	5.45E-05	6.59E-05
1	9.01E-06	1.13E-05	1.69E-05	2.68E-05	4.16E-05	6.29E-05	7.51E-05
2	9.00E-06	1.49E-05	2.85E-05	5.47E-05	1.05E-04	1.70E-04	2.19E-04
5	5.60E-07	1.00E-06	3.09E-06	1.02E-05	2.76E-05	5.25E-05	8.01E-05
8	8.12E-09	2.29E-08	1.26E-07	5.92E-07	2.08E-06	5.77E-06	9.61E-06
10	8.87E-11	6.33E-10	7.85E-09	6.38E-08	3.27E-07	1.25E-06	2.44E-06
20	0	0	0	0	8.60E-13	6.40E-11	3.41E-10
50	0	0	0	0	0	0	0

Table E-2--cont'd

AI Tissues (2 years, Light Exertion)

Diameter	5%	10%	25%	50%	75%	90%	95%
0.1	1.18E-04	1.49E-04	2.08E-04	2.96E-04	4.36E-04	5.80E-04	6.72E-04
0.2	6.48E-05	7.95E-05	1.11E-04	1.58E-04	2.30E-04	3.12E-04	3.58E-04
0.5	4.20E-05	5.32E-05	7.55E-05	1.09E-04	1.56E-04	2.12E-04	2.52E-04
0.8	4.95E-05	6.37E-05	9.18E-05	1.36E-04	2.04E-04	2.77E-04	3.36E-04
1	5.15E-05	6.95E-05	1.02E-04	1.56E-04	2.41E-04	3.36E-04	4.01E-04
2	3.54E-05	5.36E-05	1.02E-04	2.11E-04	3.55E-04	5.15E-04	6.34E-04
5	3.61E-06	5.83E-06	1.56E-05	5.57E-05	1.24E-04	2.23E-04	2.88E-04
8	1.73E-08	5.33E-08	3.08E-07	1.66E-06	7.87E-06	2.08E-05	3.53E-05
10	4.96E-11	3.02E-10	4.95E-09	7.23E-08	6.83E-07	2.59E-06	5.31E-06
20	0	0	0	0	2.34E-16	3.14E-13	5.48E-12
50	0	0	0	0	0	0	0

LNth Tissues (2 years, Light Exertion)

Diameter	5%	10%	25%	50%	75%	90%	95%
0.1	2.79E-04	4.28E-04	1.01E-03	2.32E-03	4.50E-03	7.05E-03	9.15E-03
0.2	1.54E-04	2.36E-04	5.55E-04	1.27E-03	2.44E-03	3.82E-03	5.00E-03
0.5	1.03E-04	1.52E-04	3.74E-04	8.52E-04	1.63E-03	2.65E-03	3.47E-03
0.8	1.15E-04	2.03E-04	4.66E-04	1.04E-03	2.13E-03	3.61E-03	4.75E-03
1	1.35E-04	2.41E-04	5.71E-04	1.28E-03	2.56E-03	4.53E-03	5.99E-03
2	2.05E-04	3.53E-04	8.24E-04	2.23E-03	5.01E-03	9.80E-03	1.30E-02
5	9.22E-05	1.69E-04	5.35E-04	1.97E-03	5.11E-03	1.02E-02	1.31E-02
8	3.00E-05	5.69E-05	1.99E-04	7.67E-04	2.10E-03	4.39E-03	5.75E-03
10	1.64E-05	3.06E-05	1.09E-04	4.16E-04	1.15E-03	2.42E-03	3.31E-03
20	2.29E-06	4.25E-06	1.35E-05	5.01E-05	1.38E-04	3.03E-04	4.26E-04
50	2.11E-07	3.90E-07	1.07E-06	3.60E-06	9.72E-06	2.08E-05	2.88E-05

Lung, Combined (2 years, Light Exertion)

Diameter	5%	10%	25%	50%	75%	90%	95%
0.1	6.41E-05	8.19E-05	1.16E-04	1.65E-04	2.36E-04	3.23E-04	3.78E-04
0.2	3.58E-05	4.59E-05	6.43E-05	9.15E-05	1.30E-04	1.76E-04	2.06E-04
0.5	2.23E-05	2.85E-05	4.25E-05	6.40E-05	9.33E-05	1.39E-04	1.63E-04
0.8	2.65E-05	3.40E-05	5.36E-05	8.64E-05	1.36E-04	2.24E-04	2.94E-04
1	3.02E-05	4.00E-05	6.37E-05	1.04E-04	1.78E-04	3.05E-04	4.10E-04
2	3.23E-05	5.07E-05	9.57E-05	2.00E-04	3.89E-04	7.56E-04	1.03E-03
5	3.38E-06	6.23E-06	1.74E-05	6.19E-05	1.48E-04	2.60E-04	3.81E-04
8	4.29E-07	8.19E-07	2.90E-06	1.17E-05	3.13E-05	6.89E-05	1.15E-04
10	1.82E-07	3.51E-07	1.27E-06	5.05E-06	1.55E-05	3.68E-05	6.56E-05
20	2.21E-08	3.88E-08	1.54E-07	5.89E-07	1.80E-06	4.56E-06	7.96E-06
50	2.10E-09	3.58E-09	1.23E-08	4.16E-08	1.23E-07	3.19E-07	5.38E-07

Table E-2--cont'd

BB Secretory Cells (5 years, Light Exertion)

Diameter	5%	10%	25%	50%	75%	90%	95%
0.1	1.93E-05	2.49E-05	3.79E-05	6.13E-05	9.77E-05	1.45E-04	1.90E-04
0.2	1.19E-05	1.55E-05	2.34E-05	3.77E-05	6.04E-05	8.91E-05	1.18E-04
0.5	1.06E-05	1.35E-05	2.34E-05	3.96E-05	6.94E-05	1.29E-04	1.84E-04
0.8	1.84E-05	2.37E-05	4.35E-05	8.10E-05	1.57E-04	2.95E-04	4.51E-04
1	2.58E-05	3.43E-05	6.16E-05	1.21E-04	2.37E-04	4.42E-04	7.04E-04
2	5.09E-05	8.00E-05	1.45E-04	3.07E-04	6.66E-04	1.38E-03	2.24E-03
5	3.46E-06	6.97E-06	1.88E-05	6.68E-05	2.24E-04	5.42E-04	9.27E-04
8	9.82E-07	1.68E-06	5.14E-06	2.18E-05	6.73E-05	1.94E-04	3.27E-04
10	5.55E-07	9.90E-07	3.17E-06	1.26E-05	4.12E-05	1.12E-04	2.06E-04
20	8.51E-08	1.58E-07	4.90E-07	1.70E-06	5.86E-06	1.57E-05	2.81E-05
50	8.36E-09	1.50E-08	4.17E-08	1.34E-07	4.27E-07	1.09E-06	1.93E-06

BB Basal Cells (5 years, Light Exertion)

Diameter	5%	10%	25%	50%	75%	90%	95%
0.1	1.53E-06	2.32E-06	5.33E-06	2.24E-05	6.49E-05	1.21E-04	1.80E-04
0.2	9.82E-07	1.45E-06	3.33E-06	1.39E-05	4.05E-05	7.49E-05	1.11E-04
0.5	8.96E-07	1.37E-06	3.82E-06	1.48E-05	4.44E-05	9.49E-05	1.49E-04
0.8	1.68E-06	2.76E-06	8.28E-06	2.98E-05	9.14E-05	2.14E-04	3.38E-04
1	2.36E-06	4.01E-06	1.17E-05	4.30E-05	1.33E-04	3.23E-04	5.11E-04
2	5.66E-06	9.21E-06	3.01E-05	1.11E-04	3.59E-04	9.57E-04	1.58E-03
5	2.78E-06	4.42E-06	1.29E-05	4.82E-05	1.51E-04	3.64E-04	6.89E-04
8	1.13E-06	1.89E-06	5.21E-06	2.06E-05	6.51E-05	1.60E-04	2.67E-04
10	7.44E-07	1.21E-06	3.31E-06	1.28E-05	4.09E-05	1.05E-04	1.67E-04
20	1.18E-07	1.95E-07	5.18E-07	1.77E-06	5.60E-06	1.45E-05	2.32E-05
50	1.11E-08	1.84E-08	4.72E-08	1.38E-07	4.04E-07	1.04E-06	1.64E-06

bb Secretory Cells (5 years, Light Exertion)

Diameter	5%	10%	25%	50%	75%	90%	95%
0.1	4.90E-05	6.29E-05	8.65E-05	1.22E-04	1.82E-04	2.57E-04	3.03E-04
0.2	2.71E-05	3.45E-05	4.73E-05	6.73E-05	9.95E-05	1.42E-04	1.68E-04
0.5	1.33E-05	1.69E-05	2.34E-05	3.38E-05	5.02E-05	6.92E-05	8.29E-05
0.8	1.13E-05	1.37E-05	2.01E-05	2.94E-05	4.41E-05	6.15E-05	7.30E-05
1	1.14E-05	1.41E-05	2.11E-05	3.16E-05	4.88E-05	7.16E-05	8.40E-05
2	1.38E-05	1.91E-05	3.47E-05	6.38E-05	1.17E-04	1.98E-04	2.56E-04
5	9.55E-07	1.54E-06	4.16E-06	1.30E-05	3.82E-05	7.38E-05	1.04E-04
8	3.03E-08	7.15E-08	3.14E-07	1.18E-06	4.06E-06	9.97E-06	1.73E-05
10	1.04E-09	4.37E-09	3.40E-08	1.91E-07	8.47E-07	2.73E-06	5.95E-06
20	0	0	0	2.31E-13	2.90E-11	8.56E-10	3.03E-09
50	0	0	0	0	0	0	0

Table E-2--cont'd

AI Tissues (5 years, Light Exertion)

Diameter	5%	10%	25%	50%	75%	90%	95%
0.1	1.30E-04	1.60E-04	2.18E-04	3.12E-04	4.46E-04	5.89E-04	6.96E-04
0.2	6.98E-05	8.69E-05	1.17E-04	1.66E-04	2.38E-04	3.20E-04	3.75E-04
0.5	4.84E-05	6.07E-05	8.24E-05	1.18E-04	1.64E-04	2.25E-04	2.65E-04
0.8	5.81E-05	7.40E-05	1.02E-04	1.49E-04	2.15E-04	3.01E-04	3.59E-04
1	6.19E-05	8.05E-05	1.14E-04	1.71E-04	2.56E-04	3.56E-04	4.33E-04
2	4.80E-05	6.54E-05	1.12E-04	2.14E-04	3.68E-04	5.62E-04	7.07E-04
5	5.09E-06	7.64E-06	1.82E-05	6.16E-05	1.60E-04	2.91E-04	3.88E-04
8	6.21E-08	1.62E-07	6.92E-07	2.81E-06	1.36E-05	3.39E-05	5.90E-05
10	4.06E-10	1.79E-09	2.15E-08	2.02E-07	1.58E-06	5.36E-06	1.01E-05
20	0	0	0	0	2.53E-14	5.24E-12	5.46E-11
50	0	0	0	0	0	0	0

LNth Tissues (5 years, Light Exertion)

Diameter	5%	10%	25%	50%	75%	90%	95%
0.1	2.52E-04	3.89E-04	9.50E-04	2.22E-03	4.32E-03	6.80E-03	8.97E-03
0.2	1.37E-04	2.17E-04	5.18E-04	1.20E-03	2.38E-03	3.70E-03	4.87E-03
0.5	8.86E-05	1.46E-04	3.53E-04	8.08E-04	1.59E-03	2.54E-03	3.43E-03
0.8	1.10E-04	1.78E-04	4.48E-04	9.88E-04	2.08E-03	3.38E-03	4.62E-03
1	1.27E-04	2.14E-04	5.42E-04	1.16E-03	2.44E-03	4.26E-03	5.71E-03
2	1.93E-04	3.32E-04	7.72E-04	1.91E-03	4.16E-03	8.73E-03	1.12E-02
5	7.89E-05	1.47E-04	3.79E-04	1.26E-03	4.30E-03	9.64E-03	1.27E-02
8	3.00E-05	4.94E-05	1.38E-04	5.10E-04	1.93E-03	4.20E-03	5.95E-03
10	1.69E-05	2.59E-05	7.64E-05	2.88E-04	1.08E-03	2.46E-03	3.51E-03
20	2.24E-06	3.78E-06	1.05E-05	3.73E-05	1.36E-04	3.12E-04	4.65E-04
50	2.03E-07	3.47E-07	9.49E-07	2.91E-06	9.52E-06	2.10E-05	3.20E-05

Lung, Combined (5 years, Light Exertion)

Diameter	5%	10%	25%	50%	75%	90%	95%
0.1	6.31E-05	8.37E-05	1.17E-04	1.68E-04	2.39E-04	3.27E-04	3.91E-04
0.2	3.54E-05	4.64E-05	6.57E-05	9.23E-05	1.30E-04	1.80E-04	2.12E-04
0.5	2.27E-05	2.96E-05	4.31E-05	6.53E-05	9.44E-05	1.34E-04	1.62E-04
0.8	2.86E-05	3.45E-05	5.44E-05	8.65E-05	1.32E-04	2.10E-04	2.55E-04
1	3.37E-05	4.21E-05	6.59E-05	1.04E-04	1.68E-04	2.69E-04	3.47E-04
2	4.01E-05	5.60E-05	9.77E-05	1.85E-04	3.38E-04	6.26E-04	8.33E-04
5	4.66E-06	7.44E-06	1.62E-05	5.47E-05	1.46E-04	2.85E-04	3.84E-04
8	5.91E-07	9.44E-07	2.65E-06	1.05E-05	3.14E-05	7.53E-05	1.25E-04
10	2.16E-07	3.93E-07	1.16E-06	4.70E-06	1.56E-05	4.08E-05	6.93E-05
20	2.22E-08	4.54E-08	1.33E-07	5.11E-07	1.81E-06	5.43E-06	9.27E-06
50	2.13E-09	4.09E-09	1.25E-08	3.99E-08	1.29E-07	3.74E-07	6.32E-07

Table E-2--cont'd

BB Secretory Cells (10 years, Light Exertion)

Diameter	5%	10%	25%	50%	75%	90%	95%
0.1	1.68E-05	2.20E-05	3.34E-05	5.31E-05	8.56E-05	1.26E-04	1.66E-04
0.2	1.04E-05	1.37E-05	2.07E-05	3.31E-05	5.33E-05	7.83E-05	1.04E-04
0.5	9.21E-06	1.18E-05	1.98E-05	3.37E-05	5.94E-05	1.13E-04	1.56E-04
0.8	1.54E-05	2.12E-05	3.70E-05	6.93E-05	1.32E-04	2.58E-04	3.81E-04
1	2.22E-05	3.02E-05	5.40E-05	1.00E-04	1.91E-04	3.71E-04	5.75E-04
2	4.95E-05	7.25E-05	1.22E-04	2.39E-04	5.13E-04	1.04E-03	1.66E-03
5	3.75E-06	6.08E-06	1.53E-05	4.32E-05	1.38E-04	3.79E-04	7.20E-04
8	1.19E-06	1.71E-06	4.35E-06	1.23E-05	4.37E-05	1.45E-04	2.82E-04
10	7.33E-07	1.10E-06	2.60E-06	7.78E-06	2.77E-05	8.90E-05	1.73E-04
20	1.14E-07	1.77E-07	4.10E-07	1.25E-06	4.47E-06	1.32E-05	2.71E-05
50	1.10E-08	1.71E-08	3.91E-08	1.17E-07	3.70E-07	9.33E-07	1.81E-06

BB Basal Cells (10 years, Light Exertion)

Diameter	5%	10%	25%	50%	75%	90%	95%
0.1	1.34E-06	2.03E-06	4.59E-06	1.95E-05	5.68E-05	1.05E-04	1.57E-04
0.2	8.33E-07	1.26E-06	2.89E-06	1.22E-05	3.49E-05	6.55E-05	9.58E-05
0.5	7.59E-07	1.18E-06	3.28E-06	1.26E-05	3.77E-05	8.15E-05	1.27E-04
0.8	1.44E-06	2.35E-06	7.10E-06	2.59E-05	7.59E-05	1.83E-04	2.91E-04
1	2.02E-06	3.41E-06	1.05E-05	3.64E-05	1.08E-04	2.73E-04	4.22E-04
2	4.50E-06	8.13E-06	2.58E-05	8.76E-05	2.75E-04	7.32E-04	1.16E-03
5	3.00E-06	4.71E-06	1.05E-05	2.84E-05	9.54E-05	2.48E-04	4.53E-04
8	1.40E-06	2.07E-06	4.30E-06	1.20E-05	4.41E-05	1.16E-04	2.08E-04
10	9.56E-07	1.33E-06	2.84E-06	7.69E-06	2.87E-05	7.63E-05	1.37E-04
20	1.51E-07	2.16E-07	4.66E-07	1.25E-06	4.21E-06	1.15E-05	2.12E-05
50	1.45E-08	2.08E-08	4.38E-08	1.13E-07	3.44E-07	8.71E-07	1.51E-06

bb Secretory Cells (10 years, Light Exertion)

Diameter	5%	10%	25%	50%	75%	90%	95%
0.1	5.97E-05	7.62E-05	1.05E-04	1.49E-04	2.20E-04	3.12E-04	3.72E-04
0.2	3.29E-05	4.21E-05	5.78E-05	8.19E-05	1.22E-04	1.71E-04	2.03E-04
0.5	1.66E-05	2.14E-05	2.94E-05	4.19E-05	6.23E-05	8.55E-05	1.01E-04
0.8	1.45E-05	1.81E-05	2.56E-05	3.75E-05	5.53E-05	7.50E-05	8.96E-05
1	1.52E-05	1.89E-05	2.72E-05	4.08E-05	6.25E-05	8.68E-05	1.06E-04
2	2.02E-05	2.58E-05	4.42E-05	7.58E-05	1.34E-04	2.20E-04	2.87E-04
5	1.51E-06	2.33E-06	5.02E-06	1.23E-05	3.25E-05	8.29E-05	1.18E-04
8	8.28E-08	1.69E-07	4.40E-07	1.42E-06	4.51E-06	1.23E-05	2.18E-05
10	5.08E-09	1.62E-08	7.55E-08	3.09E-07	1.17E-06	3.59E-06	6.89E-06
20	0	0	0	3.82E-12	2.06E-10	3.26E-09	1.10E-08
50	0	0	0	0	0	0	0

Table E-2--cont'd

AI Tissues (10 years, Light Exertion)

Diameter	5%	10%	25%	50%	75%	90%	95%
0.1	1.49E-04	1.84E-04	2.50E-04	3.56E-04	5.22E-04	6.91E-04	8.12E-04
0.2	8.13E-05	9.92E-05	1.35E-04	1.93E-04	2.81E-04	3.73E-04	4.45E-04
0.5	5.60E-05	6.86E-05	9.43E-05	1.39E-04	1.95E-04	2.61E-04	3.13E-04
0.8	6.68E-05	8.73E-05	1.22E-04	1.77E-04	2.55E-04	3.61E-04	4.22E-04
1	7.41E-05	9.90E-05	1.39E-04	2.02E-04	2.96E-04	4.26E-04	4.94E-04
2	6.69E-05	8.85E-05	1.40E-04	2.25E-04	3.90E-04	6.09E-04	7.46E-04
5	8.98E-06	1.24E-05	2.42E-05	5.34E-05	1.45E-04	3.04E-04	4.51E-04
8	2.16E-07	4.28E-07	1.34E-06	4.30E-06	1.40E-05	4.36E-05	7.46E-05
10	3.52E-09	1.27E-08	7.45E-08	4.69E-07	2.15E-06	8.11E-06	1.51E-05
20	0	0	0	7.95E-16	1.15E-12	8.00E-11	5.98E-10
50	0	0	0	0	0	0	0

LNth Tissues (10 years, Light Exertion)

Diameter	5%	10%	25%	50%	75%	90%	95%
0.1	2.63E-04	4.19E-04	1.02E-03	2.49E-03	4.80E-03	7.70E-03	1.03E-02
0.2	1.44E-04	2.31E-04	5.64E-04	1.35E-03	2.62E-03	4.19E-03	5.52E-03
0.5	9.35E-05	1.53E-04	3.86E-04	8.90E-04	1.81E-03	2.89E-03	3.88E-03
0.8	1.15E-04	1.93E-04	4.90E-04	1.15E-03	2.31E-03	3.85E-03	5.08E-03
1	1.34E-04	2.26E-04	5.63E-04	1.33E-03	2.75E-03	4.44E-03	6.24E-03
2	2.05E-04	3.24E-04	8.19E-04	1.92E-03	3.93E-03	7.50E-03	1.11E-02
5	9.29E-05	1.67E-04	3.74E-04	1.04E-03	2.88E-03	7.95E-03	1.23E-02
8	3.41E-05	5.86E-05	1.36E-04	3.70E-04	1.21E-03	3.63E-03	6.29E-03
10	1.94E-05	3.14E-05	7.40E-05	2.05E-04	6.98E-04	2.12E-03	3.57E-03
20	2.41E-06	4.44E-06	1.04E-05	2.88E-05	9.32E-05	2.90E-04	4.64E-04
50	2.30E-07	4.25E-07	9.84E-07	2.62E-06	7.46E-06	2.03E-05	3.26E-05

Lung, Combined (10 years, Light Exertion)

Diameter	5%	10%	25%	50%	75%	90%	95%
0.1	6.96E-05	9.50E-05	1.31E-04	1.91E-04	2.73E-04	3.80E-04	4.60E-04
0.2	3.88E-05	5.31E-05	7.32E-05	1.05E-04	1.51E-04	2.09E-04	2.53E-04
0.5	2.56E-05	3.28E-05	4.82E-05	7.33E-05	1.04E-04	1.49E-04	1.82E-04
0.8	3.07E-05	3.85E-05	6.05E-05	9.64E-05	1.45E-04	2.10E-04	2.67E-04
1	3.77E-05	4.64E-05	7.30E-05	1.14E-04	1.75E-04	2.66E-04	3.43E-04
2	5.10E-05	6.59E-05	1.06E-04	1.78E-04	3.03E-04	5.46E-04	7.44E-04
5	6.67E-06	9.78E-06	1.77E-05	3.84E-05	1.05E-04	2.48E-04	3.67E-04
8	9.31E-07	1.44E-06	3.01E-06	7.35E-06	2.36E-05	6.18E-05	1.06E-04
10	3.06E-07	5.29E-07	1.18E-06	3.38E-06	1.10E-05	3.10E-05	5.68E-05
20	2.88E-08	5.06E-08	1.23E-07	4.05E-07	1.40E-06	4.06E-06	7.94E-06
50	2.69E-09	4.88E-09	1.16E-08	3.67E-08	1.12E-07	3.03E-07	5.42E-07

Table E-2--cont'd

BB Secretory Cells (Females, 15 years, Light Exertion)

Diameter	5%	10%	25%	50%	75%	90%	95%
0.1	1.55E-05	2.07E-05	3.04E-05	4.86E-05	7.79E-05	1.15E-04	1.53E-04
0.2	9.65E-06	1.27E-05	1.89E-05	3.04E-05	4.87E-05	7.20E-05	9.50E-05
0.5	7.79E-06	9.74E-06	1.61E-05	2.63E-05	4.56E-05	8.37E-05	1.15E-04
0.8	1.18E-05	1.60E-05	2.73E-05	5.06E-05	9.33E-05	1.86E-04	2.65E-04
1	1.65E-05	2.25E-05	3.91E-05	7.32E-05	1.37E-04	2.72E-04	3.99E-04
2	3.98E-05	5.66E-05	9.54E-05	1.80E-04	3.51E-04	7.13E-04	9.86E-04
5	3.56E-06	5.45E-06	1.38E-05	3.30E-05	8.22E-05	2.00E-04	3.13E-04
8	1.25E-06	1.75E-06	3.65E-06	9.74E-06	2.92E-05	7.43E-05	1.37E-04
10	7.96E-07	1.17E-06	2.38E-06	6.33E-06	1.88E-05	4.78E-05	8.86E-05
20	1.33E-07	2.00E-07	4.28E-07	1.05E-06	3.14E-06	8.45E-06	1.43E-05
50	1.29E-08	1.91E-08	4.05E-08	1.01E-07	2.94E-07	7.71E-07	1.16E-06

BB Basal Cells (Females, 15 years, Light Exertion)

Diameter	5%	10%	25%	50%	75%	90%	95%
0.1	1.23E-06	1.87E-06	4.23E-06	1.80E-05	5.20E-05	9.54E-05	1.44E-04
0.2	7.68E-07	1.17E-06	2.64E-06	1.12E-05	3.22E-05	5.94E-05	8.90E-05
0.5	6.16E-07	9.33E-07	2.43E-06	9.64E-06	3.00E-05	6.24E-05	9.40E-05
0.8	1.07E-06	1.70E-06	5.04E-06	1.89E-05	5.36E-05	1.35E-04	2.14E-04
1	1.52E-06	2.46E-06	7.46E-06	2.71E-05	7.73E-05	1.98E-04	3.19E-04
2	3.67E-06	6.28E-06	1.86E-05	6.80E-05	1.91E-04	4.96E-04	8.25E-04
5	2.77E-06	4.20E-06	8.59E-06	2.20E-05	5.85E-05	1.40E-04	2.36E-04
8	1.53E-06	2.07E-06	3.91E-06	9.45E-06	2.50E-05	6.51E-05	1.05E-04
10	1.02E-06	1.38E-06	2.75E-06	6.26E-06	1.69E-05	4.31E-05	6.89E-05
20	1.70E-07	2.53E-07	4.84E-07	1.11E-06	2.89E-06	7.39E-06	1.23E-05
50	1.60E-08	2.45E-08	4.66E-08	1.07E-07	2.68E-07	6.72E-07	9.84E-07

bb Secretory Cells (Females, 15 years, Light Exertion)

Diameter	5%	10%	25%	50%	75%	90%	95%
0.1	6.59E-05	8.21E-05	1.13E-04	1.62E-04	2.37E-04	3.37E-04	4.03E-04
0.2	3.68E-05	4.58E-05	6.30E-05	8.98E-05	1.32E-04	1.87E-04	2.26E-04
0.5	1.87E-05	2.35E-05	3.23E-05	4.66E-05	6.83E-05	9.42E-05	1.11E-04
0.8	1.70E-05	2.10E-05	2.83E-05	4.25E-05	6.09E-05	8.18E-05	9.79E-05
1	1.76E-05	2.27E-05	3.12E-05	4.65E-05	6.84E-05	9.31E-05	1.10E-04
2	2.55E-05	3.16E-05	4.74E-05	7.90E-05	1.27E-04	2.01E-04	2.63E-04
5	2.22E-06	3.16E-06	5.97E-06	1.20E-05	2.55E-05	5.78E-05	9.40E-05
8	1.75E-07	3.48E-07	7.01E-07	1.76E-06	4.10E-06	1.03E-05	2.07E-05
10	1.93E-08	5.26E-08	1.58E-07	5.13E-07	1.28E-06	3.92E-06	6.89E-06
20	0	0	4.96E-13	5.84E-11	1.29E-09	1.19E-08	2.88E-08
50	0	0	0	0	0	0	0

Table E-2--cont'd

AI Tissues (Females, 15 years, Light Exertion)

Diameter	5%	10%	25%	50%	75%	90%	95%
0.1	1.20E-04	1.49E-04	2.06E-04	2.95E-04	4.35E-04	5.79E-04	6.81E-04
0.2	6.56E-05	8.15E-05	1.12E-04	1.60E-04	2.37E-04	3.16E-04	3.81E-04
0.5	4.57E-05	5.72E-05	8.02E-05	1.18E-04	1.69E-04	2.25E-04	2.68E-04
0.8	5.94E-05	7.40E-05	1.05E-04	1.54E-04	2.19E-04	3.06E-04	3.65E-04
1	6.73E-05	8.74E-05	1.22E-04	1.78E-04	2.57E-04	3.62E-04	4.30E-04
2	7.05E-05	8.92E-05	1.33E-04	2.01E-04	3.08E-04	4.51E-04	5.85E-04
5	1.15E-05	1.66E-05	2.79E-05	5.21E-05	9.68E-05	1.94E-04	2.92E-04
8	5.37E-07	1.01E-06	2.60E-06	6.16E-06	1.42E-05	3.12E-05	5.30E-05
10	3.24E-08	6.77E-08	2.77E-07	1.01E-06	2.95E-06	7.89E-06	1.42E-05
20	0	0	2.09E-16	4.79E-13	5.07E-11	1.14E-09	4.93E-09
50	0	0	0	0	0	0	0

LNth Tissues (Females, 15 years, Light Exertion)

Diameter	5%	10%	25%	50%	75%	90%	95%
0.1	2.13E-04	3.40E-04	8.32E-04	2.04E-03	3.93E-03	6.37E-03	8.50E-03
0.2	1.18E-04	1.87E-04	4.65E-04	1.12E-03	2.16E-03	3.48E-03	4.64E-03
0.5	7.53E-05	1.25E-04	3.14E-04	7.46E-04	1.50E-03	2.43E-03	3.27E-03
0.8	9.34E-05	1.52E-04	4.03E-04	9.57E-04	1.94E-03	3.12E-03	4.32E-03
1	1.13E-04	1.83E-04	4.68E-04	1.13E-03	2.26E-03	3.63E-03	5.19E-03
2	1.64E-04	2.68E-04	6.77E-04	1.54E-03	3.11E-03	5.22E-03	7.31E-03
5	8.35E-05	1.35E-04	3.16E-04	7.08E-04	1.58E-03	3.37E-03	6.10E-03
8	3.32E-05	5.33E-05	1.17E-04	2.58E-04	6.00E-04	1.50E-03	3.20E-03
10	1.79E-05	2.95E-05	6.61E-05	1.45E-04	3.40E-04	8.78E-04	1.95E-03
20	2.43E-06	4.21E-06	9.24E-06	2.07E-05	4.76E-05	1.26E-04	2.49E-04
50	2.34E-07	4.10E-07	8.70E-07	1.97E-06	4.49E-06	1.09E-05	1.96E-05

Lung, Combined (Females, 15 years, Light Exertion)

Diameter	5%	10%	25%	50%	75%	90%	95%
0.1	6.66E-05	8.58E-05	1.21E-04	1.73E-04	2.47E-04	3.38E-04	4.15E-04
0.2	3.75E-05	4.80E-05	6.82E-05	9.62E-05	1.38E-04	1.86E-04	2.28E-04
0.5	2.32E-05	3.06E-05	4.36E-05	6.56E-05	9.32E-05	1.31E-04	1.58E-04
0.8	2.81E-05	3.70E-05	5.44E-05	8.38E-05	1.23E-04	1.80E-04	2.19E-04
1	3.37E-05	4.41E-05	6.50E-05	9.97E-05	1.48E-04	2.21E-04	2.77E-04
2	5.27E-05	6.38E-05	9.78E-05	1.52E-04	2.41E-04	3.77E-04	5.47E-04
5	7.30E-06	1.09E-05	1.83E-05	3.41E-05	6.72E-05	1.40E-04	2.56E-04
8	1.19E-06	1.81E-06	3.50E-06	6.92E-06	1.56E-05	3.83E-05	7.32E-05
10	4.29E-07	6.59E-07	1.38E-06	2.99E-06	7.74E-06	2.01E-05	3.55E-05
20	3.07E-08	5.34E-08	1.24E-07	3.38E-07	9.43E-07	2.58E-06	5.09E-06
50	2.92E-09	5.05E-09	1.18E-08	3.20E-08	8.72E-08	2.27E-07	4.16E-07

Table E-2--cont'd

BB Secretory Cells (Females, 18-24 years, Light Exertion)

Diameter	5%	10%	25%	50%	75%	90%	95%
0.1	1.53E-05	2.09E-05	3.04E-05	4.89E-05	7.94E-05	1.18E-04	1.55E-04
0.2	9.63E-06	1.29E-05	1.91E-05	3.06E-05	4.98E-05	7.39E-05	9.77E-05
0.5	7.44E-06	9.48E-06	1.58E-05	2.54E-05	4.51E-05	7.96E-05	1.07E-04
0.8	1.10E-05	1.49E-05	2.61E-05	4.73E-05	8.71E-05	1.76E-04	2.49E-04
1	1.53E-05	2.06E-05	3.64E-05	6.95E-05	1.29E-04	2.52E-04	3.66E-04
2	3.64E-05	5.26E-05	9.04E-05	1.69E-04	3.29E-04	6.55E-04	9.14E-04
5	3.50E-06	5.26E-06	1.33E-05	3.16E-05	8.05E-05	2.00E-04	2.96E-04
8	1.24E-06	1.72E-06	3.66E-06	9.68E-06	2.90E-05	7.35E-05	1.39E-04
10	8.11E-07	1.16E-06	2.44E-06	6.48E-06	1.93E-05	4.92E-05	9.10E-05
20	1.34E-07	2.02E-07	4.29E-07	1.09E-06	3.33E-06	8.66E-06	1.53E-05
50	1.31E-08	1.93E-08	4.15E-08	1.05E-07	3.03E-07	7.84E-07	1.22E-06

BB Basal Cells (Females, 18-24 years, Light Exertion)

Diameter	5%	10%	25%	50%	75%	90%	95%
0.1	1.19E-06	1.85E-06	4.24E-06	1.78E-05	5.39E-05	9.67E-05	1.43E-04
0.2	7.65E-07	1.18E-06	2.67E-06	1.12E-05	3.34E-05	6.09E-05	9.01E-05
0.5	5.86E-07	9.02E-07	2.33E-06	9.33E-06	2.89E-05	5.99E-05	8.86E-05
0.8	9.87E-07	1.61E-06	4.59E-06	1.78E-05	5.04E-05	1.25E-04	1.97E-04
1	1.40E-06	2.32E-06	6.73E-06	2.60E-05	7.34E-05	1.80E-04	2.93E-04
2	3.45E-06	5.94E-06	1.68E-05	6.46E-05	1.88E-04	4.60E-04	7.68E-04
5	2.69E-06	3.92E-06	8.27E-06	2.11E-05	5.64E-05	1.37E-04	2.21E-04
8	1.52E-06	2.08E-06	3.98E-06	9.43E-06	2.49E-05	6.48E-05	1.04E-04
10	1.03E-06	1.38E-06	2.79E-06	6.32E-06	1.72E-05	4.23E-05	7.57E-05
20	1.71E-07	2.57E-07	4.94E-07	1.14E-06	3.05E-06	7.60E-06	1.28E-05
50	1.64E-08	2.49E-08	4.80E-08	1.09E-07	2.81E-07	7.01E-07	1.05E-06

bb Secretory Cells (Females, 18-24 years, Light Exertion)

Diameter	5%	10%	25%	50%	75%	90%	95%
0.1	6.64E-05	8.29E-05	1.16E-04	1.66E-04	2.46E-04	3.45E-04	4.17E-04
0.2	3.79E-05	4.70E-05	6.52E-05	9.31E-05	1.39E-04	1.94E-04	2.35E-04
0.5	1.99E-05	2.44E-05	3.40E-05	4.91E-05	7.16E-05	9.86E-05	1.20E-04
0.8	1.83E-05	2.21E-05	3.03E-05	4.49E-05	6.42E-05	8.62E-05	1.05E-04
1	1.87E-05	2.41E-05	3.31E-05	5.02E-05	7.17E-05	9.65E-05	1.18E-04
2	2.64E-05	3.28E-05	4.84E-05	8.06E-05	1.30E-04	1.96E-04	2.63E-04
5	2.30E-06	3.44E-06	6.20E-06	1.23E-05	2.57E-05	5.80E-05	8.95E-05
8	1.88E-07	3.77E-07	7.72E-07	1.90E-06	4.36E-06	1.11E-05	2.14E-05
10	2.19E-08	6.21E-08	1.80E-07	5.71E-07	1.43E-06	4.27E-06	7.29E-06
20	0	0	8.98E-13	9.87E-11	1.99E-09	1.65E-08	3.63E-08
50	0	0	0	0	0	0	0

Table E-2--cont'd

AI Tissues (Females, 18-24 years, Light Exertion)

Diameter	5%	10%	25%	50%	75%	90%	95%
0.1	1.12E-04	1.41E-04	1.97E-04	2.95E-04	4.41E-04	5.93E-04	6.79E-04
0.2	6.24E-05	7.69E-05	1.08E-04	1.63E-04	2.44E-04	3.28E-04	3.78E-04
0.5	4.47E-05	5.53E-05	7.90E-05	1.19E-04	1.73E-04	2.39E-04	2.85E-04
0.8	5.86E-05	7.19E-05	1.07E-04	1.56E-04	2.27E-04	3.12E-04	3.83E-04
1	6.62E-05	8.39E-05	1.23E-04	1.78E-04	2.61E-04	3.66E-04	4.39E-04
2	7.19E-05	8.91E-05	1.35E-04	2.03E-04	3.12E-04	4.50E-04	5.70E-04
5	1.20E-05	1.66E-05	2.78E-05	5.11E-05	9.23E-05	1.94E-04	2.91E-04
8	5.40E-07	1.06E-06	2.63E-06	6.18E-06	1.38E-05	3.17E-05	5.53E-05
10	3.35E-08	8.08E-08	3.08E-07	1.09E-06	3.18E-06	7.82E-06	1.49E-05
20	0	0	1.41E-15	1.14E-12	8.60E-11	1.70E-09	6.04E-09
50	0	0	0	0	0	0	0

LNth Tissues (Females, 18-24 years, Light Exertion)

Diameter	5%	10%	25%	50%	75%	90%	95%
0.1	1.86E-04	3.05E-04	7.31E-04	1.63E-03	2.87E-03	4.49E-03	5.87E-03
0.2	1.03E-04	1.71E-04	4.05E-04	9.13E-04	1.60E-03	2.48E-03	3.29E-03
0.5	7.10E-05	1.09E-04	2.88E-04	6.22E-04	1.10E-03	1.81E-03	2.32E-03
0.8	8.67E-05	1.37E-04	3.65E-04	7.63E-04	1.45E-03	2.26E-03	3.03E-03
1	1.03E-04	1.62E-04	4.33E-04	8.98E-04	1.69E-03	2.66E-03	3.57E-03
2	1.42E-04	2.36E-04	5.78E-04	1.19E-03	2.29E-03	3.68E-03	5.22E-03
5	7.09E-05	1.12E-04	2.49E-04	5.25E-04	1.08E-03	2.38E-03	4.18E-03
8	2.73E-05	4.35E-05	9.22E-05	1.91E-04	4.08E-04	1.08E-03	2.23E-03
10	1.45E-05	2.40E-05	5.03E-05	1.07E-04	2.33E-04	6.50E-04	1.41E-03
20	2.00E-06	3.31E-06	7.11E-06	1.52E-05	3.34E-05	9.26E-05	1.95E-04
50	1.90E-07	3.25E-07	6.77E-07	1.46E-06	3.18E-06	7.68E-06	1.36E-05

Lung, Combined (Females, 18-24 years, Light Exertion)

Diameter	5%	10%	25%	50%	75%	90%	95%
0.1	6.48E-05	8.36E-05	1.20E-04	1.76E-04	2.47E-04	3.43E-04	4.22E-04
0.2	3.77E-05	4.74E-05	6.76E-05	9.84E-05	1.41E-04	1.92E-04	2.33E-04
0.5	2.31E-05	2.97E-05	4.33E-05	6.64E-05	9.62E-05	1.34E-04	1.66E-04
0.8	2.73E-05	3.61E-05	5.43E-05	8.28E-05	1.23E-04	1.78E-04	2.19E-04
1	3.31E-05	4.34E-05	6.39E-05	9.82E-05	1.52E-04	2.20E-04	2.72E-04
2	5.21E-05	6.34E-05	9.71E-05	1.49E-04	2.33E-04	3.76E-04	5.39E-04
5	7.30E-06	1.06E-05	1.78E-05	3.36E-05	6.45E-05	1.32E-04	2.46E-04
8	1.21E-06	1.83E-06	3.41E-06	6.84E-06	1.56E-05	3.71E-05	7.13E-05
10	4.36E-07	6.54E-07	1.37E-06	2.98E-06	7.52E-06	1.99E-05	3.80E-05
20	3.02E-08	5.15E-08	1.22E-07	3.40E-07	9.40E-07	2.70E-06	5.31E-06
50	2.74E-09	4.69E-09	1.15E-08	3.19E-08	8.90E-08	2.36E-07	4.48E-07

Table E-2--cont'd

BB Secretory Cells (Females, 25-34 years, Light Exertion)

Diameter	5%	10%	25%	50%	75%	90%	95%
0.1	1.57E-05	2.14E-05	3.13E-05	5.03E-05	8.10E-05	1.19E-04	1.57E-04
0.2	9.91E-06	1.33E-05	1.95E-05	3.15E-05	5.07E-05	7.44E-05	9.86E-05
0.5	7.71E-06	9.96E-06	1.63E-05	2.63E-05	4.67E-05	8.21E-05	1.11E-04
0.8	1.14E-05	1.56E-05	2.71E-05	4.91E-05	9.02E-05	1.82E-04	2.55E-04
1	1.60E-05	2.15E-05	3.84E-05	7.19E-05	1.32E-04	2.59E-04	3.77E-04
2	3.74E-05	5.41E-05	9.27E-05	1.74E-04	3.37E-04	6.88E-04	9.46E-04
5	3.53E-06	5.29E-06	1.35E-05	3.21E-05	8.08E-05	2.01E-04	3.08E-04
8	1.25E-06	1.72E-06	3.70E-06	9.65E-06	2.94E-05	7.58E-05	1.43E-04
10	8.11E-07	1.17E-06	2.46E-06	6.44E-06	1.93E-05	5.05E-05	9.46E-05
20	1.36E-07	2.01E-07	4.29E-07	1.08E-06	3.33E-06	8.95E-06	1.59E-05
50	1.32E-08	1.93E-08	4.14E-08	1.03E-07	3.01E-07	8.17E-07	1.26E-06

BB Basal Cells (Females, 25-34 years, Light Exertion)

Diameter	5%	10%	25%	50%	75%	90%	95%
0.1	1.24E-06	1.89E-06	4.31E-06	1.82E-05	5.48E-05	9.82E-05	1.46E-04
0.2	7.91E-07	1.20E-06	2.75E-06	1.14E-05	3.39E-05	6.22E-05	9.20E-05
0.5	6.16E-07	9.22E-07	2.43E-06	9.62E-06	3.00E-05	6.28E-05	9.06E-05
0.8	1.03E-06	1.65E-06	4.84E-06	1.84E-05	5.24E-05	1.30E-04	2.02E-04
1	1.46E-06	2.38E-06	7.06E-06	2.70E-05	7.64E-05	1.89E-04	2.99E-04
2	3.55E-06	6.05E-06	1.75E-05	6.69E-05	1.91E-04	4.74E-04	7.84E-04
5	2.68E-06	4.04E-06	8.46E-06	2.15E-05	5.71E-05	1.42E-04	2.31E-04
8	1.54E-06	2.09E-06	4.00E-06	9.50E-06	2.53E-05	6.66E-05	1.07E-04
10	1.04E-06	1.39E-06	2.79E-06	6.34E-06	1.73E-05	4.37E-05	7.37E-05
20	1.71E-07	2.57E-07	4.92E-07	1.13E-06	3.03E-06	7.77E-06	1.30E-05
50	1.64E-08	2.49E-08	4.78E-08	1.09E-07	2.76E-07	7.04E-07	1.05E-06

bb Secretory Cells (Females, 25-34 years, Light Exertion)

Diameter	5%	10%	25%	50%	75%	90%	95%
0.1	6.83E-05	8.54E-05	1.19E-04	1.70E-04	2.50E-04	3.49E-04	4.23E-04
0.2	3.92E-05	4.86E-05	6.65E-05	9.60E-05	1.41E-04	1.97E-04	2.39E-04
0.5	2.08E-05	2.53E-05	3.50E-05	5.07E-05	7.29E-05	1.01E-04	1.23E-04
0.8	1.89E-05	2.31E-05	3.12E-05	4.62E-05	6.59E-05	8.80E-05	1.06E-04
1	1.96E-05	2.49E-05	3.39E-05	5.11E-05	7.28E-05	9.86E-05	1.19E-04
2	2.66E-05	3.26E-05	4.92E-05	8.16E-05	1.30E-04	2.01E-04	2.64E-04
5	2.28E-06	3.38E-06	6.06E-06	1.21E-05	2.50E-05	5.69E-05	9.07E-05
8	1.76E-07	3.59E-07	7.28E-07	1.83E-06	4.12E-06	1.10E-05	2.20E-05
10	1.99E-08	5.58E-08	1.61E-07	5.32E-07	1.35E-06	4.26E-06	7.23E-06
20	0	0	6.61E-13	8.17E-11	1.75E-09	1.47E-08	3.44E-08
50	0	0	0	0	0	0	0

Table E-2--cont'd

AI Tissues (Females, 25-34 years, Light Exertion)

Diameter	5%	10%	25%	50%	75%	90%	95%
0.1	1.13E-04	1.39E-04	1.90E-04	2.85E-04	4.20E-04	5.65E-04	6.58E-04
0.2	6.18E-05	7.66E-05	1.06E-04	1.59E-04	2.33E-04	3.14E-04	3.63E-04
0.5	4.43E-05	5.47E-05	7.82E-05	1.15E-04	1.67E-04	2.28E-04	2.73E-04
0.8	5.78E-05	7.23E-05	1.05E-04	1.50E-04	2.19E-04	3.02E-04	3.58E-04
1	6.54E-05	8.22E-05	1.20E-04	1.71E-04	2.50E-04	3.53E-04	4.15E-04
2	6.82E-05	8.57E-05	1.27E-04	1.94E-04	2.93E-04	4.24E-04	5.52E-04
5	1.06E-05	1.50E-05	2.52E-05	4.61E-05	8.53E-05	1.77E-04	2.62E-04
8	4.70E-07	9.19E-07	2.29E-06	5.36E-06	1.21E-05	2.86E-05	4.86E-05
10	2.80E-08	6.81E-08	2.59E-07	9.25E-07	2.71E-06	7.01E-06	1.31E-05
20	0	0	8.08E-16	7.96E-13	6.83E-11	1.44E-09	4.90E-09
50	0	0	0	0	0	0	0

LNth Tissues (Females, 25-34 years, Light Exertion)

Diameter	5%	10%	25%	50%	75%	90%	95%
0.1	1.76E-04	2.92E-04	7.03E-04	1.55E-03	2.74E-03	4.30E-03	5.53E-03
0.2	9.83E-05	1.63E-04	3.93E-04	8.66E-04	1.53E-03	2.37E-03	3.13E-03
0.5	6.81E-05	1.06E-04	2.76E-04	5.90E-04	1.05E-03	1.73E-03	2.19E-03
0.8	8.55E-05	1.33E-04	3.53E-04	7.20E-04	1.37E-03	2.17E-03	2.92E-03
1	9.88E-05	1.57E-04	4.14E-04	8.60E-04	1.61E-03	2.46E-03	3.41E-03
2	1.33E-04	2.23E-04	5.33E-04	1.11E-03	2.12E-03	3.45E-03	4.87E-03
5	6.31E-05	1.00E-04	2.21E-04	4.67E-04	9.74E-04	2.10E-03	3.74E-03
8	2.40E-05	3.76E-05	8.04E-05	1.67E-04	3.61E-04	9.82E-04	1.97E-03
10	1.27E-05	2.11E-05	4.40E-05	9.44E-05	2.06E-04	5.83E-04	1.27E-03
20	1.75E-06	2.90E-06	6.17E-06	1.33E-05	2.93E-05	8.48E-05	1.70E-04
50	1.69E-07	2.77E-07	5.91E-07	1.28E-06	2.78E-06	6.82E-06	1.24E-05

Lung, Combined (Females, 25-34 years, Light Exertion)

Diameter	5%	10%	25%	50%	75%	90%	95%
0.1	6.72E-05	8.49E-05	1.19E-04	1.73E-04	2.44E-04	3.32E-04	4.12E-04
0.2	3.82E-05	4.84E-05	6.77E-05	9.79E-05	1.40E-04	1.88E-04	2.29E-04
0.5	2.36E-05	3.04E-05	4.39E-05	6.54E-05	9.48E-05	1.33E-04	1.58E-04
0.8	2.76E-05	3.73E-05	5.43E-05	8.23E-05	1.24E-04	1.77E-04	2.18E-04
1	3.35E-05	4.46E-05	6.48E-05	9.74E-05	1.50E-04	2.18E-04	2.64E-04
2	5.21E-05	6.26E-05	9.53E-05	1.48E-04	2.27E-04	3.74E-04	5.24E-04
5	7.04E-06	1.02E-05	1.70E-05	3.25E-05	6.10E-05	1.29E-04	2.25E-04
8	1.13E-06	1.74E-06	3.23E-06	6.35E-06	1.52E-05	3.63E-05	7.42E-05
10	3.97E-07	6.09E-07	1.30E-06	2.86E-06	7.46E-06	2.01E-05	3.88E-05
20	2.94E-08	4.80E-08	1.19E-07	3.33E-07	9.29E-07	2.82E-06	5.43E-06
50	2.68E-09	4.50E-09	1.12E-08	3.15E-08	8.77E-08	2.34E-07	4.48E-07

Table E-2--cont'd

BB Secretory Cells (Males, 15 years, Light Exertion)

Diameter	5%	10%	25%	50%	75%	90%	95%
0.1	1.61E-05	2.14E-05	3.18E-05	5.09E-05	8.25E-05	1.22E-04	1.61E-04
0.2	1.00E-05	1.33E-05	1.98E-05	3.17E-05	5.14E-05	7.62E-05	1.01E-04
0.5	8.64E-06	1.09E-05	1.83E-05	3.06E-05	5.46E-05	1.01E-04	1.41E-04
0.8	1.41E-05	1.93E-05	3.36E-05	6.14E-05	1.16E-04	2.24E-04	3.33E-04
1	2.02E-05	2.78E-05	4.86E-05	9.00E-05	1.68E-04	3.36E-04	4.89E-04
2	4.76E-05	6.75E-05	1.17E-04	2.17E-04	4.33E-04	8.56E-04	1.20E-03
5	4.12E-06	6.31E-06	1.62E-05	3.84E-05	9.75E-05	2.39E-04	3.86E-04
8	1.38E-06	1.96E-06	4.08E-06	1.08E-05	3.27E-05	8.08E-05	1.54E-04
10	8.69E-07	1.28E-06	2.64E-06	7.00E-06	2.10E-05	5.15E-05	9.82E-05
20	1.41E-07	2.11E-07	4.53E-07	1.13E-06	3.39E-06	9.19E-06	1.56E-05
50	1.36E-08	2.04E-08	4.31E-08	1.08E-07	3.14E-07	8.36E-07	1.27E-06

BB Basal Cells (Males, 15 years, Light Exertion)

Diameter	5%	10%	25%	50%	75%	90%	95%
0.1	1.29E-06	1.95E-06	4.39E-06	1.90E-05	5.53E-05	1.01E-04	1.52E-04
0.2	8.13E-07	1.23E-06	2.81E-06	1.18E-05	3.41E-05	6.24E-05	9.42E-05
0.5	6.92E-07	1.05E-06	2.87E-06	1.15E-05	3.49E-05	7.41E-05	1.13E-04
0.8	1.29E-06	2.10E-06	6.18E-06	2.36E-05	6.72E-05	1.67E-04	2.65E-04
1	1.86E-06	3.06E-06	9.29E-06	3.45E-05	9.56E-05	2.47E-04	3.87E-04
2	4.43E-06	7.70E-06	2.23E-05	8.38E-05	2.41E-04	6.08E-04	1.02E-03
5	3.13E-06	4.85E-06	1.00E-05	2.55E-05	6.92E-05	1.70E-04	2.69E-04
8	1.73E-06	2.32E-06	4.44E-06	1.06E-05	2.87E-05	7.15E-05	1.18E-04
10	1.12E-06	1.52E-06	3.05E-06	6.86E-06	1.88E-05	4.72E-05	7.70E-05
20	1.79E-07	2.67E-07	5.17E-07	1.18E-06	3.13E-06	7.78E-06	1.32E-05
50	1.69E-08	2.59E-08	4.94E-08	1.13E-07	2.86E-07	7.15E-07	1.06E-06

bb Secretory Cells (Males, 15 years, Light Exertion)

Diameter	5%	10%	25%	50%	75%	90%	95%
0.1	7.28E-05	9.13E-05	1.27E-04	1.82E-04	2.67E-04	3.78E-04	4.53E-04
0.2	4.07E-05	5.10E-05	7.08E-05	9.99E-05	1.49E-04	2.11E-04	2.53E-04
0.5	2.08E-05	2.62E-05	3.63E-05	5.18E-05	7.62E-05	1.05E-04	1.25E-04
0.8	1.85E-05	2.32E-05	3.14E-05	4.68E-05	6.81E-05	9.11E-05	1.09E-04
1	1.99E-05	2.51E-05	3.45E-05	5.22E-05	7.60E-05	1.04E-04	1.25E-04
2	2.83E-05	3.56E-05	5.32E-05	8.86E-05	1.44E-04	2.27E-04	3.02E-04
5	2.29E-06	3.36E-06	6.39E-06	1.29E-05	2.74E-05	6.34E-05	1.04E-04
8	1.45E-07	3.31E-07	6.89E-07	1.76E-06	4.10E-06	1.08E-05	1.99E-05
10	1.32E-08	4.05E-08	1.33E-07	4.65E-07	1.22E-06	3.70E-06	6.23E-06
20	0	0	9.97E-14	2.29E-11	7.29E-10	8.20E-09	1.82E-08
50	0	0	0	0	0	0	0

Table E-2--cont'd

AI Tissues (Males, 15 years, Light Exertion)

Diameter	5%	10%	25%	50%	75%	90%	95%
0.1	1.30E-04	1.64E-04	2.23E-04	3.22E-04	4.80E-04	6.38E-04	7.47E-04
0.2	7.05E-05	8.75E-05	1.21E-04	1.74E-04	2.62E-04	3.48E-04	4.07E-04
0.5	4.86E-05	6.09E-05	8.54E-05	1.28E-04	1.82E-04	2.48E-04	2.96E-04
0.8	6.20E-05	7.81E-05	1.12E-04	1.66E-04	2.36E-04	3.33E-04	3.96E-04
1	7.03E-05	9.09E-05	1.31E-04	1.91E-04	2.75E-04	3.88E-04	4.64E-04
2	7.55E-05	9.24E-05	1.38E-04	2.09E-04	3.25E-04	4.78E-04	6.25E-04
5	1.13E-05	1.64E-05	2.72E-05	5.14E-05	9.74E-05	2.01E-04	3.09E-04
8	4.26E-07	7.87E-07	2.24E-06	5.65E-06	1.35E-05	3.04E-05	5.32E-05
10	1.84E-08	4.23E-08	2.02E-07	8.38E-07	2.59E-06	7.33E-06	1.31E-05
20	0	0	1.08E-19	1.32E-13	2.03E-11	5.98E-10	2.49E-09
50	0	0	0	0	0	0	0

LNth Tissues (Males, 15 years, Light Exertion)

Diameter	5%	10%	25%	50%	75%	90%	95%
0.1	2.28E-04	3.75E-04	9.04E-04	2.24E-03	4.30E-03	7.10E-03	9.37E-03
0.2	1.28E-04	2.05E-04	4.97E-04	1.23E-03	2.35E-03	3.82E-03	5.10E-03
0.5	8.24E-05	1.34E-04	3.43E-04	8.14E-04	1.61E-03	2.68E-03	3.62E-03
0.8	1.05E-04	1.65E-04	4.40E-04	1.05E-03	2.10E-03	3.48E-03	4.75E-03
1	1.23E-04	2.05E-04	5.13E-04	1.23E-03	2.44E-03	4.06E-03	5.61E-03
2	1.82E-04	2.96E-04	7.41E-04	1.72E-03	3.37E-03	5.75E-03	8.24E-03
5	9.12E-05	1.47E-04	3.50E-04	7.64E-04	1.70E-03	3.76E-03	6.70E-03
8	3.58E-05	5.65E-05	1.29E-04	2.78E-04	6.47E-04	1.71E-03	3.51E-03
10	1.93E-05	3.19E-05	7.14E-05	1.54E-04	3.69E-04	9.85E-04	2.17E-03
20	2.59E-06	4.52E-06	1.00E-05	2.22E-05	5.15E-05	1.40E-04	3.04E-04
50	2.51E-07	4.40E-07	9.52E-07	2.11E-06	4.85E-06	1.17E-05	2.17E-05

Lung, Combined (Males, 15 years, Light Exertion)

Diameter	5%	10%	25%	50%	75%	90%	95%
0.1	7.29E-05	9.40E-05	1.32E-04	1.91E-04	2.72E-04	3.71E-04	4.56E-04
0.2	4.06E-05	5.16E-05	7.41E-05	1.06E-04	1.52E-04	2.06E-04	2.52E-04
0.5	2.58E-05	3.31E-05	4.82E-05	7.18E-05	1.03E-04	1.45E-04	1.73E-04
0.8	3.16E-05	4.13E-05	6.04E-05	9.21E-05	1.36E-04	2.00E-04	2.46E-04
1	3.83E-05	4.89E-05	7.28E-05	1.11E-04	1.64E-04	2.47E-04	3.07E-04
2	5.76E-05	7.10E-05	1.09E-04	1.67E-04	2.72E-04	4.32E-04	6.38E-04
5	7.69E-06	1.13E-05	1.94E-05	3.61E-05	7.06E-05	1.53E-04	2.84E-04
8	1.19E-06	1.86E-06	3.54E-06	7.08E-06	1.64E-05	4.01E-05	7.81E-05
10	4.32E-07	6.75E-07	1.42E-06	3.12E-06	7.96E-06	2.12E-05	3.95E-05
20	3.27E-08	5.74E-08	1.32E-07	3.59E-07	9.93E-07	2.80E-06	5.71E-06
50	3.11E-09	5.42E-09	1.26E-08	3.39E-08	9.46E-08	2.48E-07	4.55E-07

Table E-2--cont'd

BB Secretory Cells (Males, 18-24 years, Light Exertion)

Diameter	5%	10%	25%	50%	75%	90%	95%
0.1	1.69E-05	2.30E-05	3.36E-05	5.39E-05	8.63E-05	1.25E-04	1.68E-04
0.2	1.06E-05	1.43E-05	2.10E-05	3.37E-05	5.41E-05	7.88E-05	1.06E-04
0.5	8.84E-06	1.15E-05	1.88E-05	3.08E-05	5.38E-05	9.99E-05	1.34E-04
0.8	1.42E-05	1.93E-05	3.31E-05	6.14E-05	1.13E-04	2.22E-04	3.23E-04
1	2.00E-05	2.74E-05	4.80E-05	8.85E-05	1.64E-04	3.30E-04	4.80E-04
2	4.74E-05	6.69E-05	1.15E-04	2.15E-04	4.18E-04	8.50E-04	1.19E-03
5	4.24E-06	6.53E-06	1.64E-05	3.89E-05	9.92E-05	2.44E-04	3.95E-04
8	1.46E-06	2.07E-06	4.33E-06	1.15E-05	3.47E-05	9.07E-05	1.70E-04
10	9.51E-07	1.36E-06	2.83E-06	7.41E-06	2.29E-05	5.90E-05	1.12E-04
20	1.54E-07	2.28E-07	4.86E-07	1.23E-06	3.79E-06	1.02E-05	1.83E-05
50	1.49E-08	2.18E-08	4.68E-08	1.18E-07	3.42E-07	9.26E-07	1.43E-06

BB Basal Cells (Males, 18-24 years, Light Exertion)

Diameter	5%	10%	25%	50%	75%	90%	95%
0.1	1.34E-06	2.01E-06	4.59E-06	1.96E-05	5.85E-05	1.05E-04	1.55E-04
0.2	8.51E-07	1.30E-06	2.93E-06	1.24E-05	3.66E-05	6.57E-05	9.73E-05
0.5	6.89E-07	1.07E-06	2.81E-06	1.12E-05	3.46E-05	7.43E-05	1.09E-04
0.8	1.27E-06	2.02E-06	6.01E-06	2.29E-05	6.38E-05	1.60E-04	2.57E-04
1	1.81E-06	2.95E-06	8.85E-06	3.30E-05	9.29E-05	2.35E-04	3.80E-04
2	4.34E-06	7.49E-06	2.20E-05	8.29E-05	2.35E-04	5.91E-04	9.75E-04
5	3.30E-06	4.93E-06	1.00E-05	2.61E-05	7.06E-05	1.74E-04	2.82E-04
8	1.81E-06	2.46E-06	4.62E-06	1.11E-05	3.04E-05	8.01E-05	1.36E-04
10	1.17E-06	1.64E-06	3.27E-06	7.38E-06	2.04E-05	5.31E-05	9.27E-05
20	1.88E-07	2.91E-07	5.59E-07	1.29E-06	3.47E-06	8.92E-06	1.55E-05
50	1.84E-08	2.81E-08	5.40E-08	1.25E-07	3.20E-07	8.15E-07	1.24E-06

bb Secretory Cells (Males, 18-24 years, Light Exertion)

Diameter	5%	10%	25%	50%	75%	90%	95%
0.1	8.31E-05	1.03E-04	1.41E-04	2.02E-04	2.95E-04	4.16E-04	5.04E-04
0.2	4.73E-05	5.82E-05	7.95E-05	1.13E-04	1.67E-04	2.35E-04	2.87E-04
0.5	2.49E-05	3.02E-05	4.20E-05	5.97E-05	8.66E-05	1.18E-04	1.45E-04
0.8	2.26E-05	2.78E-05	3.77E-05	5.56E-05	7.83E-05	1.04E-04	1.26E-04
1	2.39E-05	3.04E-05	4.12E-05	6.12E-05	8.79E-05	1.18E-04	1.42E-04
2	3.20E-05	3.97E-05	6.01E-05	9.77E-05	1.57E-04	2.46E-04	3.21E-04
5	2.64E-06	3.95E-06	7.00E-06	1.41E-05	2.98E-05	6.47E-05	1.09E-04
8	1.70E-07	3.61E-07	7.88E-07	2.01E-06	4.60E-06	1.22E-05	2.28E-05
10	1.79E-08	5.09E-08	1.65E-07	5.39E-07	1.46E-06	4.59E-06	7.50E-06
20	0	0	2.67E-13	4.31E-11	1.18E-09	1.16E-08	2.68E-08
50	0	0	0	0	0	0	0

Table E-2--cont'd

AI Tissues (Males, 18-24 years, Light Exertion)

Diameter	5%	10%	25%	50%	75%	90%	95%
0.1	1.28E-04	1.54E-04	2.13E-04	3.12E-04	4.55E-04	6.06E-04	7.02E-04
0.2	6.97E-05	8.45E-05	1.18E-04	1.73E-04	2.54E-04	3.39E-04	3.93E-04
0.5	4.94E-05	6.12E-05	8.54E-05	1.26E-04	1.80E-04	2.44E-04	2.89E-04
0.8	6.33E-05	8.04E-05	1.14E-04	1.64E-04	2.36E-04	3.23E-04	3.89E-04
1	7.00E-05	9.23E-05	1.32E-04	1.88E-04	2.71E-04	3.83E-04	4.50E-04
2	7.28E-05	9.13E-05	1.38E-04	2.10E-04	3.17E-04	4.56E-04	5.88E-04
5	1.06E-05	1.54E-05	2.63E-05	4.88E-05	9.18E-05	1.92E-04	2.81E-04
8	4.49E-07	8.54E-07	2.19E-06	5.45E-06	1.24E-05	3.02E-05	5.15E-05
10	2.23E-08	5.69E-08	2.36E-07	8.71E-07	2.66E-06	7.14E-06	1.31E-05
20	0	0	2.35E-16	4.98E-13	4.77E-11	9.94E-10	3.63E-09
50	0	0	0	0	0	0	0

LNth Tissues (Males, 18-24 years, Light Exertion)

Diameter	5%	10%	25%	50%	75%	90%	95%
0.1	1.90E-04	3.12E-04	7.59E-04	1.68E-03	2.98E-03	4.62E-03	6.03E-03
0.2	1.06E-04	1.75E-04	4.24E-04	9.30E-04	1.66E-03	2.58E-03	3.35E-03
0.5	7.36E-05	1.17E-04	3.02E-04	6.44E-04	1.17E-03	1.88E-03	2.42E-03
0.8	9.22E-05	1.45E-04	3.91E-04	8.02E-04	1.52E-03	2.35E-03	3.16E-03
1	1.07E-04	1.74E-04	4.62E-04	9.42E-04	1.78E-03	2.70E-03	3.77E-03
2	1.45E-04	2.48E-04	5.91E-04	1.24E-03	2.35E-03	3.80E-03	5.32E-03
5	6.96E-05	1.07E-04	2.46E-04	5.17E-04	1.08E-03	2.46E-03	4.56E-03
8	2.54E-05	4.08E-05	8.83E-05	1.85E-04	3.99E-04	1.09E-03	2.32E-03
10	1.37E-05	2.29E-05	4.82E-05	1.02E-04	2.26E-04	6.64E-04	1.44E-03
20	1.86E-06	3.15E-06	6.76E-06	1.45E-05	3.19E-05	9.47E-05	1.96E-04
50	1.81E-07	2.99E-07	6.47E-07	1.40E-06	3.05E-06	7.85E-06	1.41E-05

Lung, Combined (Males, 18-24 years, Light Exertion)

Diameter	5%	10%	25%	50%	75%	90%	95%
0.1	7.59E-05	9.64E-05	1.36E-04	1.96E-04	2.76E-04	3.75E-04	4.47E-04
0.2	4.35E-05	5.45E-05	7.72E-05	1.10E-04	1.53E-04	2.09E-04	2.53E-04
0.5	2.73E-05	3.54E-05	5.06E-05	7.45E-05	1.06E-04	1.47E-04	1.78E-04
0.8	3.32E-05	4.38E-05	6.30E-05	9.33E-05	1.40E-04	2.00E-04	2.47E-04
1	3.96E-05	5.28E-05	7.56E-05	1.11E-04	1.67E-04	2.48E-04	3.03E-04
2	5.80E-05	7.34E-05	1.11E-04	1.70E-04	2.66E-04	4.34E-04	6.23E-04
5	7.93E-06	1.14E-05	1.92E-05	3.61E-05	6.89E-05	1.49E-04	2.68E-04
8	1.21E-06	1.88E-06	3.52E-06	7.05E-06	1.70E-05	4.11E-05	8.40E-05
10	4.30E-07	6.76E-07	1.44E-06	3.23E-06	8.46E-06	2.32E-05	4.44E-05
20	3.27E-08	5.44E-08	1.32E-07	3.76E-07	1.09E-06	3.25E-06	6.17E-06
50	3.02E-09	5.04E-09	1.27E-08	3.56E-08	1.01E-07	2.69E-07	5.07E-07

Table E-2--cont'd

BB Secretory Cells (Males, 25-34 years, Light Exertion)

Diameter	5%	10%	25%	50%	75%	90%	95%
0.1	1.73E-05	2.33E-05	3.42E-05	5.49E-05	8.79E-05	1.27E-04	1.71E-04
0.2	1.08E-05	1.45E-05	2.14E-05	3.44E-05	5.52E-05	8.02E-05	1.08E-04
0.5	9.10E-06	1.17E-05	1.94E-05	3.19E-05	5.55E-05	1.03E-04	1.39E-04
0.8	1.48E-05	1.98E-05	3.45E-05	6.39E-05	1.17E-04	2.30E-04	3.33E-04
1	2.08E-05	2.84E-05	4.93E-05	9.21E-05	1.70E-04	3.41E-04	4.99E-04
2	4.84E-05	6.89E-05	1.17E-04	2.21E-04	4.30E-04	8.69E-04	1.22E-03
5	4.28E-06	6.60E-06	1.66E-05	3.95E-05	1.01E-04	2.45E-04	4.06E-04
8	1.47E-06	2.09E-06	4.39E-06	1.17E-05	3.53E-05	9.22E-05	1.76E-04
10	9.51E-07	1.38E-06	2.85E-06	7.47E-06	2.31E-05	6.01E-05	1.18E-04
20	1.54E-07	2.28E-07	4.88E-07	1.23E-06	3.81E-06	1.03E-05	1.90E-05
50	1.49E-08	2.18E-08	4.66E-08	1.17E-07	3.41E-07	9.42E-07	1.46E-06

BB Basal Cells (Males, 25-34 years, Light Exertion)

Diameter	5%	10%	25%	50%	75%	90%	95%
0.1	1.35E-06	2.04E-06	4.63E-06	1.99E-05	5.99E-05	1.07E-04	1.58E-04
0.2	8.65E-07	1.32E-06	2.96E-06	1.26E-05	3.72E-05	6.74E-05	9.91E-05
0.5	7.08E-07	1.09E-06	2.89E-06	1.16E-05	3.61E-05	7.68E-05	1.13E-04
0.8	1.32E-06	2.08E-06	6.22E-06	2.37E-05	6.62E-05	1.65E-04	2.66E-04
1	1.86E-06	3.06E-06	9.14E-06	3.43E-05	9.57E-05	2.44E-04	3.98E-04
2	4.43E-06	7.64E-06	2.26E-05	8.47E-05	2.39E-04	6.06E-04	9.92E-04
5	3.34E-06	5.01E-06	1.01E-05	2.64E-05	7.19E-05	1.76E-04	2.88E-04
8	1.81E-06	2.49E-06	4.67E-06	1.12E-05	3.07E-05	8.19E-05	1.42E-04
10	1.18E-06	1.64E-06	3.27E-06	7.42E-06	2.07E-05	5.42E-05	9.55E-05
20	1.88E-07	2.90E-07	5.58E-07	1.29E-06	3.47E-06	9.00E-06	1.59E-05
50	1.83E-08	2.82E-08	5.40E-08	1.24E-07	3.21E-07	8.17E-07	1.24E-06

bb Secretory Cells (Males, 25-34 years, Light Exertion)

Diameter	5%	10%	25%	50%	75%	90%	95%
0.1	8.49E-05	1.06E-04	1.44E-04	2.06E-04	3.01E-04	4.22E-04	5.15E-04
0.2	4.87E-05	5.99E-05	8.13E-05	1.16E-04	1.71E-04	2.41E-04	2.94E-04
0.5	2.58E-05	3.12E-05	4.26E-05	6.09E-05	8.84E-05	1.21E-04	1.47E-04
0.8	2.32E-05	2.88E-05	3.87E-05	5.68E-05	7.99E-05	1.07E-04	1.26E-04
1	2.48E-05	3.11E-05	4.22E-05	6.23E-05	8.89E-05	1.20E-04	1.43E-04
2	3.19E-05	4.03E-05	6.12E-05	9.88E-05	1.58E-04	2.46E-04	3.23E-04
5	2.63E-06	3.88E-06	6.90E-06	1.39E-05	2.95E-05	6.43E-05	1.09E-04
8	1.61E-07	3.49E-07	7.54E-07	1.96E-06	4.45E-06	1.21E-05	2.22E-05
10	1.62E-08	4.67E-08	1.54E-07	5.12E-07	1.42E-06	4.49E-06	7.24E-06
20	0	0	1.90E-13	3.52E-11	1.06E-09	1.06E-08	2.49E-08
50	0	0	0	0	0	0	0

Table E-2--cont'd

AI Tissues (Males, 25-34 years, Light Exertion)

Diameter	5%	10%	25%	50%	75%	90%	95%
0.1	1.21E-04	1.50E-04	2.03E-04	2.98E-04	4.35E-04	5.76E-04	6.61E-04
0.2	6.69E-05	8.17E-05	1.14E-04	1.66E-04	2.41E-04	3.24E-04	3.76E-04
0.5	4.80E-05	6.01E-05	8.26E-05	1.22E-04	1.71E-04	2.35E-04	2.78E-04
0.8	6.11E-05	7.77E-05	1.10E-04	1.57E-04	2.25E-04	3.11E-04	3.72E-04
1	6.82E-05	8.93E-05	1.26E-04	1.79E-04	2.57E-04	3.65E-04	4.30E-04
2	6.83E-05	8.68E-05	1.31E-04	1.98E-04	2.96E-04	4.29E-04	5.67E-04
5	9.61E-06	1.40E-05	2.37E-05	4.36E-05	8.32E-05	1.74E-04	2.51E-04
8	3.80E-07	7.34E-07	1.90E-06	4.79E-06	1.10E-05	2.68E-05	4.56E-05
10	1.78E-08	4.50E-08	2.01E-07	7.39E-07	2.27E-06	6.15E-06	1.15E-05
20	0	0	9.81E-17	3.64E-13	3.55E-11	7.39E-10	2.81E-09
50	0	0	0	0	0	0	0

LNth Tissues (Males, 25-34 years, Light Exertion)

Diameter	5%	10%	25%	50%	75%	90%	95%
0.1	1.78E-04	2.92E-04	7.06E-04	1.58E-03	2.80E-03	4.32E-03	5.60E-03
0.2	9.84E-05	1.63E-04	3.97E-04	8.82E-04	1.57E-03	2.44E-03	3.18E-03
0.5	6.94E-05	1.11E-04	2.87E-04	6.10E-04	1.10E-03	1.79E-03	2.25E-03
0.8	8.62E-05	1.37E-04	3.69E-04	7.56E-04	1.43E-03	2.22E-03	3.00E-03
1	9.99E-05	1.65E-04	4.30E-04	8.92E-04	1.69E-03	2.55E-03	3.54E-03
2	1.34E-04	2.26E-04	5.42E-04	1.15E-03	2.18E-03	3.50E-03	4.93E-03
5	6.18E-05	9.35E-05	2.17E-04	4.61E-04	9.60E-04	2.18E-03	4.11E-03
8	2.19E-05	3.54E-05	7.73E-05	1.63E-04	3.52E-04	9.81E-04	2.07E-03
10	1.21E-05	1.99E-05	4.23E-05	8.94E-05	2.00E-04	5.83E-04	1.30E-03
20	1.62E-06	2.76E-06	5.93E-06	1.27E-05	2.82E-05	8.67E-05	1.72E-04
50	1.58E-07	2.64E-07	5.72E-07	1.22E-06	2.65E-06	6.83E-06	1.28E-05

Lung, Combined (Males, 25-34 years, Light Exertion)

Diameter	5%	10%	25%	50%	75%	90%	95%
0.1	7.56E-05	9.55E-05	1.35E-04	1.90E-04	2.69E-04	3.66E-04	4.37E-04
0.2	4.34E-05	5.38E-05	7.70E-05	1.08E-04	1.52E-04	2.06E-04	2.46E-04
0.5	2.71E-05	3.53E-05	5.06E-05	7.38E-05	1.04E-04	1.45E-04	1.73E-04
0.8	3.30E-05	4.38E-05	6.28E-05	9.29E-05	1.37E-04	1.97E-04	2.41E-04
1	3.96E-05	5.22E-05	7.49E-05	1.11E-04	1.65E-04	2.42E-04	3.03E-04
2	5.78E-05	7.22E-05	1.10E-04	1.68E-04	2.62E-04	4.28E-04	6.25E-04
5	7.71E-06	1.08E-05	1.83E-05	3.44E-05	6.64E-05	1.45E-04	2.62E-04
8	1.17E-06	1.80E-06	3.35E-06	6.77E-06	1.64E-05	4.09E-05	7.96E-05
10	4.08E-07	6.48E-07	1.37E-06	3.16E-06	8.14E-06	2.33E-05	4.49E-05
20	3.21E-08	5.18E-08	1.31E-07	3.75E-07	1.08E-06	3.26E-06	6.26E-06
50	2.96E-09	4.85E-09	1.26E-08	3.53E-08	1.00E-07	2.69E-07	5.05E-07

Table E-3. Geometric means (Sv per Bq-hr/m^3) and gometric standard deviations versus particle diameter (assuming monodisperse, unit density spheres) for equivalent dose per unit activity exposure, H/A_E, for all population groups and all exertion levels.

Children, 2 years, Resting

	BB Secretory		BB Basal		bb Secretory		AI Tissues		LNth Tissues		Lung, Combined	
Diameter	GM	GSD	GM	GSD	GM	GSD	GM	GSD	GM	GSD	GM	GSD
0.1	4.39E-05	2.00	1.40E-05	4.56	5.63E-05	1.70	1.21E-04	1.66	9.28E-04	2.80	7.54E-05	1.63
0.2	2.77E-05	2.00	8.84E-06	4.55	3.19E-05	1.70	6.73E-05	1.67	5.27E-04	2.79	4.33E-05	1.62
0.5	1.54E-05	2.01	4.91E-06	4.57	1.67E-05	1.71	4.99E-05	1.69	3.36E-04	2.89	2.75E-05	1.70
0.8	1.50E-05	2.08	4.74E-06	4.62	1.45E-05	1.72	6.76E-05	1.72	3.92E-04	3.04	3.18E-05	1.82
1	1.79E-05	2.18	5.67E-06	4.72	1.53E-05	1.75	8.07E-05	1.74	4.57E-04	3.09	3.72E-05	1.86
2	4.47E-05	2.46	1.43E-05	5.01	2.42E-05	2.00	1.12E-04	1.90	7.06E-04	3.17	6.02E-05	1.97
5	1.30E-05	4.07	8.74E-06	4.18	5.83E-06	3.17	5.37E-05	2.70	5.33E-04	3.75	2.49E-05	2.89
8	5.43E-06	4.59	5.22E-06	4.21	1.38E-06	3.81	1.23E-05	3.33	2.54E-04	4.07	7.26E-06	3.37
10	3.94E-06	4.71	3.96E-06	4.26	5.30E-07	4.29	3.53E-06	3.86	1.52E-04	4.16	3.29E-06	3.65
20	8.28E-07	4.71	8.55E-07	4.19	-1	-1	-1	-1	2.16E-05	4.21	2.66E-07	4.92
50	7.10E-08	4.44	7.33E-08	3.93	-1	-1	-1	-1	1.81E-06	3.97	2.19E-08	4.77

Children, 2 years, Sitting

	BB Secretory		BB Basal		bb Secretory		AI Tissues		LNth Tissues		Lung, Combined	
Diameter	GM	GSD	GM	GSD	GM	GSD	GM	GSD	GM	GSD	GM	GSD
0.1	5.11E-05	2.00	1.62E-05	4.56	6.77E-05	1.70	1.52E-04	1.66	1.14E-03	2.81	9.20E-05	1.64
0.2	3.20E-05	2.00	1.02E-05	4.56	3.80E-05	1.71	8.33E-05	1.67	6.37E-04	2.80	5.21E-05	1.63
0.5	1.90E-05	2.03	6.05E-06	4.57	1.95E-05	1.71	6.05E-05	1.68	4.03E-04	2.90	3.31E-05	1.71
0.8	2.33E-05	2.20	7.42E-06	4.73	1.67E-05	1.72	8.11E-05	1.72	4.79E-04	3.03	3.98E-05	1.83
1	3.11E-05	2.32	9.91E-06	4.85	1.75E-05	1.77	9.62E-05	1.75	5.63E-04	3.06	4.75E-05	1.87
2	8.46E-05	2.57	2.71E-05	5.15	2.93E-05	2.07	1.32E-04	1.97	9.06E-04	3.17	8.11E-05	2.06
5	2.40E-05	4.32	1.64E-05	4.44	7.34E-06	3.39	6.14E-05	2.89	7.60E-04	3.85	3.29E-05	3.08
8	9.30E-06	4.80	9.06E-06	4.40	1.44E-06	4.22	1.11E-05	3.74	3.60E-04	4.20	8.77E-06	3.70
10	6.37E-06	4.88	6.45E-06	4.42	4.44E-07	5.16	2.40E-06	4.82	2.12E-04	4.30	3.85E-06	4.11
20	1.12E-06	4.83	1.15E-06	4.33	-1	-1	-1	-1	2.87E-05	4.33	3.49E-07	5.22
50	8.98E-08	4.52	9.28E-08	4.03	-1	-1	-1	-1	2.29E-06	4.03	2.77E-08	4.92

Notes: GM = geometric mean (Sv per Bq-hr/m^3); GSD = geometric standard deviation.
Values given as "-1" serve as flags to indicate that some trials resulted in no dose (zero) to the tissue and a GM and GSD was not computed.

Table E-3--cont'd

Children, 2 years, Light Exertion

	BB Secretory		BB Basal		bb Secretory		Al Tissues		LNth Tissues		Lung, Combined	
Diameter	GM	GSD	GM	GSD	GM	GSD	GM	GSD	GM	GSD	GM	GSD
0.1	7.71E-05	2.01	2.44E-05	4.59	1.13E-04	1.74	2.95E-04	1.70	2.04E-03	2.88	1.63E-04	1.71
0.2	4.79E-05	2.02	1.52E-05	4.58	6.17E-05	1.74	1.57E-04	1.70	1.11E-03	2.87	9.00E-05	1.70
0.5	5.27E-05	2.43	1.69E-05	4.97	3.01E-05	1.75	1.07E-04	1.72	7.32E-04	2.93	6.32E-05	1.83
0.8	1.09E-04	2.73	3.52E-05	5.31	2.49E-05	1.81	1.35E-04	1.80	9.44E-04	3.04	8.71E-05	2.06
1	1.60E-04	2.81	5.15E-05	5.41	2.66E-05	1.92	1.54E-04	1.87	1.14E-03	3.10	1.08E-04	2.19
2	4.14E-04	3.27	1.34E-04	6.03	5.25E-05	2.60	1.85E-04	2.41	1.97E-03	3.55	1.96E-04	2.83
5	8.07E-05	5.50	5.64E-05	5.50	8.63E-06	4.65	4.30E-05	4.06	1.52E-03	4.76	4.90E-05	4.27
8	2.15E-05	5.78	2.13E-05	5.25	4.41E-07	9.10	1.32E-06	10.62	5.91E-04	5.14	9.16E-06	5.37
10	1.23E-05	5.76	1.26E-05	5.19	-1	-1	-1	-1	3.27E-04	5.20	4.27E-06	5.86
20	1.62E-06	5.51	1.67E-06	4.94	-1	-1	-1	-1	4.11E-05	5.00	4.98E-07	5.99
50	1.22E-07	5.01	1.26E-07	4.46	-1	-1	-1	-1	3.11E-06	4.51	3.77E-08	5.43

Children, 2 years, Heavy Exertion

	BB Secretory		BB Basal		bb Secretory		Al Tissues		LNth Tissues		Lung, Combined	
Diameter	GM	GSD	GM	GSD	GM	GSD	GM	GSD	GM	GSD	GM	GSD
0.1	1.13E-04	1.99	3.55E-05	4.59	1.79E-04	1.71	5.35E-04	1.61	3.48E-03	2.88	2.75E-04	1.69
0.2	7.89E-05	2.05	2.51E-05	4.59	9.65E-05	1.71	2.81E-04	1.61	1.88E-03	2.86	1.53E-04	1.68
0.5	2.35E-04	2.57	7.57E-05	5.06	4.75E-05	1.73	1.91E-04	1.63	1.57E-03	2.84	1.49E-04	1.96
0.8	6.01E-04	2.62	1.94E-04	5.11	4.23E-05	1.77	2.45E-04	1.69	2.50E-03	2.89	2.53E-04	2.27
1	9.16E-04	2.63	2.96E-04	5.13	5.09E-05	1.85	2.86E-04	1.72	3.35E-03	2.92	3.44E-04	2.39
2	2.67E-03	2.66	8.64E-04	5.17	1.58E-04	2.23	3.66E-04	1.89	7.75E-03	2.96	8.07E-04	2.69
5	3.88E-04	3.66	2.74E-04	3.56	1.02E-05	5.15	2.13E-05	5.03	5.44E-03	3.07	1.31E-04	3.27
8	7.52E-05	3.77	7.50E-05	3.27	-1	-1	-1	-1	1.82E-03	3.22	2.35E-05	3.86
10	3.85E-05	3.77	3.94E-05	3.26	-1	-1	-1	-1	9.67E-04	3.26	1.19E-05	3.96
20	4.35E-06	3.77	4.50E-06	3.26	-1	-1	-1	-1	1.11E-04	3.27	1.31E-06	3.97
50	2.92E-07	3.72	3.02E-07	3.21	-1	-1	-1	-1	7.43E-06	3.21	9.00E-08	3.92

Notes: GM = geometric mean (Sv per Bq-hr/m^3); GSD = geometric standard deviation.
Values given as "-1" serve as flags to indicate that some trials resulted in no dose (zero) to the tissue and a GM and GSD was not computed.

Table E-3--cont'd

Children, 5 years, Resting

Diameter	BB Secretory		BB Basal		bb Secretory		AI Tissues		LNth Tissues		Lung, Combined	
	GM	GSD	GM	GSD	GM	GSD	GM	GSD	GM	GSD	GM	GSD
0.1	3.46E-05	2.00	1.09E-05	4.59	6.26E-05	1.69	1.29E-04	1.61	8.72E-04	2.86	7.69E-05	1.62
0.2	2.20E-05	2.00	6.96E-06	4.58	3.58E-05	1.69	7.25E-05	1.63	4.96E-04	2.86	4.43E-05	1.62
0.5	1.23E-05	2.00	3.88E-06	4.60	1.90E-05	1.69	5.47E-05	1.65	3.30E-04	2.96	2.87E-05	1.70
0.8	1.19E-05	2.05	3.71E-06	4.65	1.73E-05	1.69	7.53E-05	1.67	4.03E-04	3.10	3.40E-05	1.81
1	1.42E-05	2.13	4.44E-06	4.74	1.88E-05	1.72	9.09E-05	1.68	4.77E-04	3.13	4.02E-05	1.84
2	3.68E-05	2.35	1.17E-05	4.92	3.20E-05	1.89	1.33E-04	1.78	7.58E-04	3.16	6.72E-05	1.86
5	1.18E-05	3.68	7.78E-06	3.88	8.27E-06	2.84	6.65E-05	2.46	5.51E-04	3.60	2.91E-05	2.66
8	5.25E-06	4.27	4.97E-06	3.93	2.20E-06	3.46	1.66E-05	3.08	2.58E-04	3.91	8.86E-06	3.14
10	3.98E-06	4.45	3.95E-06	4.02	9.61E-07	3.87	5.35E-06	3.53	1.55E-04	4.00	4.12E-06	3.39
20	9.84E-07	4.58	1.01E-06	4.04	-1	-1	-1	-1	2.27E-05	4.11	3.23E-07	4.68
50	8.97E-08	4.35	9.27E-08	3.82	-1	-1	-1	-1	1.97E-06	3.89	2.70E-08	4.69

Children, 5 years, Sitting

Diameter	BB Secretory		BB Basal		bb Secretory		AI Tissues		LNth Tissues		Lung, Combined	
	GM	GSD	GM	GSD	GM	GSD	GM	GSD	GM	GSD	GM	GSD
0.1	4.02E-05	2.00	1.27E-05	4.59	7.52E-05	1.69	1.61E-04	1.62	1.07E-03	2.87	9.37E-05	1.64
0.2	2.53E-05	2.00	8.00E-06	4.59	4.25E-05	1.69	8.91E-05	1.63	6.00E-04	2.87	5.32E-05	1.63
0.5	1.50E-05	2.01	4.74E-06	4.60	2.22E-05	1.69	6.60E-05	1.65	3.94E-04	2.97	3.44E-05	1.71
0.8	1.82E-05	2.16	5.73E-06	4.73	1.98E-05	1.69	8.98E-05	1.68	4.84E-04	3.09	4.17E-05	1.81
1	2.42E-05	2.26	7.65E-06	4.83	2.14E-05	1.73	1.08E-04	1.69	5.76E-04	3.12	5.00E-05	1.83
2	6.77E-05	2.45	2.16E-05	5.02	3.75E-05	1.96	1.52E-04	1.85	9.22E-04	3.16	8.59E-05	1.92
5	2.00E-05	4.02	1.35E-05	4.17	9.76E-06	3.11	7.19E-05	2.72	7.07E-04	3.77	3.54E-05	2.89
8	8.37E-06	4.63	8.06E-06	4.23	2.26E-06	3.90	1.49E-05	3.54	3.31E-04	4.16	9.96E-06	3.52
10	6.05E-06	4.78	6.08E-06	4.30	8.38E-07	4.58	3.84E-06	4.34	1.97E-04	4.29	4.46E-06	3.90
20	1.24E-06	4.84	1.28E-06	4.30	-1	-1	-1	-1	2.77E-05	4.38	3.85E-07	5.17
50	1.06E-07	4.52	1.09E-07	3.99	-1	-1	-1	-1	2.32E-06	4.07	3.18E-08	4.93

Notes: GM = geometric mean (Sv per Bq-hr/m^3); GSD = geometric standard deviation.
Values given as "-1" serve as flags to indicate that some trials resulted in no dose (zero) to the tissue and a GM and GSD was not computed.

Table E-3--cont'd

Children, 5 years, Light Exertion

Diameter	BB Secretory		BB Basal		bb Secretory		AI Tissues		LNth Tissues		Lung, Combined	
	GM	GSD	GM	GSD	GM	GSD	GM	GSD	GM	GSD	GM	GSD
0.1	6.05E-05	2.00	1.90E-05	4.63	1.24E-04	1.72	3.08E-04	1.67	1.92E-03	2.95	1.66E-04	1.72
0.2	3.76E-05	2.01	1.18E-05	4.61	6.83E-05	1.72	1.66E-04	1.68	1.05E-03	2.94	9.14E-05	1.70
0.5	4.03E-05	2.38	1.28E-05	4.94	3.41E-05	1.72	1.15E-04	1.69	6.97E-04	3.00	6.34E-05	1.79
0.8	8.35E-05	2.66	2.68E-05	5.23	2.93E-05	1.76	1.48E-04	1.75	8.94E-04	3.08	8.56E-05	1.95
1	1.22E-04	2.71	3.92E-05	5.30	3.20E-05	1.84	1.70E-04	1.81	1.07E-03	3.11	1.06E-04	2.03
2	3.14E-04	3.06	1.01E-04	5.73	6.33E-05	2.45	2.02E-04	2.28	1.72E-03	3.44	1.83E-04	2.53
5	6.37E-05	5.38	4.42E-05	5.38	1.18E-05	4.45	5.28E-05	3.95	1.23E-03	4.75	4.81E-05	4.07
8	1.91E-05	5.88	1.88E-05	5.30	9.83E-07	7.23	2.60E-06	8.38	4.92E-04	5.29	9.35E-06	5.21
10	1.15E-05	5.91	1.17E-05	5.29	1.37E-07	13.89	-1	-1	2.76E-04	5.40	4.26E-06	5.80
20	1.65E-06	5.70	1.71E-06	5.07	-1	-1	-1	-1	3.62E-05	5.25	4.98E-07	6.20
50	1.32E-07	5.13	1.37E-07	4.54	-1	-1	-1	-1	2.90E-06	4.68	3.98E-08	5.58

Children, 5 years, Heavy Exertion

Diameter	BB Secretory		BB Basal		bb Secretory		AI Tissues		LNth Tissues		Lung, Combined	
	GM	GSD	GM	GSD	GM	GSD	GM	GSD	GM	GSD	GM	GSD
0.1	8.92E-05	1.99	2.77E-05	4.63	2.00E-04	1.71	5.92E-04	1.63	3.45E-03	2.98	2.92E-04	1.74
0.2	6.17E-05	2.03	1.94E-05	4.62	1.09E-04	1.71	3.14E-04	1.63	1.87E-03	2.97	1.61E-04	1.72
0.5	1.78E-04	2.54	5.71E-05	5.05	5.49E-05	1.72	2.18E-04	1.65	1.47E-03	2.93	1.47E-04	1.88
0.8	4.61E-04	2.59	1.49E-04	5.09	5.15E-05	1.75	2.87E-04	1.70	2.25E-03	2.95	2.41E-04	2.12
1	7.08E-04	2.61	2.29E-04	5.11	6.35E-05	1.82	3.38E-04	1.73	2.96E-03	2.94	3.25E-04	2.22
2	2.17E-03	2.66	7.02E-04	5.16	2.07E-04	2.18	4.61E-04	1.88	6.66E-03	2.95	7.76E-04	2.48
5	4.17E-04	3.71	2.93E-04	3.60	2.46E-05	4.08	4.93E-05	3.68	5.55E-03	3.07	1.65E-04	3.07
8	9.38E-05	3.81	9.35E-05	3.30	-1	-1	-1	-1	2.00E-03	3.24	2.99E-05	3.86
10	4.97E-05	3.82	5.10E-05	3.29	-1	-1	-1	-1	1.08E-03	3.29	1.51E-05	4.04
20	5.82E-06	3.83	6.01E-06	3.31	-1	-1	-1	-1	1.27E-04	3.32	1.75E-06	4.10
50	3.94E-07	3.77	4.07E-07	3.25	-1	-1	-1	-1	8.63E-06	3.26	1.19E-07	4.04

Notes: GM = geometric mean (Sv per Bq-hr/m^3); GSD = geometric standard deviation.
Values given as "-1" serve as flags to indicate that some trials resulted in no dose (zero) to the tissue and a GM and GSD was not computed.

Table E-3--cont'd

Children, 10 years, Resting

Diameter	BB Secretory		BB Basal		bb Secretory		AI Tissues		LNth Tissues		Lung, Combined	
	GM	GSD	GM	GSD	GM	GSD	GM	GSD	GM	GSD	GM	GSD
0.1	3.00E-05	1.99	9.43E-06	4.59	7.47E-05	1.69	1.37E-04	1.63	8.96E-04	2.89	8.20E-05	1.64
0.2	1.91E-05	1.99	6.01E-06	4.59	4.27E-05	1.69	7.67E-05	1.64	5.11E-04	2.89	4.72E-05	1.64
0.5	1.08E-05	1.99	3.37E-06	4.61	2.31E-05	1.69	5.82E-05	1.66	3.44E-04	2.99	3.08E-05	1.71
0.8	1.04E-05	2.04	3.21E-06	4.66	2.20E-05	1.69	8.08E-05	1.69	4.29E-04	3.12	3.70E-05	1.81
1	1.24E-05	2.12	3.83E-06	4.75	2.45E-05	1.72	9.82E-05	1.69	5.14E-04	3.14	4.40E-05	1.83
2	3.27E-05	2.30	1.03E-05	4.88	4.36E-05	1.84	1.49E-04	1.73	8.40E-04	3.11	7.55E-05	1.80
5	1.08E-05	3.30	7.05E-06	3.52	1.09E-05	2.52	7.62E-05	2.17	5.99E-04	3.31	3.26E-05	2.37
8	4.82E-06	3.74	4.50E-06	3.44	2.98E-06	2.98	1.99E-05	2.65	2.73E-04	3.48	1.00E-05	2.71
10	3.70E-06	3.91	3.64E-06	3.52	1.39E-06	3.31	6.95E-06	3.00	1.64E-04	3.54	4.73E-06	2.87
20	1.03E-06	4.12	1.06E-06	3.60	1.48E-08	10	0	12	2.48E-05	3.67	3.59E-07	4.03
50	1.02E-07	4.01	1.05E-07	3.49	-1	-1	-1	-1	2.26E-06	3.56	3.08E-08	4.27

Children, 10 years, Sitting

Diameter	BB Secretory		BB Basal		bb Secretory		AI Tissues		LNth Tissues		Lung, Combined	
	GM	GSD	GM	GSD	GM	GSD	GM	GSD	GM	GSD	GM	GSD
0.1	3.50E-05	1.98	1.10E-05	4.60	9.02E-05	1.69	1.74E-04	1.63	1.12E-03	2.91	1.01E-04	1.66
0.2	2.20E-05	1.99	6.93E-06	4.59	5.11E-05	1.70	9.65E-05	1.64	6.28E-04	2.90	5.76E-05	1.65
0.5	1.31E-05	2.00	4.11E-06	4.61	2.70E-05	1.69	7.20E-05	1.66	4.18E-04	3.00	3.74E-05	1.72
0.8	1.57E-05	2.15	4.91E-06	4.74	2.49E-05	1.68	9.86E-05	1.69	5.22E-04	3.12	4.56E-05	1.81
1	2.09E-05	2.25	6.54E-06	4.84	2.75E-05	1.71	1.19E-04	1.69	6.25E-04	3.14	5.47E-05	1.83
2	5.86E-05	2.38	1.86E-05	4.94	4.91E-05	1.89	1.71E-04	1.78	1.00E-03	3.12	9.36E-05	1.83
5	1.67E-05	3.57	1.11E-05	3.73	1.17E-05	2.74	7.77E-05	2.39	6.95E-04	3.46	3.64E-05	2.54
8	6.90E-06	4.04	6.58E-06	3.69	2.83E-06	3.35	1.73E-05	3.02	3.12E-04	3.72	1.03E-05	2.99
10	5.08E-06	4.20	5.07E-06	3.77	1.16E-06	3.86	5.06E-06	3.60	1.85E-04	3.81	4.65E-06	3.25
20	1.17E-06	4.35	1.21E-06	3.83	-1	-1	-1	-1	2.70E-05	3.94	3.77E-07	4.48
50	1.09E-07	4.16	1.13E-07	3.65	-1	-1	-1	-1	2.42E-06	3.73	3.29E-08	4.45

Notes: GM = geometric mean (Sv per Bq-hr/m^3); GSD = geometric standard deviation.
Values given as "-1" serve as flags to indicate that some trials resulted in no dose (zero) to the tissue and a GM and GSD was not computed.

Table E-3--cont'd

Children, 10 years, Light Exertion

Diameter	BB Secretory		BB Basal		bb Secretory		AI Tissues		LNth Tissues		Lung, Combined	
	GM	GSD	GM	GSD	GM	GSD	GM	GSD	GM	GSD	GM	GSD
0.1	5.31E-05	1.99	1.65E-05	4.64	1.52E-04	1.73	3.56E-04	1.69	2.12E-03	3.00	1.87E-04	1.75
0.2	3.31E-05	2.00	1.03E-05	4.62	8.37E-05	1.72	1.92E-04	1.69	1.16E-03	2.99	1.04E-04	1.73
0.5	3.46E-05	2.37	1.09E-05	4.93	4.23E-05	1.72	1.35E-04	1.70	7.73E-04	3.06	7.07E-05	1.80
0.8	7.08E-05	2.64	2.26E-05	5.21	3.72E-05	1.73	1.74E-04	1.75	9.86E-04	3.12	9.33E-05	1.91
1	1.03E-04	2.68	3.31E-05	5.25	4.11E-05	1.80	2.00E-04	1.78	1.17E-03	3.13	1.14E-04	1.96
2	2.54E-04	2.85	8.18E-05	5.44	7.55E-05	2.27	2.28E-04	2.10	1.73E-03	3.29	1.82E-04	2.26
5	4.65E-05	4.72	3.21E-05	4.70	1.29E-05	3.85	5.79E-05	3.40	1.03E-03	4.27	4.39E-05	3.46
8	1.43E-05	5.17	1.41E-05	4.66	1.39E-06	5.72	4.15E-06	6.13	4.04E-04	4.74	8.55E-06	4.32
10	8.96E-06	5.24	9.13E-06	4.69	2.59E-07	9.49	-1	-1	2.28E-04	4.87	3.76E-06	4.86
20	1.41E-06	5.16	1.46E-06	4.58	-1	-1	-1	-1	3.13E-05	4.82	4.27E-07	5.49
50	1.23E-07	4.72	1.27E-07	4.17	-1	-1	-1	-1	2.72E-06	4.36	3.70E-08	5.04

Children, 10 years, Heavy Exertion

Diameter	BB Secretory		BB Basal		bb Secretory		AI Tissues		LNth Tissues		Lung, Combined	
	GM	GSD	GM	GSD	GM	GSD	GM	GSD	GM	GSD	GM	GSD
0.1	7.91E-05	1.97	2.43E-05	4.66	2.48E-04	1.70	7.24E-04	1.64	4.00E-03	3.04	3.46E-04	1.78
0.2	5.43E-05	2.02	1.69E-05	4.64	1.35E-04	1.71	3.86E-04	1.65	2.17E-03	3.03	1.90E-04	1.76
0.5	1.51E-04	2.55	4.83E-05	5.07	6.98E-05	1.71	2.73E-04	1.67	1.66E-03	3.01	1.63E-04	1.85
0.8	3.92E-04	2.62	1.26E-04	5.12	6.76E-05	1.74	3.62E-04	1.72	2.48E-03	3.02	2.59E-04	2.04
1	6.06E-04	2.63	1.95E-04	5.13	8.38E-05	1.82	4.30E-04	1.75	3.21E-03	3.01	3.45E-04	2.11
2	1.89E-03	2.73	6.10E-04	5.24	2.60E-04	2.19	6.00E-04	1.90	6.91E-03	3.02	8.01E-04	2.37
5	4.32E-04	3.87	3.03E-04	3.80	4.32E-05	3.64	1.01E-04	3.11	6.33E-03	3.19	2.06E-04	2.95
8	1.11E-04	3.92	1.10E-04	3.47	-1	-1	-1	-1	2.46E-03	3.38	3.78E-05	3.77
10	6.09E-05	3.92	6.24E-05	3.46	-1	-1	-1	-1	1.36E-03	3.45	1.90E-05	4.05
20	7.43E-06	3.93	7.68E-06	3.46	-1	-1	-1	-1	1.65E-04	3.47	2.24E-06	4.17
50	5.12E-07	3.84	5.29E-07	3.37	-1	-1	-1	-1	1.14E-05	3.37	1.55E-07	4.08

Notes: GM = geometric mean (Sv per Bq-hr/m^3); GSD = geometric standard deviation.
Values given as "-1" serve as flags to indicate that some trials resulted in no dose (zero) to the tissue and a GM and GSD was not computed.

Table E-3--cont'd

Females, 15 years, Resting

Diameter	BB Secretory		BB Basal		bb Secretory		AI Tissues		LNth Tissues		Lung, Combined	
	GM	GSD	GM	GSD	GM	GSD	GM	GSD	GM	GSD	GM	GSD
0.1	2.73E-05	1.98	8.58E-06	4.59	7.92E-05	1.69	1.04E-04	1.64	6.86E-04	2.89	7.18E-05	1.62
0.2	1.75E-05	1.98	5.50E-06	4.58	4.56E-05	1.69	5.86E-05	1.66	3.94E-04	2.89	4.17E-05	1.62
0.5	9.76E-06	1.99	3.06E-06	4.61	2.53E-05	1.69	4.50E-05	1.68	2.69E-04	2.99	2.71E-05	1.67
0.8	8.71E-06	2.00	2.68E-06	4.65	2.54E-05	1.70	6.29E-05	1.70	3.40E-04	3.10	3.23E-05	1.75
1	9.81E-06	2.07	3.01E-06	4.73	2.91E-05	1.73	7.68E-05	1.70	4.10E-04	3.12	3.85E-05	1.77
2	2.46E-05	2.25	7.68E-06	4.87	5.28E-05	1.81	1.21E-04	1.69	6.85E-04	3.05	6.74E-05	1.72
5	8.99E-06	2.98	5.75E-06	3.28	1.26E-05	2.28	6.55E-05	1.92	4.97E-04	3.03	2.92E-05	2.10
8	4.11E-06	3.29	3.77E-06	3.04	3.55E-06	2.57	1.80E-05	2.25	2.24E-04	3.05	9.24E-06	2.31
10	3.20E-06	3.41	3.11E-06	3.07	1.76E-06	2.82	6.82E-06	2.51	1.35E-04	3.05	4.56E-06	2.42
20	1.00E-06	3.64	1.03E-06	3.14	3.73E-08	6.56	1.97E-08	7.76	2.09E-05	3.12	3.75E-07	3.49
50	1.09E-07	3.67	1.13E-07	3.16	-1	-1	-1	-1	1.98E-06	3.13	3.20E-08	4.01

Females, 15 years, Sitting

Diameter	BB Secretory		BB Basal		bb Secretory		AI Tissues		LNth Tissues		Lung, Combined	
	GM	GSD	GM	GSD	GM	GSD	GM	GSD	GM	GSD	GM	GSD
0.1	3.18E-05	1.98	9.94E-06	4.60	9.63E-05	1.69	1.35E-04	1.65	8.68E-04	2.91	8.98E-05	1.64
0.2	2.01E-05	1.98	6.31E-06	4.59	5.49E-05	1.70	7.54E-05	1.66	4.92E-04	2.91	5.14E-05	1.63
0.5	1.16E-05	1.99	3.63E-06	4.61	2.95E-05	1.69	5.69E-05	1.68	3.32E-04	3.01	3.31E-05	1.68
0.8	1.25E-05	2.09	3.86E-06	4.72	2.83E-05	1.68	7.87E-05	1.70	4.18E-04	3.12	3.97E-05	1.76
1	1.58E-05	2.20	4.89E-06	4.82	3.19E-05	1.71	9.53E-05	1.70	5.01E-04	3.13	4.76E-05	1.77
2	4.36E-05	2.32	1.37E-05	4.90	5.70E-05	1.83	1.41E-04	1.71	8.11E-04	3.06	8.25E-05	1.73
5	1.31E-05	3.16	8.56E-06	3.36	1.26E-05	2.40	6.62E-05	2.03	5.41E-04	3.10	3.15E-05	2.19
8	5.45E-06	3.47	5.12E-06	3.16	3.19E-06	2.78	1.60E-05	2.44	2.35E-04	3.16	9.18E-06	2.46
10	4.09E-06	3.58	4.04E-06	3.18	1.43E-06	3.14	5.35E-06	2.82	1.40E-04	3.17	4.35E-06	2.64
20	1.07E-06	3.76	1.11E-06	3.25	1.13E-08	12.11	4.06E-09	15.97	2.09E-05	3.26	3.57E-07	3.84
50	1.08E-07	3.74	1.12E-07	3.22	-1	-1	-1	-1	1.96E-06	3.22	3.17E-08	4.10

Notes: GM = geometric mean (Sv per Bq-hr/m^3); GSD = geometric standard deviation.
Values given as "-1" serve as flags to indicate that some trials resulted in no dose (zero) to the tissue and a GM and GSD was not computed.

Table E-3--cont'd

Females, 15 years, Light Exertion

Diameter	BB Secretory		BB Basal		bb Secretory		AI Tissues		LNth Tissues		Lung, Combined	
	GM	GSD	GM	GSD	GM	GSD	GM	GSD	GM	GSD	GM	GSD
0.1	4.87E-05	1.98	1.50E-05	4.64	1.64E-04	1.72	2.95E-04	1.71	1.73E-03	3.02	1.71E-04	1.73
0.2	3.03E-05	1.99	9.42E-06	4.63	9.15E-05	1.72	1.60E-04	1.71	9.53E-04	3.01	9.55E-05	1.71
0.5	2.72E-05	2.28	8.54E-06	4.87	4.68E-05	1.71	1.15E-04	1.72	6.38E-04	3.08	6.34E-05	1.77
0.8	5.18E-05	2.59	1.64E-05	5.18	4.19E-05	1.70	1.50E-04	1.74	8.09E-04	3.15	8.14E-05	1.85
1	7.52E-05	2.63	2.39E-05	5.22	4.62E-05	1.75	1.74E-04	1.75	9.58E-04	3.14	9.85E-05	1.88
2	1.87E-04	2.65	5.97E-05	5.22	7.93E-05	2.05	2.02E-04	1.90	1.36E-03	3.12	1.56E-04	2.01
5	3.37E-05	3.92	2.30E-05	3.93	1.27E-05	3.09	5.38E-05	2.66	7.15E-04	3.53	3.69E-05	2.75
8	1.07E-05	4.23	1.05E-05	3.75	1.76E-06	4.20	5.84E-06	4.05	2.76E-04	3.74	7.71E-06	3.36
10	6.95E-06	4.27	7.05E-06	3.75	4.38E-07	6.16	8.32E-07	7.06	1.56E-04	3.81	3.36E-06	3.80
20	1.20E-06	4.28	1.24E-06	3.72	-1	-1	-1	-1	2.19E-05	3.83	3.56E-07	4.67
50	1.12E-07	4.09	1.15E-07	3.54	-1	-1	-1	-1	2.02E-06	3.62	3.28E-08	4.49

Females, 15 years, Heavy Exertion

Diameter	BB Secretory		BB Basal		bb Secretory		AI Tissues		LNth Tissues		Lung, Combined	
	GM	GSD	GM	GSD	GM	GSD	GM	GSD	GM	GSD	GM	GSD
0.1	7.31E-05	1.96	2.22E-05	4.67	2.71E-04	1.70	6.26E-04	1.65	3.40E-03	3.06	3.22E-04	1.75
0.2	4.83E-05	1.99	1.49E-05	4.65	1.49E-04	1.70	3.37E-04	1.65	1.85E-03	3.06	1.78E-04	1.73
0.5	1.09E-04	2.51	3.45E-05	5.05	7.80E-05	1.70	2.42E-04	1.67	1.37E-03	3.06	1.43E-04	1.80
0.8	2.80E-04	2.61	8.98E-05	5.13	7.59E-05	1.71	3.27E-04	1.72	1.99E-03	3.07	2.20E-04	1.96
1	4.35E-04	2.63	1.40E-04	5.14	9.24E-05	1.78	3.91E-04	1.75	2.54E-03	3.06	2.91E-04	2.03
2	1.39E-03	2.74	4.48E-04	5.25	2.60E-04	2.13	5.65E-04	1.89	5.18E-03	3.05	6.71E-04	2.28
5	3.81E-04	3.95	2.66E-04	3.90	5.71E-05	3.29	1.51E-04	2.67	5.10E-03	3.24	2.14E-04	2.84
8	1.12E-04	4.01	1.12E-04	3.58	2.57E-06	7.72	2.95E-06	9.65	2.14E-03	3.42	4.25E-05	3.64
10	6.51E-05	4.02	6.66E-05	3.56	-1	-1	-1	-1	1.21E-03	3.51	2.07E-05	4.06
20	8.38E-06	4.03	8.66E-06	3.57	-1	-1	-1	-1	1.52E-04	3.56	2.46E-06	4.34
50	5.87E-07	3.91	6.06E-07	3.45	-1	-1	-1	-1	1.06E-05	3.43	1.72E-07	4.22

Notes: GM = geometric mean (Sv per Bq-hr/m^3); GSD = geometric standard deviation.
Values given as "-1" serve as flags to indicate that some trials resulted in no dose (zero) to the tissue and a GM and GSD was not computed.

Table E-3--cont'd

Females, 18-24 years, Resting

Diameter	BB Secretory		BB Basal		bb Secretory		AI Tissues		LNth Tissues		Lung, Combined	
	GM	GSD	GM	GSD	GM	GSD	GM	GSD	GM	GSD	GM	GSD
0.1	2.65E-05	1.98	8.31E-06	4.61	7.62E-05	1.71	7.89E-05	1.71	4.53E-04	2.60	6.21E-05	1.64
0.2	1.70E-05	1.99	5.33E-06	4.60	4.39E-05	1.71	4.46E-05	1.73	2.60E-04	2.60	3.61E-05	1.64
0.5	9.48E-06	1.99	2.96E-06	4.63	2.44E-05	1.71	3.43E-05	1.75	1.77E-04	2.69	2.32E-05	1.68
0.8	8.35E-06	2.01	2.56E-06	4.68	2.45E-05	1.72	4.81E-05	1.77	2.24E-04	2.78	2.72E-05	1.75
1	9.28E-06	2.08	2.83E-06	4.76	2.81E-05	1.76	5.88E-05	1.77	2.69E-04	2.79	3.23E-05	1.77
2	2.29E-05	2.28	7.10E-06	4.93	5.14E-05	1.83	9.31E-05	1.75	4.54E-04	2.73	5.74E-05	1.73
5	8.60E-06	2.98	5.48E-06	3.30	1.22E-05	2.27	5.17E-05	1.94	3.39E-04	2.73	2.47E-05	2.08
8	3.98E-06	3.27	3.64E-06	3.06	3.49E-06	2.56	1.45E-05	2.25	1.56E-04	2.79	7.97E-06	2.29
10	3.12E-06	3.40	3.02E-06	3.08	1.76E-06	2.80	5.54E-06	2.50	9.52E-05	2.82	4.03E-06	2.41
20	1.00E-06	3.63	1.03E-06	3.15	4.19E-08	6.35	1.79E-08	7.51	1.52E-05	2.93	3.63E-07	3.52
50	1.10E-07	3.66	1.14E-07	3.17	-1	-1	-1	-1	1.44E-06	2.96	3.10E-08	4.11

Females, 18-24 years, Sitting

Diameter	BB Secretory		BB Basal		bb Secretory		AI Tissues		LNth Tissues		Lung, Combined	
	GM	GSD	GM	GSD	GM	GSD	GM	GSD	GM	GSD	GM	GSD
0.1	3.13E-05	1.99	9.76E-06	4.63	9.46E-05	1.71	1.12E-04	1.70	6.08E-04	2.64	8.12E-05	1.65
0.2	1.99E-05	1.99	6.22E-06	4.62	5.42E-05	1.72	6.29E-05	1.72	3.46E-04	2.64	4.68E-05	1.65
0.5	1.14E-05	2.00	3.56E-06	4.64	2.92E-05	1.71	4.77E-05	1.74	2.34E-04	2.72	2.99E-05	1.70
0.8	1.20E-05	2.10	3.70E-06	4.75	2.81E-05	1.70	6.59E-05	1.76	2.95E-04	2.82	3.54E-05	1.76
1	1.50E-05	2.21	4.62E-06	4.86	3.17E-05	1.73	7.99E-05	1.76	3.54E-04	2.83	4.23E-05	1.78
2	4.08E-05	2.35	1.28E-05	4.96	5.66E-05	1.83	1.19E-04	1.76	5.72E-04	2.76	7.39E-05	1.74
5	1.26E-05	3.16	8.24E-06	3.39	1.26E-05	2.37	5.59E-05	2.05	3.83E-04	2.82	2.79E-05	2.17
8	5.36E-06	3.46	5.01E-06	3.17	3.23E-06	2.75	1.36E-05	2.44	1.68E-04	2.92	8.27E-06	2.45
10	4.04E-06	3.57	3.98E-06	3.20	1.48E-06	3.10	4.61E-06	2.82	1.01E-04	2.96	4.01E-06	2.64
20	1.09E-06	3.77	1.12E-06	3.27	1.36E-08	11.39	4.17E-09	15.12	1.54E-05	3.09	3.51E-07	3.92
50	1.10E-07	3.75	1.14E-07	3.25	-1	-1	-1	-1	1.44E-06	3.06	3.11E-08	4.24

Notes: GM = geometric mean (Sv per Bq-hr/m^3); GSD = geometric standard deviation.
Values given as "-1" serve as flags to indicate that some trials resulted in no dose (zero) to the tissue and a GM and GSD was not computed.

Table E-3--cont'd

Females, 18-24 years, Light Exertion

Diameter	BB Secretory		BB Basal		bb Secretory		AI Tissues		LNth Tissues		Lung, Combined	
	GM	GSD	GM	GSD	GM	GSD	GM	GSD	GM	GSD	GM	GSD
0.1	4.91E-05	1.99	1.51E-05	4.69	1.69E-04	1.73	2.90E-04	1.75	1.38E-03	2.78	1.71E-04	1.75
0.2	3.09E-05	1.99	9.54E-06	4.67	9.49E-05	1.73	1.60E-04	1.75	7.70E-04	2.77	9.63E-05	1.74
0.5	2.66E-05	2.27	8.29E-06	4.89	4.91E-05	1.72	1.16E-04	1.76	5.23E-04	2.84	6.41E-05	1.80
0.8	4.89E-05	2.59	1.54E-05	5.22	4.44E-05	1.71	1.52E-04	1.78	6.62E-04	2.90	8.14E-05	1.87
1	7.05E-05	2.65	2.23E-05	5.27	4.88E-05	1.74	1.76E-04	1.78	7.79E-04	2.90	9.81E-05	1.89
2	1.75E-04	2.66	5.60E-05	5.27	8.08E-05	2.02	2.03E-04	1.90	1.07E-03	2.89	1.53E-04	2.00
5	3.28E-05	3.90	2.24E-05	3.96	1.31E-05	3.02	5.29E-05	2.63	5.29E-04	3.30	3.59E-05	2.74
8	1.08E-05	4.24	1.05E-05	3.79	1.90E-06	4.11	5.91E-06	3.93	2.04E-04	3.56	7.61E-06	3.37
10	7.06E-06	4.30	7.13E-06	3.79	4.95E-07	5.93	8.98E-07	6.58	1.16E-04	3.65	3.35E-06	3.83
20	1.24E-06	4.32	1.28E-06	3.77	-1	-1	-1	-1	1.63E-05	3.70	3.54E-07	4.83
50	1.15E-07	4.13	1.19E-07	3.59	-1	-1	-1	-1	1.51E-06	3.49	3.25E-08	4.66

4. Females, 18-24 years, Heavy Exertion

Diameter	BB Secretory		BB Basal		bb Secretory		AI Tissues		LNth Tissues		Lung, Combined	
	GM	GSD	GM	GSD	GM	GSD	GM	GSD	GM	GSD	GM	GSD
0.1	7.51E-05	1.96	2.27E-05	4.73	2.82E-04	1.69	6.33E-04	1.60	2.79E-03	2.76	3.26E-04	1.72
0.2	4.94E-05	1.98	1.51E-05	4.69	1.57E-04	1.69	3.45E-04	1.60	1.54E-03	2.75	1.82E-04	1.71
0.5	1.02E-04	2.52	3.24E-05	5.09	8.32E-05	1.68	2.52E-04	1.62	1.14E-03	2.77	1.45E-04	1.77
0.8	2.60E-04	2.64	8.33E-05	5.18	8.14E-05	1.69	3.40E-04	1.67	1.62E-03	2.79	2.20E-04	1.92
1	4.03E-04	2.66	1.29E-04	5.19	9.79E-05	1.75	4.06E-04	1.69	2.05E-03	2.79	2.89E-04	1.98
2	1.29E-03	2.76	4.16E-04	5.28	2.57E-04	2.08	5.82E-04	1.83	3.97E-03	2.81	6.48E-04	2.23
5	3.80E-04	3.93	2.65E-04	3.92	5.92E-05	3.15	1.62E-04	2.60	3.78E-03	3.04	2.16E-04	2.82
8	1.19E-04	4.01	1.18E-04	3.59	3.09E-06	7.19	3.90E-06	8.87	1.65E-03	3.25	4.45E-05	3.66
10	7.00E-05	4.02	7.15E-05	3.58	-1	-1	-1	-1	9.42E-04	3.35	2.17E-05	4.13
20	9.21E-06	4.05	9.48E-06	3.59	-1	-1	-1	-1	1.20E-04	3.42	2.[illegible]E-06	4.49
50	6.45E-07	3.93	6.64E-07	3.48	-1	-1	-1	-1	8.41E-06	3.30	1.81E-07	4.38

Notes: GM = geometric mean (Sv per Bq-hr/m^3); GSD = geometric standard deviation.
Values given as "-1" serve as flags to indicate that some trials resulted in no dose (zero) to the tissue and a GM and GSD was not computed.

Table E-3--cont'd

Females, 25-34 years, Resting

Diameter	BB Secretory		BB Basal		bb Secretory		AI Tissues		LNth Tissues		Lung, Combined	
	GM	GSD	GM	GSD	GM	GSD	GM	GSD	GM	GSD	GM	GSD
0.1	2.70E-05	1.98	8.46E-06	4.60	7.78E-05	1.71	7.59E-05	1.69	4.26E-04	2.61	6.18E-05	1.63
0.2	1.73E-05	1.98	5.44E-06	4.59	4.50E-05	1.71	4.31E-05	1.71	2.45E-04	2.61	3.61E-05	1.63
0.5	9.68E-06	1.99	3.03E-06	4.62	2.49E-05	1.70	3.32E-05	1.73	1.68E-04	2.69	2.31E-05	1.66
0.8	8.58E-06	2.00	2.64E-06	4.67	2.51E-05	1.71	4.65E-05	1.75	2.13E-04	2.78	2.70E-05	1.72
1	9.59E-06	2.08	2.93E-06	4.76	2.87E-05	1.75	5.67E-05	1.75	2.56E-04	2.80	3.20E-05	1.74
2	2.37E-05	2.28	7.37E-06	4.93	5.20E-05	1.82	8.88E-05	1.73	4.26E-04	2.74	5.65E-05	1.71
5	8.80E-06	2.97	5.59E-06	3.30	1.22E-05	2.26	4.78E-05	1.93	3.08E-04	2.74	2.35E-05	2.06
8	4.06E-06	3.27	3.70E-06	3.05	3.46E-06	2.56	1.31E-05	2.25	1.40E-04	2.81	7.55E-06	2.27
10	3.17E-06	3.40	3.07E-06	3.08	1.74E-06	2.81	4.96E-06	2.52	8.48E-05	2.83	3.84E-06	2.41
20	1.01E-06	3.62	1.03E-06	3.15	3.98E-08	6.52	1.50E-08	7.77	1.34E-05	2.95	3.56E-07	3.56
50	1.10E-07	3.66	1.13E-07	3.16	-1	-1	-1	-1	1.27E-06	2.96	3.06E-08	4.16

Females, 25-34 years, Sitting

Diameter	BB Secretory		BB Basal		bb Secretory		AI Tissues		LNth Tissues		Lung, Combined	
	GM	GSD	GM	GSD	GM	GSD	GM	GSD	GM	GSD	GM	GSD
0.1	3.18E-05	1.98	9.93E-06	4.61	9.66E-05	1.71	1.09E-04	1.68	5.75E-04	2.64	8.08E-05	1.64
0.2	2.03E-05	1.98	6.34E-06	4.60	5.54E-05	1.71	6.13E-05	1.69	3.28E-04	2.64	4.67E-05	1.64
0.5	1.17E-05	1.99	3.64E-06	4.63	3.00E-05	1.70	4.67E-05	1.72	2.24E-04	2.73	2.99E-05	1.68
0.8	1.24E-05	2.09	3.82E-06	4.74	2.88E-05	1.69	6.44E-05	1.74	2.83E-04	2.82	3.53E-05	1.74
1	1.55E-05	2.20	4.79E-06	4.85	3.24E-05	1.72	7.79E-05	1.74	3.39E-04	2.83	4.21E-05	1.75
2	4.21E-05	2.34	1.33E-05	4.95	5.71E-05	1.83	1.14E-04	1.74	5.39E-04	2.77	7.30E-05	1.72
5	1.28E-05	3.16	8.38E-06	3.39	1.25E-05	2.38	5.17E-05	2.04	3.46E-04	2.84	2.67E-05	2.16
8	5.44E-06	3.49	5.08E-06	3.18	3.18E-06	2.78	1.23E-05	2.45	1.50E-04	2.94	7.84E-06	2.45
10	4.09E-06	3.60	4.03E-06	3.21	1.44E-06	3.14	4.09E-06	2.83	8.94E-05	2.98	3.82E-06	2.67
20	1.09E-06	3.80	1.12E-06	3.28	1.25E-08	11.96	3.37E-09	15.97	1.35E-05	3.11	3.45E-07	4.00
50	1.10E-07	3.78	1.14E-07	3.26	-1	-1	-1	-1	1.27E-06	3.08	3.07E-08	4.32

Notes: GM = geometric mean (Sv per Bq-hr/m^3); GSD = geometric standard deviation.
Values given as "-1" serve as flags to indicate that some trials resulted in no dose (zero) to the tissue and a GM and GSD was not computed.

Table E-3--cont'd

Females, 25-34 years, Light Exertion

Diameter	BB Secretory		BB Basal		bb Secretory		AI Tissues		LNth Tissues		Lung, Combined	
	GM	GSD	GM	GSD	GM	GSD	GM	GSD	GM	GSD	GM	GSD
0.1	5.02E-05	1.98	1.54E-05	4.68	1.72E-04	1.73	2.81E-04	1.73	1.31E-03	2.77	1.69E-04	1.73
0.2	3.16E-05	1.98	9.74E-06	4.66	9.72E-05	1.73	1.55E-04	1.73	7.31E-04	2.77	9.57E-05	1.72
0.5	2.75E-05	2.26	8.57E-06	4.89	5.04E-05	1.71	1.13E-04	1.74	5.00E-04	2.84	6.39E-05	1.77
0.8	5.08E-05	2.59	1.60E-05	5.21	4.55E-05	1.69	1.48E-04	1.76	6.33E-04	2.89	8.11E-05	1.85
1	7.32E-05	2.64	2.32E-05	5.26	4.99E-05	1.73	1.70E-04	1.76	7.43E-04	2.89	9.76E-05	1.88
2	1.79E-04	2.65	5.74E-05	5.25	8.11E-05	2.02	1.93E-04	1.89	9.92E-04	2.89	1.50E-04	2.00
5	3.31E-05	3.89	2.26E-05	3.94	1.28E-05	3.03	4.82E-05	2.64	4.73E-04	3.32	3.43E-05	2.74
8	1.08E-05	4.25	1.06E-05	3.78	1.82E-06	4.19	5.17E-06	4.01	1.80E-04	3.59	7.26E-06	3.42
10	7.08E-06	4.31	7.17E-06	3.79	4.66E-07	6.13	7.63E-07	6.83	1.02E-04	3.68	3.24E-06	3.91
20	1.24E-06	4.34	1.28E-06	3.78	-1	-1	-1	-1	1.44E-05	3.73	3.49E-07	4.93
50	1.15E-07	4.15	1.19E-07	3.60	-1	-1	-1	-1	1.32E-06	3.52	3.20E-08	4.75

Females, 25-34 years, Heavy Exertion

Diameter	BB Secretory		BB Basal		bb Secretory		AI Tissues		LNth Tissues		Lung, Combined	
	GM	GSD	GM	GSD	GM	GSD	GM	GSD	GM	GSD	GM	GSD
0.1	7.59E-05	1.95	2.29E-05	4.71	2.83E-04	1.68	5.73E-04	1.56	2.51E-03	2.73	3.08E-04	1.68
0.2	5.02E-05	1.97	1.53E-05	4.68	1.57E-04	1.68	3.13E-04	1.56	1.38E-03	2.73	1.72E-04	1.67
0.5	1.06E-04	2.51	3.36E-05	5.08	8.31E-05	1.67	2.28E-04	1.58	1.03E-03	2.74	1.39E-04	1.74
0.8	2.70E-04	2.63	8.65E-05	5.17	8.11E-05	1.67	3.07E-04	1.63	1.47E-03	2.76	2.12E-04	1.90
1	4.18E-04	2.65	1.34E-04	5.18	9.76E-05	1.73	3.67E-04	1.66	1.85E-03	2.76	2.79E-04	1.97
2	1.33E-03	2.76	4.29E-04	5.28	2.58E-04	2.09	5.21E-04	1.80	3.57E-03	2.79	6.36E-04	2.25
5	3.85E-04	3.95	2.69E-04	3.91	5.76E-05	3.19	1.40E-04	2.64	3.36E-03	3.04	2.08E-04	2.85
8	1.19E-04	4.01	1.18E-04	3.58	2.86E-06	7.56	3.08E-06	9.78	1.46E-03	3.26	4.34E-05	3.72
10	7.02E-05	4.03	7.18E-05	3.58	-1	-1	-1	-1	8.32E-04	3.35	2.14E-05	4.19
20	9.20E-06	4.05	9.50E-06	3.59	-1	-1	-1	-1	1.06E-04	3.42	2.56E-06	4.54
50	6.44E-07	3.94	6.65E-07	3.47	-1	-1	-1	-1	7.41E-06	3.30	1.79E-07	4.42

Notes: GM = geometric mean (Sv per Bq-hr/m^3); GSD = geometric standard deviation.
Values given as "-1" serve as flags to indicate that some trials resulted in no dose (zero) to the tissue and a GM and GSD was not computed.

Table E-3--cont'd

Males, 15 years, Resting

Diameter	BB Secretory		BB Basal		bb Secretory		AI Tissues		LNth Tissues		Lung, Combined	
	GM	GSD	GM	GSD	GM	GSD	GM	GSD	GM	GSD	GM	GSD
0.1	2.88E-05	1.98	9.11E-06	4.58	8.79E-05	1.69	1.07E-04	1.66	7.19E-04	2.89	7.65E-05	1.63
0.2	1.83E-05	1.98	5.81E-06	4.57	5.03E-05	1.70	6.01E-05	1.67	4.09E-04	2.89	4.41E-05	1.63
0.5	1.03E-05	1.99	3.25E-06	4.59	2.76E-05	1.69	4.58E-05	1.69	2.77E-04	2.99	2.84E-05	1.67
0.8	9.71E-06	2.02	3.03E-06	4.64	2.76E-05	1.70	6.39E-05	1.71	3.49E-04	3.10	3.38E-05	1.74
1	1.14E-05	2.11	3.56E-06	4.73	3.16E-05	1.74	7.81E-05	1.71	4.22E-04	3.11	4.05E-05	1.76
2	3.05E-05	2.27	9.67E-06	4.85	5.80E-05	1.82	1.23E-04	1.71	7.12E-04	3.04	7.22E-05	1.72
5	1.06E-05	3.04	6.90E-06	3.28	1.34E-05	2.31	6.62E-05	1.94	5.25E-04	3.02	3.07E-05	2.11
8	4.73E-06	3.32	4.40E-06	3.05	3.69E-06	2.61	1.80E-05	2.27	2.39E-04	3.05	9.63E-06	2.33
10	3.65E-06	3.43	3.58E-06	3.08	1.79E-06	2.87	6.67E-06	2.55	1.44E-04	3.05	4.74E-06	2.45
20	1.09E-06	3.64	1.12E-06	3.15	2.98E-08	7.48	1.46E-08	8.86	2.25E-05	3.12	3.93E-07	3.56
50	1.15E-07	3.66	1.19E-07	3.16	-1	-1	-1	-1	2.13E-06	3.12	3.40E-08	4.02

Males, 15 years, Sitting

Diameter	BB Secretory		BB Basal		bb Secretory		AI Tissues		LNth Tissues		Lung, Combined	
	GM	GSD	GM	GSD	GM	GSD	GM	GSD	GM	GSD	GM	GSD
0.1	3.35E-05	1.98	1.05E-05	4.62	1.07E-04	1.70	1.41E-04	1.67	9.23E-04	2.92	9.64E-05	1.65
0.2	2.11E-05	1.99	6.61E-06	4.61	6.09E-05	1.70	7.84E-05	1.68	5.19E-04	2.91	5.49E-05	1.64
0.5	1.24E-05	2.00	3.88E-06	4.63	3.25E-05	1.70	5.86E-05	1.70	3.47E-04	3.01	3.50E-05	1.69
0.8	1.44E-05	2.14	4.49E-06	4.75	3.11E-05	1.69	8.07E-05	1.72	4.36E-04	3.12	4.21E-05	1.75
1	1.90E-05	2.24	5.91E-06	4.85	3.50E-05	1.72	9.77E-05	1.72	5.25E-04	3.13	5.08E-05	1.76
2	5.38E-05	2.34	1.70E-05	4.92	6.33E-05	1.84	1.44E-04	1.74	8.57E-04	3.05	8.94E-05	1.73
5	1.55E-05	3.22	1.02E-05	3.41	1.36E-05	2.43	6.65E-05	2.08	5.79E-04	3.10	3.31E-05	2.21
8	6.28E-06	3.53	5.93E-06	3.20	3.32E-06	2.84	1.57E-05	2.50	2.53E-04	3.16	9.53E-06	2.50
10	4.65E-06	3.63	4.60E-06	3.22	1.44E-06	3.23	5.06E-06	2.92	1.50E-04	3.19	4.50E-06	2.70
20	1.16E-06	3.80	1.19E-06	3.29	-1	-1	-1	-1	2.25E-05	3.28	3.77E-07	3.91
50	1.15E-07	3.77	1.19E-07	3.26	-1	-1	-1	-1	2.11E-06	3.23	3.39E-08	4.11

Notes: GM = geometric mean (Sv per Bq-hr/m^3); GSD = geometric standard deviation.
Values given as "-1" serve as flags to indicate that some trials resulted in no dose (zero) to the tissue and a GM and GSD was not computed.

Table E-3--cont'd

Males, 15 years, Light Exertion

Diameter	BB Secretory		BB Basal		bb Secretory		AI Tissues		LNth Tissues		Lung, Combined	
	GM	GSD	GM	GSD	GM	GSD	GM	GSD	GM	GSD	GM	GSD
0.1	5.12E-05	1.99	1.59E-05	4.67	1.85E-04	1.73	3.22E-04	1.73	1.89E-03	3.04	1.88E-04	1.74
0.2	3.19E-05	1.99	9.95E-06	4.65	1.03E-04	1.73	1.74E-04	1.73	1.04E-03	3.03	1.04E-04	1.73
0.5	3.17E-05	2.34	1.00E-05	4.94	5.21E-05	1.72	1.24E-04	1.73	6.95E-04	3.10	6.99E-05	1.78
0.8	6.37E-05	2.62	2.03E-05	5.22	4.67E-05	1.71	1.60E-04	1.76	8.85E-04	3.15	9.05E-05	1.86
1	9.29E-05	2.65	2.97E-05	5.24	5.16E-05	1.76	1.85E-04	1.77	1.05E-03	3.14	1.10E-04	1.89
2	2.27E-04	2.66	7.30E-05	5.25	8.93E-05	2.08	2.11E-04	1.93	1.48E-03	3.13	1.74E-04	2.04
5	3.92E-05	3.96	2.69E-05	3.97	1.36E-05	3.16	5.32E-05	2.72	7.80E-04	3.55	3.92E-05	2.81
8	1.21E-05	4.27	1.18E-05	3.79	1.71E-06	4.44	5.17E-06	4.34	2.99E-04	3.77	7.96E-06	3.45
10	7.69E-06	4.31	7.79E-06	3.79	3.87E-07	6.86	6.52E-07	8.09	1.68E-04	3.84	3.48E-06	3.90
20	1.29E-06	4.32	1.33E-06	3.76	-1	-1	-1	-1	2.37E-05	3.85	3.81E-07	4.70
50	1.19E-07	4.12	1.23E-07	3.57	-1	-1	-1	-1	2.19E-06	3.64	3.50E-08	4.50

4. Males, 15 years, Heavy Exertion

Diameter	BB Secretory		BB Basal		bb Secretory		AI Tissues		LNth Tissues		Lung, Combined	
	GM	GSD	GM	GSD	GM	GSD	GM	GSD	GM	GSD	GM	GSD
0.1	7.73E-05	1.96	2.35E-05	4.70	3.08E-04	1.70	7.03E-04	1.65	3.80E-03	3.08	3.60E-04	1.76
0.2	5.23E-05	2.01	1.61E-05	4.68	1.69E-04	1.70	3.77E-04	1.66	2.07E-03	3.07	1.99E-04	1.74
0.5	1.35E-04	2.54	4.31E-05	5.09	8.79E-05	1.70	2.70E-04	1.68	1.55E-03	3.07	1.64E-04	1.82
0.8	3.51E-04	2.62	1.13E-04	5.15	8.60E-05	1.72	3.62E-04	1.73	2.27E-03	3.07	2.55E-04	1.98
1	5.44E-04	2.64	1.76E-04	5.16	1.06E-04	1.79	4.31E-04	1.76	2.92E-03	3.06	3.39E-04	2.05
2	1.72E-03	2.74	5.57E-04	5.27	3.03E-04	2.15	6.14E-04	1.90	6.01E-03	3.06	7.87E-04	2.32
5	4.51E-04	3.94	3.15E-04	3.90	6.03E-05	3.39	1.46E-04	2.78	5.80E-03	3.25	2.36E-04	2.92
8	1.28E-04	4.02	1.26E-04	3.59	2.13E-06	9.00	2.10E-06	11.64	2.40E-03	3.45	4.61E-05	3.74
10	7.28E-05	4.03	7.43E-05	3.58	-1	-1	-1	-1	1.36E-03	3.53	2.27E-05	4.12
20	9.25E-06	4.04	9.52E-06	3.58	-1	-1	-1	-1	1.70E-04	3.58	2.72E-06	4.35
50	6.46E-07	3.92	6.65E-07	3.46	-1	-1	-1	-1	1.18E-05	3.45	1.90E-07	4.23

Notes: GM = geometric mean (Sv per Bq-hr/m^3); GSD = geometric standard deviation.
Values given as "-1" serve as flags to indicate that some trials resulted in no dose (zero) to the tissue and a GM and GSD was not computed.

Table E-3--cont'd

Males, 18-24 years, Resting

Diameter	BB Secretory		BB Basal		bb Secretory		AI Tissues		LNth Tissues		Lung, Combined	
	GM	GSD	GM	GSD	GM	GSD	GM	GSD	GM	GSD	GM	GSD
0.1	2.92E-05	1.97	9.10E-06	4.59	9.56E-05	1.69	9.41E-05	1.64	5.01E-04	2.63	7.45E-05	1.62
0.2	1.87E-05	1.97	5.86E-06	4.58	5.54E-05	1.70	5.37E-05	1.65	2.89E-04	2.63	4.35E-05	1.62
0.5	1.06E-05	1.97	3.29E-06	4.61	3.10E-05	1.69	4.15E-05	1.68	2.01E-04	2.71	2.82E-05	1.65
0.8	9.84E-06	2.00	3.00E-06	4.68	3.18E-05	1.71	5.78E-05	1.70	2.58E-04	2.80	3.34E-05	1.71
1	1.14E-05	2.08	3.47E-06	4.77	3.67E-05	1.74	7.04E-05	1.70	3.11E-04	2.81	3.98E-05	1.72
2	2.96E-05	2.26	9.20E-06	4.89	6.61E-05	1.82	1.09E-04	1.69	5.10E-04	2.75	7.00E-05	1.69
5	1.08E-05	2.98	6.90E-06	3.29	1.51E-05	2.26	5.57E-05	1.91	3.54E-04	2.77	2.80E-05	2.04
8	4.95E-06	3.30	4.54E-06	3.06	4.18E-06	2.58	1.47E-05	2.26	1.58E-04	2.83	8.78E-06	2.28
10	3.85E-06	3.43	3.74E-06	3.08	2.06E-06	2.85	5.45E-06	2.54	9.52E-05	2.86	4.43E-06	2.44
20	1.18E-06	3.66	1.21E-06	3.16	3.97E-08	7.13	1.40E-08	8.36	1.49E-05	2.98	4.07E-07	3.65
50	1.26E-07	3.68	1.30E-07	3.17	-1	-1	-1	-1	1.40E-06	2.99	3.49E-08	4.21

Males, 18-24 years, Sitting

Diameter	BB Secretory		BB Basal		bb Secretory		AI Tissues		LNth Tissues		Lung, Combined	
	GM	GSD	GM	GSD	GM	GSD	GM	GSD	GM	GSD	GM	GSD
0.1	3.43E-05	1.96	1.07E-05	4.61	1.17E-04	1.70	1.29E-04	1.63	6.60E-04	2.65	9.53E-05	1.63
0.2	2.18E-05	1.97	6.81E-06	4.59	6.74E-05	1.70	7.29E-05	1.65	3.77E-04	2.65	5.51E-05	1.63
0.5	1.29E-05	1.98	3.99E-06	4.62	3.67E-05	1.69	5.55E-05	1.67	2.59E-04	2.74	3.55E-05	1.66
0.8	1.46E-05	2.10	4.48E-06	4.75	3.58E-05	1.68	7.65E-05	1.69	3.31E-04	2.82	4.24E-05	1.71
1	1.89E-05	2.21	5.82E-06	4.85	4.06E-05	1.71	9.23E-05	1.69	3.98E-04	2.83	5.09E-05	1.72
2	5.25E-05	2.32	1.65E-05	4.92	7.15E-05	1.82	1.34E-04	1.70	6.28E-04	2.77	8.83E-05	1.70
5	1.57E-05	3.16	1.03E-05	3.38	1.51E-05	2.36	5.85E-05	2.03	3.92E-04	2.86	3.11E-05	2.14
8	6.58E-06	3.50	6.20E-06	3.19	3.74E-06	2.79	1.34E-05	2.47	1.68E-04	2.97	8.97E-06	2.46
10	4.92E-06	3.61	4.87E-06	3.21	1.66E-06	3.18	4.35E-06	2.89	9.96E-05	3.02	4.35E-06	2.69
20	1.26E-06	3.80	1.30E-06	3.29	-1.00E+00	-1.00	-1.00E+00	-1.00	1.49E-05	3.15	3.92E-07	4.05
50	1.26E-07	3.77	1.30E-07	3.26	-1	-1	-1	-1	1.40E-06	3.10	3.49E-08	4.33

Notes: GM = geometric mean (Sv per Bq-hr/m^3); GSD = geometric standard deviation.
Values given as "-1" serve as flags to indicate that some trials resulted in no dose (zero) to the tissue and a GM and GSD was not computed.

Table E-3--cont'd

Males, 18-24 years, Light Exertion

Diameter	BB Secretory		BB Basal		bb Secretory		AI Tissues		LNth Tissues		Lung, Combined	
	GM	GSD	GM	GSD	GM	GSD	GM	GSD	GM	GSD	GM	GSD
0.1	5.37E-05	1.96	1.64E-05	4.67	2.05E-04	1.72	3.08E-04	1.70	1.42E-03	2.77	1.91E-04	1.71
0.2	3.38E-05	1.97	1.04E-05	4.65	1.16E-04	1.72	1.70E-04	1.71	7.95E-04	2.76	1.08E-04	1.71
0.5	3.21E-05	2.30	1.00E-05	4.91	5.99E-05	1.70	1.24E-04	1.72	5.46E-04	2.83	7.25E-05	1.75
0.8	6.27E-05	2.59	1.98E-05	5.20	5.46E-05	1.68	1.61E-04	1.74	6.97E-04	2.88	9.31E-05	1.83
1	9.10E-05	2.63	2.89E-05	5.23	6.03E-05	1.72	1.86E-04	1.75	8.20E-04	2.87	1.13E-04	1.85
2	2.23E-04	2.65	7.14E-05	5.24	9.84E-05	2.02	2.09E-04	1.89	1.10E-03	2.89	1.76E-04	2.01
5	4.02E-05	3.93	2.75E-05	3.98	1.49E-05	3.05	5.08E-05	2.68	5.23E-04	3.36	3.87E-05	2.78
8	1.29E-05	4.29	1.26E-05	3.83	1.96E-06	4.34	5.14E-06	4.18	1.98E-04	3.65	8.10E-06	3.49
10	8.29E-06	4.35	8.42E-06	3.84	4.71E-07	6.60	7.16E-07	7.29	1.12E-04	3.74	3.62E-06	4.00
20	1.42E-06	4.38	1.46E-06	3.83	-1	-1	-1	-1	1.58E-05	3.78	3.95E-07	4.98
50	1.31E-07	4.17	1.36E-07	3.63	-1	-1	-1	-1	1.46E-06	3.56	3.63E-08	4.78

4. Males, 18-24 years, Heavy Exertion

Diameter	BB Secretory		BB Basal		bb Secretory		AI Tissues		LNth Tissues		Lung, Combined	
	GM	GSD	GM	GSD	GM	GSD	GM	GSD	GM	GSD	GM	GSD
0.1	8.26E-05	1.94	2.48E-05	4.72	3.42E-04	1.68	6.58E-04	1.59	2.85E-03	2.76	3.59E-04	1.70
0.2	5.55E-05	1.98	1.69E-05	4.68	1.91E-04	1.68	3.59E-04	1.60	1.57E-03	2.76	2.01E-04	1.68
0.5	1.31E-04	2.52	4.16E-05	5.07	1.01E-04	1.67	2.63E-04	1.62	1.18E-03	2.77	1.65E-04	1.76
0.8	3.37E-04	2.61	1.08E-04	5.14	9.94E-05	1.67	3.53E-04	1.67	1.69E-03	2.79	2.54E-04	1.92
1	5.21E-04	2.63	1.68E-04	5.15	1.20E-04	1.74	4.20E-04	1.69	2.14E-03	2.78	3.34E-04	2.00
2	1.65E-03	2.74	5.33E-04	5.26	3.10E-04	2.08	5.90E-04	1.84	4.09E-03	2.81	7.59E-04	2.29
5	4.68E-04	3.97	3.27E-04	3.93	6.39E-05	3.25	1.49E-04	2.70	3.78E-03	3.07	2.40E-04	2.92
8	1.42E-04	4.05	1.41E-04	3.62	2.73E-06	8.42	3.01E-06	9.94	1.64E-03	3.31	4.99E-05	3.81
10	8.28E-05	4.06	8.48E-05	3.62	-1	-1	-1	-1	9.41E-04	3.40	2.48E-05	4.27
20	1.08E-05	4.08	1.12E-05	3.63	-1	-1	-1	-1	1.20E-04	3.46	2.59E-06	4.60
50	7.57E-07	3.96	7.82E-07	3.50	-1	-1	-1	-1	8.42E-06	3.33	2.09E-07	4.47

Notes: GM = geometric mean (Sv per Bq-hr/m^3); GSD = geometric standard deviation.
Values given as "-1" serve as flags to indicate that some trials resulted in no dose (zero) to the tissue and a GM and GSD was not computed.

Table E-3--cont'd

Males, 25-34 years, Resting

Diameter	BB Secretory		BB Basal		bb Secretory		AI Tissues		LNth Tissues		Lung, Combined	
	GM	GSD	GM	GSD	GM	GSD	GM	GSD	GM	GSD	GM	GSD
0.1	2.95E-05	1.96	9.19E-06	4.60	9.71E-05	1.69	8.91E-05	1.62	4.65E-04	2.63	7.33E-05	1.61
0.2	1.90E-05	1.97	5.93E-06	4.59	5.64E-05	1.70	5.10E-05	1.64	2.69E-04	2.63	4.30E-05	1.61
0.5	1.08E-05	1.97	3.34E-06	4.62	3.16E-05	1.69	3.95E-05	1.66	1.88E-04	2.72	2.77E-05	1.64
0.8	1.01E-05	2.00	3.07E-06	4.69	3.22E-05	1.70	5.50E-05	1.68	2.41E-04	2.80	3.27E-05	1.69
1	1.18E-05	2.08	3.57E-06	4.78	3.71E-05	1.73	6.68E-05	1.68	2.91E-04	2.81	3.89E-05	1.70
2	3.06E-05	2.26	9.50E-06	4.90	6.63E-05	1.81	1.02E-04	1.67	4.72E-04	2.75	6.82E-05	1.67
5	1.11E-05	2.98	7.05E-06	3.29	1.50E-05	2.25	5.08E-05	1.91	3.18E-04	2.78	2.66E-05	2.03
8	5.04E-06	3.30	4.63E-06	3.06	4.13E-06	2.58	1.32E-05	2.26	1.40E-04	2.84	8.29E-06	2.28
10	3.91E-06	3.43	3.80E-06	3.09	2.04E-06	2.86	4.83E-06	2.55	8.42E-05	2.86	4.21E-06	2.45
20	1.18E-06	3.67	1.22E-06	3.17	3.76E-08	7.33	1.17E-08	8.59	1.31E-05	2.99	4.01E-07	3.70
50	1.26E-07	3.69	1.30E-07	3.18	-1	-1	-1	-1	1.23E-06	2.99	3.45E-08	4.26

Males, 25-34 years, Sitting

Diameter	BB Secretory		BB Basal		bb Secretory		AI Tissues		LNth Tissues		Lung, Combined	
	GM	GSD	GM	GSD	GM	GSD	GM	GSD	GM	GSD	GM	GSD
0.1	3.48E-05	1.96	1.08E-05	4.61	1.19E-04	1.69	1.23E-04	1.62	6.15E-04	2.66	9.39E-05	1.62
0.2	2.22E-05	1.96	6.90E-06	4.60	6.87E-05	1.70	6.95E-05	1.64	3.52E-04	2.66	5.45E-05	1.62
0.5	1.31E-05	1.98	4.06E-06	4.63	3.74E-05	1.68	5.31E-05	1.66	2.44E-04	2.74	3.50E-05	1.65
0.8	1.50E-05	2.10	4.61E-06	4.76	3.64E-05	1.67	7.31E-05	1.68	3.12E-04	2.83	4.17E-05	1.70
1	1.96E-05	2.21	6.01E-06	4.86	4.12E-05	1.70	8.80E-05	1.68	3.75E-04	2.83	5.00E-05	1.70
2	5.42E-05	2.32	1.71E-05	4.92	7.19E-05	1.82	1.26E-04	1.69	5.82E-04	2.77	8.63E-05	1.69
5	1.61E-05	3.17	1.05E-05	3.39	1.51E-05	2.36	5.33E-05	2.03	3.53E-04	2.87	2.96E-05	2.13
8	6.69E-06	3.50	6.30E-06	3.19	3.69E-06	2.80	1.20E-05	2.47	1.49E-04	2.98	8.49E-06	2.46
10	4.99E-06	3.62	4.94E-06	3.22	1.63E-06	3.21	3.83E-06	2.90	8.80E-05	3.03	4.15E-06	2.72
20	1.27E-06	3.81	1.31E-06	3.30	-1	-1	-1	-1	1.31E-05	3.15	3.87E-07	4.10
50	1.26E-07	3.78	1.30E-07	3.27	-1	-1	-1	-1	1.23E-06	3.11	3.45E-08	4.38

Notes: GM = geometric mean (Sv per Bq-hr/m^3); GSD = geometric standard deviation.
Values given as "-1" serve as flags to indicate that some trials resulted in no dose (zero) to the tissue and a GM and GSD was not computed.

Table E-3--cont'd

Males, 25-34 years, Light Exertion

Diameter	BB Secretory		BB Basal		bb Secretory		AI Tissues		LNth Tissues		Lung, Combined	
	GM	GSD	GM	GSD	GM	GSD	GM	GSD	GM	GSD	GM	GSD
0.1	5.47E-05	1.96	1.66E-05	4.68	2.09E-04	1.71	2.94E-04	1.69	1.34E-03	2.78	1.88E-04	1.70
0.2	3.45E-05	1.97	1.06E-05	4.66	1.18E-04	1.71	1.63E-04	1.70	7.49E-04	2.77	1.06E-04	1.69
0.5	3.32E-05	2.30	1.03E-05	4.93	6.13E-05	1.69	1.19E-04	1.71	5.18E-04	2.84	7.18E-05	1.74
0.8	6.50E-05	2.59	2.05E-05	5.21	5.58E-05	1.67	1.54E-04	1.73	6.60E-04	2.88	9.22E-05	1.82
1	9.42E-05	2.62	2.99E-05	5.24	6.15E-05	1.71	1.77E-04	1.74	7.74E-04	2.88	1.11E-04	1.85
2	2.28E-04	2.65	7.31E-05	5.24	9.89E-05	2.02	1.97E-04	1.88	1.02E-03	2.90	1.73E-04	2.02
5	4.08E-05	3.95	2.79E-05	3.99	1.46E-05	3.06	4.60E-05	2.69	4.67E-04	3.38	3.71E-05	2.80
8	1.30E-05	4.31	1.27E-05	3.85	1.90E-06	4.40	4.49E-06	4.24	1.75E-04	3.67	7.78E-06	3.54
10	8.37E-06	4.37	8.50E-06	3.86	4.48E-07	6.78	6.07E-07	7.49	9.86E-05	3.76	3.52E-06	4.07
20	1.42E-06	4.40	1.47E-06	3.85	-1	-1	-1	-1	1.39E-05	3.80	3.91E-07	5.06
50	1.32E-07	4.19	1.36E-07	3.65	-1	-1	-1	-1	1.28E-06	3.58	3.60E-08	4.85

Males, 25-34 years, Heavy Exertion

Diameter	BB Secretory		BB Basal		bb Secretory		AI Tissues		LNth Tissues		Lung, Combined	
	GM	GSD	GM	GSD	GM	GSD	GM	GSD	GM	GSD	GM	GSD
0.1	8.35E-05	1.93	2.50E-05	4.72	3.44E-04	1.67	6.00E-04	1.56	2.58E-03	2.75	3.41E-04	1.67
0.2	5.64E-05	1.97	1.71E-05	4.68	1.92E-04	1.67	3.28E-04	1.57	1.43E-03	2.75	1.92E-04	1.65
0.5	1.36E-04	2.52	4.31E-05	5.07	1.01E-04	1.66	2.40E-04	1.59	1.08E-03	2.75	1.60E-04	1.73
0.8	3.50E-04	2.61	1.12E-04	5.14	9.97E-05	1.66	3.22E-04	1.64	1.54E-03	2.77	2.47E-04	1.92
1	5.40E-04	2.63	1.73E-04	5.15	1.21E-04	1.72	3.83E-04	1.66	1.95E-03	2.76	3.26E-04	2.00
2	1.70E-03	2.75	5.49E-04	5.27	3.12E-04	2.09	5.34E-04	1.81	3.70E-03	2.80	7.49E-04	2.31
5	4.78E-04	3.97	3.34E-04	3.93	6.30E-05	3.27	1.30E-04	2.74	3.37E-03	3.07	2.33E-04	2.96
8	1.44E-04	4.05	1.43E-04	3.63	2.56E-06	8.77	2.41E-06	10.71	1.46E-03	3.31	4.93E-05	3.87
10	8.39E-05	4.07	8.59E-05	3.62	-1	-1	-1	-1	8.34E-04	3.41	2.47E-05	4.34
20	1.09E-05	4.09	1.13E-05	3.64	-1	-1	-1	-1	1.07E-04	3.47	2.99E-06	4.66
50	7.65E-07	3.96	7.90E-07	3.51	-1	-1	-1	-1	7.46E-06	3.34	2.09E-07	4.53

Notes: GM = geometric mean (Sv per Bq-hr/m^3); GSD = geometric standard deviation.
Values given as "-1" serve as flags to indicate that some trials resulted in no dose (zero) to the tissue and a GM and GSD was not computed.

REFERENCES

Abramowitz, M.; Stegun, I.A. Handbook of Mathematical Functions with Formulas, Graphs, and Mathematical Tables. Applied Mathematics Series 55. National Bureau of Statistics; 1964.

ACGIH (American Conference of Governmental Industrial Hygienists). Particle size-selective sampling in the workplace. Report of the ACGIH Technical Committee on Air Sampling Procedures. Cincinnati, OH; 1985.

Altman, P.L.; Dittmer, D.S., eds. Biological Handbooks: Metabolism. Bethesda, Maryland: Federation of American Societies for Experimental Biology ; 1968.

Altman, P.L.; Dittmer, D.S., eds. Biological Handbooks: Respiration and Circulation. Bethesda, MD: Federation of American Societies for Experimental Biology; 1971.

Andres, T.H. Statistical sampling strategies. In: Proceedings of an NEA Workshop on Uncertainty Analysis for Performance Assessments of Radioactive Waste Disposal Systems, pp. 70-84. Paris, France: OECD (Organization for Economic Cooperation and Development); 1987.

Armbruster, L.; Breuer, H. Investigations into defining inhalable dust. In: Walton, W. H; Critchlow, A.; Coppocl, S., eds. Inhaled Particles V. Proceedings of an International Symposium Organized by the British Occupational Hygiene Society. Ann. Occup. Hyg. 26:21-32; 1982.

Ayers, M.M.; Jeffery, P.K. Proliferation and differentiation in mammalian airway epithelium. J. Eur. Respir. 1:58-80; 1988.

Bailey, M.R.; Roy, M. Clearance of particles from the respiratory tract. Annex E. In: ICRP Publication 66 Human Respiratory Tract Model for Radiological Protection. Annals of the ICRP. 24(1-3):301-413; 1994.

Bair, W.J.; Metivier, H.; Park, J. F. Comparison of early mortality in baboons and dogs after inhalation of $^{239}PuO_2$. Radiat. Res. 82:588-610; 1980.

Bair, W.J.; Park, J.F.; Dagle, G.E.; James, A.C. Overview of biological consequences of exposure to plutonium and higher actinides. Radiat. Protect. Dosim. 26:125-135; 1989.

Baldwin, F.; Hovey, A.; McEwen, T.; O'Connor, R.; Unruh, H.; Bowden, D.H. Surface to nuclear distances in human bronchial epithelium: Relationships to penetration by Rn daughters. Health Phys. 60(2):155-162; 1991.

Bartels, H. The human lungs. In: Reznik-Schuller, H. M., ed. Vol. 1, Comparative Respiratory Tract Carcinogenesis, pp. 19-54. Boca Raton, Florida: CRC Press Inc; 1983.

Bateman, H. The solution of a system of differential equations occurring in the theory of radioactive transformations. Proc. Camb. Phil. Soc. 15:423-427; 1910.

Birchall, A. A microcomputer algorithm for solving compartmental models involving radionuclide transformations. Health Phys. 50(3):389-397; 1986.

Birchall, A.; James, A.C. Uncertainty analysis of the effective dose for unit exposure from radon progeny and its implications for ICRP risk-weighting factors. Radiat. Protect. Dosim. 53(1-4):133-140; 1994.

Bo, G. Standards of reference in medicine. In: Normal Values for Respiratory Function in Man. Proceedings of the International Symposium of the Societas Europaea Physiologiae Clinicae Respiratoriae, pp. 5-14. Alghero, Italy : Panminerva Medica; 1969.

Bouleau, N. Numerical Methods for Stochastics Processes. New York: Wiley; 1994.

Bowden, D.H.; Baldwin, F. Measurement of the Thickness of the Bronchial Epithelium. Research Report of the Atomic Energy Control Board, pp. 1-21. Ottawa, Canada; 1989.

Brooks, G.A.; Fahey, T.D. Exercise Physiology: Human Bioenergetics and Its Applications. New York: Wiley; 1984.

Bruce, R.A. Normal values for Vo_2 and the Vo_2-HR relationship. Am. Rev. Respir. Dis. 129:S41-S43; 1984.

Camner, P.; Bakke, B. Nose or mouth breathing. Environ. Res. 21:394-398; 1980.

Caretti, D.M.; Szlyk, P.C.; Sils, I.V. Effects of exercise modality on patterns of ventilation and respiratory timing. Respir. Physiol. 90:201-211; 1992.

Carter, L.L.; Cashwell, E.D. Particle-Transport Simulation with the Monte Carlo Method. Report TID-26607. Available from the National Technical Information Service. Springfield, Virginia; 1975.

Carter, R.F.; Stewart, K. On the oxide formed by the combustion of plutonium and uranium. In: Walton, W. H., ed. Inhaled Particles III. Vol. 2, pp. 819-838. Oxford, United Kingdom: Pergamon Press; 1971.

Cashwell, E.D.; Everett, C.J. A Practical Manual on the Monte Carlo Method for Random Walk Problems. New York: Pergamon Press; 1959.

Chadha, T.S.; Birch, S.; Sackner, M.A. Oronasal distribution of ventilation during exercise in normal subjects and patients with asthma and rhinitis. Chest. 92:1037-1041; 1987.

Chamberlain, A.C. Radioactive Aerosols Cambridge Environmental Chemistry Series 3. Cambridge: Cambridge University Press; 1991.

Chan, T.L.; Lippmann, M. Experimental measurements and empirical modelling of the regional deposition of inhaled particles in humans. Am. Ind. Hyg. Assoc. J. 41:399-409; 1980.

ChemRisk (A Division of McLaren/Hart Environmental Engineering). Project Task 6 Report: Exposure Pathway Identification and Transport Modeling. Prepared by ChemRisk for the Colorado Department of Public Health and Environment, 4300 Cherry Creek Drive South, Denver, Colorado; 1994.

Chung, I.P.; Phalen, R.F.; Dunn-Rankin, D. Predicted aerosol aspiration efficiency for infants, children, and adults. Appl. Occup. Environ. Hyg. 8:639-644; 1993.

Clark, J.M.; Hagerman, F.C.; Gelfand, R. Breathing patterns during submaximal and maximal exercise in elite oarsmen. J. Appl. Physiol.: Respirat. Environ. Exercise Physiol. 55:440-446; 1983.

Conover, W.J. Practical Nonparameteric Statistics, 2nd ed. New York: Wiley; 1980.

Cook, C.D.; Cherry, R.B.; O'Brien, D.; Karlberg, P.; Smith, C.A. Studies of respiratory physiology in the newborn infant. I. Observations on normal premature and full-term infants. J. Clin. Invest. 34:975-982; 1955.

Cooper, D.M.; Weiler-Ravell, D. Gas exchange response to exercise in children. Am. Rev. Respir. Dis. 129:S47-S48; 1984.

Cotes, J.E. Lung Function Assessment and Application in Medicine, Fourth Edition. Oxford: Blackwell Scientific Publications; 1979.

Crick, M.J.; Hill, M.D.; Charles, D. The role of sensitivity analysis in assessing uncertainty. In: Proceedings of an NEA Workshop on Uncertainty Analysis for Performance Assessments of Radioactive Waste Disposal Systems, pp. 116-130. Paris, France: OECD (Organization for Economic Cooperation and Development); 1987.

Cuddihy, R.G. Mathematical models for predicting clearance of inhaled radioactive substances. In: Smith, H. and Gerber, G., eds. Lung Modelling for Inhalation of Radioactive Materials, pp. 167-179. Report EUR 9384. Luxembourg: Commission of the European Communities; 1984.

Cuddihy, R.G. Respiratory tract retention of inhaled particles in experimental animals. In: Inhalation Toxicology Research Institute Annual Report 1975-1976, pp. 137-142. Report LF-56. Lovelace Foundation, Albuquerque, New Mexico. Available from the National Technical Information Service, Springfield, Virginia; 1976.

Cuddihy, R.G.; Boecker, B.B.; Griffith, W.C. Modelling the deposition and clearance of inhaled radionuclides. In: Biological Implications of Radionuclides Released from Nuclear Industries, Vol. 2, pp. 77-90. Proceedings of an International Atomic Energy Agency Conference. Vienna: International Atomic Energy Agency; 1979.

Cuddihy, R.G.; Yeh, H.C. Respiratory tract clearance of particles and substances dissociated from particles. In: Mohr, U., ed. Inhalation Toxicology: The Design and Interpretation of Inhalation Studies and Their Use in Risk Assessment, pp. 169-193. Berlin: Springer-Verlag; 1988.

D'Agostino, R.B. An omnibus test of normality for moderate and large size samples. Biometrika. 58:341-348; 1971.

Dab, I. Spirometry at adolescence. Bull. Eur. Physiopathol. Respir. 18:21-29; 1982.

DeGroot, M.H. Optimal Statistical Decision. New York: McGraw-Hill; 1970.

Desmet, G., ed. Reliability of Radioactive Transfer Models. New York: Elsevier Applied Science; 1988.

DuBois, E.F. Basal Metabolism in Health and Disease (Third Edition). Philadelphia: Lea & Febiger; 1936.

Eckerman, K.F.; Wolbarst, A.B.; Richardson, A. Limiting Values of Radionuclide Intake and Air Concentration and Dose Conversion Factors for Inhalation, Submersion, and Ingestion. Federal Guidance Report No. 11, EPA 520/1-88-020. United States Environmental Protection Agency; 1988.

Egan, M.; Nixon, W. A model of aerosol deposition in the lung for use in inhalation dose assessments. Radiat. Protect. Dosim. 11:5-17; 1985.

Egan, M.J.; Nixon, W.; Robinson, N.I.; James, A.C.; Phalen, R.F. Inhaled aerosol transport and deposition calculations for the ICRP task group. J. Aerosol Sci. 20:1305-1308; 1989.

Eidson, A.F.; Mewhinney, J.A. In vitro dissolution of respirable aerosols of industrial uranium and plutonium mixed-oxide nuclear fuels. Health Phys. 45(6):1023-1037; 1983.

Elder, J.C.; Gonzales, M.; Ettinger, H.J. Plutonium aerosol size characteristics. Health Phys. 27:45-53; 1974.

Engel, S. Form, lage und lageveranderungen des bronchialbaumes im kindesalter. Arch. Kinderhielk. 60:267-288; 1913.

Evans, M.J.; Shami, S.G.; Cabral-Anderson, L.J.; Dekkar, N.P. Role of nonciliated cells in the renewal of the bronchial epithelium of rats exposed to NO_2. Am. J. Pathol. 123:126-133; 1986.

Filley, G.F.; Gregoire, F.; Wright, G.W. Alveolar and arterial oxygen tensions and the significance of the alveolar-arterial oxygen tension difference in normal men. J. Clin. Invest. 33:517-529; 1954.

Filliben, J.J. The probability plot correlation coefficient test for normality. Technometrics. 17:111-117; 1975.

Flandrois, R.; Grandmontagne, M.; Mayet, M.; Favier, R.; Frutoso, J. Maximum oxygen uptake in french children in relation to age, sex, and physical training. J. Physiol. (Paris). 78:186-194; 1982.

Fleisch, A. Le metabolisme basal standard et sa determination au moyer du metabocalculator. Helv. Med. Acta. 18:23; 1951.

Garn, S.M.; Leonard, W.R.; Hawthorne, V.M. Three limitations of the body mass index. Am. J. Clin. Nutr. 44:996-997; 1986.

Garten, C.T. Statistical uncertainties in predicting plutonium dose to lung and bone from contaminated soils. Health Phys. 39:99-102; 1980.

Gastineau, R.M.; Walsh, P.J.; Underwood, N. Thickness of bronchial epithelium with relation to exposure to radon. Health Phys. 23:857-860; 1972.

Gaultier, C. Developpement des Volumes Pulmonaires Pendant les 36 Premiers Mois de la Vie chez l'Homme. Ph.D. Thesis. Paris: CHU St-Antoine; 1978.

Gaultier, C.; Boule, M.; Allaire, Y.; Clement, A; Girard, F. Growth of lung volumes during the first three years of life. Bull. Eur. Physiopathol. Respir. 15:1103-1116; 1979.

Gaultier, C.; Perret, L.; Boule, M.; Buvry, A.; Girard, F. Occlusion pressure and breathing pattern in healthy children. Respir. Physiol. 46:71-80; 1981.

Gehr, P. Anatomy and morphology of the respiratory tract. In: Annex A. Human Respiratory Tract Model for Radiological Protection. ICRP Publication 66. Annals of the ICRP, 24(1-3):121-166; 1994.

Gehr, P. Inhalation pathway in infants and children. In: Gerber, G.B.; Métivier, H.; Smith, H., eds. Age-Related Factors in Radionuclide Metabolism and Dosimetry, pp. 67-78. Dordrecht, Netherlands: Martinus, Nijhoff Publishers; 1987.

Gies, R.A.; Cross, F.T.; Dagle, G.E. A histologic study of the influence of cigarette smoking in suppressing radon daughter carcinogenesis in dogs. Health Phys. 53(5):527-529; 1987.

Gilbert, R.; Auchincloss, J.H. ,. Jr.; Baule, G.; Peppi, D.; Long, D. Breathing pattern during CO_2 inhalation obtained from motion of the chest and abdomen. Respir. Physiol. 13:238-252; 1971.

Gilbert, R.O. Statistical Methods for Environmental Pollution Monitoring. New York: Van Nostrand Reinhold Company; 1987.

Godfrey, S. Exercise Testing in Children. London, United Kingdom: Saunders; 1973.

Godfrey, S.; Davies, C. T. M.; Wozniak, E.; Barnes, C. A. Cardio-respiratory response to exercise in normal children. Clin. Sci. 40:419-431; 1971.

Grodins, F.S. Analysis of factors concerned in regulation of breathing in exercise. Physiol. Rev. 30:220-239; 1950.

Guyton, A.C. , M.D. Textbook of Medical Physiology, Eighth Edition. Philadelphia: W.B. Saunders Company; 1991.

Hahn, G.J.; Shapiro, S.S. Statistical Models in Engineering. New York: Wiley; 1967.

Hamby, D.M. A comparison of sensitivity analysis techniques. Health Phys. 68(2):195-204; 1995.

Hansen, J.E.; Ampaya, E.P. Human air space, shapes, sizes, areas and volumes. J. Appl. Physiol. 38:990-995; 1975.

Harley, N.H.; Pasternack, B. S. Alpha absorption measurements applied to lung dose from radon daughters. Health Phys. 23:771-782; 1972.

Hart, M.; Orzalesi, M.; Cook, L. Relation between anatomic respiratory dead space and body size and lung volume. J. Appl. Physiol. 18:519-522; 1963.

Hastings, C. Approximations for Digital Computers. Princeton, NJ: Princeton University Press; 1955.

Helliesen, P.J.; Cook, C.D.; Friedlander, L.; Agathon, S. Studies of respiratory physiology in children I. Mechanics of respiration and lung volumes in 85 normal children 5 to 17 years of age. Pediatrics. 22:80-93; 1958.

Hey, E.N.; Lloyd, B.B.; Cunningham, D.J.C.; Jukes, M.G.M.; Bolton, D.P.G. Effects of various respiratory stimuli on the depth and frequency of breathing in man. Respir. Physiol. 1:193-205; 1966.

Heyder, J.; Rudolf, G. Mathematical models of particle deposition in the human respiratory tract. J. Aerosol Science. 15:697-707; 1984.

Hinds, W.C. Aerosol Technology: Properties, Behavior and Measurement of Airborne Particles. New York: Wiley & Sons; 1982.

Hoffman, F.O.; Baes; C.F. A Statistical Analysis of Selected Parameters for Predicting Food Chain Transport and Internal Dose of Radionuclides. Report NUREG/CR-1004. Oak Ridge Nat. Lab., Oak Ridge, TN. Available from National Technical Information Service, Springfield, Virginia; 1979.

Hoffman, F.O.; Gardner, R.H. Evaluation of uncertainties in radiological assessment models. In: Till, J. E. and Meyer, H. R., eds. Radiological Assessment: A Textbook on Environmental Dose Analysis. NUREG/CR-3332. U.S. Government Printing Office; 1983.

Hofmann, W. Cellular lung dosimetry for inhaled radon decay products as a base for radiation-induced lung cancer risk assessment. I. Calculation of mean cellular doses. Radiat. Environ. Biophys. 20:95-112; 1982a.

Hofmann, W. Dose calculations for the respiratory tract from inhaled natural radioactive nuclides as a function of age. II. Basal cell dose distributions and associated lung cancer risk. Health Phys. 43:31-45; 1982b.

Hofmann, W.; Daschil, F. Biological variability influencing lung dosimetry for inhaled Rn-222 and Rn-220 decay products. Health Phys. 50:345-367; 1986.

Horsfield, K.; Cumming, G. Morphology of the bronchial tree in man. J. Appl. Physiol. 24:373-383; 1968.

Horsfield, K.; Dart, G.; Olson, D.E.; Filley, G.F.; Cumming, G. Models of the human bronchial tree. J. Appl. Physiol. 31:207-217; 1971.

Hunacek, M.M.; Kathren, R.L. Alpha radiation risk coefficients for liver cancer, bone sarcomas, and leukemia. Health Phys. 68:41-49; 1995.

IAEA (International Atomic Energy Agency). Evaluating the Reliability of Predictions Made Using Environmental Transfer Models. Safety Series No. 100. Vienna, Austria: International Atomic Energy Agency; 1989.

ICRP (International Commission on Radiological Protection). 1990 Recommendations of the ICRP. ICRP Publication 60. Annals of the ICRP. 21(1-3); 1991a.

ICRP (International Commission on Radiological Protection). Age-Dependent Dose to Members of the Public from Intake of Radionuclides: Part 1. ICRP Publication 56. Annals of the ICRP. 20(2); 1989.

ICRP (International Commission on Radiological Protection). Annual Limits on Intake of Radionuclides by Workers Based on the 1990 Recommendations. ICRP Publication 61. Annals of the ICRP. 21(4); 1991b.

ICRP (International Commission on Radiological Protection). Biological effects of inhaled radionuclides. ICRP Publication 31. Oxford, United Kingdom:Pergamon Press; 1980.

ICRP(International Commission on Radiological Protection). Human respiratory tract model for radiological protection. ICRP Publication 66. Annals of the ICRP. 24 (1-3); 1994.

ICRP (International Commission on Radiological Protection). Limits for Intakes of Radionuclides by Workers. ICRP Publication 30, Part 1. Annals of the ICRP. 2(3/4); 1979.

ICRP (International Commission on Radiological Protection). The Metabolism of Plutonium and Other Actinides. ICRP Publication 19. Oxford, United Kingdom: Pergamon Press; 1972.

ICRP (International Commission on Radiological Protection). The Metabolism of Plutonium and Related Elements. ICRP Publication 48. Annals of the ICRP. 16 (2/3); 1986.

ICRP (International Commission on Radiological Protection). Recommendations of the ICRP. Report of Committee II on Permissible Dose for Internal Radiation (1959). ICRP Publication 2. 1960.

ICRP (International Commission on Radiological Protection). Report of the Task Group on Reference Man. ICRP Publication 23. Oxford, United Kingdom: Pergamon Press; 1975.

ICRU (International Commission on Radiation Units and Measurements). Stopping Powers and Ranges for Protons and Alpha Particles. ICRU Report No. 49. Bethesda, MD: ICRU Publications; 1993.

Iman, R.L.; Conover, W.J. A distribution-free approach to inducing rank correlation among input variables, Commun. Stat., Part B: Simul. Comput. 11(3):311-334; 1982.

Iman, R.L.; Helton, J.C. A Comparison on Uncertainty and Sensitivity Analysis Techniques for Computer Models. NUREG/CR-3904, Sandia Natl. Labs, Albuquerque, New Mexico. Available from the National Technical Information Service, Springfield, Virginia; 1995.

Iman, R.L.; Helton, J.C. An investigation of uncertainty and sensitivity analysis techniques for computer models. Risk Analysis. 8(1):71-90; 1988.

Iman, R.L.; Shortencarier, M.J. A Fortran 77 Program and User's Guide for the Generation of Latin Hypercube and Random Samples for Use with Computer Models. Report NUREG/CR-3624, Sandia Natl. Labs, Albuquerque, New Mexico. Available from the National Technical Information Service, Springfield, Virginia; 1984.

Iman, R.L.; Shortencarier, M.J.; Johnson, J.D. A Fortran 77 Program and User's Guide for the Calculation of Partial Correlation and Standardized Regression Coefficients. Report NUREG/CR-4122, Sandia Natl. Labs, Albuquerque, New Mexico. Available from the National Technical Information Service, Springfield, Virginia; 1985.

James, A.C. Lung dosimetry. In: Nazaroff, W. W. and Nero, A. V., Jr., eds. Radon and Its Decay Products in Indoor Air, pp. 259-309. New York: John Wiley and Sons, Inc; 1988.

James, A.C.; Akabani, G.; Birchall, A.; Jarvis, N. S.; Briant, J. K.; Durham, J. S. Absorbed fractions for alpha, electron, and beta emissions. In: Annex H. Human Respiratory Tract Model for Radiological Protection. ICRP Publication 66. Annals of the ICRP. 24(1-3):459-482; 1994a.

James, A.C.; Birchall, A.; Cross, F.T.; Cuddihy, R.G.; Johnson, J.R. The current approach of the ICRP tash group for modeling doses to respiratory tract tissues. Health Phys. 57(S1):271-282; 1989.

James, A.C.; Stahlhofen, W.; Rudolf, G.; Kobrich, R.; Briant, J.K.; Egan, M.J.; Nixon, W.; Birchall, A. Deposition of inhaled particles. In: Annex D. Human Respiratory Tract Model for Radiological Protection. ICRP Publication 66. Annals of the ICRP. 24(1-3):231-299; 1994b.

Jarvis, N.S.; Birchall, A.; James, A.C.; Bailey, M.R.; Dorrian, M. LUDEP 1.0: Personal Computer Program for Calculating Internal Doses Using the New ICRP Respiratory Tract Model. Oxon, England: National Radiological Protection Board; 1993.

Kay, J.D.S.; Petersen, E.; Vejby-Christensen, H. Mean and breath-by-breath pattern of breathing in man during steady-state exercise. J. Physiol. Lond. 251:444-669; 1975.

Keenan, K.P.; Combs, J.W.; McDowell, E.M. Regeneration of hamster tracheal epithelium after mechanical injury. I. Focal lesions: Quantitative morphological study of cell proliferation. Virchows Arch. (Cell Pathol.). 41:193-214; 1982a.

Keenan, K.P.; Combs, J.W.; McDowell, E.M. Regeneration of hamster tracheal epithelium after mechanical injury. II. Multifocal lesions: Stathmokinetic and autoradiographic studies of cell proliferation. Virchows Arch. (Cell Pathol.). 41:215-229; 1982b.

King, J.R. Probability Charts for Decision Making. New York: Industrial Press; 1971.

Landahl, H. On the removal of air-borne droplets by the human respiratory tract. Bulletin of Mathematical Biology. 12:43-56; 1950.

Layton, D.W. Metabolically consistent breathing rates for use in dose assessments. Health Phys. 64:23-36; 1993.

Lee, S.Y.; Bondietti, E.A.; Tamura, T. Dissolution characteristics of Pu-contaminated soils and sediments in lung serum simulant solution. Health Phys. 43(5):663-668; 1982.

Lentner, C., ed. Geigy Scientific Tables. Vol. 1: Units of Measurements, Body Fluids, Composition of the Body, Nutrition. Eighth Edition. Basle, Switzerland: Ciba-Geigy Ltd.; 1981.

Lewis, H.W. Report of the Risk Assessment Review Group. NUREG/CR-0400, U.S. Nuclear Regulatory Commission, Washington, DC. Available from the National Technical Information Service, Springfield, Virginia; 1978.

Liebetrau, A.M.; Doctor, P.G. The generation of dependent input variables to a performance assessment simulation code. In: Proceedings of an NEA Workshop on Uncertainty Analysis for Performance Assessments of Radioactive Waste Disposal Systems, pp. 85-115. Paris, France: OECD (Organization for Economic Cooperation and Development); 1987.

Lilliefors, H.W. Correction to the paper "On the Kolmogorov-Smirnov test for normality with mean and variance unknown." J. Amer. Statist. Assoc. 64:1702; 1969.

Lilliefors, H.W. On the Kolmogorov-Smirnov test for normality with mean and variance unknown. J. Amer. Statist. Assoc. 62:399-402; 1967.

Lind, F.; Hesser, C.M. Breathing pattern and lung volumes during exercise. Acta. Physiol. Scand. 120:123-129; 1984.

Lippmann, M. Regional deposition of particles in the human respiratory tract. In: Handbook of Physiology--Reactions to Environmental Agents, pp. 213-232. Bethesda, Maryland: American Physiological Society; 1977.

Little, C.A.; Miller, C.W. The Uncertainty Associated with Selected Environmental Transport Models. Report ORNL-5528. Oak Ridge Nat. Lab., Oak Ridge, TN. Available from National Technical Information Service, Springfield, Virginia; 1979.

Mann, J.R.; Kirchner, R.A. Evaluation of lung burdens following acute inhalation exposure to highly insoluble PuO_2. Health Phys. 13:877-882; 1967.

Masse, R.; Cross, F.T. Effects of radiation on the respiratory tract. In: Annex C. Human Respiratory Tract Model for Radiological Protection. ICRP Publication 66. Annals of the ICRP. 24(1-3):203-230; 1994.

Masse, R.; Cross, F.T. Risk considerations related to lung modeling. Health Phys. 57(Supp. 1):283-289; 1989.

Matheson, H.W.; Gray, J.S. Ventilatory function tests. III. Resting ventilation, metabolism, and derived measures. J. Clin. Invest. 20:688-692; 1950.

McDowell, E.M.; Keenan, K.P.; Huang, M. Restoration of mucociliary tracheal epithelium following deprivation of vitamin A. Virchows Arch. (Cell Pathol.). 45:221-240; 1984.

McDowell, E.M.; Newkirk, C.; Coleman, B. Development of hamster tracheal epithelium. II. Cell proliferation in the fetus. Anat. Rec. 213:448-456; 1985.

McKay, M.D.; Beckman, R.J.; Conover, W.J. A comparison of three methods for selecting values of input variables in the analysis of output from a computer code. Technometrics. 21(2):239-245; 1979.

Mercer, R.R.; Russell M.L.; Crapo, J.D. Radon dosimetry based on the depth distribution of nuclei in human and rat lungs. Health Phys. 61(1):117-130; 1991.

Mercier, J.; Varray, A.; Ramonatxo, M.; Mercier, B.; Prefaut, C. Influence of anthropometric characteristics on changes in maximal exercise ventilation and breathing patterns during growth in boys. Eur. J. Appl. Physiol. 63:235-241; 1991.

Miller, F.J.; Martonen, T.B.; Menache, M.G.; Graham, R.C.; Spektor, D.M.; Lipmann, M. Influence of breathing mode and activity level on the regional deposition of inhaled particles and implications for regulatory standards. Ann. Occup. Hyg. 32:3-10; 1988.

Morgan, M.G.; Henrion, M. Uncertainty: A Guide to Dealing with Uncertainty in Quantitative Risk and Policy Analysis. New York: Cambridge University Press; 1990.

Moss, W.D.; Hyatt, E.C.; Schulte, H.F. Particle size studies on plutonium aerosols. Health Phys. 5: 212-218; 1961.

Najjar, M.F.; Rowland, M. Anthropometric reference data and prevalence of overweight, United States, 1976-80. Vital and Health Satistics, Series 11, No. 238. DHHS Pub. No. (PHS) 87-1688. Washington, D.C.: Government Printing Office; 1987.

NCRP (National Council on Radiation Protection and Measurements). Deposition, Retention, and Dosimetry of Inhaled Substances. Draft report of the NCRP. Bethesda, MD: NCRP; 1993.

NCRP (National Council on Radiation Protection and Measurements). Radiological Assessment: Predicting the Transport, Bioaccumulation, and Uptake by Man of Radionuclides Released to the Environment. NCRP Report No. 76; Bethesda, MD: NCRP; 1984.

Niinimaa, V.; Cole, P.; Mintz, S.; Shephard, R. J. Oronasal distribution of respiratory airflow. Respir. Physiol. 43:69-75; 1981.

Niinimaa, V.; Cole, P.; Mintz, S.; Shephard, R. J. The switching point from nasal to oronasal breathing. Respir. Physiol. 42:61-71; 1980.

Nixon, W.; Egan, M. J. Modelling study of regional deposition of inhaled aerosols with special reference to effects of ventilation asymmetry. J. Aerosol Sci. 18:563-579; 1987.

Nowak, E.; Hofer, E. A program package to support the probabilistic modelling of parameter uncertainties. In: Desmet, G., ed. Reliability of Radioactive Transfer Models, pp. 305-317. New York: Elsevier Applied Science; 1987.

OECD (Organization for Economic Cooperation and Development). Proceedings of an NEA Workshop on Uncertainty Analysis for Performance Assessments of Radioactive Waste Disposal Systems. Paris, France: OECD; 1987.

Ogden, T.L.; Birkett, J.L. The human head as a dust sampler. In: Walton, W.H.; McGovern, B., eds. Inhaled Particles IV, Part 2, Proceedings of an International Symposium Organized by the British Occupational Hygiene Society, pp. 93-105. Oxford, United Kingdom: Pergamon Press; 1977.

Olson, D.E.; Dart, G.A.; Filley, G. F. Pressure drop and fluid flow regime of air inspired into the human lung. J. Appl. Physiol. 28:482-494; 1970.

Paek, D.; McCool, F.D. Breathing patterns during varied activities. J. Appl. Physiol. 73:887-893; 1992.

Park, S.K.; Miller, K.W. Random number generators: Good ones are hard to find. Communications of the ACM. 31(10):1192-1201; 1988.

Paschoa, A.S.; Wrenn, M.E. Uncertainty analysis for ranking parameters in environmental methematical modelling. In: Desmet, G., ed. Reliability of Radioactive Transfer Models, pp. 331-338. New York: Elsevier Applied Science; 1987.

Patrick, J.M.; Howard, A. The influence of age, sex, body size and lung size on the control and pattern of breathing during CO_2 inhalation in caucasians. Respir. Physiol. 16:337-350; 1972.

Phalen, R.; Oldham, M.; Beaucage, C.; Crocker, T.; Mortensen, J. Postnatal enlargement of human tracheobronchial airways and implications for particle deposition. Anat. Rec. 212:368-380; 1985.

Phalen, R.; Schum, G.; Oldham, M. The sensitivity of an inhaled aerosol tracheobronchial deposition model to input parameters. J. Aerosol Medicine. 3:271-282; 1990.

PNL (Pacific Northwest Laboratory). Air Pathway Report. Phase I of the Hanford Environmental Dose Reconstruction Project. PNL-7412, HEDR Rev. 1. Richland, WA: Pacific Northwest Laboratory; 1991a.

PNL (Pacific Northwest Laboratory). Columbia River Pathway Report, Phase I of the Hanford Environmental Dose Reconstruction Project. PNL-7411, HEDR Rev. 1. Richland, WA: Pacific Northwest Laboratory; 1991b.

PNL (Pacific Northwest Laboratory). Summary Report. Phase I of the Hanford Environmental Dose Reconstruction Project. PNL-7410, HEDR Rev. 1. Richland, WA: Pacific Northwest Laboratory; 1991c.

Poon, C. Effects of inspiratory resistive load on respiratory control in hypercapnia and exercise. J. Appl. Physiol. 66:2391-9; 1989.

Powers, S.K.; Howley, E.T. Exercise Physiology: Theory and Application to Fitness and Performance. Dubuque, Iowa: William C. Brown Publishers; 1990.

Press, W.H.; Flannery, B.P.; Teukolsky, S.A.; Vetterling, W.T. Numerical Recipes: The Art of Scientific Computing. New York: Cambridge University Press; 1986.

Quanjer, H.; Andersen, L. H.; Tammeling, G. J.,eds. Static lung volumes and capacities. Bull. Europ. Physiopath. Resp. 19:11-21, 48-53; 1983.

Ramamurthi, M.; Hopke, P. K. On improving the validity of wire screen unattached fraction Rn daughter measurements. Health Phys. 56:189-194; 1989.

Rasmussen, N.C. Reactor Safety Study: An Assessment of Accident Risks in U.S. Commercial Nuclear Power Plants. Report NUREG-75/014 (WASH-1400). Nuclear Regulatory Commission, Washington, DC. Available from the National Technical Information Service, Springfield, Virginia; 1975.

Rodenstein, D.O.; Stanescu, D.C. Soft palate and oronasal breathing in humans. J. Appl. Physiol. 57:651-657; 1984.

Rohrer, F. Physiologie der Atembewegung. In: Bethe et al.,eds. Handbuch der Normalen und Path. Physiologie, Vol. 2, pp. 70-127. Berlin: Springer; 1925.

Roy, M.; Courtay, C. Daily activities and breathing parameters for use in respiratory tract dosimetry. Radiat. Protect. Dosim. 35:179-186; 1991.

Royston, J.P. An extension of Shapiro and Wilk's W test for normality to large samples. Applied Statistics. 31:115-124; 1982.

Rubinstein, R.Y. Simulation and the Monte Carlo Method. New York: Wiley; 1981.

Rudolf, G.; Gebhart, J.; Heyder, J.; Scheuch, G.; Stahlhofen, W. Modelling the deposition of aerosol particles in the human respiratory tract. J. Aerosol Sci. 14:188-192; 1983.

Rudolf, G.; Gebhart, J.; Heyder, J.; Schiller, C. F.; Stahlhofen, W. An empirical formula describing aerosol deposition in man for any particle size. J. Aerosol Sci. 17:350-355; 1986.

Rudolf, G.; Kobrich, R.; Stahlhofen, W. Modelling and algebraic formulation of regional aerosol deposition in man. J. Aerosol Sci. 21:S403-S406; 1990.

Rudolf, G.; Kobrich, R.; Stahlhofen, W.; James, A. C. Regional airway deposition in man--a statistical and algebraic model. In: Dodgson, J. and McCallum, R. L., eds. Inhaled Particles VII. Proceedings of an International Symposium on Inhaled Particles Organized by the British Occupational Hygiene Society. Ann. Occup. Hygiene; 1994.

Sachs, L. Applied Statistics: A Handbook of Techniques. New York: Springer-Verlag; 1984.

Saibene, F.; Mognoni, P.; Lafortuna, C. L.; Mostardi, R. Oronasal breathing during exercise. Pfluegers Arch. 378:65-69; 1978.

Saltin, B.; Astrand, P. Maximal oxygen uptake in athletes. J. Appl. Physiol. 23:353-358; 1967.

Scheuch, G. Die Dispersion, Deposition und Clearance von Aerosolpartikelen in den menschlichen Atemwegen (PhD Thesis). Frankfurt am Main, Germany: J.W. Goethe-Universitat; 1991.

Scheuch, G.; Kreyling, W.; Haas, F.; Stahlhofen, W. The clearance of polystyrene particles from human intrathoracic airways. J. Aerosol Med. 6(Suppl.):47; 1993.

Scheuch, G.; Stahlhofen, W. Particle depositon of inhaled aerosol boluses in the upper human airways. J. Aerosol Med. 1:29-36; 1988.

Schofield, W.N. Predicting basal metabolic rate, new standards and review of previous work. Hum. Nutr. Clin. Nutr. 39C:5-41; 1985.

Schum, G.; Phalen, R.; Oldham, M. The effect of dead space on inhaled particle deposition. J. Aerosol Med. 4:297-311; 1991.

Shapiro, S.S.; Wilk, M.B. An analysis of variance test for normality (complete samples). Biometrika. 52:591-611; 1965.

Skrable, K.W.; French, C.; Chabot, G.; Major, A. A general equation for the kinetics of linear first order phenomena and suggested applications. Health Phys. 27:155-157; 1974.

Smalley, K.J.; Knew, A.N.; Kendrick, Z.V.; Colliver, J.A.; Owen, Q.E. Reassessment of body mass indicies. Am. J. Clin. Nutr. 52:405-408; 1990.

Stahlhofen, W. Human lung clearance following bolus inhalation of radioaerosols. In: Extrapolation of Dosimetric Relationships for Inhaled Particles and Gases, pp. 153-166. Washington, DC: Academic Press; 1989.

Stahlhofen, W.; Gebhart, J.; Rudolf, G.; Scheuch, G. Measurement of lung clearance with pulses of radioactively-labelled aerosols. J. Aerosol Sci. 17:333-336; 1986a.

Stahlhofen, W.; Gebhart, J.; Rudolf, G.; Scheuch, G. Retention of radioactivity labelled Fe_2O_3-particles in human lungs. In: Hofmann, W., ed. Deposition and Clearance of Aerosols in the Human Respiratory Tract. Second International Symposium, Salzburg, Austria, September 18-20, 1986, pp. 123-128. Vienna, Austria: Facultas Universitätsverlag Ges.m.b.H.; 1987a.

Stahlhofen, W.; Gebhart, J.; Rudolf, G.; Scheuch, G.; Bailey, M. R. Human lung clearance of inhaled radioactively labelled particles in horizontal and vertical position of the inhaling person. J. Aerosol Sci. 18:741-744; 1987b.

Stahlhofen, W.; Gebhart, J.; Rudolf, G.; Scheuch, G.; Philipson, K. Clearance from the human airways of particles of different sizes deposited from inhaled aerosol boli. In: Aerosols: Formation and Reactivity. Second International Aerosol Conference, West Berlin, Germany, Sept.22-26, 1986, pp. 192-196. Oxford, England: Pergamon Press; 1986b.

Stahlhofen, W.; Koebrich, R.; Rudolf, G.; Scheuch, G. Short term and long term clearance of particles from the upper human respiratory tract as function of particle size. J. Aerosol Sci. 12:S407-S410; 1990.

Stahlhofen, W.; Rudolf, G.; James, A.C. Intercomparison of experimental regional aerosol deposition data. J. Aerosol Med. 2:285-308; 1989.

Stahlhofen, W.; Scheuch, G.; Bailey, M. R. Measurement of the tracheobronchial clearance of particles after aerosol bolus inhalation. In: Dodgson, J. and McCallum, R. I., eds. Inhaled Particles VII, Proceedings of an International Symposium on Inhaled Particles Organized by the British Occupational Hygiene Society. Ann. Occup. Hyg.; 1994.

Stahlman, M.T.; Meece, N. J. Pulmonary ventilation and diffusion in the human newborn infant. J. Clin. Invest. 36:1081-1091; 1957.

Sutherland, J.W. Estimation of lung cancer risk from environmental exposure to airborne plutonium from the Rocky Flats plant. In: Current Concepts in Lung Dosimetry, Proceedings of a Special Workshop, pp. 157-167. PNL-SA-11049. Available from the National Technical Information Service, Springfield, VA; 1983.

Swift, D.L.; Montassier, N.; Hopke, P.K.; Karpen-Hayes, K.; Cheng, Y.S.; Su, Y.F.; Yeh, H.C.; Strong, J.C. Inspiratory deposition of ultrafine particles in human nasal replicate cast. J. Aerosol Sci. 23:65-72; 1992.

Taussig, L.M.; Harris, T.R.; Leboowitz, M.D. Lung function in infants and young children. Am. Rev. Respir. Dis. 116:233-239; 1977.

Taylor, L.S. The Tri-Partite Conferences on Radiation Protection. Canada, United States (1949-1953). U.S. DOE Report HVO-270 (DE 84016028). Available from the National Technical Information Service, Springfield, VA; 1984.

TGLD (Task Group on Lung Dynamics). Deposition and retention models for internal dosimetry of the human respiratory tract. Health Phys. 12:173-207; 1966.

Till, J.E.; Meyer, H.R. , Radiological Assessment: A Textbook on Environmental Dose Analysis. U.S. Government Printing Office, NUREG/CR-3332:; 1983.

Trevisani, L.; Sartori, S.; Bovolenta, M. R.; Mazzoni, M.; Pazzi, P.; Putinati, S.; Potena, A. Structural characterization of the bronchial epithelium of subjects with chronic bronchitis and in asymptomatic smokers. Respiration. 59:136-144; 1992.

Uddstromer, M. Nasal respiration. Acta Otolaryngol. 42, Suppl.:3-146; 1940.

USDA (U.S. Department of Agriculture). Nutrient Intakes: Individuals in the United States, year 1977-1978, NFCS 1977-1978. Report No. I-2. Washington, DC: U.S. Dept. of Agriculture, Human Nutrition Information Service; 1984.

USDHHS (U.S. Department of Health and Human Services). Dietary Intakes Source Data: United States, 1976-1980. DHHS Publication No. (PHS) 83-1681. Hyattsville, MD: National Center for Health Statistics; 1983.

USNRC (U.S. Nuclear Regulatory Commission). Standards for protection against radiation. Title 10 Part 20 Code of Federal Regulations (10CFR20). Washington, DC: Government Printing Office; 1992.

Vashi, V.D.; Suryanarayanan, C.S.; Kotrappa, P. Dissolution characteristics of plutonium aerosols in lung serum simulant. Health Phys. 39:105-108; 1980.

Vincent, J.H.; Mark, D. Application of blunt sampler theory to the definition and measurement of inhalable dust. In: Walton, W. H; Critchlow, A.; Coppock, S., eds. Inhaled Particles V. Proceedings of an International Symposium Organized by the British Occupational Hygiene Society. Ann. Occup. Hyg. 26:3-19; 1982.

Vincent, J.H.; Mark, D.; Miller, B.G.; Armbruster, L.; Ogden, T.L. Aerosol inhalability at higher windspeeds. J. Aerosol Sci. 21:577-586; 1990.

Vogel, R.M. The probability plot correlation coefficient test for normal, lognormal and gumbel distributional hypothesis. Water Resources Research. 22(4):587-590; 1986.

Voillequé, P.G.; Mis, F.J.; Warren, S.B.; Harrison, M.C. Solubility of transuranic nuclides in aerosols in two Ginna steam generator work environments. In: Power Reactor Health Physics, Proceedings of the Twenty-First Midyear Topical Meeting of the Health Physics Society, pp. 251-259. McLean, Virginia: Health Physics Society; 1987.

Walker, J.T. An empirical model descibing the postnatal growth of organs in ICRP reference humans: I. The lungs. Radiat. Prot. Dosim. 38:7-13; 1991.

Warren, D.W.; Hairfile, W.M.; Dalston, E.T. Effect of age on nasal cross-sectional area and respiratory mode in children. Laryngoscope 100:89-93; 1990.

Weast, R.C., ed. CRC Handbook of Chemistry and Physics, 59th Edition. West Palm Beach, Florida: CRC Press, Inc.; 1978.

Weibel, E.R. The Normal Human Lung. New York: Academic Press Inc; 1963.

Wheatley, J.R.; Amis, T.C.; Engel, L.A. Oronasal partitioning of ventilation during exercise in humans. J. Appl. Physiol. 71:546-551; 1991.

Wise, K.N. The effect of uncertainty of model parameters of estimates of committed dose equivalent. Health Phys. 48 (4):501-508; 1985.

Wood, L.; Prichard, S.; Weng, T.; Kruger, K.; Bryan, A.; Levison, H. Relationship between anatomical dead space and body size in health, asthma, and cystic fibrosis. Am. Rev. Respir. Dis. 104:215-222; 1971.

Yeh, H.; Schum, G. Models of human lung airways and their application to inhaled particle deposition. Bull. of Mathematical Biology. 42:461-480; 1980.

Younes, M. Determinants of thoracic excursions. In: Whipp, B. J.; Wasserman, K., eds. Exercise: Pulmonary Physiology and Pathophysiology, pp. 13-17. New York: Marcel Dekker, Inc; 1991.

Yu, C.; Diu, C.K. A comparative study of aerosol deposition in different lung models. J. Am. Ind. Hyg. Assoc. 43:54-56; 1982.

Yu, C.P.; Diu, C.K.; Soong, T.T. Statistical analysis of aerosol deposition in nose and mouth. J. Am. Ind. Hyg. Assoc. 42:726-733; 1981.

Zapletal, A.; Šamánek, M.; Paul, T. Lung Function in Children and Adolescents. Methods, References Values. (Herzog, H., ed.). Basel, Switzerland: Karger; 1987.

BIOGRAPHICAL SKETCH

Thomas Edward Huston was born in North Little Rock, Arkansas, on May 20, 1968. He lived in North Little Rock through his childhood and received his elementary and secondary education through the public school system, graduating from North Little Rock Ole Main High School in June, 1986.

Following high school, Thomas was awarded a Trustee's Scholarship and an Arkansas Governor's Scholarship to attend Hendrix College in Conway, Arkansas, where he majored in physics. While at Hendrix College, Thomas was awarded the Barry M. Goldwater Excellence in Science Foundation Scholarship and the 1990 Hendrix College President's Medal. He also served on the student senate during his senior year. During all but the first summer of his enrollment at Hendrix, Thomas participated in summer internships at Oak Ridge National Laboratory in Tennessee. In the spring of 1990, Thomas was offered a United States Department of Energy (DOE) Environmental Restoration and Waste Management Fellowship to attend graduate school in health physics. Thomas graduated Summa Cum Laude from Hendrix College in June of 1990, receiving a Bachelor of Arts degree with distinction in physics.

He accepted the DOE fellowship and was admitted into the Department of Nuclear Engineering Sciences at the University of Florida in the Health Physics Program. After two years including course work, research, and a practicum experience at Oak Ridge

National Laboratory, Thomas received his Master of Science degree in August of 1992. After that date Thomas began his work toward the doctoral degree in health physics.

During February of 1993 Thomas was fortunate to have received the James E. Swander Memorial Scholarship which recognizes outstanding graduate students in the Department of Nuclear Engineering Sciences. In November of 1993 Thomas passed his qualifying exam and became an official PhD candidate. In January of 1994 Thomas became an Associate Member of the American Academy of Health Physics, resulting from his successful completion of Part I of the certification exam administered by the American Board of Health Physics. His appointment as a DOE fellow ended in August of 1994 at which time he began work on a research assistantship provided through the Department of Environmental Engineering Sciences.

Thomas is a member of the national Health Physics Society, the Florida Chapter of Health Physics Society, and the American Nuclear Society. Thomas is happily married to the former Rhonda Michelle Wood, who is also a native of North Little Rock, Arkansas. He has one son, Hayden Edward Huston, born July 24, 1995.

I certify that I have read this study and that in my opinion it conforms to acceptable standards of scholarly presentation and is fully adequate, in scope and quality, as a dissertation for the degree of Doctor of Philosophy.

William G. Vernetson, Chairman
Associate Engineer of Nuclear
Engineering Sciences

I certify that I have read this study and that in my opinion it conforms to acceptable standards of scholarly presentation and is fully adequate, in scope and quality, as a dissertation for the degree of Doctor of Philosophy.

W. Emmett Bolch, Jr., Cochair
Professor of Environmental Engineering
Sciences

I certify that I have read this study and that in my opinion it conforms to acceptable standards of scholarly presentation and is fully adequate, in scope and quality, as a dissertation for the degree of Doctor of Philosophy.

Marc J. Jaeger
Professor of Physiology

I certify that I have read this study and that in my opinion it conforms to acceptable standards of scholarly presentation and is fully adequate, in scope and quality, as a dissertation for the degree of Doctor of Philosophy.

David E. Hintenlang
Associate Professor of Nuclear
Engineering Sciences

I certify that I have read this study and that in my opinion it conforms to acceptable standards of scholarly presentation and is fully adequate, in scope and quality, as a dissertation for the degree of Doctor of Philosophy.

William S. Properzio
Associate Professor of Environmental Engineering Sciences

I certify that I have read this study and that in my opinion it conforms to acceptable standards of scholarly presentation and is fully adequate, in scope and quality, as a dissertation for the degree of Doctor of Philosophy.

Wesley E. Bolch
Associate Professor of Nuclear Engineering Sciences

This dissertation was submitted to the Graduate Faculty of the College of Engineering and to the Graduate School and was accepted as partial fulfillment of the requirements for the degree of Doctor of Philosophy.

August 1995

Winfred M. Phillips
Dean, College of Engineering

Karen A. Holbrook
Dean, Graduate School

LD
1780
1995
.H972

UNIVERSITY OF FLORIDA
3 1262 08553 7123